**NTNU – Trondheim**
Norwegian University of
Science and Technology

# Hot gas cleaning

Milly Kure

Chemical Engineering
Submission date: June 2014
Supervisor: Edd Anders Blekkan, IKP
Co-supervisor: Svatopluk Chytil, SINTEF

Norwegian University of Science and Technology
Department of Chemical Engineering

**Preface**

This thesis is made as a completion of the MSc. degree in Chemical engineering. The study presented in this report has been carried out at NTNU, Chemical engineering department.

Many people have contributed to this study either academically, practically or with support and motivation. I would therefore like to thank my supervisor, Edd Blekkan (Professor NTNU) and co-supervisor, Svatopluk Chytil (Sintef) for their valuable input and support throughout the course of the study.

Furthermore I would like to thank Karin Dragsten, Andrey Volynkin, Fengliu Lou, Eirik Pedersen and Nikolaos Tsakoumis for their patience and support offered through training in use of various instruments.

Finally I would like to thank my family and friends for their support throughout my two-year masters study.

**Declaration of compliance**

I declare that this is an independent work according to the exam regulations of the Norwegian University of Science and Technology (NTNU).

Place and date: Signature:

## TABLE OF CONTENTS

## Summary

Five $H_2S$ adsorbent materials for hot gas cleaning of biomass-derived synthesis gas were prepared. Three of the new sorbents were prepared based on a novel manganese-based sorbent that uses alumina support. The new adsorbent materials were prepared with 15 wt% manganese loading on different supports as $ZrO_2$, $TiO_2$ and $CeO_2$. The supports have different physico-chemical properties. Two alumina based sorbents were prepared with 15 and 30wt% manganese loading on the alumina support. All the sorbents were prepared by single impregnation method except for the 30wt% loading which was prepared by double impregnation. This study required to investigate the sorption activities of the new developed materials and compare their performance with the novel alumina based sorbents.

The new sorbents were characterized along-side the alumina based sorbents using nitrogen adsorption, X-ray diffraction, Thermogravimetric Analysis, Temperature Programmed Reduction and oxygen pulse chemisorption methods. Raman spectroscopy analysis was also carried out however due to inability to replicate results for a reference manganese oxide sorbent the results have not been included in the main report but have been attached to the appendix for the interested reader.

A new laboratory based set-up unit was to be used to test sorption activities. Various challenges were faced while ensuring that the new laboratory set up was running safely and efficiently, and as a result, the remaining time was not enough to test all the five sorbents that were prepared. The sorption tests were only performed on the alumina based sorbents, in duplicate. The second set of experiments was performed with doubled amounts of sorbents, sorption gases and regeneration gases. This in a way, served to confirm reproducibility of results with the new laboratory setup. The new developed sorbent materials have been handed over to the supervisors and left as future work.

The sorption studies of the alumina based sorbents were performed by carrying out repeated sulfidation and regeneration reaction cycles $450^0$C. The results were monitored and measured by a mass spectrometer. A total of thirteen sorption cycles were performed in each experiment by using a sorption gas mixture of $N_2$, $H_2$ and $H_2S$ (Ar) with $H_2S$ concentration of 0.4% in the feed for the sulfidation reaction and $O_2$ diluted in $N_2$ (10% $O_2$) gas for the regeneration reactions. The first and last sorption cycles were measured as full sorption cycles meaning they were allowed to go to maximum saturation of the sorbent with $H_2S$. Cycles 2 to 12 were performed as short sorption cycles and were not allowed to reach maximum saturation. The sulfidation reaction was stopped when the $H_2S$ concentration in the outlet gas reached 0.1%. This allowed as many as 5 sorption cycles to be carried out in one day. The steps involved in each sorption cycle can be summarized as flushing, sulfidation, flushing and regeneration. One short sorption cycle took approximately one and a half hours.

Sorption capacities for the alumina based sorbents have been calculated as $gH_2S/gSorbent$ from the measurement data obtained through sorption studies. A breakthrough point of 0.02% $H_2S$ concentration was used.

# Chapter 1 Introduction

## 1.1 Biomass renewable energy

Biomass gasification is a process that converts biomass into synthesis gas at temperatures close to $800^0$C in the presence of gasifying oxidants such as oxygen, air and steam. Biomass is made up of recently living carbonaceous type of material which when heated in the presence of gasifying oxidants is converted into a valuable combustible gaseous fuel known as synthesis gas. Synthesis gas is a mixture of $H_2$ and CO which can be used to generate heat, power or converted into different types of chemicals.

Biomass gasification hence provides a means of converting biomass into valuable forms both economically and industrially. But synthesis gas is not the only product from biomass gasification. Other gaseous products and solid waste materials are produced concurrently and some of these products have a negative impact on the downstream instruments that use the synthesis gas.

Synthesis gas can also be produced through processes such as coal gasification, partial oxidation of heavy oil fraction, steam and auto thermal reforming of natural gas. The various processes make it possible to use other forms of carbonaceous feedstock such as the traditional fossil fuels; coal, heavy oil fraction from petroleum oil and natural gas to produce synthesis gas. However biomass gasification possesses certain advantages over the traditional fossil fuels.

In the present time, fossil fuels dominate the heat and power industry partly due to their relatively cheaper cost and the availability of commercial technology. A similar dominant trend is observed when it comes to emission of the environmentally harmful greenhouse gas, carbon dioxide ($CO_2$). In 2011, about 99% of the $CO_2$ emissions was produced through combustion of coal, oil and gas with coal contributing the most contribution at 44% [2].

Greenhouse gas contributes negatively to the global climate change through global warming. There are numerous reports that also look into, and further explain the ecological and social negative impacts of global warming examples of which include floods (due to melting of glaciers) and economic consequences caused by poor yields of agricultural products [3, 4].

Fossil fuels are also made up of carbon-containing compounds that are stored in geological reservoirs. The carbon is released into the atmosphere during combustion introducing new carbon dioxide into the atmosphere. Biomass on the other hand is considered to be $CO_2$-neutral because the net emission of carbon dioxide from biomass is relatively zero. Biomass (plants), through photosynthesis, captures carbon dioxide from the air and releases it during combustion making biomass an attractive $CO_2$-emission-free renewable energy source.

The predicted dwindling of fossil fuel reserves and an ever increasing global demand for energy have partly contributed to the increased focus on renewable energy sources. Despite the prediction, fossil fuels are still expected to be the major source of energy in 2035 [5]. Based on 2011 inventory and rate of production, the existing coal reserves were estimated to last for a little over 100 years [5]. Biomass, in

contrast to the fossil fuels, can be obtained from renewable materials such as wood and agricultural waste.

The economic development of countries is closely linked to availability and deliverability of raw materials and products. This is aided by an improved production and transportation sector i.e. roads, sea and aviation all of which need fuel. Hence the levels of economic development is also linked to the use of fossil fuels [5]. Most industrial production processes such as the steel industry and chemical industries require a lot of energy and fossil fuels are a cheap source of energy with already existing conversion technology that is commercially available.

The close link between fossil fuels and economic development can be hampered by the geographically-limited fossil-fuel sources. Fossil fuel is not evenly distributed on the globe and this is a potential source of national and economic insecurity to the countries that have to import fossil fuels. Biomass however is abundant and a more evenly distributed energy resource even at a local level.

The price of fossil fuels is on a steady rise [5] bringing about potential for the biomass-derived fuel to be available at a competitive cost in future. To increase cost-competitiveness and benefits from using biomass renewable energy, it is necessary to maximize efficiency of the biomass conversion routes. The efficiency has to be extended to gas cleaning due to the strict quality requirements of downstream processes for the synthesis gas.

It should be noted that obtaining benefits such as heat and electricity from biomass is not limited to biomass gasification. Other routes include direct combustion, thermochemical conversion, pyrolysis to produce char and liquid bio-oil and bio-chemical conversion routes such as fermentation and anaerobic digestion to produce ethanol and biogas [6, 7].

## 1.2 Biomass feedstock and contaminants

Biomass is a term used to refer to biodegradable organic materials from living or dead plants and animals that has not been fossilized. This includes wood and plants from forests, agricultural waste and biodegradable municipal waste. On a whole, differences in biomass extend to their shape, size and make-up composition for example, the mineral content and moisture content can vary even within the same species of plants.

Huber et al [8] presents a summary of potential biomass feedstock as;

- Unwanted agricultural and urban waste.
- Forest products such as wood, trees, shrubs and residues from logging.
- Energy crops such as starchy crops (i.e. corn and wheat), grass, and sugar crops.
- Water-based biomass such as algae and water hyacinth.

The biomass feedstock can further be classified according to their chemical structures [8, 9] as;

- Starch-based feedstock which include food crops like corn, barley, wheat and sugarcane.
- Lipid-based feedstock which includes both plants and animals with fatty acids. Examples of lipid based plants are soy beans and algae.

- Lignocellulosic-based feedstock is predominantly wood based and includes non-food plants such as agricultural residues and forest plants or waste. This type of feedstock is mostly considered for use in biomass gasifiers because they do not compete with the food-based biomass.

Lignocellulosic materials are composed of 3 different fractions of chemical species known as cellulose (40-80%), hemicellulose (15-30%) and lignin (10-25%) [8 and references there-in]. Formation of these structures starts with the sugar building blocks, $(CH_2O)_n$ in plants which are formed when the plants combine carbon dioxide ($CO_2$) from the atmosphere and water ($H_2O$) using energy from the sun. The sugar is stored within the plants as naturally occurring polymers such as starch, cellulose and hemicellulose. Figure 1-1 to Figure 1-3 show the chemical structures of cellulose, hemicellulose and softwood lignin [10, 11].

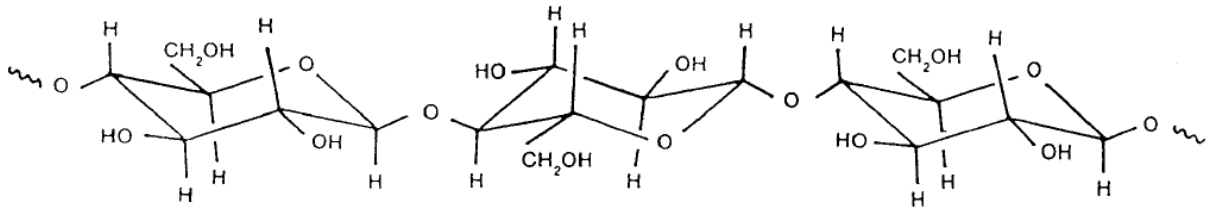

Figure 1-1 Chemical structure of cellulose

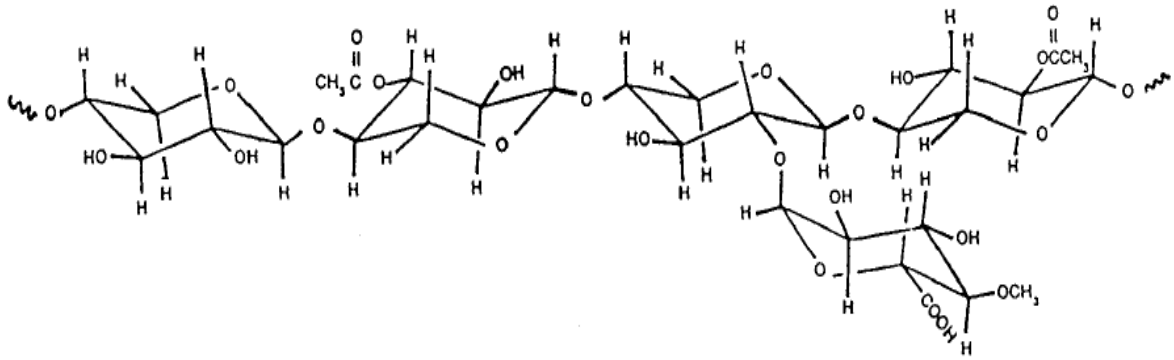

Figure 1-2 Chemical structure of hemicellulose

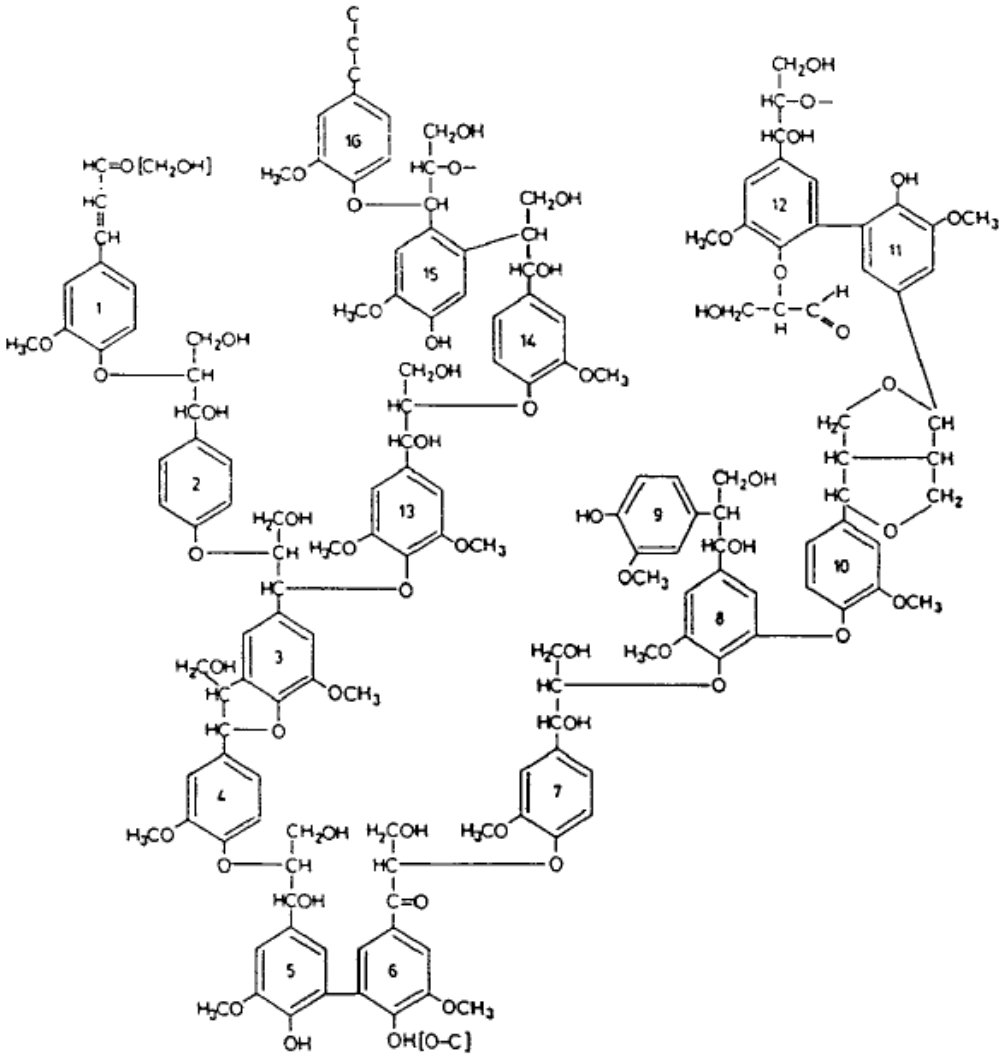

Figure 1-3 Chemical structure of softwood lignin

Cellulose is highly crystalline and provides strength at a cellular level to the cell wall. Hemicellulose has a chemical structure similar to cellulose but does not form crystalline polymers and lignin is polyphenolic with a chemical structure based on benzene rings.

The energy content of biomass can be estimated from the elemental composition making it possible to estimate the potential energy output from biomass gasification. Different types of biomass have different energy content although it usually ranges from 15,500 – 16,500 kJ/Kg [12].

Table 1-1 shows proximate and ultimate analyses together with the higher heating energy value for different types of wood-based materials, agricultural residues and animal waste.

Table 1-1 Typical proximate and ultimate analysis and higher heating calorific values for some biomass feedstock's [1]

| Fuel | Proximate analysis, ar* (wt %) | | | | Ultimate analysis, daf** (wt %) | | | | | | HHV*** (MJ/kg) (dry) |
|---|---|---|---|---|---|---|---|---|---|---|---|
| | Moisture | Volatile Matter | Fixed Carbon | Ash | C | H | O | N | S | Cl | |
| Wood pine chips | 4 | 81.3 | 14.6 | 0.1 | 52 | 6.2 | 41.59 | 0.12 | 0.08 | 0.01 | 20.23 |
| Miscanthus giganteus | 14.2 | 70.4 | 14.1 | 1.3 | 49.1 | 6.4 | 43.98 | 0.26 | 0.13 | 0.13 | 19.88 |
| Switch Grass | 7.17 | 73.05 | 15.16 | 4.62 | 49.4 | 5.7 | 44.25 | 0.45 | 0.1 | 0.1 | 17.82 |
| Straw-wheat straw | 7.78 | 68.83 | 17.09 | 6.3 | 49.23 | 5.78 | 43.99 | 0.64 | 0.1 | 0.26 | 17.42 |
| Rice husks | 9.4 | 74 | 13.2 | 12.8 | 42.3 | 6.1 | 50.56 | 1.1 | 0.1 | 0.04 | 16.3 |
| Palm PKE | 7.6 | 72.12 | 16.18 | 4.1 | 51.12 | 7.37 | 38.21 | 2.8 | 0.3 | 0.2 | 20 |
| Sugar cane bagasse | 10.4 | 76.7 | 14.7 | 2.2 | 49.9 | 6 | 43.15 | 0.4 | 0.04 | 0.51 | 19.47 |
| Olive residue | 6.4 | 65.13 | 19.27 | 9.2 | 54.42 | 6.82 | 37.29 | 1.4 | 0.05 | 0.04 | 19.67 |
| Cow dung | 13.9 | 60.5 | 11.9 | 13.7 | 54 | 6.4 | 36.7 | 0.83 | 0.03 | 1 | 17.36 |

**ar - as received*

***daf - dry and ash-free*

****Higher Heating Value*

The ultimate analysis provides the elemental biomass composition as carbon (C), hydrogen (H), oxygen (O), sulphur (S), nitrogen (N) and halides while the proximate analysis provides the weight % measurement of the fixed carbon, moisture, volatile matter and ash content.

The composition values are measured as weight percentage (wt %) based on the weight of the feedstock as dry and ash free (daf) as well as the weight as received (ar), which includes the ash and moisture content.

The amount of moisture in the biomass affects its combustion properties and biomass has relatively high moisture content. The moisture prevents the immediate combustion of biomass and reduces its energy value hence low moisture content in biomass is preferred in biomass gasification. Drying of the biomass is a pre-requisite for biomass gasification as a way of increasing the energy values. Particle size is another problem area that needs to be addressed as part of pre-treatment for the biomass feedstock.

Table 1-2 shows a comparison of energy content and elemental composition of some biomass and mineral coal [12]. Straw and wood have a much higher volatile matter contents compared to mineral coal and charcoal and the energy content is reflected inversely. Broadly speaking, the energy content is however positively linked to the carbon content.

**Table 1-2 Chemical composition and calorific value of different fuel feedstock's [12]**

| Fuel feedstock | Volatile Matter (%) | Calorific Value (MJ/Kg) | Ash (%) | C (%) | O (%) | H (%) | N (%) | S (%) |
|---|---|---|---|---|---|---|---|---|
| Straw | 80.3 | 14.2 | 4.3 | 44.0 | 35.0 | 5.0 | 0.5 | 0.1 |
| Wood | 85.0 | 15.3 | 0.5 | 43.0 | 37.0 | 5.0 | 0.1 | - |
| Charcoal | 23.0 | 30.1 | 0.7 | 71.0 | 11.0 | 3.0 | 0.1 | - |
| Mineral coal | 26.0 | 29.5 | 1-15 | 73.0 | 5.0 | 4.0 | 1.4 | 1.0 |

When biomass is heated to high temperatures, the chemical structures decompose and many gaseous products are released. The gaseous product is primarily of a mixture of hydrogen ($H_2$), carbon monoxide (CO), carbon dioxide ($CO_2$), water ($H_2O$) and methane ($CH_4$). The main gases of interest are $H_2$ and CO which make up the synthesis gas. Other unwanted byproducts that are produced include tars, sulfur compounds, particulate matter, nitrogen compounds, chlorine and alkali metals.

**Tars** are made up of condensable hydrocarbons such as heavy deoxygenated hydrocarbons and polycyclic aromatic hydrocarbons (PAH) which are formed through incomplete combustion and gasification of some parts of the biomass. Tars can condense on the walls of downstream equipment such as heat exchangers and reactors causing fouling and clogging of filters and lines. Tars can also deactivate catalysts that are used in the downstream processes for further conversion of the synthesis gas into other products.

**Sulfur** is primarily present as hydrogen sulfide ($H_2S$). Smaller amounts of carbonyl sulfide (COS) are also produced. Sulphur compounds are acidic and can cause corrosion of metal surfaces as well as deactivate catalyst. Its oxidized form (sulfur dioxide ($SO_2$)) is a pollutant that requires strict emission control.

**Particulate matter** is made up mostly of inorganic compounds (ash) and residual solid carbon (char) from the unconverted biomass material. It may also include bed materials from the gasifier. The particles vary in size from less than 1µm to more than 100µm [13] and can deposit in downstream process equipment causing plugging. Other potential problems with particulate matter include fouling, corrosion and erosion of equipment.

**Nitrogen** from a biomass gasifier is primarily present as ammonia ($NH_3$) and in lesser amounts as molecular nitrogen and hydrogen cyanide (HCN). Due to the high concentration of hydrogen in the gasifier product gas, the HCN is usually converted to $NH_3$ [13, and references there-in]. At typical gasification temperatures, the $NH_3$ decomposes to molecular nitrogen. Molecular nitrogen is a potential source of thermal $NO_x$ emissions from the downstream processes and catalyst poisoning. It is therefore necessary to reduce the nitrogen content from the biomass-derived synthesis gas.

**Chlorine** in the biomass-derived synthesis gas is present as hydrochloric acid (HCl). The chlorine from the biomass is vaporized during gasification and can react with water vapor present to form hydrochloric acid. Its presence can be detrimental because it can lead to corrosion of metallic equipment and catalyst poisoning.

**Alkali compounds** from biomass mostly include potassium and sodium. The compounds are volatile and will vaporize at temperatures above $600^0$C in the gasifier [13, 14]. Due to their high reactivity, when condensed, the alkali compounds can react with the species that are present in the gasifier such as chlorine to form chlorides, hydroxides and sulfates. These compounds are detrimental can lead to corrosion and fouling in equipment's [15]. The alkali compounds also deactivate catalysts in downstream processes such as tar cracking and reforming.

The concentrations of the unwanted byproducts (contaminants) depend on a number of factors such as the type of feedstock, gasifier technology used and the gasifier process conditions.

## 1.3 Biomass gasification technology

Various gasification technologies which use different types of feedstock are available. Focus on development of large scale gasifiers has been on coal gasification since the 1930s but was hampered by the availability of cheap oil and gas[16]. Rising prices of oil and gas have played a part in the recent renewed interest in biomass and coal gasification processes. Biomass gasifier technology is similar to the coal gasifiers with modifications done to incorporate the different quality of feedstock. The biomass gasification technologies however, should be both economically viable and environmentally friendly to be a sustainable industry.

During the gasification process, the solid biomass is reacted with an oxidizing agent such as steam and/or oxygen or air at high temperatures to produce synthesis gas. As mentioned earlier, other byproducts are produced alongside the synthesis gas. The major reactions that occur during gasification

include pyrolysis, partial oxidation, steam reforming, Boudouard reaction, the water gas shift reaction and methanation [17]. Table 1-3 shows chemical reactions that occur during gasification of a selected cellulose [8].

**Table 1-3 Reactions during gasification of selected cellulose [8]**

| Classification | Stoichiometric equation | Enthalpy (KJ/g.mol) ref temp. 300K | Equation No. |
|---|---|---|---|
| Pyrolysis | $C_6H_{10}O_5 \longrightarrow 5CO + 5H_2 + C$ | 180 | 1-1 |
| | $C_6H_{10}O_5 \longrightarrow 5CO + CH_4 + 3H_2$ | 300 | 1-2 |
| | $C_6H_{10}O_5 \longrightarrow 3CO + CO_2 + 2CH_4 + H_2$ | -142 | 1-3 |
| Partial oxidation | $C_6H_{10}O_5 + 0.5O_2 \longrightarrow 6CO + 5H_2$ | 71 | 1-4 |
| | $C_6H_{10}O_5 + O_2 \longrightarrow 5CO + CO_2 + 5H_2$ | -213 | 1-5 |
| | $C_6H_{10}O_5 + 2O_2 \longrightarrow 3CO + 3CO_2 + 5H_2$ | -778 | 1-6 |
| Steam gasification | $C_6H_{10}O_5 + H_2O \longrightarrow 6CO + 6H_2$ | 310 | 1-7 |
| | $C_6H_{10}O_5 + 3H_2O \longrightarrow 4CO + 2CO_2 + 8H_2$ | 230 | 1-8 |
| | $C_6H_{10}O_5 + 7H_2O \longrightarrow 6CO_2 + 12H_2$ | 64 | 1-9 |
| Water-gas shift | $CO + H_2O \longrightarrow CO_2 + H_2$ | -41 | 1-10 |
| Methanation | $CO + 3H_2 \longrightarrow CH_4 + H_2O$ | -206 | 1-11 |

Since biomass feedstock is available in various forms such as agricultural residues, wood and urban waste, standardizing the gasifier technology is a challenge. Different technologies exist. The conventional gasifier reactor design include the moving-bed reactor gasifier, fluidized bed reactor gasifier and the entrained flow reactor gasifier [16, 17]. The differences can be seen in the direction of flow of the feed and oxidant when they are introduced into the gasifier.

The moving bed gasifiers are further classified into the up-draft moving bed gasifiers and down-draft moving-bed gasifiers. Both designs have the feed introduced from the top but the oxidant for the up-draft gasifier is introduced from the bottom in a counter-current flow as seen in Figure 1-4. The technology is referred to as moving-bed because the feed that is introduced from the top of the gasifier steadily moves towards the bottom as the gasification process proceeds. The gaseous product exits from the top of the gasifier at temperatures of about $500^0$C [17]. The heat from the exiting gas helps to heat and subsequently dry and devolatilize the new biomass feed before followed by gasification. Due to the excess amount of oxygen at the bottom of the reactor where the oxidant is introduced, complete combustion occurs at the bottom and steam and $CO_2$ are formed. The oxidized hot gases are reduced to $H_2$ and CO as they diffuse upwards through the reactor bed. This type of reactor can work with biomass that contains high moisture content because the design allows for easy drying of the feed, however the gasifier has a high tar yield.

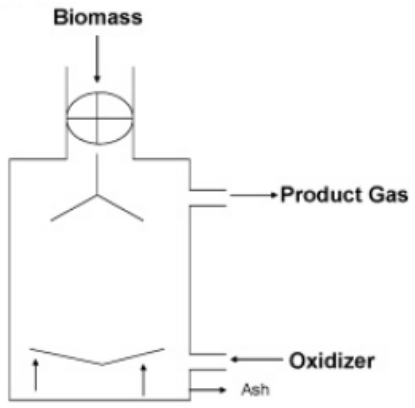


Figure 1-4 Principal design of the updraft gasifier[8]

The down draft gasifier has a set-up that is similar to the updraft gasifier except the oxidant is introduced from the top of the reactor allowing for co-current flow of the gasifier feedstock and the oxidant. See Figure 1-5. Compared to the updraft gasifier, this design has a lower tar yield.

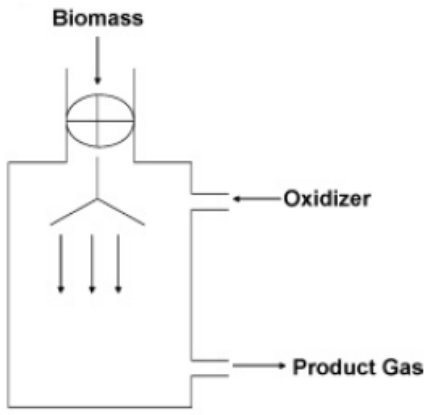


Figure 1-5 Principal design of the downdraft gasifier [8]

Figure 1-6 shows the design of a fluidized bed gasifier. Both the biomass feedstock and the oxidant are fed from the bottom of the reactor and the product gas exits from the top of the reactor. The bed is made up of an inert solid material such as sand which is fluidized by the upward flow of the oxidant.

The reactor is called a bubbling fluidized bed gasifier when the oxidant flows at a minimum fluidization velocity such that the gas just bubbles through the fluid media. A circulating fluidized bed gasifier has the oxidant flowing at a flowrate that is higher than the minimum fluidization velocity and the inert particles and feed particles are entrained within the gas stream. The particle size has to be small enough

for it to be easily fluidized by the flowing oxidant. The inert materials can be removed from the product gas by use of cyclones and then put back into the reactor.

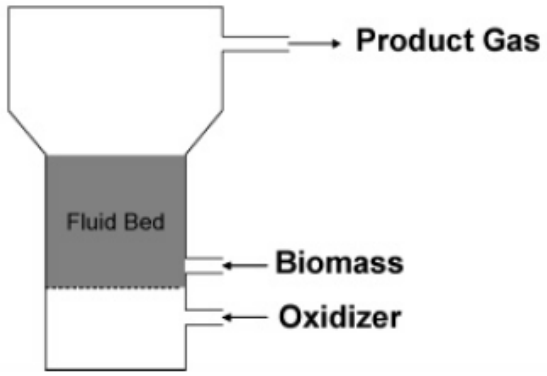


Figure 1-6 Principal design of the fluidized bed gasifier [8]

Figure 1-7 shows the schematic diagram of an entrained flow gasifier. The fuel feed reacts with both steam and oxygen (or air) concurrently. The feedstock for this gasifier has to be reduced to fine particles (pulverized) and the residence time of the feed particles in the reactor is very short, just a few seconds [8, 16].

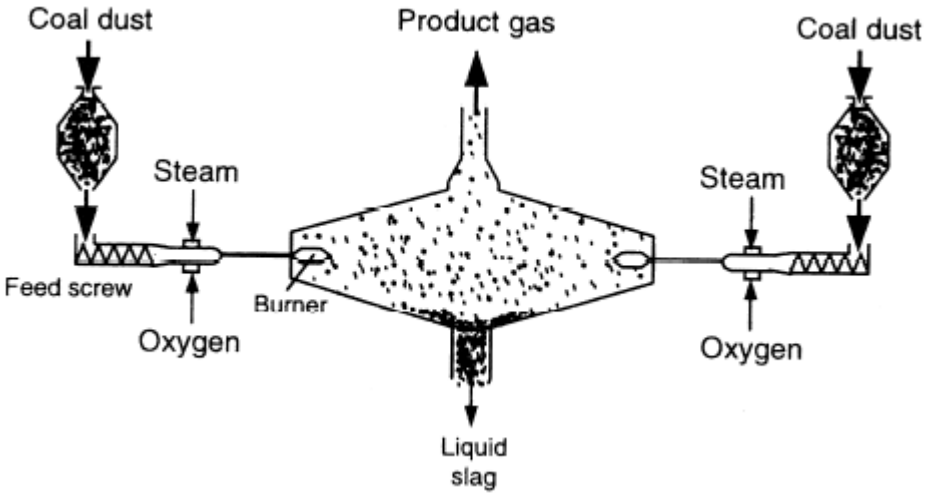


Figure 1-7 Schematic diagram of an entrained flow gasifier [16]

## 1.4 Sulfur contaminants

### 1.4.1 Sulfur formation

The downstream processes for the biomass-derived gaseous product as well as the environmental emission standards dictate the amount of effort that will be put in cleaning the gas product.

Sulfur content in biomass is reported to be very low however the detrimental effect it has in industrial systems is quite significant to warrant the multitude of research studies on sulfur removal processes. $H_2S$ concentration in the raw synthesis gas is reported to be about 100 ppmv and even higher if black liquor from the pulp and paper industry is used[18, 19].

Sulfur compounds are formed through various chemical reactions that take place during biomass gasification. The sulfur from biomass is mainly converted to $H_2S$ with smaller amounts of carbonyl sulfide (COS) [20]. Other organic sulfur compounds produced are mercaptans, carbon disulfide ($CS_2$) and thiopene. Focus on removing sulfur compounds is focused on removing $H_2S$.

When biomass is introduced into a gasifier, it gets devolatilized producing volatile hydrocarbons and solid char [1, 19, 20]. The volatile hydrocarbons undergo further reactions in the gasifier to produce synthesis gas. The gaseous sulfur compounds $H_2S$ and COS are also produced as byproducts. The sulfur-containing-char is further gasified in the presence of an oxidant to also give sulfur-containing gaseous compounds. Table 1-4 shows a summarized form of the sulfur forming equation.

**Table 1-4 Reactions showing sulfur formation during gasification [1, 17, 19]**

| Chemical reaction | | Equation No. |
|---|---|---|
| Biomass devolatilization | Biomass-**S** + heat → $H_2$**S** + CO**S** + $CO_2$ … + Char-**S** | 1-12 |
| Volatile gas phase reactions | $H_2$**S** + 1.5$O_2$ → **S**$O_2$ + $H_2O$ | 1-13 |
| | $CO_2$ + $H_2$**S** ↔ CO**S** + $H_2O$ | 1-14 |
| | $H_2$**S** + CO ↔ $H_2$ + CO**S** | 1-15 |
| | CO**S** + $H_2$**S** ↔ C**S**$_2$ + H2O | 1-16 |
| | C**S**$_2$ ↔ C + 2/x **S**$_x$ | 1-17 |
| | **S**$O_2$ + 0.5$O_2$ ↔ **S**$O_3$ | 1-18 |
| | $H_2O$ + **S**O3 ↔ $H_2$**S**$O_4$ | 1-19 |
| Char oxidation | Char-**S** + $O_2$ → **S**$O_2$ + ... | 1-20 |
| | Char-**S** + $H_2O$ → $H_2$**S** + … | 1-21 |
| | Char-**S** + $CO_2$ → CO**S** + … | 1-22 |

### 1.4.2 Sulfur capture

Despite the low levels of sulfur in the raw synthesis gas, some downstream industrial applications have even lower sulfur tolerance levels. X. Meng et al. have listed a summary allowable sulfur contents for different industrial processes as reported by different literatures [19]. A brief summary of the listed allowable sulfur levels based on lowest reported levels can be seen in Table 1-5.

Table 1-5 Allowable Sulfur content for different industrial applications [19]

| Industrial Application | Sulfur Requirement (ppmv) |
|---|---|
| Ammonia production | < 0.1 |
| Methanol synthesis | < 0.5 |
| Solid oxide fuel cell | < 0.1 |
| Fischer-Tropsch process | < 0.1 |
| Gas turbines | < 100 |

Beyond the allowable levels, sulfur can negatively affect the performance of the various downstream industrial applications as well as increase sulfur emission levels from the industrial applications to levels above the set environmental emission requirements. $SO_2$ has strict emission requirements and sulfur compounds in biomass are a precursor to $SO_2$ as seen in the reaction in Table 1-4.

Other negative effects caused by the sulfur include increased corrosion rates, plugging of tubes hence limiting plant life and increasing maintenance hours and deactivate catalysts. Sulfur can deactivate the ruthenium and cobalt catalysts that are used in the Fischer-Tropsch process. Consequently, it is essential to remove the sulfur chemical species from the biomass-derived synthesis gas before they are used in the downstream processes.

Various methods exist for removing sulfur compounds from synthesis gas. Most current research however is focused on obtaining sulfur cleaning methods that can work efficiently at high temperature hence improving thermal efficiency of the process. This is critical because synthesis has exits the gasifier at high temperatures and the downstream processes operate have high temperature synthesis gas requirements. Cleaning the gas at the high temperatures (hot gas cleaning) provides better thermal efficiency than cooling the gas, cleaning it and re-heating it for the downstream processes.

The optimal hot gas cleaning temperature could be debatable based on overall economic benefits and thermal efficiency. Different temperatures have been mentioned in the literature. Woolcock et al. [13] reports of thermodynamic benefits from hot gas cleaning for temperatures above $200^0$C. Cheah et al. [21] mention 300-$600^0$C as the optimum hot gas cleaning temperature in the coal industry if removal of alkali is to also be considered. The operating temperatures must be below alkali metal condensation temperature such that the alkali metals can be condensed and collected. Bakker et al. [22] point out that $400^0$C should be an optimal cleaning temperature because at that temperature clear benefits of hot gas cleaning exist. They explain that the higher temperatures would lead to phase transitions of materials and hence it would be required to use materials that can withstand high temperatures and these are more costly even though large savings can be achieved if the process is dedicated to the high temperatures thereby omitting heat exchangers.

Some of these shall be briefly described. The different sulfur removal methods can generally be classified based on where along the gasification process they are applied. The methods shall be briefly discussed in the subchapters below.

### 1.4.2.1 In-bed sulfur capture

In-bed sulfur capture methods involve using sorbents that are placed within the bed of the gasifier. This helps to reduce the amount of downstream equipment used in the gasification process hence simplifying operation.

The most commonly used sorbents are the calcium based sorbents such as limestone ($CaCO_3$) and dolomite ($CaCO_3.MgCO_3$). The calcium based sorbents react with $H_2S$ to form CaS. However, in the presence of oxygen, CaS undergoes an unwanted side reaction to form a stable $CaSO_4$ which forms a layer on the sorbent hence reducing its activity. See equations 1-23 and 1-24 below.

$$CaCO_3 + H_2S \rightarrow CaS + CO_2 + H_2O \quad (1\text{-}23)$$

$$CaS + 2O_2 \rightarrow CaSO_4 \quad (1\text{-}24)$$

The $CaCO_3$ can decompose in the gasifier at high temperatures of approximately $880^0$C to form calcium oxide (CaO) and $CO_2$. The produced CaO also reacts with $H_2S$ to form CaS and water hence giving the highest activity for $H_2S$ removal [23]. This process is known as calcination.

The spent sorbent containing CaS requires stabilization before it is released for disposal. Stabilization can be done by oxidizing the CaS to the stable $CaSO_4$ which is more acceptable for disposal. CaS is unstable and can react with water in the environment to form $H_2S$.

The desulfurization capacity of the lime-based sorbents is said to be dependent on reaction temperature and partial pressures of $CO_2$ and steam and are also affected by attrition and partial conversion of $H_2S$ to CaS at temperatures below the calcination point [7, 21].

Different types of research have been carried out on improving desulfurization capability of the calcium based sorbent. Details of the various research, including a silica-supported lime regenerative sorbent will not be mentioned in this report however X. Meng et al. [19] provides a summary of some of the research work.

### 1.4.2.2 Downstream sulfur capture

A traditional downstream sulfur capture method involves the use of low temperature amine scrubbers. These amine i.e. monoethanol amine (MEA) and diethanol amine (DEA) absorb the gaseous sulfur compounds. However the amine scrubbers require cooling of the raw synthesis gas from the gasifier exit temperatures of at least over $500^0$C to approximately 50-$60^0$C for cleaning, and then reheating for use in the downstream processes[13, 17]. These systems exhibit high thermal inefficiency coupled with high operational costs due to the cooling and re-heating of the synthesis gas.

Most downstream sulfur capture methods are based on the use of regenerative metal oxide based sorbents. In the mid 1970's Westmoreland and Harrison [24] screened 28 metal oxides using a thermodynamic feasibility study in order to determine their potential for high temperature (up to $1500^0$C) desulfurization.

Metal oxides were rejected for having a less than adequate desulfurization capacity at the interested temperatures even if the capacity was favorable below the interested temperatures. Metal oxides were

also rejected for forming stable and chemically inactive oxides or carbonates in the interested temperature range.

Cheah et al. [21] and Bakker et al. [22] have listed some factors that are considered important in designing and selecting a desulfurization sorbent that will realize economic and operational benefits. These are summarized as follows:

- Fast $H_2S$ adsorption kinetics with high equilibrium constant in order for the sorbent to retain $H_2S$.
- High capacity for sulfur adsorption in order to reduce the quantity of sorbent used and consequently the size of equipment used.
- High selectivity for $H_2S$ capture with minimal side reactions such as sulphate forming reactions.
- High thermal and chemical stability. The sorbent should not experience loss of activity due to evaporation or sintering at high temperatures. The sorbent should also be stable in the reducing environment provided by the raw synthesis gas.
- High mechanical stability to minimize thermal degradation and attrition rate.
- Ability to regenerate the sorbent. This is critical.

Out of the 28 metals investigated by Westmoreland and Harrison, 11 were identified to have high high-temperature desulfurization potential. These include iron, zinc, molybdenum, manganese, vanadium, calcium, strontium, barium, cobalt, copper and tungsten. The most studied metal oxides include zinc, copper, calcium, manganese and iron [7, 21].

**Zinc-based sorbents** show favorable desulfurization thermodynamics with high sorption capacity [7]. However zinc oxide is unstable. It is easily reduced to its elemental form in the reducing atmosphere provided by the synthesis gas as shown in equations 1-25 and 1-26. To increase stability of the sorbent, the thermodynamics of the reduction equations should be unfavorable because the reduced elemental form is easily vaporized at temperatures exceeding $600^0$C. Melting points of metals are relatively lower than the melting points of their respective oxides. Consequently zinc-based sorbents are best used at temperatures less than $400^0$C.

$$MeO\ (s) + H_2\ (g) \rightarrow Me\ (S) + H_2O \qquad 1\text{-}25$$

$$MeO\ (s) + CO\ (g) \rightarrow Me\ (s) + CO_2\ (g) \qquad 1\text{-}26$$

Most research on zinc-based sorbents is focused on increasing the stability of the sorbent at high temperatures. Zinc ferrite ($ZnFe_2O_4$) and zinc titanate (a mixture of zinc and titanium oxide) perhaps exhibit the most successful stability properties to-date for the zinc-based properties. Zinc ferrite has shown an improved desulfurization capacity at temperatures close to $500^0$C although it disintegrates at higher temperatures (approximately $700^0$C) to give $Fe_2O_3$ and $ZnO_2$ followed by reduction of the chemical species depending on the reduction potential in the reactor [25]. Zinc titanate is reported to be more successful compared to the ferrite with reduction not taking place temperatures up to $700^0$C [21, 26].

**Copper-based sorbents** have probably been studied just as much as the zinc-based sorbents. They are able to remove $H_2S$ to very low levels giving out a clean gas product. However, like zinc, in its uncombined form, copper oxide is readily reducible by the $H_2$ and CO in the synthesis gas to its elemental form. Researches looking at mixed and dispersed copper-based sorbents to stabilize the metal oxide are reported to be yielding promising results [27, 28]

**Manganese oxide** was predicted by Westmoreland and Harrison to have desulfurization potential at temperatures of 600-700$^0$C where the other metal oxides experienced challenges [24]. They determined that the active MnO phase is stable up to temperatures exceeding 1000$^0$C. This offers a wider sulfidation and regeneration temperatures choice without risking loss of the sorbent. The MnO phase does not reduce to its elemental Manganese form in the reducing atmosphere offered by the synthesis gas[29]. Its great challenge however is sulfate formation during oxidative regeneration at low temperatures[30].

**Iron oxide** was also reported by Westmoreland and Harrison to have a suitable desulfurization capacity up to 700$^0$C [24]. Iron oxide, even in its reduced state, is said to still have good desulfurization capabilities since the metallic iron reacts with $H_2S$ to form FeS [21, 31].

A general desulfurization equation for the metal oxides is shown in equation 1-27.

$$Me_xO_y\,(s) + xH_2S\,(g) + (y-x)H_2\,(g) \rightarrow xMeS\,(s) + yH_2O\,(g) \qquad 1\text{-}27$$

Me represents a suitable metal

# Chapter 2 Theoretical concepts of experimental methods

## 2.1 Regenerative high temperature desulfurization

### 2.1.1 The active element

In this study, manganese oxide has been chosen as the active element. As mentioned in the previous chapter, manganese oxide has relatively low volatility and exhibit high temperature stability up to temperatures exceeding $1000^0$C.The MnO phase exhibits a uniqueness among the other transition metals mentioned in the previous chapter, in that it is not reduced any further due to thermodynamic limitations[21, 29].

Manganese oxide exists in different phases. Figure 2-1 shows the important manganese oxide phases and their transition temperatures in the presence of air. The figure shows manganese oxide being reduced from $Mn^{4+}$ ($MnO_2$) to $Mn^{2+}$ (MnO). The re-oxidation is reversible up to $Mn^{3+}$ ($Mn_2O_3$) while re-oxidation to $Mn^{4+}$ requires pure oxygen and pressures of about 3000bars [32]. The reduction-oxidation properties of manganese oxide play a key role in producing a regenerative desulfurization sorbent.

$$MnO_2 \xrightarrow{500^0C} Mn_2O_3 \xrightarrow{900^0C} Mn_3O_4 \xrightarrow{1700^0C} MnO$$

Figure 2-1 Common manganese oxide phases at different tamperatures in air [32]

A number of researches have been done on manganese based sorbents for high temperature desulfurization but only a few of these will be mentioned in this report.

Bakker et al.[22] prepared a particle-based and monolith-based regenerable sorbents and found the sorbents to be stable even after at least 100 sulfidation and regeneration cycles in the temperature range of 400 to $1000^0$C.

Ben-Slimane and Hepworth [30] carried out some sulfidation and regeneration tests on different formulations of manganese based sorbents using a TGA apparatus in $H_2S$-$H_2$ gas atmosphere at temperatures of 700-$1000^0$C with the aim of studying the feasibility of using the manganese-based sorbents in the desulfurization of fuel gas obtained from coal gasification. They concluded that regeneration of the sulfided sorbent in air at temperatures above $900^0$C was necessary to prevent sulfate formation.

Wakker et al. [33] developed manganese oxide and iron oxide sorbents supported on alumina support and tested them in a laboratory set-up at 400-$800^0$C for over 400 cycles to study the influence of the coal-gasification-derived raw gas, operating temperatures and pressure on the sorbents. They were able to determine that most of the deactivation of the sorbent occurred within the first 10 cycles.

### 2.1.2 The support

In this study, supported manganese oxide will be used. The support lends its textural properties and provides a large surface area onto which the metal oxide is dispersed. The support has an influence on the desulfurization activity of the metal oxide with higher reaction rates observed [34].

Ideal supports would thermally and chemically stable with high mechanical strength and a controlled surface area and porosity[35]. The most common supports used in the industry are alumina, carbon, silica and for certain applications, magnesium oxide, titanium oxide, zirconium oxide, zinc oxide, silicon carbide, zeolites[35].

Four different supports with different textures have been chosen to study their influence on the sorption capacity of the manganese oxide. The different supports used include gamma alumina (ɣ-$Al_2O_3$), zirconium oxide ($ZrO_2$), titanium oxide ($TiO_2$) and cerium oxide ($CeO_2$).

- **Gamma-Alumina**

  Aluminium oxide has been widely used in the catalysis industry as a support due to its high thermal and mechanical stability. The oxide exists in different phases and the three most popular include the nonporous, crystalline α-$Al_2O_3$ and the amorphous and porous η- and ɣ-$Al_2O_3$ phases[35]. ɣ-$Al_2O_3$ is the most used and it has a high surface area in the range of 50-300 $m^2/g$ with surface hydroxyls in the range of 10-15 $OH/nm^2$ [35].

  Alumina supports can be obtained commercially or prepared locally by thermal dehydration of boehmite (AlOOH) or $Al(OH)_3$.

- **Zirconium Oxide**

  Zirconium oxide is a chemically unreactive crystalline compound available in 3 phases with different crystalline structure. The monoclinic phase exists at temperatures < $1170^0$C, the tetragonal phase at 1170-$2370^0$C and the cubic phase at temperatures > $2370^0$C [36].

  However, zirconium oxide exhibits poor thermal surface-texture-stability with the surface area reducing with increasing calcination temperature [36, 37]. Table 2-1 shows surface areas $ZrO_2$ calcined at different temperatures [36].

**Table 2-1 Specific surface area of ZrO treated at different calcination temperatures**

| Calcination temperature ($^0$C) | Surface area $m^2/g$ |
|---|---|
| 300 | 175.5 |
| 400 | 109.0 |
| 500 | 64.5 |
| 600 | 32.1 |
| 700 | 21.4 |
| 800 | 10.8 |
| 900 | 9.9 |

❖ **Titanium Oxide**

Titanium (IV) oxide, $TiO_2$ exists in nature in different crystalline forms and the most abundant forms include rutile (tetragonal), anatase (tetragonal) and brookite (orthorhombic)[38].

Rutile is the thermodynamically stable form of $TiO_2$ while the anatase and brookite are metastable. Anatase and brookite can be converted into rutile when heated at temperatures higher than the ranges 600-1100$^0$C and 500-700$^0$C respectively [38].

❖ **Cerium Oxide**

Cerium is a rare earth metal and in the oxide form, cerium has the oxidation number 4+ (in $CeO_2$) and 3+ (in $Ce_2O_3$) with the latter reported to be a more stable form . $CeO_2$ is a pale yellow-white substance that can be reduced at high temperatures in the presence of hydrogen to form $Ce_2O_3$ which is gold yellow.

### 2.1.3 Sulfidation reaction

The sulfidation reaction between a metal oxide and $H_2S$ proceeds via an O-S exchange as seen in equation 2-1

$$MeO\ (s) + H_2S\ (g) \rightarrow MeS\ (s) + H_2O\ (g) \qquad 2\text{-}1$$

Equations 2-2 to 2-5 are sulfidation chemical reactions of the different manganese oxide phases which occur at temperatures of approximately 325$^0$C while equation 2-6 occurs at temperatures higher than 325$^0$C[34].

**Table 2-2 Manganese oxide sulfidation reactions [34]**

| Chemical reaction | Equation No. |
|---|---|
| $MnO_2 + 2H_2S \rightarrow MnS_2 + 2H_2O$ | 2-2 |
| $Mn_2O_3 + 3H_2S \leftrightarrow MnS + MnS_2 + 3H_2O$ | 2-3 |
| $Mn_3O_4 + 4H_2S \leftrightarrow 2MnS + MnS_2 + 4H_2O$ | 2-4 |
| $MnO + H_2S \leftrightarrow MnS + H_2O$ | 2-5 |
| $MnS_2 + H_2 \leftrightarrow MnS + H_2S$ | 2-6 |

### 2.1.4 Sorbent regeneration pathways

Regenerating a sorbent involves an O-S exchange and therefore requires an oxidizing regenerant. Not all metal oxide sorbents can be regenerated. Other sorbents, such as calcium based sorbents, can generally be classified as disposable sorbents because they must be disposed when they are used up. Disposable sorbents are mostly used within the gasifier (in-situ) while the regenerable sorbents are used in a separate reactor from the gasifier.

The regeneration step is critical and it offers more advantages if it can be done in an economic way and still maintain the sulfur sorption capacity after repeated sulfidation and regeneration cycles.

There different pathways for regenerating sulfide metal oxides involve using different types of regenerants, each of which produces a different sulfur based product. The different regenerants include oxygen, sulfur dioxide and water (steam) and the sulfur based products given out are sulfur dioxide, elemental sulfur and hydrogen sulfide respectively. Equations 2-7 to 2-9 illustrate the chemical reactions taking place in each case.

$MeS\ (s) + 1.5O_2\ (g) \rightarrow MeO\ (s) + SO_2\ (g)$ **2-7**

$MeS\ (s) + 0.5SO_2\ (g) \rightarrow MeO\ (s) + S\ (g)$ **2-8**

$MeS\ (s) + H_2O\ (g) \rightarrow MeO\ (s) + H_2S\ (g)$ **2-9**

Obtaining elemental sulfur is perhaps more advantageous because a separate Claus process would be eliminated however regenerating with sulfur dioxide leads to the unacceptable sulfate compound unless regeneration is carried out at temperatures above $500^0$C [22]. The reaction with oxygen is exothermic and it is necessary to dilute the oxygen with an inert chemical compound in order to avoid overheating. Using water as a regenerant requires a sulfiding system that is not sensitive to water. $SO_2$ is the least preferred product.

### 2.1.5 Thermodynamics

The sulfidation reaction is a solid-gas phase reaction and based on the equilibrated general sulfidation reaction equation 2-1, the equilibrium constant can be expressed as;

$$K_{eq} = \frac{[H2O][sulfided\ surface\ sites]}{[H2S][\ free\ surface\ sites]} \qquad \textbf{2-10}$$

A higher equilibrium constant implies better desulfurization capabilities. This can also be achieved by having a sorbent with high surface area [22].

Figure 2-2 shows variation of equilibrium constants with temperature different manganese oxide phases and a supported manganese aluminate for the sulfidation reaction with $H_2S$ [22]. The equilibrium constants decrease with increasing temperature and the unsupported manganese oxide phases have a higher equilibrium constants compared to the supported manganese oxide, manganese aluminate ($MnAl_2O_4$).

Figure 2-3 shows the variation of thermodynamic constants of the regeneration reactions with the various regenerants [22].

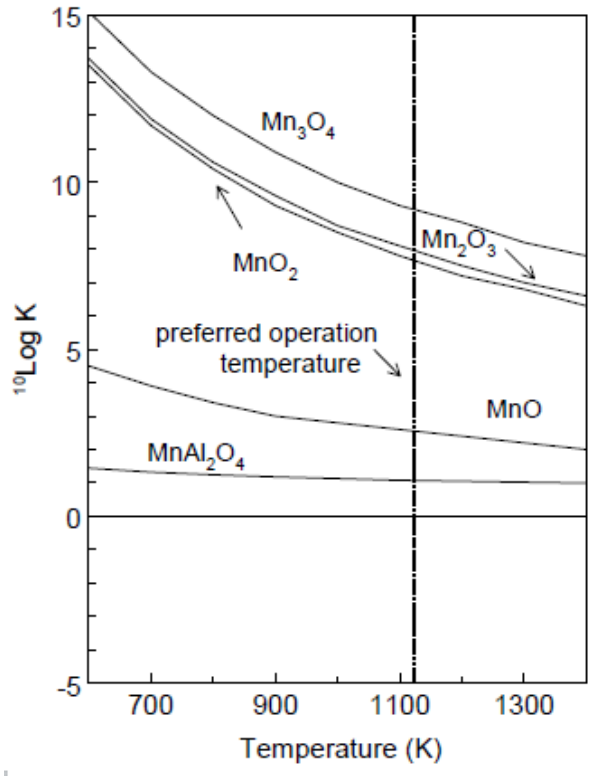


Figure 2-2 Equilibrium constants of different phases of manganese oxides and manganese aluminate ($MnAl_2O_4$) [22]

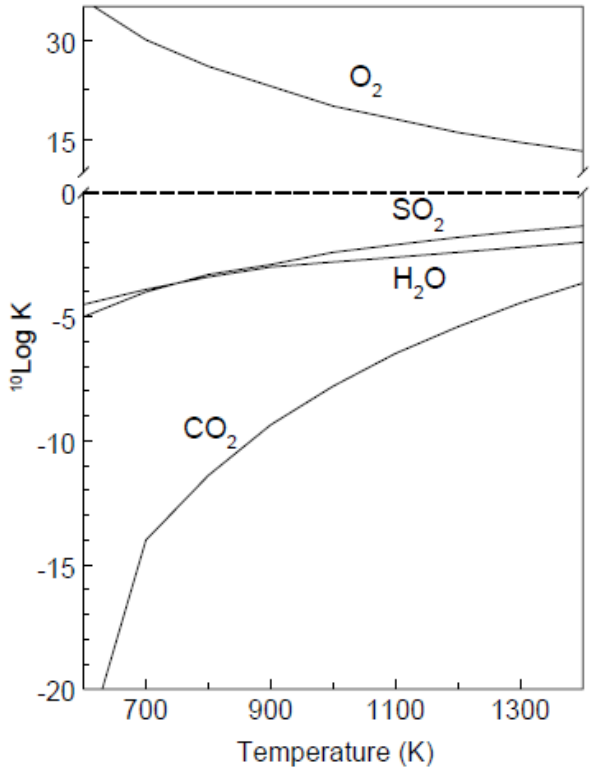


Figure 2-3 Equilibrium constants for the regeneration reaction of MnS to MnO with the different regeneration species [22]

## 2.2 Kinetics

The rate at which desulfurization occurs is an important factor. Figure 2-4 shows sulfidation rate constants of some metal oxides that were obtained based on initial rates of sulfidation reaction with the order of reaction with respect to the solid metal oxide and H2S equal to one. The results show $Fe_2O_3$ and MnO exhibiting faster sulfidation reaction rates compared to zinc oxide and calcium oxide.

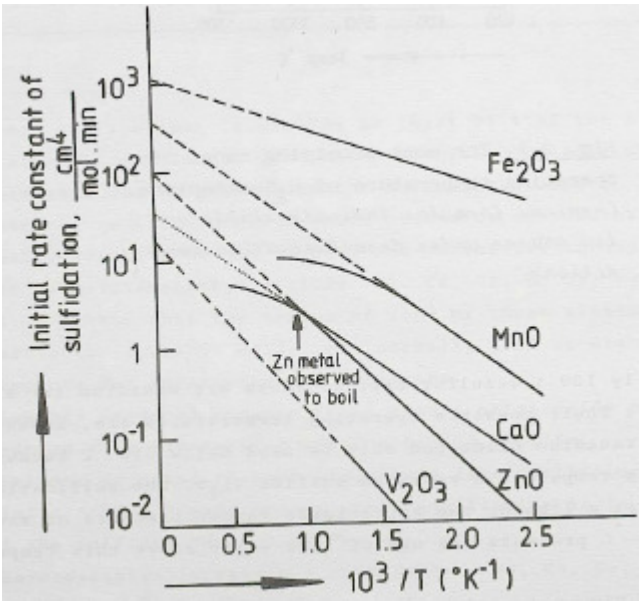


**Figure 2-4 Initial sulfidation rate constant for some selected metal oxides. Solid lines for experimental data, broken lines for extrapolations of the Arrhenius plots for a reaction-controlled sulfidation [39].**

## 2.3 Sorbent preparation

### 2.3.1 Incipient wetness impregnation

Incipient wetness impregnation method in sorbent preparation is a method that aims at loading a support material with an active phase. The active phase is a metal that has active sites on which a chemical reaction occurs. The support is usually an oxide that provides a surface area on which the active phase is dispersed.

The unsupported metal phase is usually unstable [35]. For example, if used at high chemical reaction temperatures, they are likely to undergo sintering. The support therefore helps to stabilize the active metal phases in various ways such as by providing thermal stability, physical strength as well as selectivity in some cases. Commonly used supports include alumina, zinc oxide, zirconium oxide, titanium oxide and some of their characteristics include thermally stability and chemical inertness.

The aim of this method is to deposit the active metal phase in the pores of the support by filling the pores with a solution that contains the active metal component. This is followed by drying the mixture in order to remove the solvent and load the active metal component on the support. The solution containing the active metal component is prepared by dissolving the metal salt precursor into the

solvent. The effect that the solution of the dissolved metal precursor has on the surface of the support can determine whether a good dispersion of the metal on the surface will be achieved or not. In solution, the oxide support is hydroxylated to form hydroxyl groups onto which the active metal precursors can be anchored onto the support [35, 40].

The hydroxyl groups can be basic or acidic depending on the pH of the solution used as well as the isoelectric point of the support oxide. The isoelectric point represents the pH at which the surface of the metal oxide is neutral. If the pH of the solution is lower than the isoelectric point, the surface will have a basic charge. A charged surface oxide is preferred since it allows an oppositely charged metal precursor in the solution to bind to the ionic hydroxyl groups.

In order to limit the deposition of the active metal phase inside the pores, it is important to use a volume of solution that corresponds to the pore volume of the support material. In incipient wetness impregnation method, the pore volume of the support is determined by empirical methods i.e. verified by observation and the volume is equal to the volume that, when exceeded, the support looks wet [40].

This process can be limited by solubility of the metal precursor in the volume of solvent being used. This however can be overcome by successive impregnation with drying and/or calcining in between the impregnation steps. Co-impregnation is also possible, where more than one active metal component is introduced on the support in a single impregnation step.

## 2.4 Characterization methods

### 2.4.1 Nitrogen adsorption

Nitrogen adsorption is an analytical technique used for characterization of porous solid materials using nitrogen at 77K. The method is used to determine surface area, pore volume and pore size distribution of the porous materials. Liquid nitrogen is used to cool the samples to cryogenic temperatures and nitrogen is also the adsorptive gas used.

Nitrogen can form multilayer adsorption and the Brunauer-Emmett-Teller (BET) method uses a multilayer molecular adsorption model to determine the surface area of porous materials [41]. BET is an extension of the Langmuir theory which assumes monolayer adsorption. According to the Langmuir model, the plateau on type 1 adsorption isotherm corresponds to the amount of adsorbed gas that forms a complete monolayer. An adsorption isotherm shows the amount of gas adsorbed and its pressure at constant temperature.

Equation 2-11 shows the BET equation that was developed by Brunauer, Emmett and Teller based on the langmuir theory [42].

$$\frac{P}{V(Po - P)} = \frac{1}{VmC} + \frac{(C-1)P}{VmCPo} \qquad 2\text{-}11$$

Where P is the partial pressure of nitrogen

$P_o$ is the saturation pressure at the experimental temperature
V is the volume of nitrogen gas adsorbed at the partial pressure, P
$V_m$ is the volume of nitrogen gas adsorbed at monolayer coverage
C is the BET constant

A plot of $\frac{P}{V(Po-P)}$ against $\frac{P}{Po}$ gives a straight line with a slope equal to $\frac{(C-1)}{VmC}$ and the y-intercept is equal to $\frac{1}{VmC}$. From this, it is possible to calculate the volume of gas adsorbed at monolayer. The calculated volume can be converted into number of molecules, and by knowing the area of each gas molecule, the total area occupied by the gas molecules can be determined[35]. At 77K, the nitrogen molecule occupies an area of 16.2Å$^2$.

The Barrett, Joyner and Halend (BJH) method also uses the nitrogen adsorption to determine pore volume and pore size distribution using adsorption-desorption techniques. The adsorption-desorption is determined over a wide range of relative pressure while allowing for a slow attainment of equilibrium[43].

### 2.4.2 Thermogravimetric Analysis (TGA)

Thermogravimetric Analysis provides a weight change profile of materials with increasing temperature a controlled atmosphere. The sample is generally heated in either an inert atmosphere or reactive gas atmosphere and its weight is measured as a function of both time and temperature. The heating rate can be programmed to increase linearly with time or create isothermal conditions for a desired length of time.

The instrument includes a sensitive micro-balance pan which is used to measure the weight of the samples, a furnace to provide heat and a thermocouple to measure the temperature. The atmosphere can be changed by passing either an inert gas (such as argon) or a reactive gas (such as air or hydrogen) over the sample. To prevent any chemical reactions, an inert gas is used.

A weight loss can be attributed to release of weakly adsorbed species, loss of volatile species, decomposition of the sample or reductive chemical reactions. A weight gain could be due to oxidation or absorption.

The TGA instrument on its own cannot provide information regarding the volatile products given off during analysis. However, the TGA can be coupled with a mass spectrometer which is able to analyze and give chemical information regarding the volatile products.

It is also possible to have simultaneous TGA and differential thermal calorimetry (DSC) measurement on the same sample. DSC measures the heat flow of the sample making it possible to determine if the sample has absorbed or released heat.

The results from the TGA can be graphically reported as a curve showing weight change (or lack of) against temperature or time. The results make it possible to study of thermal stability of materials as well as obtain decomposition and volatility characteristics. Absence of a slope on the curve means there

is no observed mass change. This would imply that the sample is stable within the measured temperature range. A dramatic loss in weight could be due to decomposition of the sample.

### 2.4.3 Temperature Programmed Reduction (TPR)

Temperature programmed reduction is a useful characterization technique that allows monitoring of a chemical reaction with increasing temperature. Informative data such as reduction profiles of metal oxides can be obtained with this technique. The method can be on metal oxides, supported metal oxides and mixed metal oxides.

The study involves passing a reducing gas (hydrogen) over the metal oxide while the temperature is set to increase linearly with time. The typical heating rate ranges from 0.1 – 20 $^{0}$C/min [35].

When reduction takes place, hydrogen gas is consumed to produce water as shown in the chemical reaction equation 2-12. A thermal conductivity detector (TCD) is used to detect the amount of hydrogen gas consumed while an electrical furnace can be used to heat up the reactor.

$$Me_xO_y + yH_2 \rightarrow xMe + yH_2O \qquad 2\text{-}12$$

The TCD detects the changes in the thermal conductivity of the gas at the outlet of the reactor. A graphical representation of the TPR results (TCD signal vs temperature) shows a reduction profile of the sample indicating temperatures at which reduction of the metal oxide occurs.

A reduction chemical reaction will contribute to a peak-shaped signal on the TPR curve. The temperature that corresponds to the maximum point of the peak represents the temperature where the rate of reduction is highest. The area under the TPR curve can be calculated by integration and it represents the total amount of hydrogen gas consumed during the reduction process.

By calibrating the TCD signal with a known amount of hydrogen gas (pulse calibration), it is possible to calculate the amount of hydrogen gas consumed during the TPR reaction. During pulse calibration, a known volume of gas is used to obtain a reference area on a TPR results plot, which is then used to calculate the amount of gas consumed during the analysis. A mass spectrometer can also be used to detect the composition of gases at the outlet.

### 2.4.4 Oxygen pulse chemisorption

Oxygen pulse chemisorption can be used to determine the dispersion of the active metal component on the surface of the support by using the amount of oxygen gas that has been chemisorbed on a pre-reduced sorbent. The stoichiometric ratio of oxygen to the metal is required to be stable [44].

The general procedure involves reducing the metal oxide as per equation 2-12 and then introducing oxygen gas which will chemisorb onto the active metal component.

The oxygen is introduced into an inert gas (a carrier) in a series of pulses of known volume and each pulse is passed through the sample placed in a reactor. The amount of oxygen gas that has not adsorbed

will exit the reactor and will be detected by a TCD. Subtracting the amount of un-adsorbed oxygen from the pulse loop volume, the amount of chemisorbed oxygen gas can be determined.

The graphical representation of the pulse chemisorption measurements involves a peak for each pulse and the peak height corresponds to the amount of oxygen detected at the outlet of the reactor. During oxygen adsorption, the peak height would be lower than when no adsorption is taking place. A breakthrough pulse is obtained when the sample is fully saturated with oxygen at which the rest of the peaks are more or less uniform.

Pulse calibration is performed in the same way as for TPR in order to determine the amount of oxygen gas that has been adsorbed.

A high purity carrier gas and reactive gas should be used to increase accuracy of measurements and this can be aided by use of water traps and suitable filters[44, 45].

### 2.4.5 X-Ray Diffraction (XRD)

X-ray diffraction is a technique used for phase identification and analysis of crystalline-based substances. It can also be used to measure particle size. The technique involves illuminating the crystalline substance with a monochromatic beam of x-rays which are then diffracted by the atoms to produce a specific diffraction pattern.

According to Braggs law (equation 2-13), the diffracted x-rays that are in phase will give constructive interference. By measuring the diffraction angles, 2θ, at which constructive interference occurs, it is possible to obtain the distance between two lattice planes of an atom [35]. This distance affects the position of the peaks on the diffraction pattern and is different for each compound because it is linked to the atomic structure. For this reason, the diffraction pattern is unique for each compound just like a fingerprint.

$$\text{Braggs Law:} \quad n\lambda = 2d\sin\theta \qquad \text{2-13}$$

Where n is an integer representing the order of reflection
λ is the wavelength of the x-rays
d is the spacing between two lattice planes
θ is the incident angle of incoming the x-rays

The uniqueness of the diffraction pattern makes it possible to identify unknown substances by comparing the x-ray diffraction pattern of the unknown substance to a library with known patterns. The comparison of the diffraction pattern can be done by using a search and match software.

More information about the substances can be obtained from the diffraction pattern. For example it is also possible to estimate the size of the crystallite particles with the Scherrer formula (see equation 2-14). The Scherrer formula relates the width of the peaks at half of the maximum peak height to the crystallite size.

$$\text{Scherrer formula:} \quad \tau = \frac{K\lambda}{\beta \cos\theta} \qquad \text{2-14}$$

Where $\boldsymbol{\tau}$ is the average particle size

K is a constant

λ is the x-ray wavelength

β is the width of the peak at half-peak height

θ is the angle of diffraction

# Chapter 3 Experimental methods, equipment and procedures

## 3.1 Sorbent preparation

Five sorbents were prepared by incipient wetness impregnation method. Manganese nitrate tetrahydrate ($Mn(NO_3)_2.4H_2O$, Sigma-Aldrich) was used as the metal precursor for all the five sorbents prepared. The supports used include ɤ-$Al_2O_3$, ZrO2, $TiO_2$, and $CeO_2$ supports.

The 5 different sorbents prepared include 15wt% Mn loaded on ɤ-$Al_2O_3$, ZrO2, $TiO_2$, and $CeO_2$ supports by single impregnation. The fifth sorbent is 30wt% Mn loaded on ɤ-$Al_2O_3$ by double impregnation.

ɤ-$Al_2O_3$ (96%, Strem chemicals) was pre-treated before impregnation by calcination in air in a high temperature furnace at $500^0$C for 10 hours. The $CeO_2$ support was obtained by calcination of cerium nitrate hexahydrate ($Ce(NO_3)_3.6H_2O$, 99%, Sigma-Aldrich) in air at $600^0$C for the same length of time [46, 47]. $TiO_2$ (≥99%, Sigma-Aldrich) was pre-treated by calcination in air at $700^0$C for 10 hours [48]. The heating rate used was $10^0$C/min. $ZrO_2$ (Alfa aeser) was supplied in pellet form as $ZrO_2$ support and the only pre-treatment of the support included grinding to a fine size before impregnation.

The pore volumes for the different supports were determined empirically by simple titration method with distilled water. Calculations used in sorbent preparation are included in Appendix A .

After dissolving the required amount of metal precursor into a volume of distilled water equivalent to the calculated pore volumes for each support, the different supports were impregnated by the dissolved metal precursor. The samples were then slowly dried by placing them in an oven at $100^0$C for 24hours and then calcined in air at $600^0$C for 5hours with a heating rate of $1^0$C/min.

For the 30 wt.% Mn sorbent, a 15 wt.% Mn loading was introduced onto the support in each of the impregnation. The second impregnation was carried out after drying from the first impregnation followed by calcination. The same calcination profile was used. Figure 3-1 shows a picture of the freshly impregnated supports, 15wt% Mn.

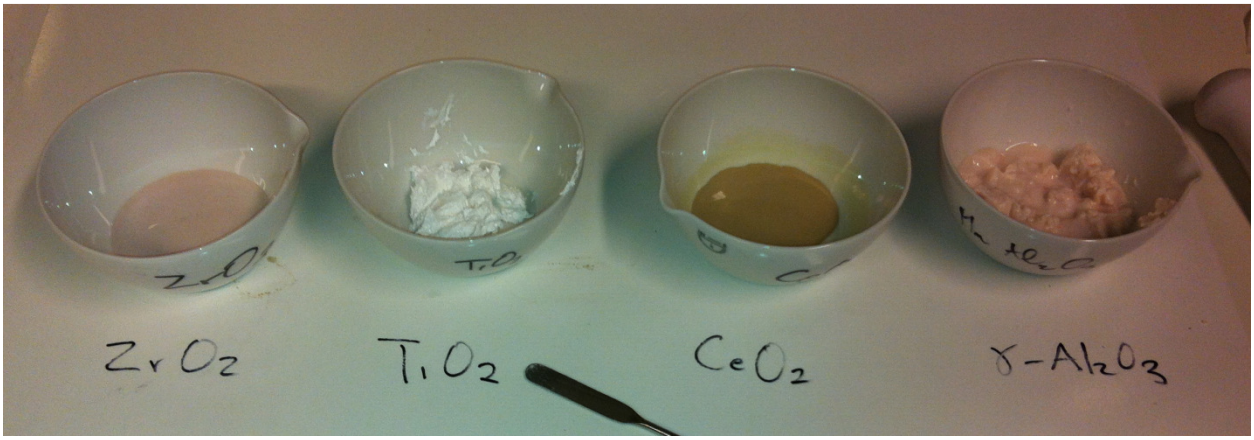


Figure 3-1 Freshly impregnated supports

The calcined sorbents were crushed with a hydraulic press at 10 tons for 30 minutes and then sieved to 150-250µm particle size.

The sieved particles (150-250µm) were used for the $H_2S$ sorption studies and nitrogen adsorption characterization. The residues were kept for the rest of the characterization methods.

## 3.2 Nitrogen adsorption

The Micromeritics Tristar 3000 Surface Area and Porosity Analyzer was used for nitrogen adsorption characterization measurements to obtain the textural properties of the five prepared sorbents.

A known amount of sample was placed into the instrument sample glass tubes and pretreated by degassing with a vacuum pump in a cooling station for one hour before being placed in the heating section at temperatures of $200^0$C overnight. The sample is ready for analysis when the degassing unit pressure is 100torr or less.

After degassing, the samples were cooled and re-weighed in case there is a decrease in weight. The sample tubes were then installed into the instrument for measurement.

## 3.3 X-Ray Diffraction (XRD)

XRD patterns were obtained for the pre-treated supports ($\gamma$-$Al_2O_3$, ZrO2, $TiO_2$, and $CeO_2$), the calcined sorbents ($Mn_xO_y$ on $\gamma$-$Al_2O_3$, ZrO2, $TiO_2$, and $CeO_2$ at 15 wt% Mn, and $Mn_xO_y$ on $\gamma$-$Al_2O_3$ at 30 wt% Mn) and the regenerated alumina based sorbents after $H_2S$ sorption measurement.

The instrument used for XRD characterization is the Bruker Diffrac (Advance Davinci X-ray Diffractometer) with a 2θ angle range of 5 and 75 degrees over a time period of 1 hour for each sample.

## 3.4 Thermogravimetric Analysis (TGA)

TGA profiles were obtained for the pre-treated supports and calcined sorbents. The instrument used is the Netzsch STA 449C Jupiter which allows for simultaneous TGA and DSC measurements. The instrument was used together with the Netzsch aërlosQMS 403C mass spectrometer to record ion current for water in the outlet gas.

The analysis was carried out on weighed samples placed on an alumina crucible and placed into the furnace chamber. The atmosphere used for analysis is a reducing gas mixture of hydrogen and argon each flowing at 20ml/min. The temperature was programmed to increase from near room temperature (approximately $30^0$C) to $900^0$C with a heating rate of $10^0$C/min. The samples were then held at this temperature for 10 minutes. The mass spectrometer was set to detect the presence of water from the outlet gas. The sample holder used on an alumina crucible and inserted into the furnace chamber.

## 3.5 Temperature Programmed Reduction

TPR spectra measurements were obtained for the $Mn_xO_y$ on $\gamma$-$Al_2O_3$, ZrO2, $TiO_2$, and $CeO_2$ at 15 wt% Mn, and $Mn_xO_y$ on $\gamma$-$Al_2O_3$ at 30 wt% Mn sorbents. The instrument used was the Altamira AMI-300 (BenchCAT 1000 Hp Hybrid).

Approximately 120mg of each sample was used in the analysis. The reactor is U-shaped and made of quartz. The samples were kept in place by a small plug of quartz wool placed both at the bottom and top of the sample. The reactor was then installed on the TPR equipment with the thermocouple placed just above the sample to measure the bed temperature. A leak test was carried out before resuming with analysis. An electrical furnace was used to provide the heating requirement.

The samples were pre-treated by heating to $350^0$C in an inert gas (Argon) atmosphere flowing at 50 ml/min. The heating rate used was $10^0$C/min. The samples were then held at the final temperature for 30 minutes before being cooled to $50^0$C.

The TPR measurement was carried out in a reducing gas mixture of 10% $H_2$ in Argon at a flow rate of 50 ml/min. the temperature range investigated was $50^0$C to $650^0$C. The same heating rate of $10^0$C/min was used. H2 concentration in the effluent gas from the reactor was monitored with a thermal conductivity detector (TCD). Pulse calibration measurements were done after the TPR measurements in order to determine the amount of hydrogen consumed during the TPR measurement. The pulse loop volume used was 50µL.

## 3.6 Oxygen pulse chemisorption

Oxygen pulse chemisorption characterization was performed by the Altamira AMI-300 (BenchCAT 1000 Hp Hybrid). The same instrument that was used for the TPR measurements.

The analysis was only performed on the alumina based samples as $Mn_xO_y/Al_2O_3$ (15 wt% and 30 wt%) calcined sorbents and the regenerated sorbent samples after the $H_2S$ sorption measurements.

Loading the sample onto the equipment is done in the same manner like for TPR measurement. The analysis started with reducing the samples by using only hydrogen gas flowing at 50 ml/min. the reduction was carried out during a temperature increment from room temperature to $250^0$C and then held at this temperature for 4 hours. The heating rate used was $5^0$C/min. Sample reduction was followed by flushing with helium gas flowing at 50 ml/min at the same temperature ($250^0$C).

Oxygen pulse chemisorption was the carried out on the reduced samples at $250^0$C. Helium gas was used as the oxygen gas carrier. The oxygen gas was introduced to the reduced samples in pulses (pulse loop volume of 50µL) with the carrier gas flowing at 30 ml/min. The instrument was programmed to run 20 chemisorption pulses. After pulse chemisorption measurements, pulse calibration was performed in order to determine the amount of oxygen that was used up.

## 3.7 UV-Raman spectroscopy

The analysis was only performed on the five sorbents prepared as well as the used and regenerated alumina based samples as $Mn_xO_y/Al_2O_3$ (15 wt% and 30 wt%).

Measurements were performed using the Horiba Jobin Yvon, LABRAM HR 800 instrument 325nm UV laser supplied externally by a Kimmon Koha instrument. The sprectra was measured over a range of 200-800 $cm^{-1}$. A D1 filter for the laser beam was used to reduce fluorescence and damage to the samples.

## 3.8 Equipment and procedures

### 3.8.1 Equipment

The $H_2S$ sorption studies and measurements were carried out using a laboratory set-up that was manually operated. The flow diagram for the equipment is shown in Figure 3-2. The risk assessment for the apparatus was carried out and a scanned copy has been attached to Appendix D

The laboratory set-up consists of a gas supply system, a reactor, a heating system and an analysis system. The pipeline is made out of stainless steel.

The set-up is relatively new and the sorption experiments carried out in this study are the first to be carried out with the new laboratory set-up. A number of challenges were encountered to have the system up and running. Some of the challenges include an $H_2S$ mass flow meter that was installed instead of a mass flow controller, the replacement of which took almost three weeks; changing the reactor system due to possible corrosion that was noticed on some of the steel fittings after a few $H_2S$ sorption trial runs; some time was spent in training and calibrating the mass spectrometer as well as determining its stability and accuracy in measuring gases of interest; replacement of the pressure reduction valve on the $H_2S$ gas bottle due to leakage and installing a vent system for the gas bottle.

#### 3.8.1.1 Gas supply

The laboratory set-up was supplied with nitrogen gas, hydrogen gas and oxygen gas from the local gas distribution line while approximately 1% $H_2S$ gas in argon was supplied from a cylinder that was placed within the laboratory set-up enclosure.

A hydrogen gas detector and an $H_2S$ gas detector were placed within the lab set-up to detect any leakages of the harmful gases. Portable detectors were also used when and as required.

#### 3.8.1.2 Mass flow controller

Bronkhorst High-Tech mass flow controllers for gases were used. The mass flow controllers have a maximum flow rate of 500ml/min and are also designed for low gas flow rates.

Communication to the mass flow controllers is made easy by using the bronkhorst flow DDE (Dynamic Data Exchange) server with the computer windows application. A DDE link can be established with more than one mass flow controller allowing for easy control of flow rates of more than one gas. Each mass flow controller has a serial number that is tagged to the gas it is being used for. The gas mass flow controllers are gas-specific. The gas specificity is also important when using corrosive gases since they may require different types of fittings to be used in the mass flow controllers.

An adjustable control valve is used for easy control of the gas flows. The valve opening is proportional to the set-point percentage which ranges from 0-100%. Hence the flow rate can be controlled by using the set-point percentages or by manually inputting the wanted flow rate in ml/min. Both the measured value and the set-point values are displayed. The mass flow controllers were calibrated for the specific gas and within the interested flow range.

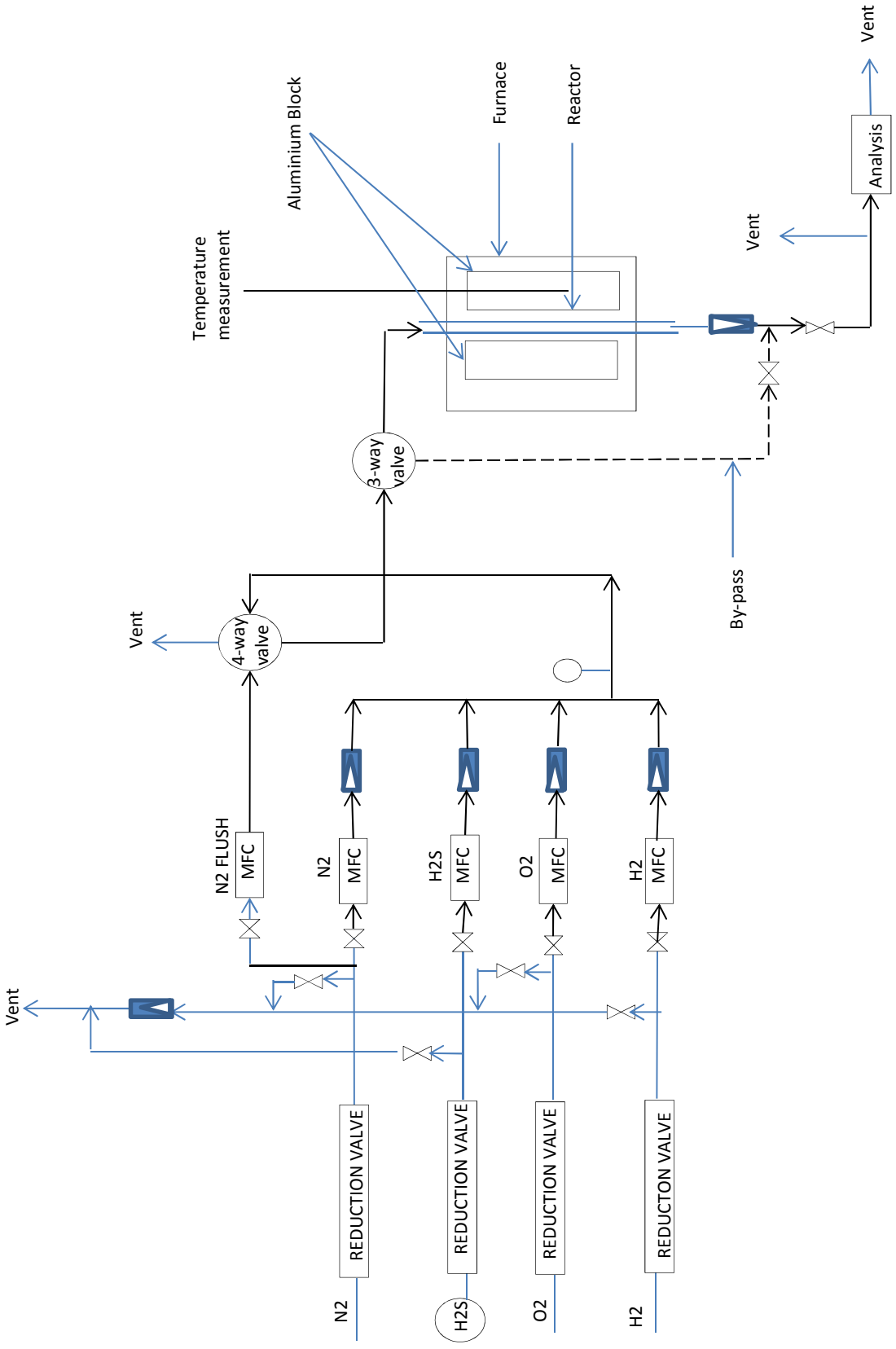


Figure 3-2 Experimental apparatus for regenerative $H_2S$ adsorption studies

Mass flow controller calibration was done using a 100ml soap bubble meter. The calibration results are attached to the Appendix E It was noted that the measured flow rates from the bubble meter were notably higher than the displayed measured flow rates on the flow DDE. Because of this, the calibration curves were used to obtain the required valve opening set-point % depending on the required flow rates during $H_2S$ sorption measurements.

Prior to calibration, the system was leak tested to ensure that there was no loss of gas along the pipelines. Both the spray detector and the portable $H_2$ gas detector were used for the leak test.

#### 3.8.1.3 Reactor

A few challenges were encountered while trying to design a good reactor. A total of three different reactors were designed and tested.

The first reactor that was designed for the laboratory set-up was a ceramic tubular reactor, 8.9mm ID, 12.7mm outside diameter and 750mm long. Installing this reactor required the use of graphite seals and steel fittings. Ensuring a leak free reactor system required with the graphite seals required some effort.

A trial $H_2S$ sorption measurement using a reference sample, $Mn_xO_y$-$Al_2O_3$ (N) [49] was attempted at temperatures of $350^0$C. To load a sample into the reactor, a plug of quartz wool was required to keep the sample in place. At the end of the attempted measurements, some discoloration was observed on the reactor steel fittings. It has not been verified but the discoloration is suspected to be corrosion. Figure 3-3 (a) and (b) show pictures of the discolored steel fittings while Figure 3-4 shows deposits on a white tissue after cleaning the steel fitting. The sample removed at the end of the experiment was also mixed with the quartz wool fibers which could compromise any tests that are carried out on the used samples.

Using a quartz reactor with steel fittings that have a Teflon lining was then investigated. A quartz reactor was with ID of 4mm was designed. This reactor shall be referred to as Quartz reactor No. 1.

This reactor was more user-friendly and required less effort to install and to ensure leak-proof. The reactor was designed with a sinter hence it was not necessary to use quartz wool when loading the sample. The advantage of this is that the used sample can be collected without the quartz wool fibers.

This reactor was used for the result-reproducibility tests which shall be further explained later in the report. However pressure build-up 0.6 bars was observed with a total gas flow rate of 50ml/min at high temperatures. This was suspected to be due to the much smaller reactor diameter that was now being used.

To allow for higher temperatures with no pressure build up, another similar quartz reactor was obtained but with a wider internal diameter (6mm). This reactor shall be referred to as Quartz reactor No. 2. Pressure build-up was not observed at a total gas flow rate of 100 ml/min and temperatures of $500^0$C. This reactor was used for the sorption studies of the prepared sorbents.

The reactors enclosed by an aluminium jacket and insulated to minimized heat loss.

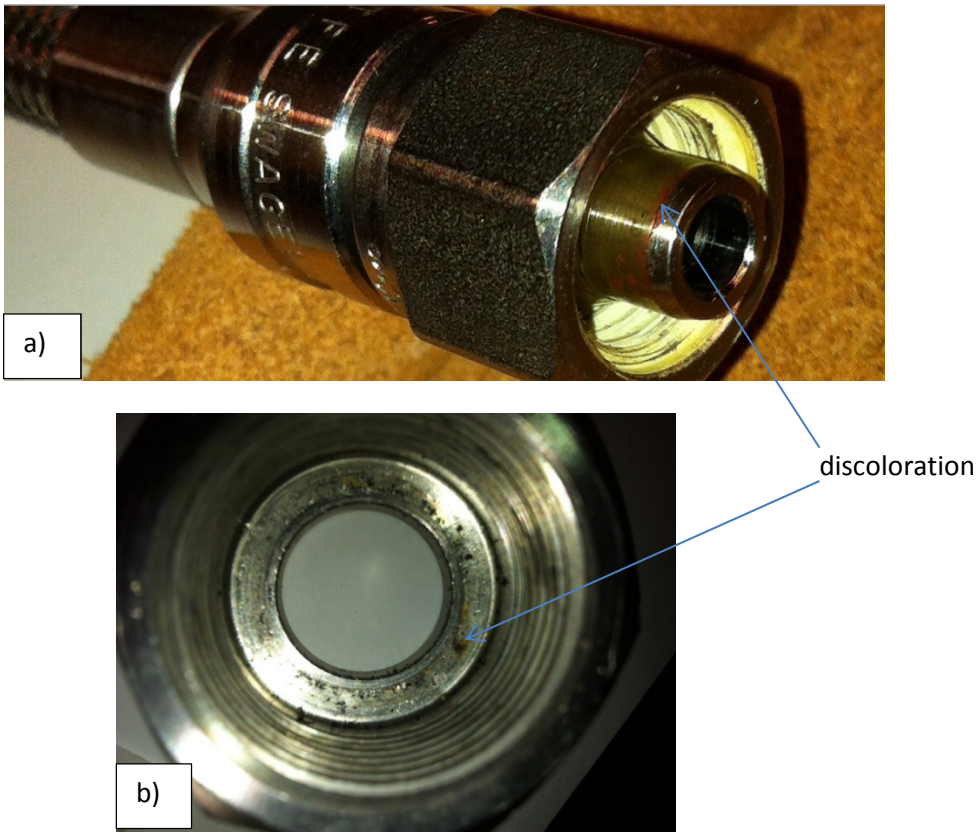


Figure 3-3 a and b Corrosion on stainless steel fittings for reactor after trial sorption cycles

Figure 3-4 Deposits from steel fitting after cleaning with white tissue paper

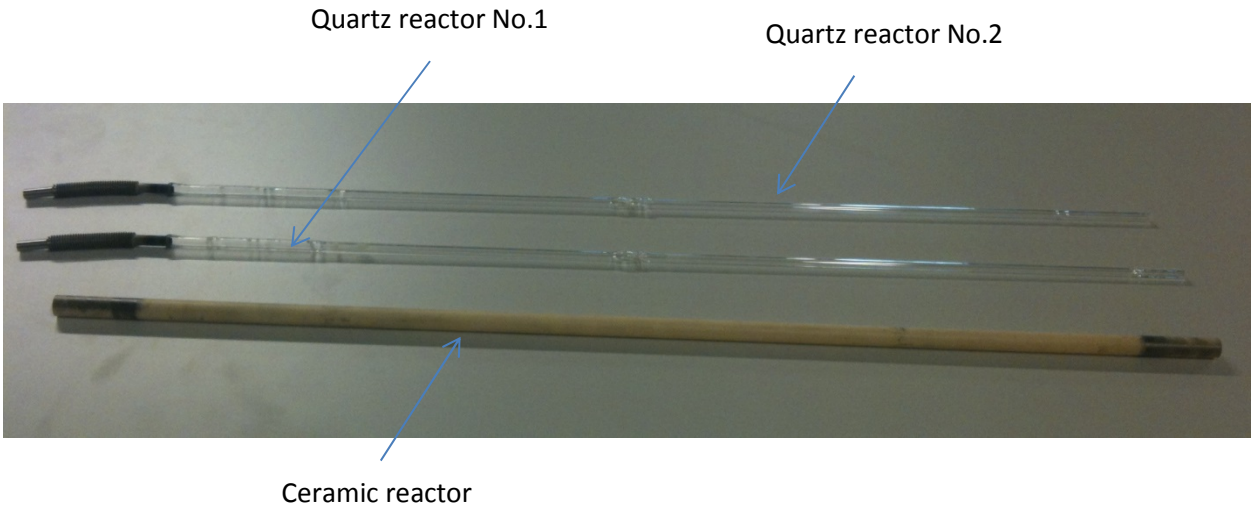


**Figure 3-5 Sorption reactors used on the $H_2S$ sorption laboratory set-up**

#### 3.8.1.4 Temperature controller

The Eurotherm 2408 PID controller with set-point programming is installed on the laboratory set-up used for temperature control in the reactor. The controller is connected to an electrical furnace and a thermocouple (for temperature measurement). The thermocouple is placed within the aluminium jacket which encloses the reactor.

The thermocouple used is a type K, with chromel-alumel alloy combination and can be used for a temperature range of -180 to $1300^0$C. The voltage difference between the two alloy conductors is converted into a temperature measurement. The voltage is created when the temperature on one end of the metal conductors (i.e. the thermocouple end) is different from the temperature at the reference point (which is on other part of the circuit). The different metal alloys produce different voltages and the electric potential, which is the difference in voltage between the two metal alloys, is then translated into a temperature measurement. The difference in voltage increases with increase in temperature.

The home display for the Eurotherm controller shows both the measured temperature value and the set-point temperature value that has been chosen by the operator. The controller also allows for automatic operation mode where the heating output from the electrical furnace is adjusted automatically to maintain the set-point temperature. An alarm-flash-message system on the home display is used to notify any alarm conditions that may have occurred such as a faulty thermocouple.

#### 3.8.1.5 Mass spectrometer

The Pfeiffer GSD320 Thermostar quadrupole mass spectrometer analytical instrument is connected to the exit gas line from the reactor. The instrument was used to monitor $H_2S$ sorption activity and sorbent regeneration by producing spectra of the gaseous species present in the exit gas line from the reactor. The mass spectrometer is made up of an ion source, a quadrupole mass filter and an ion detector.

The gaseous chemical substances from the reactor are directed to the mass spectrometer where they are converted into positively charged particles by the ion source and accelerated before being separated

according to their mass to charge ratio. An electric and/or magnetic field is used to separate the ions. The ions are then sent to the detector and the spectra of the detected ions showing their relative abundance is displayed.

The ion source of the GSD320 Thermostar comprises a filament that emits electrons which collide with gaseous chemical species knocking out electrons and forming the positively charged chemical species. The electric field is provided by a quadrupole mass filter which is made up of four distinctly aligned rods in a high vacuum chamber, to which a direct current (DC) and radio frequency (RF) voltage is applied. The detector is a faraday cup and includes a secondary electron multiplier (SEM) for amplification.

A purge line is connected to the mass spectrometer to dilute the toxic gases before they are released to the vent.

The Pfeiffer quadrupole spectrometer uses the Quadera software which links the instrument to the PC and displays the spectra of the gas species reaching the detector on the PC.

The mass spectrometer was calibrated for nitrogen, hydrogen, argon and hydrogen sulfide gases. After calibration, different gas flow compositions were set and the gas concentration measurements by the mass spectrometer were noted. The measured values were compared to the expected (calculated) values. Figure 3-6 to Figure 3-9 are the graphical representation of the measured values vs expected values for the calibrated values. The values for $H_2S$ are in agreement but the other gas compositions are not in complete agreement. Basing on the $H_2S$ values, which is the main gas of interest, the experiment was allowed to continue.

The mass spectrometer measurements can be obtained as gas concentration measurements and ion current measurements for the calibrated gaseous species. If some gas species which are not calibrated are required to be monitored, the scan analog scan measurement was used. The gases include oxygen and sulfur dioxide which are present during regeneration of the sulfided sorbents.

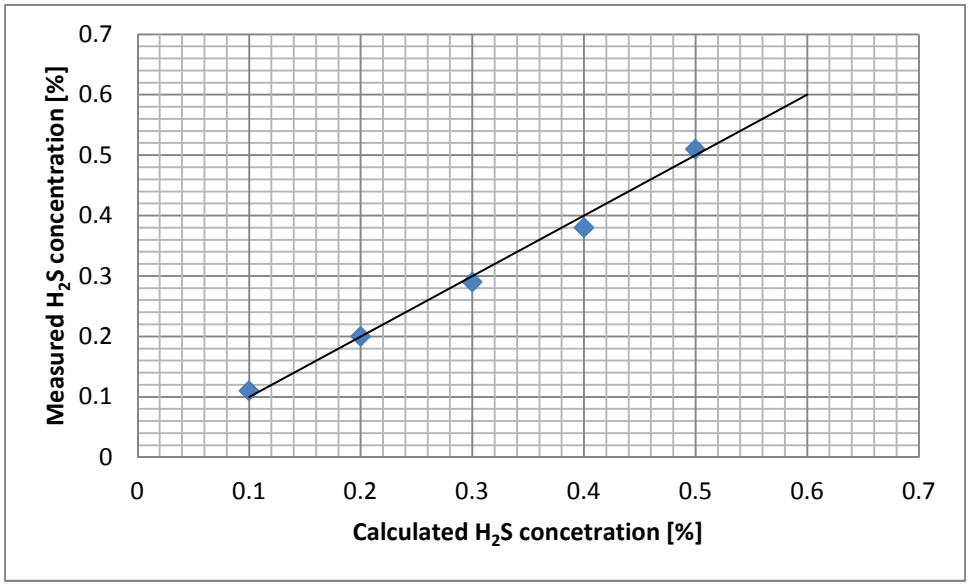


Figure 3-6 Measured vs expected $H_2S$ concentration with the Mass spectrometer

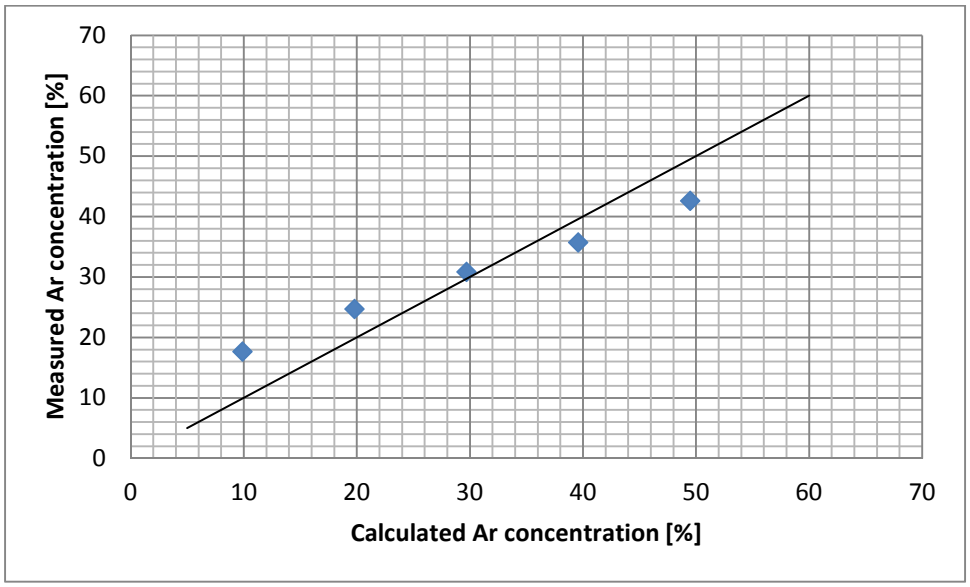


Figure 3-7 Measured vs expected Argon concentration with the Mass spectrometer

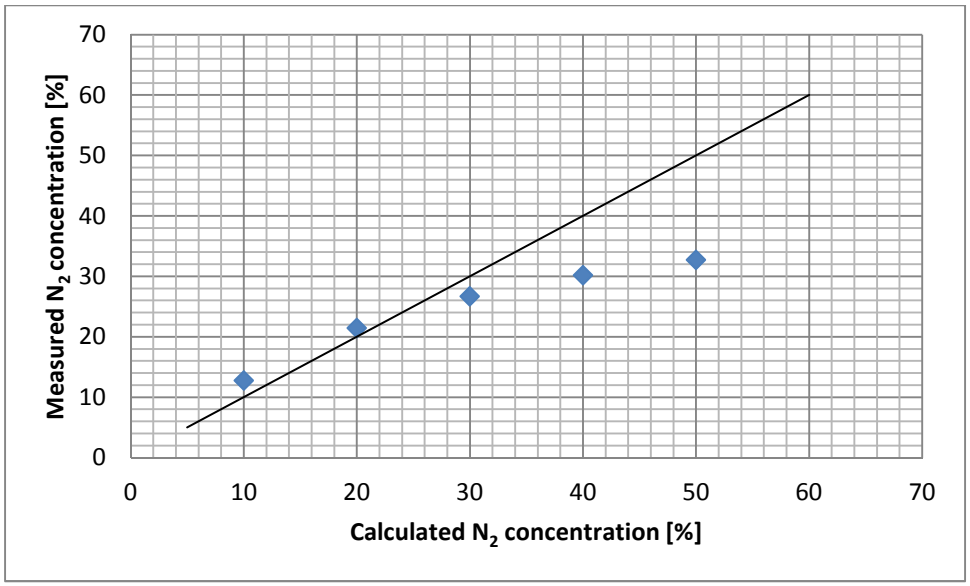


Figure 3-8 Measured vs expected Argon concentration with the Mass spectrometer

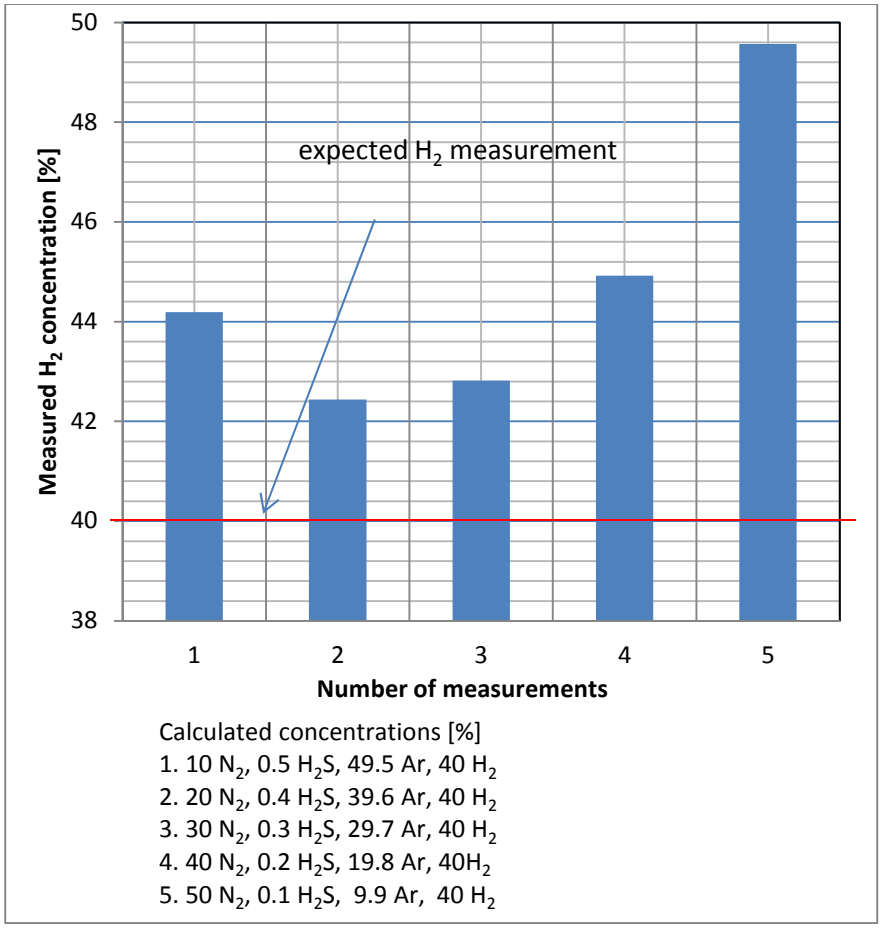


Figure 3-9 Measured vs expected $H_2$ concentration with the Mass spectrometer

## 3.9 Procedures

### 3.9.1 Leak test and pressure test

These tests were done for safety reasons and to ensure a material balance by eliminating loss of gaseous materials (reactants and products) during $H_2S$ sorption studies. This was done with a spray detector and/or $H_2$ detector which required $H_2$ gas to be flowing in the pipelines. When $H_2S$ gas was flowing in the pipeline, a portable $H_2S$ gas detector was also used to verify leak-proof. The procedures are detailed in Appendix B

### 3.9.1 $H_2S$ sorption activity measurement

The $H_2S$ sorption activity measurements were done in cycles. A cycle includes one sulfidation reaction measurement and its subsequent regeneration measurement. The procedure for this experiment is included in Appendix C but in general the $H_2S$ sorption cycle can be summarized to include these four steps: flushing, sulfiding, flushing and regeneration. Details such as the sorption gas flow rates, regeneration gas flow rates and temperatures used shall be included in the main report.

#### 3.9.1.1 Result-reproducibility

The aim of this experiment was to find out if results can be reproduced by using the new laboratory set-up. The experiment involved measuring five (5) successive sulfidation and regeneration cycles with a reference sorbent sample ($Mn_xO_y$-$Al_2O_3$ (N)) that was prepared and characterized by Chytil et al. [49] in a different study. The sorbent was used as received. This experiment was repeated 3 times and each experiment was carried out over 3 consecutive days. The first sorption cycle was done on the day 1, cycles 2 & 3 on day 2 and finally cycles 4 & 5 on day 3. The sulifdation reaction was allowed to proceed until maximum saturation of the sorbents with $H_2S$ was observed afterwhich the sorbent was regenerated to prepare for the next sorption cycle. The sorbent is saturated when the outlet $H_2S$ concentration is equal to the inlet $H_2S$ concentration.

The $H_2S$ sorption gas mixture used was $N_2$, $H_2$ and $H_2S$ (Ar) gases at flows of 10, 20 and 20 ml/min respectively. The regeneration gas used was oxygen diluted in nitrogen at flows of 5ml/min and 45ml/min respectively.

The Quartz reactor No. 1 was used for the reproducibility experiment. As mentioned before, a pressure build-up of approximately 0.6 bars was observed with a total gas flow rate of 50ml/min. The pressure build-up was observed to increase with temperature and for this reason the experiment was carried out at $400^0$C instead of the intended $500^0$C. Approximately 120mg of the sorbent was used for each experiment. The experimental activities over the 3 days for each experiment have been summarized below.

**Day 1:** The experiment starts with pre-reduction of the sorbent while the temperature is set to increase from room temperature to $400^0$C at a heating rate of $5^0$C/min. The reducing gas used was $H_2$ mixed with $N_2$ at an equal flow rate of 25 ml/min. The sorbent was then left in the reducing gas mixture at $400^0$C for 1 hour. The sorption measurements for the first cycle were then carried out.

After the sorbent got saturated with $H_2S$, the reactor was flushed with $N_2$ and regenerated. The $N_2$ flush flow rate used in this experiment was 50ml/min. Regeneration was monitored and measured by using the mass spectrometer analog scan. The reactor was then flushed again after regeneration and subsequently left overnight in the $N_2$ gas flowing at 15ml/min.

**Day 2:** A $H_2$ leak test with a $H_2$ and $N_2$ gas mixture flowing at 25ml/min each was carried out to ensure the system was still leak-proof. This was followed by flushing the reactor with nitrogen and then measuring the 2$^{nd}$ and 3$^{rd}$ sorption cycles. In between cycles, only $N_2$ flushing as part of the sorption cycle procedure was done. The regenerated sorbent after sorption cycle 3 was flushed with nitrogen and left overnight in a $H_2$ and $N_2$ gas mixture each flowing at 10ml/min.

**Day 3:** The same procedure as for day 2 was carried out to measure sorption cycles 4 and 5.

The cleaning regime for the reactor included washing with distilled water and a clean brush followed by ethanol and then subsequently rinsed with distilled water again before drying in an oven at 100$^0$C.

#### 3.9.1.2 Sorption breakthrough curve measurement

Due to limited time, this experiment was only carried out on the prepared alumina based sorbents, $Mn_xO_y/Al_2O_3$, 15 and 30 wt% Mn. The rest of the sorbents, $Mn_xO_y/ZrO_2$, $Mn_xO_y/TiO_2$ and $Mn_xO_y/CeO_2$, have been handed over to the supervisors and left as future work to be done.

The $H_2S$ sorption experiments were carried out twice for each of the alumina based sorbents at temperatures of 450$^0$C. The reactor used was Quartz reactor no.2. No pressure build-up was observed at a total gas flow rate of 100ml/min at 450$^0$C. Again, the intended temperature to be used was 500$^0$C but during some challenges experienced with the thermocouple during trial runs at 500$^0$C, and lack of extra spare thermocouples, it was decided to be safe and operate at temperatures below 500$^0$C. 450$^0$C was a preferred compromise.

The two experiments for each sorbent shall be referred to as Experiment 1 and Experiment 2. Each experiment has total of thirteen (13) $H_2S$ sorption cycles which were carried out over 4 consecutive days. Cycle 1 was measured on the first day, cycles 2-6 were carried out on the 2$^{nd}$ day, cycles 7-11 were carried out on the 3$^{rd}$ day and finally cycles 12 and 14 were carried out on the 4$^{th}$ day. The first and last sorption cycles were carried out as full sorption cycles where maximum saturation of the sorbents was allowed to be reached. The rest of the cycles (2-12) were measured as short sorption cycles and sulfidation reaction was stopped when the $H_2S$ concentration in the effluent gas from the reactor reached 0.1% $H_2S$. Maximum saturation of the sorbent was not allowed to be reached for the short sorption cycles.

In Experiment 1, approximately 120mg of the sorbent was used with a sorption gas mixture of $N_2$, $H_2$ and $H_2S$ (Ar) flowing at 10, 20 and 20 ml/min. The regeneration gas used was oxygen diluted in nitrogen at flow rates of 5 and 45 ml/min respectively. Nitrogen flushing was done at a flow rate of 100ml/min.

In Experiment 2, the mass of sorbent was doubled to approximately 240mg. Subsequently, the sorption gas flow rates and regeneration gas flow rates were also doubled to 20, 40 and 40 ml/min for the

sorption gases $N_2$, $H_2$ and $H_2S$ (Ar) respectively while the regeneration gas flows were doubled to 10 ml/min $O_2$ and 90 ml/min $N_2$. The $N_2$ flushing was maintained at 100ml/min.

The experimental activities over the four days have been summarized below.

**Day 1:** The experiment starts with pre-reduction of the sorbent while the temperature is set to increase to $450^0$C at a rate of $5^0$C/min. The reducing gas mixture of $H_2$ and $N_2$ was used at a flow rate of 25ml/min each. The sorbent is then left in the reducing gas mixture at $450^0$C for one hour before measuring the first sorption cycle to maximum saturation of sorbent. The pre-reduction gas mixture was maintained the same for both experiment 1 and experiment 2. At the end of the first sorption cycle, the sorbent was left overnight in a reducing gas atmosphere of $H_2$ and $N_2$ gas each flowing at 10 ml/min overnight at end of each day.

**Day 2:** A $H_2$ leak test with $H_2$ and $N_2$ gas each flowing at 50ml/min was performed and then the short sorption cycles 2 to 6 were measured. The sorbents were then left overnight in the same reducing gas mixture as for day 1.

**Day 3:** The procedure used here to measure cycles 7 to 11 is the same as that used on day 2.

**Day 4**: After the $H_2$ leak test, the sorbent is left in pure $H_2$ gas flow of 50ml/min for half an hour before flushing the reactor with $N_2$ and measuring the short sorption cycle number 12 and the full sorption cycle number 13.

At the end of the experiments, the regenerated sorbents were carefully collected and taken for nitrogen adsorption, XRD analysis, Raman spectroscopy and $O_2$ pulse chemisorption measurements.

## 3.10 Analysis and interpretation of results

### 3.10.1 Modes of measurement used

The $H_2S$ sorption studies on sorbents were monitored by using spectra obtained by a mass spectrometer. The spectra included concentration measurements of the calibrated gases with respect to time, ion current measurements of the gases with respect to time and analog scans that showed ion current peak intensities at the atomic mass units (amu) of the gases that are present.

Figure 3-10 shows concentration measurements of the sorption gases ($N_2$, $H_2$, Ar, and $H_2S$) that are used during sulfidation reaction in a sorption cycle. The concentrations are measured as a function of time and the time can be displayed as the actual time of measurement or as relative time (relative to the time the measurement was started).

In the graphical representation shown in Figure 3-10, the changes in concentration of $H_2S$ gas, which is the main gas of interest, can hardly be seen. This is because the gas is used in very low concentrations compared to the other gases. Figure 3-11 shows the same concentration measurement as for Figure 3-10 but with only $H_2S$ concentration measurement. The rest of the gases ($N_2$, $H_2$, and Ar) have been removed from the measurement graph. The low $H_2S$ concentrations and its changes can now be clearly seen.

In order to present changes in gas concentrations for all the gases present, the ion current measurement is used. The ion current measurements are obtained at the same time as the concentration measurements therefore the ion current measurements shown in Figure 3-12 is a direct representation of the changes taking place in gas concentrations shown in Figure 3-10. The ion current measurement makes it possible to clearly see all the gases that are present on one graphical presentation.

Some gases have not been calibrated with the mass spectrometer such as $O_2$ and $SO_2$ and these are present during regeneration of the sorbent. Therefore regeneration was monitored and measured by the mass spectrometer analog scan. Figure 3-13 shows an analog scan obtained during regeneration of a sulfided sorbent.

A complete result set for an $H_2S$ sorption cycle presented in this report will include three (3) graphical presentations as; $H_2S$ gas concentration measurement obtained during sulfidation reaction as a function of relative time; Ion current measurement graph obtained during the same sulfidation reaction as a function of relative time and will include all the calibrated gas species present during the sulfidation reaction; an analog scan profile obtained during regeneration of the sorbent showing ion current peak intensities for the gas species that are present based on their atomic mass units (amu).

### 3.10.2 Interpretation of measurements

In preparation of the sulfidation reaction, the sorption gas mixture to be used (containing $H_2S$) is allowed to flow through the bypass line in order to stabilize. It was said to have stabilized when changes in the $H_2S$ concentration measurement were minimal or hardly noticeable. This is considered as the amount of $H_2S$ gas entering the reactor once the sorption gas flowing in the bypass is switched from the bypass line to the reactor. This is done by a simple switch of a valve direction.

When sulfidation reaction takes place between the $H_2S$ gas and the sorbent that is in the reactor, the amount of $H_2S$ gas exiting the reactor will be less than the amount of gas in the inlet. This is seen as a drop in the $H_2S$ concentration measurement. This is illustrated in Figure 3-11. When the sorbent starts to get saturated with the $H_2S$, less amount of the gas will be adsorbed and the $H_2S$ concentration measurement will begin to rise. The reaction is considered complete when the outlet $H_2S$ gas concentration is equal to the inlet (bypass) gas concentration. This measurement curve is known as the breakthrough curve.

After the sulifdation reaction, all the sorption gases are switched off except for $N_2$ gas in order to flush the reactor with the inert gas and prepare for regeneration. As a result, the $H_2S$ gas concentration drops drastically. A similar $H_2S$ ion current measurement is obtained See Figure 3-12.

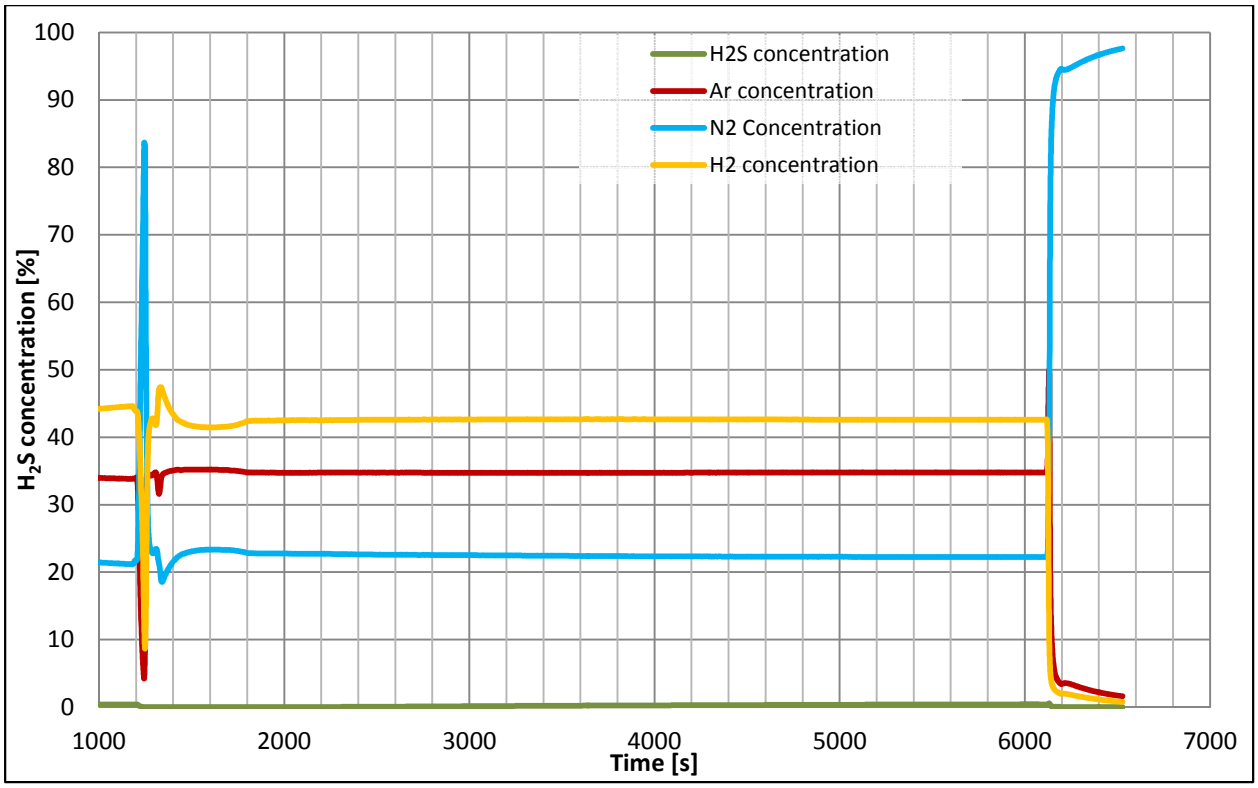


Figure 3-10 Concentration measurement of gases used during sulfidation of sorbent for a sorption cycle

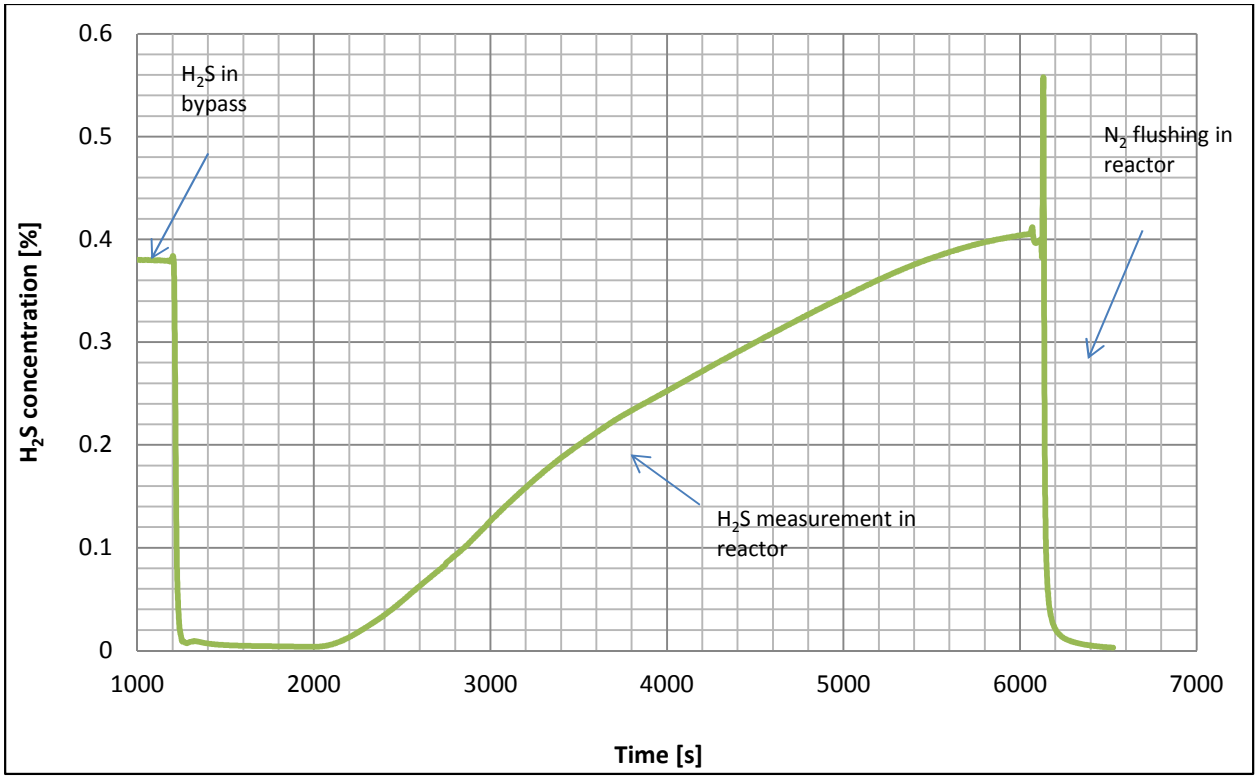


Figure 3-11 $H_2S$ concentration breakthrough curve measurement during $H_2S$ sulfidation

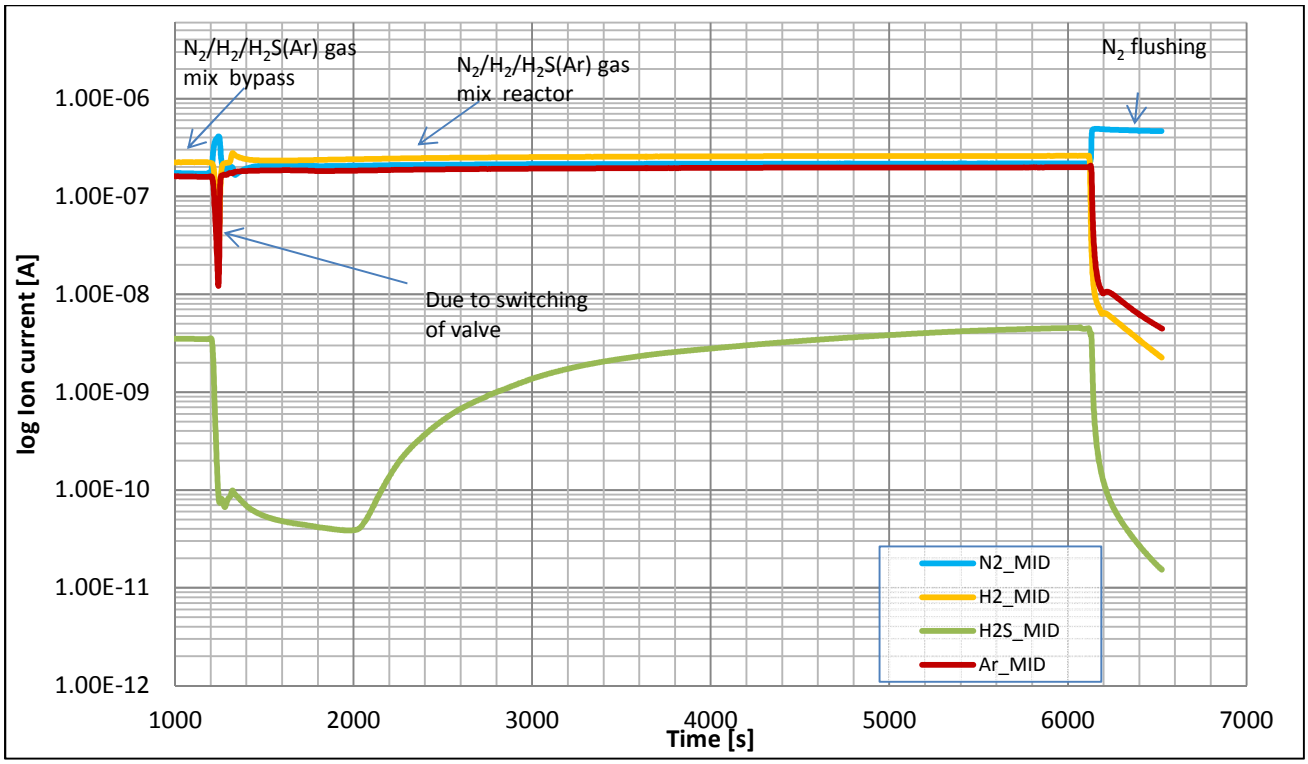


**Figure 3-12 Ion current for $H_2S$ breakthrough measurement for all gases present**

The analog scan measurement that is obtained during regeneration is presented as peak intensities at the atomic mass unit(s) of the gases that are present at the time when the scan is measured. The peak intensities get higher with higher gas concentrations. The scans are measured in series and numbered accordingly. Each scan was measured at a rate of 2 s/amu (atomic mass unit) from 0 to 70amu using the secondary electron multiplier (SEM). The range was chosen to include the expected high intensity peak for the gases that will be closely monitored during regeneration; $O_2$ and $SO_2$. Table 3-1 shows amu values for different chemical compounds.

**Table 3-1 amu values for different chemical compounds**

| Chemical compound | amu |
|---|---|
| $SO_2$ | 64, 48, 32, 16, 66 |
| $H_2S$ | 34, 32, 33, 36, 35 |
| $O_2$ | 32, 16, 34, 33 |
| $N_2$ | 28, 14, 29 |
| $H_2$ | 2, 1 |
| Ar | 40, 20, 36, 38, 18 |
| $H_2O$ | 18, 17, 16, 20,19 |

Figure 3-13 shows an analog scan obtained during regeneration of a sulfided sorbent with $O_2$ gas diluted in $N_2$. The regeneration measurement starts when stabilized peak intensities for $O_2$ and $N_2$ are obtained while the gas is flowing through the by-pass. Regeneration proceeds by O-S exchange such that oxygen is consumed and Sulfur dioxide is produced and when the regeneration gas is directed to the reactor by switch of a valve, part or all of the oxygen will be consumed by the sulfided sorbent and the peak intensities for oxygen will reduce or even completely disappear while new peaks of sulfur dioxide will appear. When regeneration is complete, the oxygen peaks will reappear as before and the sulfur dioxide peaks will disappear. The peaks for nitrogen gas will be seen throughout the regeneration.

Careful timing for switching the valve to direct the regeneration gas to the reactor must be taken into account in order to see all the $SO_2$ peaks and the disappearing of the $O_2$ peaks if the regeneration time is short.

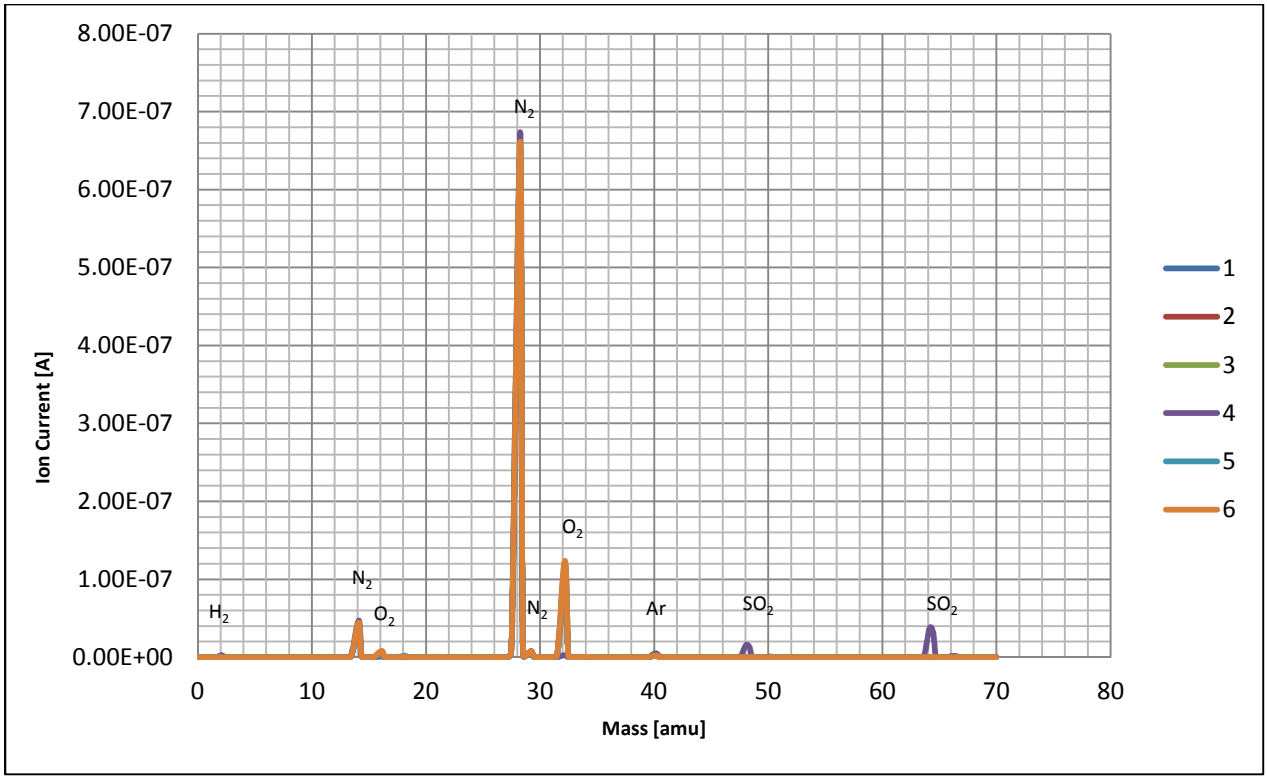


Figure 3-13 Analog scans during regeneration of $Mn_xO_y/Al_2O_3$ (N) sorbent

### 3.10.3 Effect of valve switching and loaded reactor on sorption measurements

In order to investigate the effect of valve switching and a loaded reactor on the $H_2S$ concentration measurement, an experiment was designed that involved measuring the $H_2S$ concentration as a function of time for an empty reactor and a reactor loaded with inert while following the same steps taken during sulfidation of a sorbent with $H_2S$.

The basic steps include;

1. Flushing the reactor with $N_2$ gas (100ml/min) for approximately 5 minutes
2. Switch valve from reactor to bypass and flush the by-pass with nitrogen at the same flow for approximately 5 minutes.
3. Prepare sorption gas mixture of $N_2$, $H_2$ and $H_2S$ (Ar) at flows of 10, 20 and 20 ml/min respectively and let it flow through the reactor for approximately 10 minutes.
4. Switch valve and let the sorption gas flow through the reactor for approximately 10 minutes.
5. Switch of the $H_2$ and $H_2S$ (Ar) gas flows and increase the $N_2$ gas flow to 100ml/min for at least 10 minutes.

The Quartz reactor No. 2 was used and the experiment was carried out at $500^0$C. For inert material used for the loaded reactor is the calcined $Al_2O_3$ support. Approximately 120mg was used. The lines were flushed with nitrogen for at least an hour before the experiment was done. The measured $H_2S$ concentration profiles are shown in Figure 3-14 below.

When there is no residual $H_2S$ in the pipeline, no effect of valve switching is noticed from the $H_2S$ measurement and it is hard to tell at what point the valve was switched from the reactor to the bypass.

When the sorption gas is introduced into the bypass, it took about 10 minutes for the sorption gas to stabilize in both cases. The effect of switching the valve from the bypass to the reactor when the $H_2S$ gas is in the line is quite evident. When the valve is switched to the reactor, the loaded reactor registers a larger lag time compared to the empty reactor before the $H_2S$ concentration measurement is registered by the mass spectrometer. For the empty reactor, the $H_2S$ concentration measured is almost immediately equal to the one registered in the bypass while for the loaded reactor, a slightly lower $H_2S$ concentration is obtained and it took approximately 5 to 8 minutes for the concentration to be equal to the one obtained from the bypass.

$N_2$ flushing for the empty reactor shows a very fast and drastic drop in $H_2S$ concentration while it took slightly longer (approximately an extra 5 minutes) to obtain near zero $H_2S$ concentration measurements with the loaded reactor. Even after an hour of flushing the loaded reactor, the $H_2S$ concentration measured approximately 1ppm.

From this experiment it can be said that switching the valve from a reactor to the bypass or the other way round has no major effect on the $H_2S$ concentration and it can be assumed that all the $H_2S$ directed to the bypass is also directed to the reactor assuming constant flow rates.

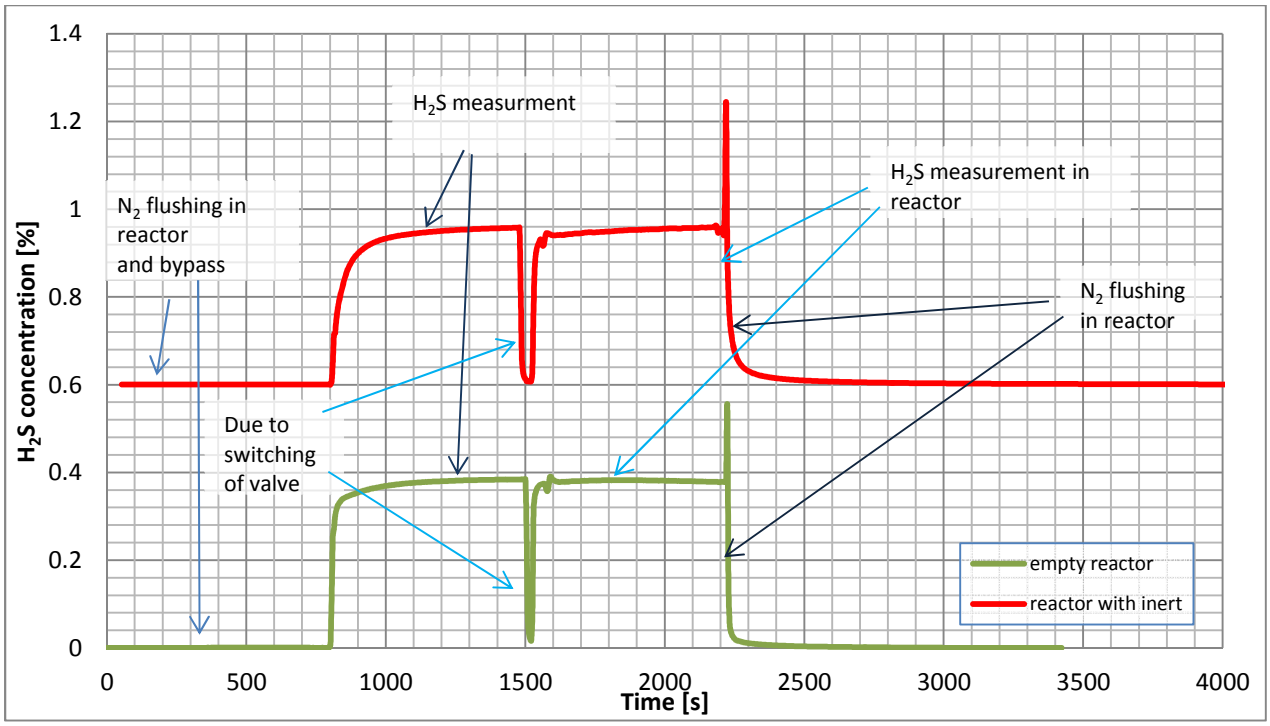


**Figure 3-14 $H_2S$ concentration measurement for an empty reactor and reactor loaded with inert at 450$^0$C**
**NB: Curves have been off-set along the x and y-axis for the sake of clarity and ease of comparison**

## 3.11 Challenges in sorption cycle measurements

An attempt was made to match the timing for $N_2$ flushing of the reactor and bypass, stabilization of the $H_2S$ concentration measurement in the bypass before sending the gas to the reactor and stabilization of the regeneration gas in the bypass before regenerating the sorbent.

Because of this, in some measurements it can be seen that a stable $H_2S$ concentration measurement had not yet been obtained within the allocated time before switching the sorption gas from the bypass to the reactor. See Figure 3-15. It should be noted that the gas flow rates were stable at all times. When a slight increment in stabilization time was done, another problem was encountered. The a maximum apparent stabilized $H_2S$ concentration measurement was obtained within the allocated time but then the value would start decreasing before the sorption gas was introduced to the reactor. See Figure 3-16. Again, the gas flow rates were stable at all times.

In some cases, when a stable $H_2S$ concentration measurement was observed, there appeared to be a drift in the concentration measurement with time because the final stabilized measured value for $H_2S$ concentration after complete sulfidation of the sorbent was seen to be higher than the value in the bypass. This drift was not limited to one sulfidation cycle but was also observed during the course of the experiment from one cycle to another. The calculated $H_2S$ concentration in the sorption gas mixture based on the flow rates is 0.4% and Figure 4-19 shows a drift in $H_2S$ concentration in the bypass from the 1$^{st}$ cycle to the 13$^{th}$ cycle.

The challenge observed in obtaining during gas regeneration, was proper timing between the position of the scan and the time for switching the valve to flow the regeneration gas mixture from the bypass to the reactor for regeneration cycles that did not require a lot of time. A mistiming would mean either only 1 of the expected 2 $SO_2$ peaks would be observed (refer to Figure 3-18) or both peaks would not be seen but the oxygen consumption would be observed as illustrated Figure 3-19a and b, where the b represents a zoomed representation of Figure 3-19a.

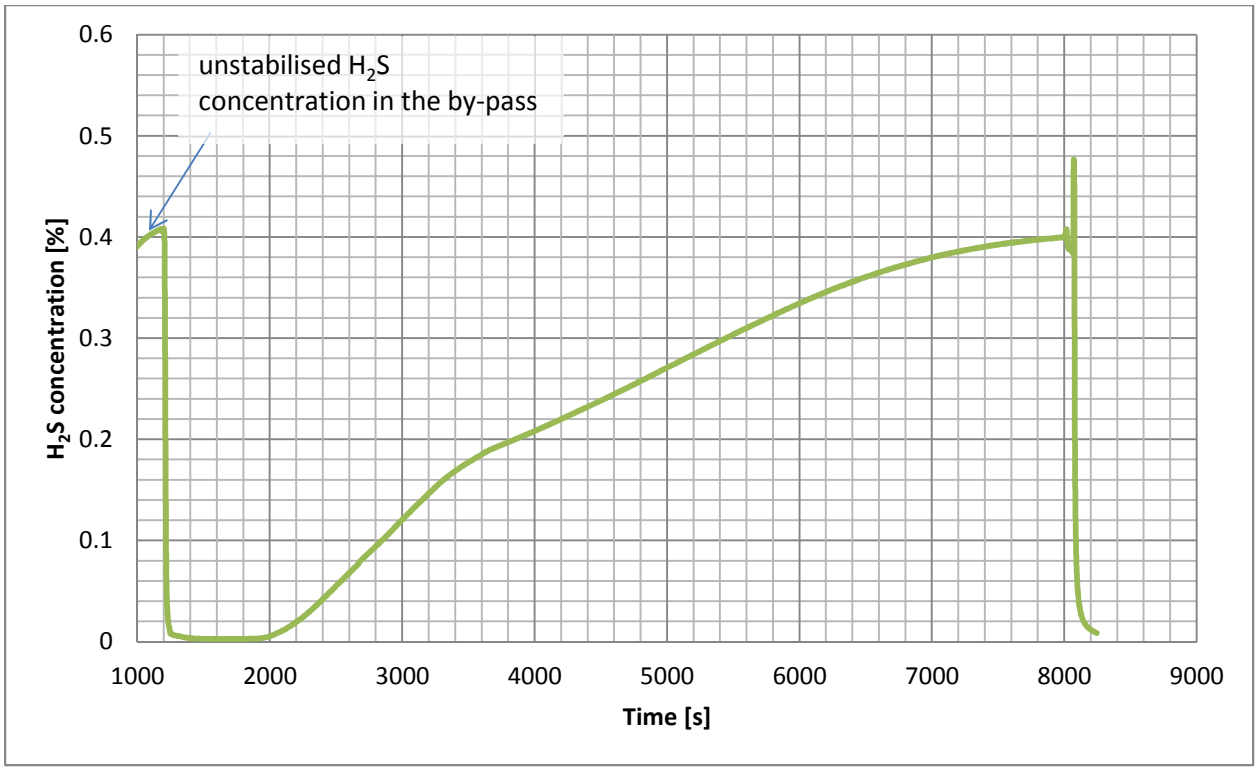


Figure 3-15 $H_2S$ breakthrough curve showing unstable $H_2S$ concentration measurement in the by-pass

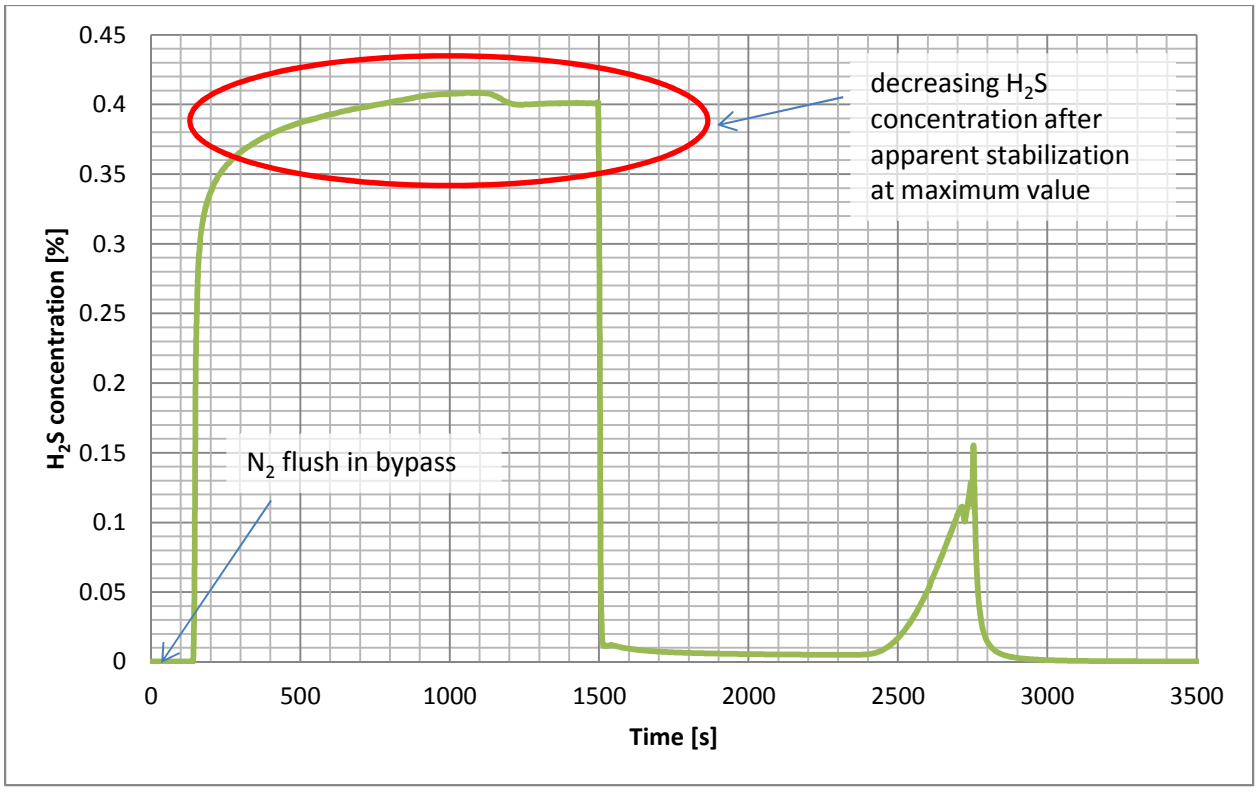


Figure 3-16 $H_2S$ breakthrough curve showing decrease $H_2S$ concentration measurement in the by-pass during the sorption gas stabilization time

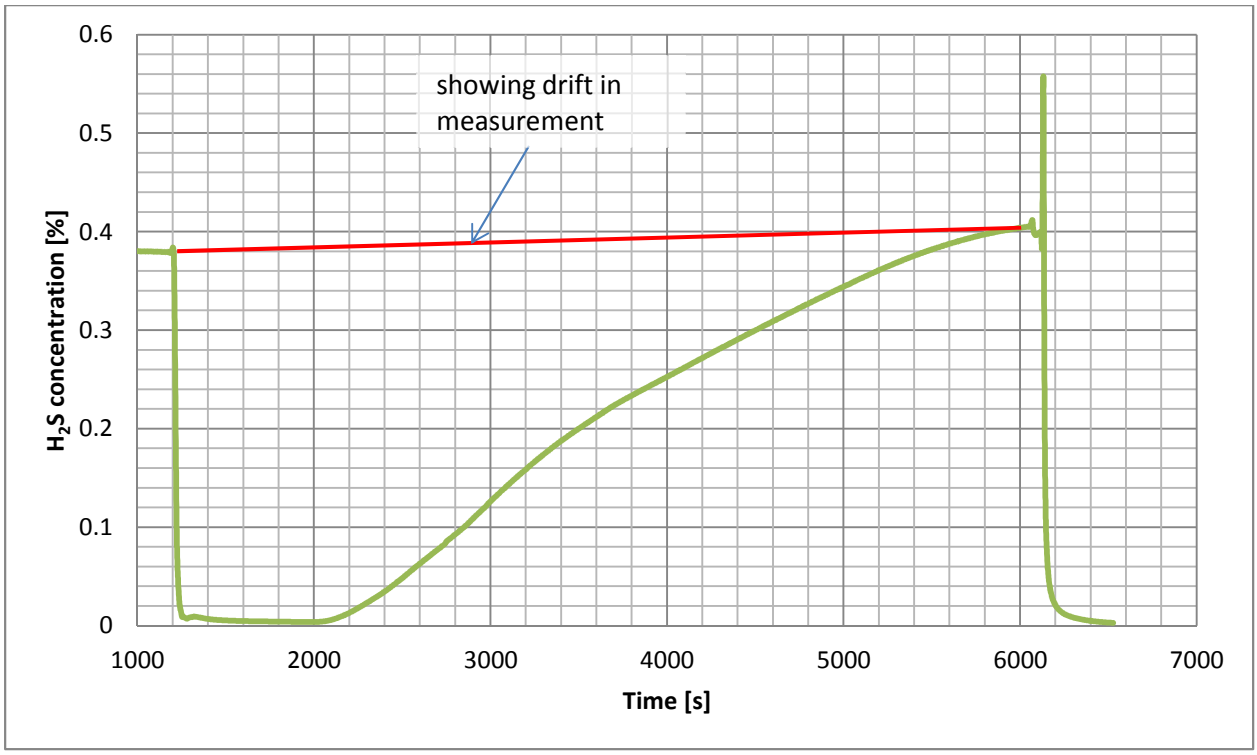


Figure 3-17 $H_2S$ breakthrough curve showing a drift in $H_2S$ concentration measurement after complete sulfidation reaction

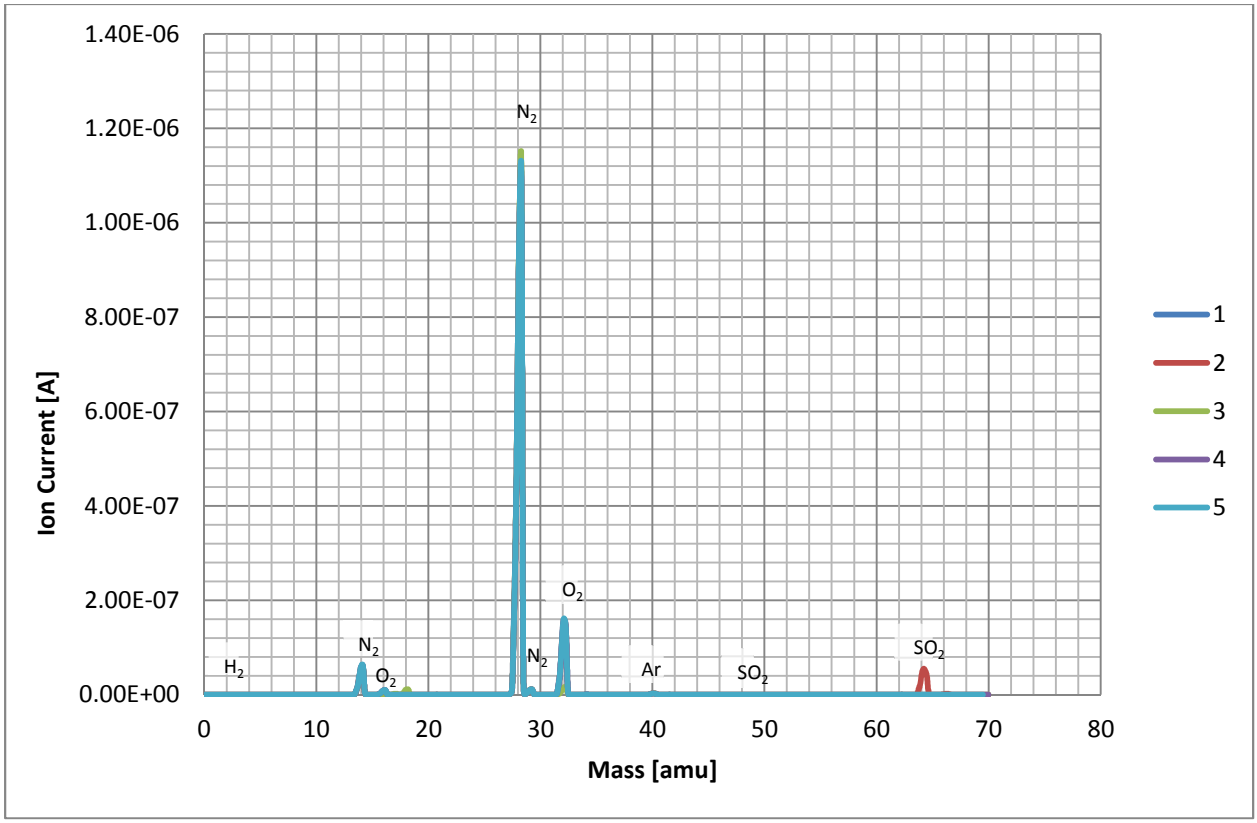


Figure 3-18 Regeneration analog scan showing only one $SO_2$ intensity peak

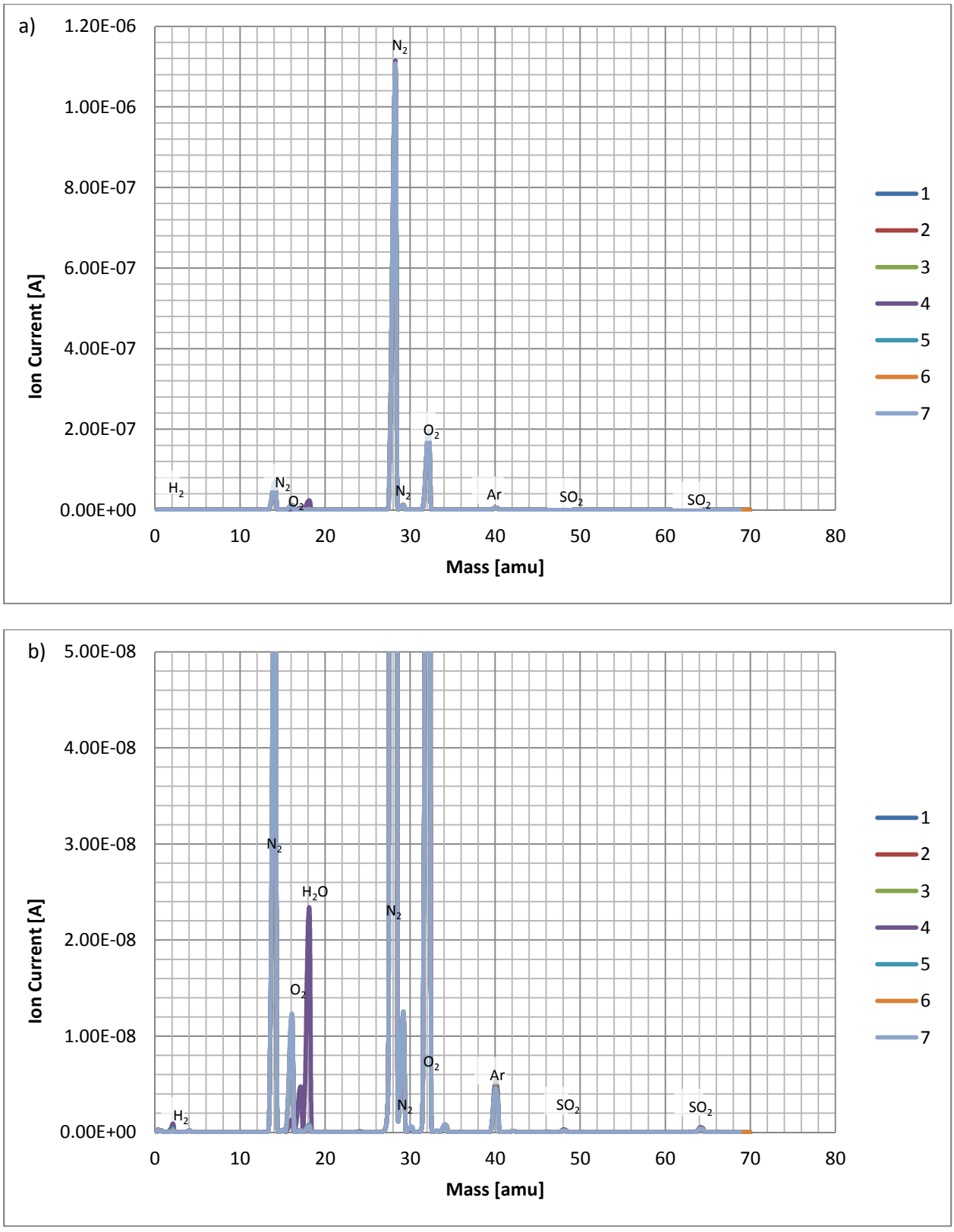


**Figure 3-19 Regeneration analog scanning showing (a) the nearly missed $SO_2$ intensity peaks and (b) the corresponding zoomed analog scan**

# Chapter 4 Results and discussion

The different properties of the supports used, ɤ-Al2$O_3$, $ZrO_2$, $TiO_2$ and $CeO_2$, and their respective manganese-based sorbents have been studied and presented in this chapter. XRD analysis has been a useful tool in identifying the manganese oxide phases present on each of the sorbents. The reduction properties of the sorbents have been studied with temperature programmed reduction (TPR) and thermogravimetric Analysis (TGA) studies. Nitrogen adsorption has been used to obtain and compare the textural properties of the sorbents.

The results obtained from the sorption studies were carried out on the two alumina based sorbents have been presented and evolution of the sorbent capacity after repeated sulfidation and regeneration cycles has been studied.

The used and regenerated alumina based sorbents have been further analyzed with a combination of nitrogen adsorption, TPR and oxygen chemisorption to show the effect of the repeated sulfidation and regeneration reactions on the sorbents.

Raman spectra for the prepared sorbents as well as the used and regenerated alumina based sorbents were obtained, however due to inability to replicate the results of the reference sample used, $Mn_xO_y$-$Al_2O_3$(A) [49], the results shall not be included in the main report and will not contribute to the discussion or conclusion made in this report. Nevertheless, the results have been attached to Appendix P for the interested reader.

## 4.1 Characterization

### 4.1.1 Nitrogen adsorption

Table 4-1 shows the BET surface area, pore volume and average pore size of the supports and prepared sorbents. The Micromeritics instrument summary reports have been attached to Appendix F

The supports exhibit different textural properties. The $Al_2O_3$ support has the highest surface area at 154$m^2$/g while $TiO_2$ support has the lowest at 8$m^2$/g. ZrO2 and CeO2 have a lower BET surface area than Al2O3 support but they have larger pore sizes. The same trend is observed with their respective sorbents although the sorbents have a reduced surface area. The 30wt% $Mn_xO_y/Al_2O_3$ sorbent which was prepared by double impregnation has a lower surface area and pore volume compared to the 15wt% $Mn_xO_y/Al_2O_3$. In general, the surface area is expected decrease with increasing loading of the metal oxide until a monolayer coverage is completed [50 and references there-in]. The difference in surface area between the supports and their respective sorbents can be explained by the calcination that part of the sorbent preparation method.

In all cases however, the average pore size remained relatively unchanged. The same has been reported by Liang et al. [51] when they studied the effect of manganese loading on alumina support. They observed a faster reduction rate with the small pores compared to the larger pores although the average pore density remained the same.

Table 4-1 Textural properties of $Mn_xO_y/Al_2O_3$ (15wt% Mn), $Mn_xO_y/Al_2O_3$ (30wt% Mn), $Mn_xO_y/ZrO_2$, $Mn_xO_y/TiO_2$ and $Mn_xO_y/CeO_2$ sorbents and their respective supports

| Sample | BET surface area ($m^2/g$) | Pore volume ($cm^3/g$) | Average pore size (nm) |
|---|---|---|---|
| $Al_2O_3$ support | 154 | 0.24 | 6 |
| $Mn_xO_y/Al_2O_3$ (15wt% Mn) | 137 | 0.24 | 7 |
| $Mn_xO_y/Al_2O_3$ (30wt% Mn) | 102 | 0.16 | 6 |
| $Mn_xO_y/Al_2O_3$ (15wt% Mn, used & regenerated) | 82 | 0.15 | 7 |
| $Mn_xO_y/Al_2O_3$ (30wt% Mn, used & regenerated) | 36 | 0.07 | 7 |
| $ZrO_2$ support | 93 | 0.29 | 12 |
| $Mn_xO_y/ZrO_2$ | 83 | 0.25 | 11 |
| $TiO_2$ support | 8 | 0.03 | 7 |
| $Mn_xO_y/TiO_2$ | 5 | 0.02 | 7 |
| $CeO_2$ support | 53 | 0.17 | 13 |
| $Mn_xO_y/CeO_2$ | 35 | 0.12 | 13 |

### 4.1.2 X-Ray Diffraction

XRD analysis has been a useful tool in identifying the manganese oxide phases present on the prepared sorbents. Only $Mn_2O_3$ phase was identified on all the prepared sorbents. This is in agreement with literature for supported manganese oxide sorbents prepared with a manganese nitrate precursor [49]. The sulfur adsorption capacity of the sorbents can be notably influenced by the crystal structure of the manganese oxide. Anatase was also identified to be the titanium oxide phase on the $Mn_2O_3/TiO_2$ sorbent.

Figure 4-1 shows the peak profiles for the sorbents used and the supports used with the positions of the $Mn_2O_3$ phases have been marked. For the alumina based sorbents, the diffraction pattern for the alumina support is hardly detected. For a manganese loading of less than 6% on alumina support, the diffraction pattern for the manganese oxide is hardly detected and this implies a strong interaction between the metal oxide and the support and hence a well dispersed system[51]. When manganese content is increased, the interaction becomes weaker.

For the sorbents prepared with $ZrO_2$, $TiO_2$ and $CeO_2$, the diffraction patterns for the supports are clearly exhibited indicating a stronger interaction between $Mn_2O_3$ and the various supports and hence a well dispersed system.

Table 1-2 shows the crystallite size of the $Mn_2O_3$ phase on the prepared sorbents as determined by both Topas and the Eva software. Eva software uses the Scherrer formula to calculate the crystallite size as FWHM (Full Width at Half Maximum) and IB (Intergral Breadth). The Scherrer formula was applied on the second $Mn_2O_3$ peak a smoothened peak, Kα stripped and background subtracted. The Topas software was used on all the $Mn_2O_3$ phase peaks that were identified. Using the Topas software requires inputing all the instrument fundamental parameters used and this was done. The Topas software

calculates a volume weighted FWHM (Lvol-FWHM) and IB (Lvol-IB). Lvol represents the volume of the average crystal.

The crystallite sizes obtained by the two methods appear to be in close agreement except for the $Mn_2O_3/ZrO_2$ sorbent which shows a significant difference between the crystallite sizes determined by Topas and the Eva-Scherrer value. The Topas software is said to work best on isolated and loosely linked peaks and this could be cause of the significant difference since the XRD pattern for $Mn_2O_3/ZrO_2$ has overlapping $Mn_2O_3$ and $ZrO_2$ peaks.

Figure 4-3 shows a comparison of the XRD pattern of the fresh alumina based sorbents and the used and regenerated sorbents after the sorption studies. The phases on the used and regenerated sorbents have not been identified although it can be mentioned though that the $Mn_2O_3$ phase peaks appear to be absent. Bakker et al. [22] performed similar studies and they were able to identify the spinel manganese aluminate ($MnAl_2O_3$) phase on a used and regenerated sorbent while studying manganese-based sorbents for regenerative high temperature desulfurization.

A spinel can be formed when two metal oxides react under favorable conditions forming a distinct compound. The equilibrium constant for sulfidation reaction of the spinel $MnAl_2O_4$ and $H_2S$ is close to 1 on the log plot shown in Figure 2-2 [22]. This implies that the sulfidation reaction is reversible and therefore it can be used for regenerative desulfurization at high temperatures. The sulfidation and regeneration reactions for the spinel manganese aluminate can be written as shown in equations 4-1 and 4-2 respectively.

$$MnAl_2O_4\ (s) + H_2S\ (g) \rightarrow MnS\ (s) + Al_2O_3\ (s) + H_2O\ (g) \qquad 4\text{-}1$$

$$MnS\ (s) + Al_2O_3\ (s) + O_2\ (g) \rightarrow MnAl_2O_4\ (s) + SO_2\ (g) \qquad 4\text{-}2$$

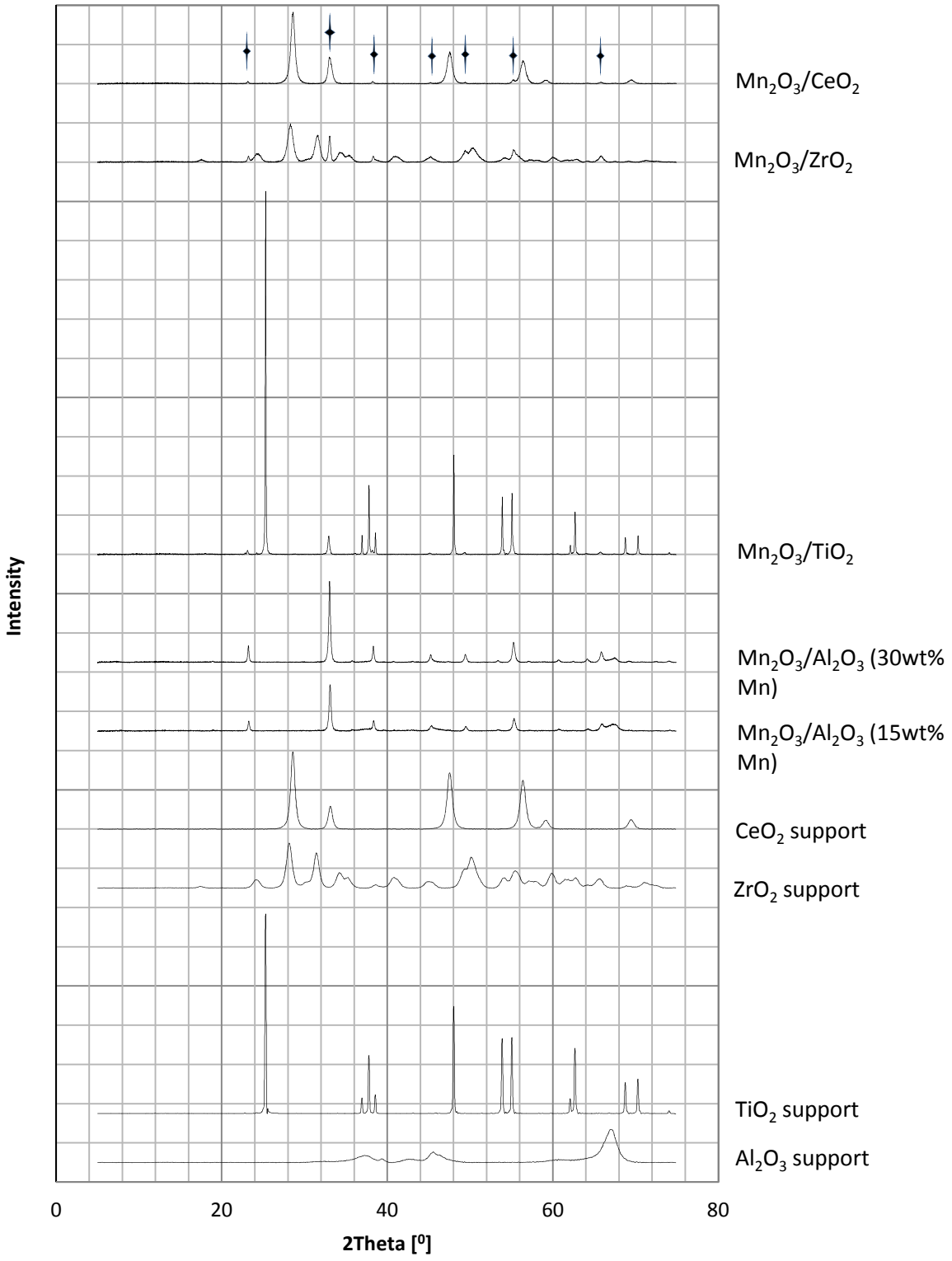


Figure 4-1 XRD patterns for supports and prepared sorbents, Symbol ♦ for $Mn_2O_3$

Table 4-2 Crystallite size of $Mn_2O_3$ phase on $Mn_2O_3$/ɣ- $Al_2O_3$ (15wt% Mn), $Mn_2O_3$/ɣ-$Al_2O_3$ (30wt% Mn), $Mn_2O_3/ZrO_2$, $Mn_2O_3/TiO_2$ and $Mn_2O_3/CeO_2$

| | Topas | | Scherrer from EVA (on the 2nd peak) | |
|---|---|---|---|---|
| **$Mn_2O_3$ phase on:** | **Lvol-IB (nm)** | **Lvol-FWHM (nm)** | **IB (nm)** | **FWHM (nm)** |
| $Mn_2O_3$/ɣ- $Al_2O_3$_15wt% Mn | 16 | 19 | 28 | 35 |
| $Mn_2O_3$/ɣ-$Al_2O_3$_30wt% Mn | 24 | 29 | 31 | 40 |
| $Mn_2O_3/ZrO_2$ | 7 | 9 | 29 | 34 |
| $Mn_2O_3/TiO_2$ | 37 | 45 | 31 | 40 |
| $Mn_2O_3/CeO_2$ | 20 | 19 | 14 | 17 |

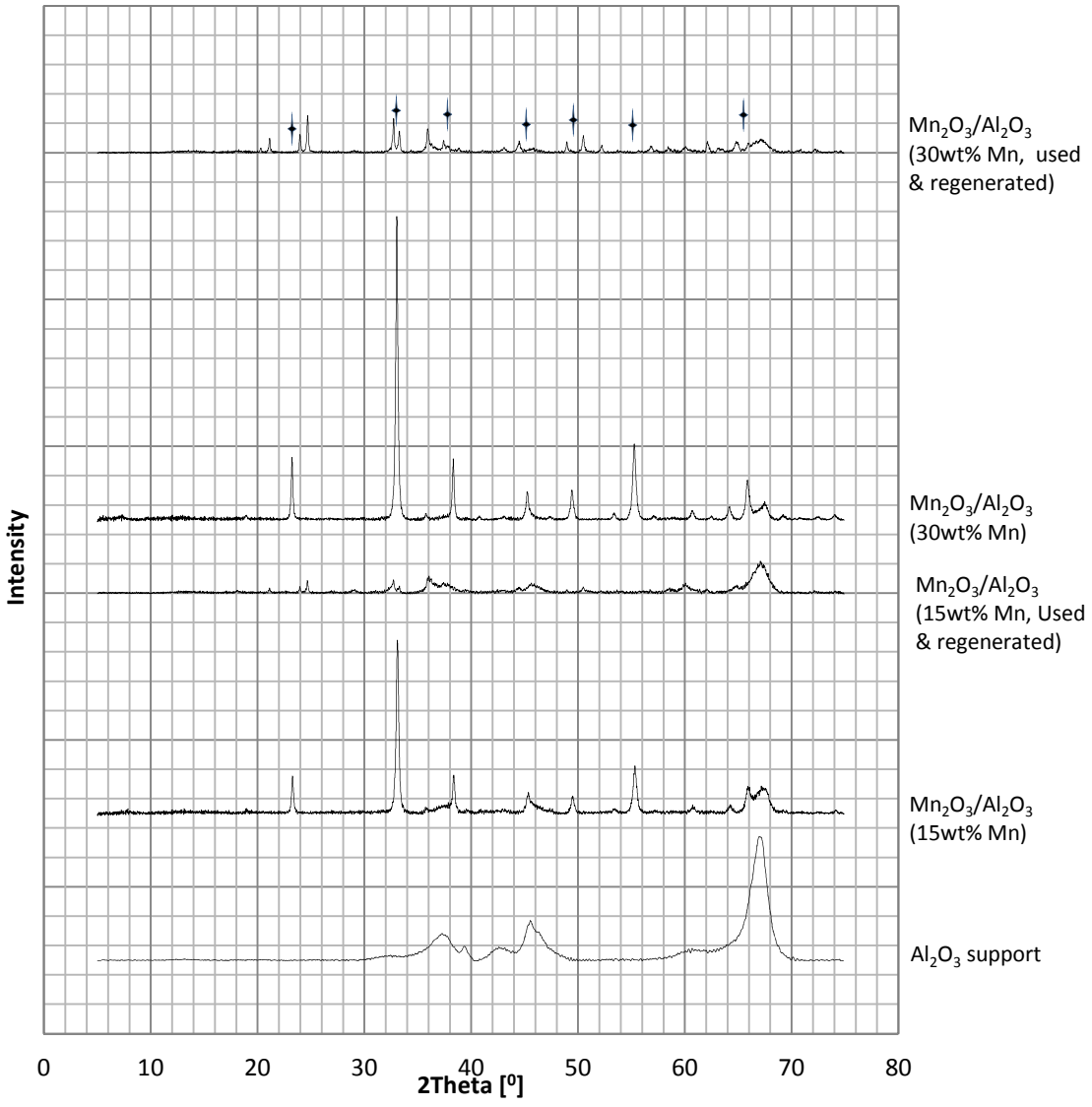


Figure 4-3 XRD patterns for the alumina support, alumina based sorbents and the used and regenerated alumna based sorbents. Symbol ✦ for $Mn_2O_3$

### 4.1.3 Temperature Programmed Reduction

The TPR profiles obtained for the five sorbents that were prepared have been shown in Figure 4-5. The experiment was carried out with 10% $H_2$ in Ar gas in order to investigate their reducibility properties of the sorbents.

The alumina based samples have similar TPR profiles with two distinct peaks. XRD analysis identified $Mn_2O_3$ as the only manganese oxide phase present on all the sorbents hence the two peaks can be attributed to the two-step reduction process of the $Mn_2O_3$ phase to MnO. Equations 4-3 and 4-4 show the reduction chemical equations for the two-step reduction process. Due to thermodynamic limitations, MnO is not be reduced further [29].

Step 1 $3Mn_2O_3 + H_2 \rightarrow 2Mn_3O_4 + H_2O$ 4-3

Step 2 $Mn_3O_4 + H_2 \rightarrow 3MnO + H_2O$ 4-4

The first peak is due to the reduction of $Mn_2O_3$ to $Mn_3O_4$ while the second peak is due to the reduction of $Mn_3O_4$ to MnO. This is consistent with literature [49, 52]. The color of the sorbents changed from a dark color to a green color after the TPR experiment indication the presence of MnO which is green. See Figure 4-6 a1 and a2.

The peak temperatures are observed to be approximately $400^0$C and $500^0$C respectively although the temperatures for the higher loading alumina based sorbent (30 wt% Mn on $Mn_2O_3/Al_2O_3$) are slightly lower. This is the effect of manganese loading on alumina. An increase in manganese loading will shift the peak temperatures to a lower value [52].

The peak intensities for the 30wt% Mn alumina based sorbent are higher than the respective 15wt% Mn and this is confirmed by the higher amount of hydrogen consumed by the sorbent. See Table 4-3. The peaks for the higher loading sample are more distinct compared to the low loading samples which appear to be overlapping. Broad and overlapping peaks are attributed to be due to a strong interaction between the metal oxide and the support and this confirms that a higher manganese loading on alumina reduces this metal-support interaction [51] [52].

$Mn_2O_3/ZrO_2$ exhibits the same 2 peak profile with a broad shoulder on the first peak. This confirms the strong metal-support interaction that was deduced from the XRD pattern and hence a good dispersion of $Mn_2O_3$ on the support. The two-step reduction processes of $Mn_2O_3$ occur at lower temperatures compared to the alumina based sorbents with the peak temperature seen at approximately $330^0$C and the second reduction peak at approximately $410^0$C. It seems the support increases the reducibility of the manganese oxide. The color of the sorbent after the TPR experiment was also green just as for the alumina based samples.

The TPR profile for $Mn_2O_3/TiO_2$ shows an overlap of the reduction peaks indicating a strong-metal interaction and hence good dispersion. This was also indicated by the XRD pattern. The diffraction pattern of a manganese oxide sorbent supported on $TiO_2$ appears to be dependent on the calcination temperature. Ettireddy et al. [50] performed characterization studies on manganese oxide sorbent supported on both anatase titanium oxide at various manganese loadings and observed four distinct

reduction peaks. The first peak at approximately 200$^0$C, was reported to be due to the reduction of $Ti^{4+}$ to $Ti^{3+}$; the second peak at approximately 320$^0$C due to the reduction of $MnO_2$ to $Mn_2O_3$; the third peak at approximately 410$^0$C due to the reduction of $Mn_2O_3$ to $Mn_3O_4$ and the last peak at approximately 460$^0$C due to the reduction of $Mn_3O_4$ to MnO. The sorbents were calcined at 250$^0$C in air for 4 hours. Thirupathi et al. [53] in their study on nickel-doped manganese oxide supported on titanium oxide support report a TPR profile of manganese oxide on $TiO_2$ (un-doped) with three peaks for the reduction of $MnO_2$ to $Mn_2O_3$, $Mn_2O_3$ to $Mn_3O_4$ and $Mn_3O_4$ to MnO respectively. A calcination temperature of 400$^0$C in air for 2 hours was used. The reduction peak of $Ti^{4+}$ to $Ti^{3+}$ was not present. Anatase is said to be quite stable, however due to its interaction with manganese oxide, the reduction of $Ti^{4+}$ to $Ti^{3+}$ can be expected to take place at temperatures less than 250$^0$C and its absence is because the sorbent was calcined at a temperature higher than 250$^0$C.

The sorbents used in this study were calcined at 600$^0$C hence the reduction peak for $Ti^{4+}$ to $Ti^{3+}$ is not expected to be seen and from XRD analysis, $MnO_2$ is not present and the reduction peak of $MnO_2$ to $Mn_2O_3$ is also not expected to be seen. The color of the sorbent changed from light grey to yellow after the TPR experiment. Refer to Figure 4-6 b.

The TPR profile for $Mn_2O_3/CeO_2$ sorbent shows three overlapping peaks again confirming the high dispersion of the metal oxide on the support as deduced by the XRD analysis. Luo et al. [54] studied $H_2$-TPR profiles of manganese oxide sorbents supported on $CeO_2$ and calcined at different temperatures and they observed for sorbents calcined at temperatures lower than 600$^0$C only two peaks were obtained and this is in agreement with the two step reduction process of $Mn_2O_3$ to MnO. However a third peak was observed when calcination temperatures were higher than 600$^0$C.

The third peak could be attributed to the reduction of the bulk $CeO_2$ according to the reaction equation 4-5 below.

$$CeO_2 + 0.5H_2 \rightarrow 0.5Ce_2O_3 + 0.5H_2O \qquad 4\text{-}5$$

Kobayashi et al. [55] studied the reduction of pure cerium oxide and a $CuO_2$-$CeO_2$ sorbent calcined at 650$^0$C and observed an appreciable reduction of the pure cerium oxide occurring at temperatures close to 650$^0$C due to the reduction of bulk oxygen of cerium. A similar explanation could be given in this case where the presence of $Mn_2O_3$ reduces the reduction temperature of the bulk $CeO_2$. The color of the $Mn_2O_3/CeO_2$ sorbent changed from a dark color to light grey after the TPR experiment. Refer to Figure 4-6.

The amount of integral hydrogen gas consumed was calculated from the TPR profiles for all the sorbents and the results are tabulated in Table 4-3. Instrument reports obtained after calculating $H_2$ consumption can be found in Appendix H . The stoichiometric factor (stoichiometric ratio of hydrogen/metal) used is 1 based on the equation 4-6.

$$Mn_2O_3 + H_2 \rightarrow 2MnO + H_2O \qquad 4\text{-}6$$

The $H_2$ consumption for $Mn_2O_3/Al_2O_3$ (30wt% Mn) is about twice as much as that of $Mn_2O_3/Al_2O_3$ (15wt% Mn). This is expected due to the doubled manganese loading. $Mn_2O_3/CeO_2$ sorbent shows the highest

hydrogen consumption among the sorbents with 15wt% manganese loading and the additional reduction of $CeO_2$ contributes to the higher observed consumption.

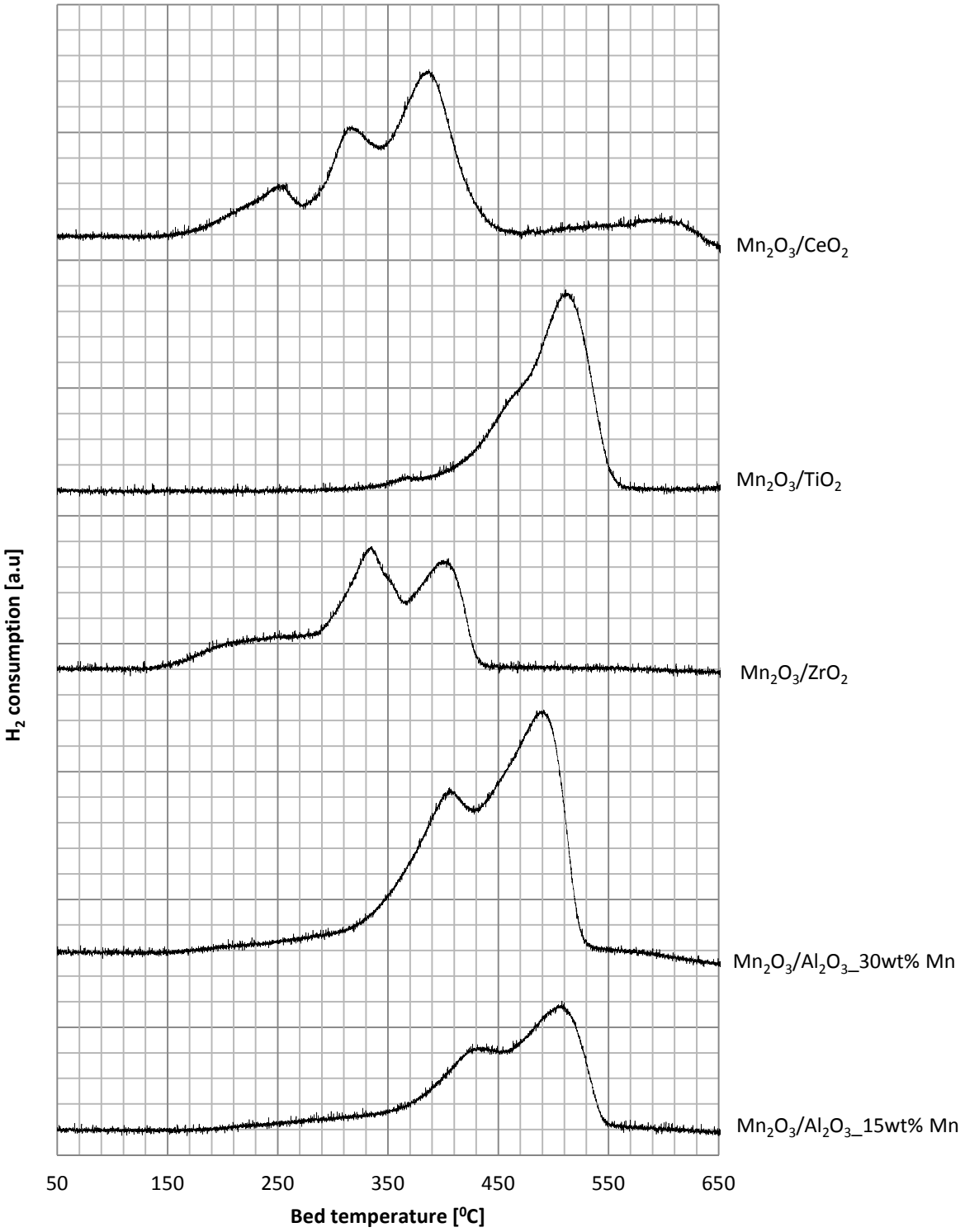


Figure 4-5 $H_2$-TPR profiles of the $Mn_xO_y$-$Al_2O_3$_15wt% Mn, -$Al_2O_3$_30wt% Mn, -$ZrO_2$, -$TiO_2$ and –$CeO_2$ sorbents

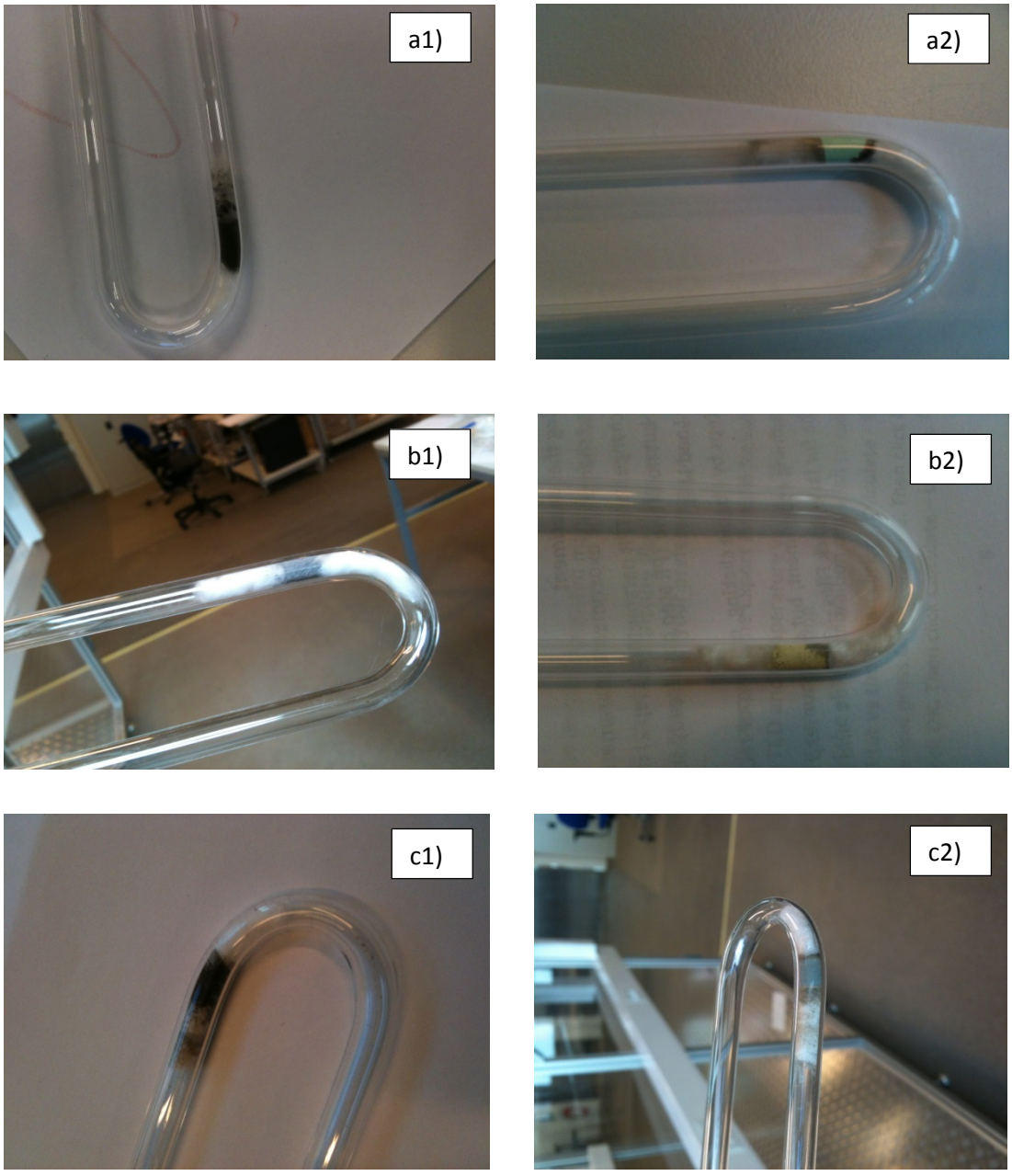


**Figure 4-6 showing samples of sorbents before and after H2-TPR measurements**
**a1, b1 and c1 for $Mn_2O_3/Al_2O_3$ (15wt% Mn), $Mn_xO_y/TiO_2$ and $Mn_xO_y/CeO_2$ respectively before analysis**
**a2, b2 and c2 for $Mn_2O_3/Al_2O_3$ (15wt% Mn), $Mn_xO_y/TiO_2$ and $Mn_xO_y/CeO_2$ respectively after analysis**

Table 4-3 $H_2$ consumption and % $H_2$ reduction obtained from $H_2$-TPR

| Sample | $H_2$ consumption (µmol/g) |
|---|---|
| $Mn_2O_3/Al_2O_3$ (15wt% Mn) | 530 |
| $Mn_2O_3/Al_2O_3$ (30wt% Mn) | 1019 |
| $Mn_2O_3/ZrO_2$ | 471 |
| $Mn_2O_3/TiO_2$ | 460 |
| $Mn_2O_3/CeO_2$ | 774 |

### 4.1.4 Thermogravimetric Analysis

The TGA profiles obtained for the sorbents agree with the two-step reduction process of $Mn_2O_3$ to MnO. The ion current profiles for water obtained by the mass spectrometer indicate two water peaks and this is the water formed from each reduction step. Figure 4-9 shows the mass spectrometer measurements. The initial peaks observed at temperatures close to $50^0$C and are due to physically adsorbed water on the sorbents. $Mn_2O_3/CeO_2$ has a third peak at approximately $520^0$C due to the reduction of $CeO_2$. It should be noted however that the temperatures for the ion current peaks obtained by the mass spectrometer and the peak temperatures for the TPR profiles are not in agreement. This deviation can be attributed to the instruments.

Figure 4-7 which shows weight loss observed from all the sorbents due to loss of the oxygen atom. The highest weight loss is exhibited by the $Mn_2O_3/Al_2O_3$ (30wt% Mn) sorbent at temperatures close to $450^0$C and then a stable weight is recorded. The weight change for $Mn_2O_3/Al_2O_3$ (15wt% Mn) occurs at the same temperature but with a lower degree. The same can be said for $Mn_2O_3/TiO_2$ and $Mn_2O_3/ZrO_2$ although weight change for the latter occurs at a lower temperature of approximately $350^0$C before the weight stabilizes. $Mn_2O_3/CeO_2$ on the other hand shows weight loss occurring at two temperatures, approximately $300^0$C and $600^0$C. A weight loss at $600^0$C is also observed for the $CeO_2$ support confirming the reduction of $CeO_2$. The rest of the supports that were used show TGA profiles with relatively stable weight and showed to be inert and unreactive in a reducing gas atmosphere.

The DSC measurements in Figure 4-8 show that heat is given out during the reduction processes with heat peaks being observed at temperatures as low as $250^0$C.

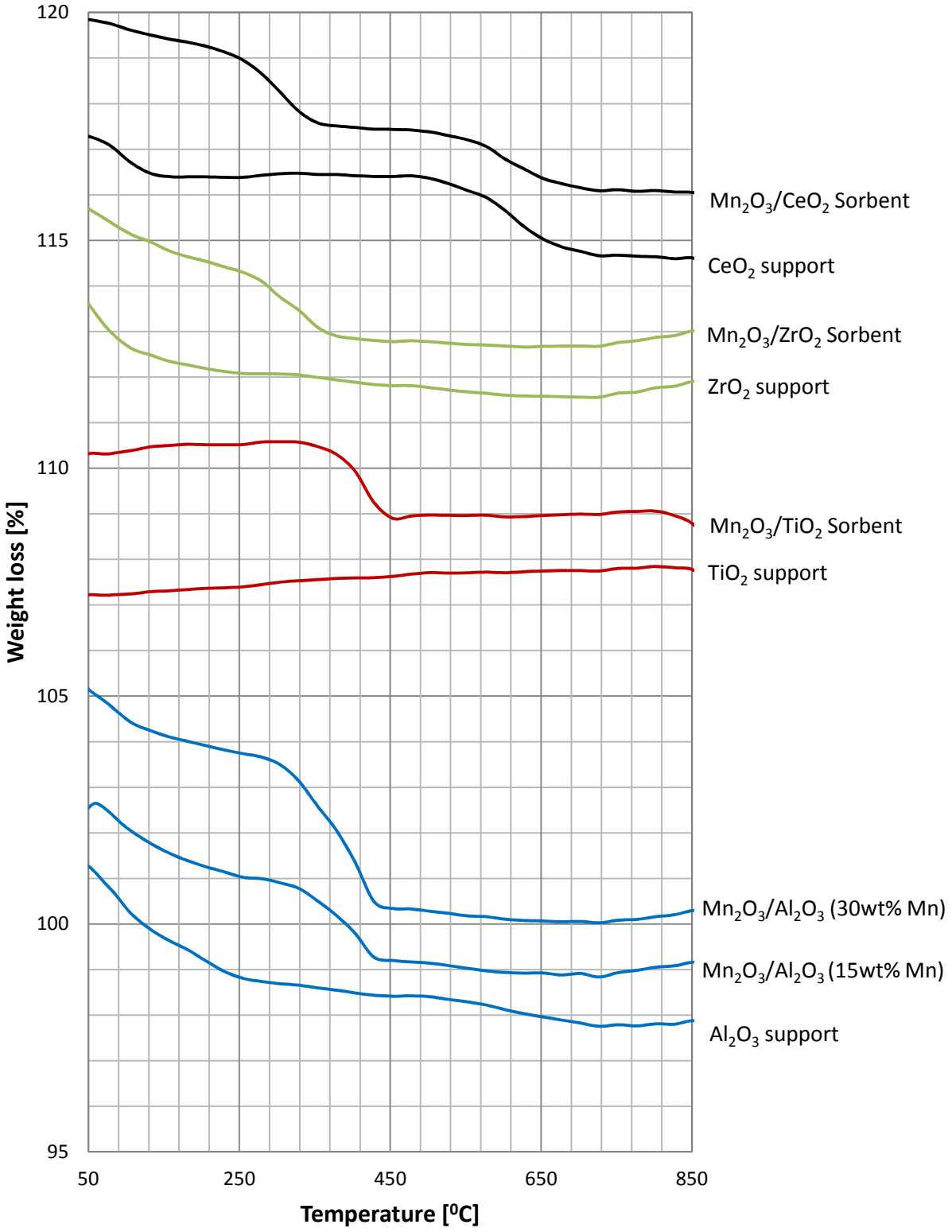


**Figure 4-7 TGA profile of $Mn_2O_3$-$Al_2O_3$ (15wt% Mn), -$Al_2O_3$ (30wt% Mn), -$ZrO_2$, -$TiO_2$ and –$CeO_2$ sorbents and their respective treated supports in 10% $H_2$ (Ar) atmosphere**
**NB: Curves have been off-set along the y-axis for the sake of clarity and ease of comparison**

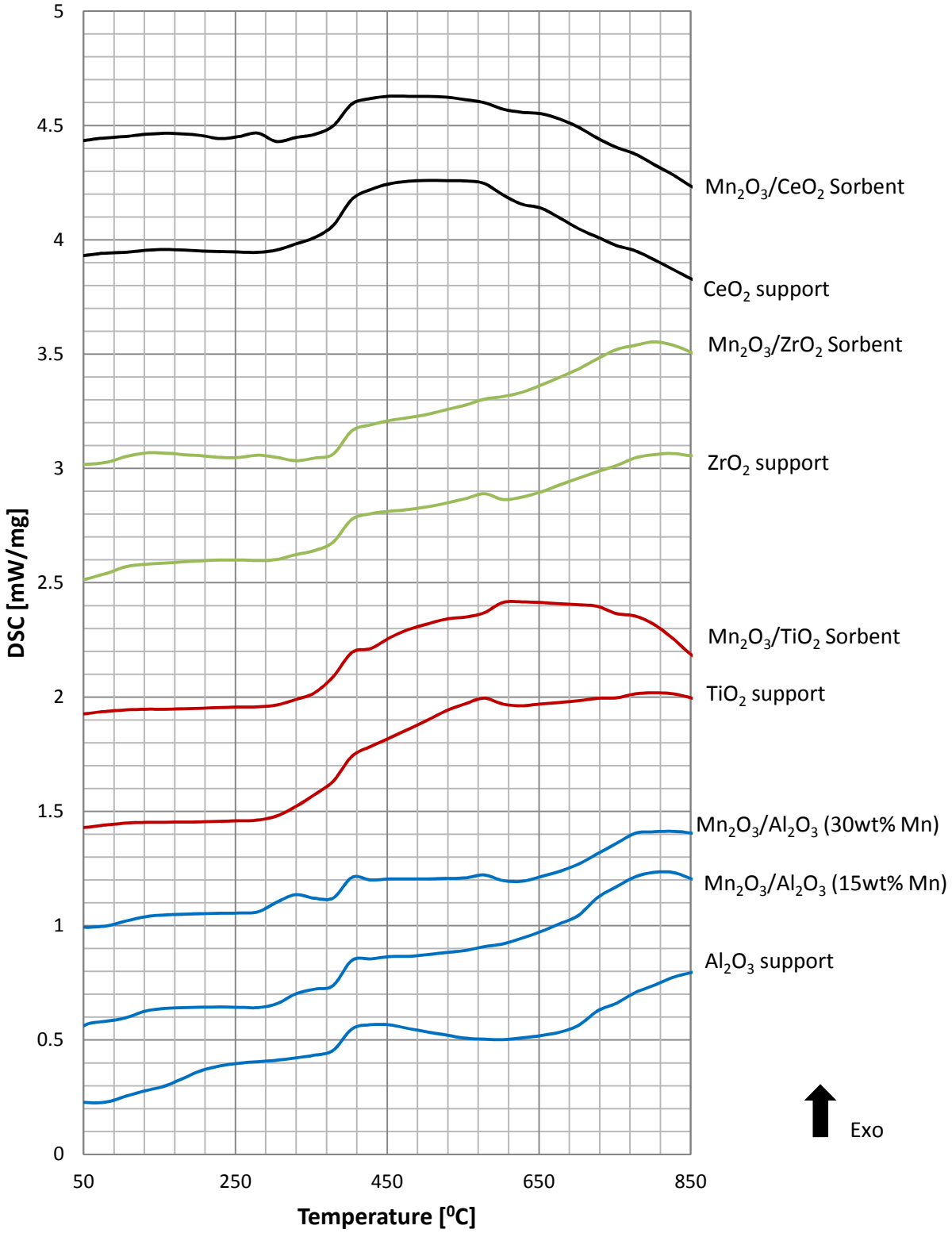


**Figure 4-8 DSC heat flow profile obtained during TGA analysis of $Mn_2O_3$-$Al_2O_3$ (15wt% Mn), -$Al_2O_3$ (30wt% Mn), -$ZrO_2$, -$TiO_2$ and –$CeO_2$ sorbents and their respective treated supports**
**NB: Curves have been off-set along the y-axis for the sake of clarity and ease of comparison**

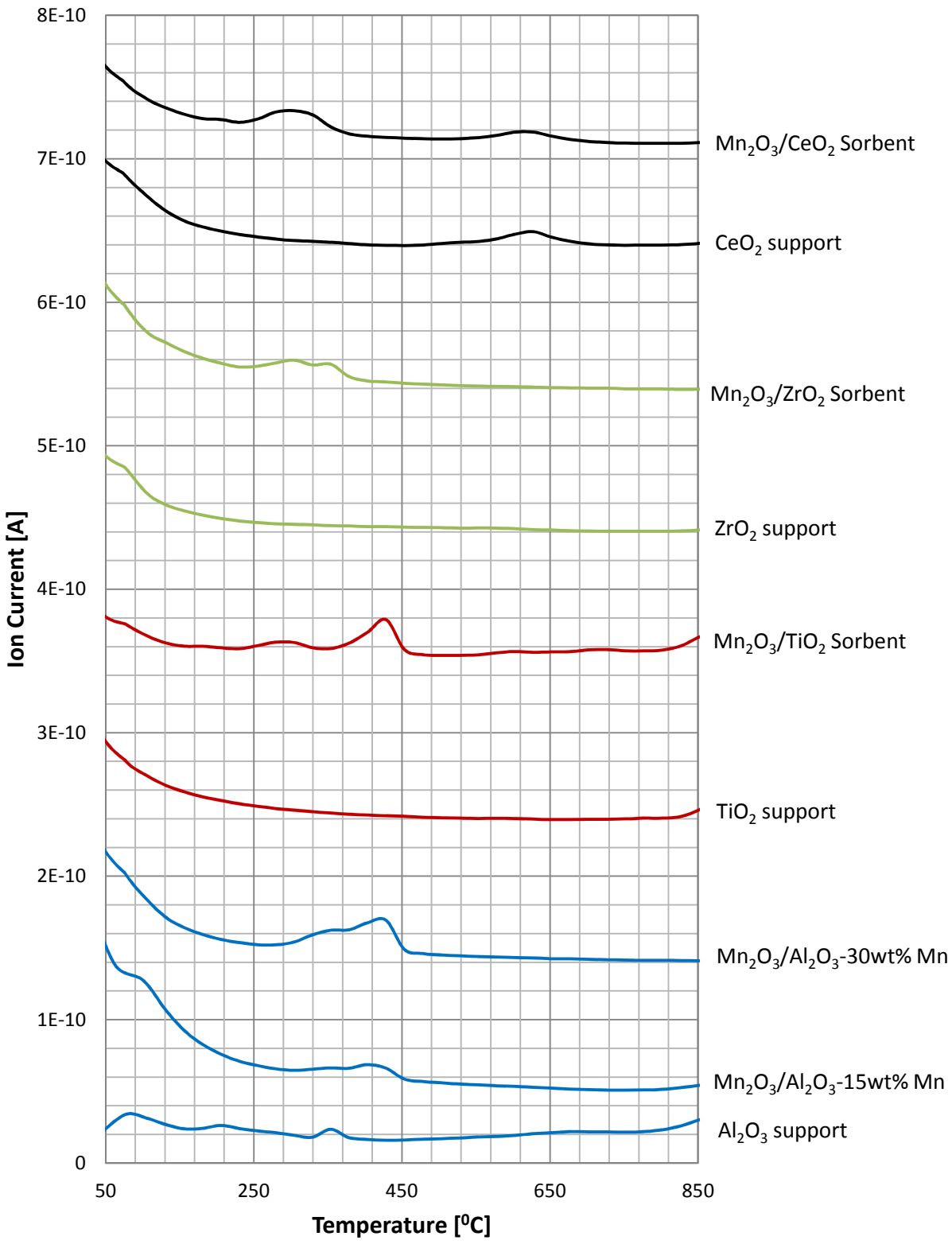


**Figure 4-9 Ion current spectra for water (mass 18) obtained by mass spectrometer during TGA analysis of $Mn_2O_3$-$Al_2O_3$ (15wt% Mn), -$Al_2O_3$ (30wt% Mn), -$ZrO_2$, -$TiO_2$ and –$CeO_2$ sorbents and their respective treated supports**
**NB: Curves have been off-set along the y-axis for the sake of clarity and ease of comparison**

### 4.1.5 Oxygen pulse chemisorption

Dispersion of the active metal was obtained for the two alumina based sorbents based on the amount of oxygen used after reducing the sorbents. The measurement was carried out twice for each sorbent and the results are shown in Table 4-4. Summarized instrument reports from calculations are attached to Appendix I . 3% dispersion of manganese was found on both the 15 and 30wt% $Mn_2O_3/Al_2O_3$ sorbents. The stoichiometric factor (stoichiometric ratio of oxygen to manganese) of 0.25 was used based on equation 4-7 below.

$$2MnO + 0.5O_2 \rightarrow Mn_2O_3 \qquad 4\text{-}7$$

No oxygen uptake was observed with the used and regenerated alumina based sorbents after the sorption studies implying no metal dispersion. This could be the case if spinel manganese aluminate, $MnAl_2O_4$ is formed during the sulfidation and regeneration reactions [22].

**Table 4-4 Oxygen uptake and metal dispersion of $Mn_2O_3/Al_2O_3$, 15wt% and 30wt% Mn**

| **Sample** | | **$O_2$ uptake (µmol/g)** | **Dispersion (%)** |
|---|---|---|---|
| $Mn_2O_3/Al_2O_3$ (15wt% Mn) | sample 5 | 19 | 3 |
| | sample 6 | 18 | 3 |
| $Mn_2O_3/Al_2O_3$ (30wt% Mn) | sample 1 | 46 | 3 |
| | sample 2 | 39 | 3 |

### 4.1.6 Raman spectroscopy

As mentioned earlier, these results shall not be included in the main report or discussed, however the results are attached to Appendix P for the interested reader.

## 4.2 $H_2S$ sorption activity measurements

### 4.2.1 Result-reproducibility

Figure 4-10 to Figure 4-12 show the results from the three experiments carried out to determine if results could be reproduced when using the new laboratory equipment. The sorption results that include the $H_2S$ sorption concentration measurement, ion current measurement and the analog scan for regeneration have been attached to Appendix L .

Based on observation minor differences are observed on the breakthrough curve measurements obtained from the three experiments. The major differences are seen from cycles 2 and 4 which were the first cycles done on a new day after the sorbents were left overnight in flowing gas mixture of nitrogen and hydrogen. A slight difference is also observed with the first cycle in terms of time taken for the breakthrough curve ($H_2S$ concentration) to start increasing.

It can be said that the results are able to be reproduced but repeating an experiment would be recommended for certainty.

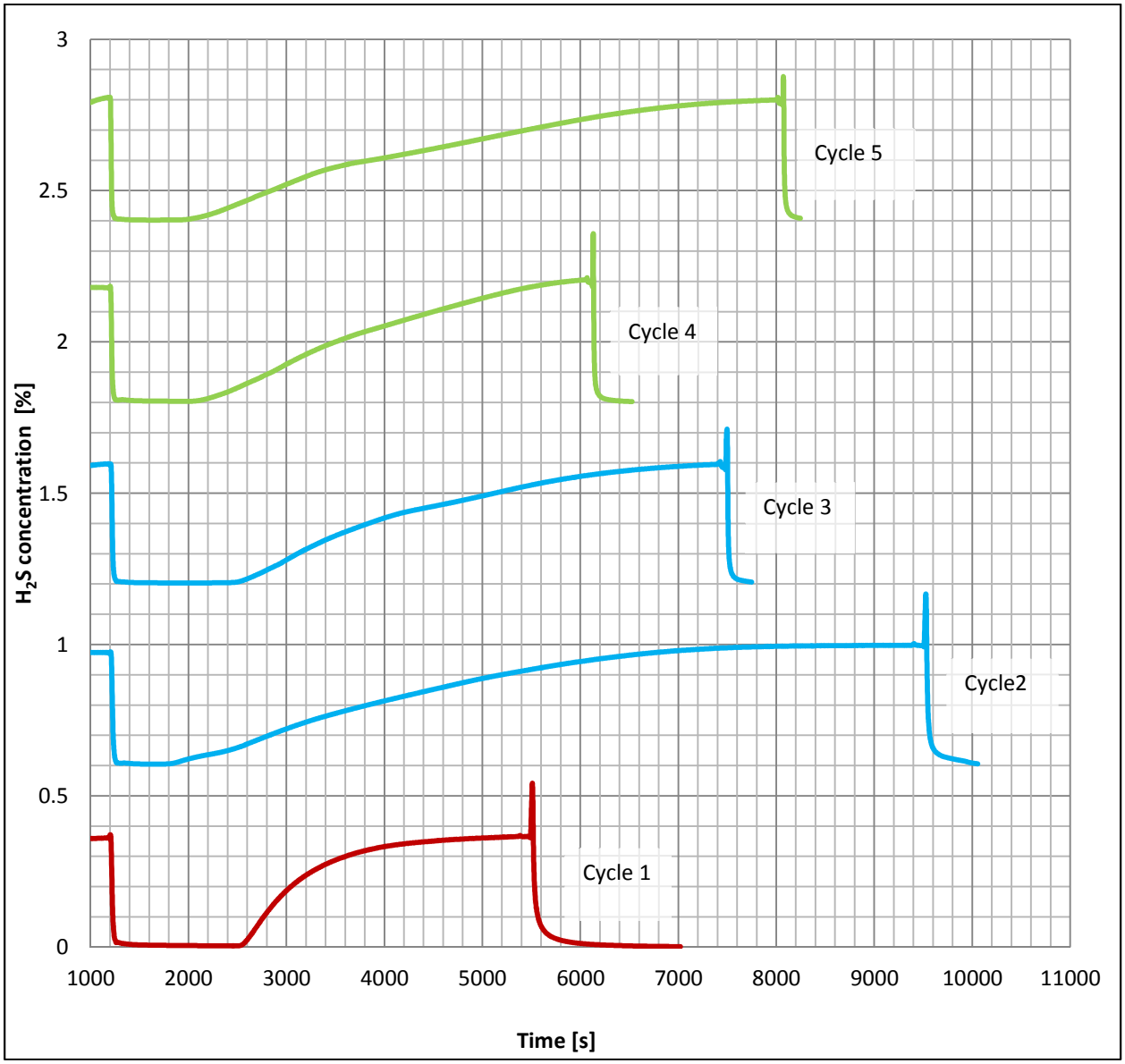


**Figure 4-10 $H_2S$ sorption breakthrough measurement on $Mn_xO_y/Al_2O_3$ (N) sorbent for Experiment 1**
**NB: Curves have been off-set along the x and y-axis for the sake of clarity and ease of comparison**

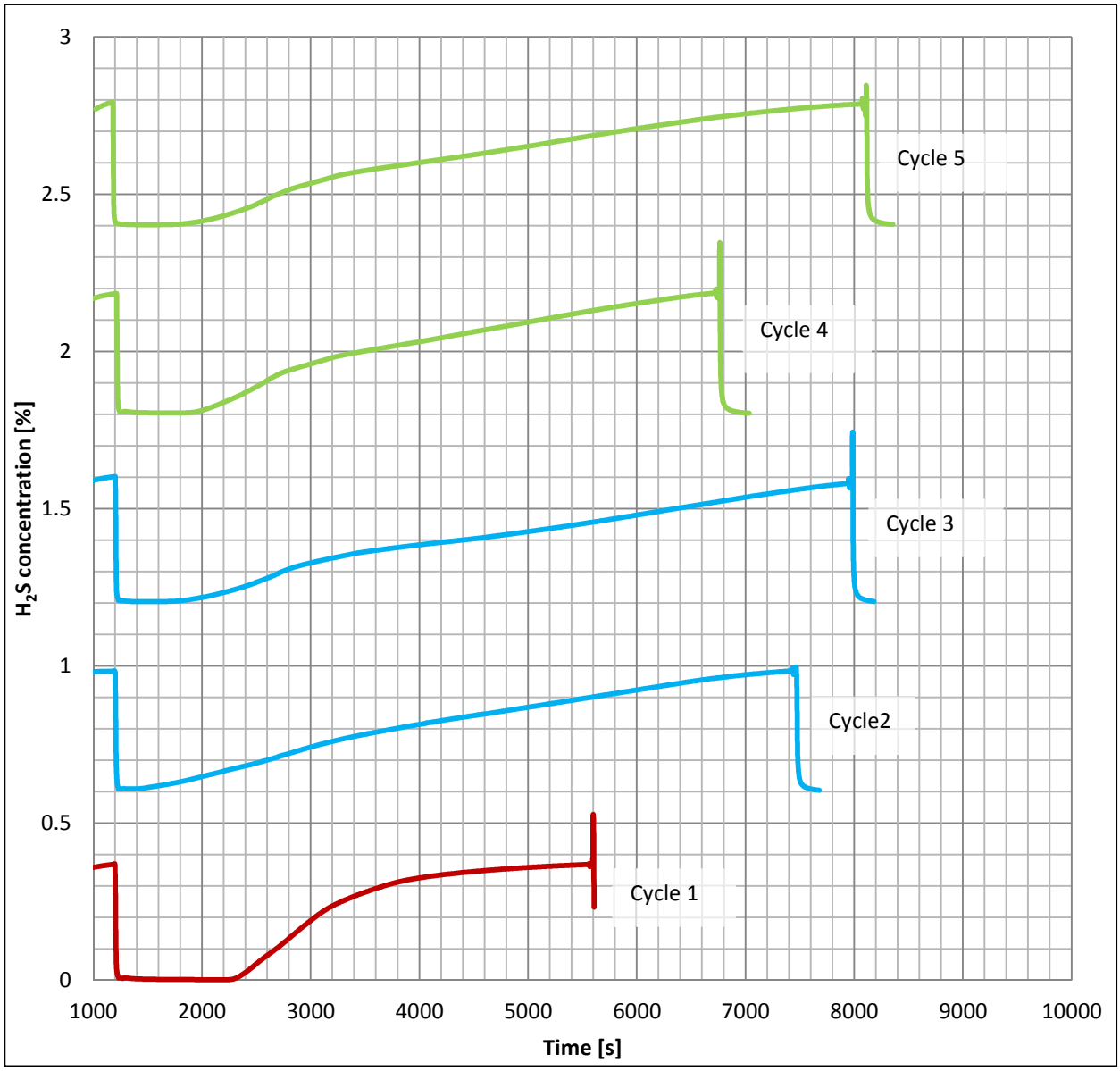


**Figure 4-11 $H_2S$ sorption breakthrough measurement on $Mn_xO_y/Al_2O_3$ (N) sorbent for Experiment 2**
**NB: Curves have been off-set along the x and y-axis for the sake of clarity and ease of comparison**

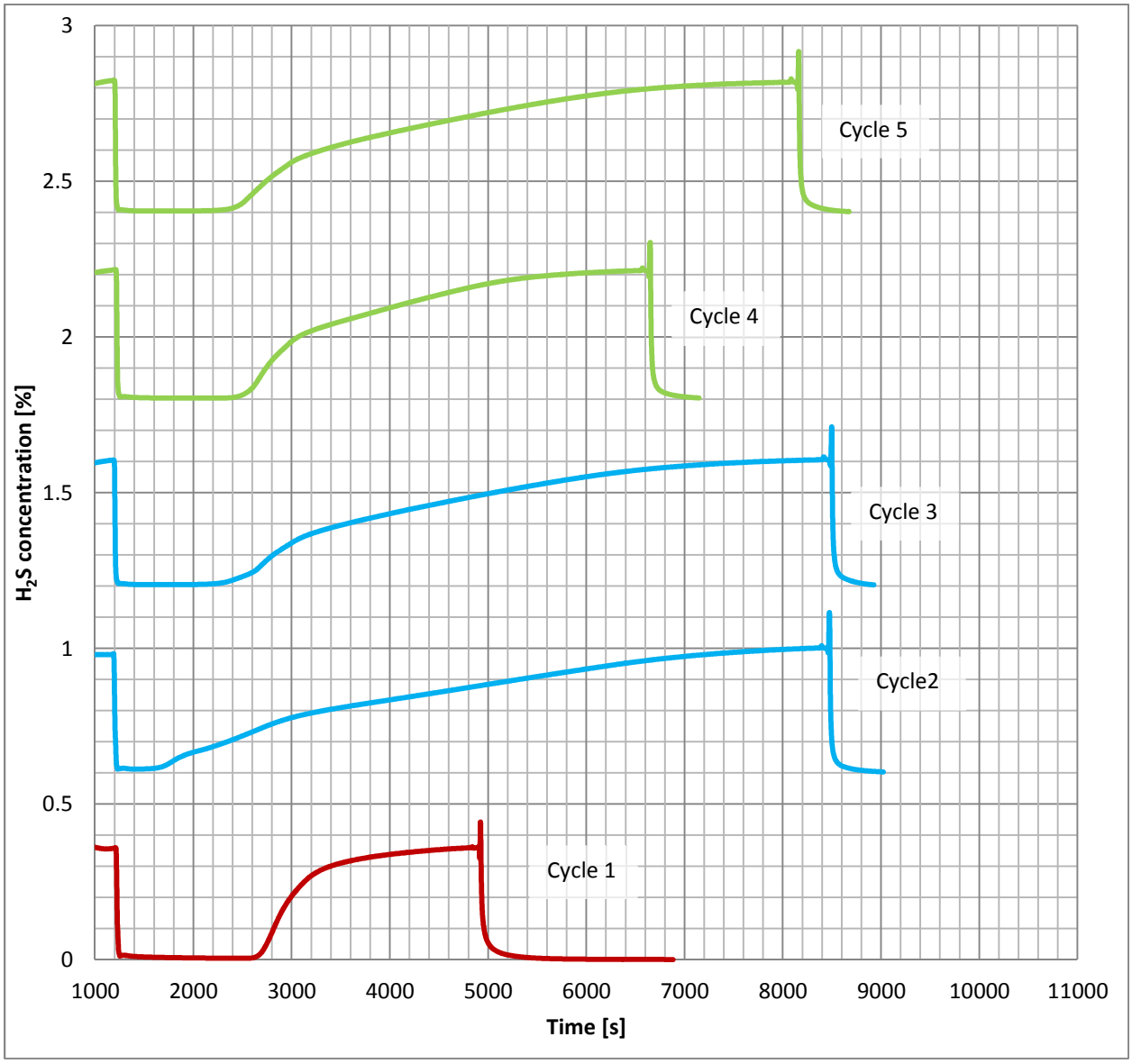


**Figure 4-12 $H_2S$ sorption breakthrough measurement on $Mn_xO_y/Al_2O_3$ (N) sorbent for Experiment 3**
**NB: Curves have been off-set along the x and y-axis for the sake of clarity and ease of comparison**

### 4.2.3 $H_2S$ Sorption breakthrough curve measurements

Appendix M and Appendix N have detailed $H_2S$ sorption measurement results obtained during sorption studies of $Mn_2O_3/Al_2O_3$ (15wt% Mn) and $Mn_2O_3/Al_2O_3$ (30wt% Mn) respectively. The results are presented as $H_2S$ sorption concentration measurement, ion current measurement and a regeneration analog scan for each sorption cycle.

As mentioned earlier, sorption studies for $Mn_2O_3/ZrO_2$, $Mn_2O_3/TiO_2$ and $Mn_2O_3/CeO_2$ sorbents were not performed and the sorbents have been handed over to the supervisor as future work.

The sorption studies for $Mn_2O_3/Al_2O_3$ (15wt% Mn) and $Mn_2O_3/Al_2O_3$ (30wt% Mn) were performed in duplicate with the amount of sorbent, sorption gas flow rates and regeneration gas flow rates doubled for the second experiment. The first cycle and last cycle ($13^{th}$) were measured as full sorption cycles while cycles 2 to 12 were measured as short cycles with the sulfidation reaction stopped when the $H_2S$ concentration measured at the outlet of the reactor reached 0.1%.

Figure 4-13 and Figure 4-14 and Figure 4-17 and Figure 4-18 show the development of the breakthrough curves with repeated sorption cycles for $Mn_2O_3/Al_2O_3$ 15 and 30wt% Mn loading respectively, experiment one and two. The sorption cycles are presented in series with the breakthrough curve for cycle 1 at the bottom and the last cycle at the top.

In general, a decrease in sorption capacity of the sorbents is observed with repeated sulfidation and regeneration cycles. A substantial decrease in activity is also observed whenever the sorbent has been left overnight in $N_2$ and $H_2$ atmosphere. It was expected that keeping the regenerated sorbent in a reducing atmosphere overnight would help to maintain the sorption activity but this was not the case. However the second breakthrough curve measured on every new day after day 1 showed an improved sorption activity when compared to last sorption cycle performed the previous day. It is possible that the activity was improved by the regeneration reaction. It can be expected that if each new day started with regeneration, instead of the flushing and sulfidation, the substantial decrease in sorption capacity would not be observed. This was however not confirmed.

The same trend was observed with the second set of experiments when the mass and flow rates used were doubled. The similarity of breakthrough curves obtained for experiment one and two in both cases suggest the absence of external diffusion.

Comparing the high loading sample and the low loading sample, the time required for the first breakthrough curve of the 30wt% loading sample to reach 0.1% is approximately twice the time required by the 15wt% loading sample. This should be expected since the metal loading has been doubled. However in terms of sorption capacity stability, the higher loading sorbent showed poor stability. The deactivation is substantial such that its last sorption cycle (cycle 13) required approximately the same time as the low loading sample to reach 0.1% and the sorption capacity registered is less than half of what it was in the first cycle.

Figure 4-15 and Figure 4-16 and Figure 4-19 and Figure 4-20 show the complete first cycle and $13^{th}$ cycle superimposed for $Mn_2O_3/Al_2O_3$ 15 and 30wt% Mn loading respectively, experiment 1 and 2. This would

have provided a better visual way of comparing the development of breakthrough curves after repeated sorption cycles however the drift in $H_2S$ concentration measurement makes this impossible. It will still be mentioned that in all the figures, the breakthrough curve of the first experiment shows lower $H_2S$ concentration values at the outlet compared to the $13^{th}$ cycle. But this could also be just a drift in measurement.

The major difference between the high loading sample and the low loading sample is in stability of the sorbent in regards to the sorption capacity. The sorption capacity for the high loading sample drops drastically after the first sorption cycles and then a steady decline is obtained. The time taken to reach 0.1% $H_2S$ concentration for the last cycle is less than half the time used in the first cycle.

It is also observed that when the higher loading sorbent starts to get saturated and the $H_2S$ concentration at the outlet starts to increase, it takes a shorter time for the concentration of the low loading sample to reach 0.1%. The time tends to drag for the higher loading sample. This could be attributed to the larger surface area of the high loading sorbent.

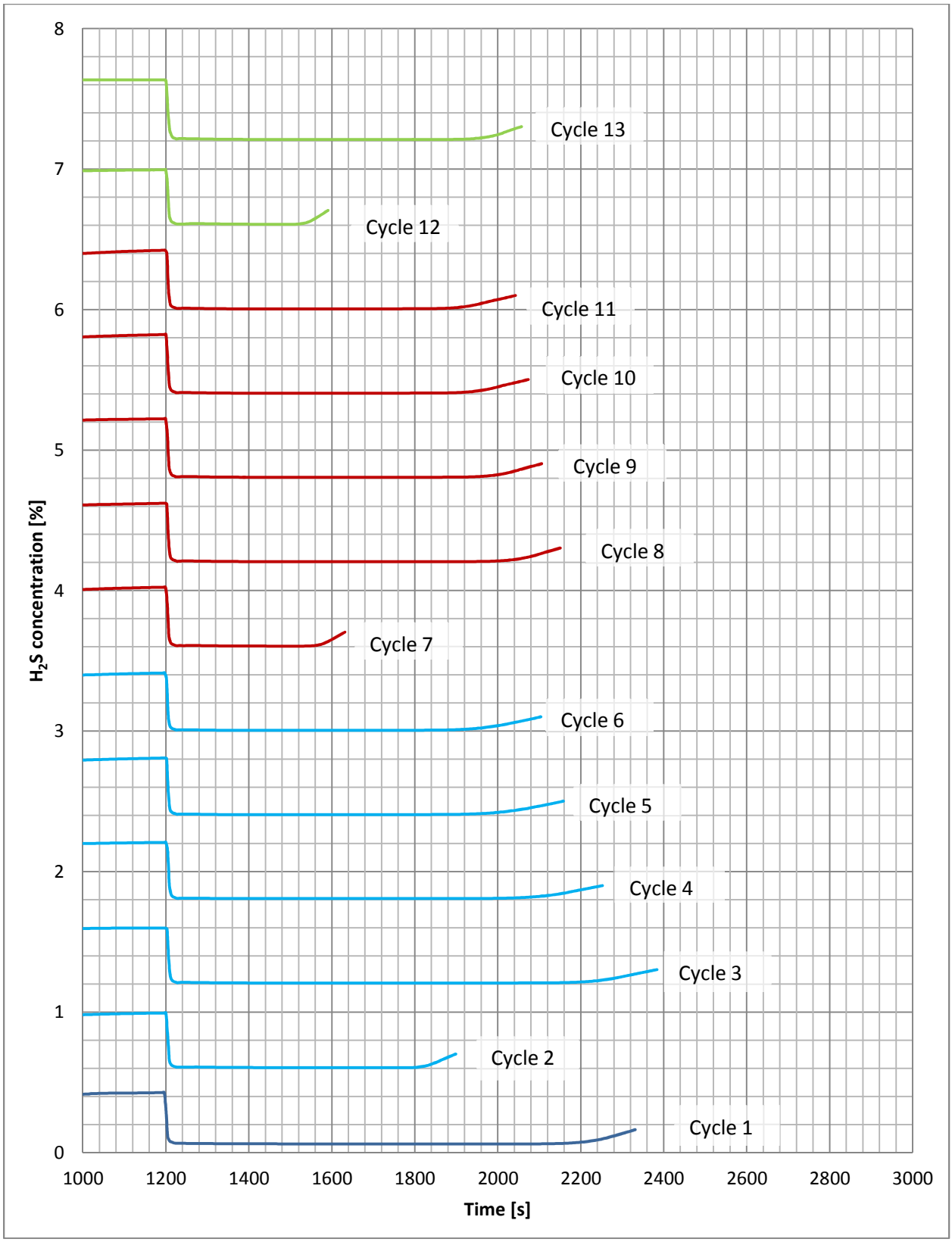


Figure 4-13 $H_2S$ sorption breakthrough curve measurement on $Mn_2O_3/Al_2O_3$ (15wt% Mn) sorbent, Experiment 1
NB: Curves have been off-set along the x and y-axis for the sake of clarity and ease of comparison

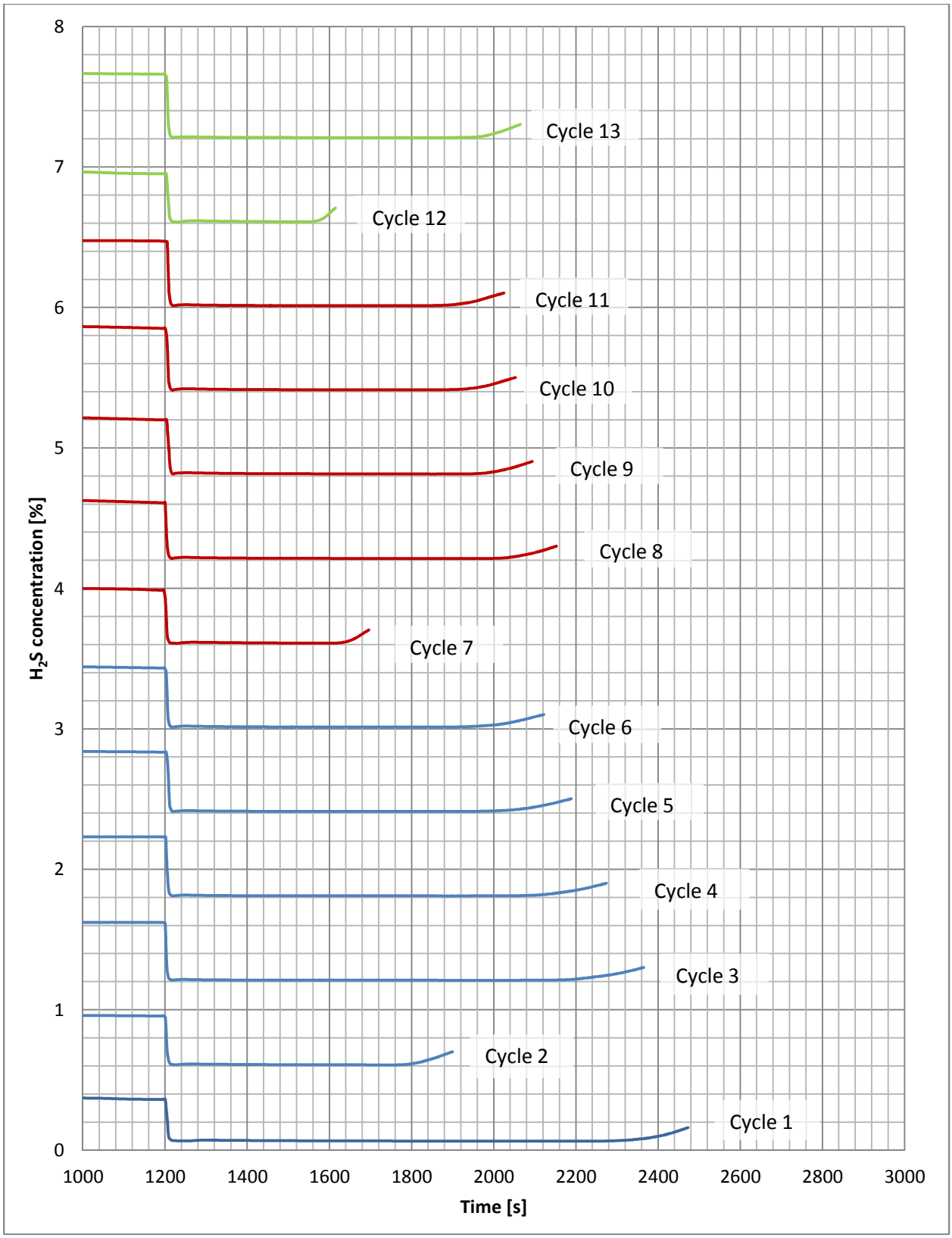


**Figure 4-14 $H_2S$ sorption breakthrough curve measurement on $Mn_2O_3/Al_2O_3$ (15wt% Mn) sorbent, Experiment 2**
**NB: Curves have been off-set along the x and y-axis for the sake of clarity and ease of comparison**

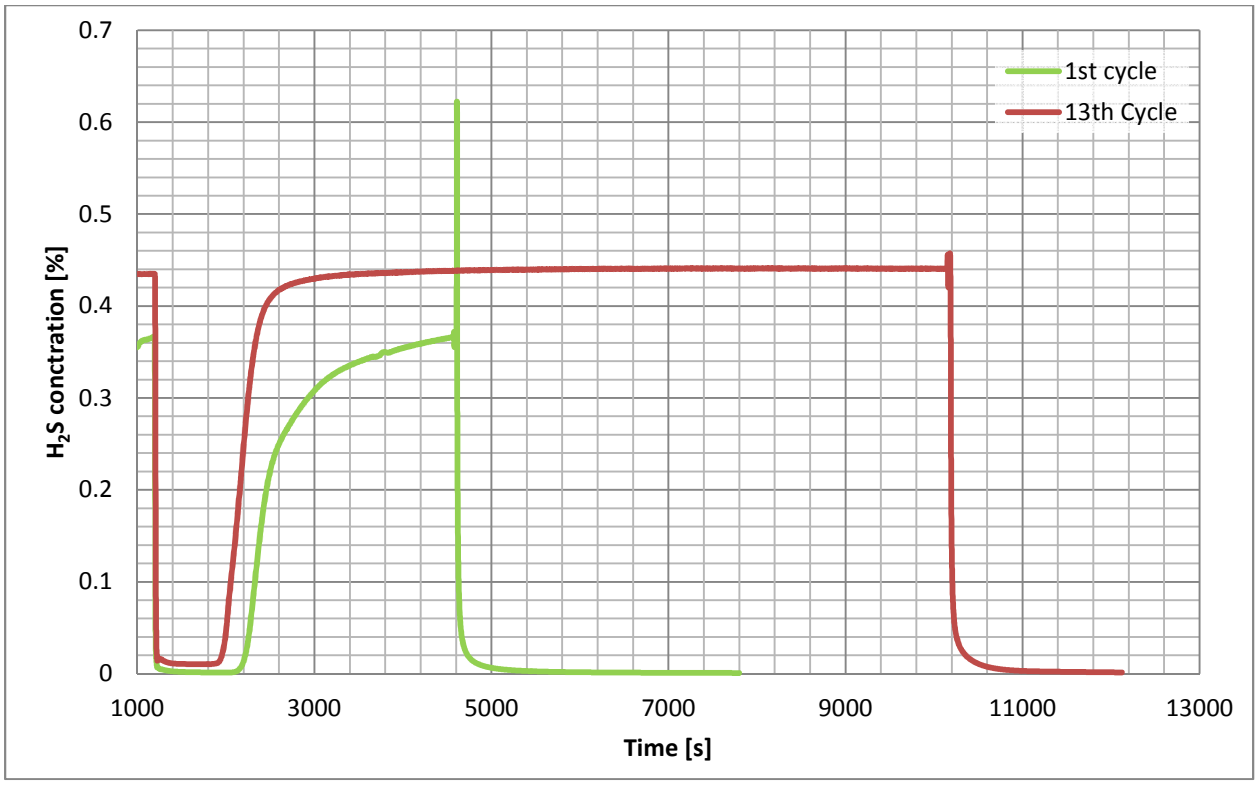


Figure 4-15 Comparison of 1st and 13th sorption breakthrough curves for $Mn_2O_3/Al_2O_3$ (15wt% Mn), Experiment 1
NB: Curves have been off-set along the x-axis for the sake of clarity and ease of comparison

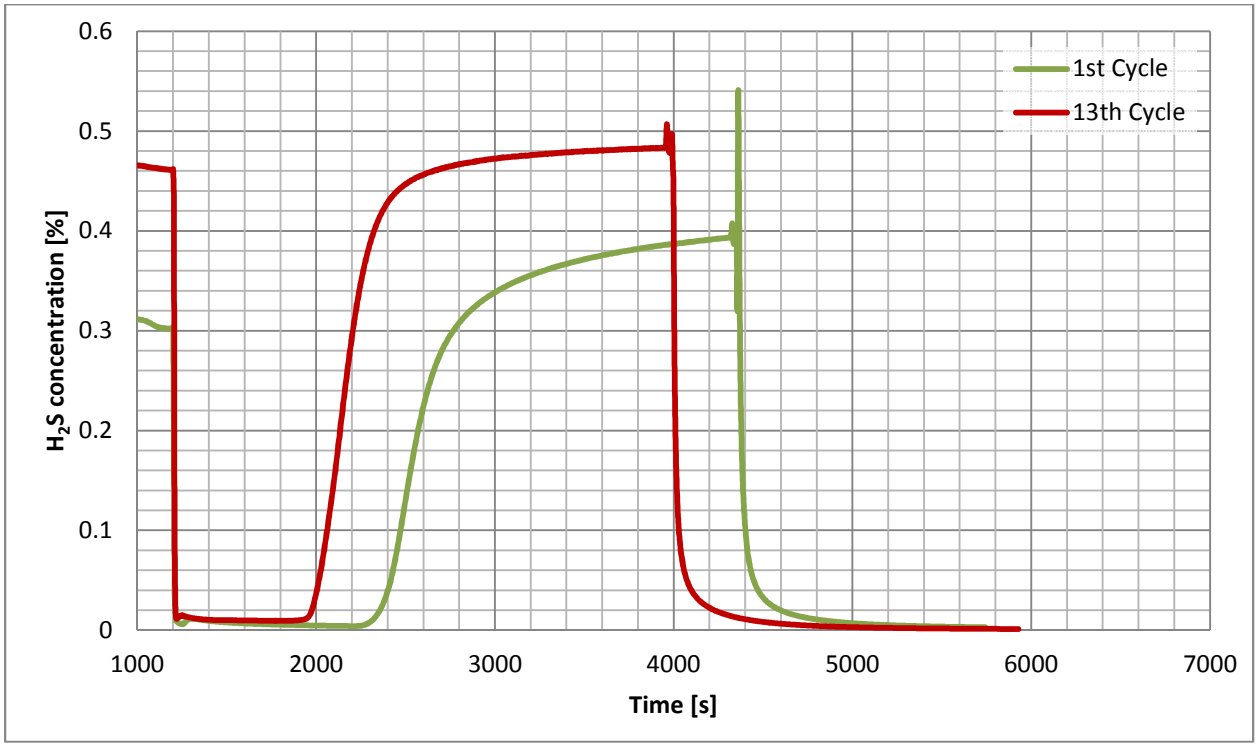


Figure 4-16 Comparison of 1st and 13th sorption breakthrough curves for $Mn_2O_3/Al_2O_3$ (15wt% Mn), Experiment 2
NB: Curves have been off-set along the x-axis for the sake of clarity and ease of comparison

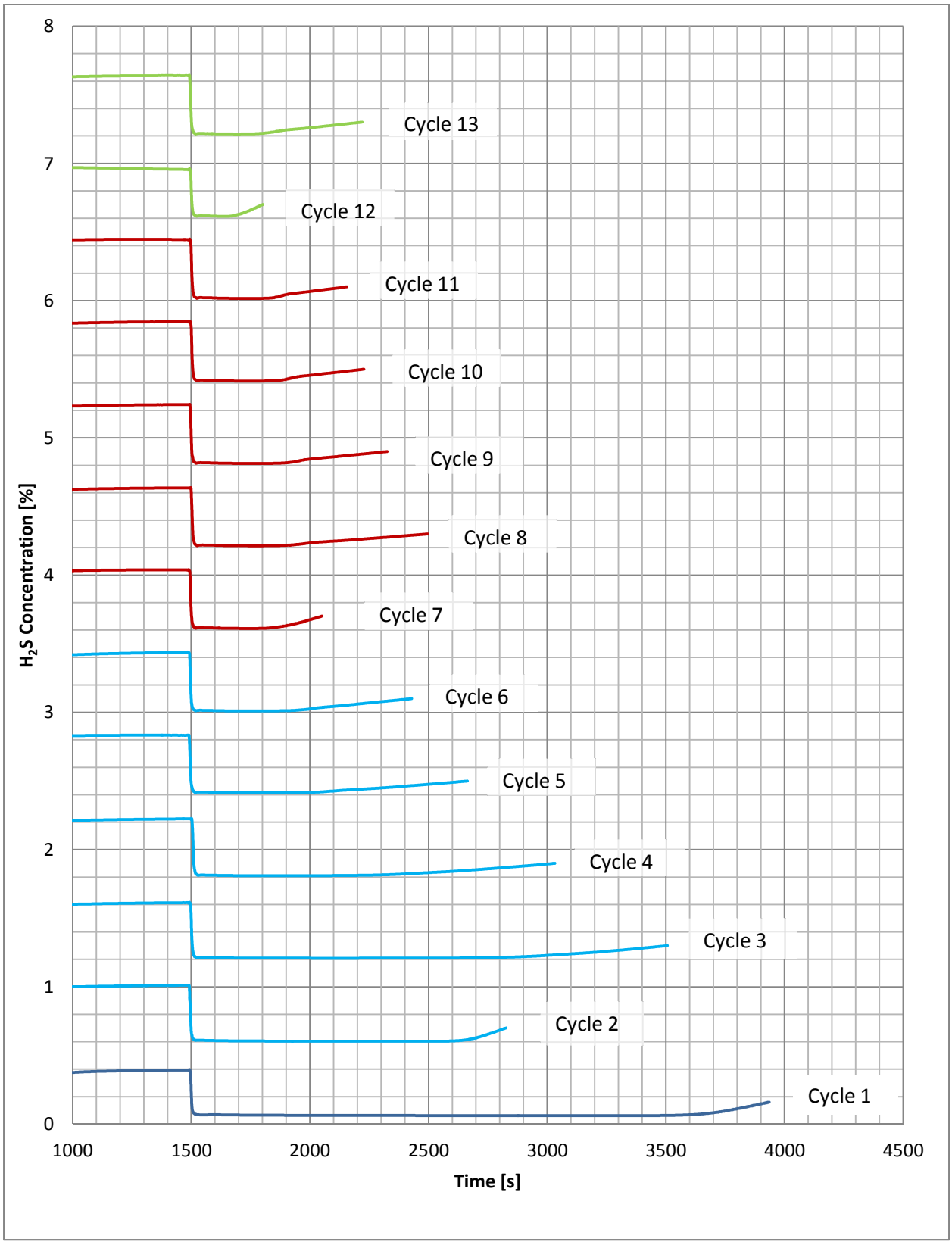


**Figure 4-17 $H_2S$ sorption breakthrough curve measurement on $Mn_2O_3/Al_2O_3$ (30wt% Mn) sorbent, Experiment 1**
**NB: Curves have been off-set along the x and y-axis for the sake of clarity and ease of comparison**

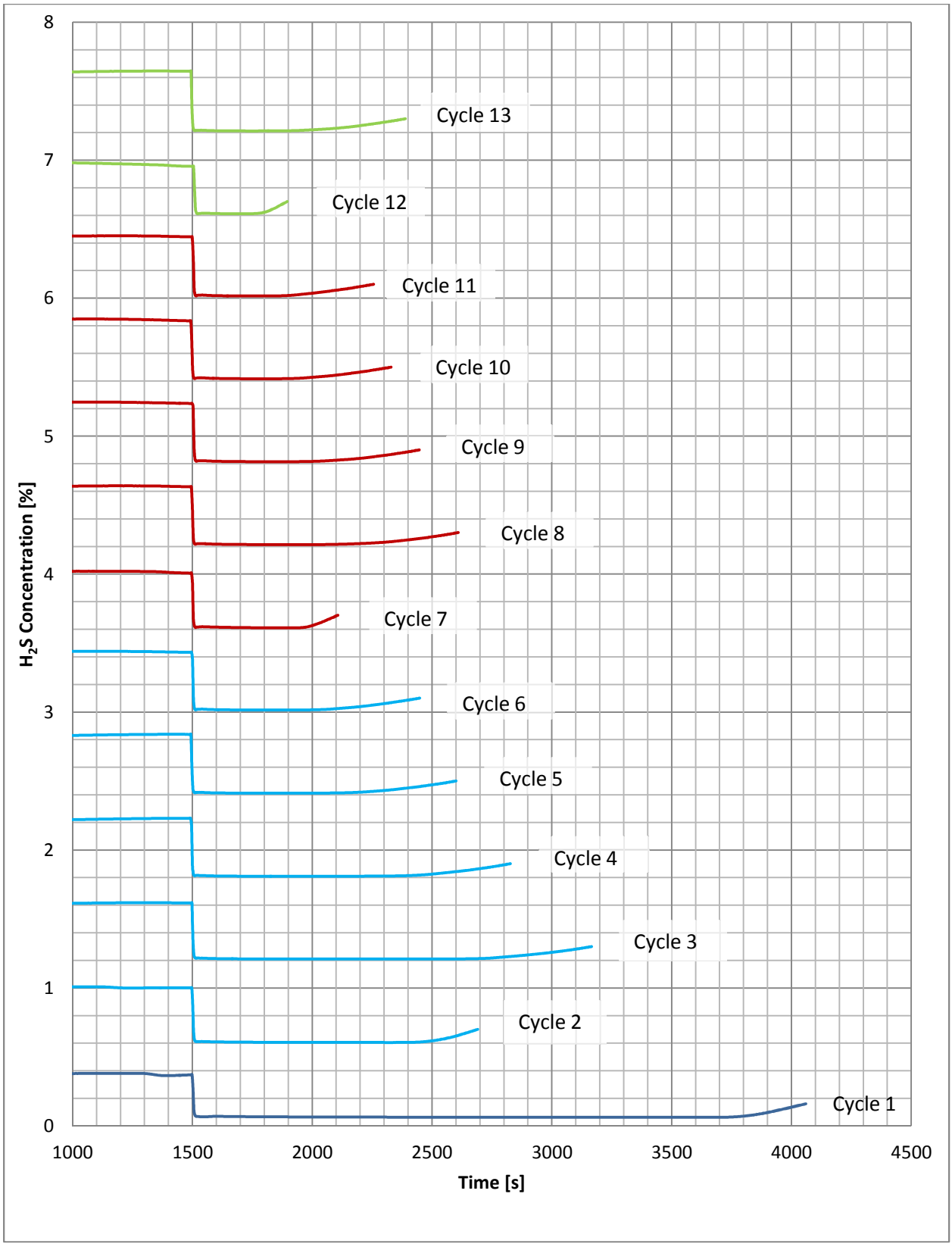


**Figure 4-18 $H_2S$ sorption breakthrough curve measurements on $Mn_2O_3/Al_2O_3$ (30wt% Mn) sorbent, Experiment 2**
**NB: Curves have been off-set along the x and y-axis for the sake of clarity and ease of comparison**

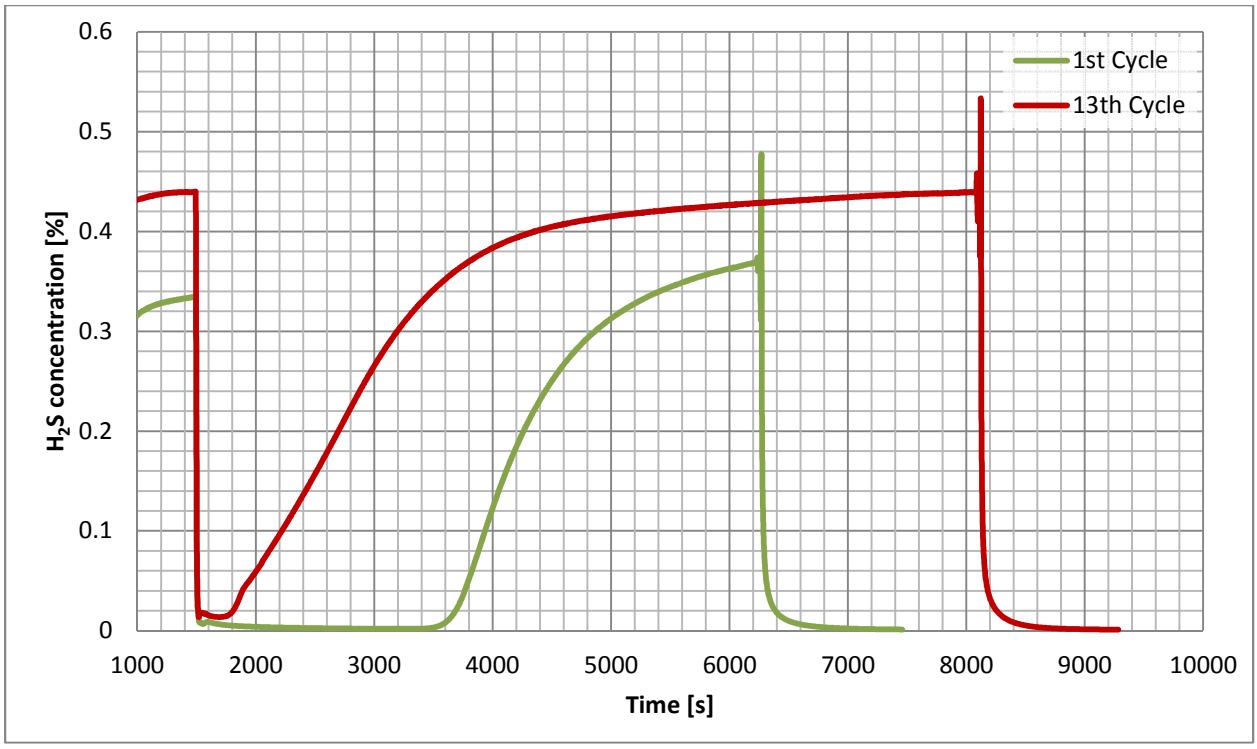


Figure 4-19 Comparison of 1st and 13th sorption breakthrough curves for $Mn_2O_3/Al_2O_3$ (30wt% Mn), Experiment 1
NB: Curves have been off-set along the x-axis for the sake of clarity and ease of comparison

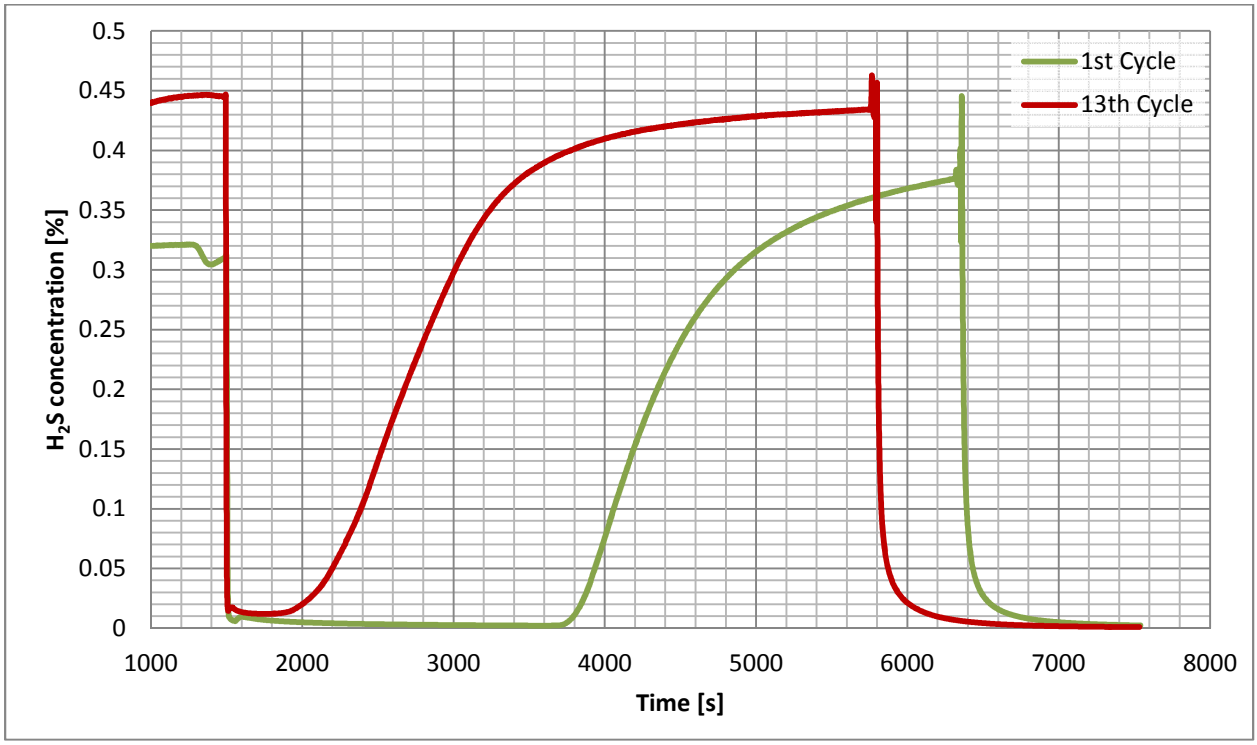


Figure 4-20 Comparison of 1st and 13th sorption breakthrough curves for $Mn_2O_3/Al_2O_3$ (30wt% Mn) Experiment 2
NB: Curves have been off-set along the x-axis for the sake of clarity and ease of comparison

Not much can be said about the regeneration reactions during the sorption studiesbecause they were not the main focus of this study however it can be noted that that the time it took to regenerate the sorbents is proportional to the time it took to measure the breakthrough curves.

A yellowish substance suspected to be sulfur because of the color, was also noticed to have settled on the inner wall of the reactor near the exit point (a cooler part of the reactor). Figure 4-21 shows a picture of the yellow substance taken after having completed one of the sorption study experiments. This was observed for all experiments including the result-reproducibility experiments.

Elemental sulfur is can be formed when $SO_2$ reacts with the sulfided metal sorbent based on the regeneration equation 2-8. It is possible that the $SO_2$ formed during regeneration with $O_2$ has enough contact time within the sorbent bed to react with the sulfided metal and form the elemental sulfur.

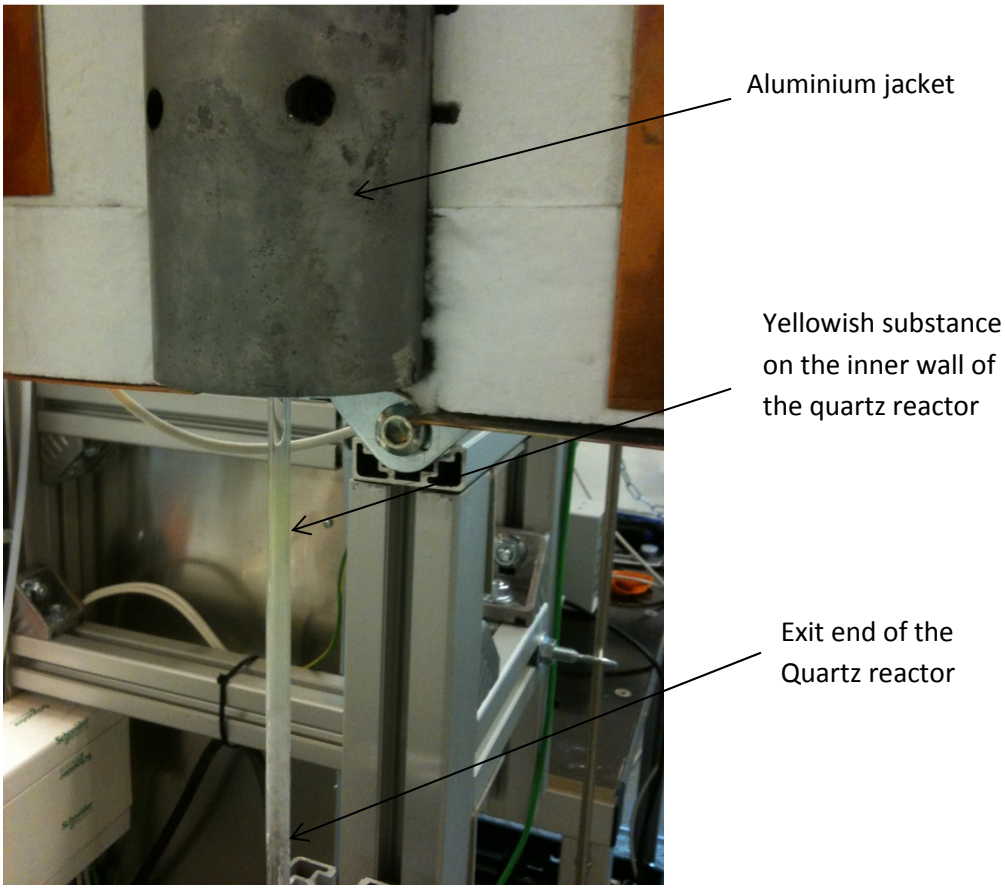


**Figure 4-21 Sulfur settled on the inner wall of the cooler part of the quartz reactor during subsequent sorption cycles**

#### 4.2.3.2 Sorption capacity

Figure 4-22 and Figure 4-23 show a clear picture that depicts reproducibility of results with the new laboratory set-p. The figures show the development of the sorbent sorption capacity as $gH_2S/gSorbent$ for $Mn_2O_3/Al_2O_3$ (15 wt%) and $Mn_2O_3/Al_2O_3$ (30wt%) respectively with the sorption capacities for experiment one and two superimposed on the same graph.

The calculations used to determine the sorption capacities are presented in Appendix O . The breakthrough point used for the calculations was 0.02% $H_2S$ concentration.

It can be said that the sorbent sorption capacities for experiment one and two are almost identical as expected and reproducibility of results is possible with the new laboratory set-up.

The sorbent capacities are being compared to the maximum expected sorption capacity. The red circles indicate the 'odd' breakthrough curve measurements which were obtained as the first cycle on a new day after leaving the sample overnight in a reducing gas mixture. If these are to be ignored, it can be said that both samples exhibit a substantial initial deactivation after the first sorption cycle and then starts to stabilize towards the last cycles. The deactivation degree is higher for the higher manganese loading sample.

It can be assumed, from studying the 15 and 30 wt% manganese oxide sorbents on alumina, that the stability of the alumina based sorbents is somehow linked to the manganese loading. A lower loading seems to be favoring sorption stability. The stability of the sorbent sorption capacity with respect to metal loading can be studied further to confirm this.

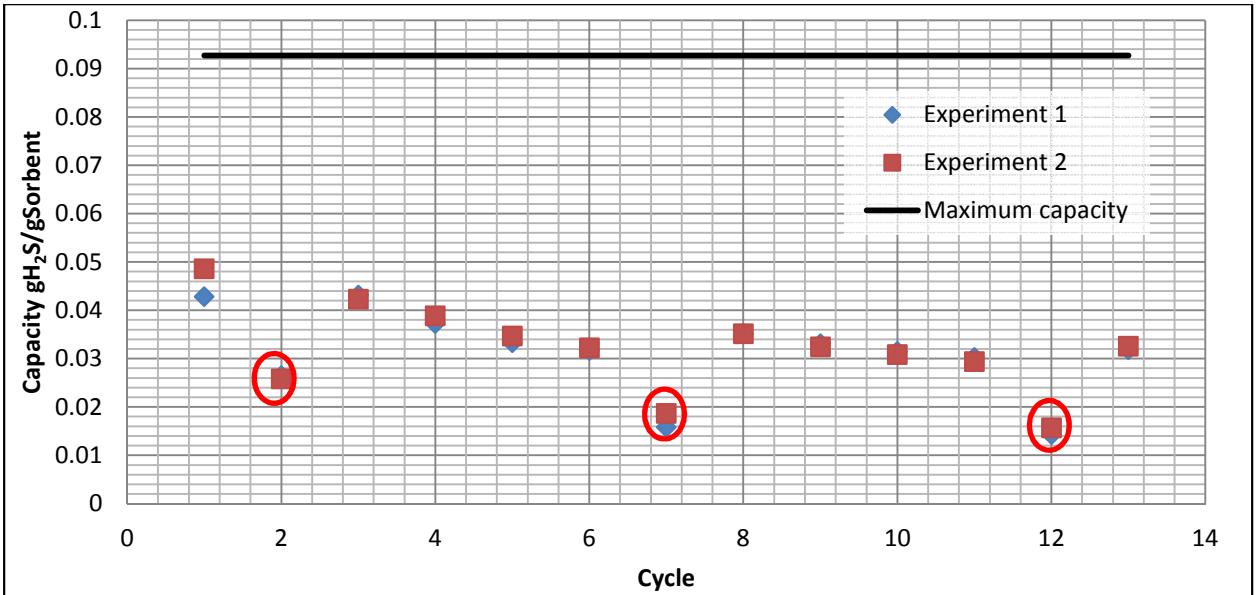


***Experiment 1: Sorbent 0.1209g, Sorption gas $N_2/H_2/H_2S(Ar)$ flow 10/20/20 ml/min, 0.4% $H_2S$ in feed***
***Regeneration gas $O_2/N_2$ flow 5/45 ml/min***
***Experiment 2: Sorbent 0.2417g, Sorption gas $N_2/H_2/H_2S(Ar)$ flow 20/40/40 ml/min, 0.4% $H_2S$ in feed***
***Regeneration gas $O_2/N_2$ flow 10/90 ml/min***

Figure 4-22 Sorption capacity development for $Mn_xO_y/Al_2O_3$_15wt% Mn sorbent with subsequent sulfidation and regeneration cycles for experiment 1 and 2

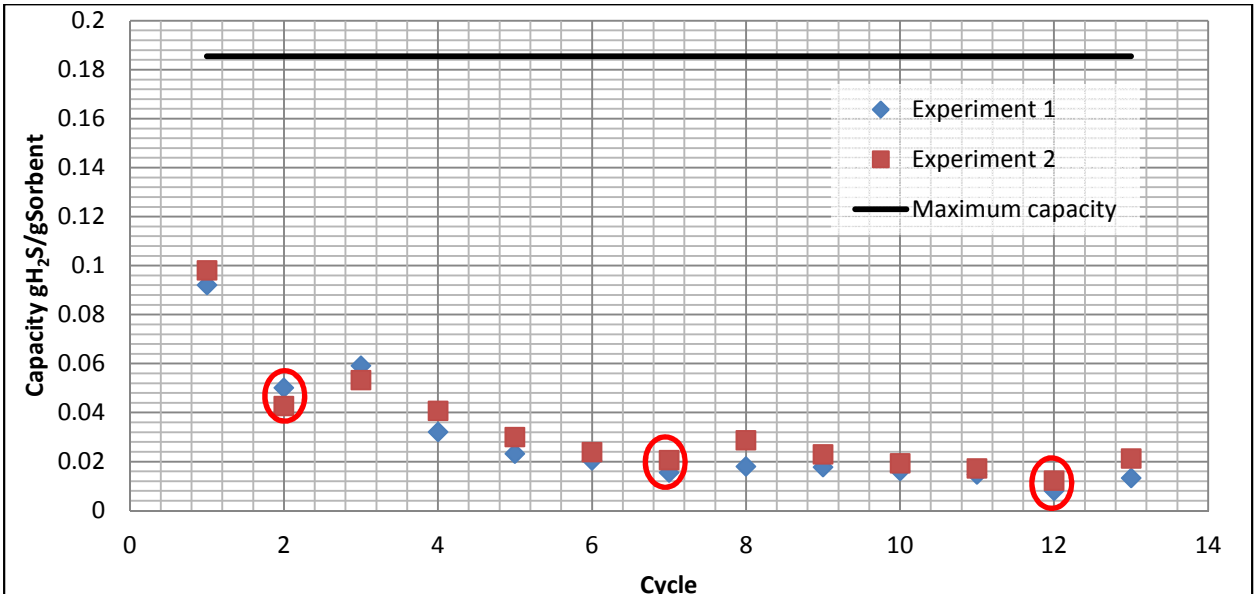


***Experiment 1: Sorbent 0.1208g, Sorption gas $N_2/H_2/H_2S(Ar)$ flow 10/20/20 ml/min, 0.4% $H_2S$ in feed***
***Regeneration gas $O_2/N_2$ flow 5/45 ml/min***
***Experiment 2: Sorbent 0.2422g, Sorption gas $N_2/H_2/H_2S(Ar)$ flow 20/40/40 ml/min, 0.4% $H_2S$ in feed***
***Regeneration gas $O_2/N_2$ flow 10/90 ml/min***

Figure 4-23 Sorption capacity development for $Mn_xO_y/Al_2O_3$_30wt% Mn sorbent with subsequent sulfidation and regeneration cycles for experiment 1 and 2

# Chapter 5 Conclusion

It is possible to reproduce sorption measurement results by using the new laboratory set-up, however it would be recommended to stabilize the sorption measurements obtained by the mass spectrometer.

The initial sorption capacity of the alumina based sorbents is proportionally dependent on the manganese loading and the opposite seems to be case in terms of sorption stability after repeated sorption cycles.

Activities of the new developed $H_2S$ adsorbent materials cannot be mentioned at this point without the investigative sorption studies. However it can be insinuated that among the 15 wt% manganese loading sorbent, the $Mn_2O_3/CeO_2$ could be expected to have the highest sorption capacity based on the amount of $H_2$ consumed during TPR experiment.

# References


1. Williams, A., et al., *Pollutants from the combustion of solid biomass fuels.* Progress in Energy and Combustion Science, 2012. **38**(2): p. 113-137.
2. Hoeven, M.V.d., *CO2 Emissions from Fuel Combustion Highlights*. 2013, International Energy Agency: Paris. p. 9.
3. Omer, A.M., *Energy, environment and sustainable development.* Renewable and Sustainable Energy Reviews, 2008. **12**(9): p. 2265-2300.
4. Grigg, J., *The health effects of fossil fuel derived particles.* Archives of Disease in Childhood, 2002. **86**(2): p. 79-83.
5. Hoeven, M.V.d., *World Energy Outlook 2012*. 2012, International Energy Agency: Paris.
6. Omer, A.M., *Green energies and the environment.* Renewable and Sustainable Energy Reviews, 2008. **12**(7): p. 1789-1821.
7. Meng, X., *Biomass gasification: the understanding of sulfur, tar, and char reduction in fluidized bed gasifiers*, in *Process and Energy*. 2012, Delft Unversity of Technology: Delft. p. 271.
8. Huber, G.W., S. Iborra, and A. Corma, *Synthesis of Transportation Fuels from Biomass: Chemistry, Catalysts, and Engineering.* Chemical Reviews, 2006. **106**(9): p. 4044-4098.
9. Serrano-Ruiz, J.C. and J.A. Dumesic, *Catalytic routes for the conversion of biomass into liquid hydrocarbon transportation fuels.* Energy & Environmental Science, 2011. **4**(1): p. 83-99.
10. O'Sullivan, A., *Cellulose: the structure slowly unravels.* Cellulose, 1997. **4**(3): p. 173-207.
11. Pandey, K.K., *A study of chemical structure of soft and hardwood and wood polymers by FTIR spectroscopy.* Journal of Applied Polymer Science, 1999. **71**(12): p. 1969-1975.
12. Strehler, A., *Technologies of wood combustion.* Ecological Engineering, 2000. **16, Supplement 1**(0): p. 25-40.
13. Woolcock, P.J. and R.C. Brown, *A review of cleaning technologies for biomass-derived syngas.* Biomass and Bioenergy, 2013. **52**(0): p. 54-84.
14. Kumar, A., D. Jones, and M. Hanna, *Thermochemical Biomass Gasification: A Review of the Current Status of the Technology.* Energies, 2009. **2**(3): p. 556-581.
15. Turn, S.Q., et al., *The fate of inorganic constituents of biomass in fluidized bed gasification.* Fuel, 1998. **77**(3): p. 135-146.
16. Moulijn, J.A., M. Makkee, and A.V. Diepen, *Chemical process technology*. 2001, West sussex: John Wiley & Soons Ltd.
17. Mondal, P., G.S. Dang, and M.O. Garg, *Syngas production through gasification and cleanup for downstream applications — Recent developments.* Fuel Processing Technology, 2011. **92**(8): p. 1395-1410.
18. Torres, W., S.S. Pansare, and J.G. Goodwin, *Hot Gas Removal of Tars, Ammonia, and Hydrogen Sulfide from Biomass Gasification Gas.* Catalysis Reviews, 2007. **49**(4): p. 407-456.
19. Meng, X., et al., *In bed and downstream hot gas desulphurization during solid fuel gasification: A review.* Fuel Processing Technology, 2010. **91**(8): p. 964-981.
20. Jazbec, M., K. Sendt, and B.S. Haynes, *Kinetic and thermodynamic analysis of the fate of sulphur compounds in gasification products.* Fuel, 2004. **83**(16): p. 2133-2138.
21. Cheah, S., D.L. Carpenter, and K.A. Magrini-Bair, *Review of Mid- to High-Temperature Sulfur Sorbents for Desulfurization of Biomass- and Coal-derived Syngas.* Energy & Fuels, 2009. **23**(11): p. 5291-5307.
22. Bakker, W.J.W., F. Kapteijn, and J.A. Moulijn, *A high capacity manganese-based sorbent for regenerative high temperature desulfurization with direct sulfur production: Conceptual process application to coal gas cleaning.* Chemical Engineering Journal, 2003. **96**(1–3): p. 223-235.

23. Fenouil, L.A. and S. Lynn, *Study of Calcium-Based Sorbents for High-Temperature H2S Removal. 2. Kinetics of H2S Sorption by Calcined Limestone.* Industrial & Engineering Chemistry Research, 1995. **34**(7): p. 2334-2342.
24. Westmoreland, P.R. and D.P. Harrison, *Evaluation of candidate solids for high-temperature desulfurization of low-Btu gases.* Environmental Science & Technology, 1976. **10**(7): p. 659-661.
25. Focht, G.D., P.V. Ranade, and D.P. Harrison, *High-temperature desulfurization using zinc ferrite: Reduction and sulfidation kinetics.* Chemical Engineering Science, 1988. **43**(11): p. 3005-3013.
26. Lew, S., A.F. Sarofim, and M. Flytzani-Stephanopoulos, *The reduction of zinc titanate and zinc oxide solids.* Chemical Engineering Science, 1992. **47**(6): p. 1421-1431.
27. Kyotani, T., et al., *Removal of H2S from hot gas in the presence of Cu-containing sorbents.* Fuel, 1989. **68**(1): p. 74-79.
28. Li, Z. and M. Flytzani-Stephanopoulos, *Cu−Cr−O and Cu−Ce−O Regenerable Oxide Sorbents for Hot Gas Desulfurization.* Industrial & Engineering Chemistry Research, 1997. **36**(1): p. 187-196.
29. Leith, I.R. and M.G. Howden, *Temperature-programmed reduction of mixed iron—manganese oxide catalysts in hydrogen and carbon monoxide.* Applied Catalysis, 1988. **37**(0): p. 75-92.
30. Ben-Slimane, R. and M.T. Hepworth, *Desulfurization of Hot Coal-Derived Fuel Gases with Manganese-Based Regenerable Sorbents. 3. Fixed-Bed Testing.* Energy & Fuels, 1995. **9**(2): p. 372-378.
31. Tamhankar, S.S., M. Hasatani, and C.Y. Wen, *Kinetic studies on the reactions involved in the hot gas desulfurization using a regenerable iron oxide sorbent—I: Reduction and sulfidation of iron oxide.* Chemical Engineering Science, 1981. **36**(7): p. 1181-1191.
32. Stobbe, E.R., B.A. de Boer, and J.W. Geus, *The reduction and oxidation behaviour of manganese oxides.* Catalysis Today, 1999. **47**(1–4): p. 161-167.
33. Wakker, J.P., A.W. Gerritsen, and J.A. Moulijn, *High temperature hydrogen sulfide and carbonyl sulfide removal with manganese oxide (MnO) and iron oxide (FeO) on .gamma.-alumina acceptors.* Industrial & Engineering Chemistry Research, 1993. **32**(1): p. 139-149.
34. Bakker, W.J.W., et al., *Hot Gas Cleaning, Sulfiding Mechanisms in Absorption of H2S by Solids*, in *Desulfurization of Hot Coal Gas*, A. Atimtay and D. Harrison, Editors. 1998, Springer Berlin Heidelberg. p. 159-178.
35. Chorkendorff, I. and J.W. Niemantsverdriet, *Concepts of Modern Catalysis and Kinetics*. 2nd ed. 2007, Weinheim: Wiley-VCH.
36. Tanabe, K., *Surface and catalytic properties of ZrO2.* Materials Chemistry and Physics, 1985. **13**(3–4): p. 347-364.
37. Mercera, P.D.L., et al., *Zirconia as a support for catalysts: Evolution of the texture and structure on calcination in air.* Applied Catalysis, 1990. **57**(1): p. 127-148.
38. Low, J., *Earth Sciences in the 21st Century : Rutile : Properties, Synthesis and Applications*. 2012, Hauppauge, NY, USA: Nova Science Publishers, Inc.
39. Case, G.D., *Chemistry of Hot Gas Cleanup in Coal Gasification and Combustion*. 1978: NTIS.
40. Haber, J., *Manual on catalyst characterization (Recommendations 1991)*, in *Pure and Applied Chemistry*. 1991. p. 1227.
41. Sing, K.S.W., *Adsorption methods for the characterization of porous materials.* Advances in Colloid and Interface Science, 1998. **76–77**(0): p. 3-11.
42. Brunauer, S., P.H. Emmett, and E. Teller, *Adsorption of Gases in Multimolecular Layers.* Journal of the American Chemical Society, 1938. **60**(2): p. 309-319.
43. Sing, K., *The use of nitrogen adsorption for the characterisation of porous materials.* Colloids and Surfaces A: Physicochemical and Engineering Aspects, 2001. **187–188**(0): p. 3-9.
44. Miura, H., et al., *An Inspection of the Purity of Helium Used as the Carrier Gas in Pulse-adsorption Experiments.* Bulletin of the Chemical Society of Japan, 1985. **58**(3): p. 1043-1044.

45. Dąbrowski, A., *Applications in Industry*. 1998: Elsevier Science.
46. Kugai, J., et al., *Effect of CeO2 support properties on structure of Pt–Cu nanoparticles synthesized by electron beam irradiation method for preferential CO oxidation.* Chemical Engineering Journal, 2013. **223**(0): p. 347-355.
47. Kugai, J., et al., *Effects of nanocrystalline CeO2 supports on the properties and performance of Ni–Rh bimetallic catalyst for oxidative steam reforming of ethanol.* Journal of Catalysis, 2006. **238**(2): p. 430-440.
48. Storsæter, S., et al., *Study of the effect of water on Fischer–Tropsch synthesis over supported cobalt catalysts.* Journal of Catalysis, 2005. **231**(2): p. 405-419.
49. Chytil, S., et al., *Preparation and Characterization of MnxOy-Al2O3 Sorbents for H2S Removal from Biomass Gasification Gas.* Energy Procedia, 2012. **26**(0): p. 98-106.
50. Ettireddy, P.R., et al., *Surface characterization studies of TiO2 supported manganese oxide catalysts for low temperature SCR of NO with NH3.* Applied Catalysis B: Environmental, 2007. **76**(1–2): p. 123-134.
51. Liang, B., et al., *Effect of manganese content on the properties of high temperature regenerative H{sub 2}S acceptor.* Journal Name: Fuel; Journal Volume: 78; Journal Issue: 3; Other Information: PBD: Feb 1999, 1999: p. pp. 319-325.
52. Kapteijn, F., et al., *Alumina-Supported Manganese Oxide Catalysts: I. Characterization: Effect of Precursor and Loading.* Journal of Catalysis, 1994. **150**(1): p. 94-104.
53. Thirupathi, B. and P.G. Smirniotis, *Nickel-doped Mn/TiO2 as an efficient catalyst for the low-temperature SCR of NO with NH3: Catalytic evaluation and characterizations.* Journal of Catalysis, 2012. **288**(0): p. 74-83.
54. Luo, M.-F., X.-M. Zheng, and Y.-J. Zhong, *CO oxidation activity and TPR characterization of CeO2-supported manganese oxide catalysts.* Indian Journal of Chemistry, 1999. **38**(7): p. 703-707.
55. Kobayashi, M. and M. Flytzani-Stephanopoulos, *Reduction and Sulfidation Kinetics of Cerium Oxide and Cu-Modified Cerium Oxide.* Industrial & Engineering Chemistry Research, 2002. **41**(13): p. 3115-3123.

# *Appendix A Sorbent preparation calculations*

**Basic information:**

Molecular weight of Mn = 55g/mol

Molecular weight of $Mn(NO_3)_2.4H_2O$ = 251g/mol

**Basis: 1g of total sorbent (manganese loading + support);**

Calculating the amount of Manganese nitrate tetra hydrate salt ($Mn(NO_3)_2.4H_2O$) needed to get 15 wt % Mn loading on sorbent:

Mass of manganese needed = $\frac{15}{100}\ x\ 1$

= 0.15 g A- 1

Mass of manganese nitrate tetrahydrate precursor, $Mn(NO_3)_2.4H_2O$ needed = $\frac{251}{55}\ x0.15$

= 0.6845g A- 2

Mass of support needed = 1 – 0.15

= 0.85 g A- 3

Table A- 1 shows results obtained from calculating pore volume; hence amount of water needed to dissolve the manganese salt precursor per gram of support.

**Table A- 1 Results obtained from calculating pore volume for the various support materials**

| Support material | Mass (g) | Water volume (ml) | Pore volume ($ml/g_{support}$) | Average pore volume ($ml/g_{support}$) |
|---|---|---|---|---|
| ɣ-$Al_2O_3$ | 0.5209 | 0.3593 | 0.6898 | 0.70 |
| | 0.7006 | 0.4949 | 0.7064 | |
| $CeO_2$ | 0.6433 | 0.3665 | 0.5697 | 0.59 |
| | 0.5648 | 0.3430 | 0.6073 | |
| TiO2 | 0.8172 | 0.4125 | 0.5048 | 0.48 |
| | 1.6783 | 0.7516 | 0.4478 | |
| $ZrO_2$ | 0.4373 | 0.2260 | 0.5168 | 0.50 |
| | 0.8800 | 0.4264 | 0.4845 | |

Since the precursor has 4 moles of water, subtracting the amount of water in the salt from the volume of water is done to obtain the corrected volume for dissolving the manganese salt precursor.

**Calculating for volume of water in precursor:**

Mass of water in 1 mole (251g) of manganese salt precursor = 4 x $M_{H2O}$

$$= 4 \times 18$$

$$= 72g \quad \text{A- 4}$$

Mass of water in the amount of precursor needed for 1 gram of total sorbent (or 0.85g of support)

$$= \frac{72}{251}\ x\ 0.6845$$

$$= 0.1964g \quad \text{A- 5}$$

Therefore, volume of water in the salt = $\frac{\text{mass of water}}{\text{density water}}$

$$= \frac{0.1964}{1}$$

$$= 0.1964ml \quad \text{A- 6}$$

Table A- 2 shows the values for corrected volume of water required to dissolve manganese precursor per 1 gram total sorbent (or 0.85g support).

**Table A- 2 Corrected volume of water for 0.85g support**

| **Support material** | **Average pore volume ($ml/g_{support}$)** | ***Calculated volume ($ml/g_{total\ sorbent}$)** | ****corrected volume ($ml/g_{total\ sorbent}$)** |
|---|---|---|---|
| ϒ-$Al_2O_3$ | 0.70 | 0.59 | 0.40 |
| $CeO_2$ | 0.59 | 0.50 | 0.30 |
| TiO2 | 0.48 | 0.40 | 0.21 |
| $ZrO_2$ | 0.50 | 0.43 | 0.23 |

* calculated volume of water = Average pore volume x 0.85

** corrected volume = Calculated volume - 0.1964

# *Appendix B Procedure for leak test and pressure test*

## Leak test procedure

Close all outlets

Fill line with inert gas (i.e. N2) at moderate pressure (5-6 bars)

If all outlets are closed, the gas inlet flow should approach zero

Listen for any huge leaks (whistling sound?)

Check for small leaks with leak detection spray

Tighten nuts/joints where there are leakages

Pressurize and isolate equipment for some time (i.e. a few hours or leave it overnight). Check for any Pressure loss (Bar/h --> ml/min)

If everything seems ok, continue at a higher pressure and start over again.

If not ok, replace inert gas with H2 gas and use a CO detector to search for leaks

Ensure leak proof at operating conditions

Note:

Always leak test when the equipment has been modified (i.e. replaced parts, after reactor dismount/remount)

## Pressure test procedure

Ensure all equipment used is certified for the operating conditions

Pressure testing should be carried out at higher pressure than desired operating conditions, at room temperature and with inert gas BUT REMEMBER Pressure tolerations are affected by temperature!

Close all outlets

Fill line with inert gas up to desired pressure

Note:

Always pressure test when the equipment has been modified (i.e. replaced parts, after reactor dismount/remount)

# *Appendix C Procedure for sorption cycle measurement*

**Start-up**

1. Ensure the Mass Spectrometer is has been switched on at least a day before the experiment starts.
2. Switch on the heater of the Mass Spectrometer at least an hour before the experiment.
3. Load the reactor with the sample and fix the reactor to the apparatus. The reactor is to be enclosed within an aluminium jacket and insulated to minimize heat loss. (Note that melting point of aluminium is around $600^0$C. For temperatures close to and above $600^0$C, the aluminium jacket should not be used).
4. Ensure the thermocouple is placed inside the aluminium block to measure temperature.
5. Perform a $H_2$-leak test and ensure there is no gas leakage.
6. Switch the 3-way valve to the by-pass
7. Ensure all the required gases ($N_2$, $O_2$, $H_2S$ (Ar), $H_2$) are available. (for safety purposes, $H_2$ and $O_2$ gases should not be mixed in the lines)

**Pre-reduction:**

8. Switch the 3-way valve to the reactor and flow the pre-reduction gas mixture through the reactor.
9. Set the required temperature programme for the reactor using the Eurotherm temperature controller
10. Switch the 3-way valve to reactor and set the pre-reduction gas mixture flow over the sorbent.
11. After pre-reduction of the sorbent, flush the reactor with nitrogen.

**Sulfidation:**

12. Switch the 3-way valve from the reactor to the bypass.
13. Prepare sorption gas mixture and let the gas flow through the by-pass for the pre-set time (or until the mass spectrometer measurement is stable).
14. Switch the 3-way valve back to the reactor and monitor the $H_2S$ concentration measurement (the breakthrough curve).
15. When sorption measurement is complete, flush the reactor with Nitrogen and save the measured data.

**Regeneration:**

16. Switch the 3-way valve to the bypass and flush the line (to remove the sorption gas).
17. Prepare the regeneration gas and let it flow through the bypass line until the analog scan measurement is stable.
18. Switch 3-way valve to reactor and monitor regeneration of the sorbent using the scan analog signal.
19. When regeneration is complete, save the measured data and flush the reactor with nitrogen gas.
20. For a new sorption cycle, repeat steps from step 12. For shut down, continue to the next step.

**Shut down**

21. When measurement is done, switch off the Mass Spectrometer.
22. Close all gas valves on apparatus as well as the $H_2S$ gas cylinder.

| NTNU HSE/KS | Risk assessment | Prepared by: Milly K | Number | Date |
|---|---|---|---|---|
| | | HSE sectior | HMS04/2603E | 04.02.2011 |
| | | Approved by: The Rector | Page 1 out of 4 | Replaces 01.12.2006 |

**Unit:** SET UP 1.2 CHEMISTRY HALL D **Date:** 08/11/2013
**Line manager:** EDD BLEKKAN
**Participants in the risk assessment (including their function):** MILLY KURE, SVATOPLUK CHYTIL, EDD BLEKKAN, KARIN DRAGSTEN

| Activity from the identification process form | Potential undesirable incident/strain | Likelihood: | Consequence: | | | Risk value | Comments/status Suggested measures |
|---|---|---|---|---|---|---|---|
| | | Likelihood (1-5) | Human (A-E) | Environment (A-E) | Economy/ material (A-E) | | |
| Operation of lab set-up | Bursting of high pressure lines | 1 | C | C | C | 1C | To set a pressure test procedure and Pressure test up to slightly above the operating pressure |
| | Gas leaks from pipelines in the set-up | 1 | C | C | C | 1C | To set a leak test procedure |
| | H2 gas explosion | 2 | C | C | C | 2C | Need a portable H2 detector to detect leakages on pipeline |
| | H2S toxic gas leak | 2 | C | C | C | 2C | Need a portable H2S detector to check for small leakages on pipelines. |
| | H2S fire hazard | 2 | C | C | C | 2C | Have a H2S detector. This has already been placed at the floor level of the set-up. |
| | H2S leakage from cylinder | 2 | C | C | C | 2C | No H2S detector outside set-up. Cylinder has been placed inside the set-up. |
| | High temperatures in reactor | 5 | C | B | B | 5C | Monitor temperature and not open reactor until system has cooled down to room temperature. |
| | Accidental mixing of H2 and O2 to cause an explosion | 1 | C | C | C | 1C | Labelling of lines and valves and setting up a procedure for running the set-up |

| NTNU HSE/KS | Risk assessment | Prepared by Milly K. | Number | Date |
|---|---|---|---|---|
| | | HSE section | HMSRV2603E | 04.02.2011 |
| | | Approved by The Rector | Page 2 out of 4 | Replaces 01.12.2006 |

| | | | | | | | |
|---|---|---|---|---|---|---|---|
| Catalyst preparation | γ-Al2O3 skin irritant, eye irritant, respiratory tract irritant | 1 | C | C | B | 1C | Use of protective equipment |
| | γ-Al2O3 spills | 1 | C | C | B | 1C | Mix with sodium carbonate and sweep up. Not to be let in drains. |
| | Manganese (2) acetate tetrahydrate skin irritant, eye irritant, respiratory tract irritant | 1 | C | C | B | 1C | Use of protective equipment |
| | Manganese (2) acetate tetrahydrate spills | 1 | C | C | B | 1C | Sweep up without creating dust and put in cosed container for disposal. Not to be let in drains. |
| | Manganese (2) nitrate tetrahydrate skin irritant, eye irritant, respiratory tract irritant | 1 | C | C | B | 1C | Use protective equipment |
| | Manganese (2) nitrate tetrahydrate fire hazard (intensifies fire with combustible material) | 1 | C | C | B | 1C | Proper storage away from combustible materials |
| | Manganese (2) nitrate tetrahydrate spills | 1 | C | C | B | 1C | Sweep up and shovel. Clean place by wet-brushing and put in closed container for disposal |
| Product from High temperature furnace | Manganese oxides skin irritant, eye irritant, respiratory tract irritant | 1 | C | C | B | 1C | Use protective equipment |
| | Manganese oxides spills | 1 | C | C | B | 1C | Put spill in disposal container and clean contaminated surface by spreading water |

| | | | | | | | |
|---|---|---|---|---|---|---|---|
| | Flammable vapour from the acetate | 1 | C | C | B | 1C | Ensure proper ventilation |

***Likelihood, e.g.:***
1. *Minimal*
2. *Low*
3. *Medium*
4. *High*
5. *Very high*

***Consequence, e.g.:***
A. *Safe*
B. *Relatively safe*
C. *Dangerous*
D. *Critical*
E. *Very critical*

***Risk value (each one to be estimated separately):***
***Human = Likelihood x Human Consequence***
***Environmental = Likelihood x Environmental consequence***
***Financial/material = Likelihood x Consequence for Economy/materiel***

**Potential undesirable incident/strain**

Identify possible incidents and conditions that may lead to situations that pose a hazard to people, the environment and any materiel/equipment involved.

**Criteria for the assessment of likelihood and consequence in relation to fieldwork**

Each activity is assessed according to a worst-case scenario. Likelihood and consequence are to be assessed separately for each potential undesirable incident. Before starting on the quantification, the participants should agree what they understand by the assessment criteria:

**Likelihood**

| Minimal 1 | Low 2 | Medium 3 | High 4 | Very high 5 |
|---|---|---|---|---|
| Once every 50 years or less | Once every 10 years or less | Once a year or less | Once a month or less | Once a week |

**Consequence**

| Grading | Human | Environment | Financial/material |
|---|---|---|---|
| E Very critical | May produce fatality/ies | Very prolonged, non-reversible damage | Shutdown of work >1 year. |
| D Critical | Permanent injury, may produce serious serious health damage/sickness | Prolonged damage. Long recovery time. | Shutdown of work 0.5-1 year. |
| C Dangerous | Serious personal injury | Minor damage. Long recovery time | Shutdown of work < 1 month |
| B Relatively safe | Injury that requires medical treatment | Minor damage. Short recovery time | Shutdown of work < 1week |
| A Safe | Injury that requires first aid | Insignificant damage. Short recovery time | Shutdown of work < 1day |

The unit makes its own decision as to whether opting to fill in or not consequences for economy/materiel, for example if the unit is going to use particularly valuable equipment. It is up to the individual unit to choose the assessment criteria for this column.

**Risk = Likelihood x Consequence**
Please calculate the risk value for "Human", "Environment" and, if chosen, "Economy/materiel", separately.

**About the column "Comments/status, suggested preventative and corrective measures":**
Measures can impact on both likelihood and consequences. Prioritise measures that can prevent the incident from occurring; in other words, likelihood-reducing measures are to be prioritised above greater emergency preparedness, i.e. consequence-reducing measures.

# *Appendix E Mass flow controller calibration results*

Calibration data measured at 23$^0$C, 1atm

| | |
|---|---|
| **Gas** | **Oxygen** |
| **Channel** | 1 |
| **User tag** | O2 |
| **Serial Number** | SMN11211984D |

| Valve opening [%] | Volume [mL] | Time [s] | [mL/min] | (Corrected volume) | Corrected [mL/min] |
|---|---|---|---|---|---|
| 30 | 9 | 3.086 | 174.9838 | 8.247945725 | 160.3618741 |
| 25 | 9 | 3.644 | 148.1888 | 8.247945725 | 135.805912 |
| 20 | 9 | 4.588 | 117.6983 | 8.247945725 | 107.8632832 |
| 15 | 9 | 6.112 | 88.35079 | 8.247945725 | 80.96805358 |
| 10 | 9 | 9.124 | 59.18457 | 8.247945725 | 54.23901178 |
| 5 | 9 | 18.014 | 29.97668 | 8.247945725 | 27.47178547 |
| 2 | 9 | 42.542 | 12.69334 | 8.247945725 | 11.63266286 |

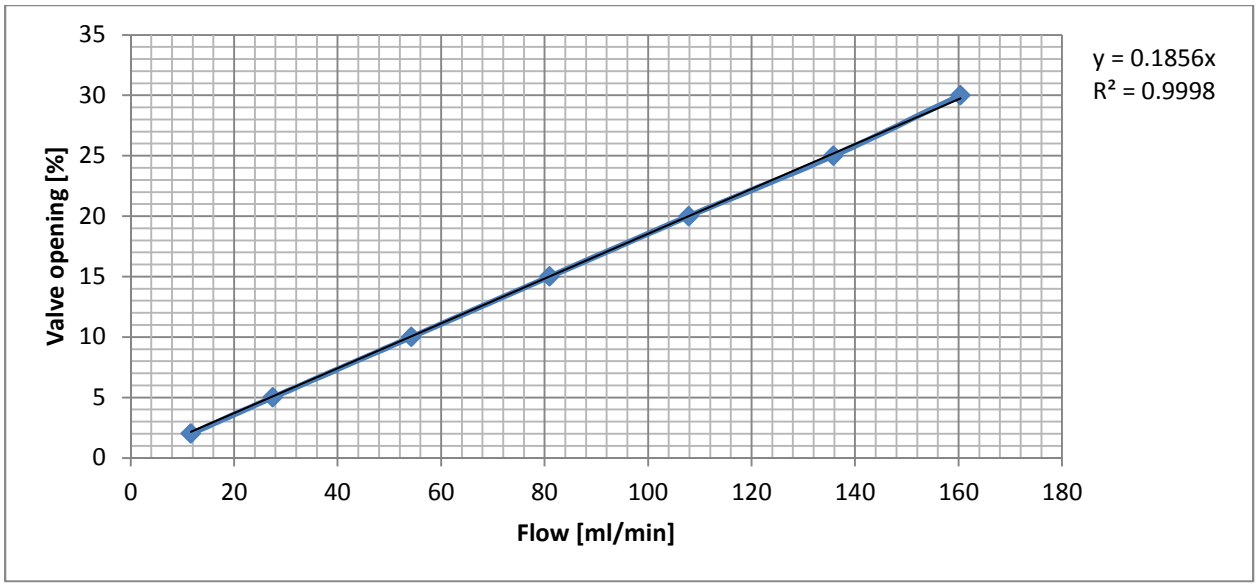

| | |
|---|---|
| **Gas** | **Hydrogen** |
| **Channel** | 2 |
| **User tag** | H2 |
| **Serial Number** | SMN11211984C |

| Valve opening [%] | Volume [mL] | Time [s] | [mL/min] | (Corrected volume) | Corrected [mL/min] |
|---|---|---|---|---|---|
| 30 | 9 | 3.028 | 178.335535 | 8.247945725 | 163.4335348 |
| 25 | 9 | 3.648 | 148.0263158 | 8.247945725 | 135.657002 |
| 20 | 9 | 4.61 | 117.1366594 | 8.247945725 | 107.3485344 |
| 15 | 9 | 6.176 | 87.43523316 | 8.247945725 | 80.12900639 |
| 10 | 9 | 9.116 | 59.23650724 | 8.247945725 | 54.28661074 |
| 5 | 9 | 17.916 | 30.1406564 | 8.247945725 | 27.62205534 |
| 2 | 9 | 42.432 | 12.72624434 | 8.247945725 | 11.66281918 |

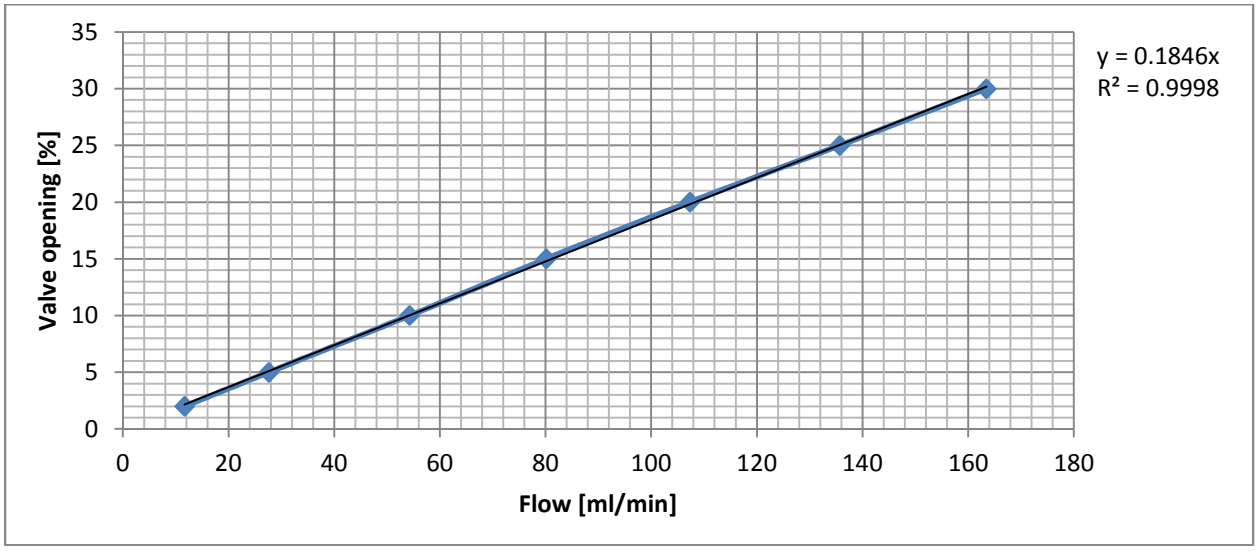

| | |
|---|---|
| **Gas** | **HYDROGEN SULPHIDE** |
| **Channel** | 3 |
| **User tag** | H2SMIX |
| **Serial Number** | SMN11211984H |

| Valve opening [%] | Volume [mL] | Time [s] | [mL/min] | (Corrected volume) | Corrected [mL/min] |
|---|---|---|---|---|---|
| 30 | 9 | 2.526 | 213.7767 | 8.247945725 | 195.9132001 |
| 25 | 9 | 3.018 | 178.9264 | 8.247945725 | 163.9750641 |
| 20 | 9 | 3.812 | 141.6579 | 8.247945725 | 129.8207617 |
| 15 | 9 | 4.984 | 108.3467 | 8.247945725 | 99.29308657 |
| 10 | 9 | 7.472 | 72.26981 | 8.247945725 | 66.23082755 |
| 5 | 9 | 14.864 | 36.32939 | 8.247945725 | 33.29364528 |
| 2 | 9 | 36.3 | 14.87603 | 8.247945725 | 13.63296814 |

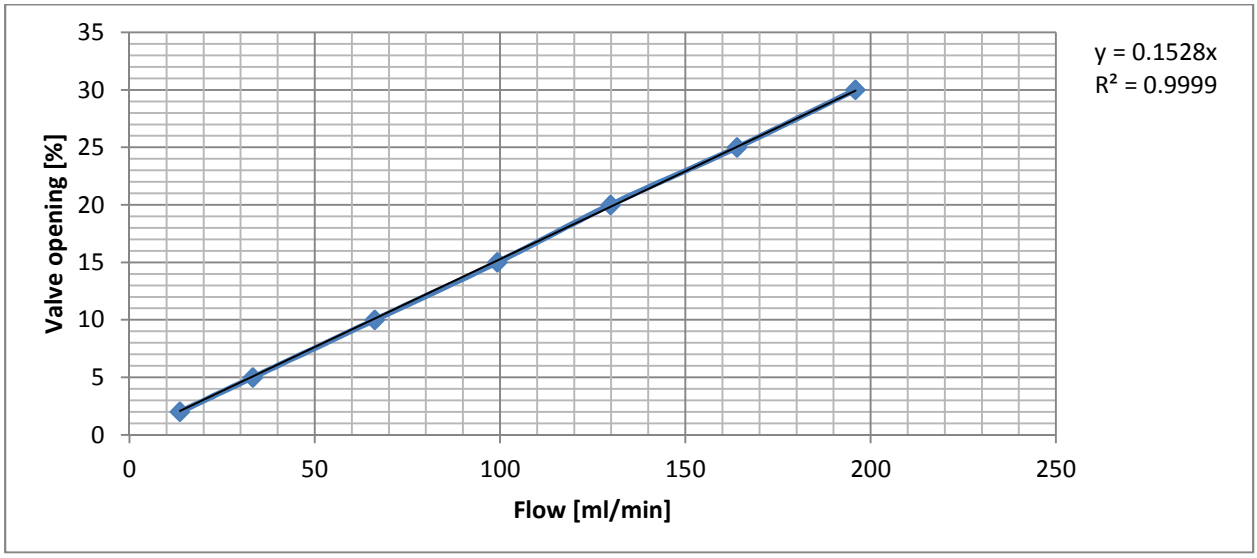

| | |
|---|---|
| **Gas** | **Nitrogen** |
| **Channel** | 4 |
| **User tag** | N2 |
| **Serial Number** | SMN11211984B |

| Valve opening [%] | Volume [mL] | Time [s] | [mL/min] | (Corrected volume) | Corrected [mL/min] |
|---|---|---|---|---|---|
| 30 | 9 | 3.162 | 170.7779886 | 8.247945725 | 156.507509 |
| 25 | 9 | 3.7 | 145.9459459 | 8.247945725 | 133.7504712 |
| 20 | 9 | 4.59 | 117.6470588 | 8.247945725 | 107.816284 |
| 15 | 9 | 6.224 | 86.76092545 | 8.247945725 | 79.5110449 |
| 10 | 9 | 9.31 | 58.00214823 | 8.247945725 | 53.15539672 |
| 5 | 9 | 18.768 | 28.77237852 | 8.247945725 | 26.36811293 |
| 2 | 9 | 47.814 | 11.29376333 | 8.247945725 | 10.35003856 |

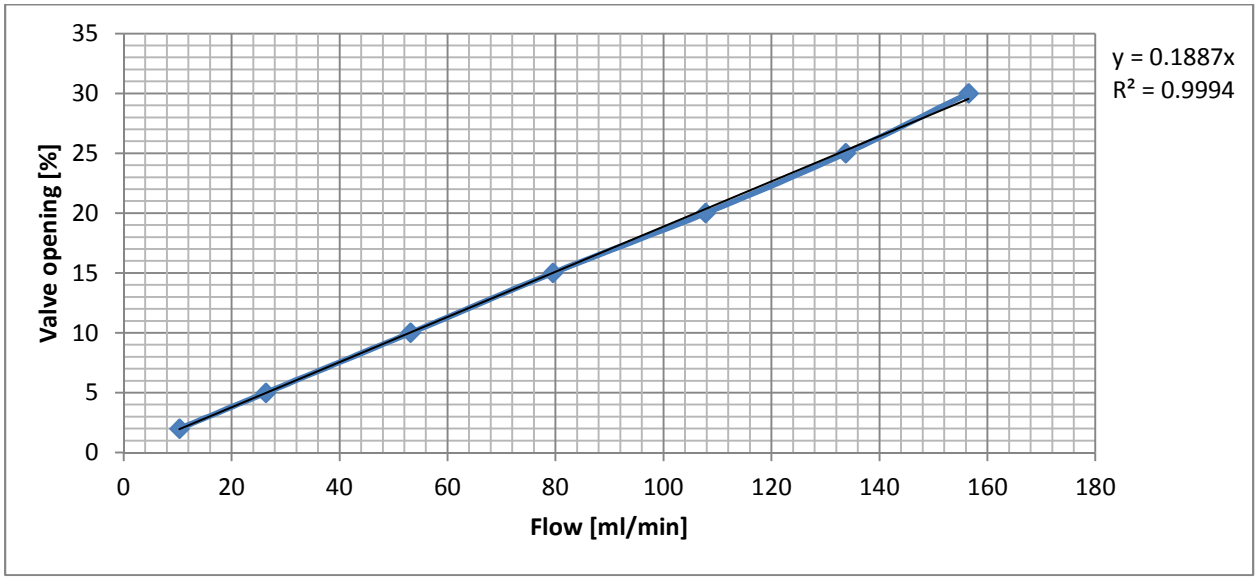

| | |
|---|---|
| **Gas** | **Nitrogen (Flush)** |
| **Channel** | 5 |
| **Usertag** | N2FLUSH |
| **Serial Number** | SMN11211984A |

| Valve opening [%] | Volume [mL] | Time [s] | [mL/min] | (Corrected volume) | Corrected [mL/min] |
|---|---|---|---|---|---|
| 30 | 9 | 2.992 | 180.4813 | 8.247945725 | 165.3999811 |
| 25 | 9 | 3.642 | 148.2702 | 8.247945725 | 135.8804897 |
| 20 | 9 | 4.486 | 120.3745 | 8.247945725 | 110.3158144 |
| 15 | 9 | 5.952 | 90.72581 | 8.247945725 | 83.14461416 |
| 10 | 9 | 8.904 | 60.6469 | 8.247945725 | 55.57914909 |
| 5 | 9 | 17.216 | 31.36617 | 8.247945725 | 28.745164 |
| 2 | 9 | 39.734 | 13.59038 | 8.247945725 | 12.45474263 |

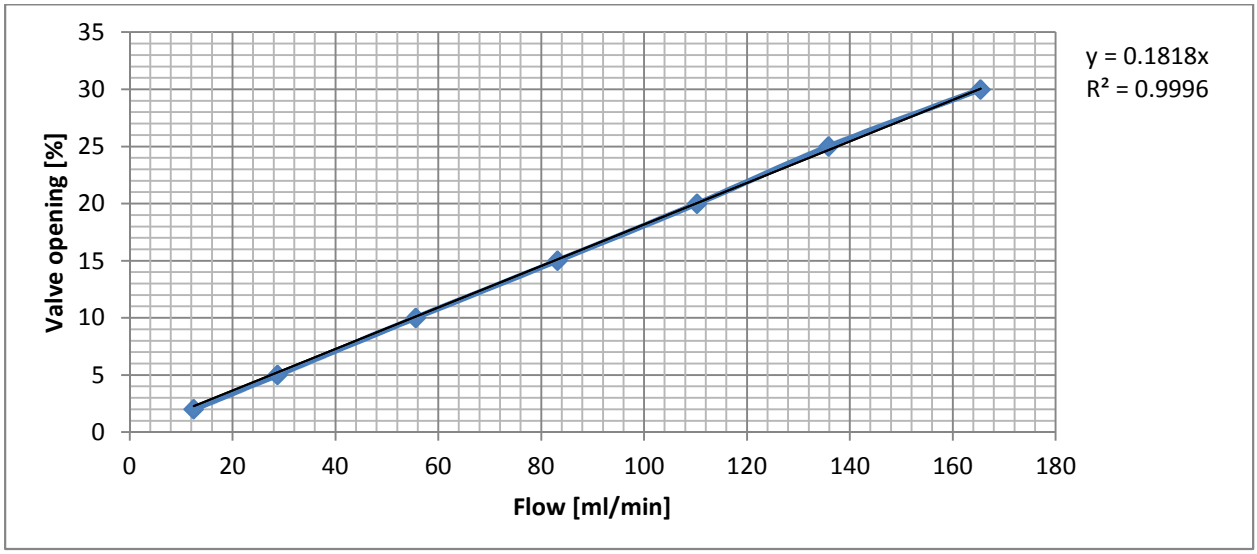

# *Appendix F Nitrogen adsorption summary reports*

## Gamma $Al_2O_3$ support

| | | | |
|---|---|---|---|
| Micromeritics Instrument Corporation | | | |
| TriStar II 3020 V1.03 (V1.03) | Unit 1 Port 2 | Serial #: 731 | Page 1 |

| | | | |
|---|---|---|---|
| Sample: | Gamma alumina support | | |
| Operator: | Milly | | |
| Submitter: | Milly | | |
| File: | C:\WIN3020\DATA\MILLY\000-022.SMP | | |
| Started: | 06.04.2014 11:08:20 | Analysis Adsorptive: | N2 |
| Completed: | 06.04.2014 14:35:30 | Analysis Bath Temp.: | -195.850 °C |
| Report Time: | 08.05.2014 15:58:37 | Sample Mass: | 0.0597 g |
| Warm Free Space: | 11.4306 cm³ Measured | Cold Free Space: | 32.9920 cm³ Measured |
| Equilibration Interval: | 5 s | Low Pressure Dose: | None |
| Sample Density: | 1.000 g/cm³ | Automatic Degas: | No |

**Summary Report**

**Surface Area**

| | |
|---|---|
| Single point surface area at P/Po = 0.299122380: | 149.2991 m²/g |
| BET Surface Area: | 153.8468 m²/g |
| Langmuir Surface Area: | 246.5905 m²/g |
| t-Plot External Surface Area: | 157.0880 m²/g |

| | |
|---|---|
| BJH Adsorption cumulative surface area of pores between 17.000 Å and 3000.000 Å diameter: | 177.116 $m^2/g$ |
| BJH Desorption cumulative surface area of pores between 17.000 Å and 3000.000 Å diameter: | 217.6133 $m^2/g$ |

**Pore Volume**

| | |
|---|---|
| Single point adsorption total pore volume of pores less than 694.181 Å diameter at P/Po = 0.971315305: | 0.227113 $cm^3/g$ |
| t-Plot micropore volume: | -0.003489 $cm^3/g$ |
| BJH Adsorption cumulative volume of pores between 17.000 Å and 3000.000 Å diameter: | 0.237222 $cm^3/g$ |
| BJH Desorption cumulative volume of pores between 17.000 Å and 3000.000 Å diameter: | 0.249843 $cm^3/g$ |

**Pore Size**

| | |
|---|---|
| Adsorption average pore width (4V/A by BET): | 59.0490 Å |
| BJH Adsorption average pore diameter (4V/A): | 53.574 Å |
| BJH Desorption average pore diameter (4V/A): | 45.924 Å |

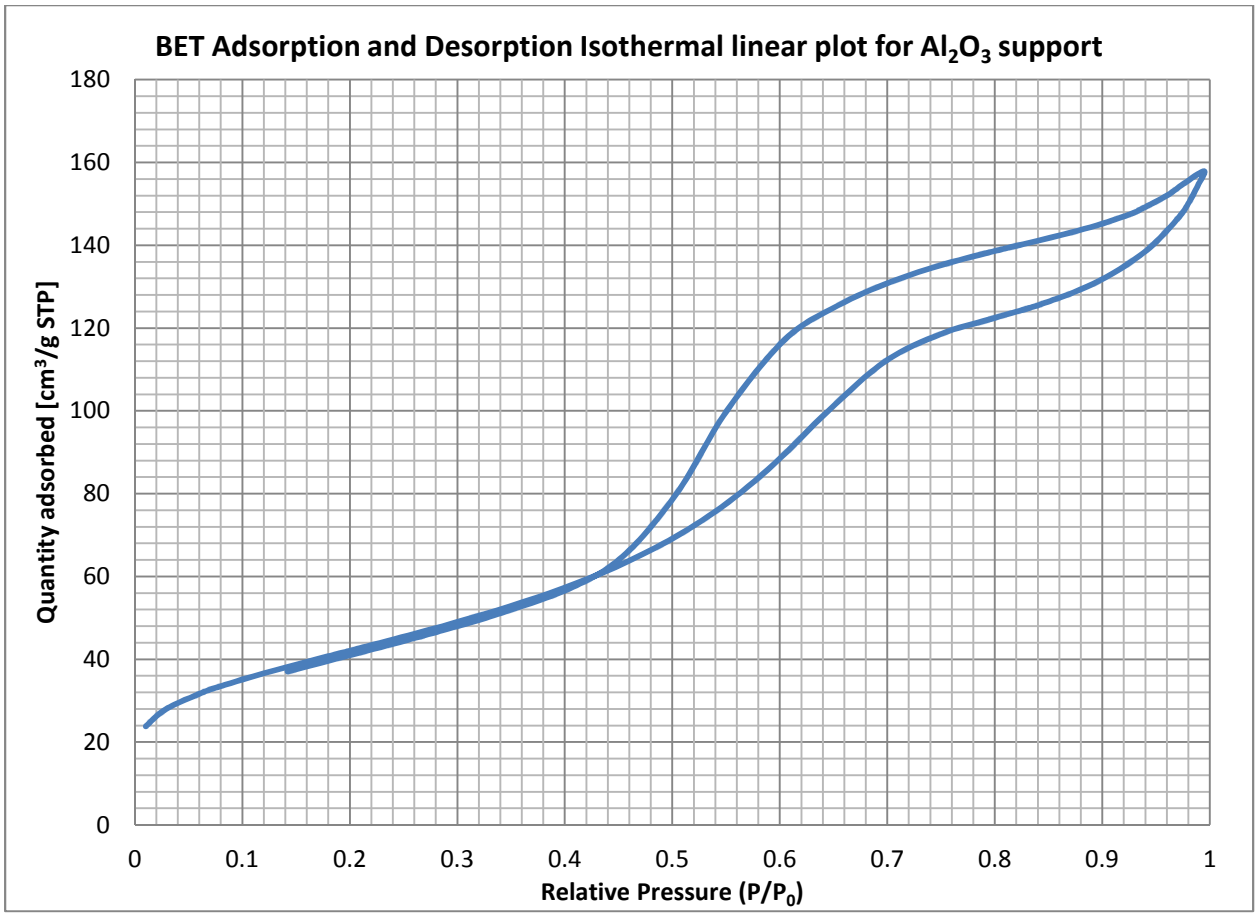
BET Adsorption and Desorption Isothermal linear plot for $Al_2O_3$ support
Quantity adsorbed [$cm^3/g$ STP]
180
160
140
120
100
80
60
40
20
0
0
0.1
0.2
0.3
0.4
0.5
0.6
0.7
0.8
0.9
1
Relative Pressure ($P/P_0$)

## $ZrO_2$ support

| | | | |
|---|---|---|---|
| Micromeritics Instrument Corporation | | | |
| TriStar II 3020 V1.03 (V1.03) | Unit 1 Port 1 | Serial #: 731 | Page 1 |

| | | | |
|---|---|---|---|
| Sample: | Zirconium oxide support | | |
| Operator: | Milly | | |
| Submitter: | Milly | | |
| File: | C:\WIN3020\DATA\MILLY\000-025.SMP | | |
| Started: | 11.04.2014 12:00:02 | Analysis Adsorptive: | N2 |
| Completed: | 11.04.2014 15:08:11 | Analysis Bath Temp.: | -195.850 °C |
| Report Time: | 08.05.2014 16:03:03 | Sample Mass: | 0.0637 g |
| Warm Free Space: | 11.3891 cm³ Measured | Cold Free Space: | 32.7246 cm³ Measured |
| Equilibration Interval: | 5 s | Low Pressure Dose: | None |
| Sample Density: | 1.000 g/cm³ | Automatic Degas: | No |

**Summary Report**

**Surface Area**

| | |
|---|---|
| Single point surface area at P/Po = 0.299079676: | 90.6300 m²/g |
| BET Surface Area: | 92.7892 m²/g |
| Langmuir Surface Area: | 147.8709 m²/g |
| t-Plot Micropore Area: | 3.3080 m²/g |
| t-Plot External Surface Area: | 89.4812 m²/g |
| BJH Adsorption cumulative surface | |

| | |
|---|---|
| area of pores between 17.000 Å and 3000.000 Å diameter: | 117.690 $m^2/g$ |
| BJH Desorption cumulative surface area of pores between 17.000 Å and 3000.000 Å diameter: | 131.0455 $m^2/g$ |

**Pore Volume**

| | |
|---|---|
| Single point adsorption total pore volume of pores less than 705.471 Å diameter at P/Po = 0.971785334: | 0.271071 $cm^3/g$ |
| t-Plot micropore volume: | 0.000686 $cm^3/g$ |
| BJH Adsorption cumulative volume of pores between 17.000 Å and 3000.000 Å diameter: | 0.294363 $cm^3/g$ |
| BJH Desorption cumulative volume of pores between 17.000 Å and 3000.000 Å diameter: | 0.296105 $cm^3/g$ |

**Pore Size**

| | |
|---|---|
| Adsorption average pore width (4V/A by BET): | 116.8545 Å |
| BJH Adsorption average pore diameter (4V/A): | 100.047 Å |
| BJH Desorption average pore diameter (4V/A): | 90.382 Å |

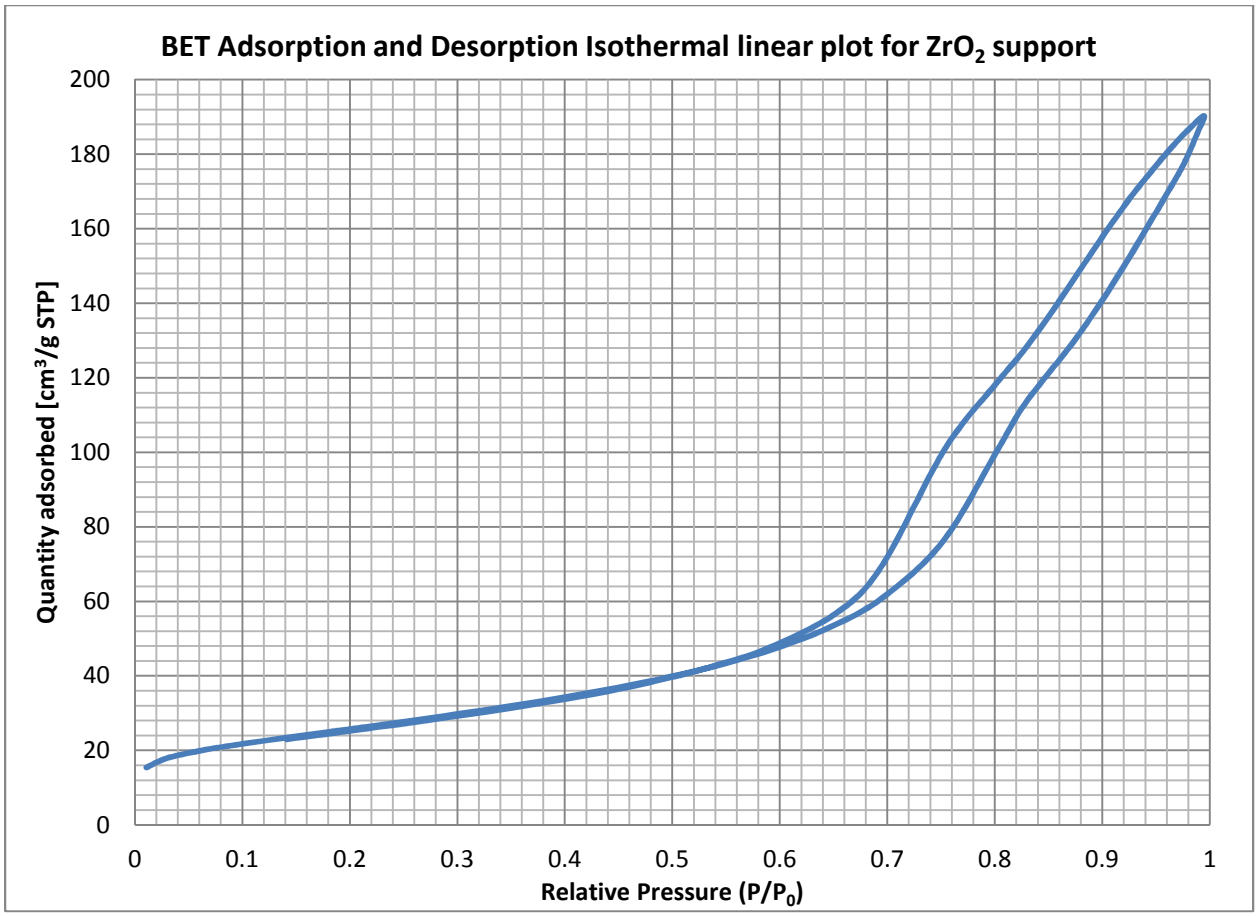
BET Adsorption and Desorption Isothermal linear plot for ZrO2 support
Quantity adsorbed [cm3/g STP]
200
180
160
140
120
100
80
60
40
20
0
0
0.1
0.2
0.3
0.4
0.5
0.6
0.7
0.8
0.9
1
Relative Pressure (P/P0)

## $TiO_2$ support

| | | | |
|---|---|---|---|
| TriStar II 3020 V1.03 (V1.03) | Unit 1 Port 1 | Serial #: 731 | Page 1 |

| | | | |
|---|---|---|---|
| Sample: | Titanium oxide support | | |
| Operator: | Milly | | |
| Submitter: | Milly | | |
| File: | C:\WIN3020\DATA\MILLY\000-023.SMP | | |
| Started: | 05.04.2014 10:53:59 | Analysis Adsorptive: | N2 |
| Completed: | 05.04.2014 14:18:41 | Analysis Bath Temp.: | -195.850 °C |
| Report Time: | 08.05.2014 16:01:57 | Sample Mass: | 0.0608 g |
| Warm Free Space: | 11.2163 cm³ Measured | Cold Free Space: | 32.1095 cm³ Measured |
| Equilibration Interval: | 5 s | Low Pressure Dose: | None |
| Sample Density: | 1.000 g/cm³ | Automatic Degas: | No |

**Summary Report**

**Surface Area**

| | |
|---|---|
| Single point surface area at P/Po = 0.299257144: | 7.6112 m²/g |
| BET Surface Area: | 7.7486 m²/g |
| Langmuir Surface Area: | 12.2589 m²/g |
| t-Plot Micropore Area: | 0.7969 m²/g |
| t-Plot External Surface Area: | 6.9517 m²/g |
| BJH Adsorption cumulative surface area of pores between 17.000 Å and 3000.000 Å | 7.268 m²/g |

diameter:

| | |
|---|---|
| BJH Desorption cumulative surface area of pores between 17.000 Å and 3000.000 Å diameter: | 7.7152 $m^2/g$ |

**Pore Volume**

| | |
|---|---|
| Single point adsorption total pore volume of pores less than 718.637 Å diameter at P/Po = 0.972314497: | 0.014301 $cm^3/g$ |
| t-Plot micropore volume: | 0.000356 $cm^3/g$ |
| BJH Adsorption cumulative volume of pores between 17.000 Å and 3000.000 Å diameter: | 0.026829 $cm^3/g$ |
| BJH Desorption cumulative volume of pores between 17.000 Å and 3000.000 Å diameter: | 0.026914 $cm^3/g$ |

**Pore Size**

| | |
|---|---|
| Adsorption average pore width (4V/A by BET): | 73.8235 Å |
| BJH Adsorption average pore diameter (4V/A): | 147.648 Å |
| BJH Desorption average pore diameter (4V/A): | 139.537 Å |

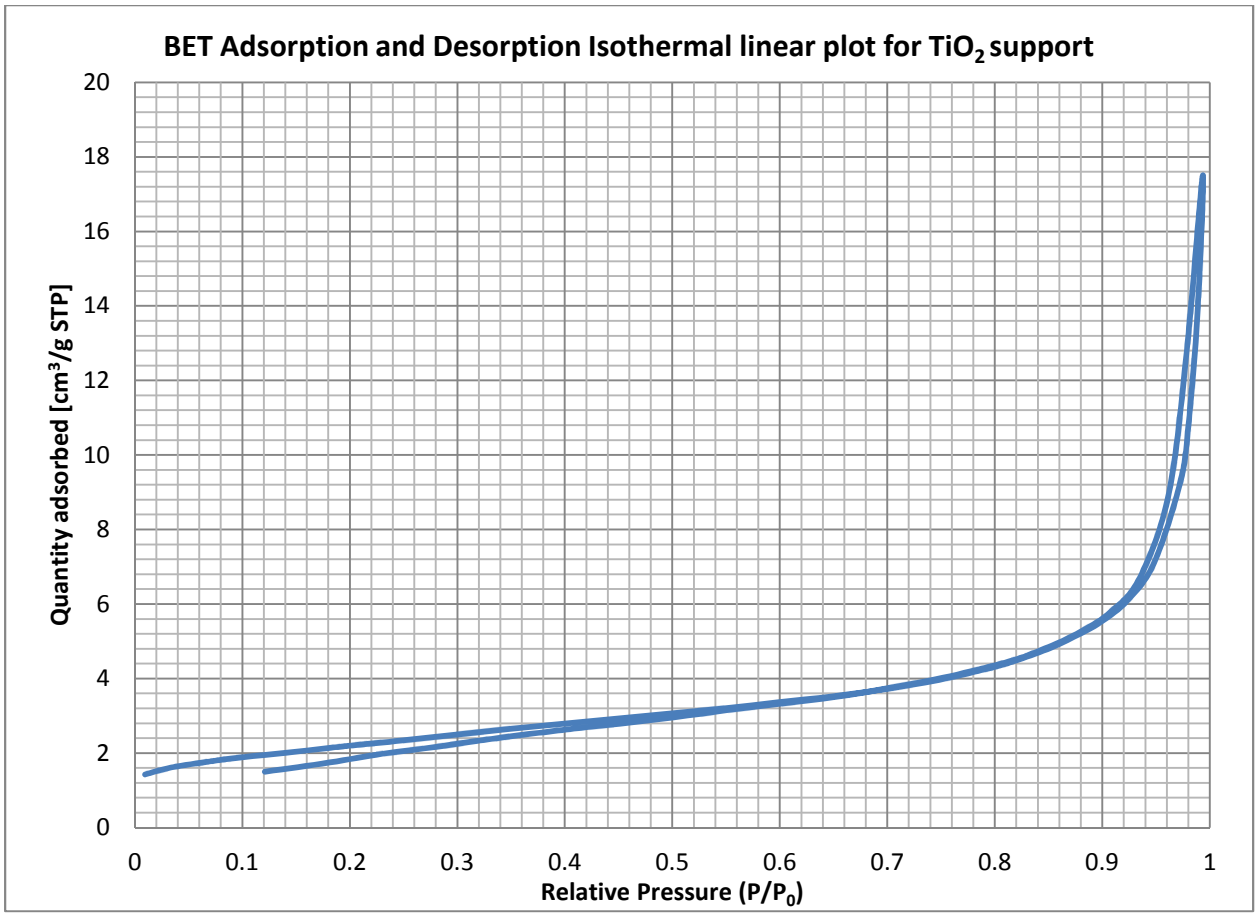
BET Adsorption and Desorption Isothermal linear plot for TiO2 support
Quantity adsorbed [cm3/g STP]
Relative Pressure (P/P0)
0
2
4
6
8
10
12
14
16
18
20
0
0.1
0.2
0.3
0.4
0.5
0.6
0.7
0.8
0.9
1

## $CeO_2$ support

| | | | |
|---|---|---|---|
| Micromeritics Instrument Corporation | | | |
| TriStar II 3020 V1.03 (V1.03) | Unit 1 Port 3 | Serial #: 731 | Page 1 |

| | | | |
|---|---|---|---|
| Sample: | Cerium oxide support | | |
| Operator: | Milly | | |
| Submitter: | Milly | | |
| File: | C:\WIN3020\DATA\MILLY\000-024.SMP | | |
| Started: | 05.04.2014 10:53:59 | Analysis Adsorptive: | N2 |
| Completed: | 05.04.2014 14:18:41 | Analysis Bath Temp.: | -195.850 °C |
| Report Time: | 08.05.2014 16:02:35 | Sample Mass: | 0.0696 g |
| Warm Free Space: | 11.4278 cm³ Measured | Cold Free Space: | 33.1628 cm³ Measured |
| Equilibration Interval: | 5 s | Low Pressure Dose: | None |
| Sample Density: | 1.000 g/cm³ | Automatic Degas: | No |

**Summary Report**

**Surface Area**

| | |
|---|---|
| Single point surface area at P/Po = 0.299733088: | 52.0794 m²/g |
| BET Surface Area: | 52.9754 m²/g |
| Langmuir Surface Area: | 84.2470 m²/g |
| t-Plot Micropore Area: | 4.3838 m²/g |
| t-Plot External Surface Area: | 48.5917 m²/g |
| BJH Adsorption cumulative surface | |

| | |
|---|---|
| area of pores between 17.000 Å and 3000.000 Å diameter: | 59.662 $m^2/g$ |
| BJH Desorption cumulative surface area of pores between 17.000 Å and 3000.000 Å diameter: | 69.3668 $m^2/g$ |

**Pore Volume**

| | |
|---|---|
| Single point adsorption total pore volume of pores less than 1249.726 Å diameter at P/Po = 0.984263404: | 0.167253 $cm^3/g$ |
| t-Plot micropore volume: | 0.001603 $cm^3/g$ |
| BJH Adsorption cumulative volume of pores between 17.000 Å and 3000.000 Å diameter: | 0.174211 $cm^3/g$ |
| BJH Desorption cumulative volume of pores between 17.000 Å and 3000.000 Å diameter: | 0.174396 $cm^3/g$ |

**Pore Size**

| | |
|---|---|
| Adsorption average pore width (4V/A by BET): | 126.2873 Å |
| BJH Adsorption average pore diameter (4V/A): | 116.797 Å |
| BJH Desorption average pore diameter (4V/A): | 100.564 Å |

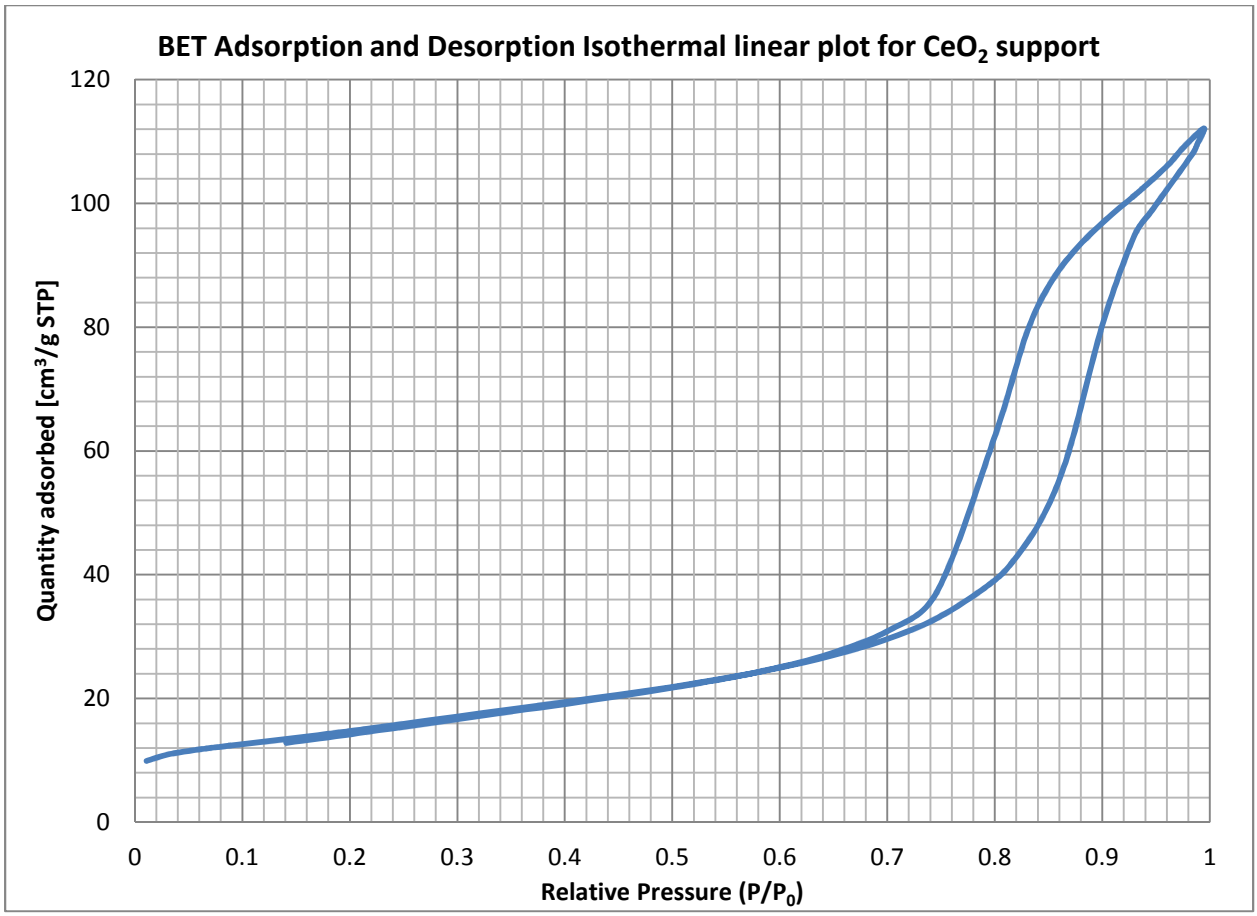
BET Adsorption and Desorption Isothermal linear plot for $CeO_2$ support
Quantity adsorbed [$cm^3/g$ STP]
120
100
80
60
40
20
0
0
0.1
0.2
0.3
0.4
0.5
0.6
0.7
0.8
0.9
1
Relative Pressure ($P/P_0$)

## $Mn_2O_3/Al_2O_3$ (15wt% Mn) sorbent

| | | | |
|---|---|---|---|
| Micromeritics Instrument Corporation | | | |
| TriStar II 3020 V1.03 (V1.03) | Unit 1 Port 1 | Serial #: 731 | Page 1 |

| | | | |
|---|---|---|---|
| Sample: | 15 wt.% $Mn\_Mn_xO_y/Al_2O_3$ | | |
| Operator: | Milly | | |
| Submitter: | Milly | | |
| File: | C:\WIN3020\DATA\MILLY\000-027.SMP | | |
| Started: | 13.04.2014 11:07:20 | Analysis Adsorptive: | N2 |
| Completed: | 13.04.2014 14:22:16 | Analysis Bath Temp.: | -195.850 °C |
| Report Time: | 08.05.2014 16:03:44 | Sample Mass: | 0.0488 g |
| Warm Free Space: | 11.4559 cm³ Measured | Cold Free Space: | 33.2420 cm³ Measured |
| Equilibration Interval: | 5 s | Low Pressure Dose: | None |
| Sample Density: | 1.000 g/cm³ | Automatic Degas: | No |

**Summary Report**

**Surface Area**

| | |
|---|---|
| Single point surface area at P/Po = 0.298895596: | 132.8847 m²/g |
| BET Surface Area: | 137.0040 m²/g |
| Langmuir Surface Area: | 220.5738 m²/g |
| t-Plot External Surface Area: | 141.2812 m²/g |
| BJH Adsorption cumulative surface area of pores between 17.000 Å and 3000.000 Å diameter: | 168.557 m²/g |

| | |
|---|---|
| BJH Desorption cumulative surface area of pores between 17.000 Å and 3000.000 Å diameter: | 205.5721 $m^2/g$ |

**Pore Volume**

| | |
|---|---|
| Single point adsorption total pore volume of pores less than 722.646 Å diameter at P/Po = 0.972471747: | 0.223655 $cm^3/g$ |
| t-Plot micropore volume: | -0.004117 $cm^3/g$ |
| BJH Adsorption cumulative volume of pores between 17.000 Å and 3000.000 Å diameter: | 0.237524 $cm^3/g$ |
| BJH Desorption cumulative volume of pores between 17.000 Å and 3000.000 Å diameter: | 0.242962 $cm^3/g$ |

**Pore Size**

| | |
|---|---|
| Adsorption average pore width (4V/A by BET): | 65.2988 Å |
| BJH Adsorption average pore diameter (4V/A): | 56.366 Å |
| BJH Desorption average pore diameter (4V/A): | 47.275 Å |

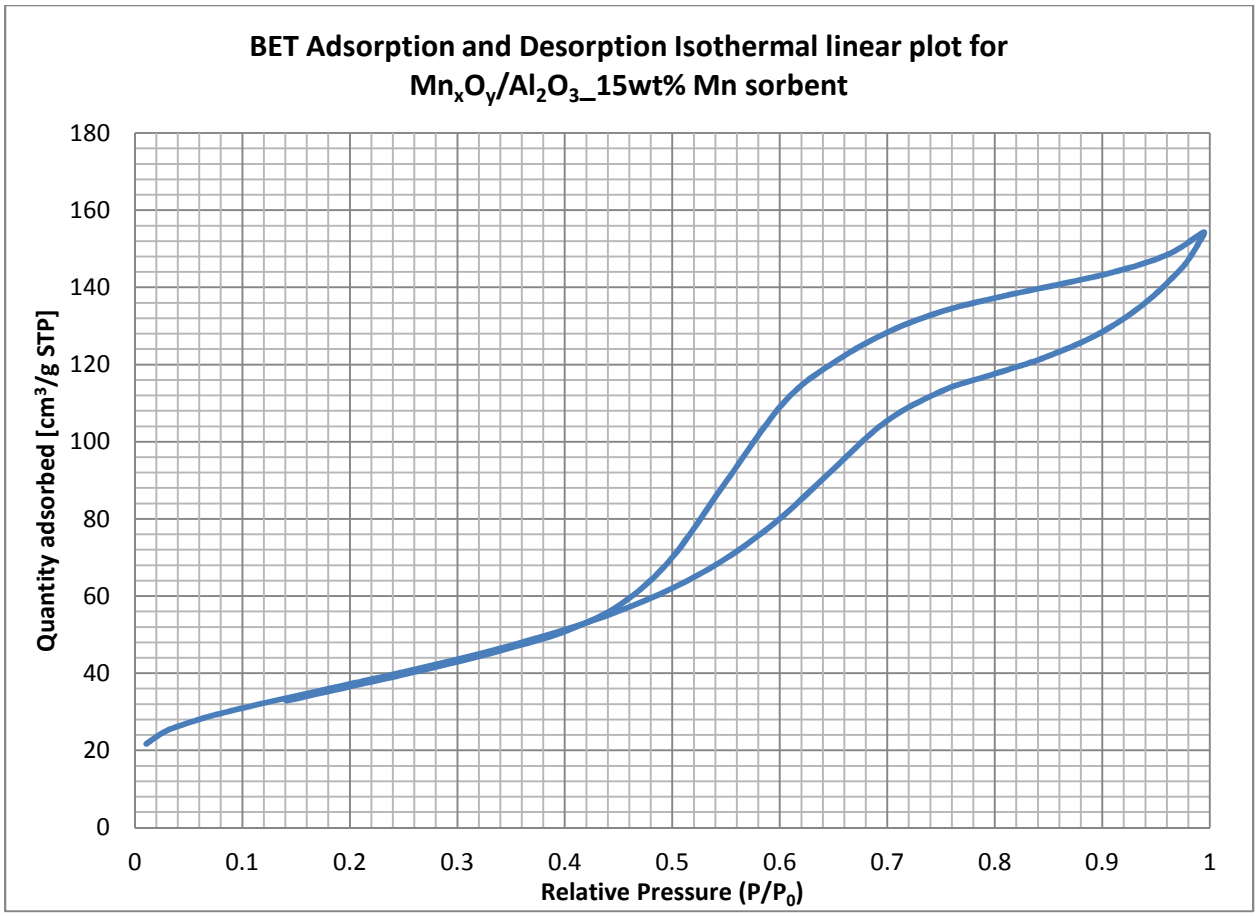
BET Adsorption and Desorption Isothermal linear plot for
$Mn_xO_y/Al_2O_3$_15wt% Mn sorbent
Quantity adsorbed [$cm^3$/g STP]
180
160
140
120
100
80
60
40
20
0
0
0.1
0.2
0.3
0.4
0.5
0.6
0.7
0.8
0.9
1
Relative Pressure ($P/P_0$)

## $Mn_2O_3/Al_2O_3$ (30wt% Mn) sorbent

| | | | |
|---|---|---|---|
| Micromeritics Instrument Corporation | | | |
| TriStar II 3020 V1.03 (V1.03) | Unit 1 Port 1 | Serial #: 731 | Page 1 |

| | | | |
|---|---|---|---|
| Sample: | 30 wt.% $Mn\_Mn_xO_y$ /$Al_2O_3$ | | |
| Operator: | Milly | | |
| Submitter: | Milly | | |
| File: | C:\WIN3020\DATA\MILLY\000-028.SMP | | |
| Started: | 23.04.2014 9:22:11 | Analysis Adsorptive: | N2 |
| Completed: | 23.04.2014 11:33:22 | Analysis Bath Temp.: | -195.850 °C |
| Report Time: | 08.05.2014 16:04:23 | Sample Mass: | 0.0536 g |
| Warm Free Space: | 11.4382 cm³ Measured | Cold Free Space: | 32.7143 cm³ Measured |
| Equilibration Interval: | 5 s | Low Pressure Dose: | None |
| Sample Density: | 1.000 g/cm³ | Automatic Degas: | No |

**Summary Report**

**Surface Area**

| | |
|---|---|
| Single point surface area at P/Po = 0.298931834: | 98.4849 m²/g |
| BET Surface Area: | 101.5020 m²/g |
| Langmuir Surface Area: | 163.5243 m²/g |
| t-Plot External Surface Area: | 104.4472 m²/g |
| BJH Adsorption cumulative surface area of pores between 17.000 Å and 3000.000 Å diameter: | 123.271 m²/g |

| | |
|---|---|
| BJH Desorption cumulative surface area of pores between 17.000 Å and 3000.000 Å diameter: | 154.2337 $m^2/g$ |

**Pore Volume**

| | |
|---|---|
| Single point adsorption total pore volume of pores less than 747.147 Å diameter at P/Po = 0.973395402: | 0.154950 $cm^3/g$ |
| t-Plot micropore volume: | -0.002955 $cm^3/g$ |
| BJH Adsorption cumulative volume of pores between 17.000 Å and 3000.000 Å diameter: | 0.158673 $cm^3/g$ |
| BJH Desorption cumulative volume of pores between 17.000 Å and 3000.000 Å diameter: | 0.163016 $cm^3/g$ |

**Pore Size**

| | |
|---|---|
| Adsorption average pore width (4V/A by BET): | 61.0630 Å |
| BJH Adsorption average pore diameter (4V/A): | 51.488 Å |
| BJH Desorption average pore diameter (4V/A): | 42.278 Å |

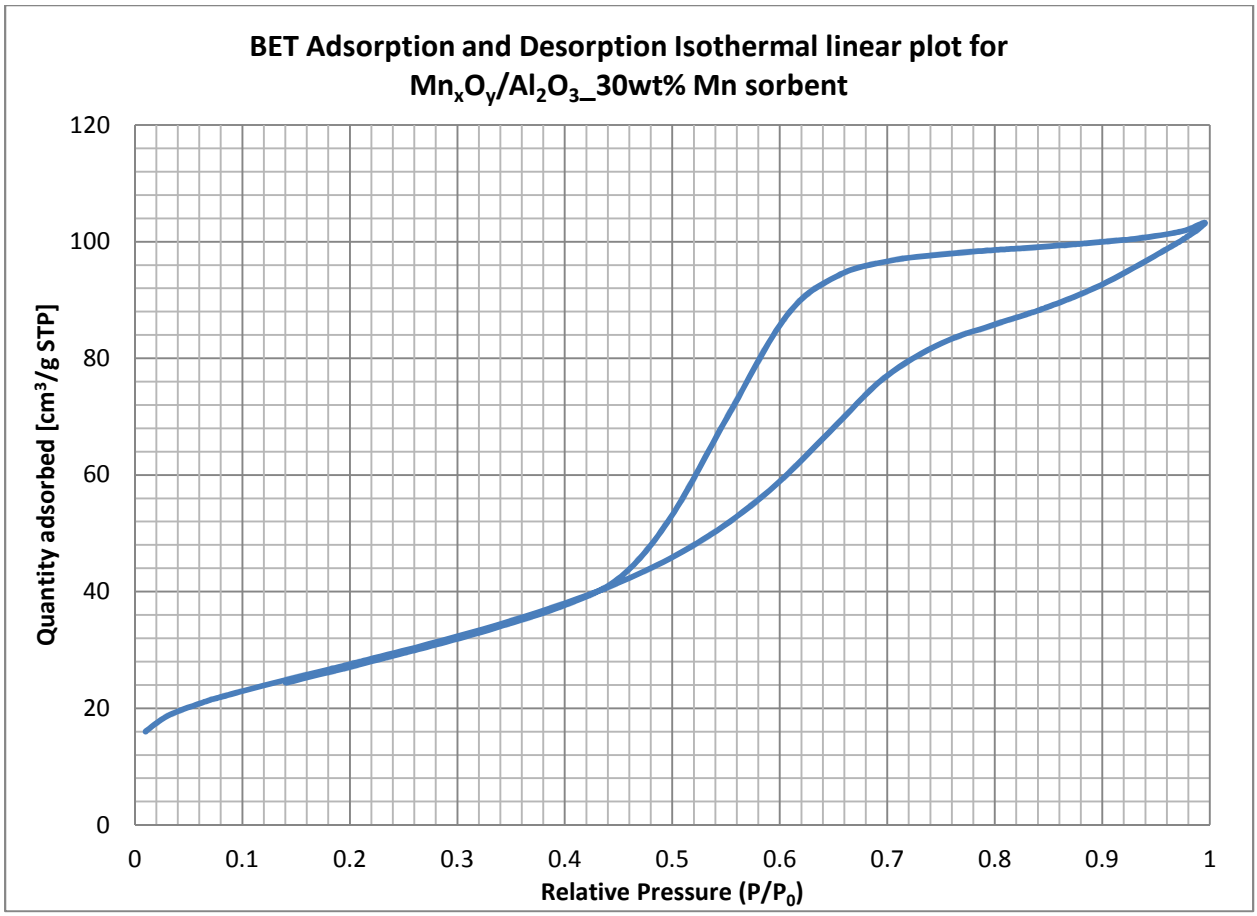
BET Adsorption and Desorption Isothermal linear plot for
$Mn_xO_y/Al_2O_3$_30wt% Mn sorbent
Quantity adsorbed [$cm^3$/g STP]
120
100
80
60
40
20
0
0
0.1
0.2
0.3
0.4
0.5
0.6
0.7
0.8
0.9
1
Relative Pressure ($P/P_0$)

# $Mn_2O_3/ZrO_2$ sorbent

| | | | |
|---|---|---|---|
| Micromeritics Instrument Corporation | | | |
| TriStar II 3020 V1.03 (V1.03) | Unit 1 Port 3 | Serial #: 731 | Page 1 |

| | | | |
|---|---|---|---|
| Sample: | 15 wt% Mn_$Mn_xO_y/ZrO_2$ | | |
| Operator: | Milly | | |
| Submitter: | | | |
| File: | C:\WIN3020\DATA\MILLY\000-029.SMP | | |
| Started: | 13.04.2014 11:07:20 | Analysis Adsorptive: | N2 |
| Completed: | 13.04.2014 14:22:16 | Analysis Bath Temp.: | -195.850 °C |
| Report Time: | 08.05.2014 16:05:10 | Sample Mass: | 0.0463 g |
| Warm Free Space: | 11.2015 cm³ Measured | Cold Free Space: | 32.2684 cm³ Measured |
| Equilibration Interval: | 5 s | Low Pressure Dose: | None |
| Sample Density: | 1.000 g/cm³ | Automatic Degas: | No |

**Summary Report**

**Surface Area**

| | |
|---|---|
| Single point surface area at P/Po = 0.299189912: | 80.6880 m²/g |
| BET Surface Area: | 82.5997 m²/g |
| Langmuir Surface Area: | 132.0368 m²/g |
| t-Plot Micropore Area: | 2.5085 m²/g |
| t-Plot External Surface Area: | 80.0912 m²/g |
| BJH Adsorption cumulative surface | |

| | |
|---|---|
| area of pores between 17.000 Å and 3000.000 Å diameter: | 105.125 $m^2/g$ |
| BJH Desorption cumulative surface area of pores between 17.000 Å and 3000.000 Å diameter: | 119.0070 $m^2/g$ |

**Pore Volume**

| | |
|---|---|
| Single point adsorption total pore volume of pores less than 697.754 Å diameter at P/Po = 0.971465738: | 0.235493 $cm^3/g$ |
| t-Plot micropore volume: | 0.000266 $cm^3/g$ |
| BJH Adsorption cumulative volume of pores between 17.000 Å and 3000.000 Å diameter: | 0.254610 $cm^3/g$ |
| BJH Desorption cumulative volume of pores between 17.000 Å and 3000.000 Å diameter: | 0.255303 $cm^3/g$ |

**Pore Size**

| | |
|---|---|
| Adsorption average pore width (4V/A by BET): | 114.0406 Å |
| BJH Adsorption average pore diameter (4V/A): | 96.879 Å |
| BJH Desorption average pore diameter (4V/A): | 85.811 Å |

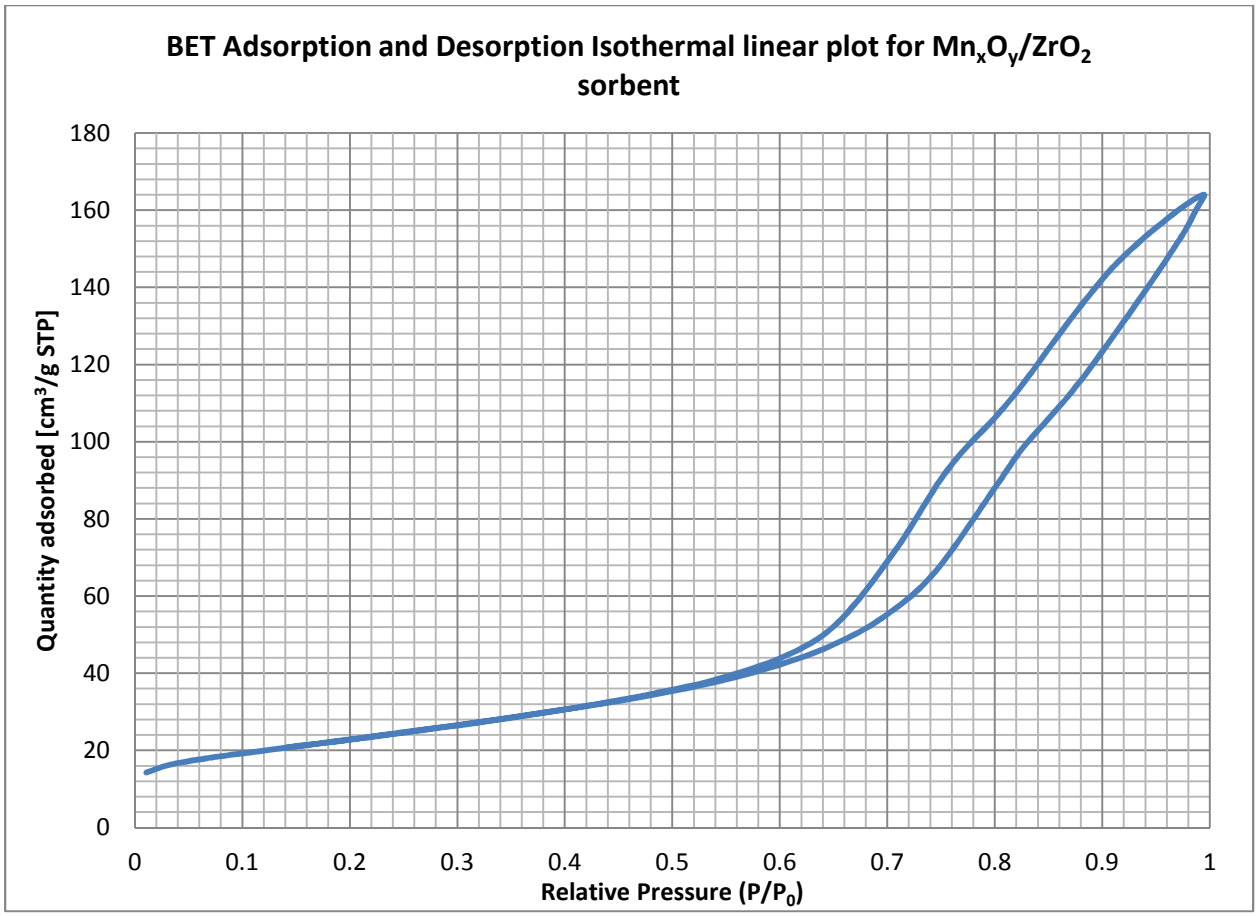
BET Adsorption and Desorption Isothermal linear plot for $Mn_xO_y/ZrO_2$ sorbent
Quantity adsorbed [$cm^3/g$ STP]
180
160
140
120
100
80
60
40
20
0
0
0.1
0.2
0.3
0.4
0.5
0.6
0.7
0.8
0.9
1
Relative Pressure ($P/P_0$)

## $Mn_2O_3/TiO_2$ sorbent

| | | | |
|---|---|---|---|
| Micromeritics Instrument Corporation | | | |
| TriStar II 3020 V1.03 (V1.03) | Unit 1 Port 1 | Serial #: 731 | Page 1 |

| | | | |
|---|---|---|---|
| Sample: | 15 wt% Mn_$Mn_xO_y/TiO_2$ | | |
| Operator: | Milly | | |
| Submitter: | | | |
| File: | C:\WIN3020\DATA\MILLY\000-034.SMP | | |
| Started: | 25.05.2014 10:42:59 | Analysis Adsorptive: | N2 |
| Completed: | 25.05.2014 13:14:00 | Analysis Bath Temp.: | -195.850 °C |
| Report Time: | 27.05.2014 12:27:22 | Sample Mass: | 0.0561 g |
| Warm Free Space: | 12.5013 cm³ Measured | Cold Free Space: | 36.8933 cm³ Measured |
| Equilibration Interval: | 5 s | Low Pressure Dose: | None |
| Sample Density: | 1.000 g/cm³ | Automatic Degas: | No |

**Summary Report**

**Surface Area**

| | |
|---|---|
| Single point surface area at P/Po = 0.299176497: | 4.6951 m²/g |
| BET Surface Area: | 4.6700 m²/g |
| Langmuir Surface Area: | 6.9883 m²/g |
| t-Plot Micropore Area: | 2.7727 m²/g |
| t-Plot External Surface Area: | 1.8974 m²/g |
| BJH Adsorption cumulative surface | |

| | |
|---|---|
| area of pores between 17.000 Å and 3000.000 Å diameter: | 1.896 $m^2/g$ |
| BJH Desorption cumulative surface area of pores between 17.000 Å and 3000.000 Å diameter: | 2.1245 $m^2/g$ |

**Pore Volume**

| | |
|---|---|
| Single point adsorption total pore volume of pores less than 714.882 Å diameter at P/Po = 0.972165626: | 0.008310 $cm^3/g$ |
| t-Plot micropore volume: | 0.001518 $cm^3/g$ |
| BJH Adsorption cumulative volume of pores between 17.000 Å and 3000.000 Å diameter: | 0.020695 $cm^3/g$ |
| BJH Desorption cumulative volume of pores between 17.000 Å and 3000.000 Å diameter: | 0.022109 $cm^3/g$ |

**Pore Size**

| | |
|---|---|
| Adsorption average pore width (4V/A by BET): | 71.1798 Å |
| BJH Adsorption average pore diameter (4V/A): | 436.573 Å |
| BJH Desorption average pore diameter (4V/A): | 416.275 Å |

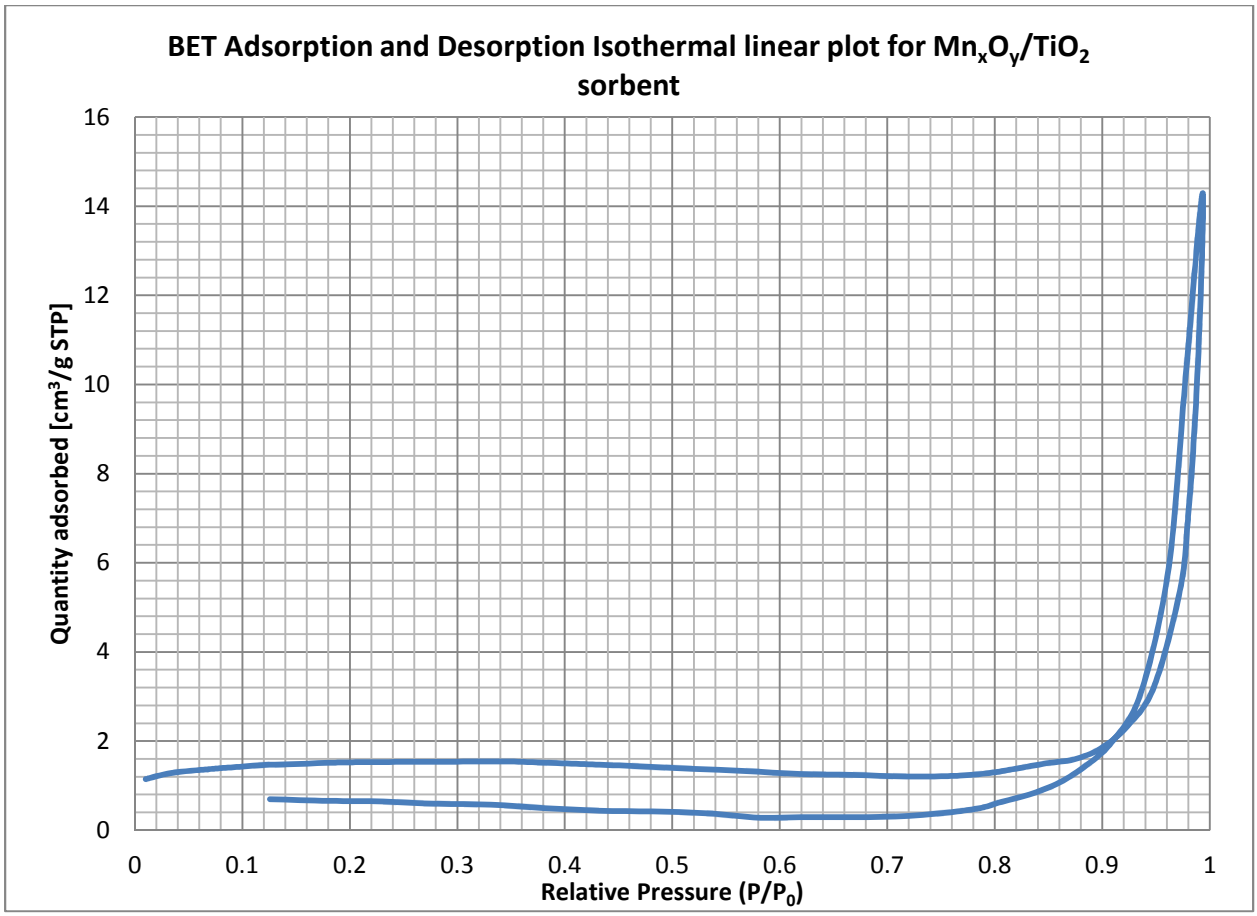
BET Adsorption and Desorption Isothermal linear plot for $Mn_xO_y/TiO_2$ sorbent
Quantity adsorbed [$cm^3$/g STP]
16
14
12
10
8
6
4
2
0
0
0.1
0.2
0.3
0.4
0.5
0.6
0.7
0.8
0.9
1
Relative Pressure ($P/P_0$)

## $Mn_2O_3/CeO_2$ sorbent

| | | | |
|---|---|---|---|
| Micromeritics Instrument Corporation | | | |
| TriStar II 3020 V1.03 (V1.03) | Unit 1 Port 2 | Serial #: 731 | Page 1 |

| | | | |
|---|---|---|---|
| Sample: | 15 wt% Mn_$Mn_xO_y/CeO_2$ | | |
| Operator: | Milly | | |
| Submitter: | | | |
| File: | C:\WIN3020\DATA\MILLY\000-035.SMP | | |
| Started: | 25.05.2014 10:42:59 | Analysis Adsorptive: | N2 |
| Completed: | 25.05.2014 13:14:00 | Analysis Bath Temp.: | -195.850 °C |
| Report Time: | 27.05.2014 12:30:31 | Sample Mass: | 0.0565 g |
| Warm Free Space: | 11.9552 cm³ Measured | Cold Free Space: | 34.9231 cm³ Measured |
| Equilibration Interval: | 5 s | Low Pressure Dose: | None |
| Sample Density: | 1.000 g/cm³ | Automatic Degas: | No |

**Summary Report**

**Surface Area**

| | |
|---|---|
| Single point surface area at P/Po = 0.299264685: | 33.9566 m²/g |
| BET Surface Area: | 34.5270 m²/g |
| Langmuir Surface Area: | 54.4565 m²/g |
| t-Plot Micropore Area: | 4.0659 m²/g |
| t-Plot External Surface Area: | 30.4611 m²/g |
| BJH Adsorption cumulative surface area of pores | |

| | |
|---|---|
| between 17.000 Å and 3000.000 Å diameter: | 36.543 $m^2/g$ |
| BJH Desorption cumulative surface area of pores between 17.000 Å and 3000.000 Å diameter: | 43.6368 $m^2/g$ |

**Pore Volume**

| | |
|---|---|
| Single point adsorption total pore volume of pores less than 640.769 Å diameter at P/Po = 0.968862995: | 0.108878 $cm^3/g$ |
| t-Plot micropore volume: | 0.001888 $cm^3/g$ |
| BJH Adsorption cumulative volume of pores between 17.000 Å and 3000.000 Å diameter: | 0.120885 $cm^3/g$ |
| BJH Desorption cumulative volume of pores between 17.000 Å and 3000.000 Å diameter: | 0.121703 $cm^3/g$ |

**Pore Size**

| | |
|---|---|
| Adsorption average pore width (4V/A by BET): | 126.1363 Å |
| BJH Adsorption average pore diameter (4V/A): | 132.320 Å |
| BJH Desorption average pore diameter (4V/A): | 111.560 Å |

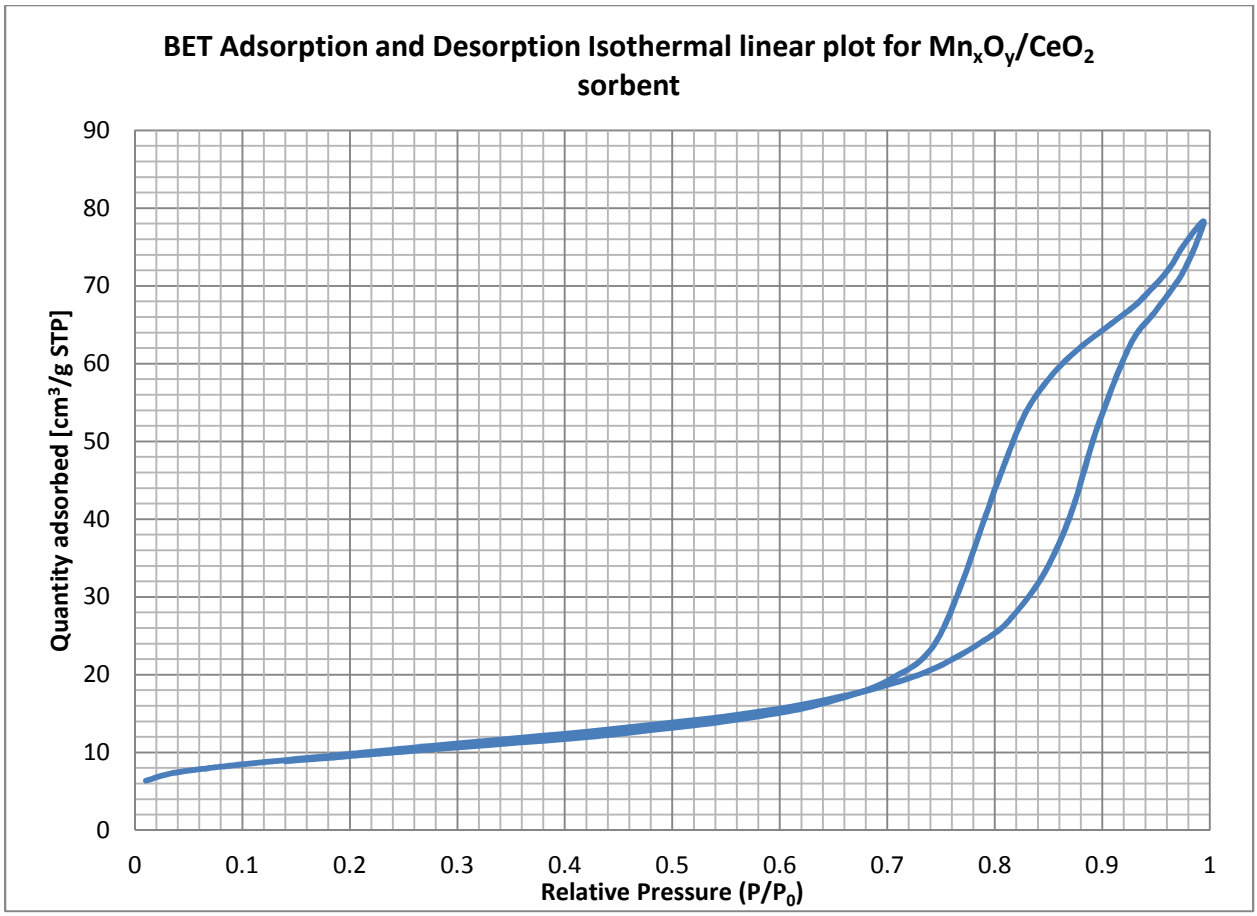
BET Adsorption and Desorption Isothermal linear plot for $Mn_xO_y/CeO_2$ sorbent
Quantity adsorbed [$cm^3/g$ STP]
90
80
70
60
50
40
30
20
10
0
0
0.1
0.2
0.3
0.4
0.5
0.6
0.7
0.8
0.9
1
Relative Pressure ($P/P_0$)

## *Appendix G Thermogravimetric Analysis results*

### Gamma $Al_2O_3$ support

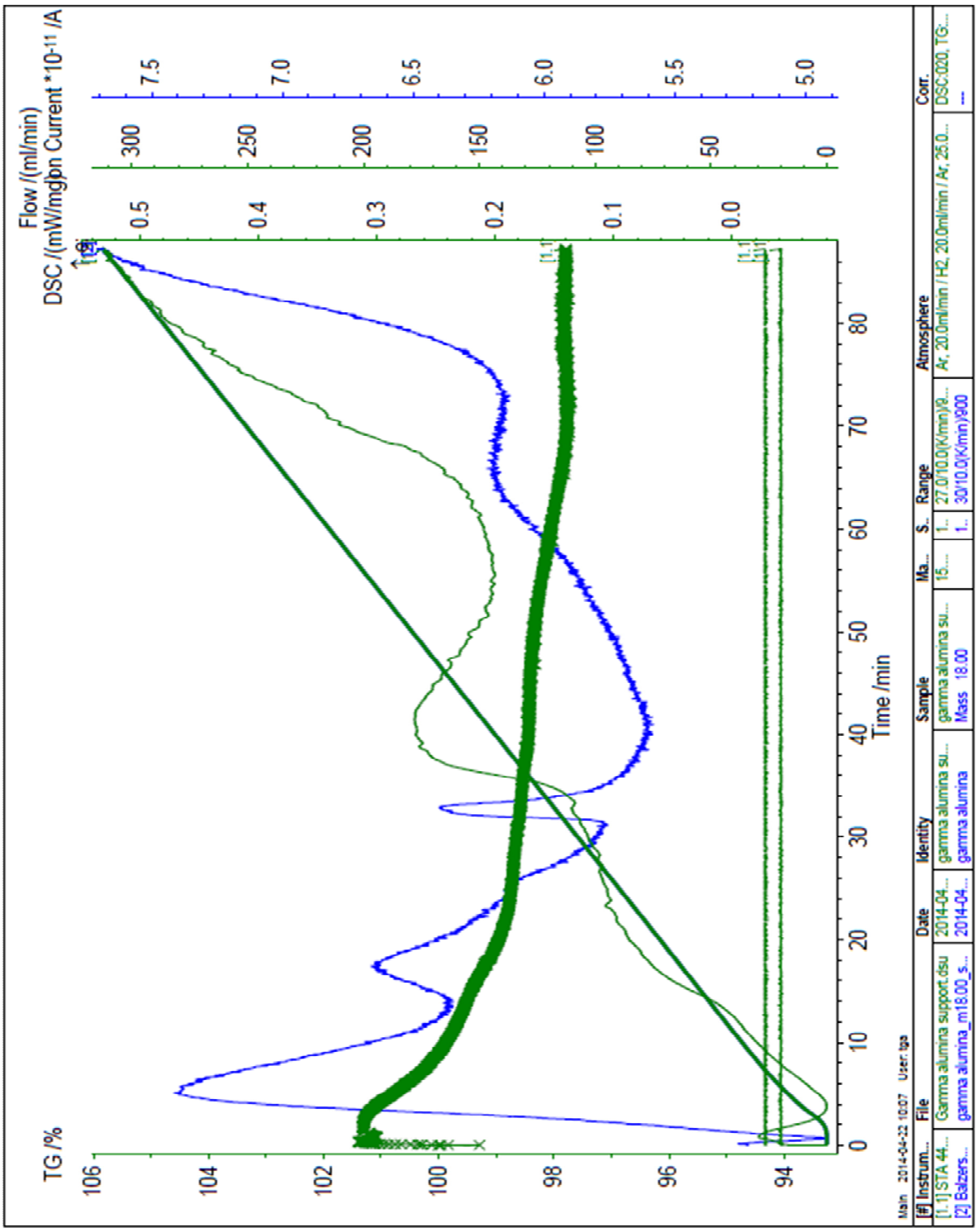

## $ZrO_2$ support

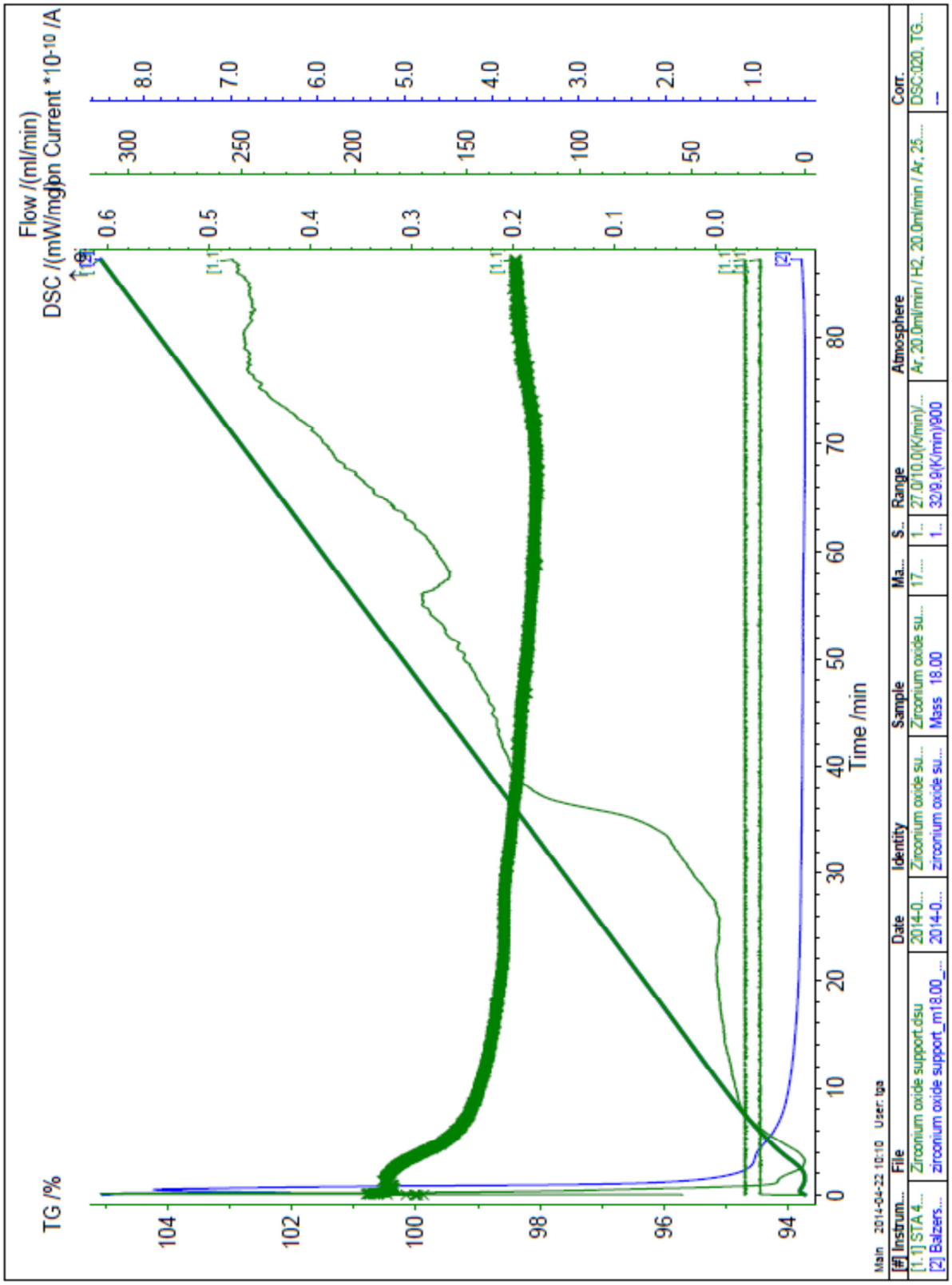

## $TiO_2$ support

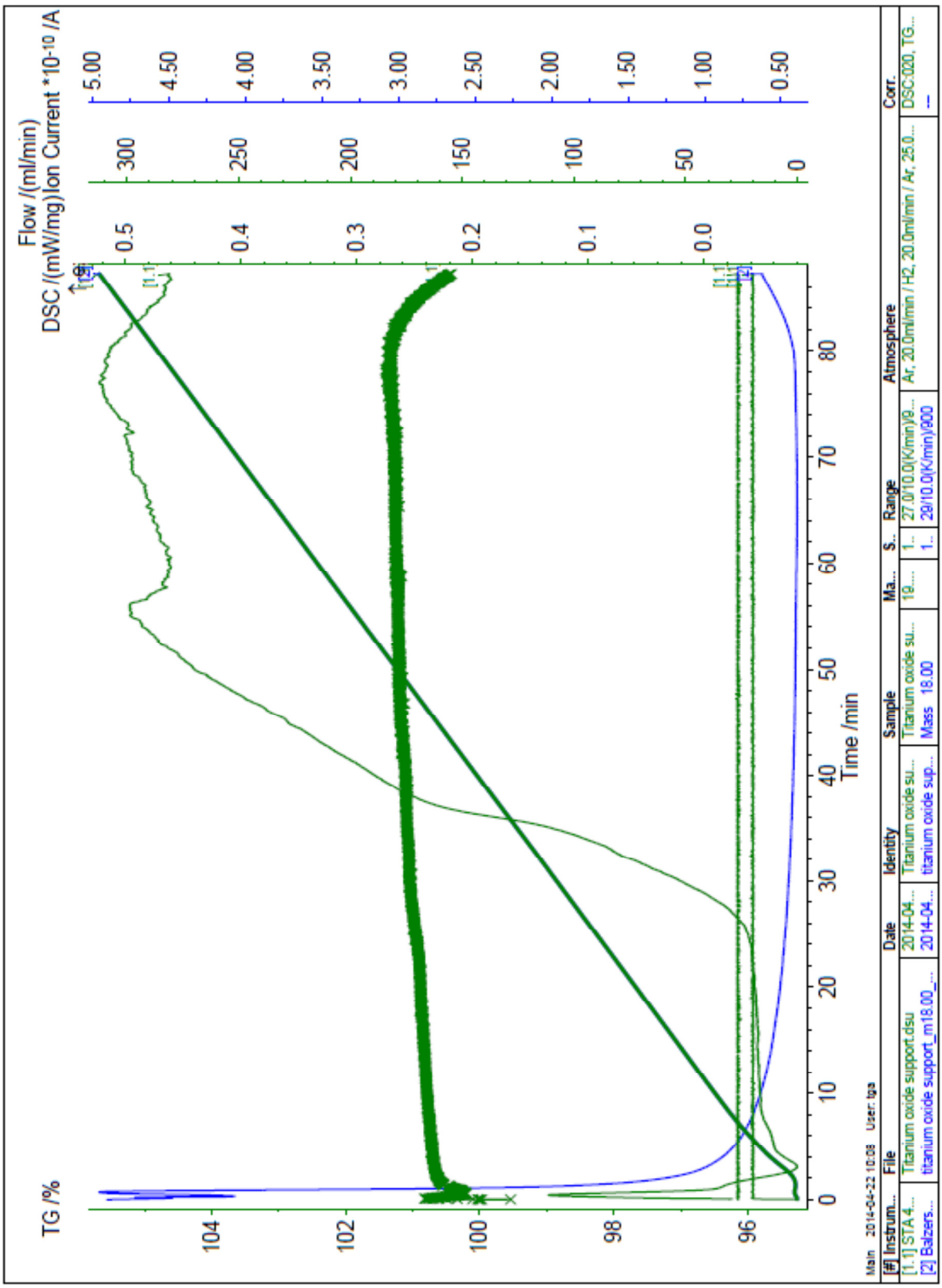

## $CeO_2$ support

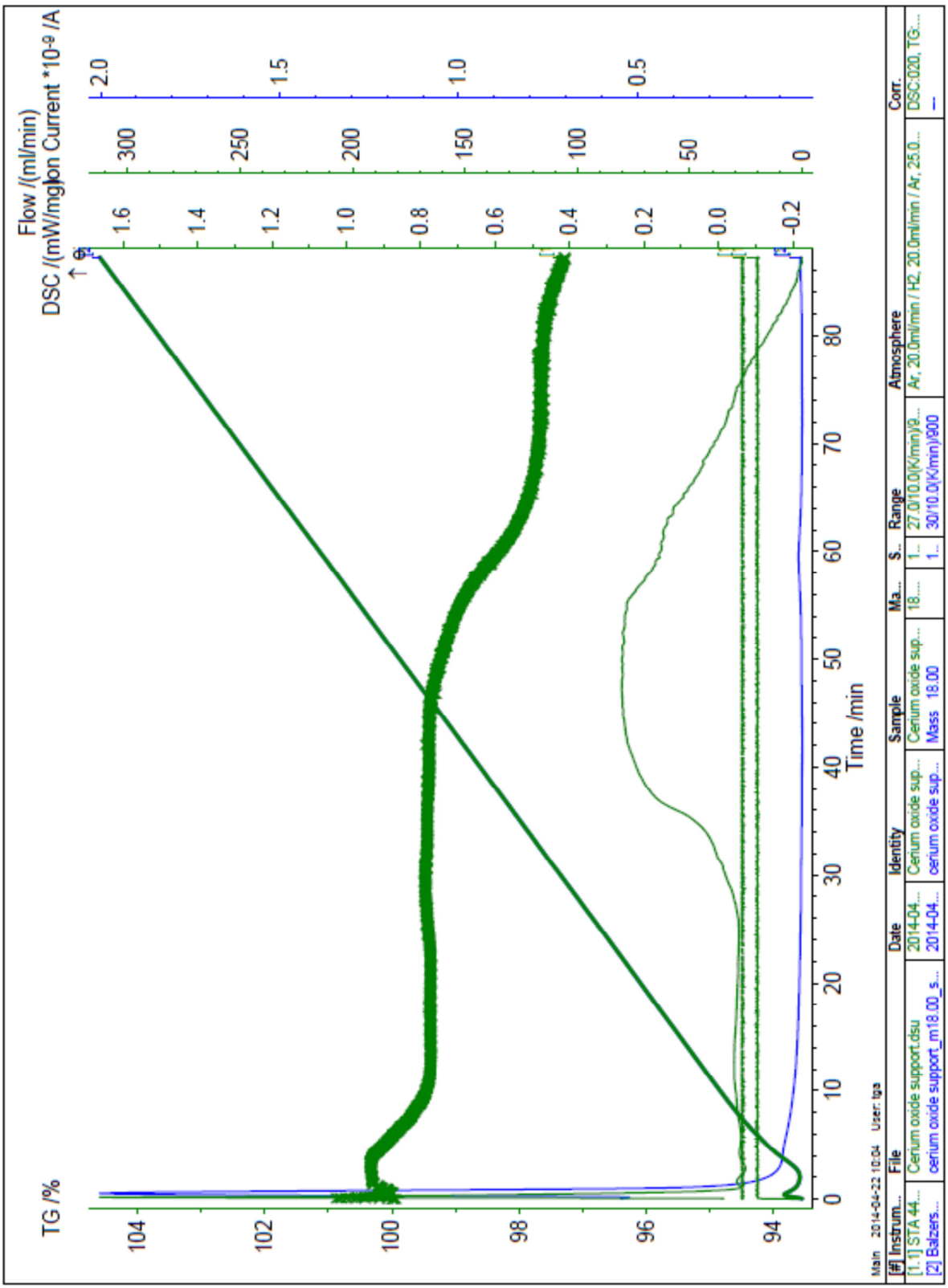

## $Mn_2O_3/Al_2O_3$ (15wt% Mn) sorbent

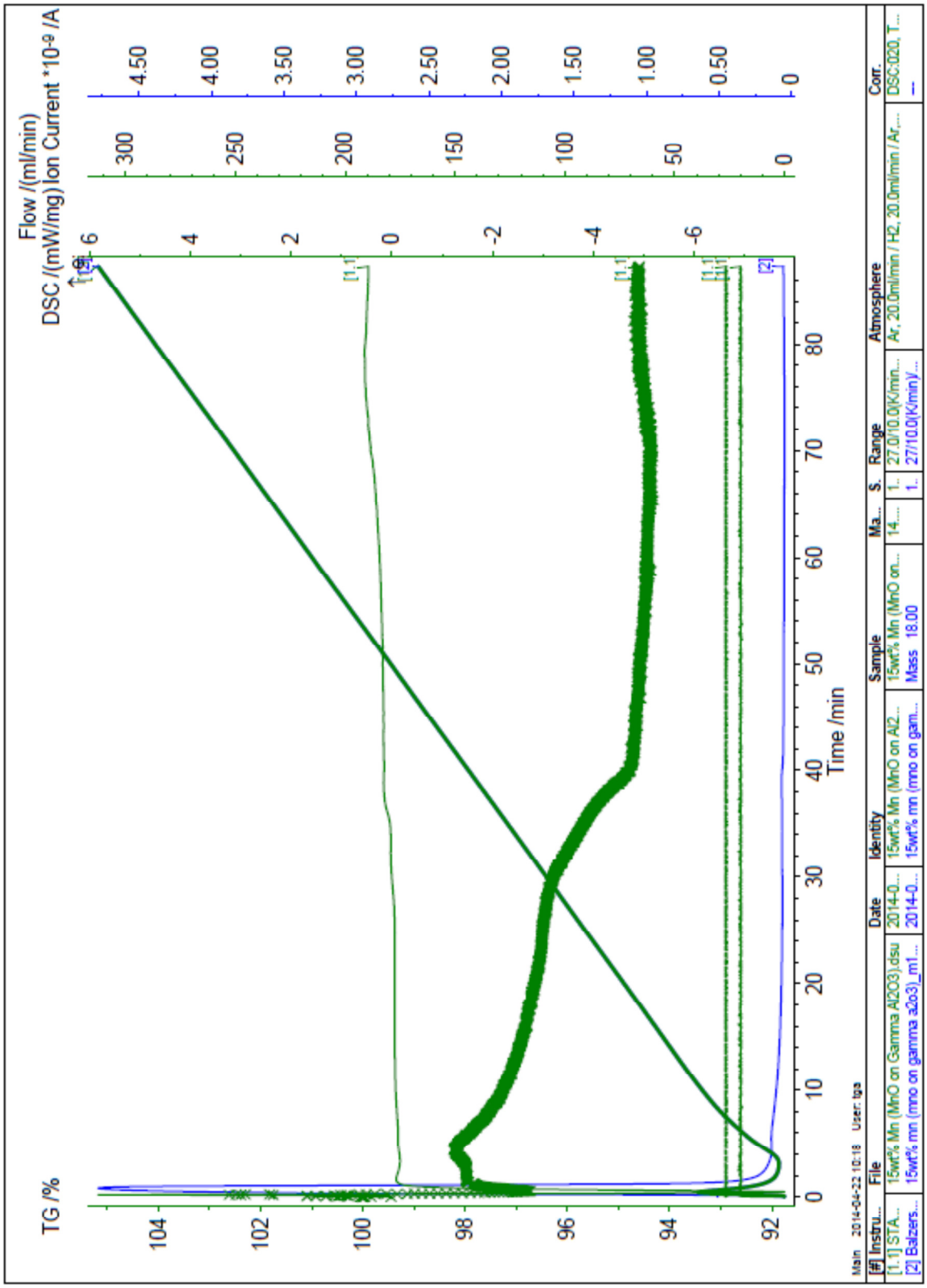

## $Mn_2O_3/Al_2O_3$ (30wt% Mn) sorbent

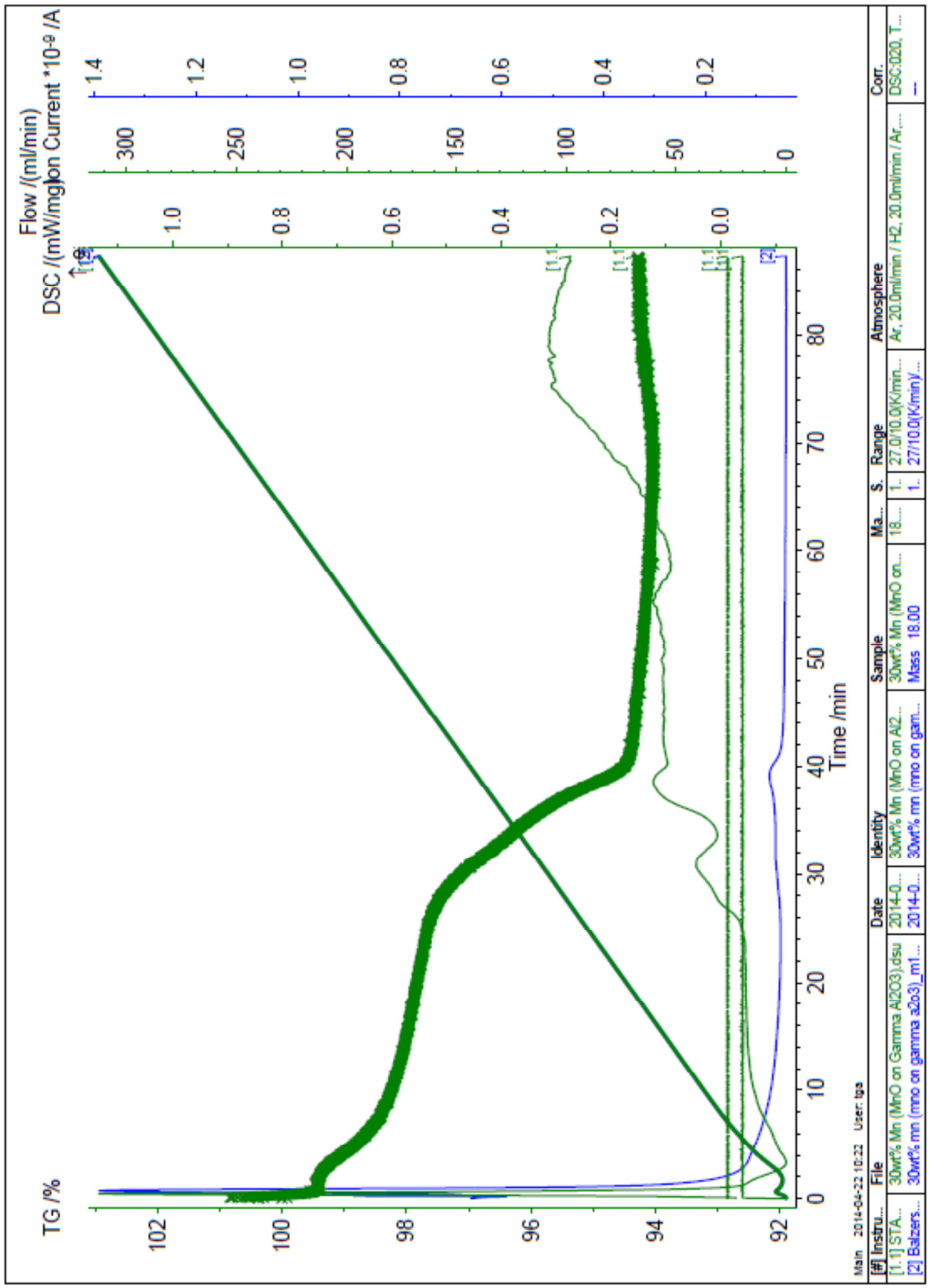

## $Mn_2O_3/ZrO_2$ sorbent

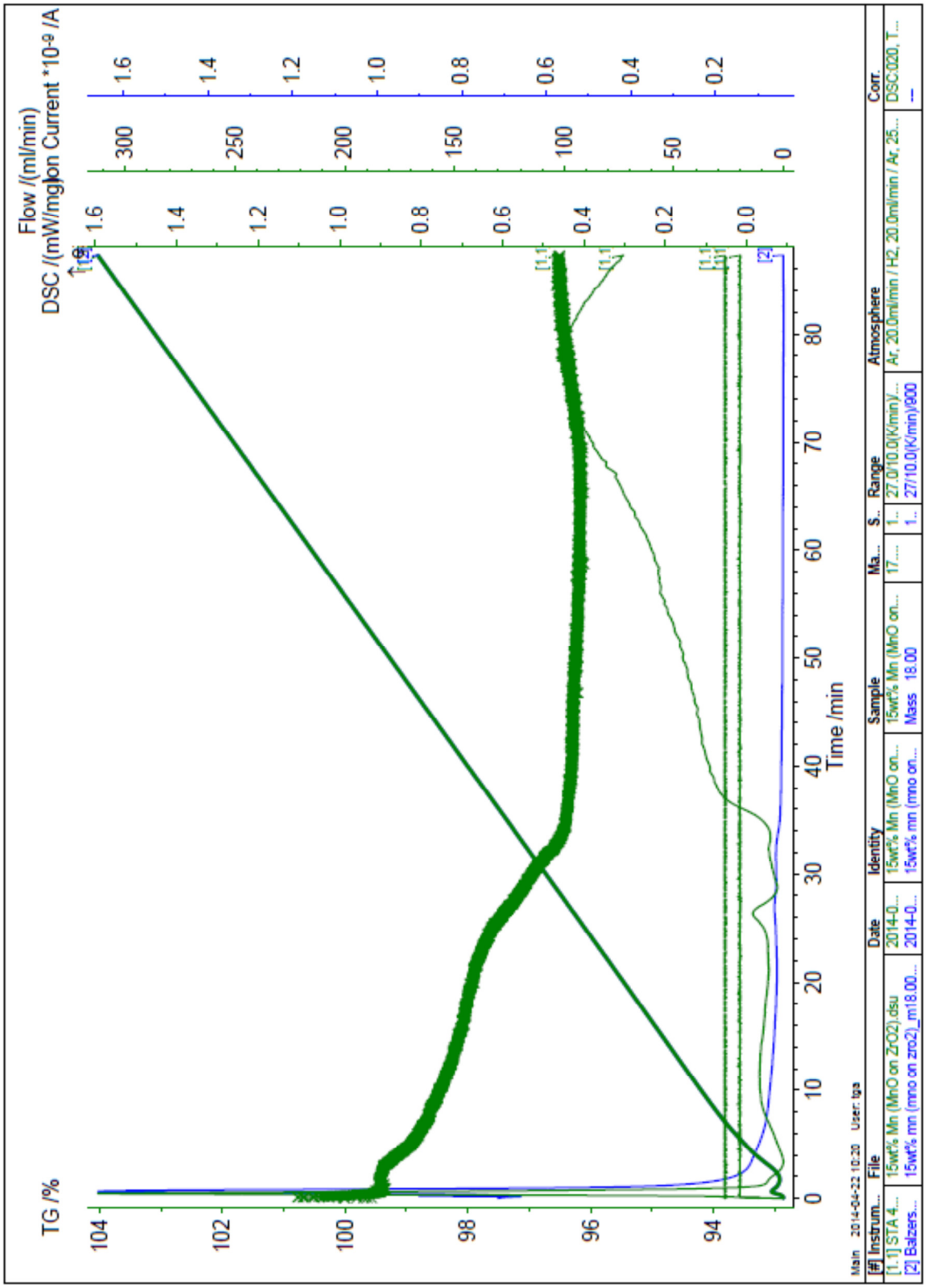

## $Mn_2O_3/TiO_2$ sorbent

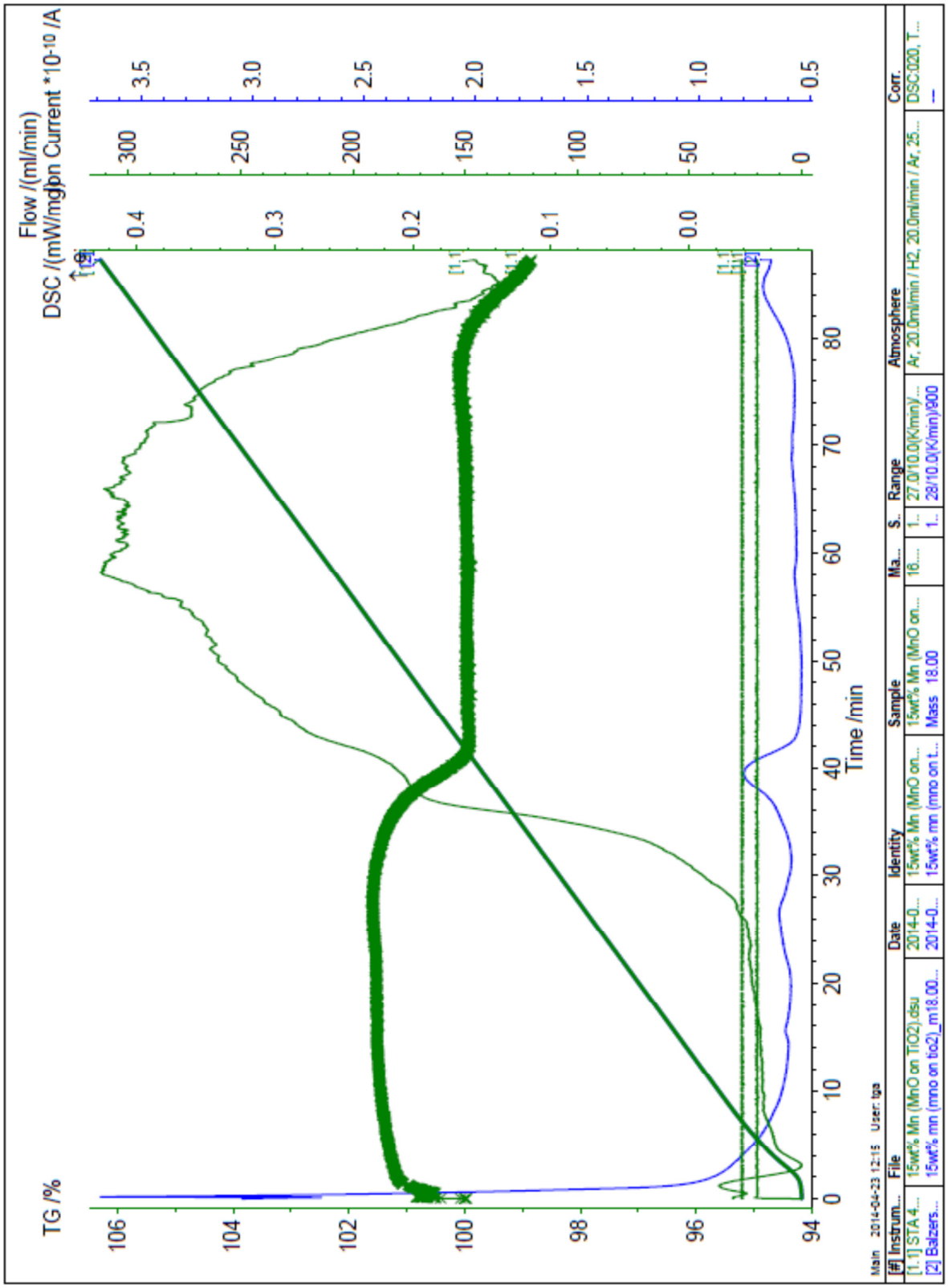

## $Mn_2O_3/CeO_2$ sorbent

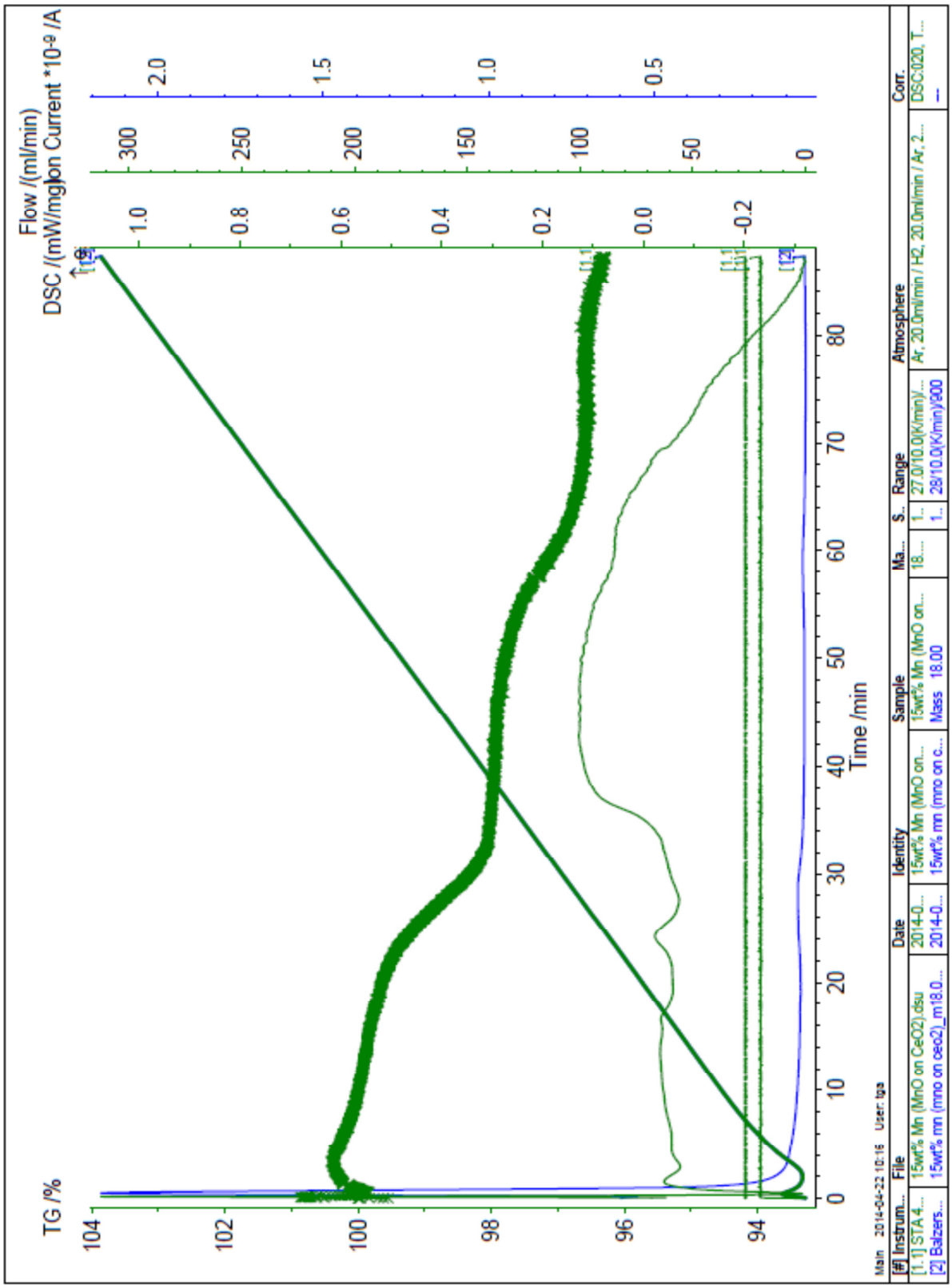

## *Appendix H TPR $H_2$-consumption Altamira summary reports*

### $Mn_2O_3/Al_2O_3$ (15wt% Mn) sorbent

Altamira Instruments

**********

| | |
|---|---|
| DFN Name : | @15wt%MnxOyonAl2O3.dfn |
| Comments : | 15wt% Mn_MnxOy on Al2O3 |
| Sample Weight : | 0.1212 (g) |
| Active Component : | Mn @ 15.0 % Loading |
| Calibration Loop Volume : | 50.0 (uL) |
| Loop Temperature : | 25.0 (Deg C) |
| Loop Pressure : | 1.0 (atm) |
| Analytical Gas : | H2 @ 10.0 % |

**********

Uptake : 529.541 (umol/g)

**********

% Reduction : 19.395

6/4/2014 2:48 PM

## $Mn_2O_3/Al_2O_3$ (30wt% Mn) sorbent

Altamira Instruments

**********

| | |
|---|---|
| DFN Name : | @30wt%MnxOyonAl2O3.dfn |
| Comments : | 30wt%Mn_MnxOy on Al2O3 |
| Sample Weight : | 0.1215 (g) |
| Active Component : | Mn @ 30.0 % Loading |
| Calibration Loop Volume : | 50.0 (uL) |
| Loop Temperature : | 25.0 (Deg C) |
| Loop Pressure : | 1.0 (atm) |
| Analytical Gas : | H2 @ 10.0 % |

**********

Uptake : 1019.300 (umol/g)

**********

% Reduction : 18.667

6/4/2014 2:54 PM

## $Mn_2O_3/ZrO_2$ sorbent

Altamira Instruments

**********

| | |
|---|---|
| DFN Name : | @15wt%MnxOyonZrO2.dfn |
| Comments : | MnxOy on ZrO2 |
| Sample Weight : | 0.1210 (g) |
| Active Component : | Mn @ 15.0 % Loading |
| Calibration Loop Volume : | 50.0 (uL) |
| Loop Temperature : | 25.0 (Deg C) |
| Loop Pressure : | 1.0 (atm) |
| Analytical Gas : | H2 @ 10.0 % |

**********

Uptake : 471.287 (umol/g)

**********

% Reduction : 17.262

6/4/2014 2:57 PM

## $Mn_2O_3/TiO_2$ sorbent

Altamira Instruments

**********

| | |
|---|---|
| DFN Name : | @15wt%MnxOyonTiO2.dfn |
| Comments : | 15wt%Mn_MnxOy on TiO2 |
| Sample Weight : | 0.1209 (g) |
| Active Component : | Mn @ 15.0 % Loading |
| Calibration Loop Volume : | 50.0 (uL) |
| Loop Temperature : | 25.0 (Deg C) |
| Loop Pressure : | 1.0 (atm) |
| Analytical Gas : | H2 @ 10.0 % |

**********

Uptake : 460.071 (umol/g)

**********

% Reduction : 16.851

6/4/2014 3:01 PM

## $Mn_2O_3/CeO_2$ sorbent

Altamira Instruments

**********

| | |
|---|---|
| DFN Name : | @15wt%MnxOyonCeO2.dfn |
| Comments : | 15wt%Mn_MnxOy on CeO2 |
| Sample Weight : | 0.1210 (g) |
| Active Component : | Mn @ 15.0 % Loading |
| Calibration Loop Volume : | 50.0 (uL) |
| Loop Temperature : | 25.0 (Deg C) |
| Loop Pressure : | 1.0 (atm) |
| Analytical Gas : | H2 @ 10.0 % |

**********

Uptake : 774.144 (umol/g)

**********

% Reduction : 28.354

6/4/2014 3:05 PM

## *Appendix I $O_2$ uptake and Dispersion Altamira summary reports*

### $Mn_2O_3/Al_2O_3$ (15wt% Mn) sorbent

Altamira Instruments

**********

DFN Name :
@sample5_15wtMnOonAl2O3_250deg_240min.dfn
Comments : 15wt % MnO on Al2O3
Sample Weight : 0.1208 (g)
Active Component : Mn @ 15.0 % Loading
Calibration Loop Volume : 50.0 (uL)
Loop Temperature : 25.0 (Deg C)
Loop Pressure : 1.0 (atm)
Analytical Gas : O2 @ 100.0 %

**********

Uptake : 19.862 (umol/g)

**********

% Dispersion : 2.910

Hemi-spherical diameter : 3.439E+2 (Angstroms)
Cubic side length : 2.866E+2 (Angstroms)

6/4/2014 3:13 PM


**********

| | |
|---|---|
| DFN Name : | @sample6_15wtMnOonAl2O3.dfn |
| Comments : | 15wt% Mn_MnxOy on Al2O3 |
| Sample Weight : | 0.1210 (g) |
| Active Component : | Mn @ 15.0 % Loading |
| Calibration Loop Volume : | 50.0 (uL) |
| Loop Temperature : | 25.0 (Deg C) |
| Loop Pressure : | 1.0 (atm) |
| Analytical Gas : | O2 @ 100.0 % |

**********

Uptake : 20.157 (umol/g)

**********

% Dispersion : 2.953

Hemi-spherical diameter : 3.388E+2 (Angstroms)
Cubic side length : 2.824E+2 (Angstroms)

6/4/2014 3:19 PM

## $Mn_2O_3/Al_2O_3$ (30wt% Mn) sorbent

Altamira Instruments

**********

| | |
|---|---|
| DFN Name : | @30wtMnOonAl2O3.dfn |
| Comments : | 30wt%Mn_MnxOy on Al2O3 |
| Sample Weight : | 0.1210 (g) |
| Active Component : | Mn @ 30.0 % Loading |
| Calibration Loop Volume : | 50.0 (uL) |
| Loop Temperature : | 25.0 (Deg C) |
| Loop Pressure : | 1.0 (atm) |
| Analytical Gas : | O2 @ 100.0 % |

**********

Uptake : 43.461 (umol/g)

**********

% Dispersion : 3.184

Hemi-spherical diameter : 3.143E+2 (Angstroms)
Cubic side length : 2.619E+2 (Angstroms)

6/4/2014 3:25 PM


**********

| | |
|---|---|
| DFN Name : | @sample2_30wtMnOonAl2O3.dfn |
| Comments : | 30wt% Mn_MnxOy on Al2O3 |
| Sample Weight : | 0.1215 (g) |
| Active Component : | Mn @ 30.0 % Loading |
| Calibration Loop Volume : | 50.0 (uL) |
| Loop Temperature : | 25.0 (Deg C) |
| Loop Pressure : | 1.0 (atm) |
| Analytical Gas : | O2 @ 100.0 % |

**********

Uptake : 37.488 (umol/g)

**********

% Dispersion : 2.746

Hemi-spherical diameter : 3.644E+2 (Angstroms)
Cubic side length : 3.036E+2 (Angstroms)

6/4/2014 3:35 PM

## *Appendix J Sorption cycle measurement results for empty reactor*

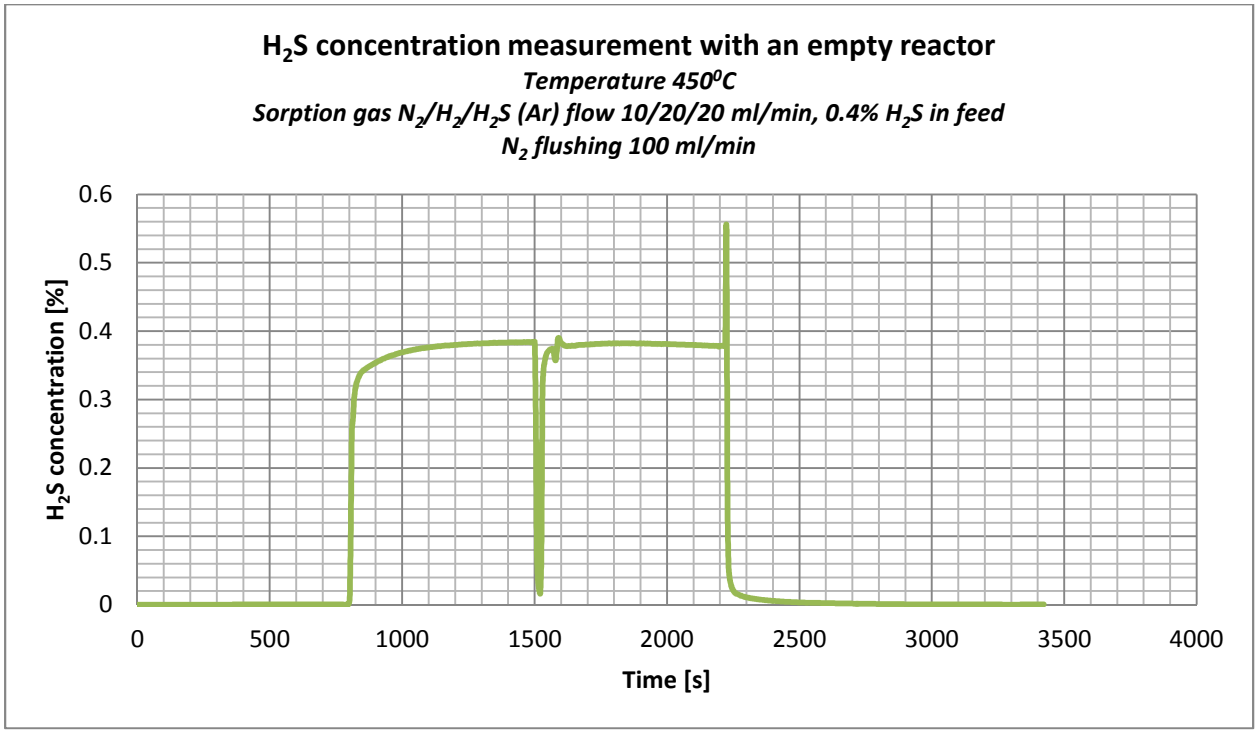


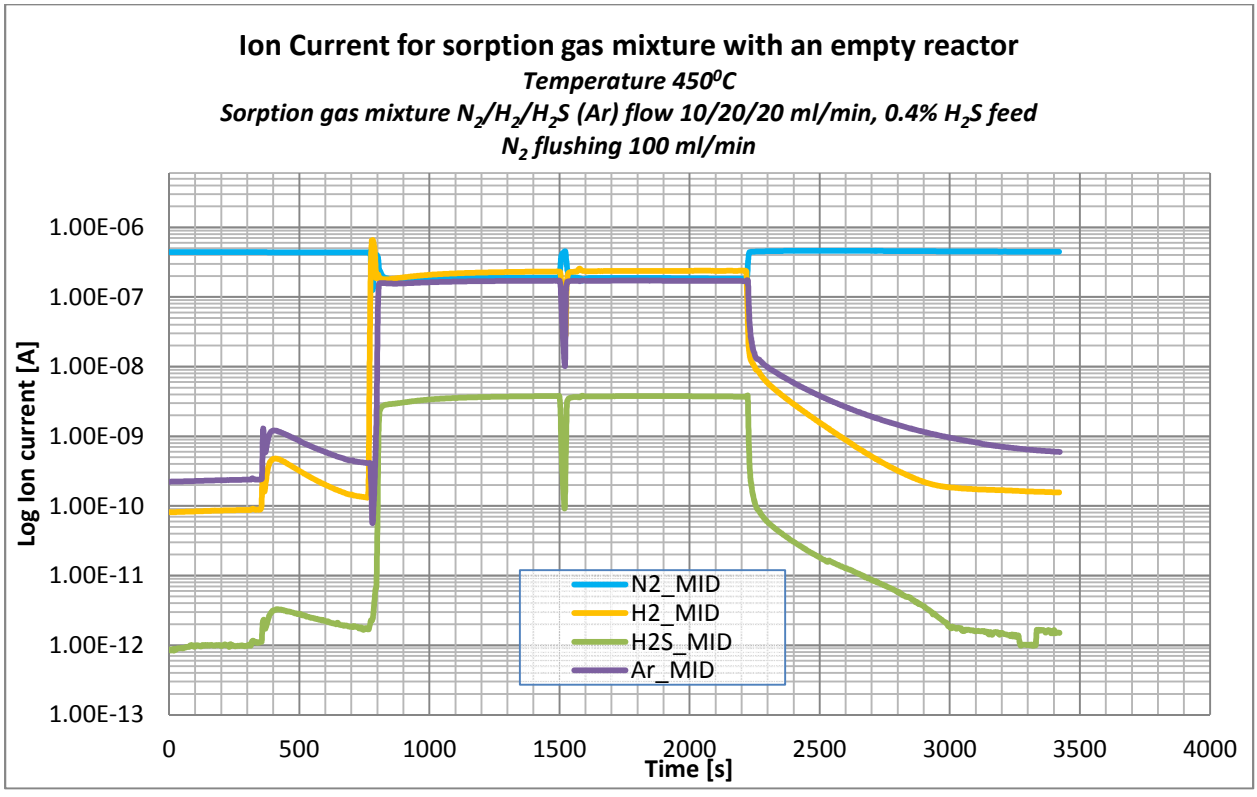

## *Appendix K Sorption cycle measurement results with an inert*

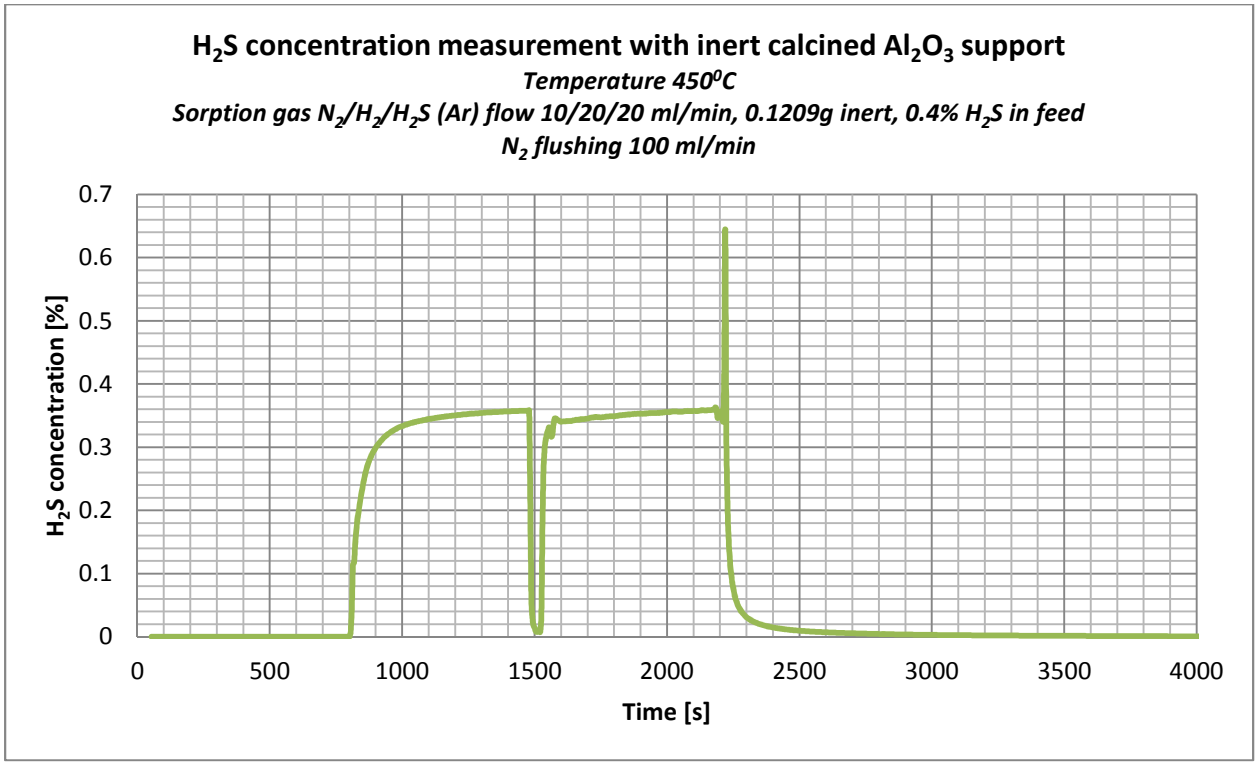


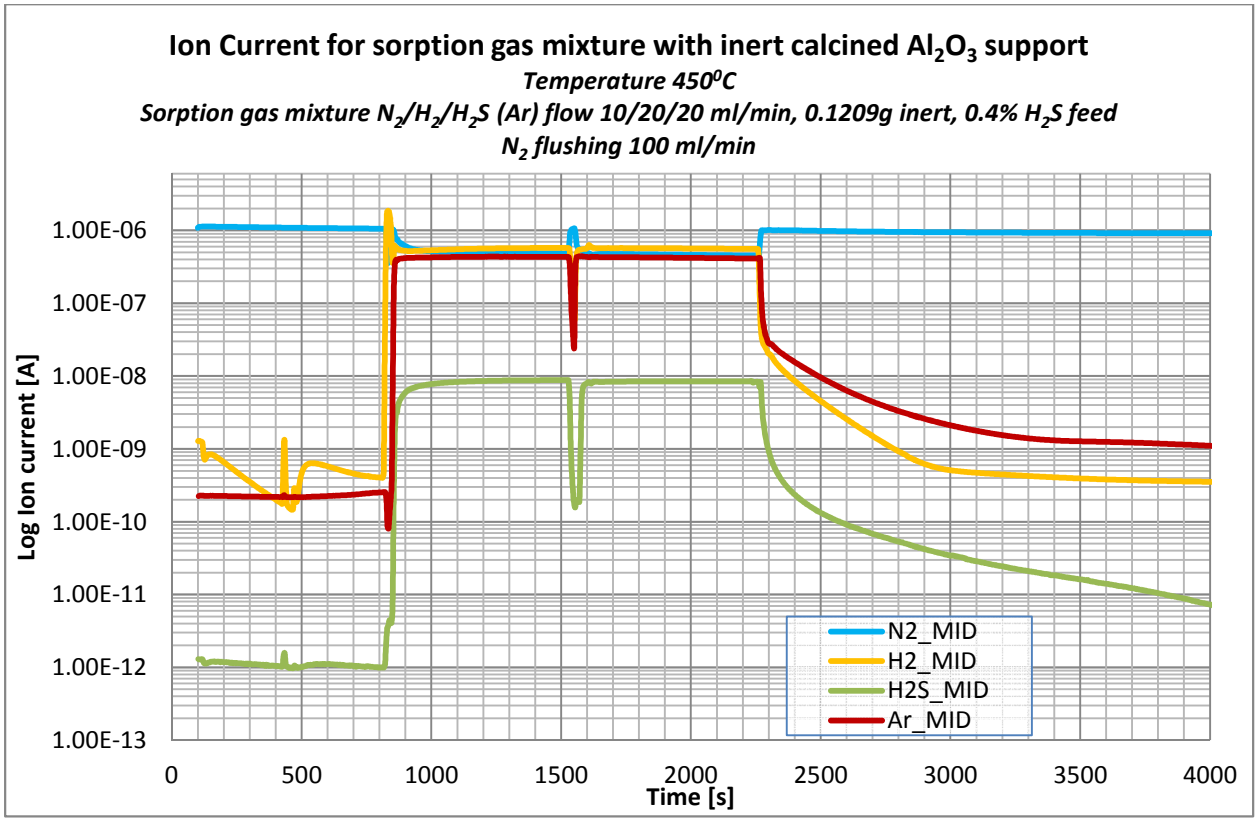

## *Appendix L Sorption cycle measurement results for Result-reproducibility experiment*

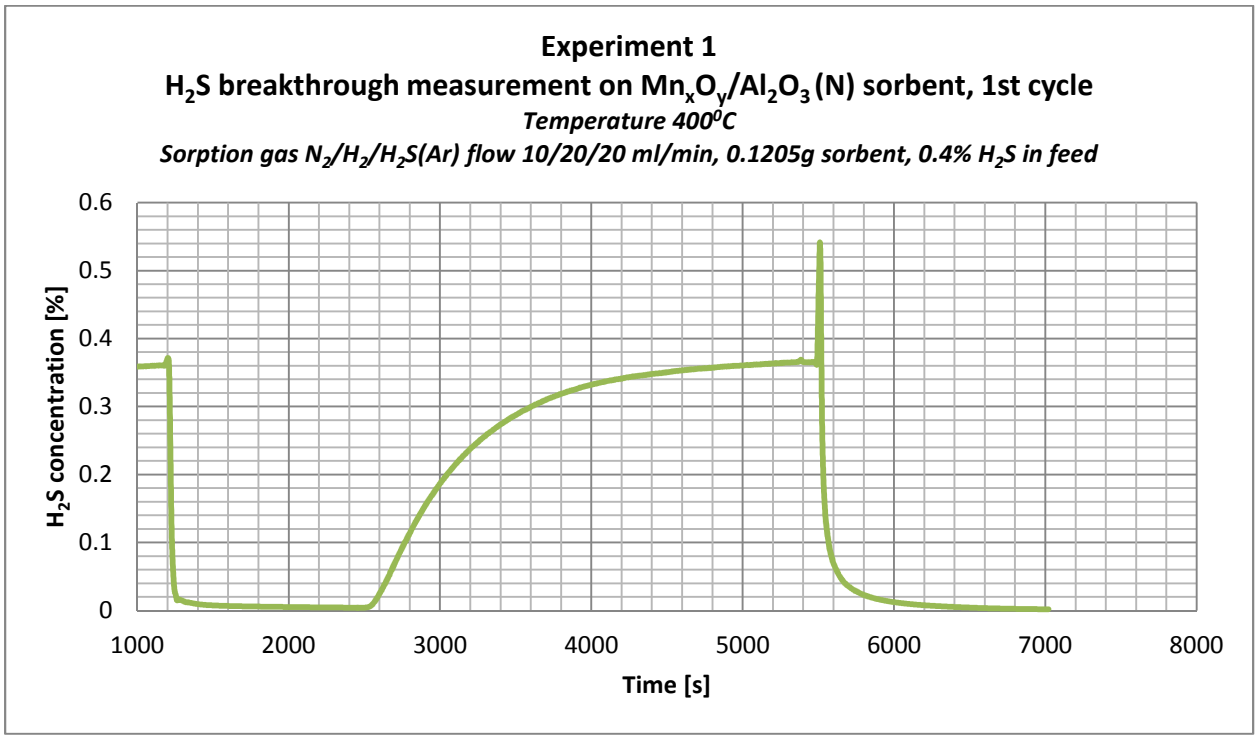


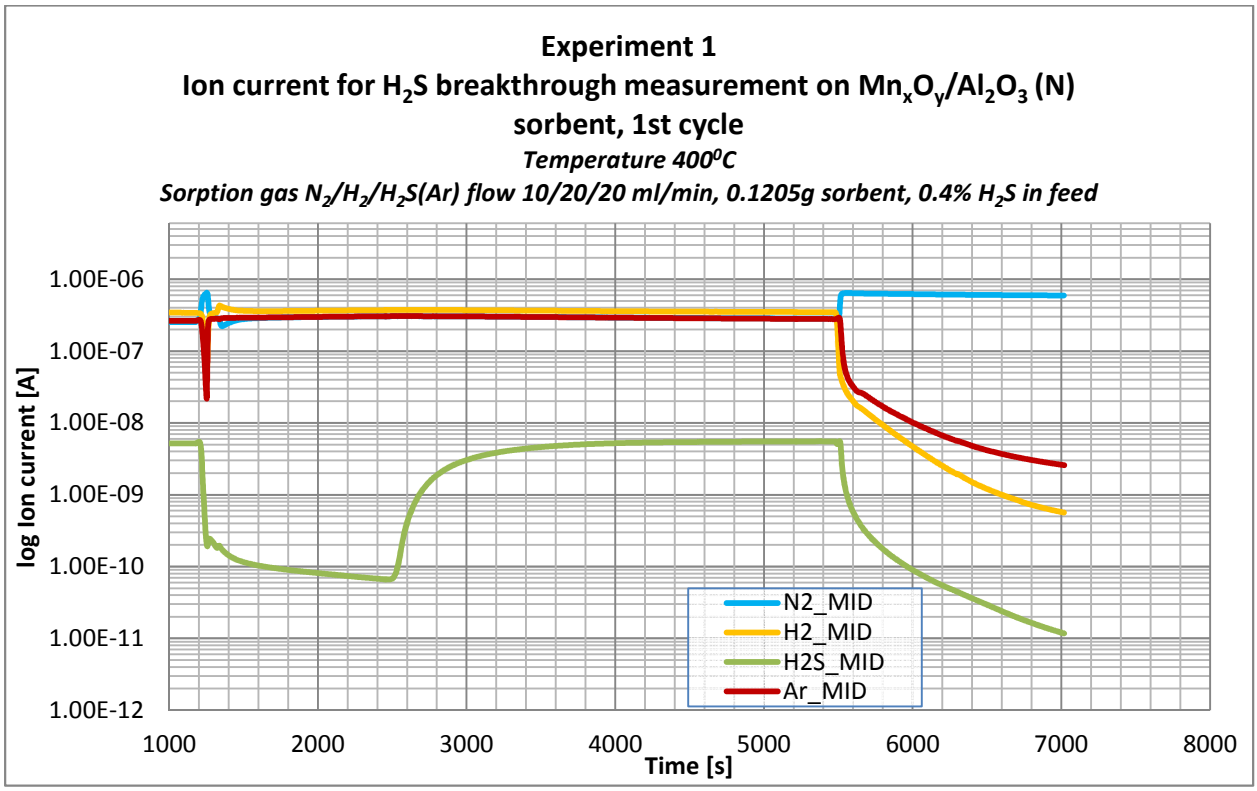

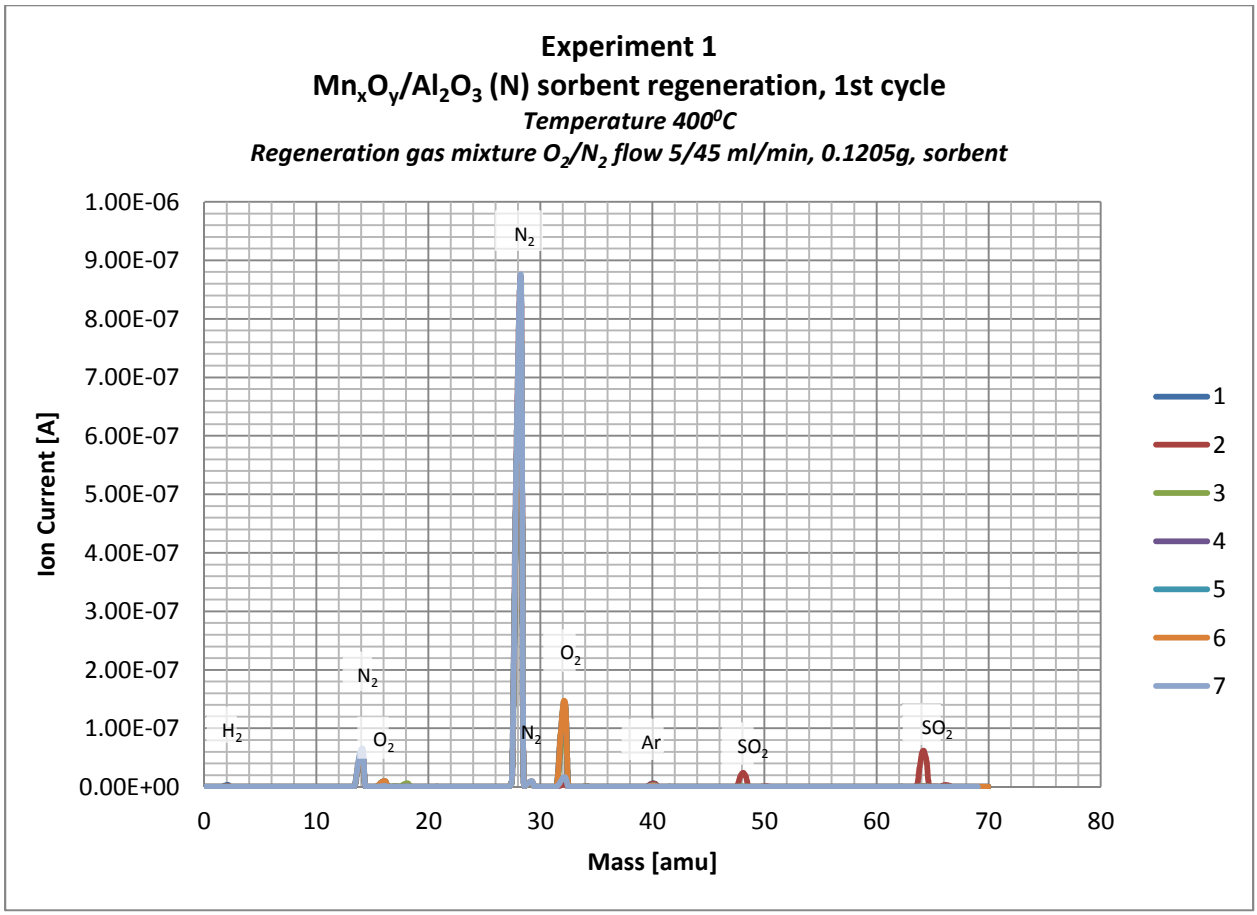
Experiment 1
Mn$_x$O$_y$/Al$_2$O$_3$ (N) sorbent regeneration, 1st cycle
Temperature 400$^0$C
Regeneration gas mixture O$_2$/N$_2$ flow 5/45 ml/min, 0.1205g, sorbent
Ion Current [A]
1.00E-06
9.00E-07
8.00E-07
7.00E-07
6.00E-07
5.00E-07
4.00E-07
3.00E-07
2.00E-07
1.00E-07
0.00E+00
0
10
20
30
40
50
60
70
80
Mass [amu]
H$_2$
N$_2$
O$_2$
N$_2$
N$_2$
O$_2$
Ar
SO$_2$
SO$_2$
1
2
3
4
5
6
7

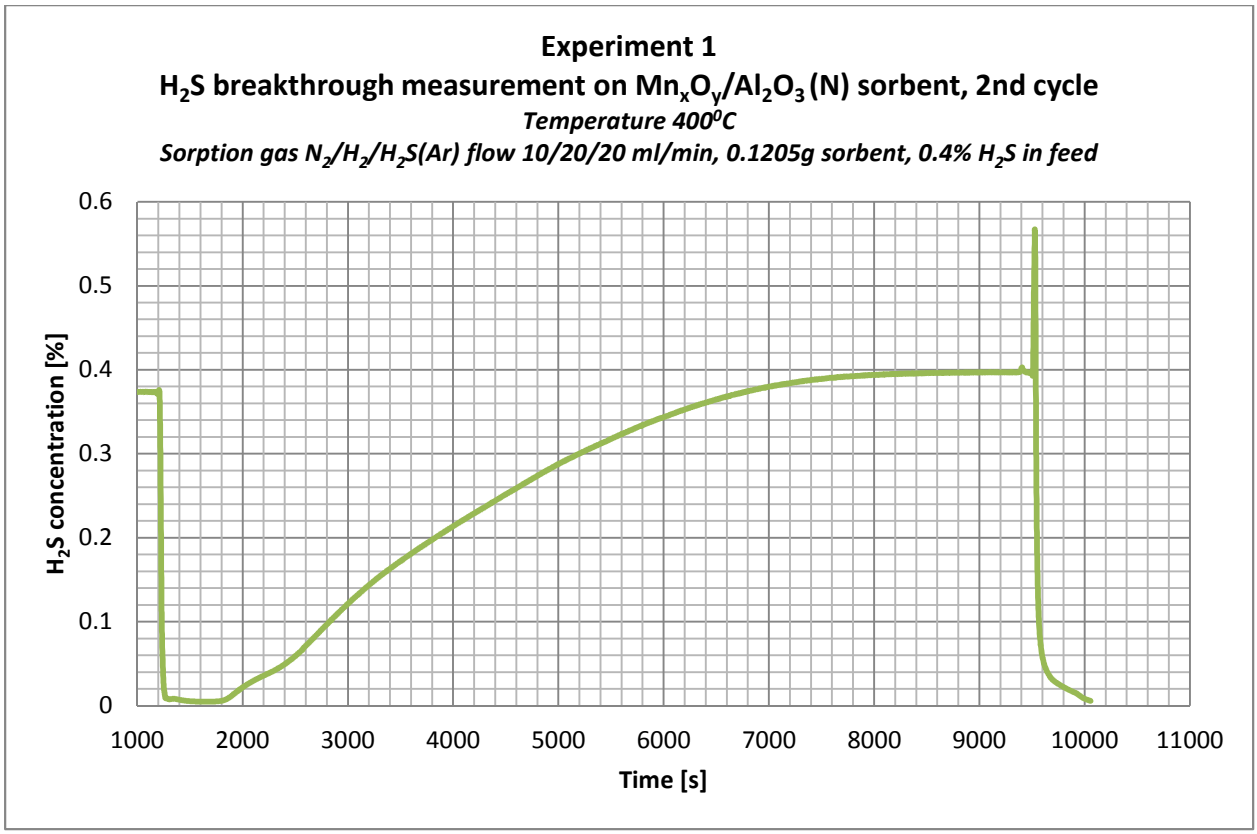
Experiment 1
H2S breakthrough measurement on MnxOy/Al2O3 (N) sorbent, 2nd cycle
Temperature 400⁰C
Sorption gas N2/H2/H2S(Ar) flow 10/20/20 ml/min, 0.1205g sorbent, 0.4% H2S in feed
H2S concentration [%]
0.6
0.5
0.4
0.3
0.2
0.1
0
1000
2000
3000
4000
5000
6000
7000
8000
9000
10000
11000
Time [s]

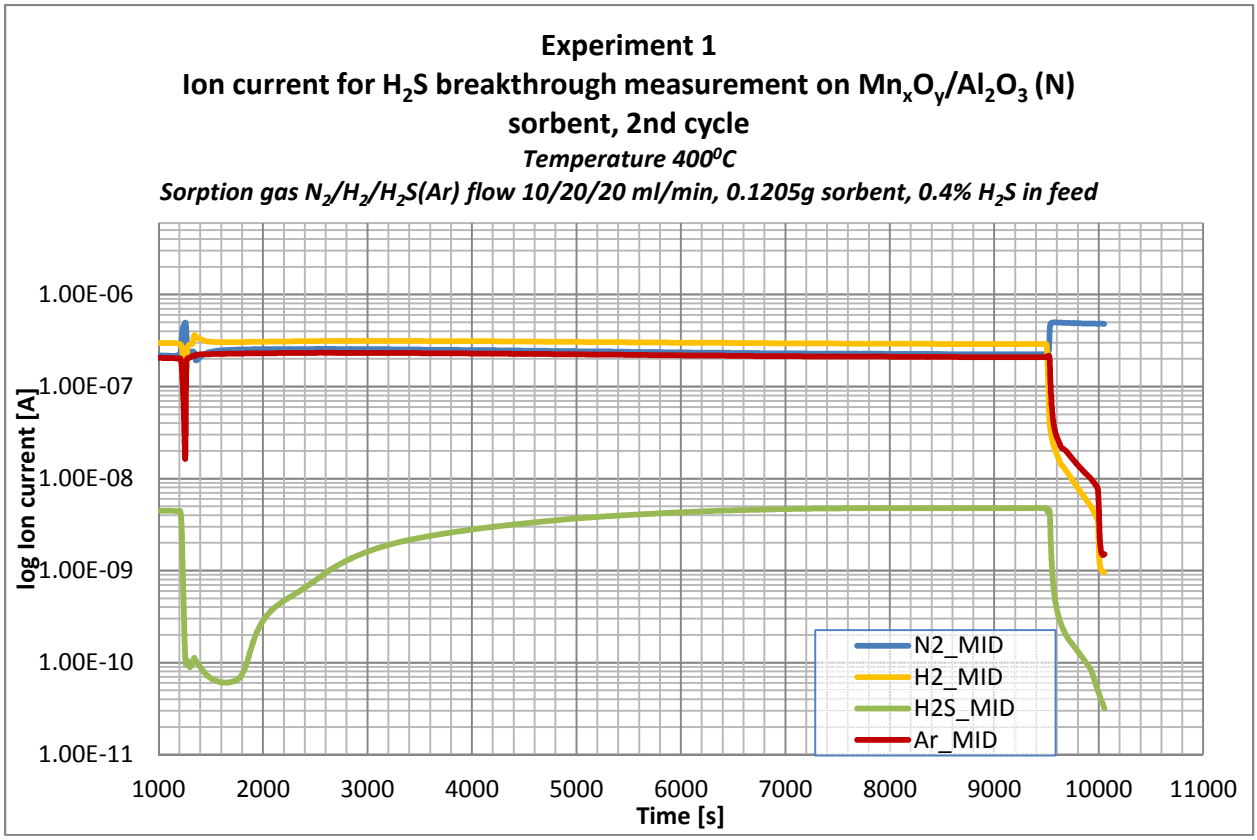
Experiment 1
Ion current for H2S breakthrough measurement on MnxOy/Al2O3 (N) sorbent, 2nd cycle
Temperature 400⁰C
Sorption gas N2/H2/H2S(Ar) flow 10/20/20 ml/min, 0.1205g sorbent, 0.4% H2S in feed
log Ion current [A]
1.00E-06
1.00E-07
1.00E-08
1.00E-09
1.00E-10
1.00E-11
1000
2000
3000
4000
5000
6000
7000
8000
9000
10000
11000
Time [s]
N2_MID
H2_MID
H2S_MID
Ar_MID

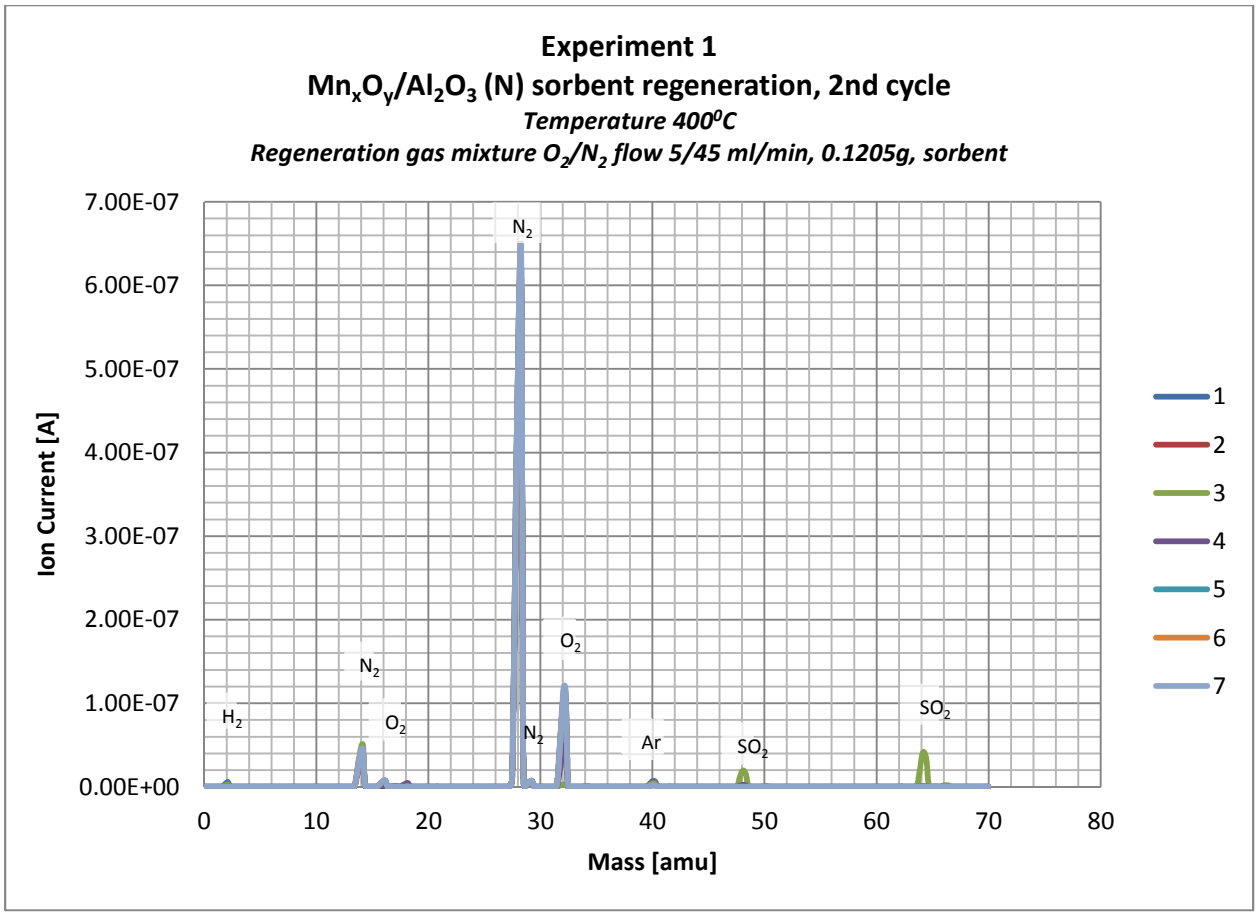
Experiment 1
Mn$_x$O$_y$/Al$_2$O$_3$ (N) sorbent regeneration, 2nd cycle
Temperature 400$^0$C
Regeneration gas mixture O$_2$/N$_2$ flow 5/45 ml/min, 0.1205g, sorbent
Ion Current [A]
7.00E-07
6.00E-07
5.00E-07
4.00E-07
3.00E-07
2.00E-07
1.00E-07
0.00E+00
0
10
20
30
40
50
60
70
80
Mass [amu]
H$_2$
N$_2$
O$_2$
N$_2$
O$_2$
N$_2$
Ar
SO$_2$
SO$_2$
1
2
3
4
5
6
7

**Experiment 1**

**$H_2S$ breakthrough measurement on $Mn_xO_y/Al_2O_3$ (N) sorbent, 3rd cycle**

***Temperature 400$^0$C***

***Sorption gas $N_2/H_2/H_2S(Ar)$ flow 10/20/20 ml/min, 0.1205g sorbent, 0.4% $H_2S$ in feed***

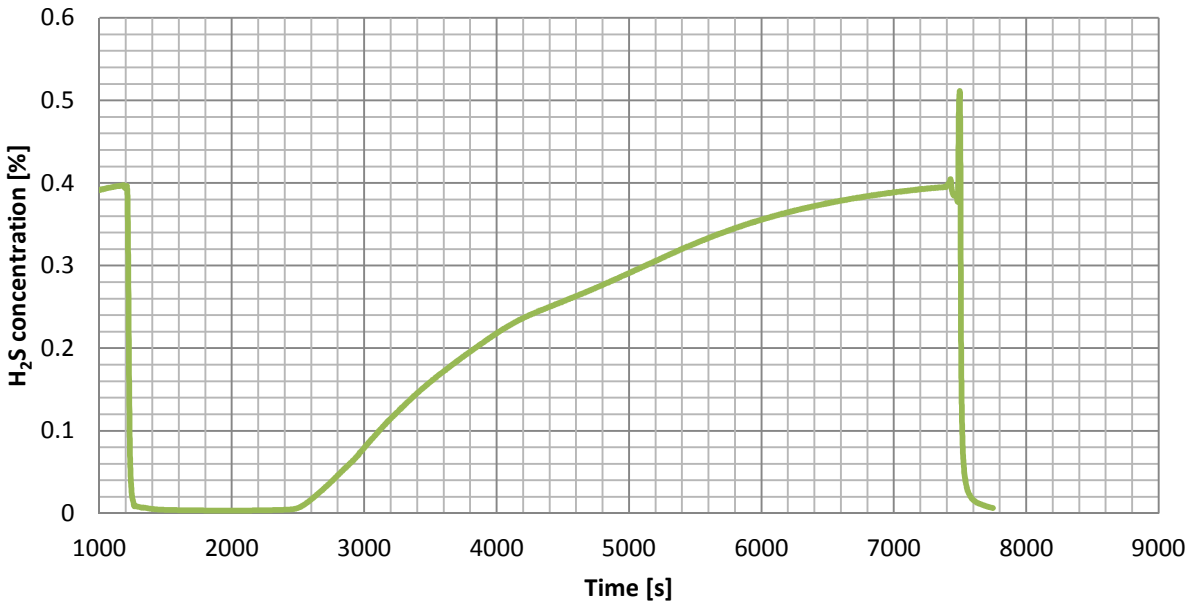


**Experiment 1**

**Ion current for $H_2S$ breakthrough measurement on $Mn_xO_y/Al_2O_3$ (N) sorbent, 3rd cycle**

***Temperature 400$^0$C***

***Sorption gas $N_2/H_2/H_2S(Ar)$ flow 10/20/20 ml/min, 0.1205g sorbent, 0.4% $H_2S$ in feed***

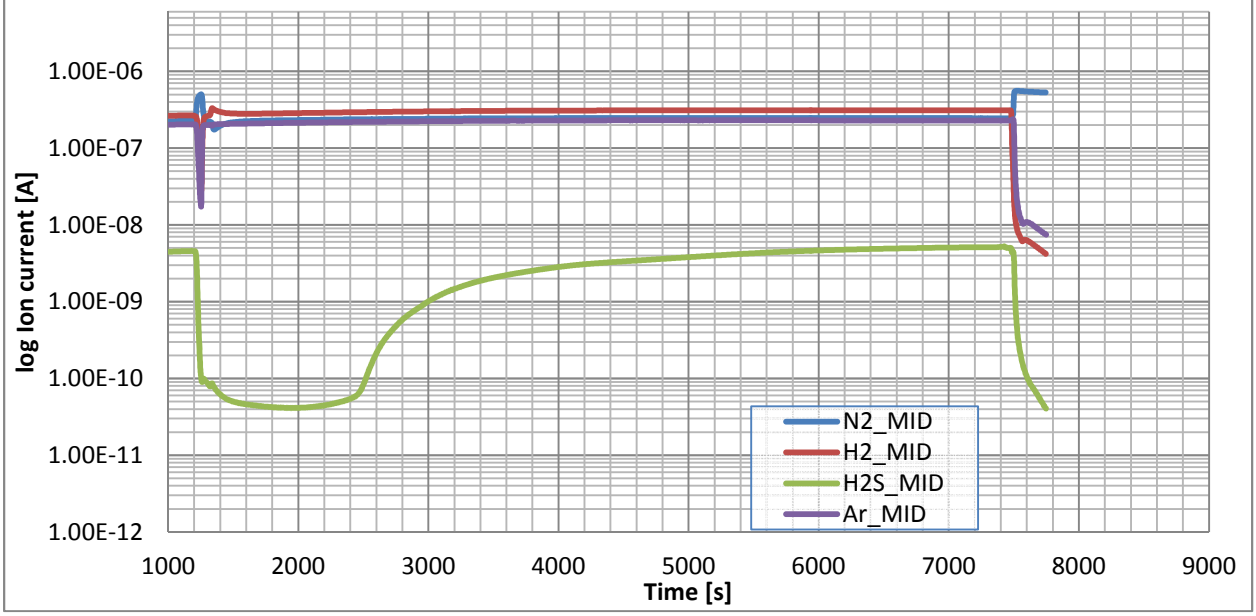

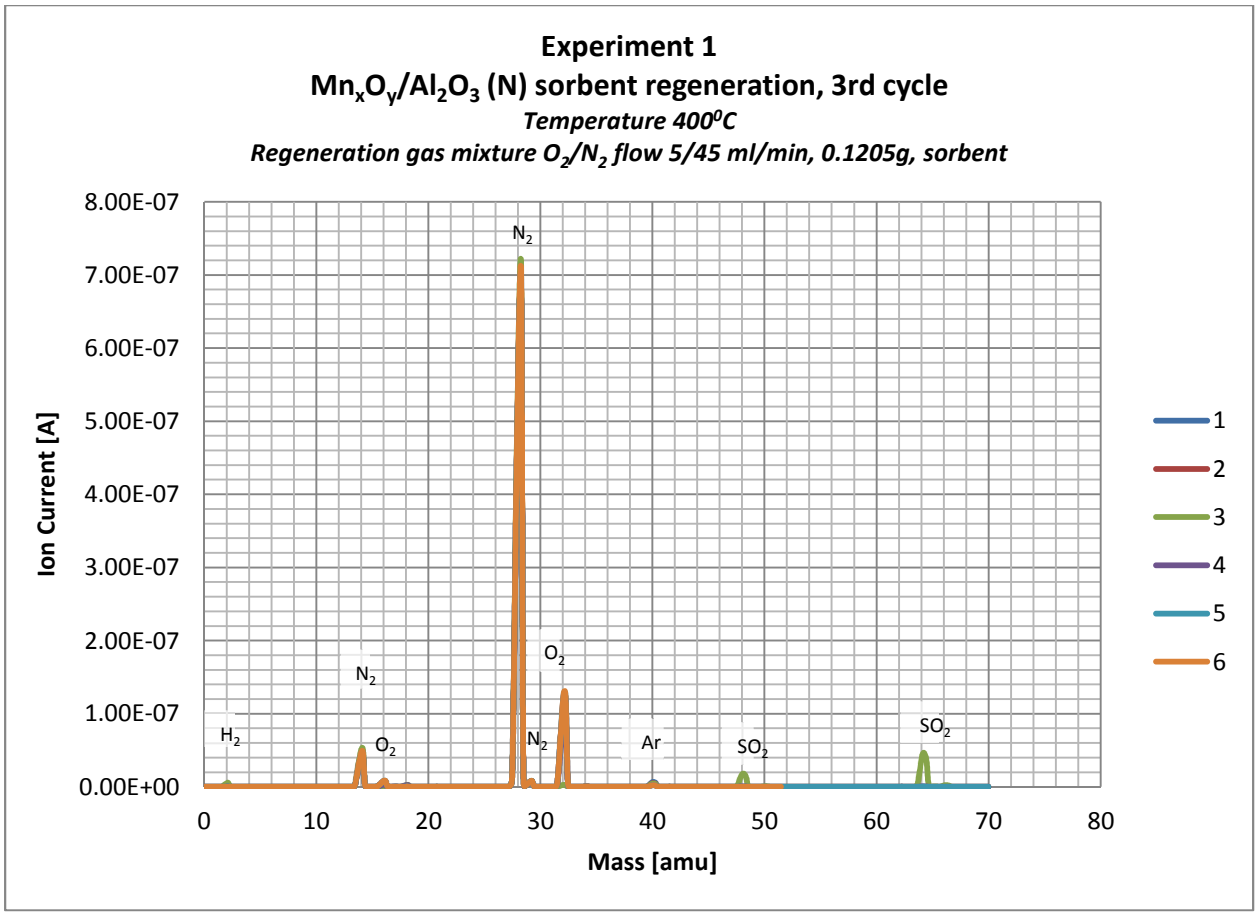
Experiment 1
Mn$_x$O$_y$/Al$_2$O$_3$ (N) sorbent regeneration, 3rd cycle
Temperature 400$^0$C
Regeneration gas mixture O$_2$/N$_2$ flow 5/45 ml/min, 0.1205g, sorbent
Ion Current [A]
8.00E-07
7.00E-07
6.00E-07
5.00E-07
4.00E-07
3.00E-07
2.00E-07
1.00E-07
0.00E+00
0
10
20
30
40
50
60
70
80
Mass [amu]
H$_2$
N$_2$
O$_2$
N$_2$
O$_2$
N$_2$
Ar
SO$_2$
SO$_2$
1
2
3
4
5
6

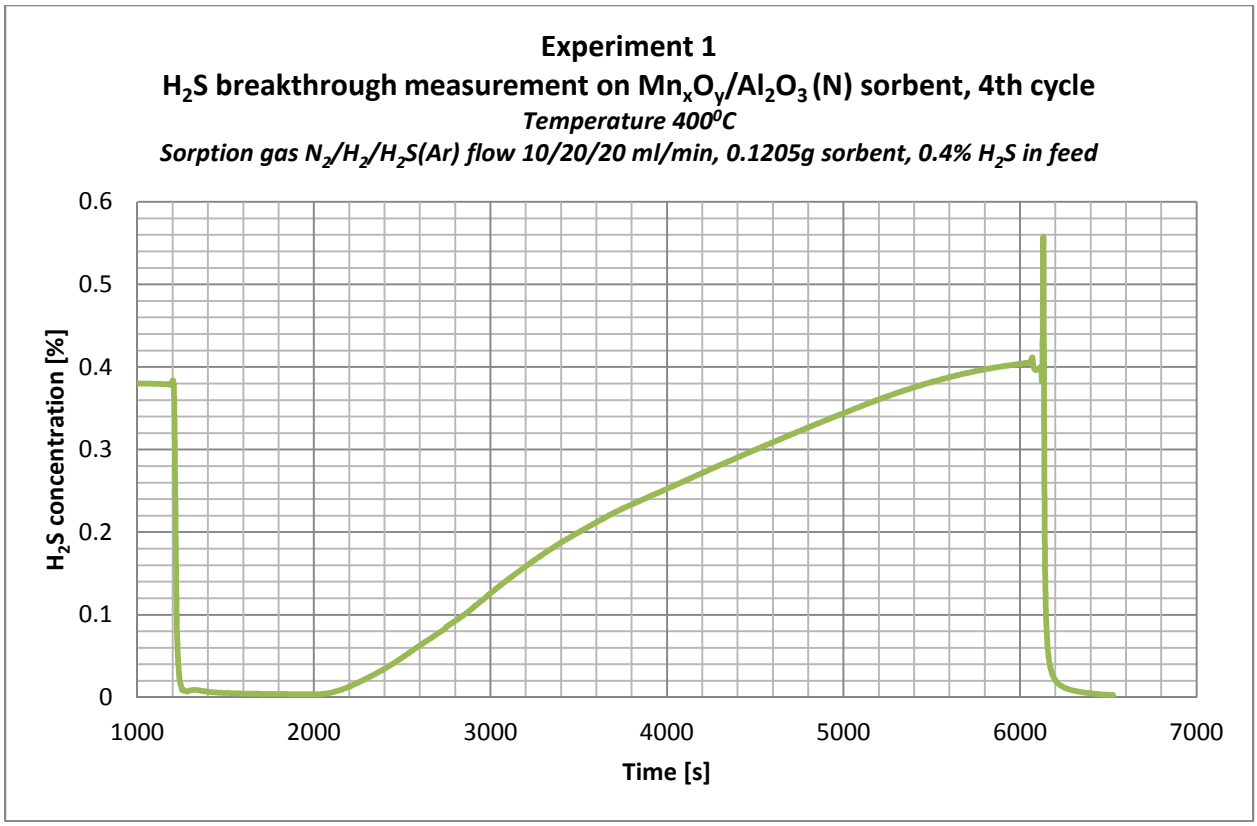
Experiment 1
H2S breakthrough measurement on MnxOy/Al2O3 (N) sorbent, 4th cycle
Temperature 400⁰C
Sorption gas N2/H2/H2S(Ar) flow 10/20/20 ml/min, 0.1205g sorbent, 0.4% H2S in feed
H2S concentration [%]
0.6
0.5
0.4
0.3
0.2
0.1
0
1000
2000
3000
4000
5000
6000
7000
Time [s]

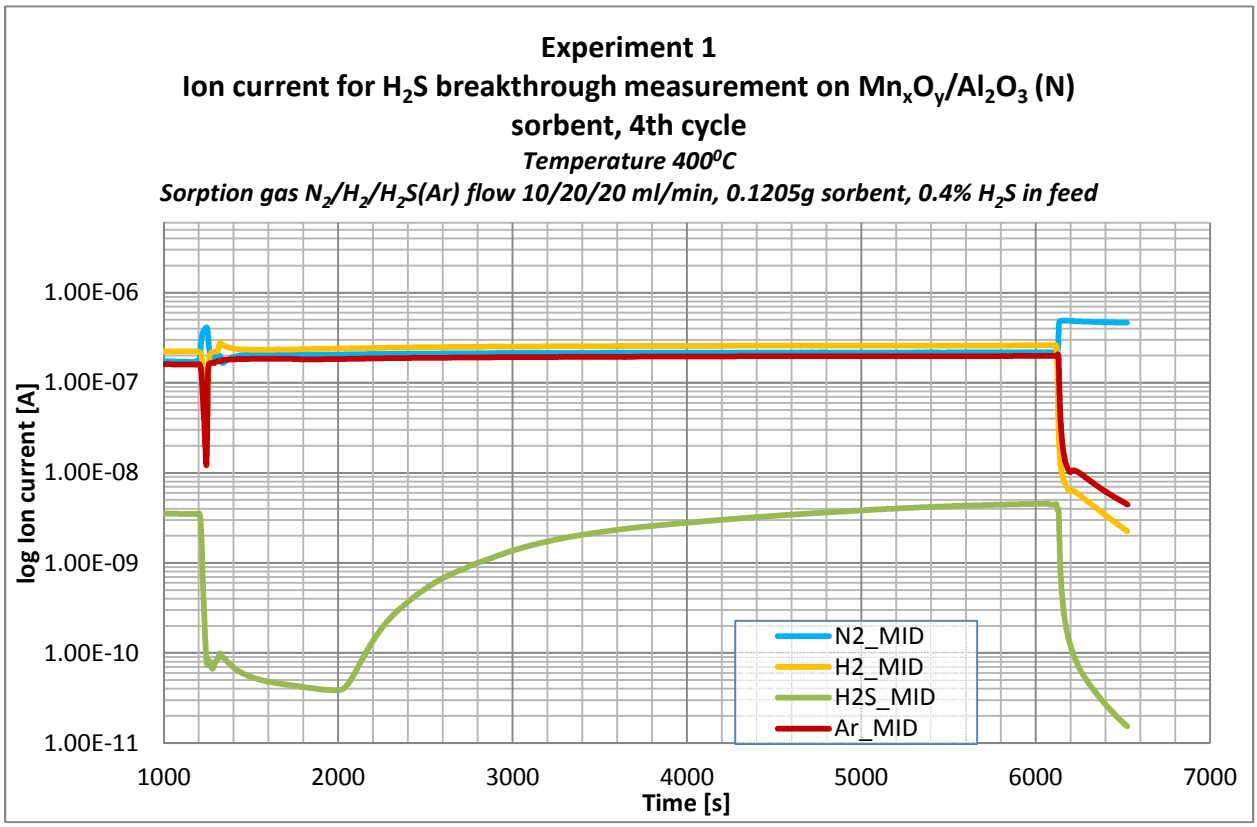
Experiment 1
Ion current for H2S breakthrough measurement on MnxOy/Al2O3 (N) sorbent, 4th cycle
Temperature 400⁰C
Sorption gas N2/H2/H2S(Ar) flow 10/20/20 ml/min, 0.1205g sorbent, 0.4% H2S in feed
log Ion current [A]
1.00E-06
1.00E-07
1.00E-08
1.00E-09
1.00E-10
1.00E-11
1000
2000
3000
4000
5000
6000
7000
Time [s]
N2_MID
H2_MID
H2S_MID
Ar_MID

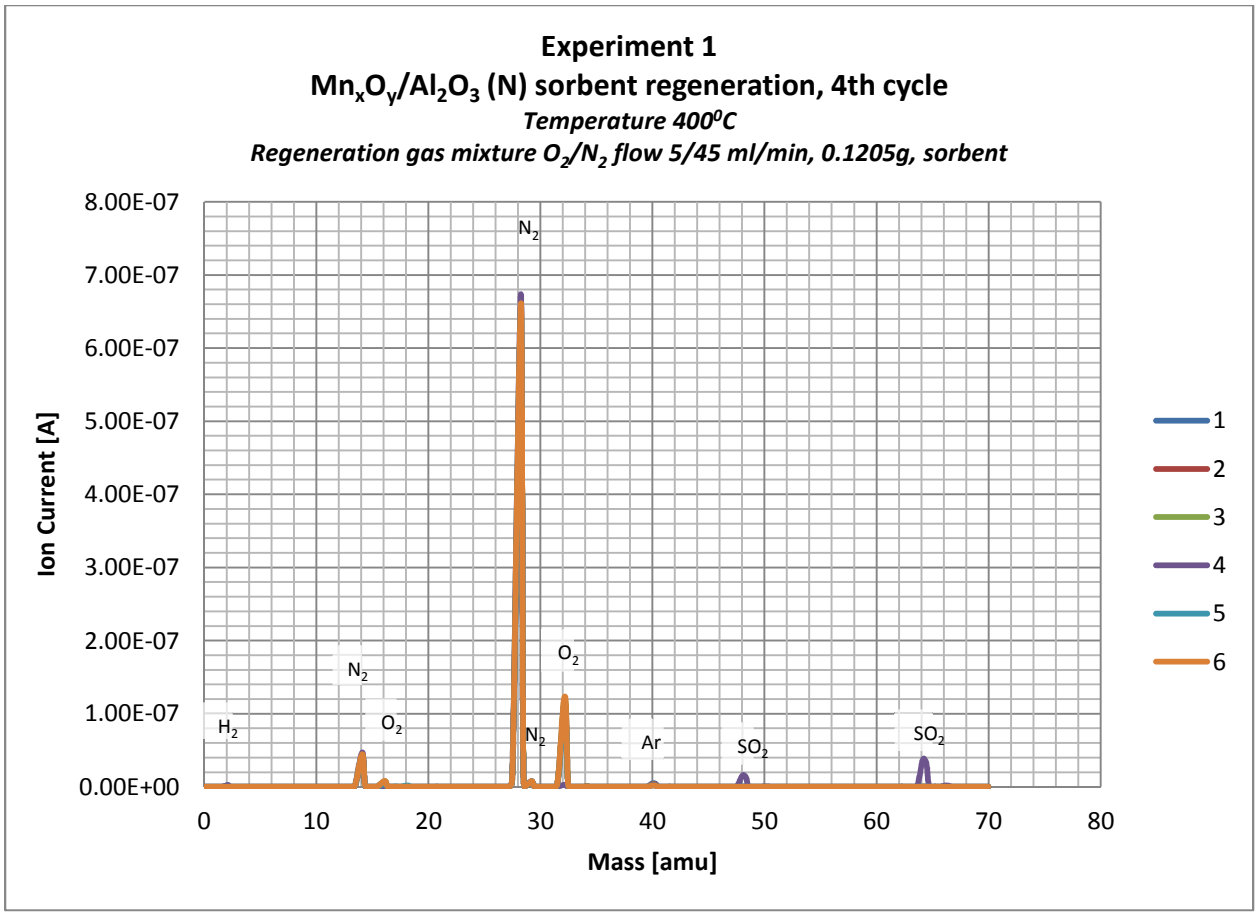
Experiment 1
Mn$_x$O$_y$/Al$_2$O$_3$ (N) sorbent regeneration, 4th cycle
Temperature 400$^0$C
Regeneration gas mixture O$_2$/N$_2$ flow 5/45 ml/min, 0.1205g, sorbent
Ion Current [A]
8.00E-07
7.00E-07
6.00E-07
5.00E-07
4.00E-07
3.00E-07
2.00E-07
1.00E-07
0.00E+00
0
10
20
30
40
50
60
70
80
Mass [amu]
N$_2$
O$_2$
H$_2$
Ar
SO$_2$
1
2
3
4
5
6

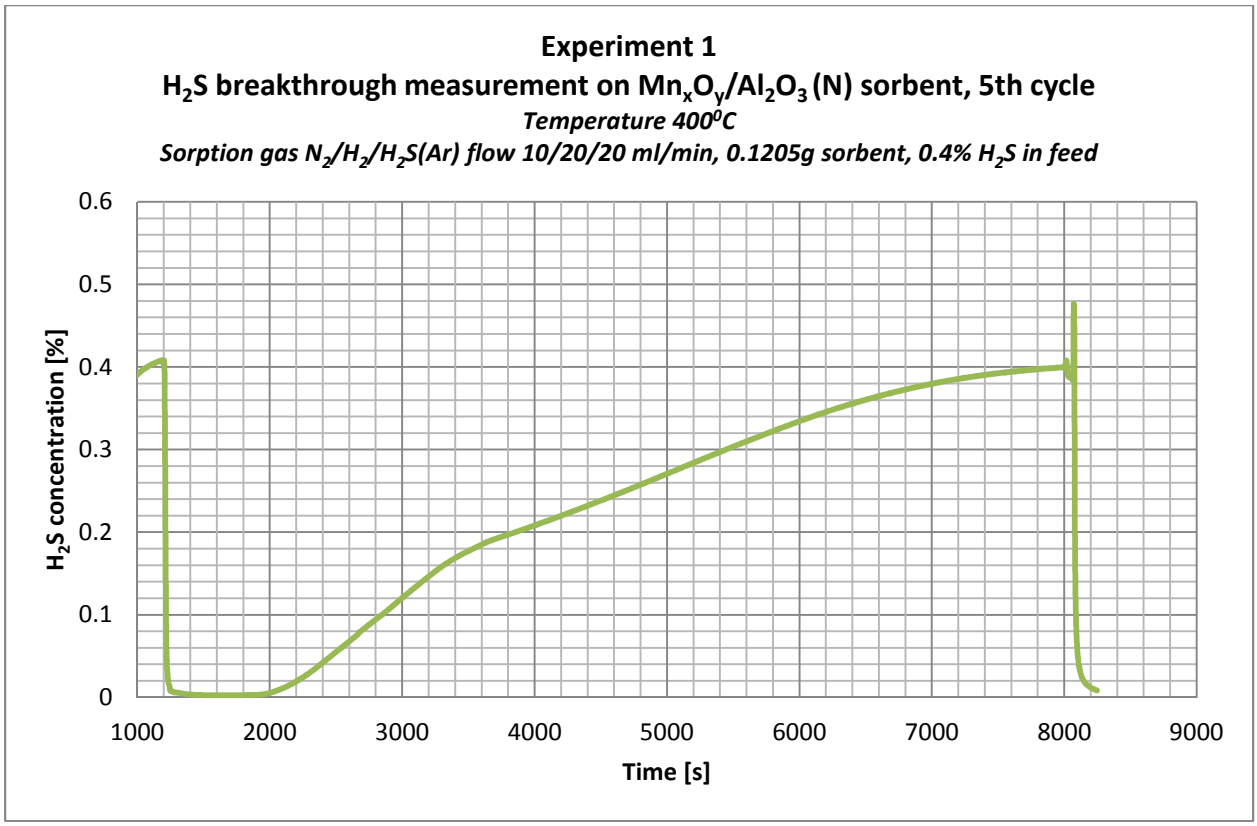
Experiment 1
H2S breakthrough measurement on MnxOy/Al2O3 (N) sorbent, 5th cycle
Temperature 400⁰C
Sorption gas N2/H2/H2S(Ar) flow 10/20/20 ml/min, 0.1205g sorbent, 0.4% H2S in feed
H2S concentration [%]
0.6
0.5
0.4
0.3
0.2
0.1
0
1000
2000
3000
4000
5000
6000
7000
8000
9000
Time [s]

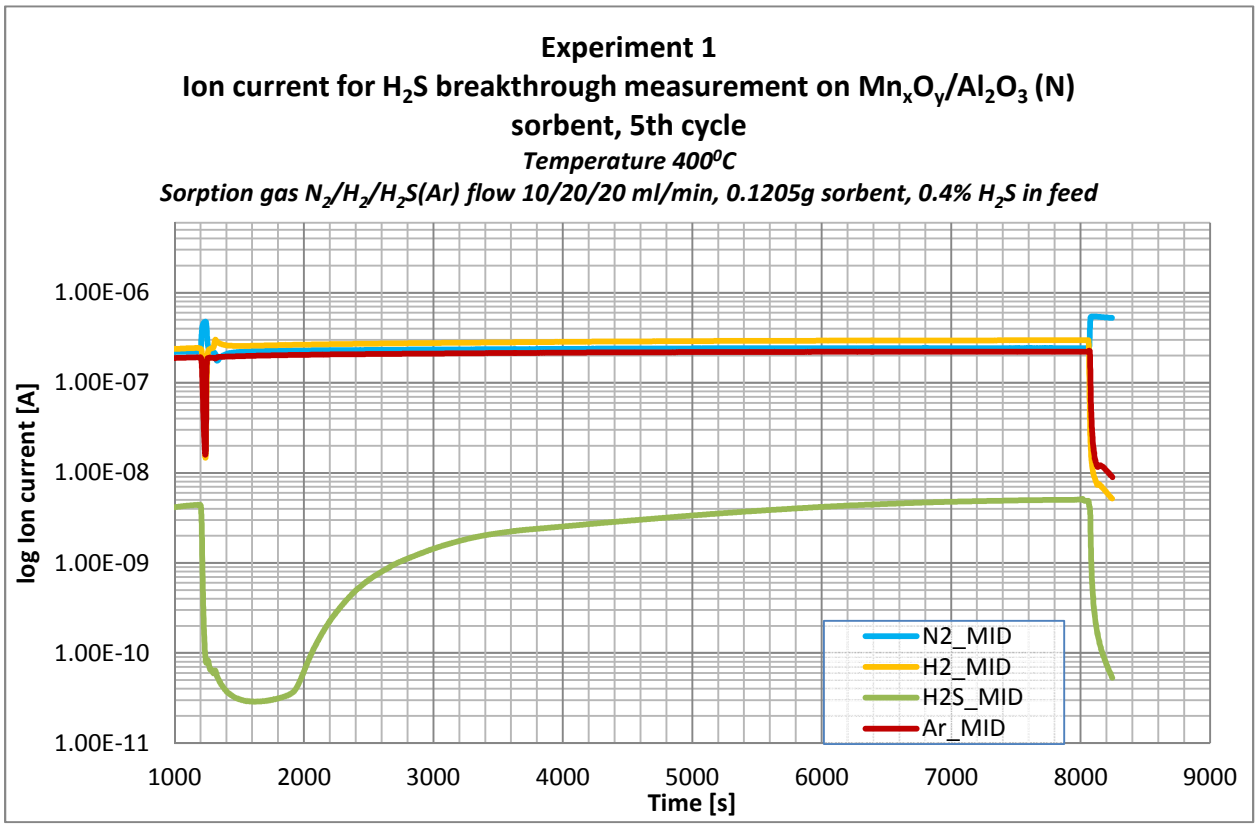
Experiment 1
Ion current for H2S breakthrough measurement on MnxOy/Al2O3 (N) sorbent, 5th cycle
Temperature 400⁰C
Sorption gas N2/H2/H2S(Ar) flow 10/20/20 ml/min, 0.1205g sorbent, 0.4% H2S in feed
log Ion current [A]
1.00E-06
1.00E-07
1.00E-08
1.00E-09
1.00E-10
1.00E-11
1000
2000
3000
4000
5000
6000
7000
8000
9000
Time [s]
N2_MID
H2_MID
H2S_MID
Ar_MID

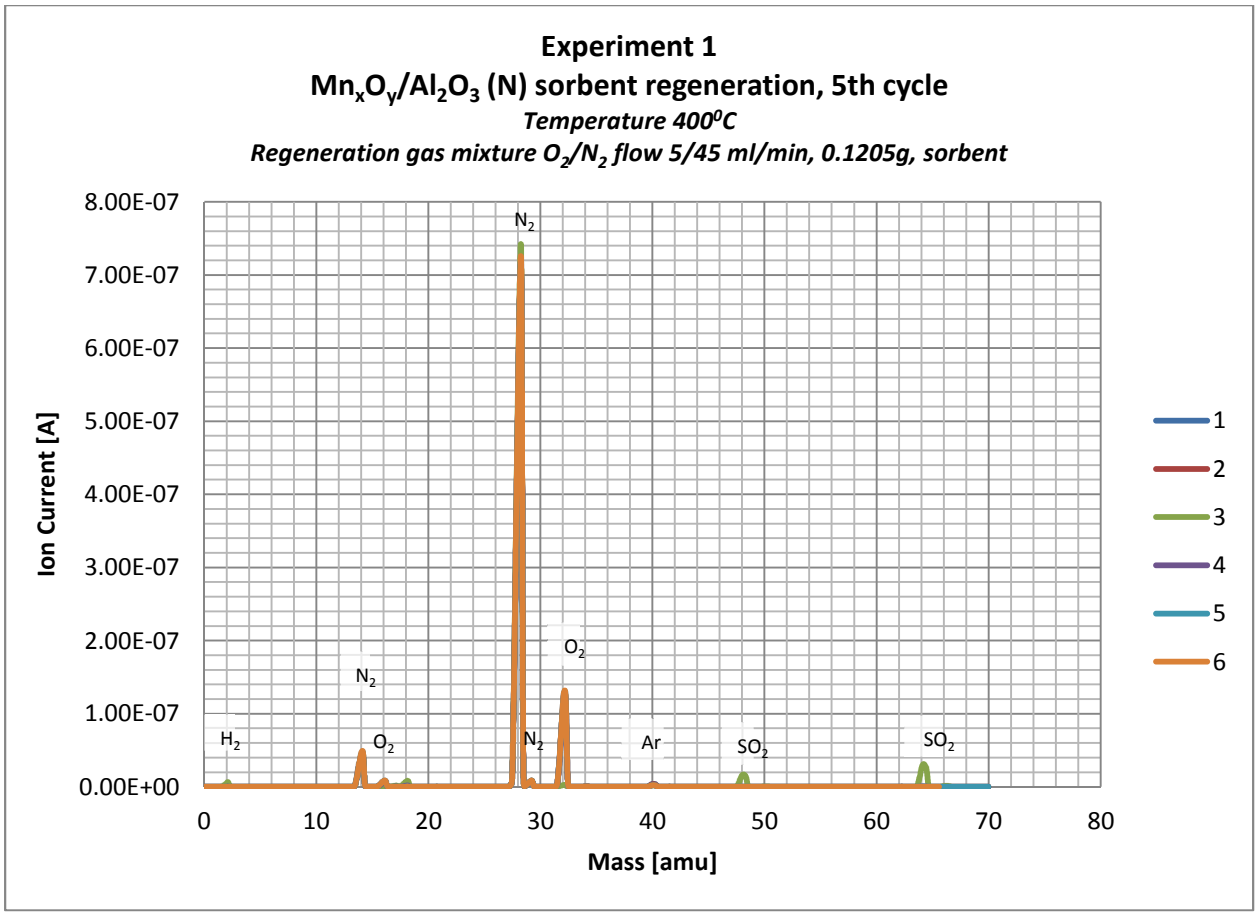
Experiment 1
Mn$_x$O$_y$/Al$_2$O$_3$ (N) sorbent regeneration, 5th cycle
Temperature 400$^0$C
Regeneration gas mixture O$_2$/N$_2$ flow 5/45 ml/min, 0.1205g, sorbent
Ion Current [A]
8.00E-07
7.00E-07
6.00E-07
5.00E-07
4.00E-07
3.00E-07
2.00E-07
1.00E-07
0.00E+00
0
10
20
30
40
50
60
70
80
Mass [amu]
N$_2$
O$_2$
N$_2$
H$_2$
O$_2$
N$_2$
Ar
SO$_2$
SO$_2$
1
2
3
4
5
6

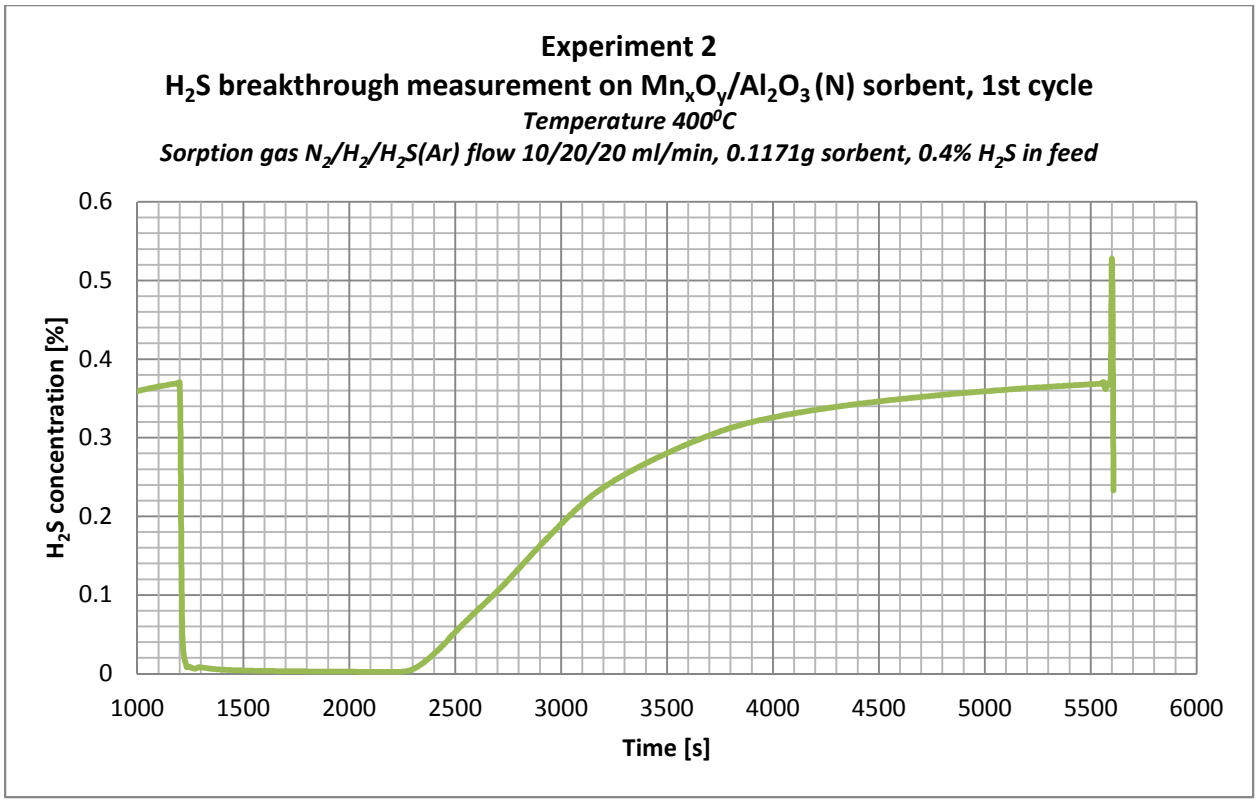
Experiment 2
H2S breakthrough measurement on MnxOy/Al2O3 (N) sorbent, 1st cycle
Temperature 400⁰C
Sorption gas N2/H2/H2S(Ar) flow 10/20/20 ml/min, 0.1171g sorbent, 0.4% H2S in feed
H2S concentration [%]
0.6
0.5
0.4
0.3
0.2
0.1
0
1000
1500
2000
2500
3000
3500
4000
4500
5000
5500
6000
Time [s]

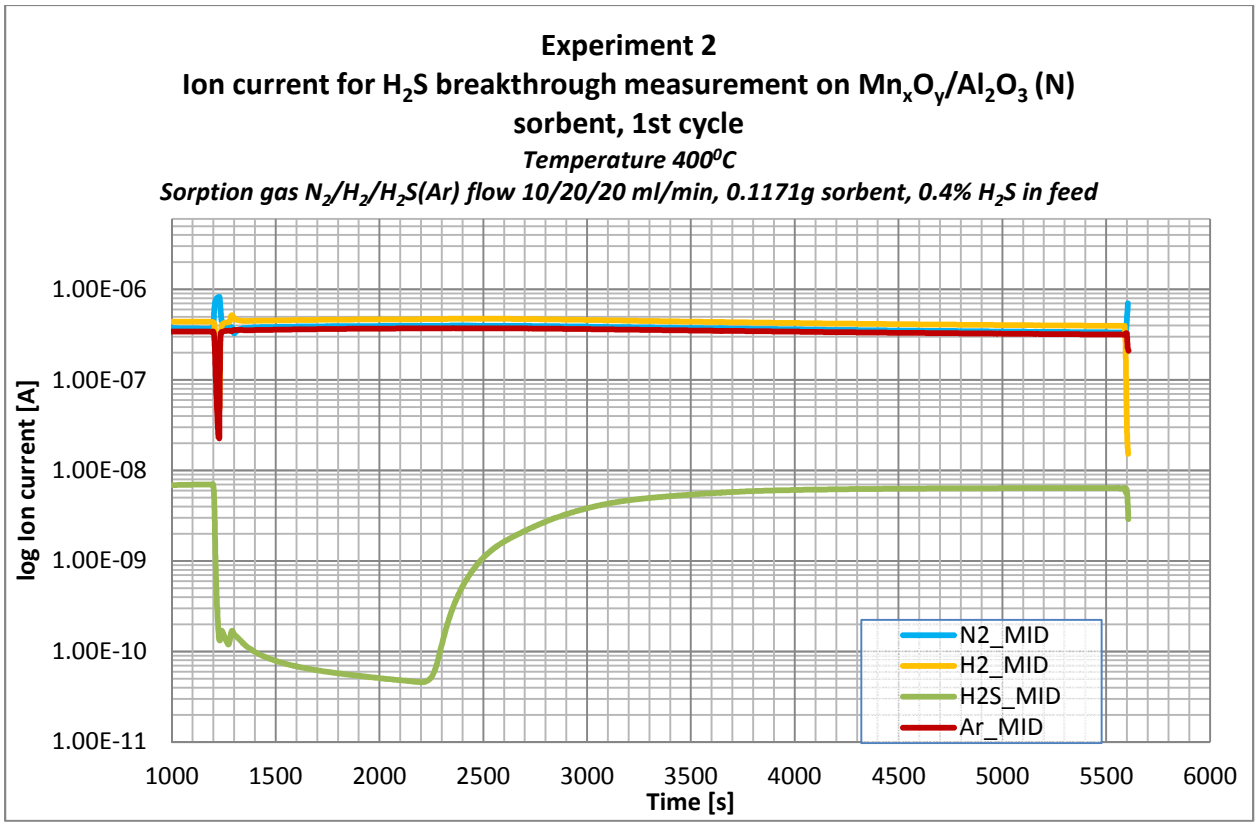
Experiment 2
Ion current for H2S breakthrough measurement on MnxOy/Al2O3 (N) sorbent, 1st cycle
Temperature 400⁰C
Sorption gas N2/H2/H2S(Ar) flow 10/20/20 ml/min, 0.1171g sorbent, 0.4% H2S in feed
log Ion current [A]
1.00E-06
1.00E-07
1.00E-08
1.00E-09
1.00E-10
1.00E-11
1000
1500
2000
2500
3000
3500
4000
4500
5000
5500
6000
Time [s]
N2_MID
H2_MID
H2S_MID
Ar_MID

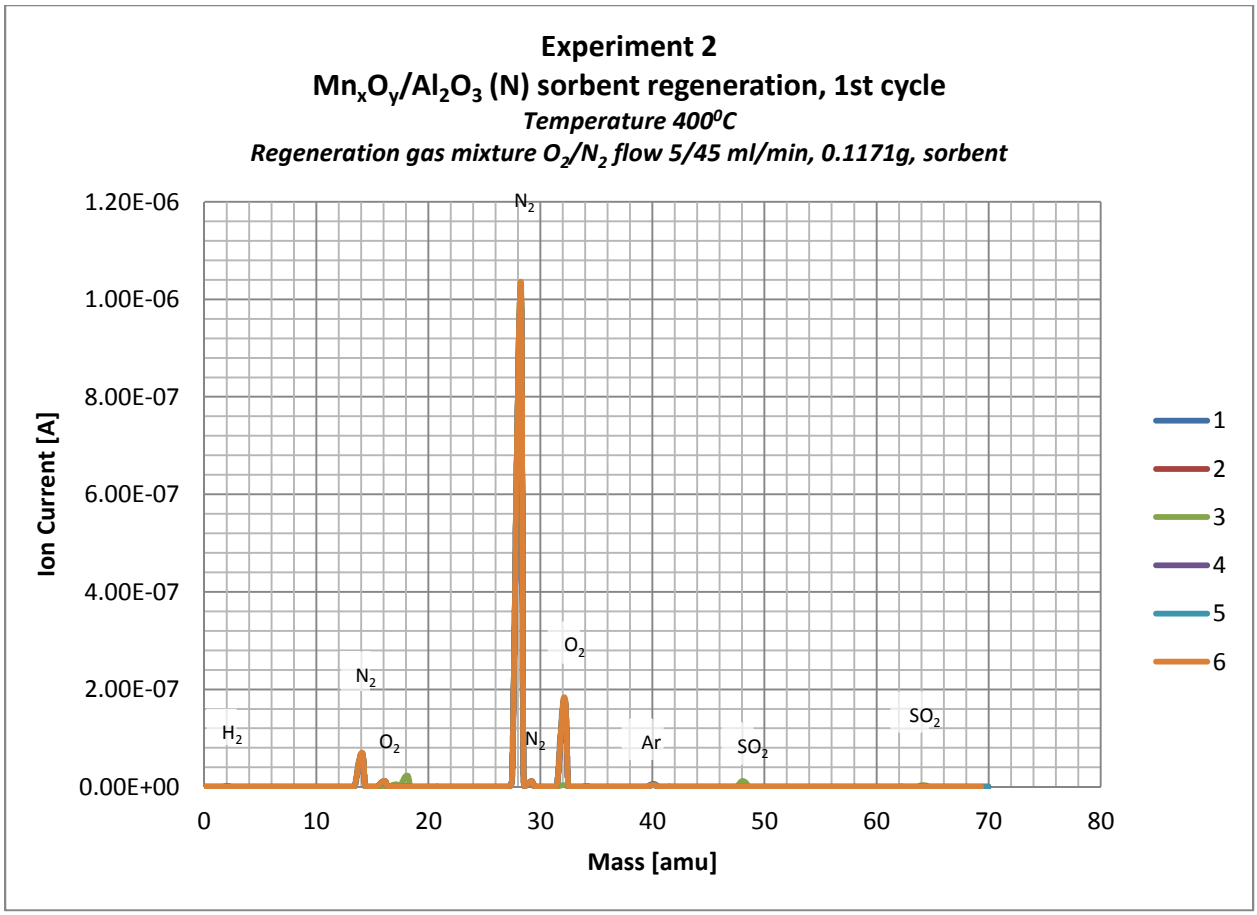
Experiment 2
Mn$_x$O$_y$/Al$_2$O$_3$ (N) sorbent regeneration, 1st cycle
Temperature 400$^0$C
Regeneration gas mixture O$_2$/N$_2$ flow 5/45 ml/min, 0.1171g, sorbent
Ion Current [A]
1.20E-06
1.00E-06
8.00E-07
6.00E-07
4.00E-07
2.00E-07
0.00E+00
0
10
20
30
40
50
60
70
80
Mass [amu]
N$_2$
O$_2$
N$_2$
H$_2$
O$_2$
N$_2$
Ar
SO$_2$
SO$_2$
1
2
3
4
5
6

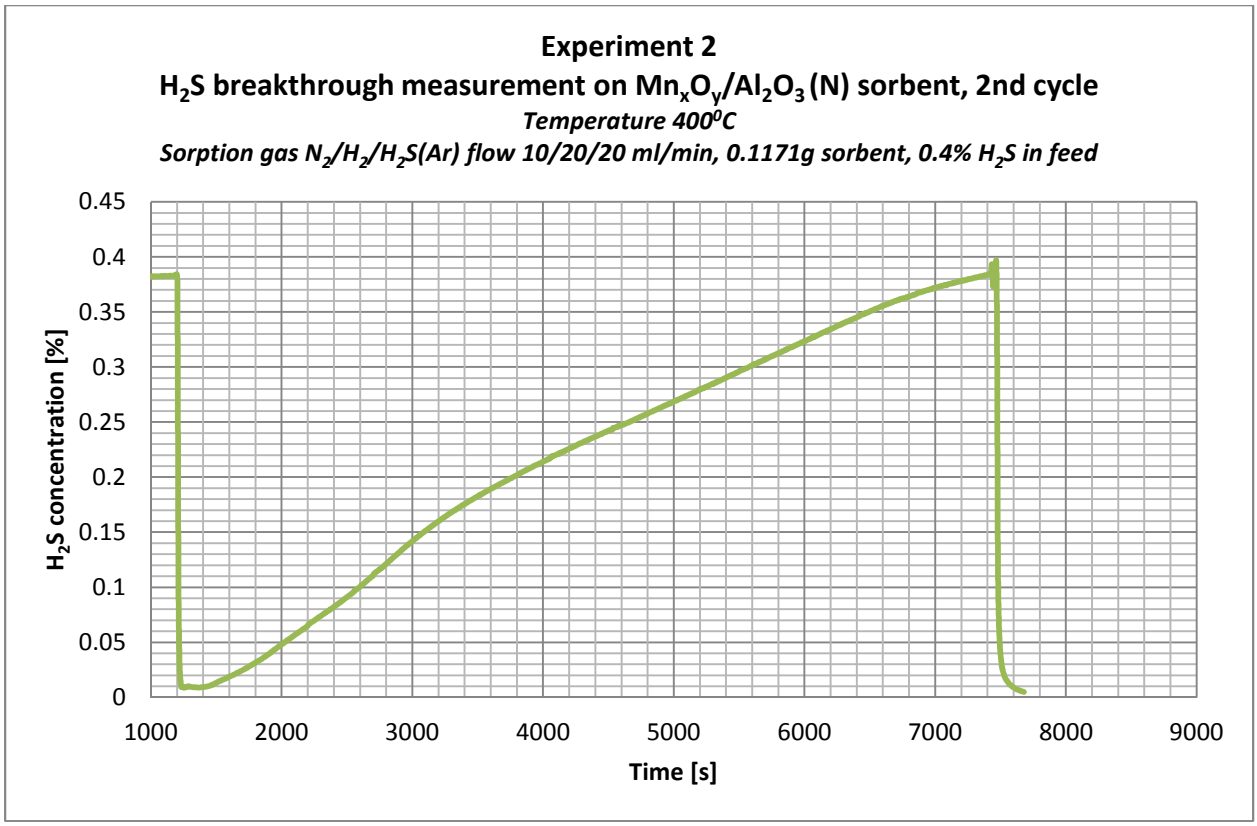
Experiment 2
H2S breakthrough measurement on MnxOy/Al2O3 (N) sorbent, 2nd cycle
Temperature 400⁰C
Sorption gas N2/H2/H2S(Ar) flow 10/20/20 ml/min, 0.1171g sorbent, 0.4% H2S in feed
H2S concentration [%]
0.45
0.4
0.35
0.3
0.25
0.2
0.15
0.1
0.05
0
1000
2000
3000
4000
5000
6000
7000
8000
9000
Time [s]

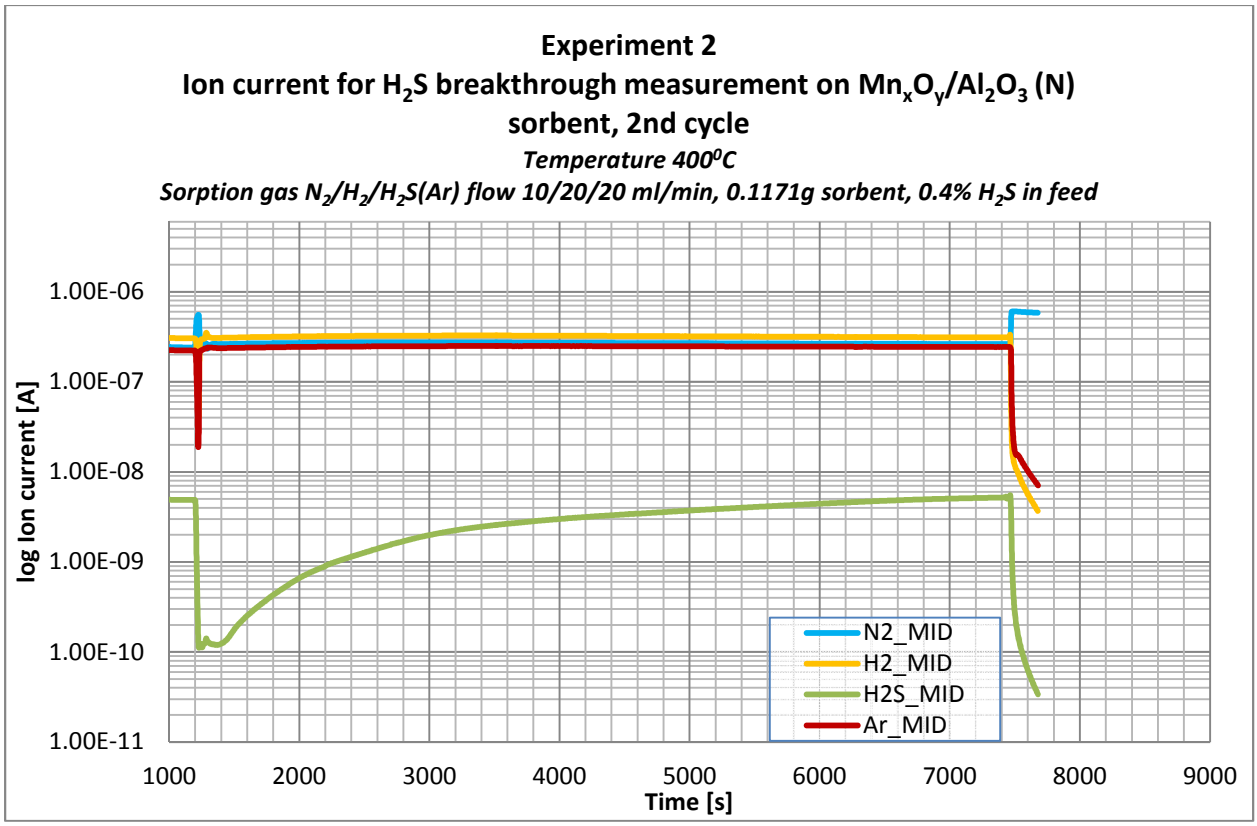
Experiment 2
Ion current for H2S breakthrough measurement on MnxOy/Al2O3 (N) sorbent, 2nd cycle
Temperature 400⁰C
Sorption gas N2/H2/H2S(Ar) flow 10/20/20 ml/min, 0.1171g sorbent, 0.4% H2S in feed
log Ion current [A]
1.00E-06
1.00E-07
1.00E-08
1.00E-09
1.00E-10
1.00E-11
1000
2000
3000
4000
5000
6000
7000
8000
9000
Time [s]
N2_MID
H2_MID
H2S_MID
Ar_MID

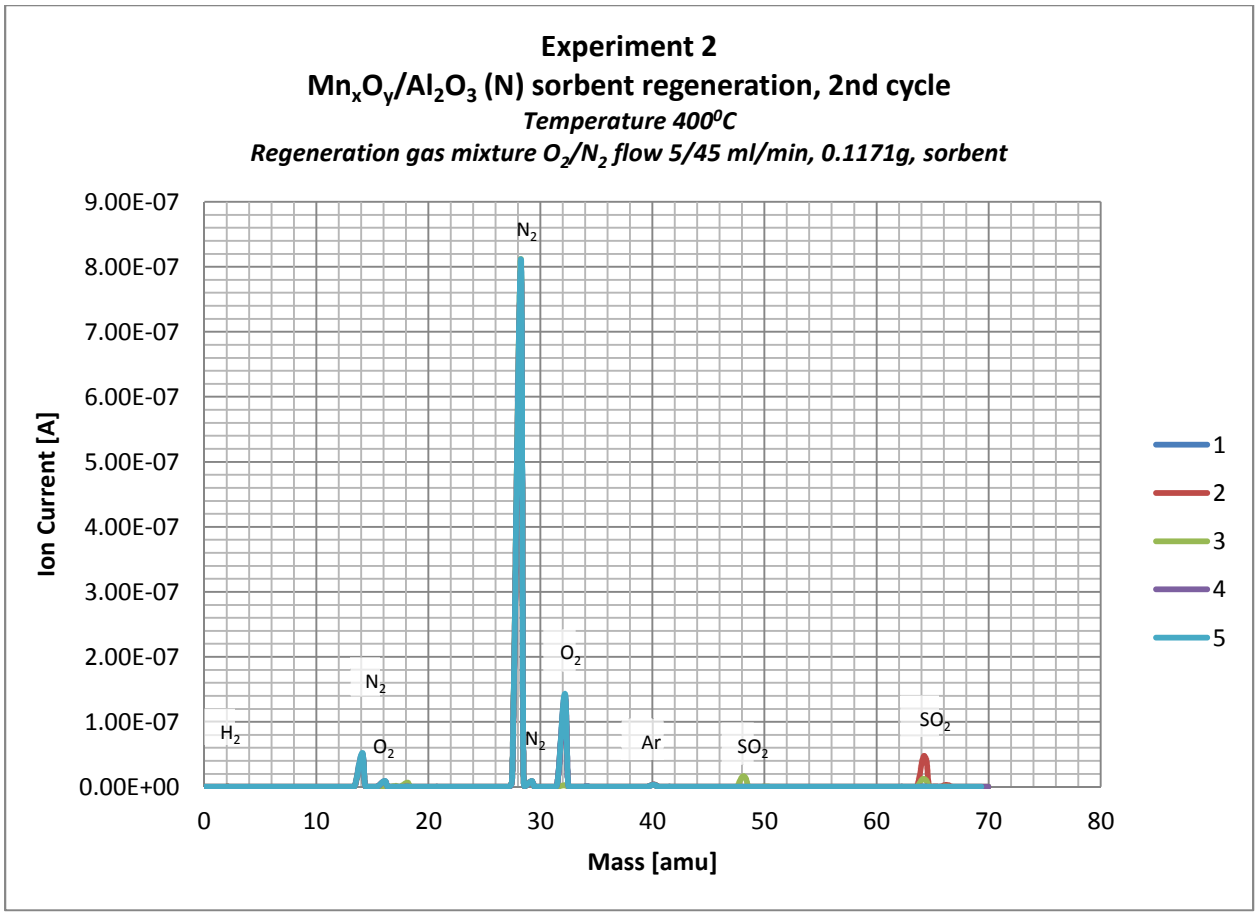
Experiment 2
$Mn_xO_y/Al_2O_3$ (N) sorbent regeneration, 2nd cycle
Temperature 400$^0$C
Regeneration gas mixture $O_2/N_2$ flow 5/45 ml/min, 0.1171g, sorbent
Ion Current [A]
9.00E-07
8.00E-07
7.00E-07
6.00E-07
5.00E-07
4.00E-07
3.00E-07
2.00E-07
1.00E-07
0.00E+00
0
10
20
30
40
50
60
70
80
Mass [amu]
$N_2$
$O_2$
$H_2$
Ar
$SO_2$
1
2
3
4
5

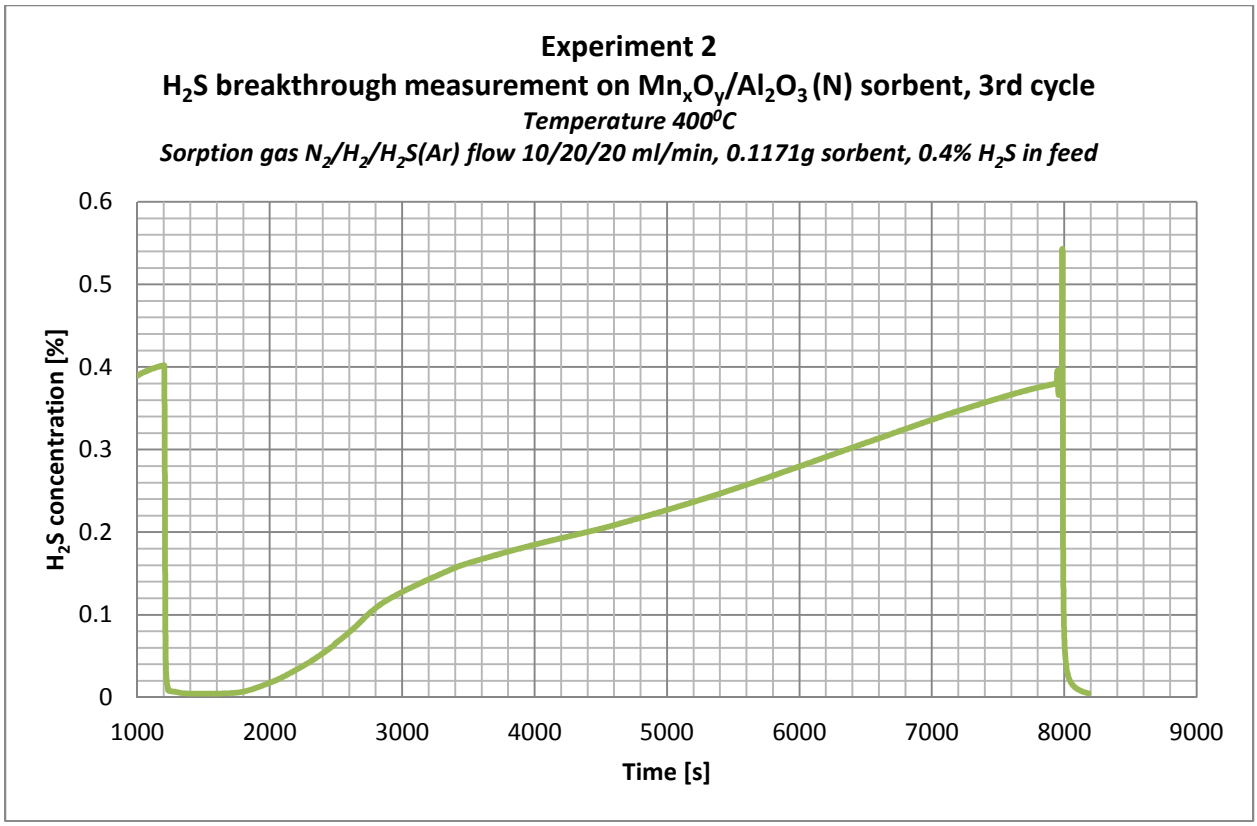
Experiment 2
H2S breakthrough measurement on MnxOy/Al2O3 (N) sorbent, 3rd cycle
Temperature 400⁰C
Sorption gas N2/H2/H2S(Ar) flow 10/20/20 ml/min, 0.1171g sorbent, 0.4% H2S in feed
H2S concentration [%]
0.6
0.5
0.4
0.3
0.2
0.1
0
1000
2000
3000
4000
5000
6000
7000
8000
9000
Time [s]

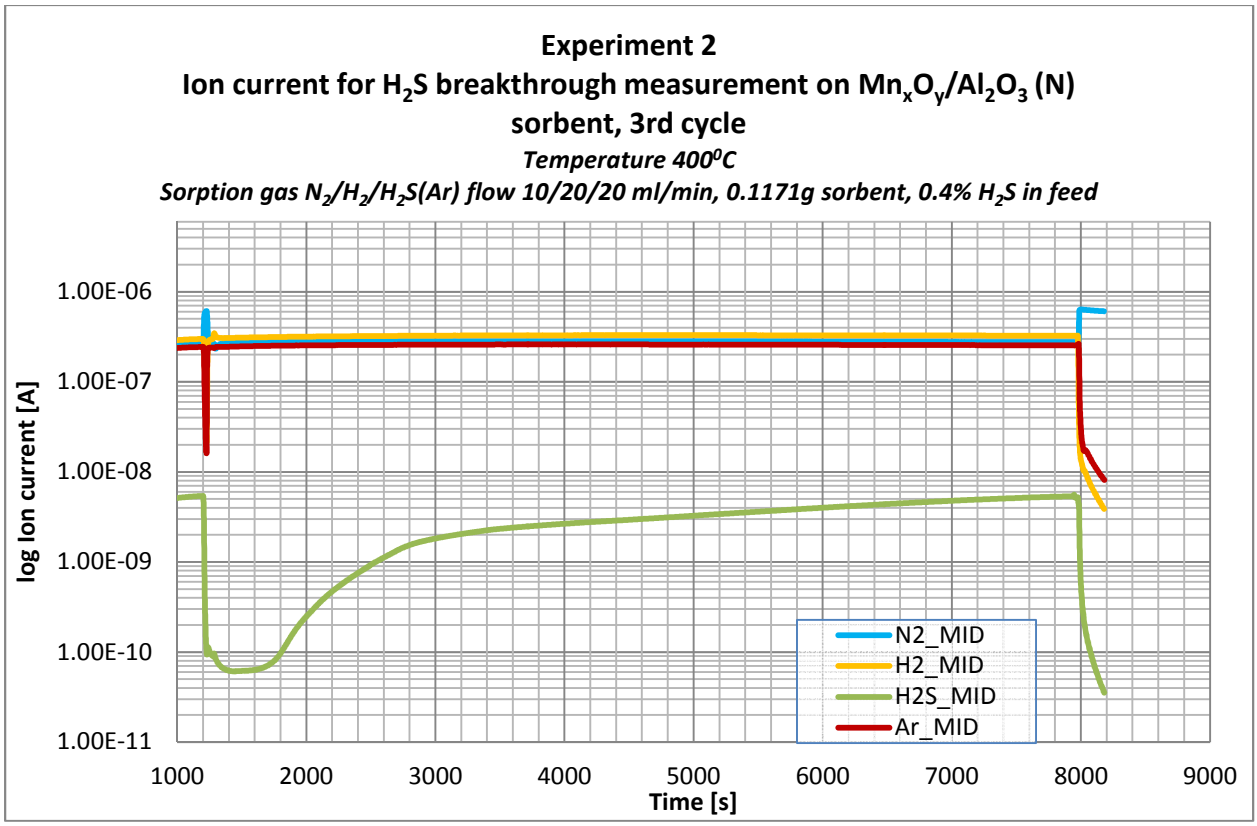
Experiment 2
Ion current for H2S breakthrough measurement on MnxOy/Al2O3 (N) sorbent, 3rd cycle
Temperature 400⁰C
Sorption gas N2/H2/H2S(Ar) flow 10/20/20 ml/min, 0.1171g sorbent, 0.4% H2S in feed
log Ion current [A]
1.00E-06
1.00E-07
1.00E-08
1.00E-09
1.00E-10
1.00E-11
1000
2000
3000
4000
5000
6000
7000
8000
9000
Time [s]
N2_MID
H2_MID
H2S_MID
Ar_MID

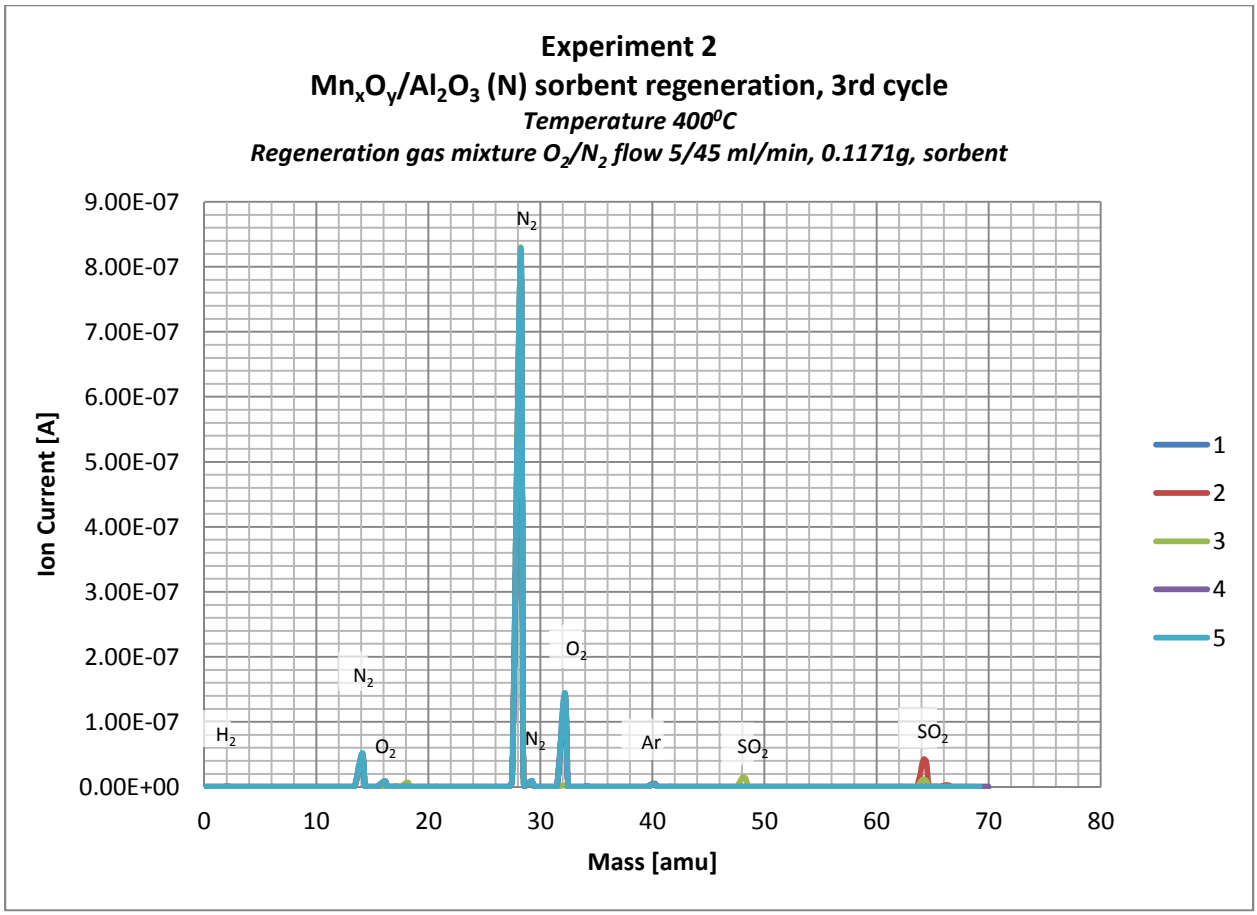
Experiment 2
Mn$_x$O$_y$/Al$_2$O$_3$ (N) sorbent regeneration, 3rd cycle
Temperature 400$^0$C
Regeneration gas mixture O$_2$/N$_2$ flow 5/45 ml/min, 0.1171g, sorbent
Ion Current [A]
9.00E-07
8.00E-07
7.00E-07
6.00E-07
5.00E-07
4.00E-07
3.00E-07
2.00E-07
1.00E-07
0.00E+00
0
10
20
30
40
50
60
70
80
Mass [amu]
N$_2$
O$_2$
H$_2$
Ar
SO$_2$
1
2
3
4
5

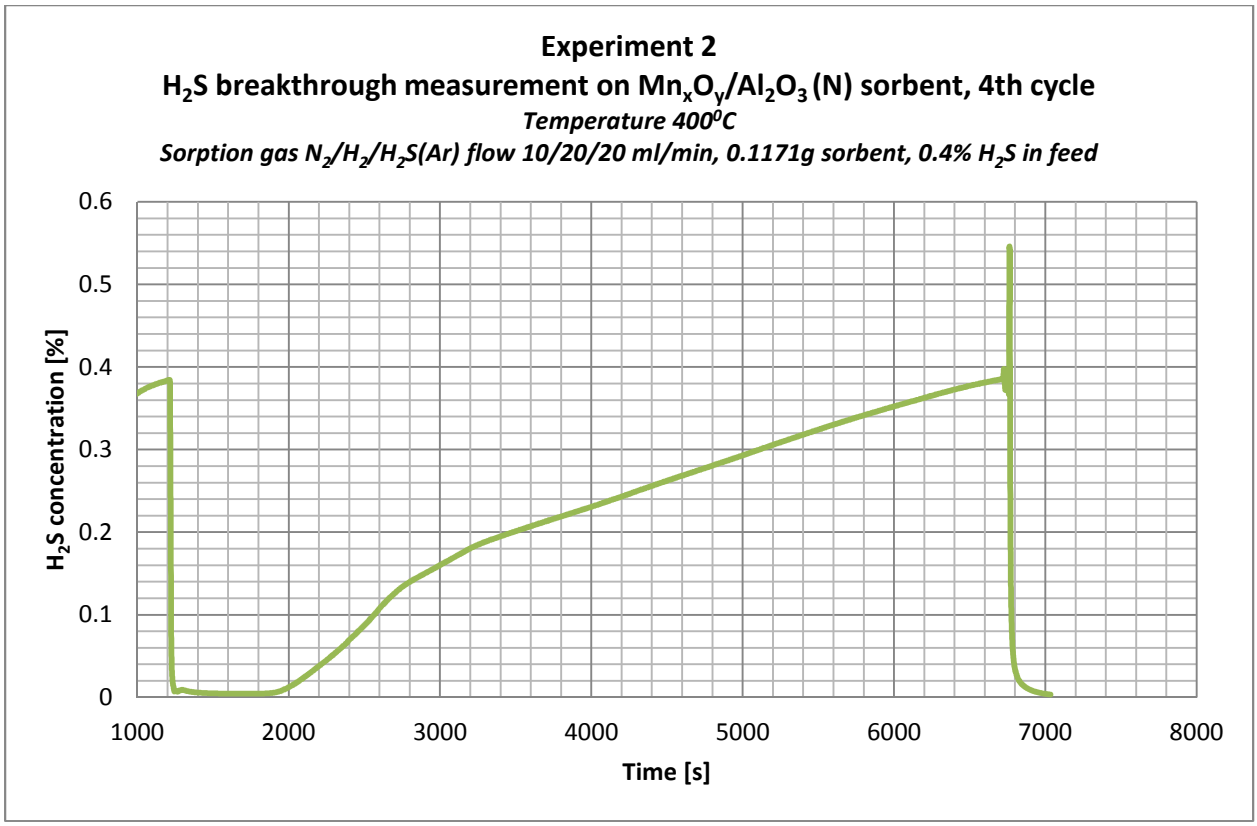
Experiment 2
H2S breakthrough measurement on MnxOy/Al2O3 (N) sorbent, 4th cycle
Temperature 400⁰C
Sorption gas N2/H2/H2S(Ar) flow 10/20/20 ml/min, 0.1171g sorbent, 0.4% H2S in feed
H2S concentration [%]
0.6
0.5
0.4
0.3
0.2
0.1
0
1000
2000
3000
4000
5000
6000
7000
8000
Time [s]

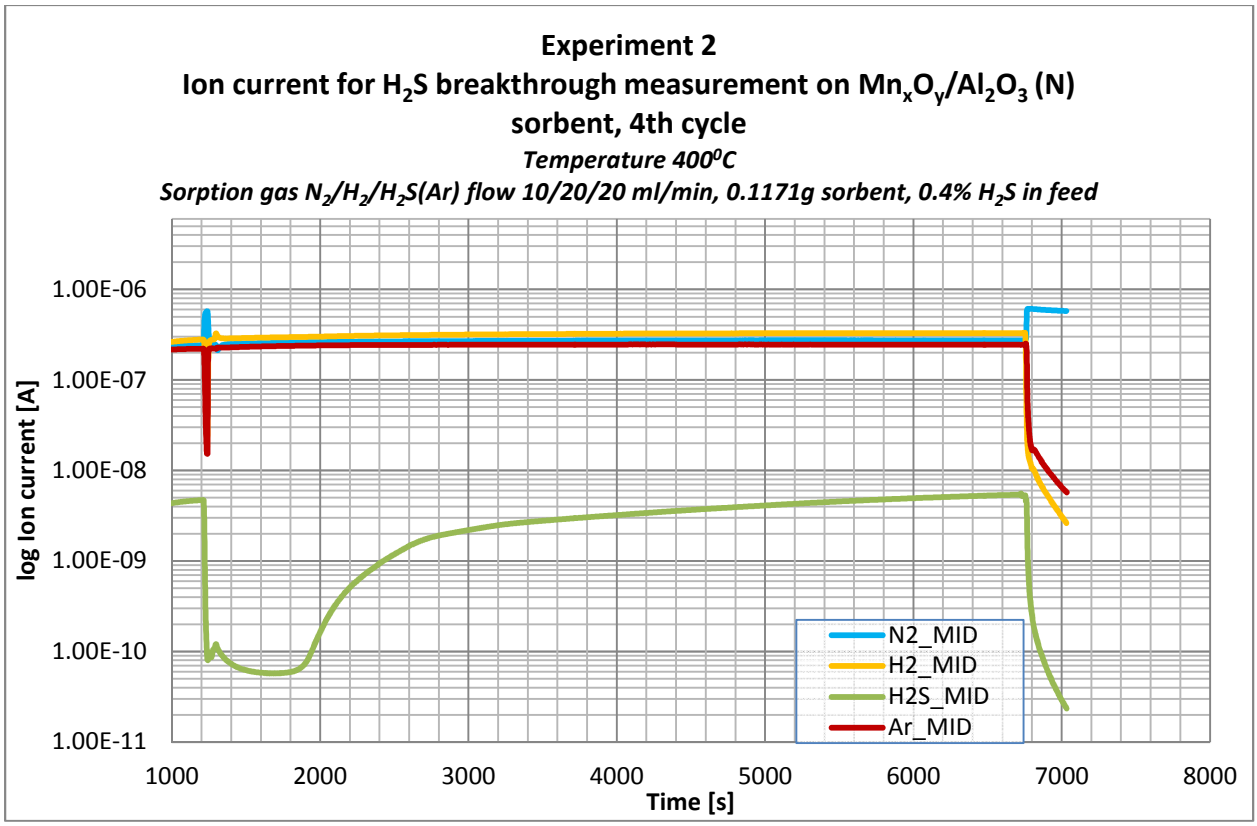
Experiment 2
Ion current for H2S breakthrough measurement on MnxOy/Al2O3 (N) sorbent, 4th cycle
Temperature 400⁰C
Sorption gas N2/H2/H2S(Ar) flow 10/20/20 ml/min, 0.1171g sorbent, 0.4% H2S in feed
log Ion current [A]
1.00E-06
1.00E-07
1.00E-08
1.00E-09
1.00E-10
1.00E-11
1000
2000
3000
4000
5000
6000
7000
8000
Time [s]
N2_MID
H2_MID
H2S_MID
Ar_MID

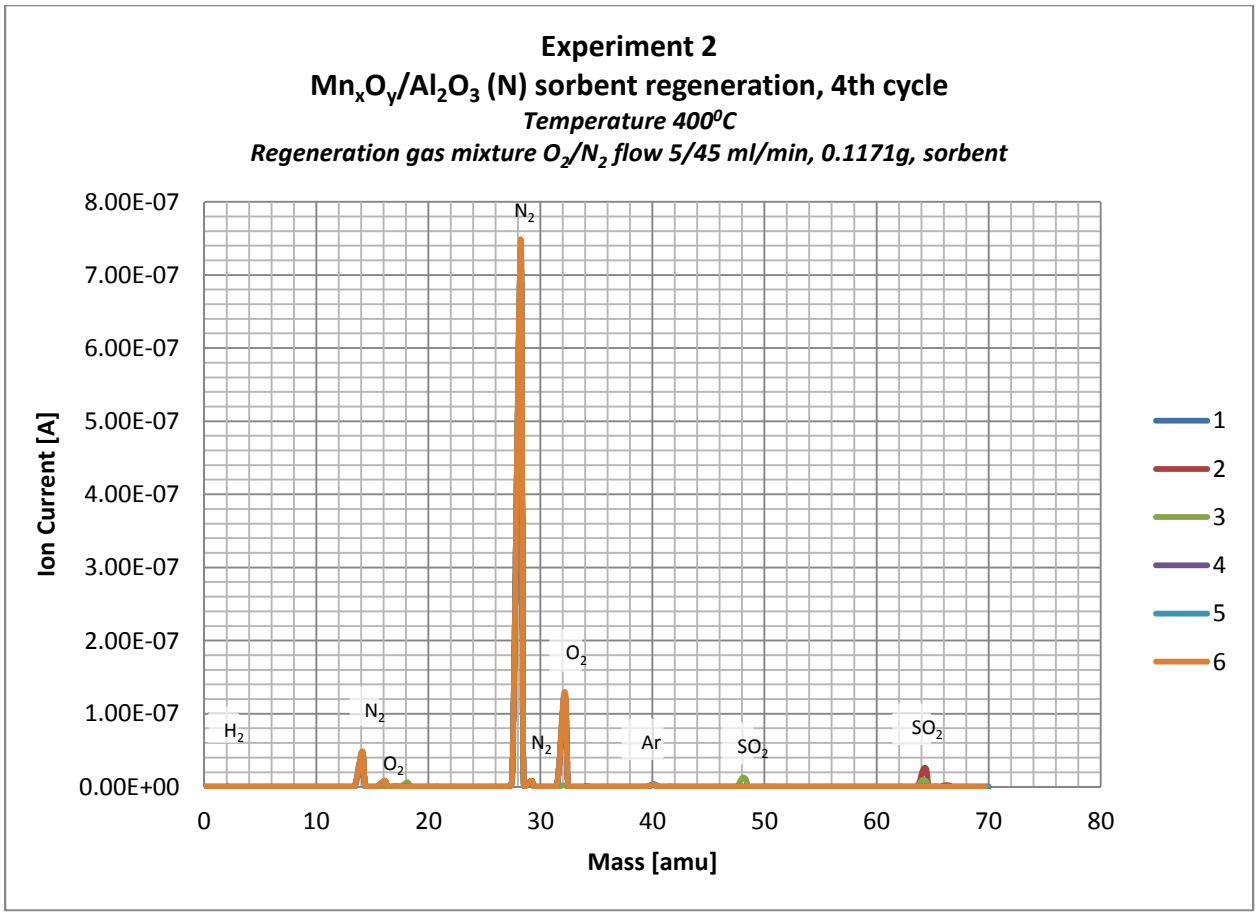
Experiment 2
Mn$_x$O$_y$/Al$_2$O$_3$ (N) sorbent regeneration, 4th cycle
Temperature 400$^0$C
Regeneration gas mixture O$_2$/N$_2$ flow 5/45 ml/min, 0.1171g, sorbent
Ion Current [A]
8.00E-07
7.00E-07
6.00E-07
5.00E-07
4.00E-07
3.00E-07
2.00E-07
1.00E-07
0.00E+00
0
10
20
30
40
50
60
70
80
Mass [amu]
N$_2$
O$_2$
H$_2$
N$_2$
O$_2$
N$_2$
Ar
SO$_2$
SO$_2$
1
2
3
4
5
6

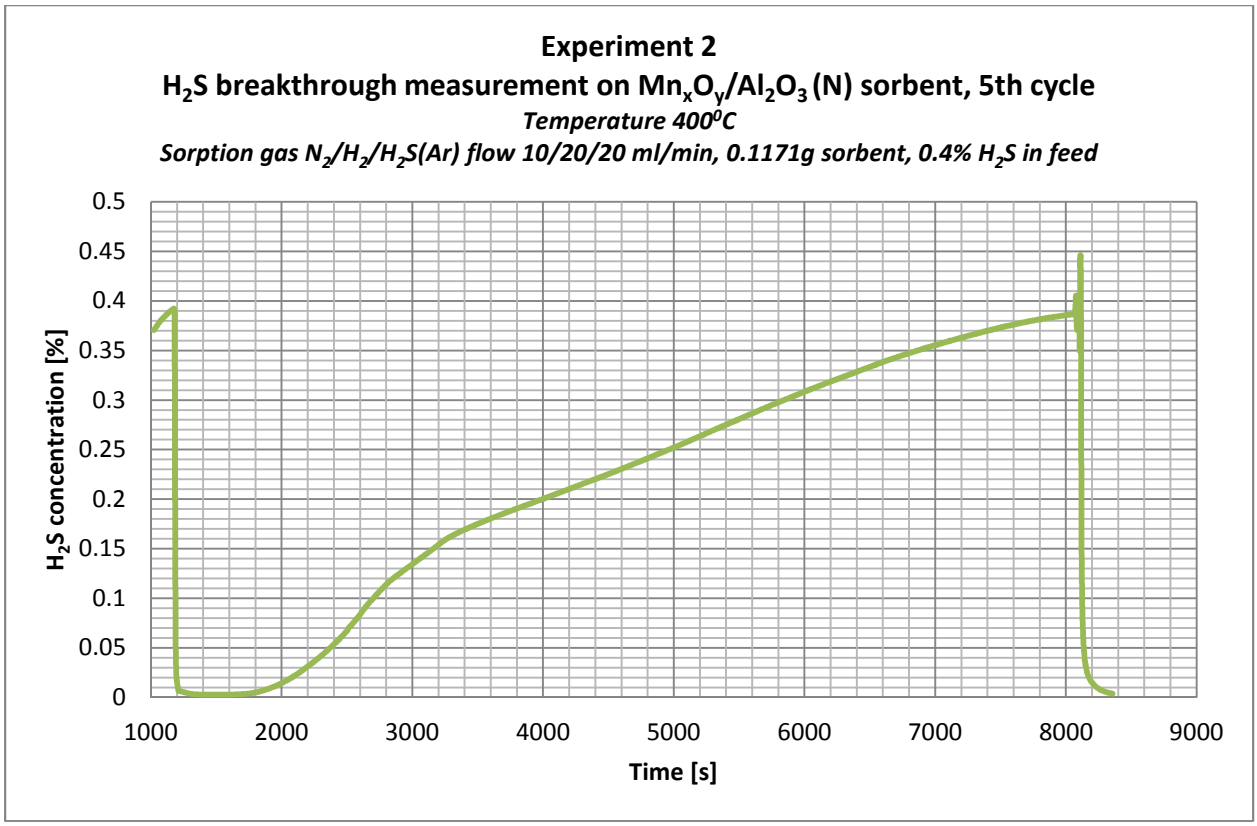
Experiment 2
H2S breakthrough measurement on MnxOy/Al2O3 (N) sorbent, 5th cycle
Temperature 400⁰C
Sorption gas N2/H2/H2S(Ar) flow 10/20/20 ml/min, 0.1171g sorbent, 0.4% H2S in feed
H2S concentration [%]
0.5
0.45
0.4
0.35
0.3
0.25
0.2
0.15
0.1
0.05
0
1000
2000
3000
4000
5000
6000
7000
8000
9000
Time [s]

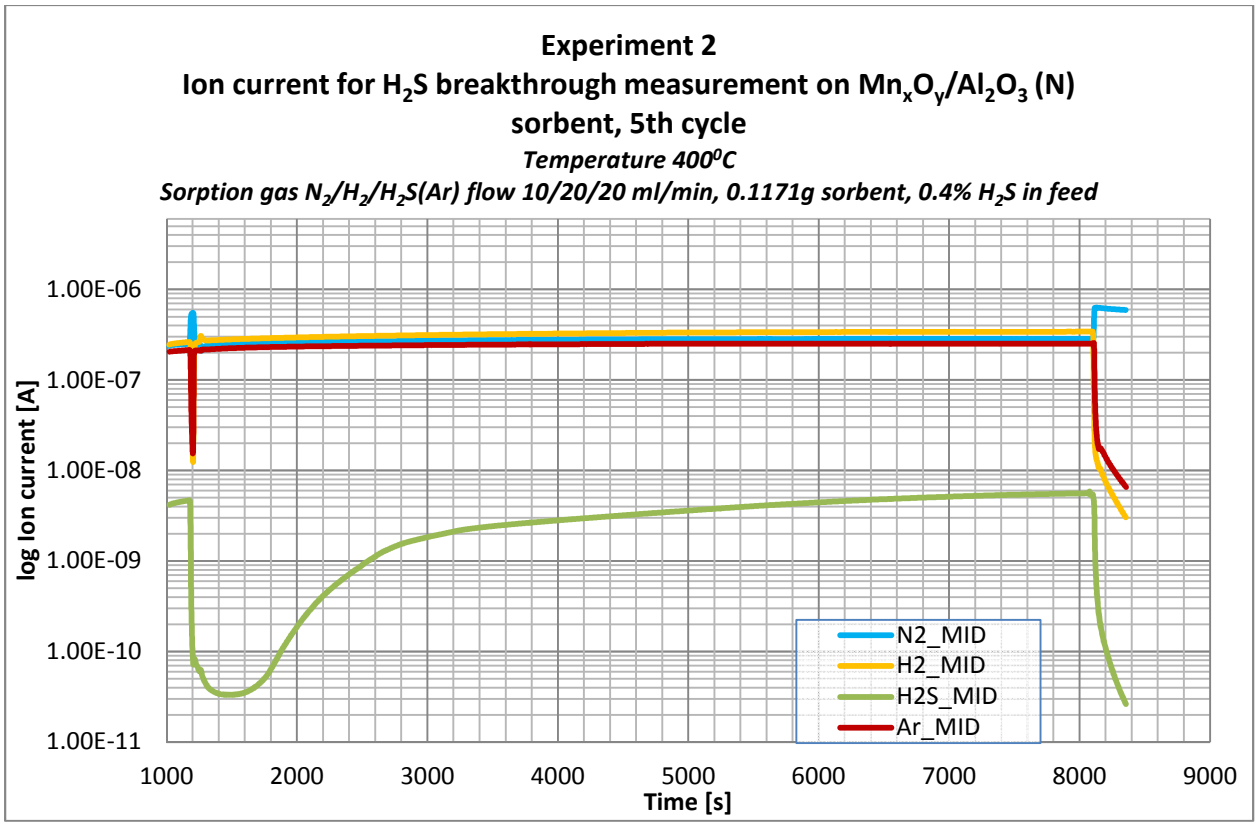
Experiment 2
Ion current for H2S breakthrough measurement on MnxOy/Al2O3 (N) sorbent, 5th cycle
Temperature 400⁰C
Sorption gas N2/H2/H2S(Ar) flow 10/20/20 ml/min, 0.1171g sorbent, 0.4% H2S in feed
log Ion current [A]
1.00E-06
1.00E-07
1.00E-08
1.00E-09
1.00E-10
1.00E-11
1000
2000
3000
4000
5000
6000
7000
8000
9000
Time [s]
N2_MID
H2_MID
H2S_MID
Ar_MID

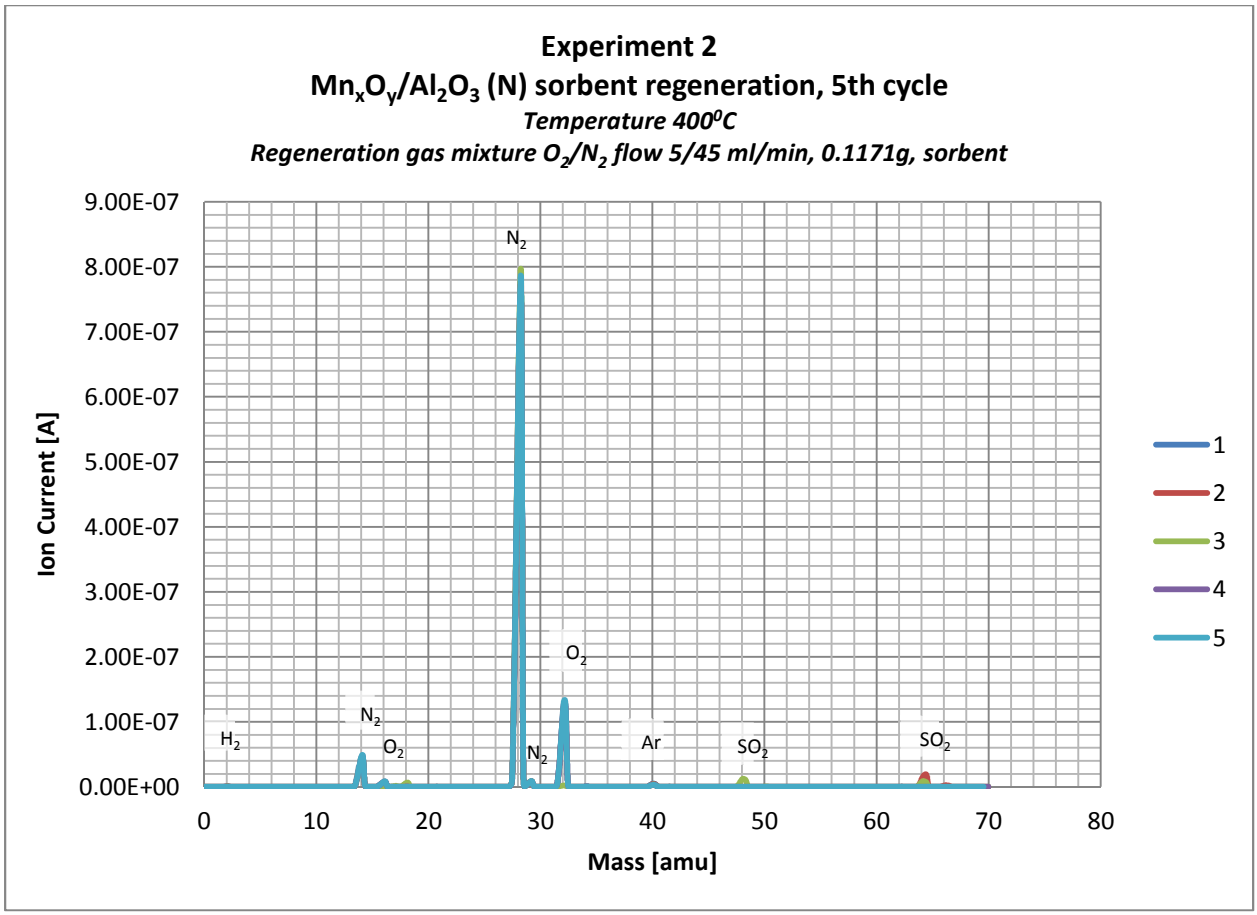
Experiment 2
Mn$_x$O$_y$/Al$_2$O$_3$ (N) sorbent regeneration, 5th cycle
Temperature 400$^0$C
Regeneration gas mixture O$_2$/N$_2$ flow 5/45 ml/min, 0.1171g, sorbent
Ion Current [A]
9.00E-07
8.00E-07
7.00E-07
6.00E-07
5.00E-07
4.00E-07
3.00E-07
2.00E-07
1.00E-07
0.00E+00
0
10
20
30
40
50
60
70
80
Mass [amu]
H$_2$
N$_2$
O$_2$
N$_2$
O$_2$
N$_2$
Ar
SO$_2$
SO$_2$
1
2
3
4
5

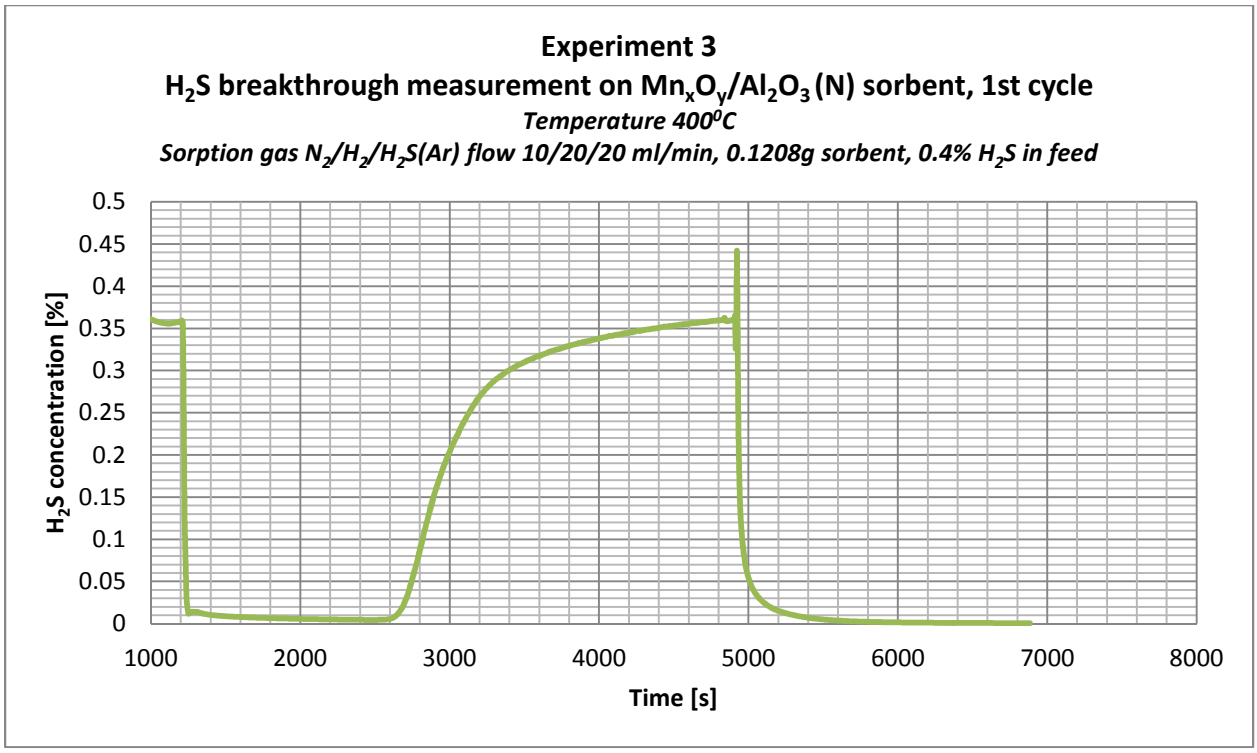
Experiment 3
H2S breakthrough measurement on MnxOy/Al2O3 (N) sorbent, 1st cycle
Temperature 400⁰C
Sorption gas N2/H2/H2S(Ar) flow 10/20/20 ml/min, 0.1208g sorbent, 0.4% H2S in feed
H2S concentration [%]
0.5
0.45
0.4
0.35
0.3
0.25
0.2
0.15
0.1
0.05
0
1000
2000
3000
4000
5000
6000
7000
8000
Time [s]

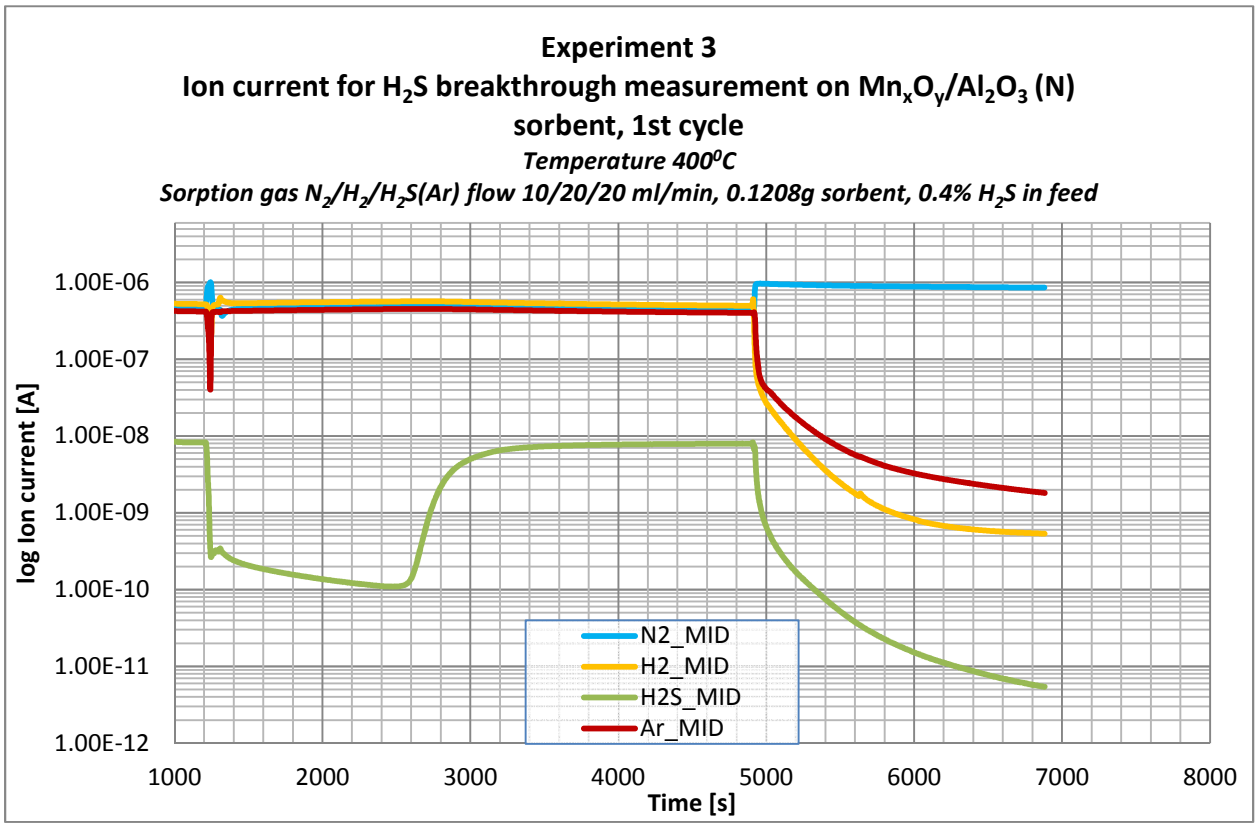
Experiment 3
Ion current for H2S breakthrough measurement on MnxOy/Al2O3 (N) sorbent, 1st cycle
Temperature 400⁰C
Sorption gas N2/H2/H2S(Ar) flow 10/20/20 ml/min, 0.1208g sorbent, 0.4% H2S in feed
log Ion current [A]
1.00E-06
1.00E-07
1.00E-08
1.00E-09
1.00E-10
1.00E-11
1.00E-12
1000
2000
3000
4000
5000
6000
7000
8000
Time [s]
N2_MID
H2_MID
H2S_MID
Ar_MID

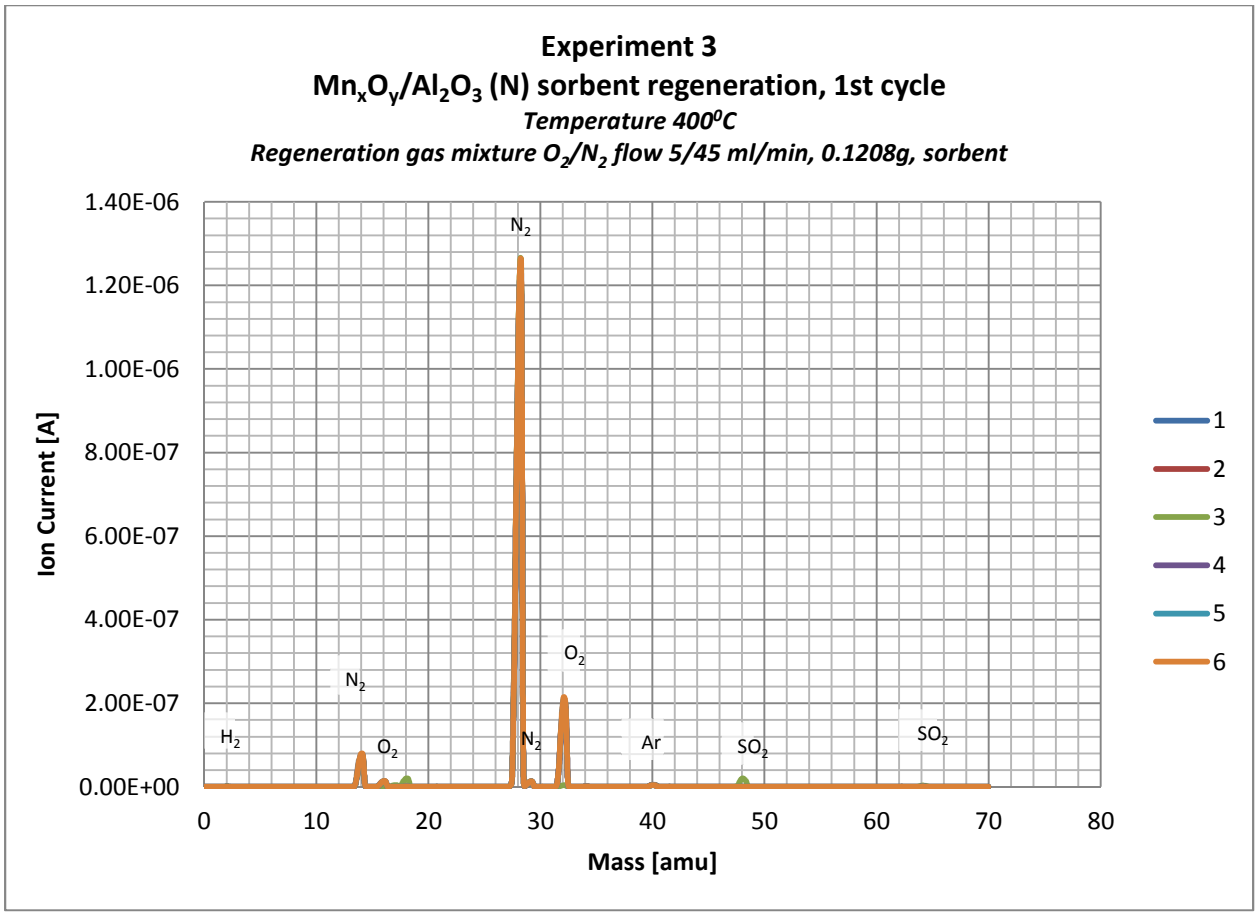
Experiment 3
Mn$_x$O$_y$/Al$_2$O$_3$ (N) sorbent regeneration, 1st cycle
Temperature 400$^0$C
Regeneration gas mixture O$_2$/N$_2$ flow 5/45 ml/min, 0.1208g, sorbent
Ion Current [A]
1.40E-06
1.20E-06
1.00E-06
8.00E-07
6.00E-07
4.00E-07
2.00E-07
0.00E+00
0
10
20
30
40
50
60
70
80
Mass [amu]
N$_2$
N$_2$
O$_2$
H$_2$
O$_2$
N$_2$
Ar
SO$_2$
SO$_2$
1
2
3
4
5
6

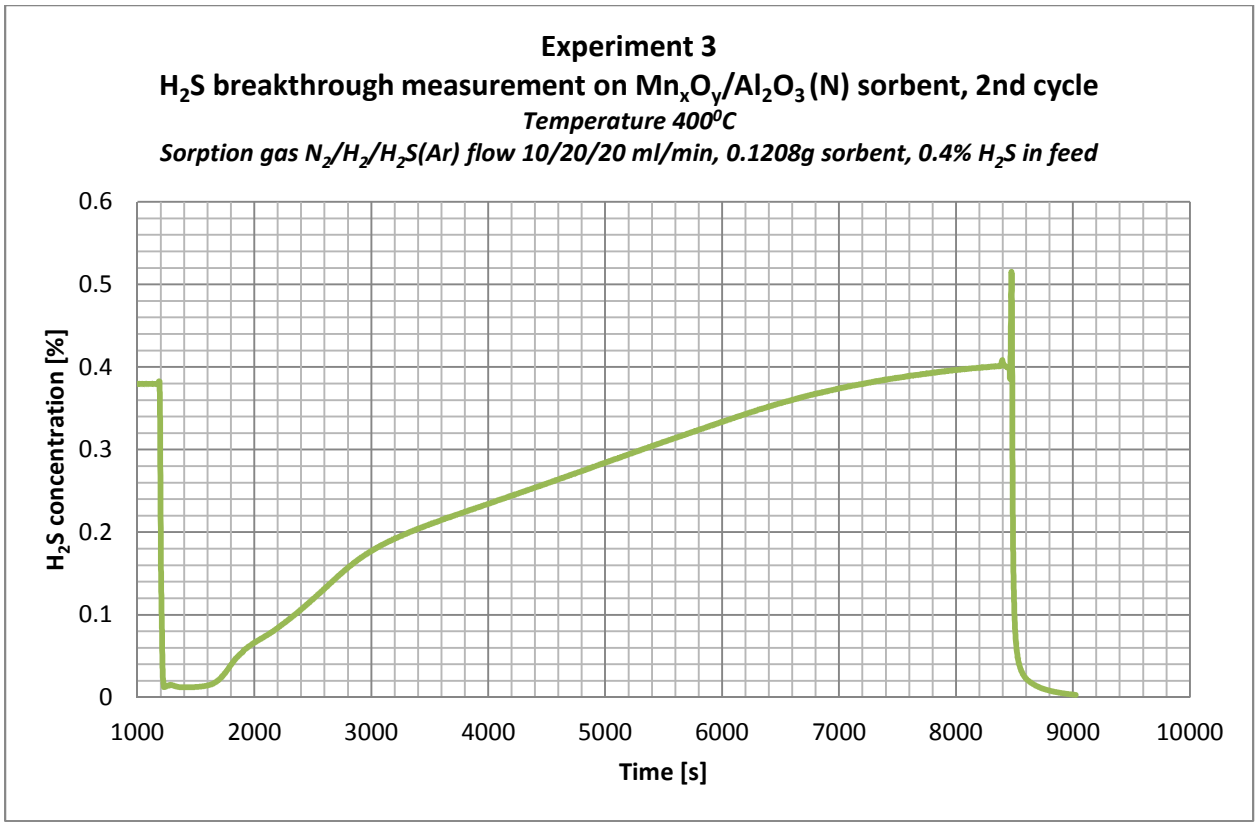
Experiment 3
H2S breakthrough measurement on MnxOy/Al2O3 (N) sorbent, 2nd cycle
Temperature 400⁰C
Sorption gas N2/H2/H2S(Ar) flow 10/20/20 ml/min, 0.1208g sorbent, 0.4% H2S in feed
H2S concentration [%]
0.6
0.5
0.4
0.3
0.2
0.1
0
1000
2000
3000
4000
5000
6000
7000
8000
9000
10000
Time [s]

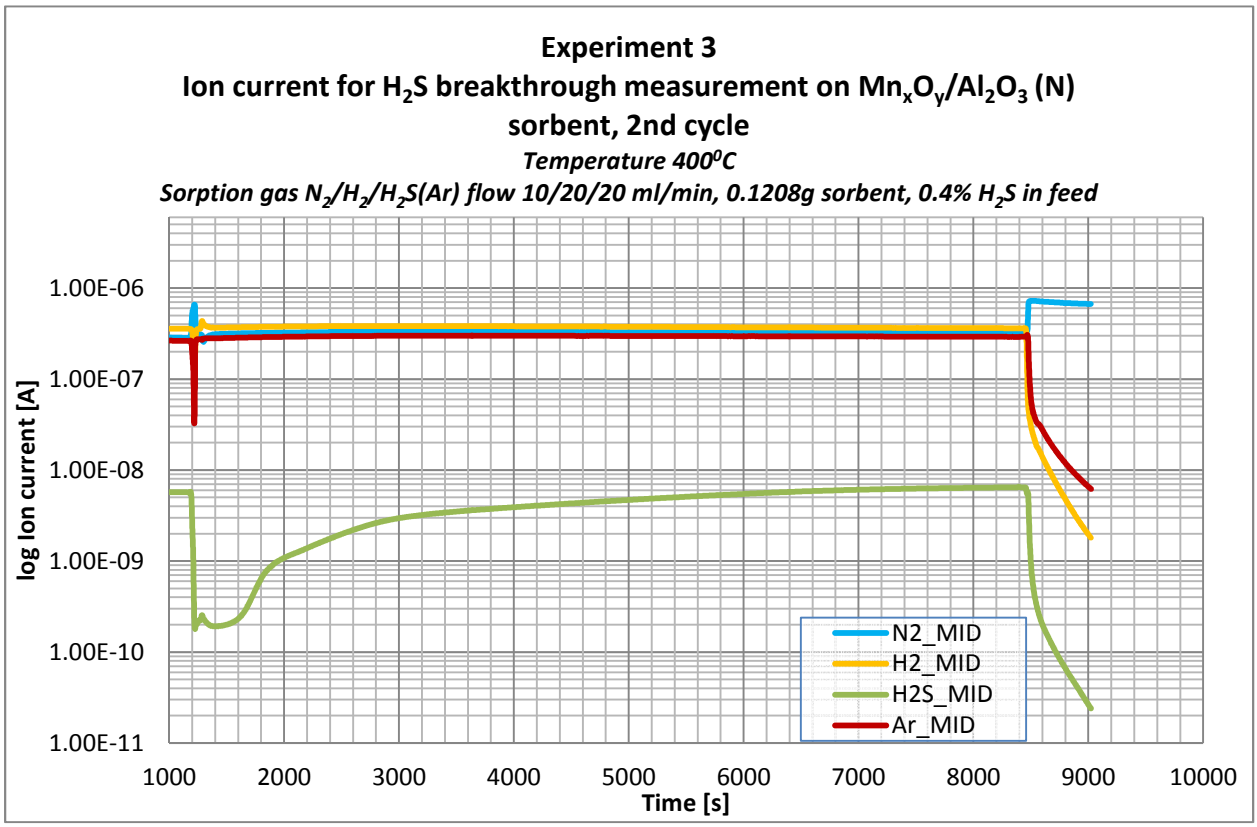
Experiment 3
Ion current for H2S breakthrough measurement on MnxOy/Al2O3 (N) sorbent, 2nd cycle
Temperature 400⁰C
Sorption gas N2/H2/H2S(Ar) flow 10/20/20 ml/min, 0.1208g sorbent, 0.4% H2S in feed
log Ion current [A]
1.00E-06
1.00E-07
1.00E-08
1.00E-09
1.00E-10
1.00E-11
1000
2000
3000
4000
5000
6000
7000
8000
9000
10000
Time [s]
N2_MID
H2_MID
H2S_MID
Ar_MID

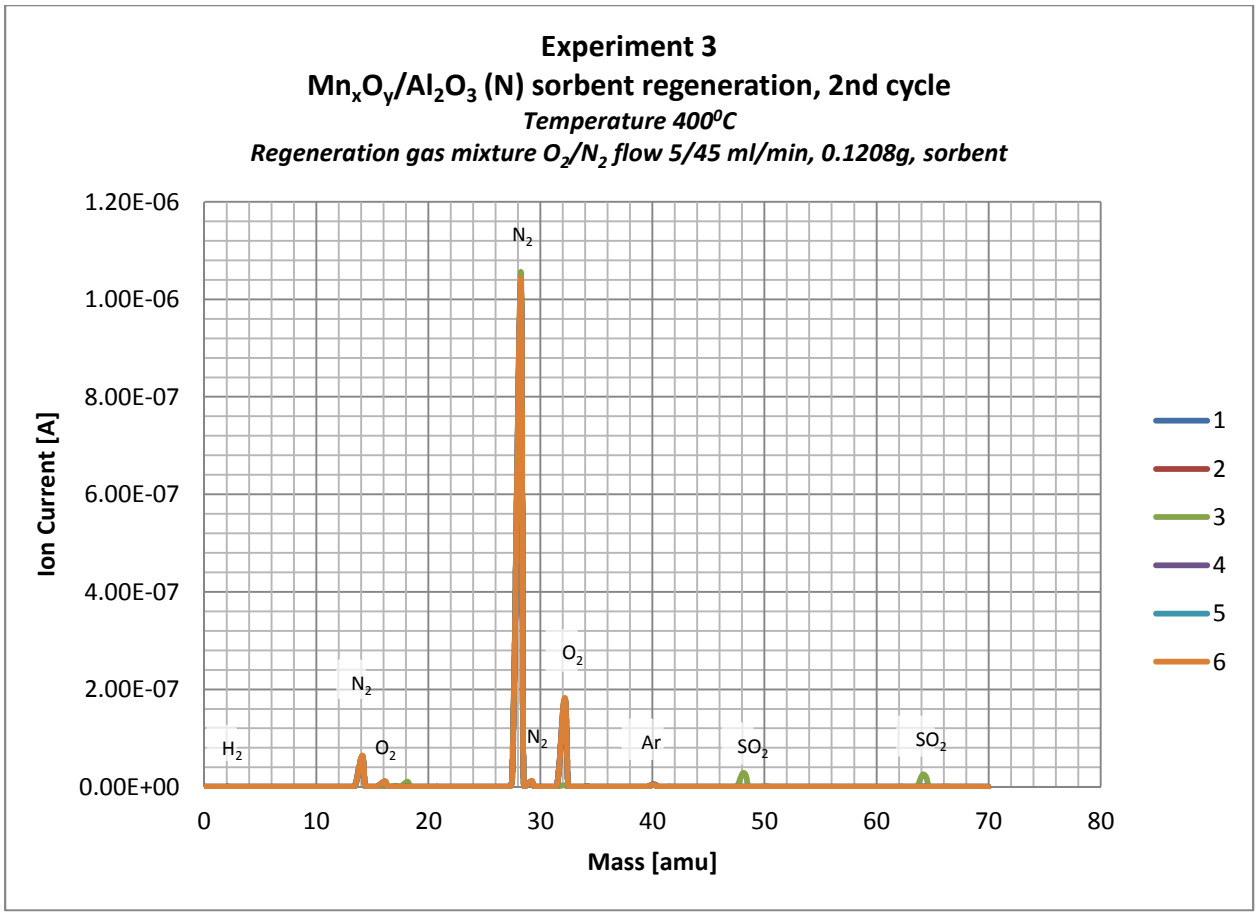
Experiment 3
Mn$_x$O$_y$/Al$_2$O$_3$ (N) sorbent regeneration, 2nd cycle
Temperature 400$^0$C
Regeneration gas mixture O$_2$/N$_2$ flow 5/45 ml/min, 0.1208g, sorbent
Ion Current [A]
1.20E-06
1.00E-06
8.00E-07
6.00E-07
4.00E-07
2.00E-07
0.00E+00
0
10
20
30
40
50
60
70
80
Mass [amu]
N$_2$
O$_2$
N$_2$
H$_2$
O$_2$
N$_2$
Ar
SO$_2$
SO$_2$
1
2
3
4
5
6

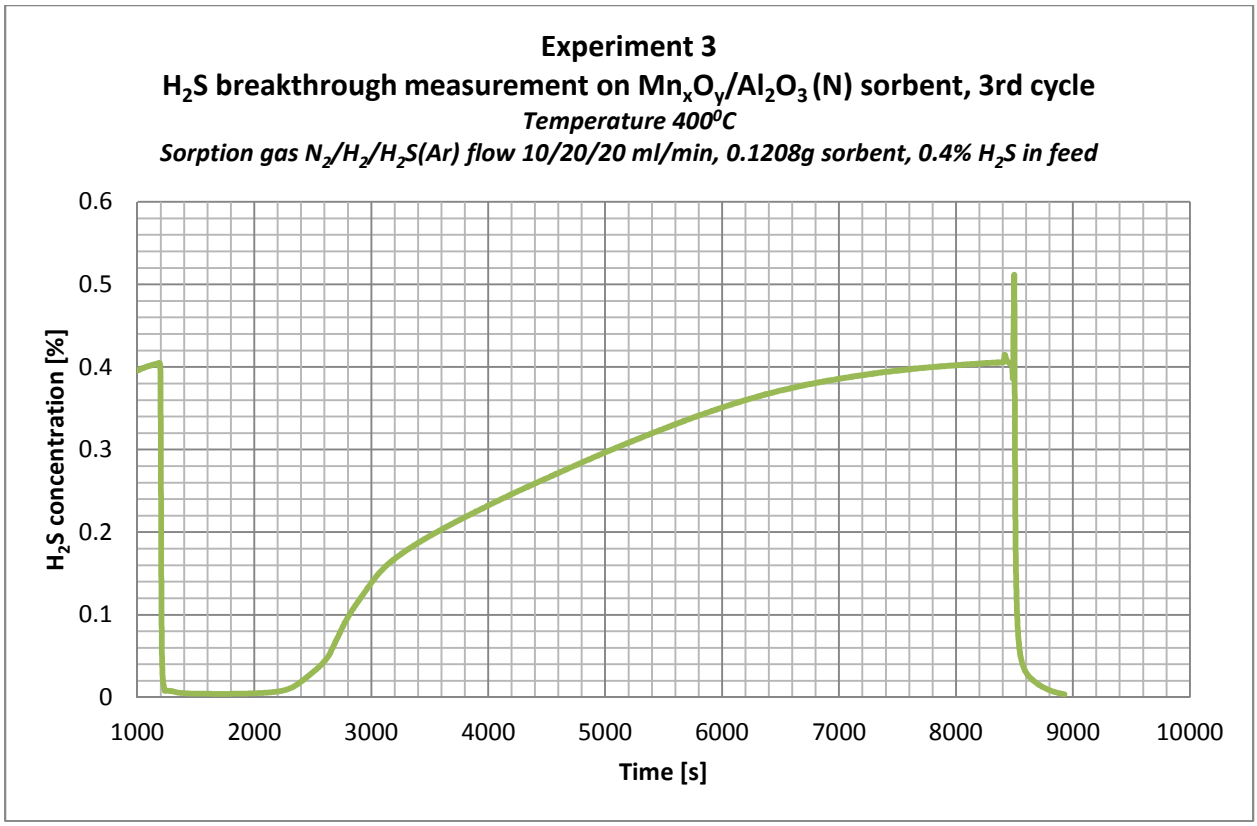
Experiment 3
H2S breakthrough measurement on MnxOy/Al2O3 (N) sorbent, 3rd cycle
Temperature 400⁰C
Sorption gas N2/H2/H2S(Ar) flow 10/20/20 ml/min, 0.1208g sorbent, 0.4% H2S in feed
H2S concentration [%]
0.6
0.5
0.4
0.3
0.2
0.1
0
1000
2000
3000
4000
5000
6000
7000
8000
9000
10000
Time [s]

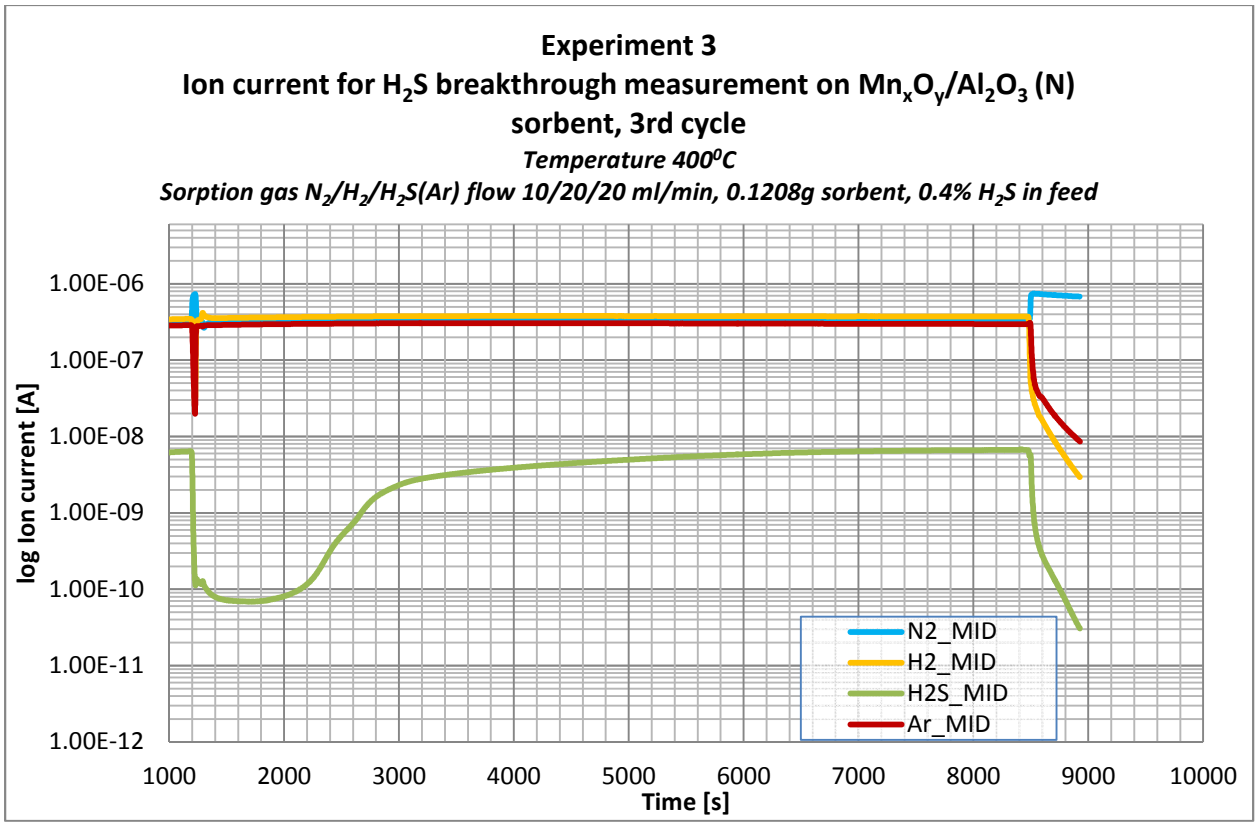
Experiment 3
Ion current for H2S breakthrough measurement on MnxOy/Al2O3 (N) sorbent, 3rd cycle
Temperature 400⁰C
Sorption gas N2/H2/H2S(Ar) flow 10/20/20 ml/min, 0.1208g sorbent, 0.4% H2S in feed
log Ion current [A]
1.00E-06
1.00E-07
1.00E-08
1.00E-09
1.00E-10
1.00E-11
1.00E-12
1000
2000
3000
4000
5000
6000
7000
8000
9000
10000
Time [s]
N2_MID
H2_MID
H2S_MID
Ar_MID

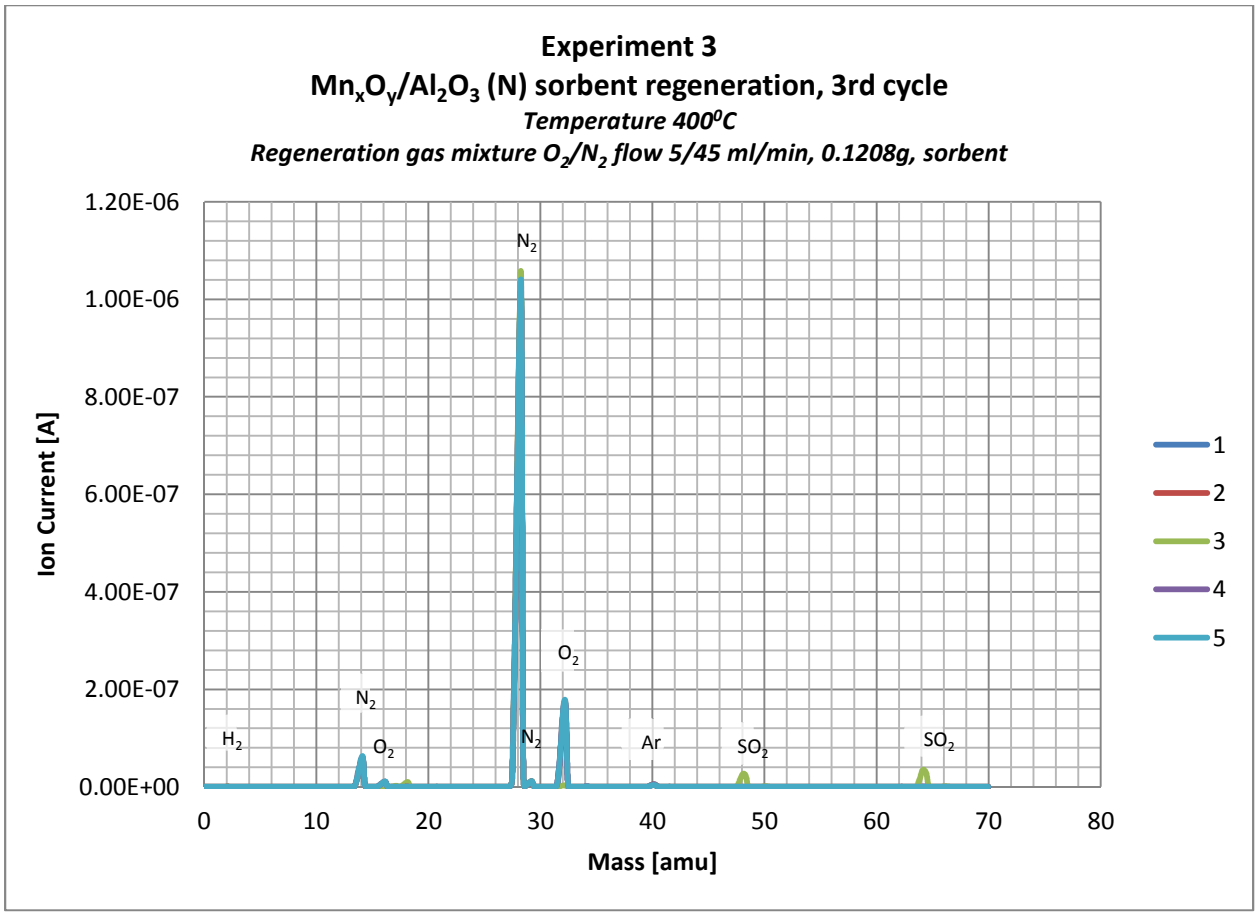
Experiment 3
Mn$_x$O$_y$/Al$_2$O$_3$ (N) sorbent regeneration, 3rd cycle
Temperature 400$^0$C
Regeneration gas mixture O$_2$/N$_2$ flow 5/45 ml/min, 0.1208g, sorbent
Ion Current [A]
1.20E-06
1.00E-06
8.00E-07
6.00E-07
4.00E-07
2.00E-07
0.00E+00
0
10
20
30
40
50
60
70
80
Mass [amu]
N$_2$
O$_2$
N$_2$
H$_2$
O$_2$
N$_2$
Ar
SO$_2$
SO$_2$
1
2
3
4
5

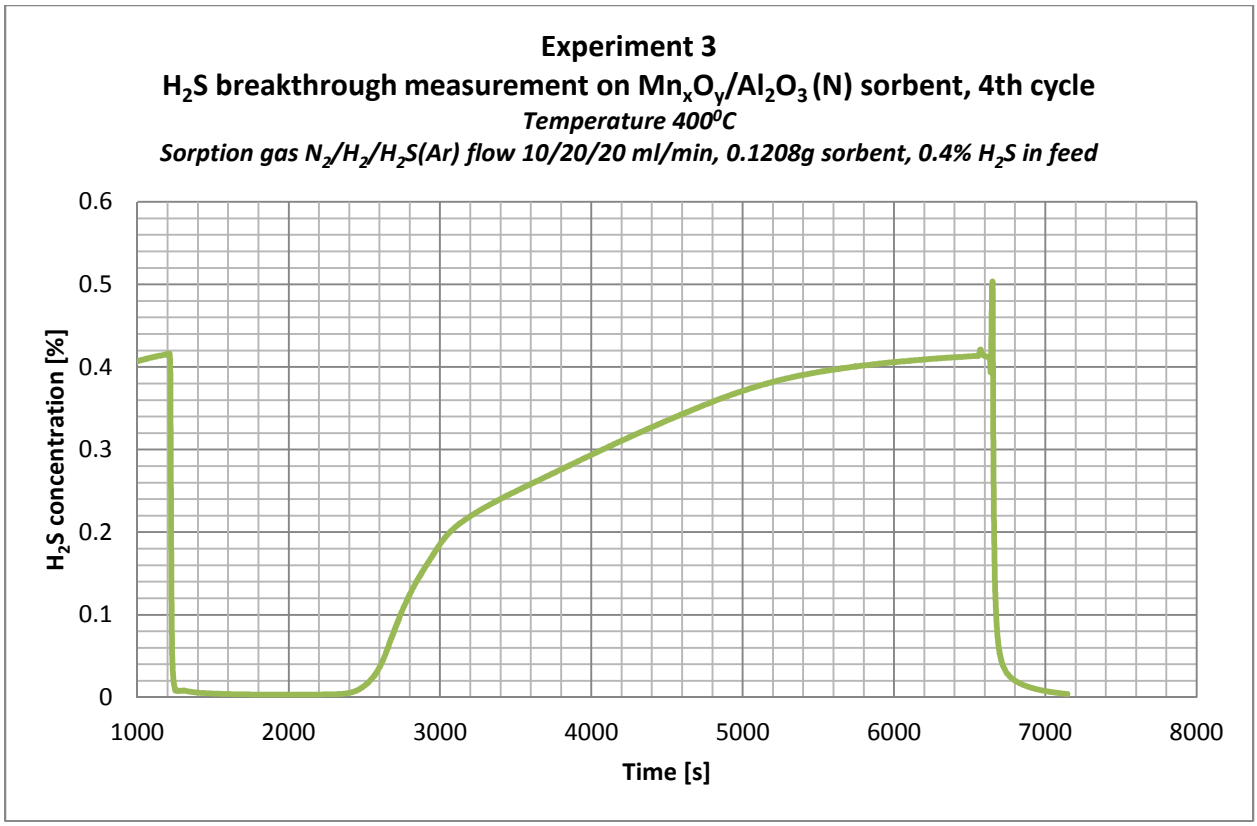
Experiment 3
H2S breakthrough measurement on MnxOy/Al2O3 (N) sorbent, 4th cycle
Temperature 400⁰C
Sorption gas N2/H2/H2S(Ar) flow 10/20/20 ml/min, 0.1208g sorbent, 0.4% H2S in feed
H2S concentration [%]
0.6
0.5
0.4
0.3
0.2
0.1
0
1000
2000
3000
4000
5000
6000
7000
8000
Time [s]

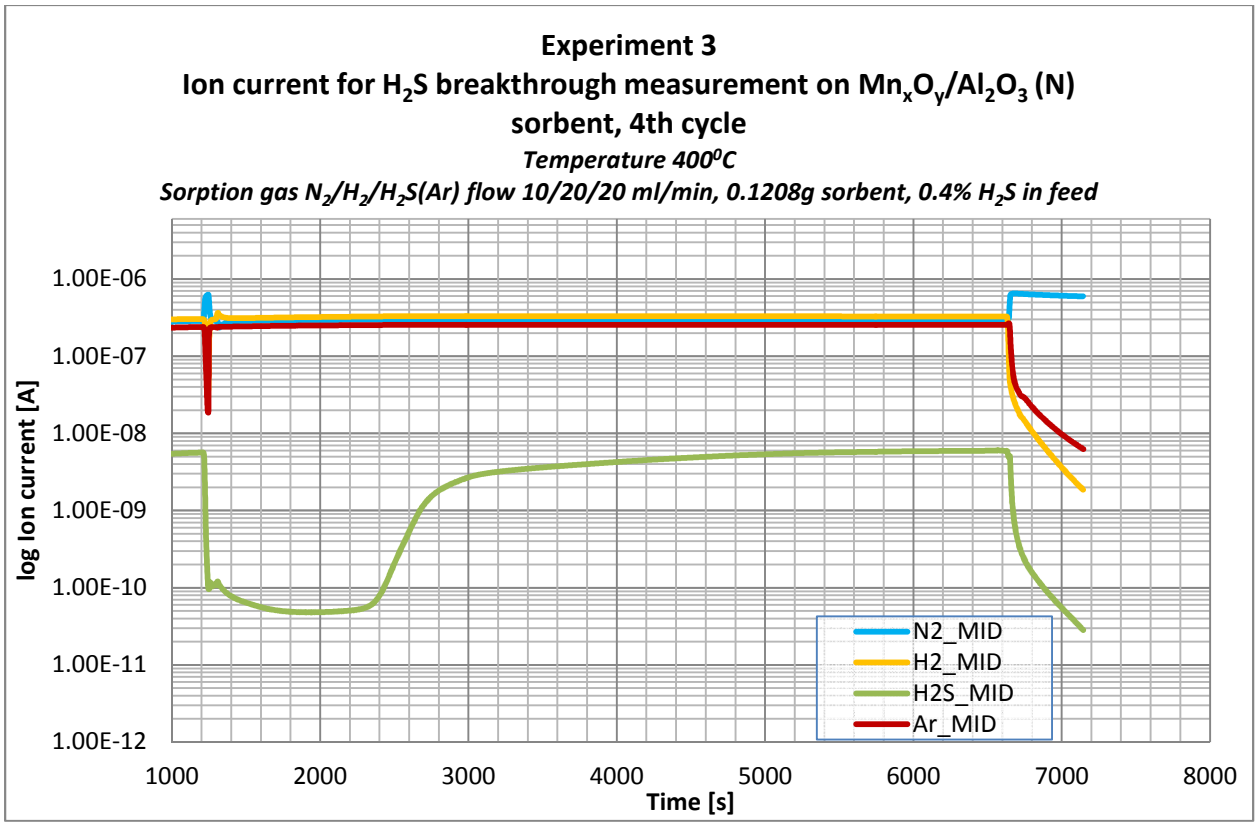
Experiment 3
Ion current for H2S breakthrough measurement on MnxOy/Al2O3 (N) sorbent, 4th cycle
Temperature 400⁰C
Sorption gas N2/H2/H2S(Ar) flow 10/20/20 ml/min, 0.1208g sorbent, 0.4% H2S in feed
log Ion current [A]
1.00E-06
1.00E-07
1.00E-08
1.00E-09
1.00E-10
1.00E-11
1.00E-12
1000
2000
3000
4000
5000
6000
7000
8000
Time [s]
N2_MID
H2_MID
H2S_MID
Ar_MID

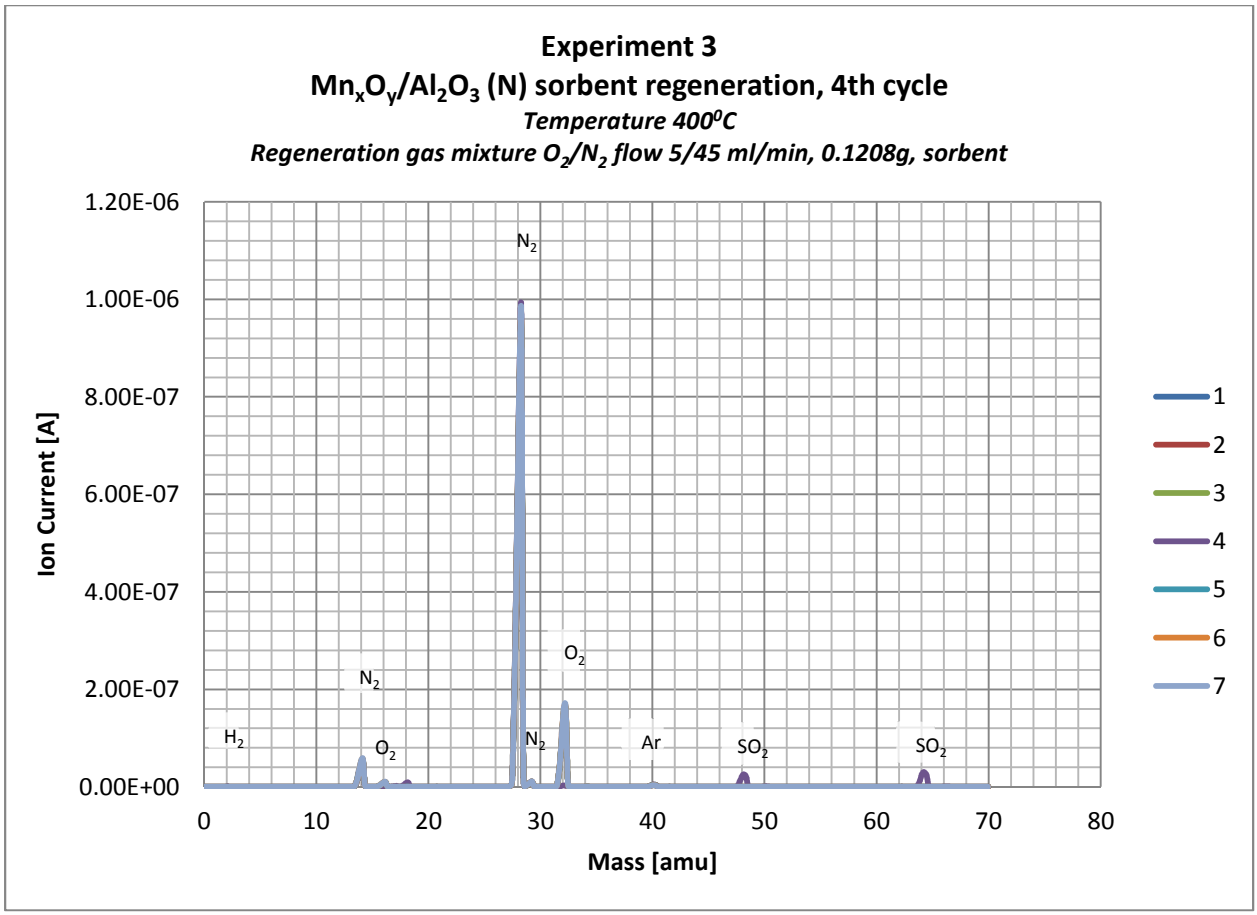
Experiment 3
Mn$_x$O$_y$/Al$_2$O$_3$ (N) sorbent regeneration, 4th cycle
Temperature 400$^0$C
Regeneration gas mixture O$_2$/N$_2$ flow 5/45 ml/min, 0.1208g, sorbent
Ion Current [A]
1.20E-06
1.00E-06
8.00E-07
6.00E-07
4.00E-07
2.00E-07
0.00E+00
0
10
20
30
40
50
60
70
80
Mass [amu]
N$_2$
O$_2$
N$_2$
H$_2$
O$_2$
N$_2$
Ar
SO$_2$
SO$_2$
1
2
3
4
5
6
7

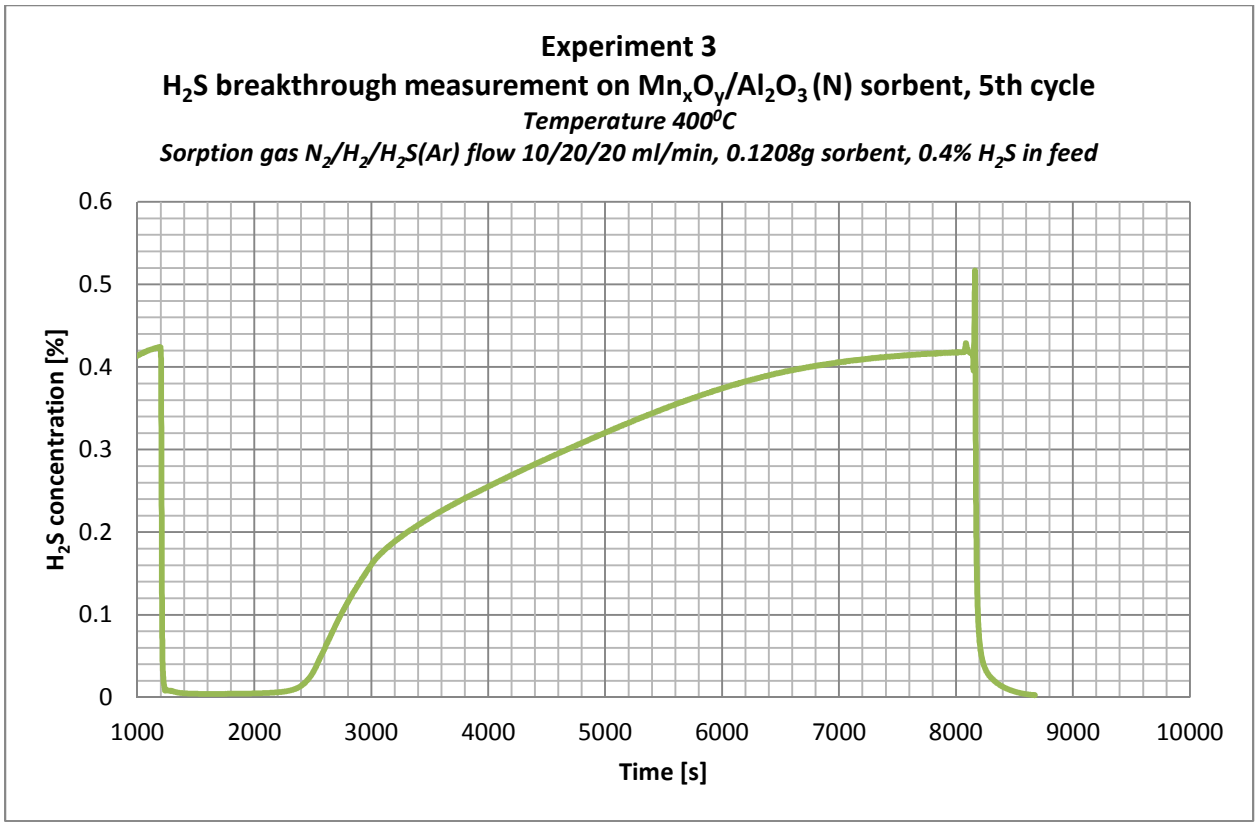
Experiment 3
H2S breakthrough measurement on MnxOy/Al2O3 (N) sorbent, 5th cycle
Temperature 400⁰C
Sorption gas N2/H2/H2S(Ar) flow 10/20/20 ml/min, 0.1208g sorbent, 0.4% H2S in feed
H2S concentration [%]
0.6
0.5
0.4
0.3
0.2
0.1
0
1000
2000
3000
4000
5000
6000
7000
8000
9000
10000
Time [s]

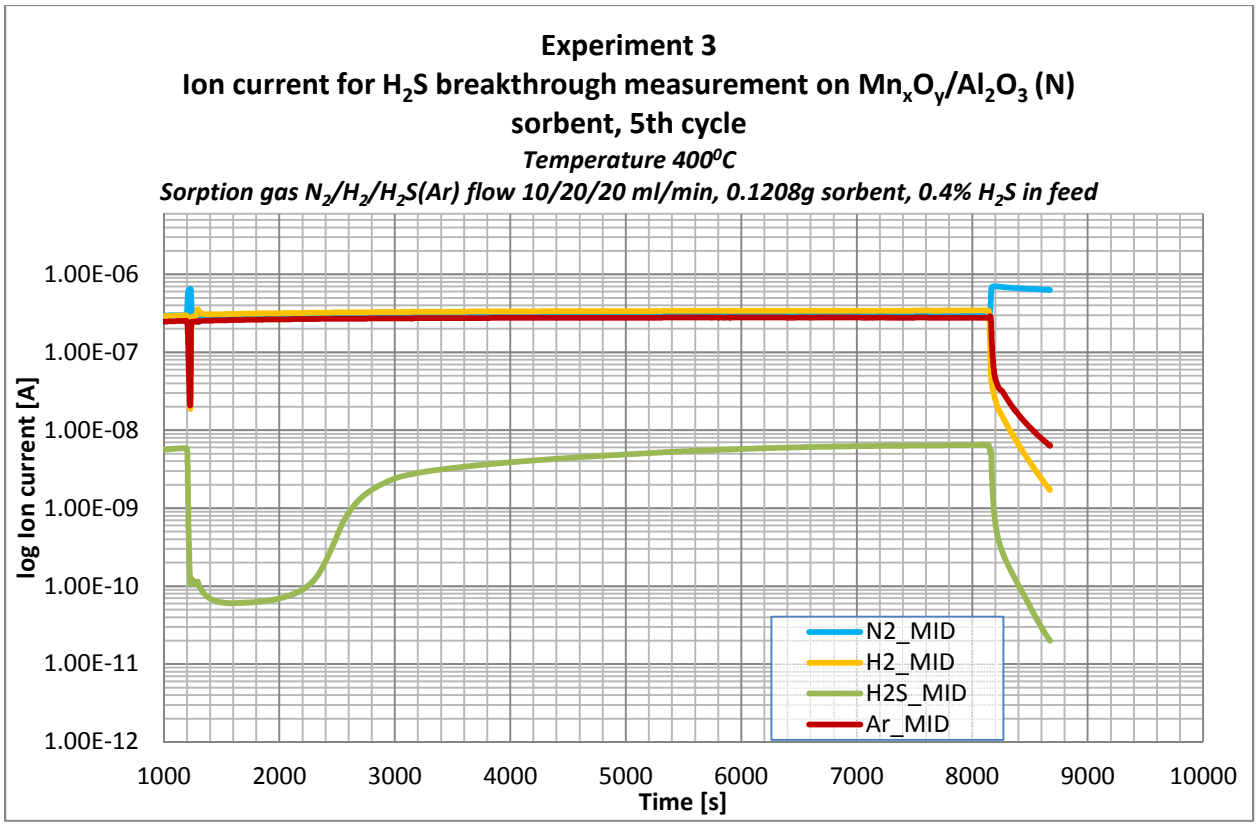
Experiment 3
Ion current for H2S breakthrough measurement on MnxOy/Al2O3 (N) sorbent, 5th cycle
Temperature 400⁰C
Sorption gas N2/H2/H2S(Ar) flow 10/20/20 ml/min, 0.1208g sorbent, 0.4% H2S in feed
log Ion current [A]
1.00E-06
1.00E-07
1.00E-08
1.00E-09
1.00E-10
1.00E-11
1.00E-12
1000
2000
3000
4000
5000
6000
7000
8000
9000
10000
Time [s]
N2_MID
H2_MID
H2S_MID
Ar_MID

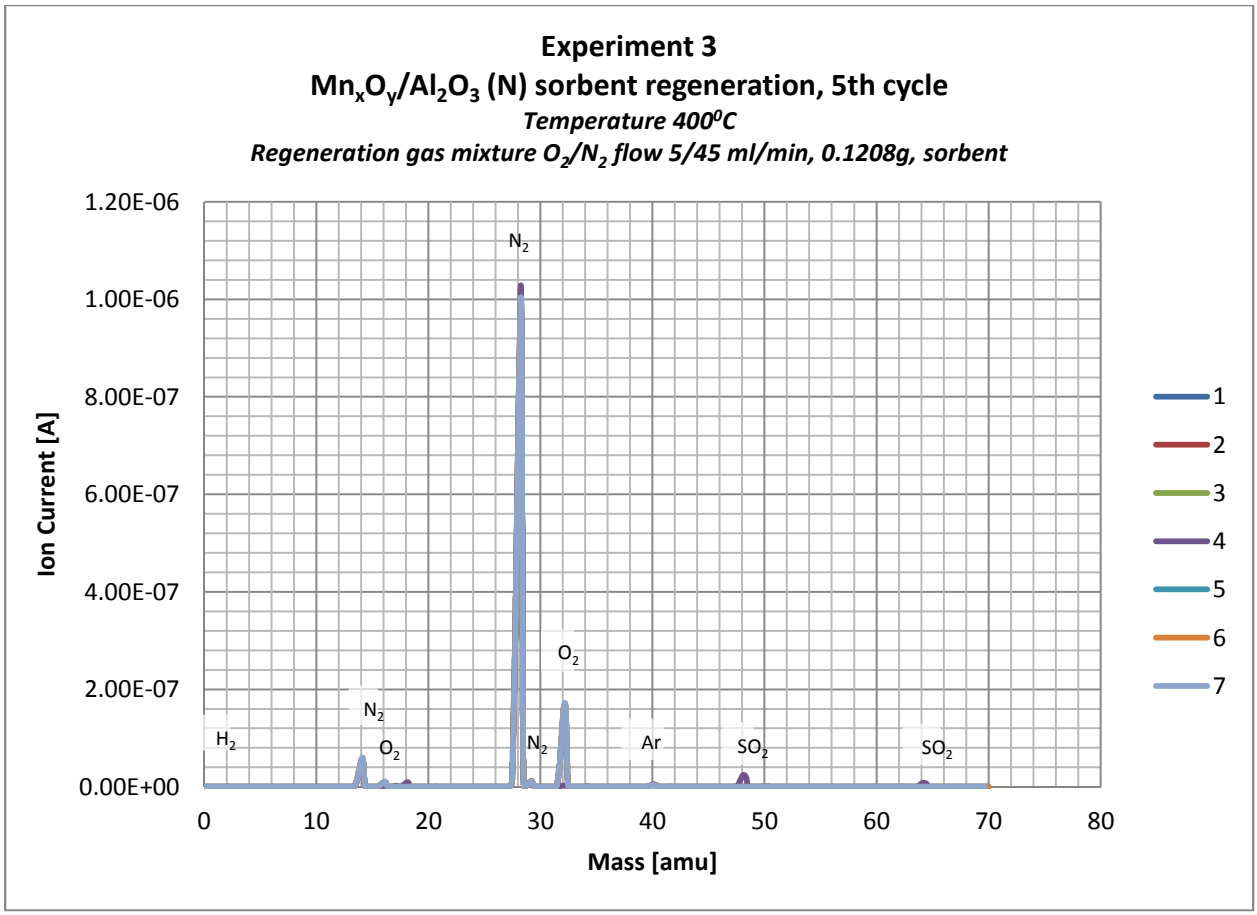
Experiment 3
Mn$_x$O$_y$/Al$_2$O$_3$ (N) sorbent regeneration, 5th cycle
Temperature 400$^0$C
Regeneration gas mixture O$_2$/N$_2$ flow 5/45 ml/min, 0.1208g, sorbent
Ion Current [A]
1.20E-06
1.00E-06
8.00E-07
6.00E-07
4.00E-07
2.00E-07
0.00E+00
0
10
20
30
40
50
60
70
80
Mass [amu]
N$_2$
O$_2$
N$_2$
H$_2$
O$_2$
N$_2$
Ar
SO$_2$
SO$_2$
1
2
3
4
5
6
7

## *Appendix M Sorption cycle measurement results for $Mn_2O_3/Al_2O_3$ (15 wt% Mn)*

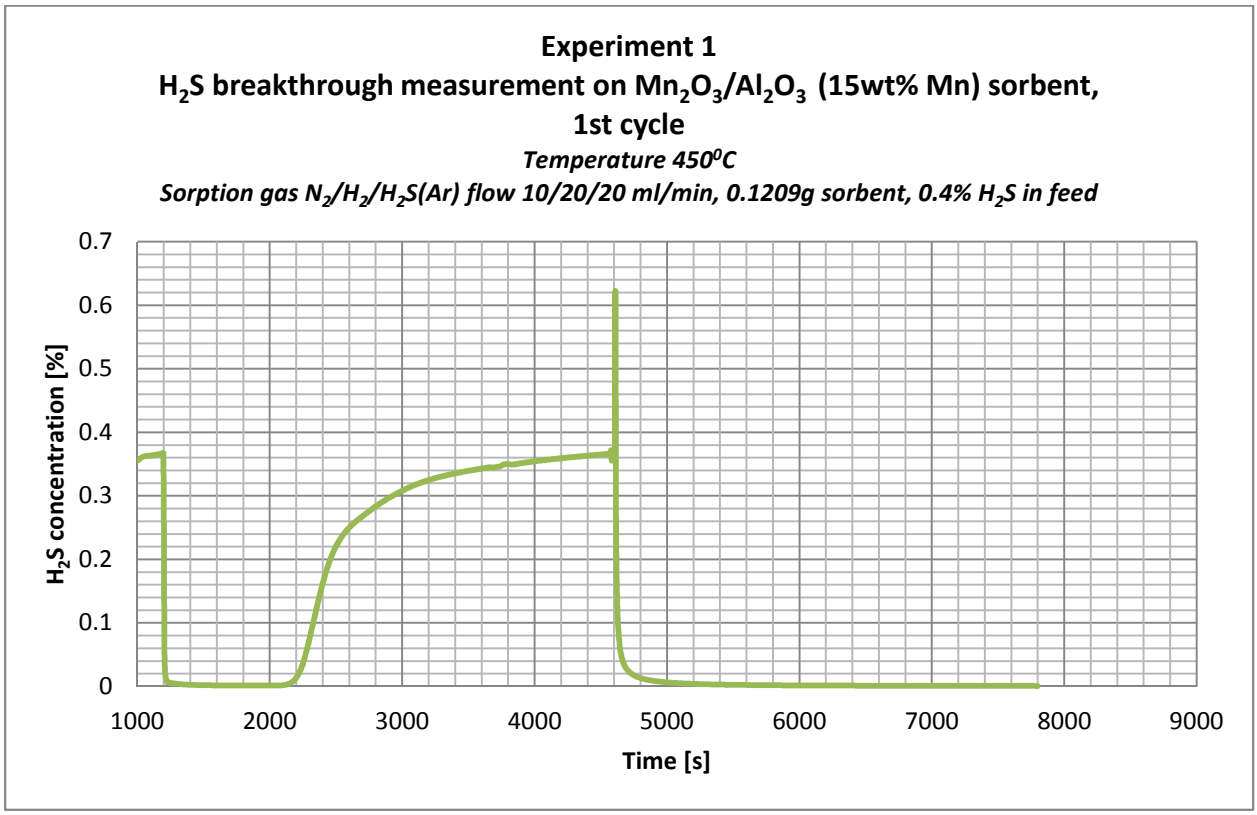


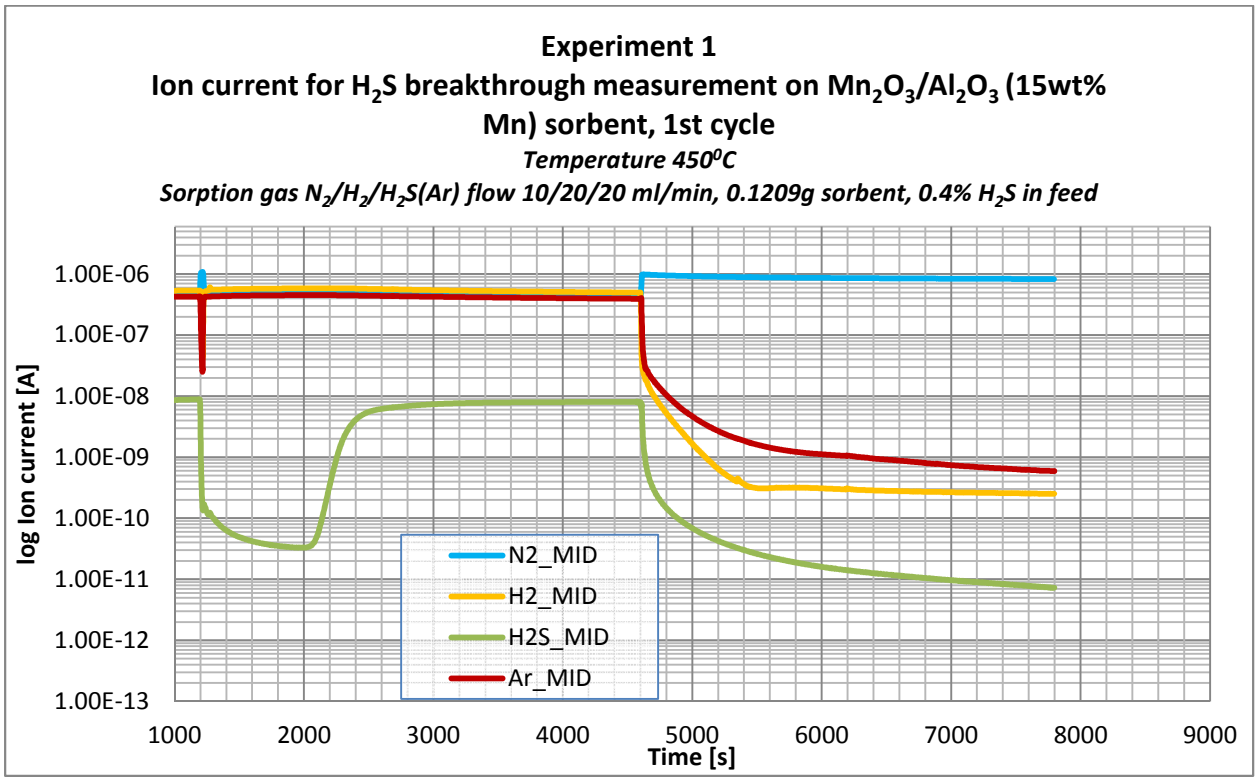

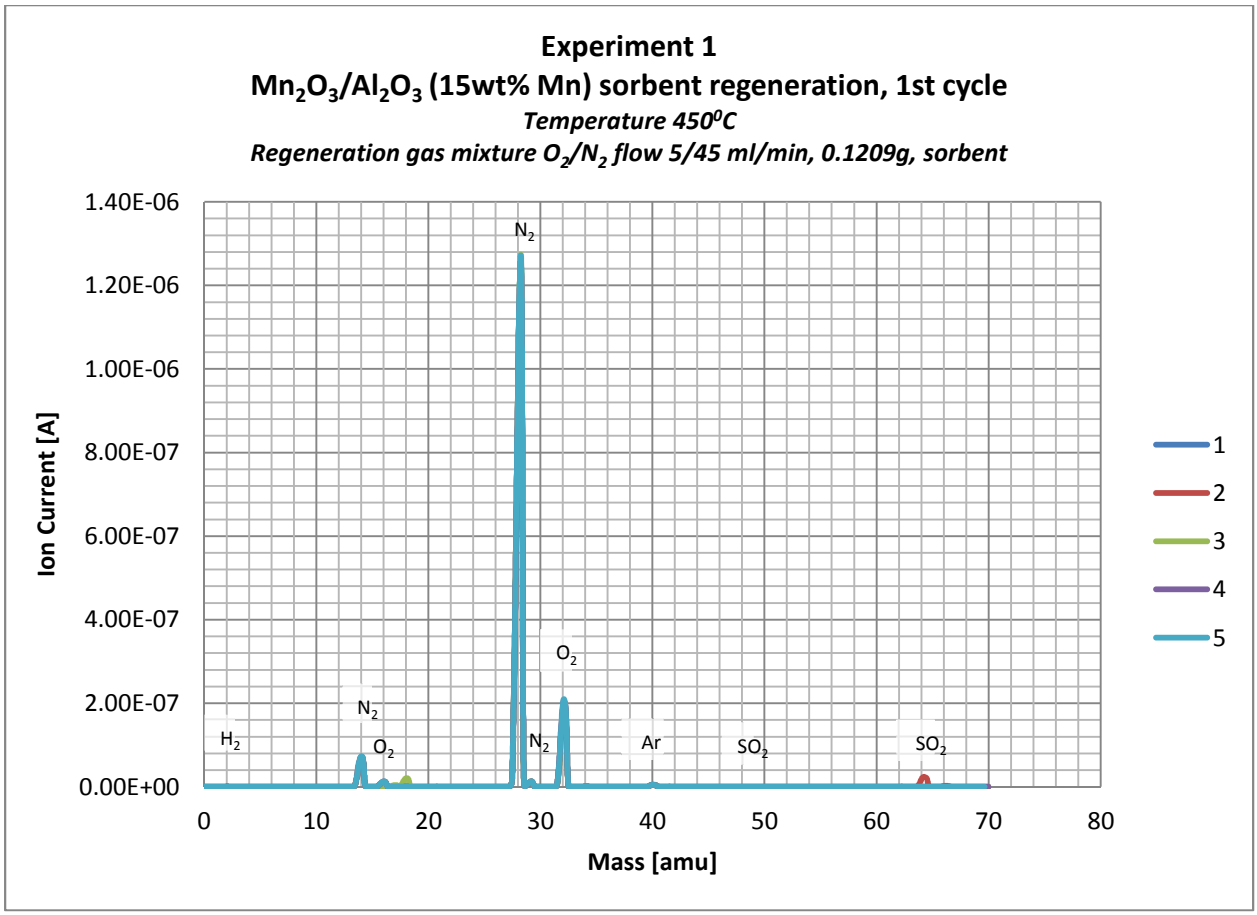
Experiment 1
Mn2O3/Al2O3 (15wt% Mn) sorbent regeneration, 1st cycle
Temperature 450⁰C
Regeneration gas mixture O2/N2 flow 5/45 ml/min, 0.1209g, sorbent
Ion Current [A]
1.40E-06
1.20E-06
1.00E-06
8.00E-07
6.00E-07
4.00E-07
2.00E-07
0.00E+00
0
10
20
30
40
50
60
70
80
Mass [amu]
N2
O2
N2
H2
N2
O2
Ar
SO2
SO2
1
2
3
4
5

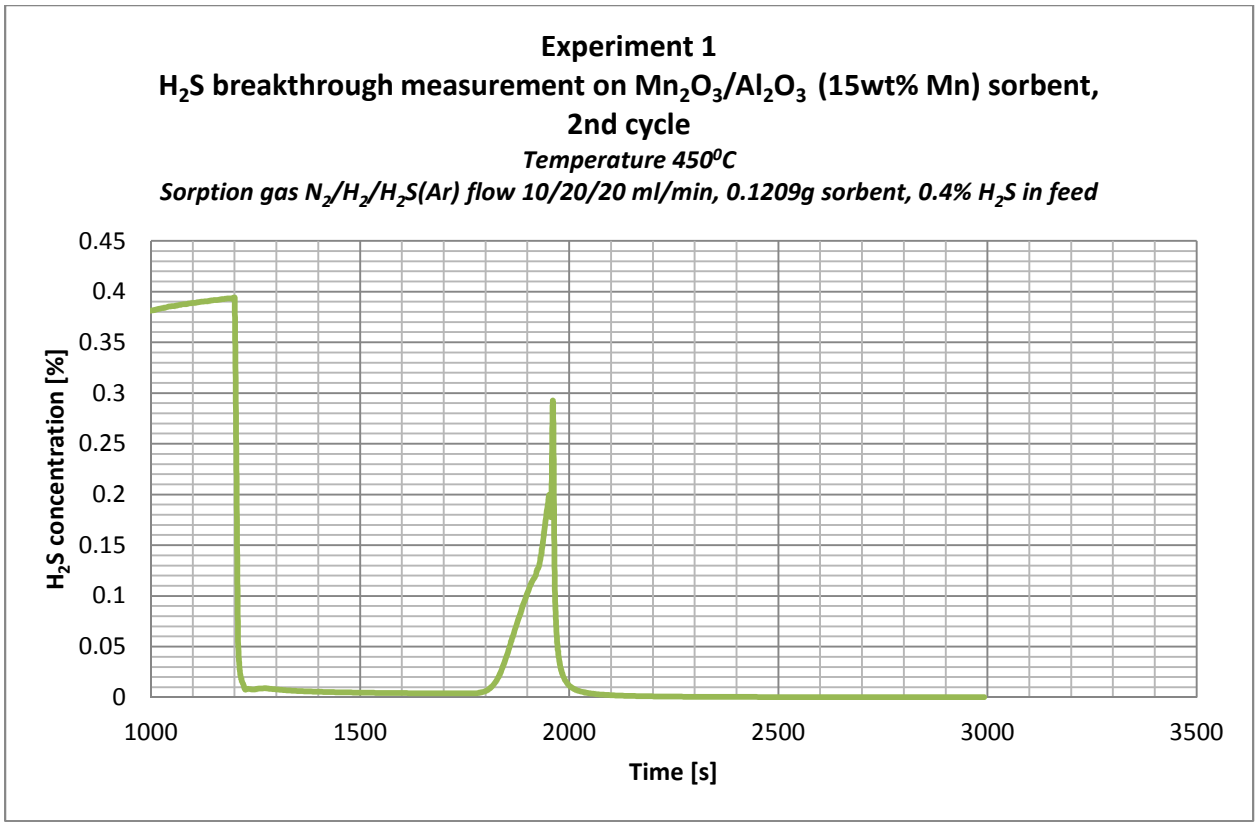
Experiment 1
H2S breakthrough measurement on Mn2O3/Al2O3 (15wt% Mn) sorbent, 2nd cycle
Temperature 450⁰C
Sorption gas N2/H2/H2S(Ar) flow 10/20/20 ml/min, 0.1209g sorbent, 0.4% H2S in feed
H2S concentration [%]
0.45
0.4
0.35
0.3
0.25
0.2
0.15
0.1
0.05
0
1000
1500
2000
2500
3000
3500
Time [s]

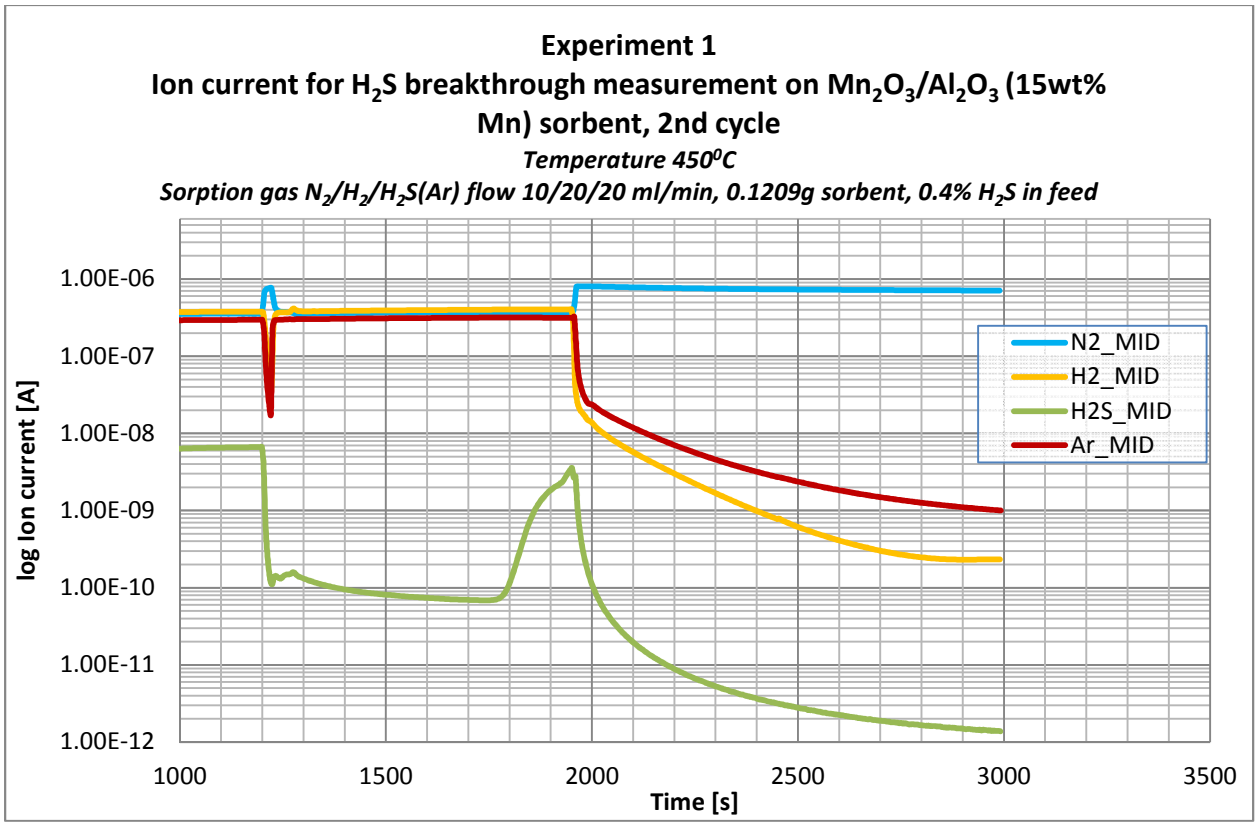
Experiment 1
Ion current for H2S breakthrough measurement on Mn2O3/Al2O3 (15wt% Mn) sorbent, 2nd cycle
Temperature 450⁰C
Sorption gas N2/H2/H2S(Ar) flow 10/20/20 ml/min, 0.1209g sorbent, 0.4% H2S in feed
log Ion current [A]
1.00E-06
1.00E-07
1.00E-08
1.00E-09
1.00E-10
1.00E-11
1.00E-12
1000
1500
2000
2500
3000
3500
Time [s]
N2_MID
H2_MID
H2S_MID
Ar_MID

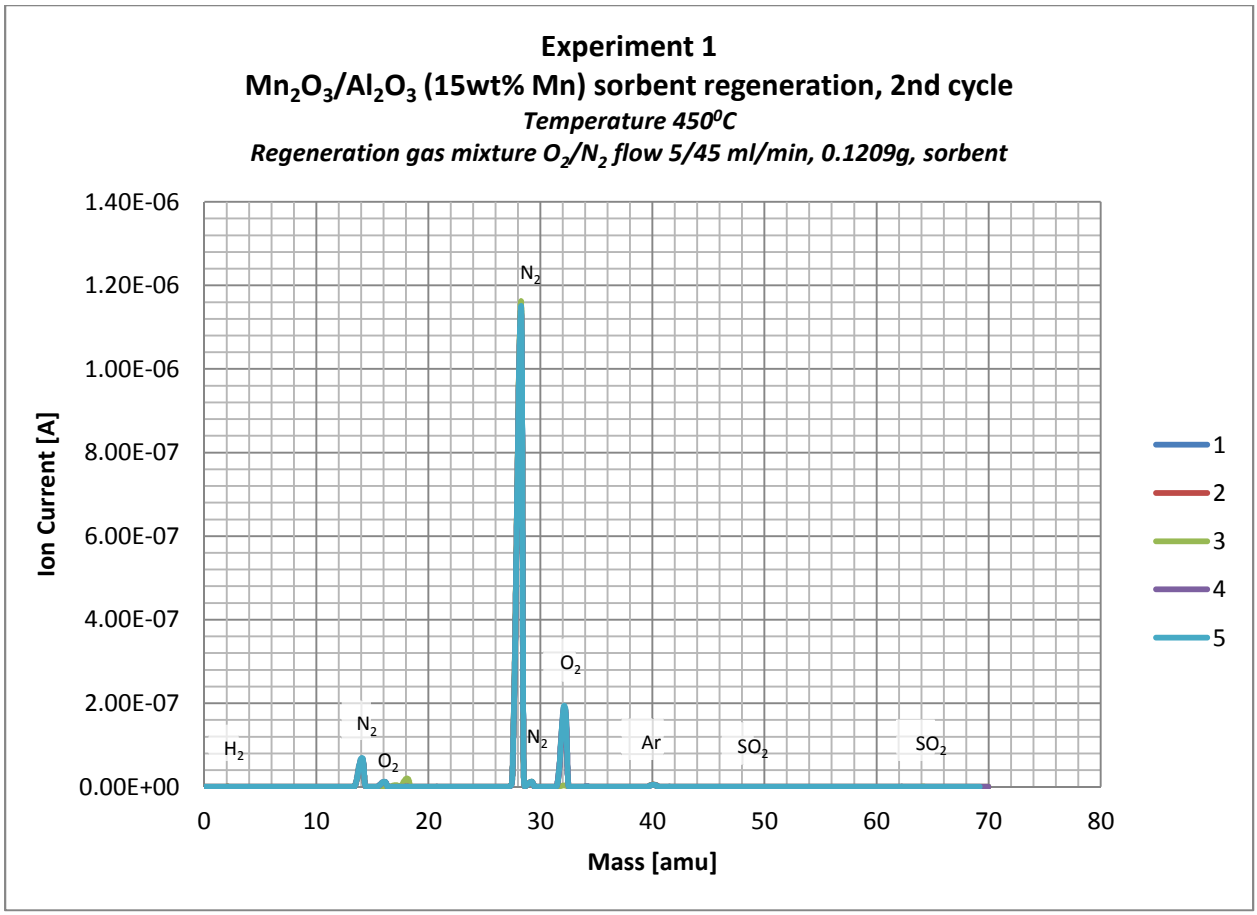
Experiment 1
Mn2O3/Al2O3 (15wt% Mn) sorbent regeneration, 2nd cycle
Temperature 450⁰C
Regeneration gas mixture O2/N2 flow 5/45 ml/min, 0.1209g, sorbent
Ion Current [A]
1.40E-06
1.20E-06
1.00E-06
8.00E-07
6.00E-07
4.00E-07
2.00E-07
0.00E+00
0
10
20
30
40
50
60
70
80
Mass [amu]
N2
O2
H2
Ar
SO2
1
2
3
4
5

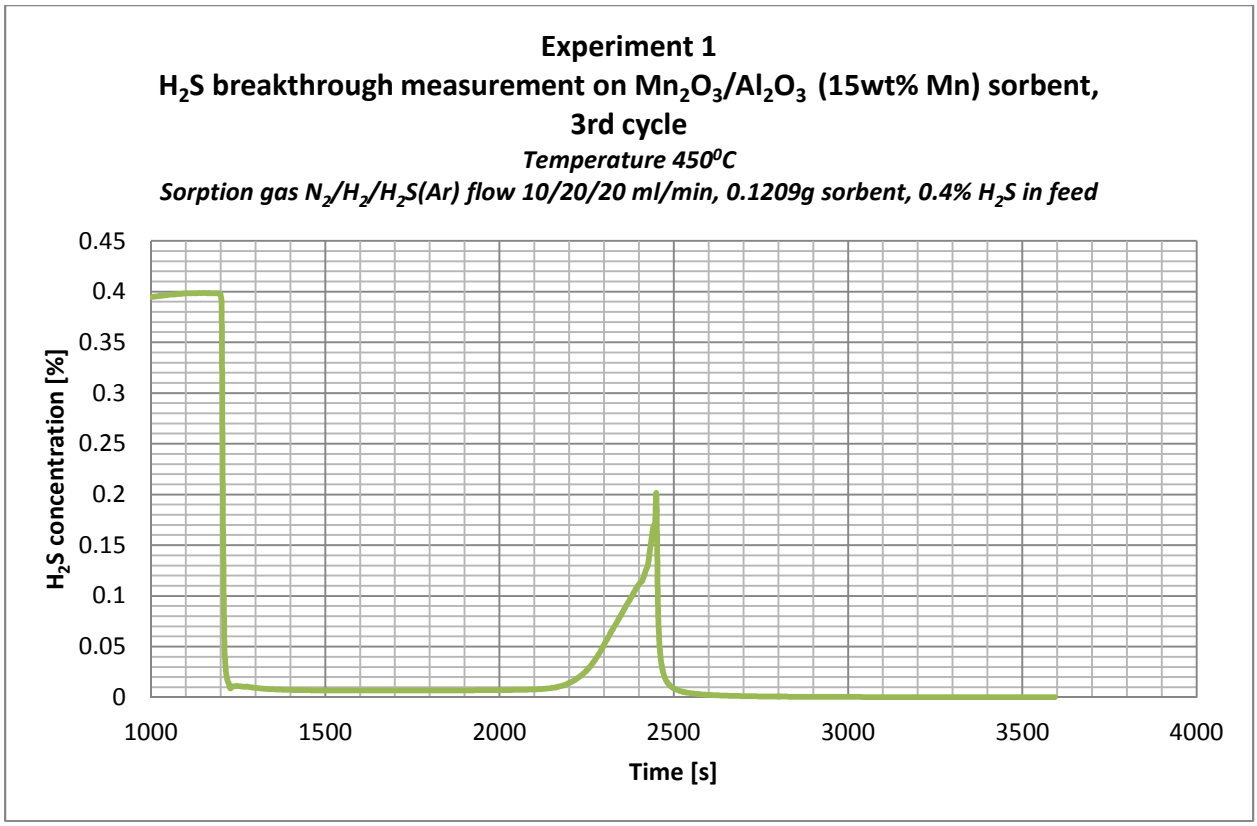
Experiment 1
H2S breakthrough measurement on Mn2O3/Al2O3 (15wt% Mn) sorbent, 3rd cycle
Temperature 450⁰C
Sorption gas N2/H2/H2S(Ar) flow 10/20/20 ml/min, 0.1209g sorbent, 0.4% H2S in feed
H2S concentration [%]
0.45
0.4
0.35
0.3
0.25
0.2
0.15
0.1
0.05
0
1000
1500
2000
2500
3000
3500
4000
Time [s]

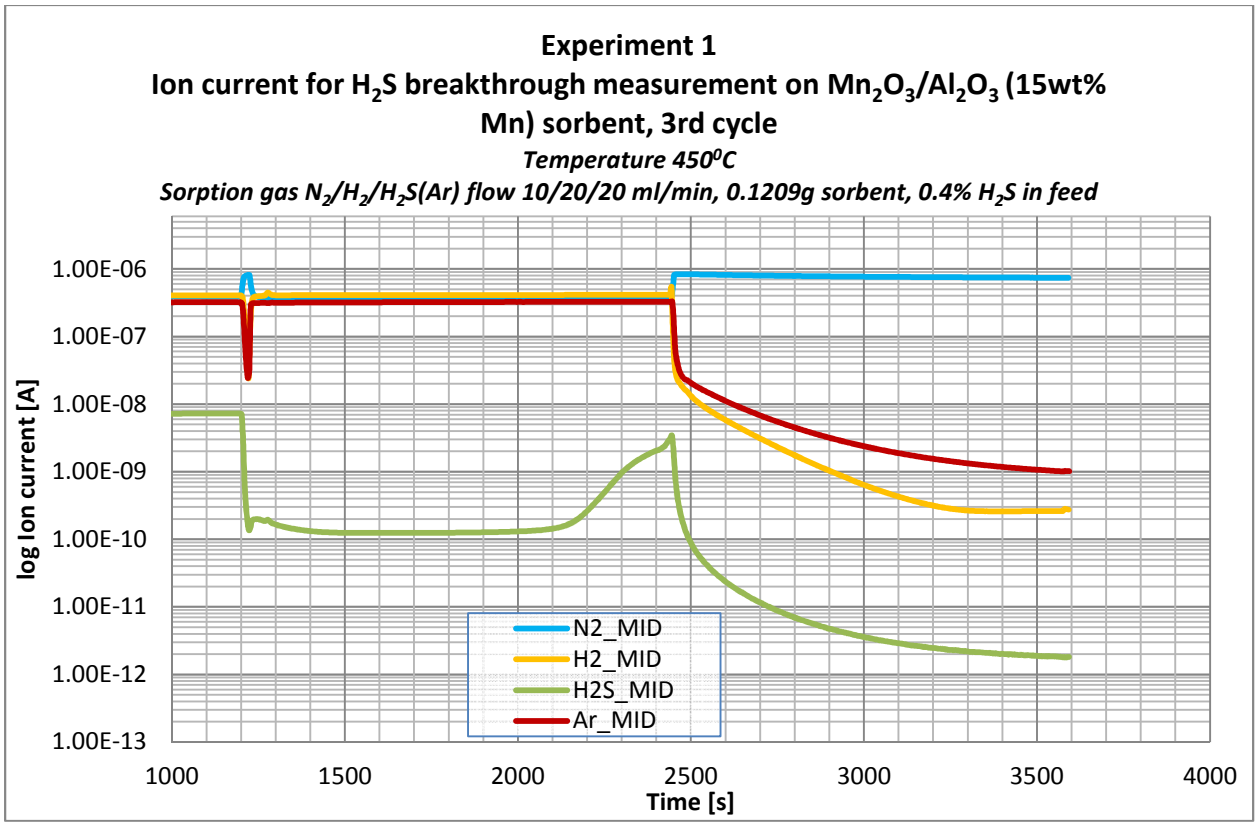
Experiment 1
Ion current for H2S breakthrough measurement on Mn2O3/Al2O3 (15wt% Mn) sorbent, 3rd cycle
Temperature 450⁰C
Sorption gas N2/H2/H2S(Ar) flow 10/20/20 ml/min, 0.1209g sorbent, 0.4% H2S in feed
log Ion current [A]
1.00E-06
1.00E-07
1.00E-08
1.00E-09
1.00E-10
1.00E-11
1.00E-12
1.00E-13
1000
1500
2000
2500
3000
3500
4000
Time [s]
N2_MID
H2_MID
H2S_MID
Ar_MID

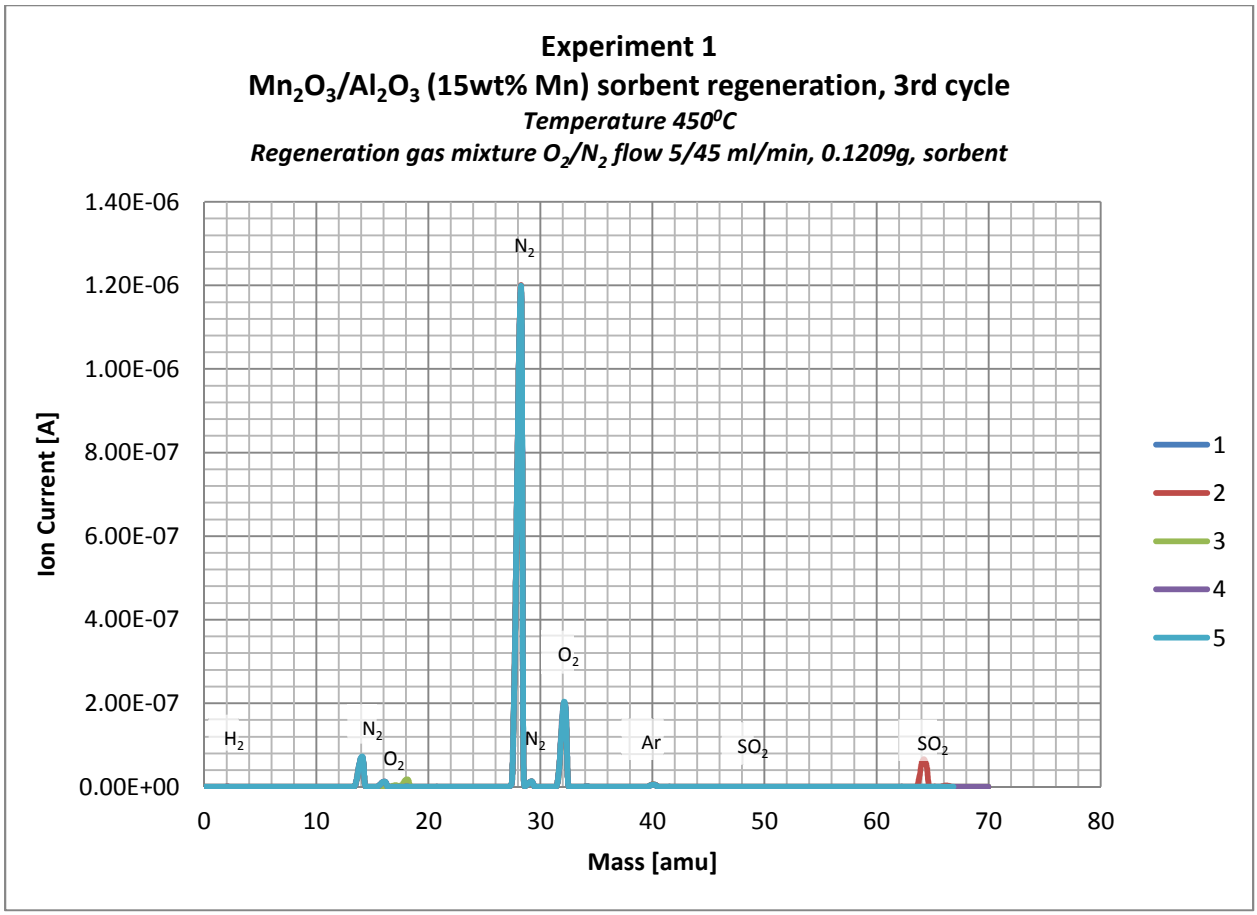
Experiment 1
Mn2O3/Al2O3 (15wt% Mn) sorbent regeneration, 3rd cycle
Temperature 450⁰C
Regeneration gas mixture O2/N2 flow 5/45 ml/min, 0.1209g, sorbent
Ion Current [A]
1.40E-06
1.20E-06
1.00E-06
8.00E-07
6.00E-07
4.00E-07
2.00E-07
0.00E+00
0
10
20
30
40
50
60
70
80
Mass [amu]
H2
N2
O2
N2
N2
O2
Ar
SO2
SO2
1
2
3
4
5

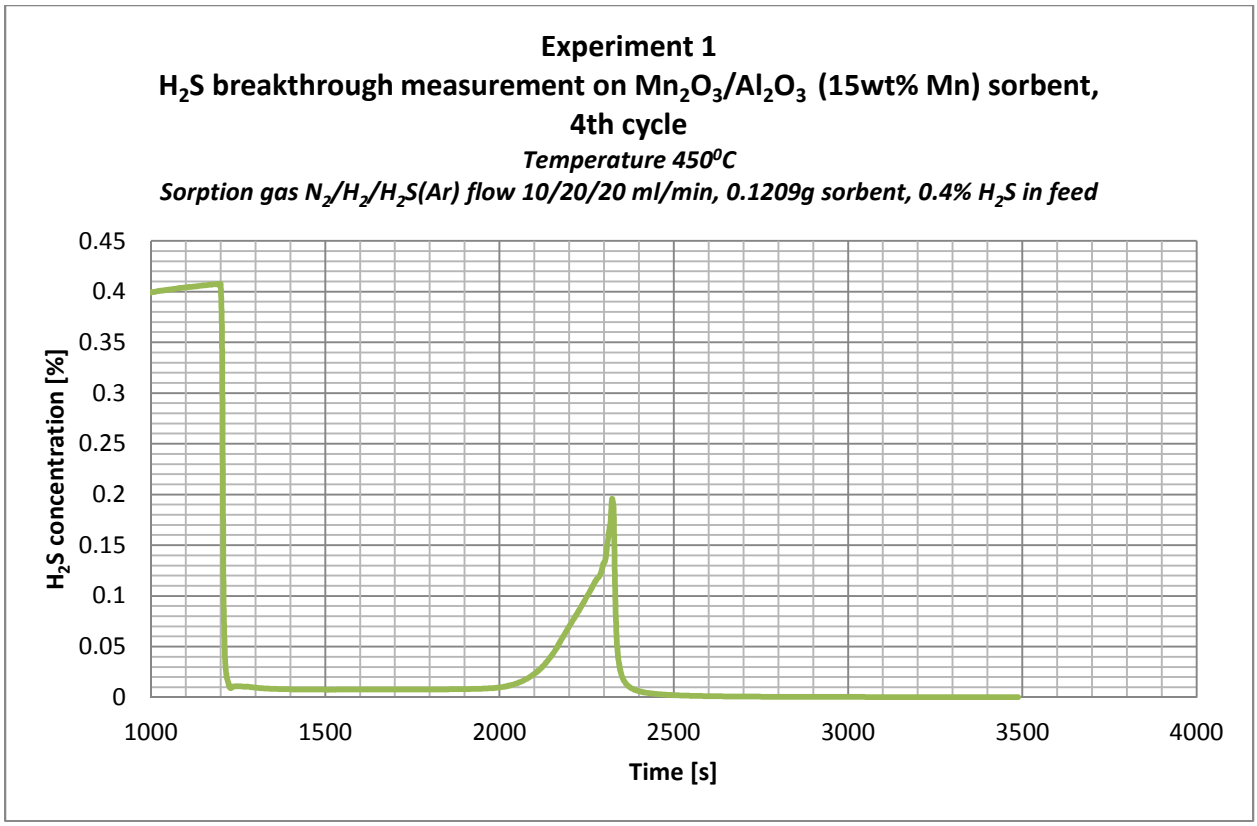
Experiment 1
H2S breakthrough measurement on Mn2O3/Al2O3 (15wt% Mn) sorbent, 4th cycle
Temperature 450⁰C
Sorption gas N2/H2/H2S(Ar) flow 10/20/20 ml/min, 0.1209g sorbent, 0.4% H2S in feed
H2S concentration [%]
0.45
0.4
0.35
0.3
0.25
0.2
0.15
0.1
0.05
0
1000
1500
2000
2500
3000
3500
4000
Time [s]

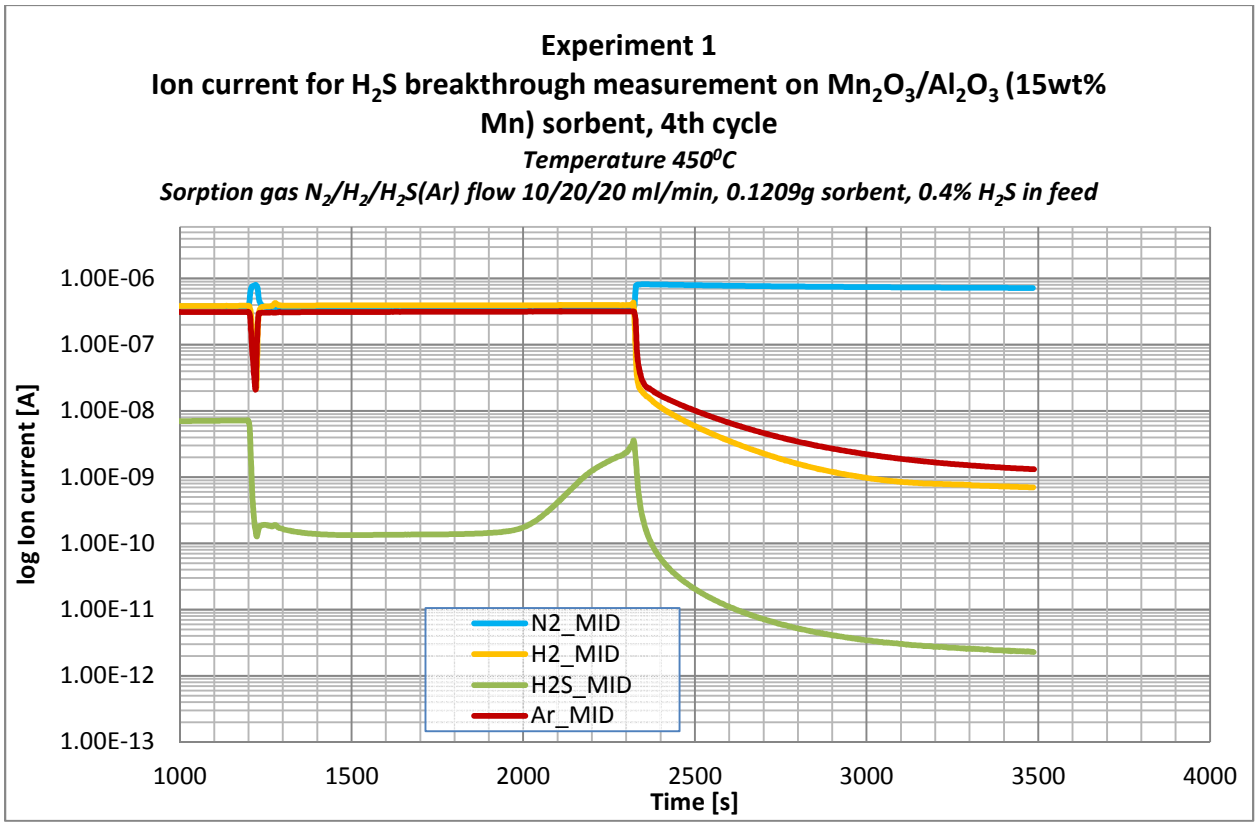
Experiment 1
Ion current for H2S breakthrough measurement on Mn2O3/Al2O3 (15wt% Mn) sorbent, 4th cycle
Temperature 450⁰C
Sorption gas N2/H2/H2S(Ar) flow 10/20/20 ml/min, 0.1209g sorbent, 0.4% H2S in feed
log Ion current [A]
1.00E-06
1.00E-07
1.00E-08
1.00E-09
1.00E-10
1.00E-11
1.00E-12
1.00E-13
1000
1500
2000
2500
3000
3500
4000
Time [s]
N2_MID
H2_MID
H2S_MID
Ar_MID

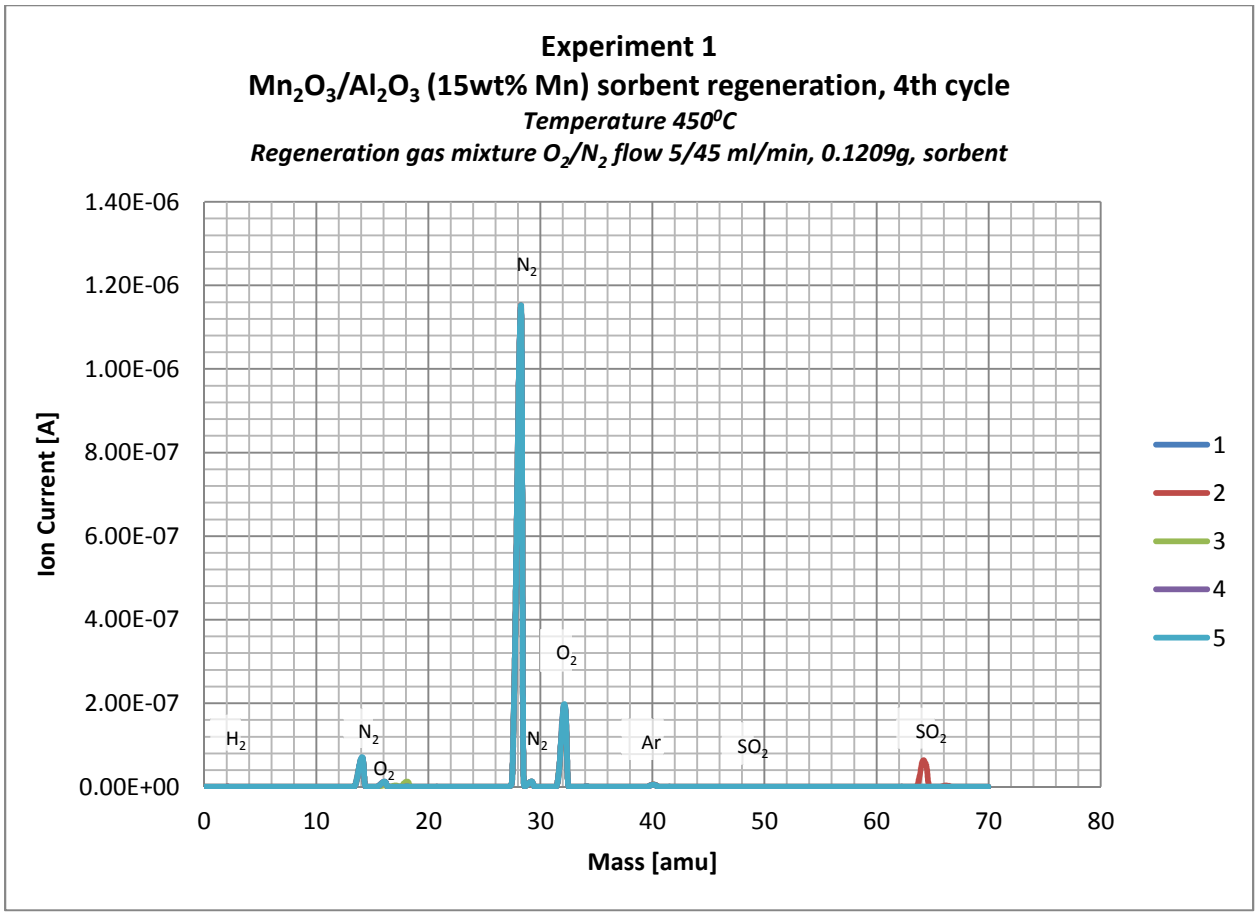
Experiment 1
Mn2O3/Al2O3 (15wt% Mn) sorbent regeneration, 4th cycle
Temperature 450⁰C
Regeneration gas mixture O2/N2 flow 5/45 ml/min, 0.1209g, sorbent
Ion Current [A]
1.40E-06
1.20E-06
1.00E-06
8.00E-07
6.00E-07
4.00E-07
2.00E-07
0.00E+00
0
10
20
30
40
50
60
70
80
Mass [amu]
N2
O2
H2
N2
O2
N2
Ar
SO2
SO2
1
2
3
4
5

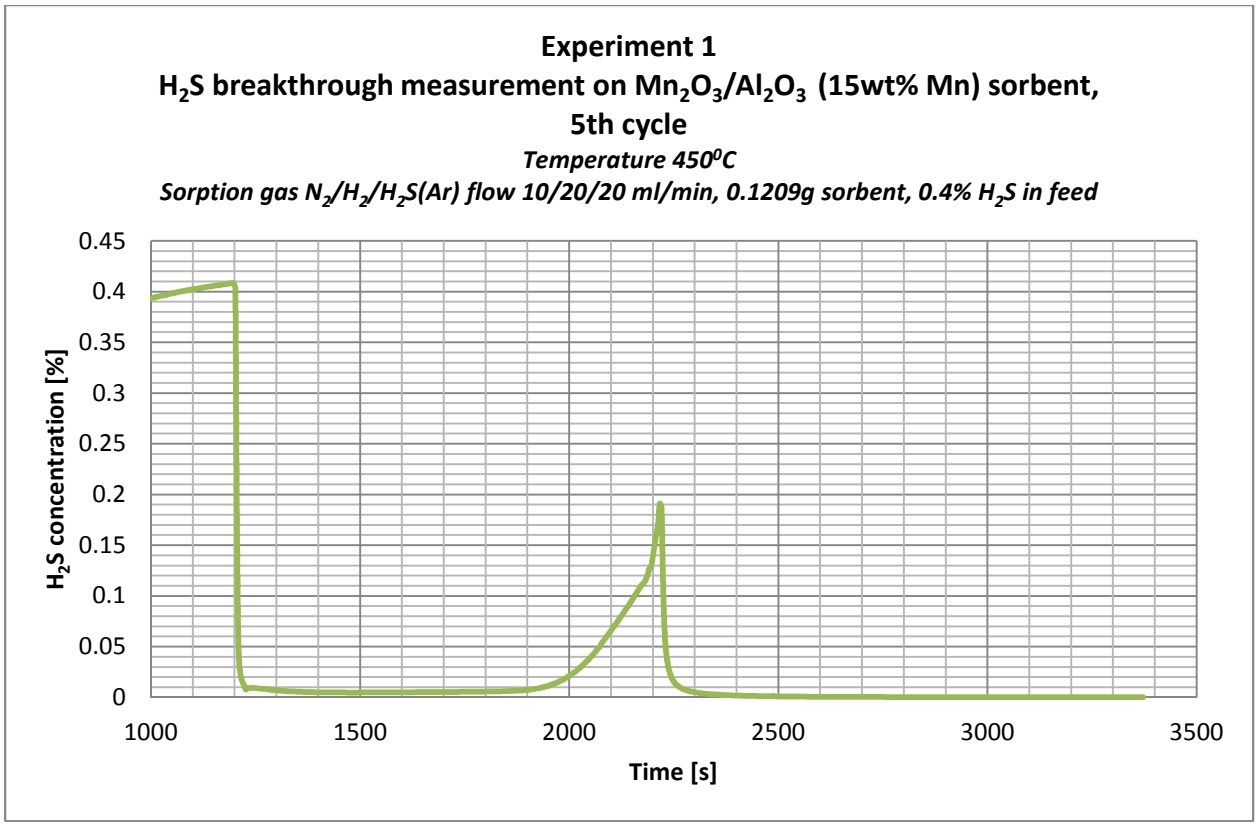
Experiment 1
H2S breakthrough measurement on Mn2O3/Al2O3 (15wt% Mn) sorbent, 5th cycle
Temperature 450⁰C
Sorption gas N2/H2/H2S(Ar) flow 10/20/20 ml/min, 0.1209g sorbent, 0.4% H2S in feed
H2S concentration [%]
0.45
0.4
0.35
0.3
0.25
0.2
0.15
0.1
0.05
0
1000
1500
2000
2500
3000
3500
Time [s]

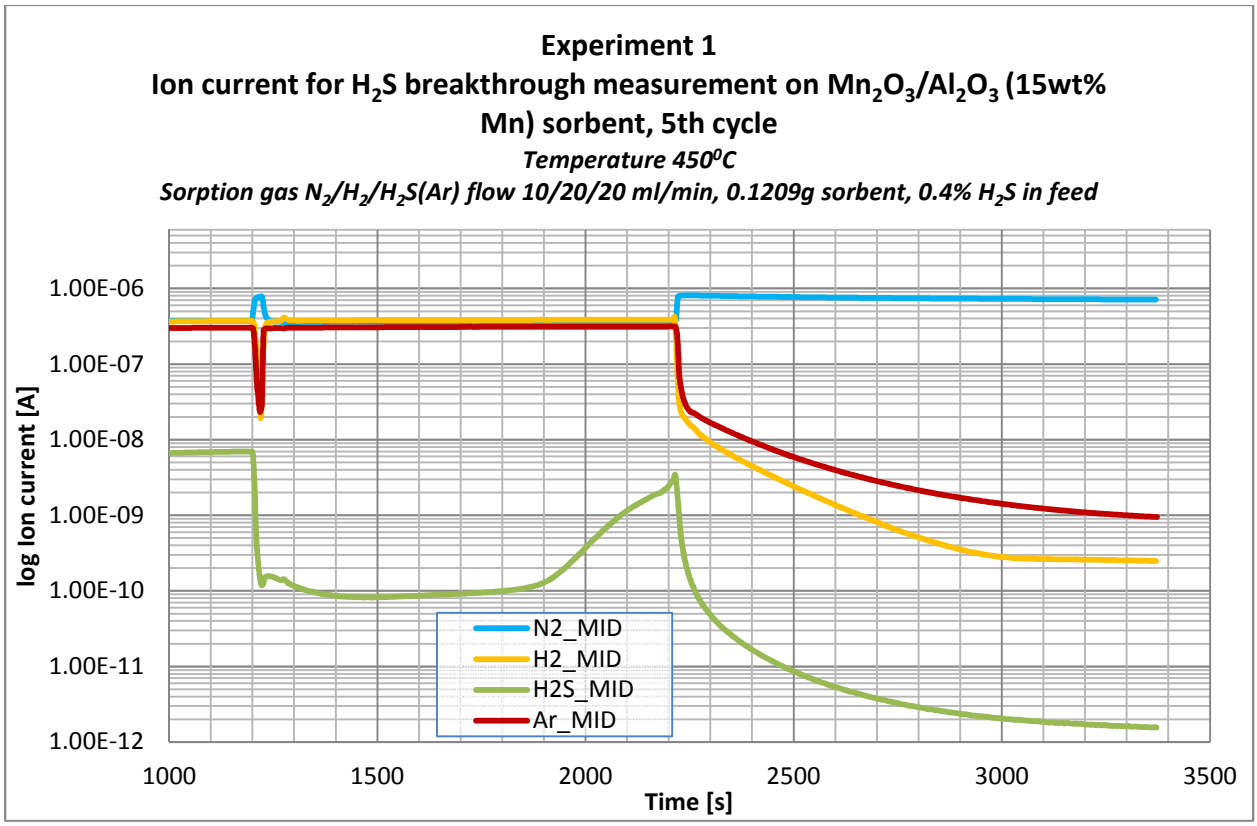
Experiment 1
Ion current for H2S breakthrough measurement on Mn2O3/Al2O3 (15wt% Mn) sorbent, 5th cycle
Temperature 450⁰C
Sorption gas N2/H2/H2S(Ar) flow 10/20/20 ml/min, 0.1209g sorbent, 0.4% H2S in feed
log Ion current [A]
1.00E-06
1.00E-07
1.00E-08
1.00E-09
1.00E-10
1.00E-11
1.00E-12
1000
1500
2000
2500
3000
3500
Time [s]
N2_MID
H2_MID
H2S_MID
Ar_MID

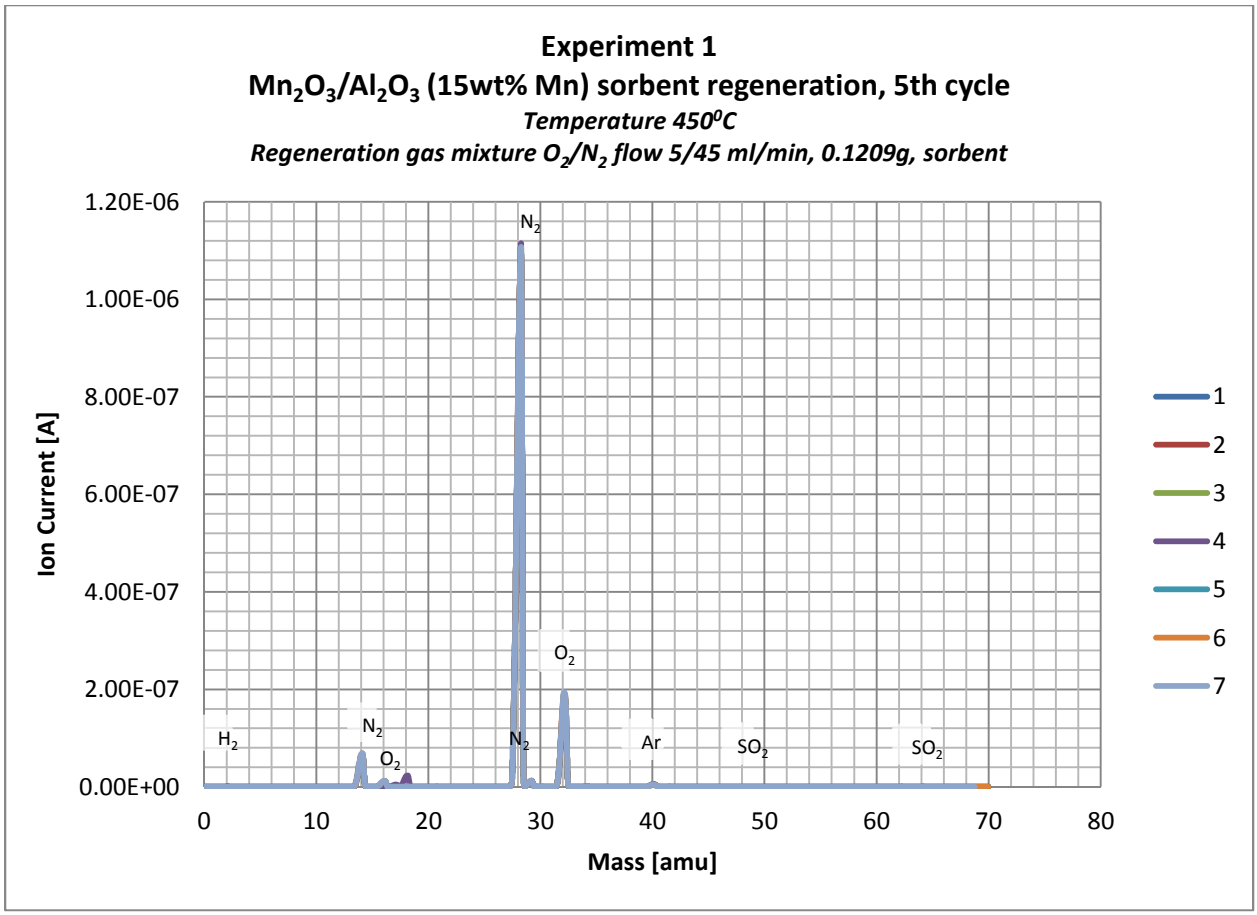
Experiment 1
Mn2O3/Al2O3 (15wt% Mn) sorbent regeneration, 5th cycle
Temperature 450⁰C
Regeneration gas mixture O2/N2 flow 5/45 ml/min, 0.1209g, sorbent
Ion Current [A]
1.20E-06
1.00E-06
8.00E-07
6.00E-07
4.00E-07
2.00E-07
0.00E+00
0
10
20
30
40
50
60
70
80
Mass [amu]
H2
N2
O2
N2
N2
O2
Ar
SO2
SO2
1
2
3
4
5
6
7

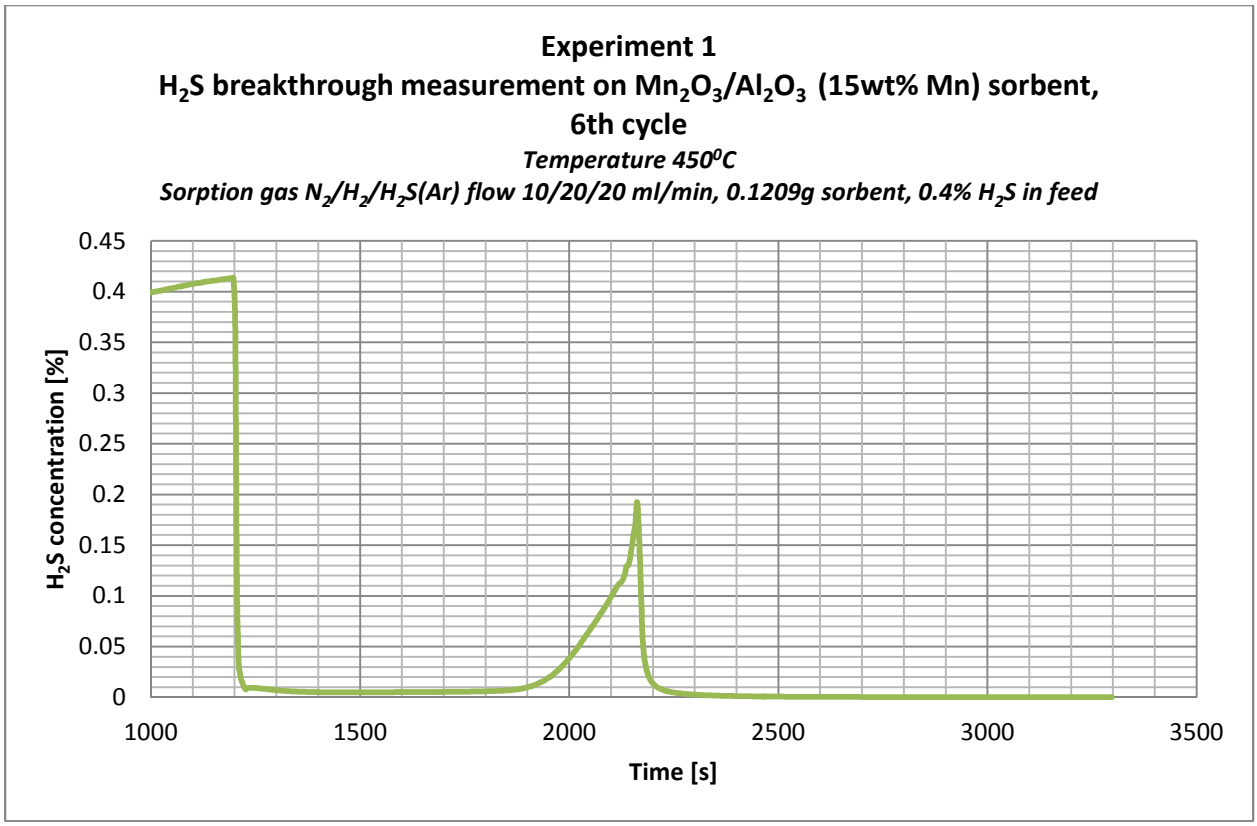
Experiment 1
H2S breakthrough measurement on Mn2O3/Al2O3 (15wt% Mn) sorbent, 6th cycle
Temperature 450⁰C
Sorption gas N2/H2/H2S(Ar) flow 10/20/20 ml/min, 0.1209g sorbent, 0.4% H2S in feed
H2S concentration [%]
0.45
0.4
0.35
0.3
0.25
0.2
0.15
0.1
0.05
0
1000
1500
2000
2500
3000
3500
Time [s]

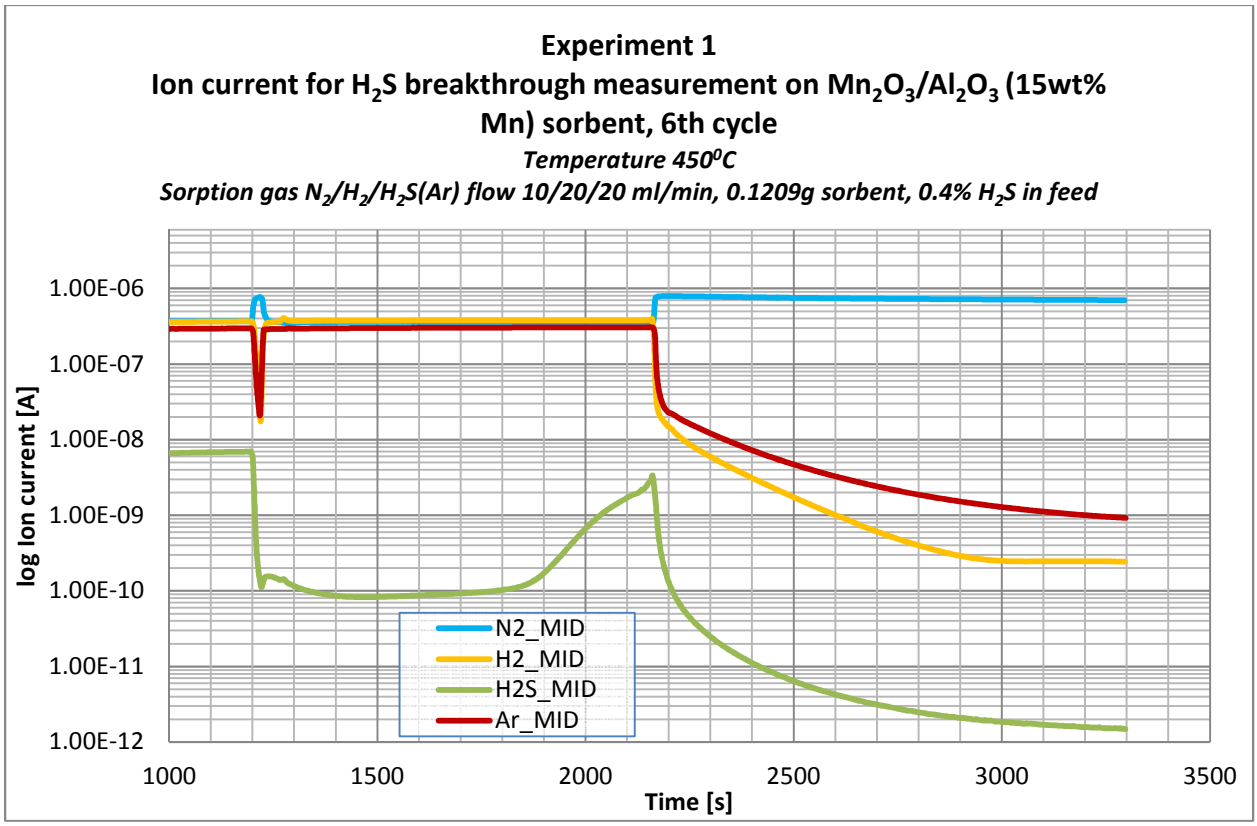
Experiment 1
Ion current for H2S breakthrough measurement on Mn2O3/Al2O3 (15wt% Mn) sorbent, 6th cycle
Temperature 450⁰C
Sorption gas N2/H2/H2S(Ar) flow 10/20/20 ml/min, 0.1209g sorbent, 0.4% H2S in feed
log Ion current [A]
1.00E-06
1.00E-07
1.00E-08
1.00E-09
1.00E-10
1.00E-11
1.00E-12
1000
1500
2000
2500
3000
3500
Time [s]
N2_MID
H2_MID
H2S_MID
Ar_MID

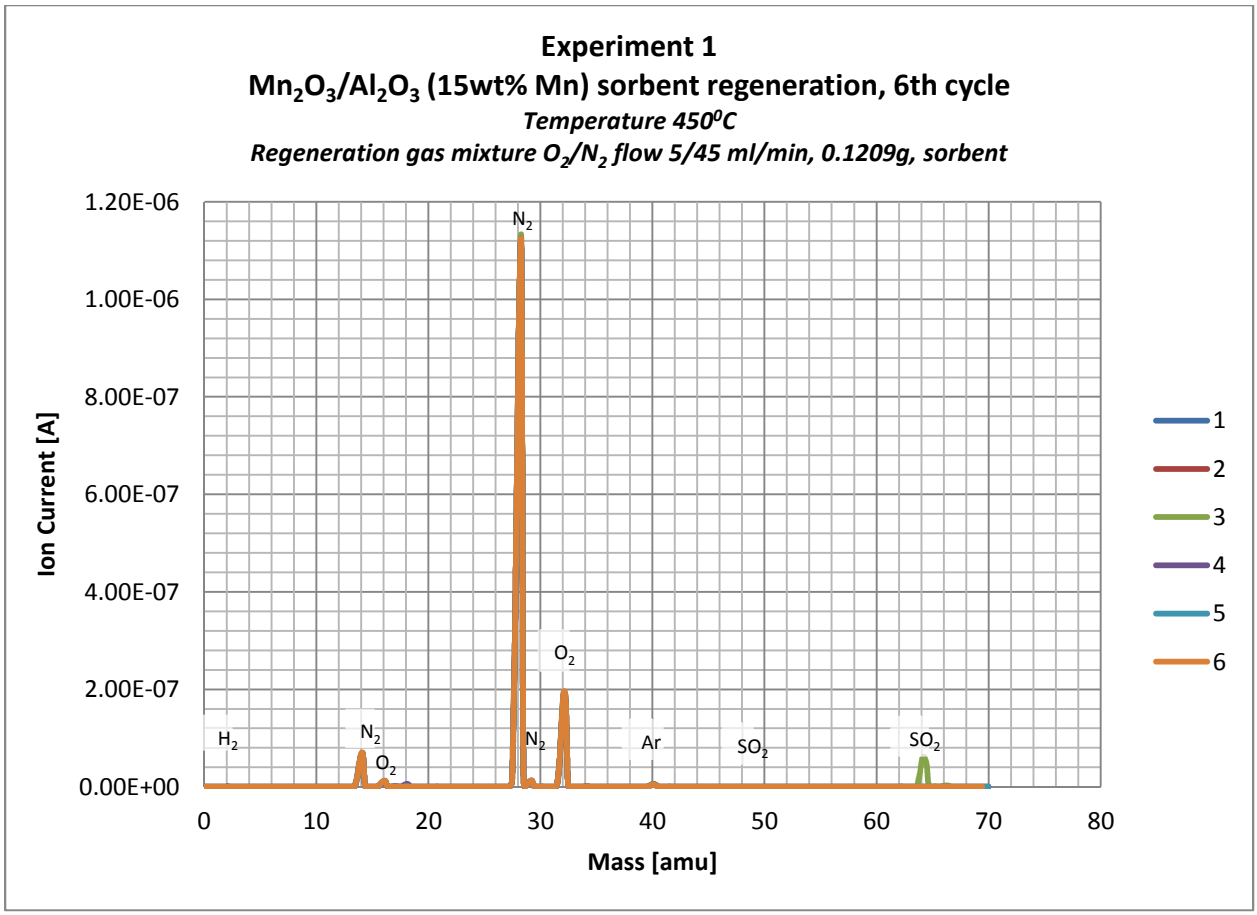
Experiment 1
Mn2O3/Al2O3 (15wt% Mn) sorbent regeneration, 6th cycle
Temperature 450⁰C
Regeneration gas mixture O2/N2 flow 5/45 ml/min, 0.1209g, sorbent
Ion Current [A]
1.20E-06
1.00E-06
8.00E-07
6.00E-07
4.00E-07
2.00E-07
0.00E+00
0
10
20
30
40
50
60
70
80
Mass [amu]
N2
O2
H2
N2
O2
N2
Ar
SO2
SO2
1
2
3
4
5
6

**Experiment 1**

**$H_2S$ breakthrough measurement on $Mn_2O_3/Al_2O_3$ (15wt% Mn) sorbent, 7th cycle**

***Temperature 450$^0$C***

***Sorption gas $N_2/H_2/H_2S$(Ar) flow 10/20/20 ml/min, 0.1209g sorbent, 0.4% $H_2S$ in feed***

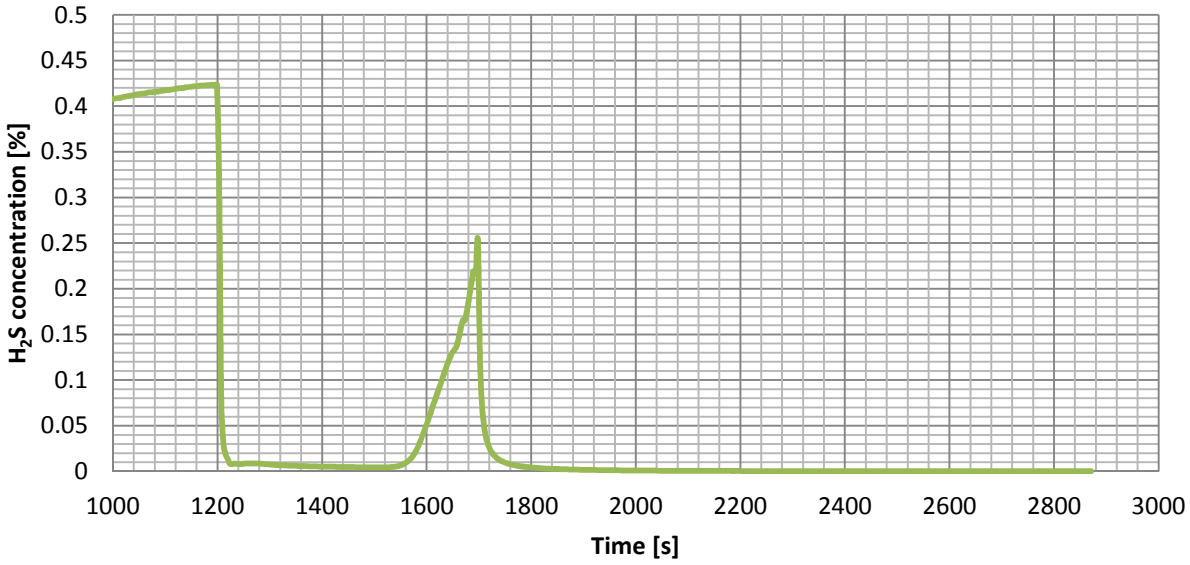


**Experiment 1**

**Ion current for $H_2S$ breakthrough measurement on $Mn_2O_3/Al_2O_3$ (15wt% Mn) sorbent, 7th cycle**

***Temperature 450$^0$C***

***Sorption gas $N_2/H_2/H_2S$(Ar) flow 10/20/20 ml/min, 0.1209g sorbent, 0.4% $H_2S$ in feed***

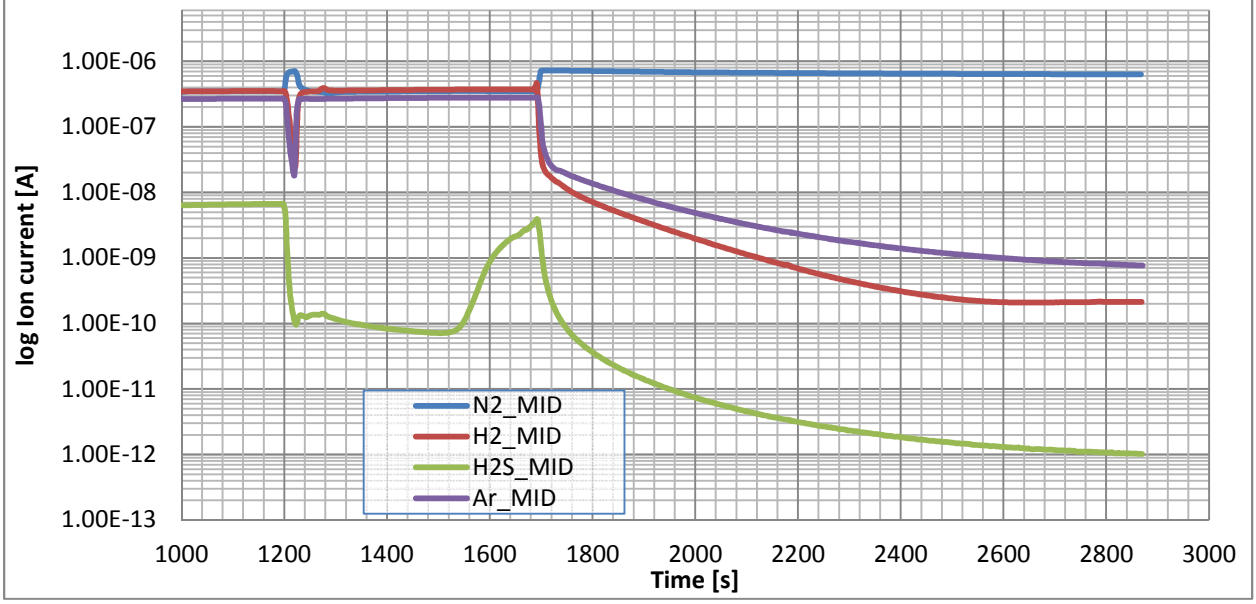

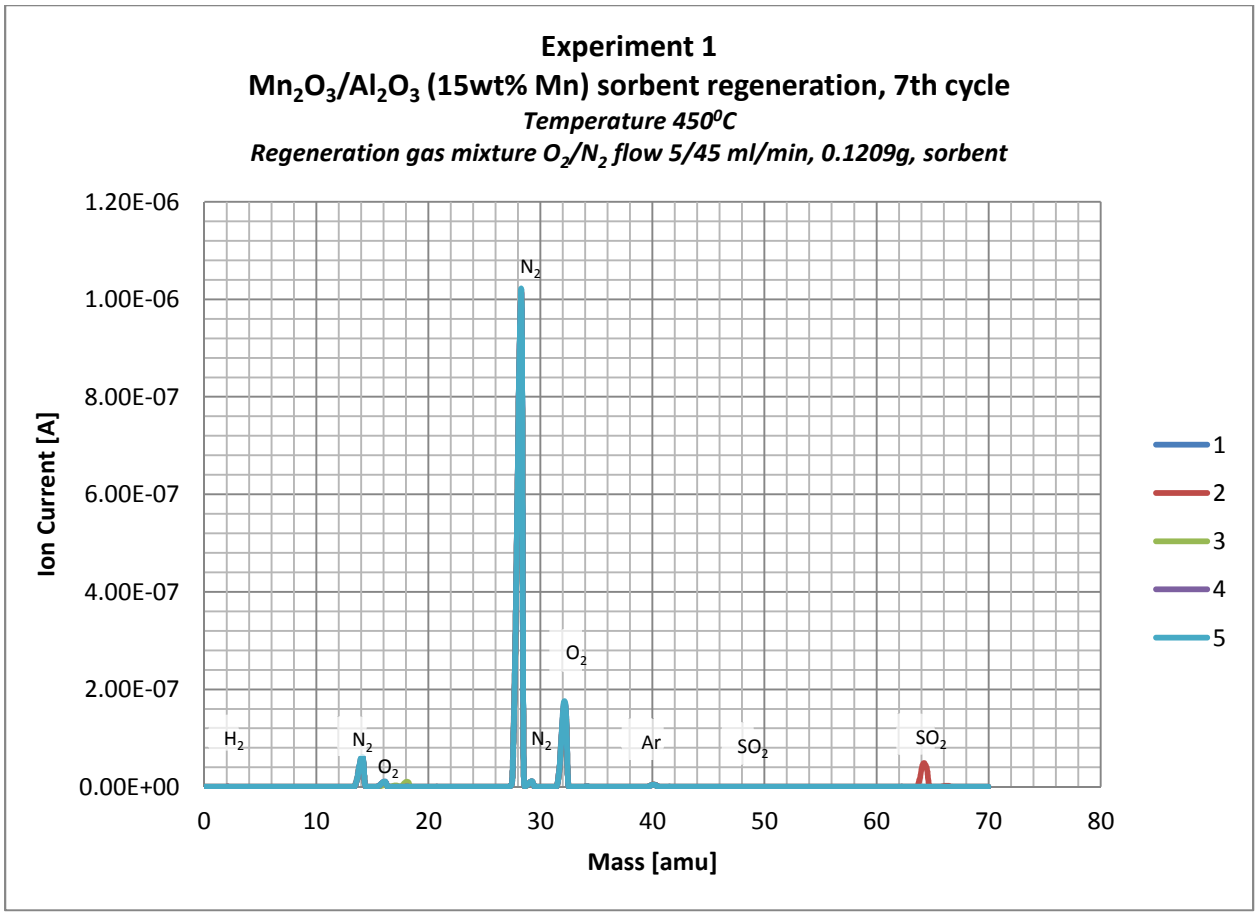
Experiment 1
Mn2O3/Al2O3 (15wt% Mn) sorbent regeneration, 7th cycle
Temperature 450⁰C
Regeneration gas mixture O2/N2 flow 5/45 ml/min, 0.1209g, sorbent
Ion Current [A]
1.20E-06
1.00E-06
8.00E-07
6.00E-07
4.00E-07
2.00E-07
0.00E+00
0
10
20
30
40
50
60
70
80
Mass [amu]
H2
N2
O2
N2
O2
N2
Ar
SO2
SO2
1
2
3
4
5

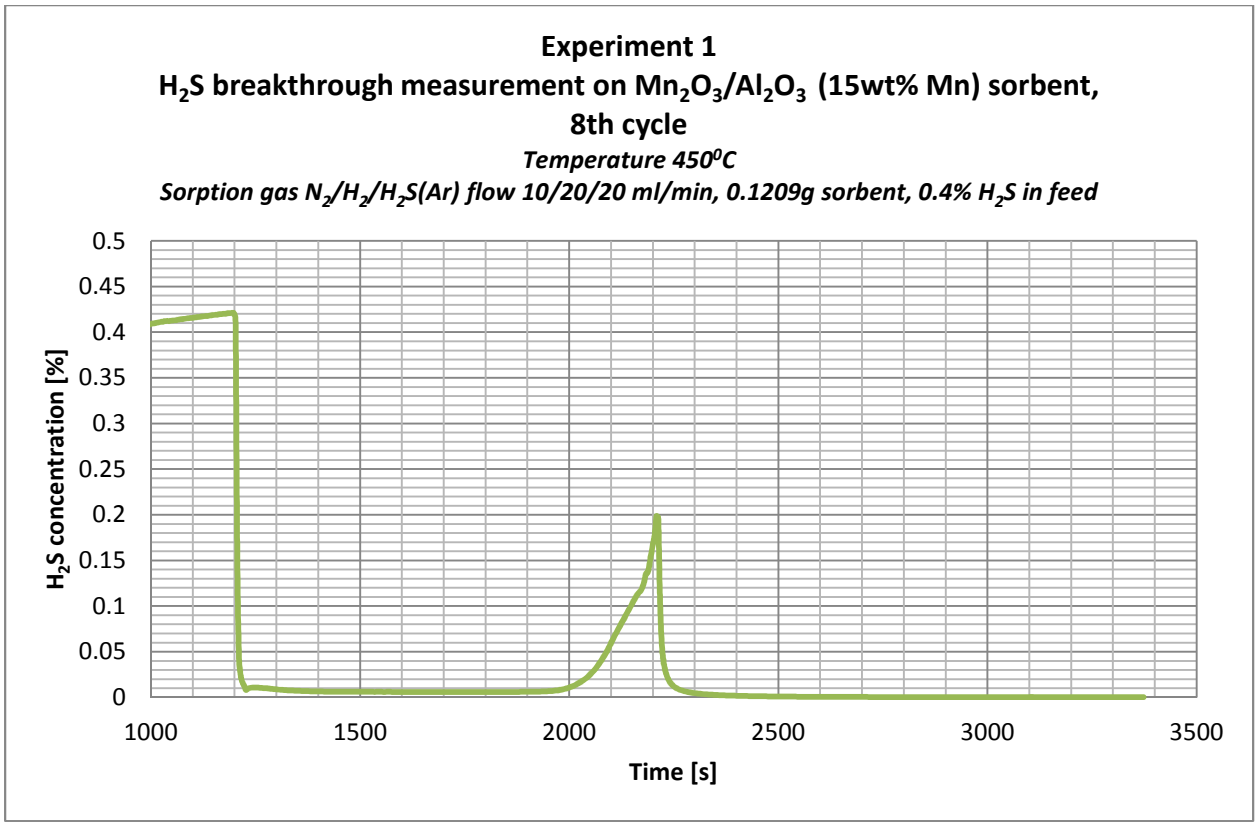
Experiment 1
H2S breakthrough measurement on Mn2O3/Al2O3 (15wt% Mn) sorbent, 8th cycle
Temperature 450⁰C
Sorption gas N2/H2/H2S(Ar) flow 10/20/20 ml/min, 0.1209g sorbent, 0.4% H2S in feed
H2S concentration [%]
0.5
0.45
0.4
0.35
0.3
0.25
0.2
0.15
0.1
0.05
0
1000
1500
2000
2500
3000
3500
Time [s]

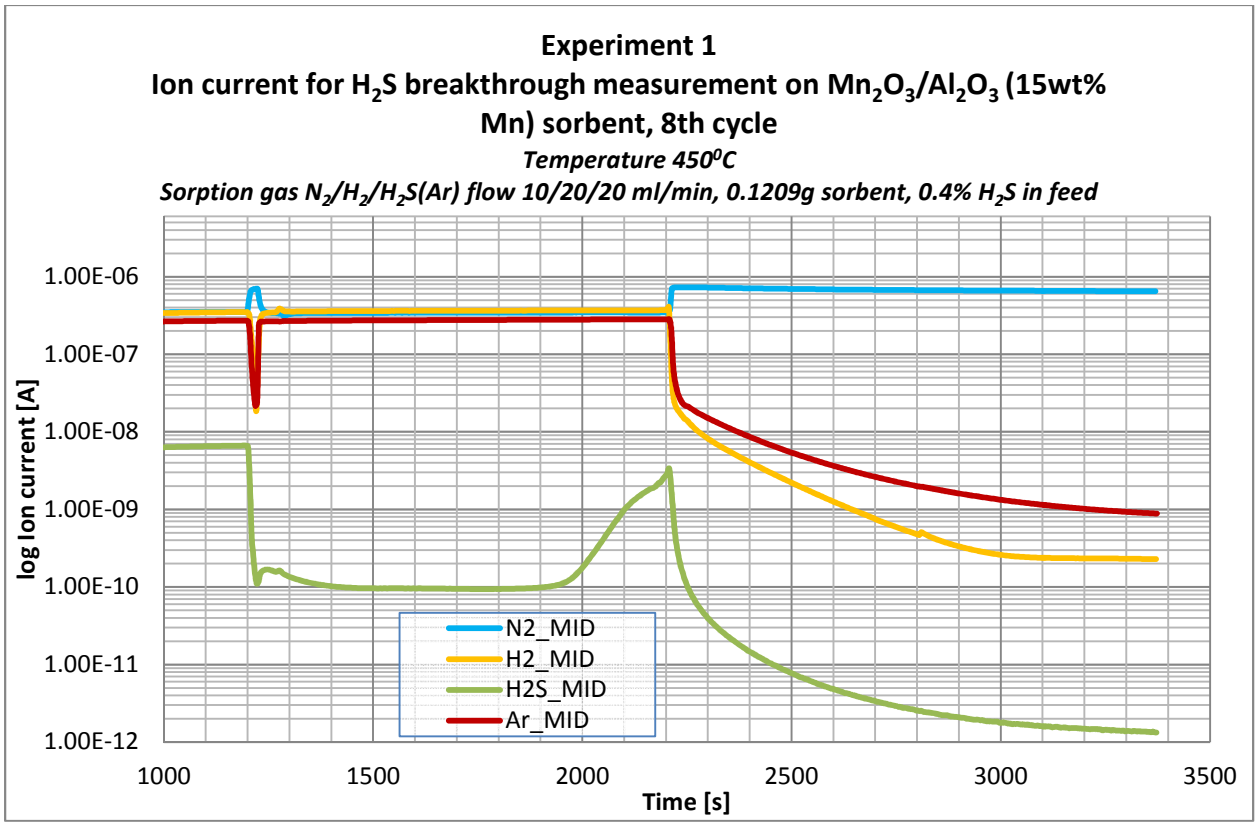
Experiment 1
Ion current for H2S breakthrough measurement on Mn2O3/Al2O3 (15wt% Mn) sorbent, 8th cycle
Temperature 450⁰C
Sorption gas N2/H2/H2S(Ar) flow 10/20/20 ml/min, 0.1209g sorbent, 0.4% H2S in feed
log Ion current [A]
1.00E-06
1.00E-07
1.00E-08
1.00E-09
1.00E-10
1.00E-11
1.00E-12
N2_MID
H2_MID
H2S_MID
Ar_MID
1000
1500
2000
2500
3000
3500
Time [s]

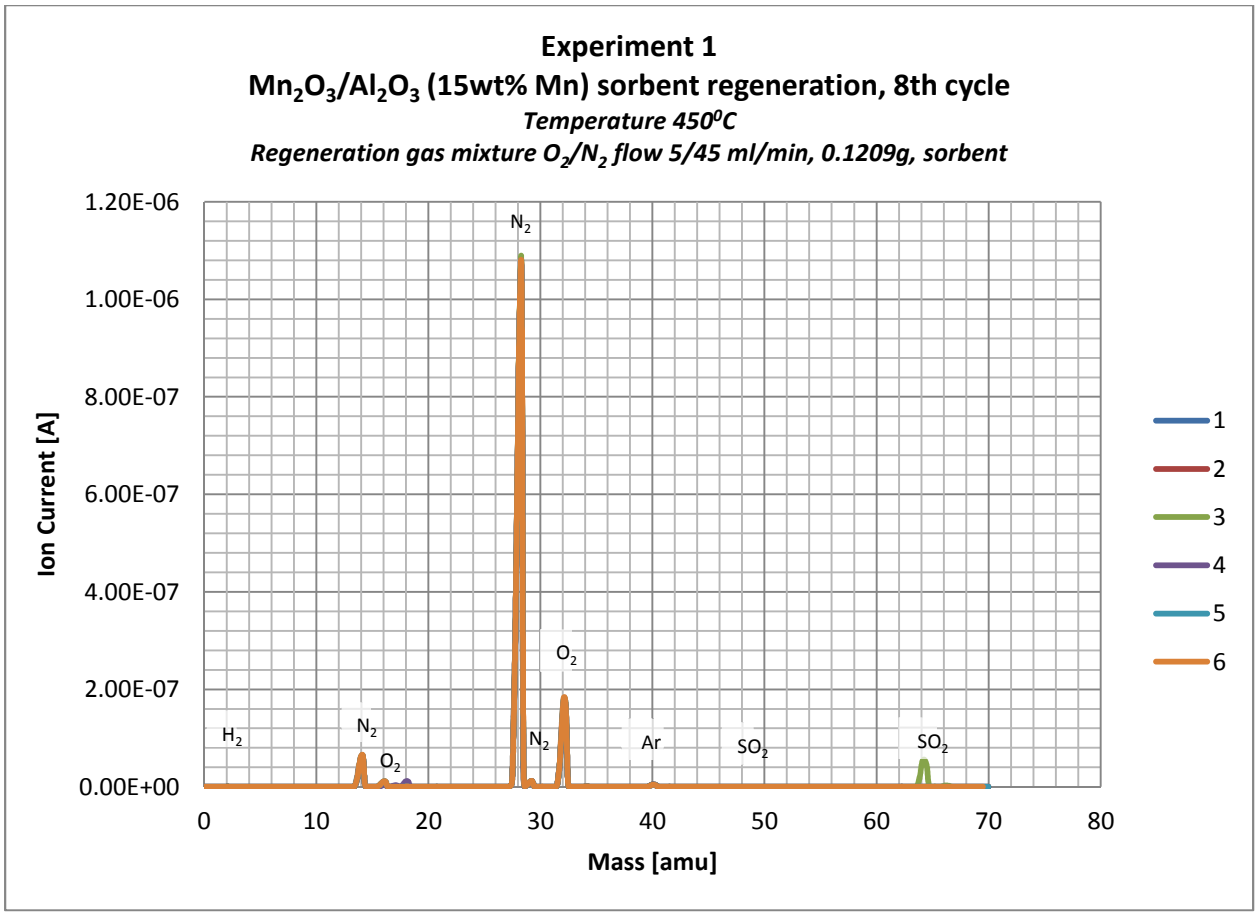
Experiment 1
Mn2O3/Al2O3 (15wt% Mn) sorbent regeneration, 8th cycle
Temperature 450⁰C
Regeneration gas mixture O2/N2 flow 5/45 ml/min, 0.1209g, sorbent
Ion Current [A]
1.20E-06
1.00E-06
8.00E-07
6.00E-07
4.00E-07
2.00E-07
0.00E+00
0
10
20
30
40
50
60
70
80
Mass [amu]
H2
N2
O2
N2
O2
N2
Ar
SO2
SO2
1
2
3
4
5
6

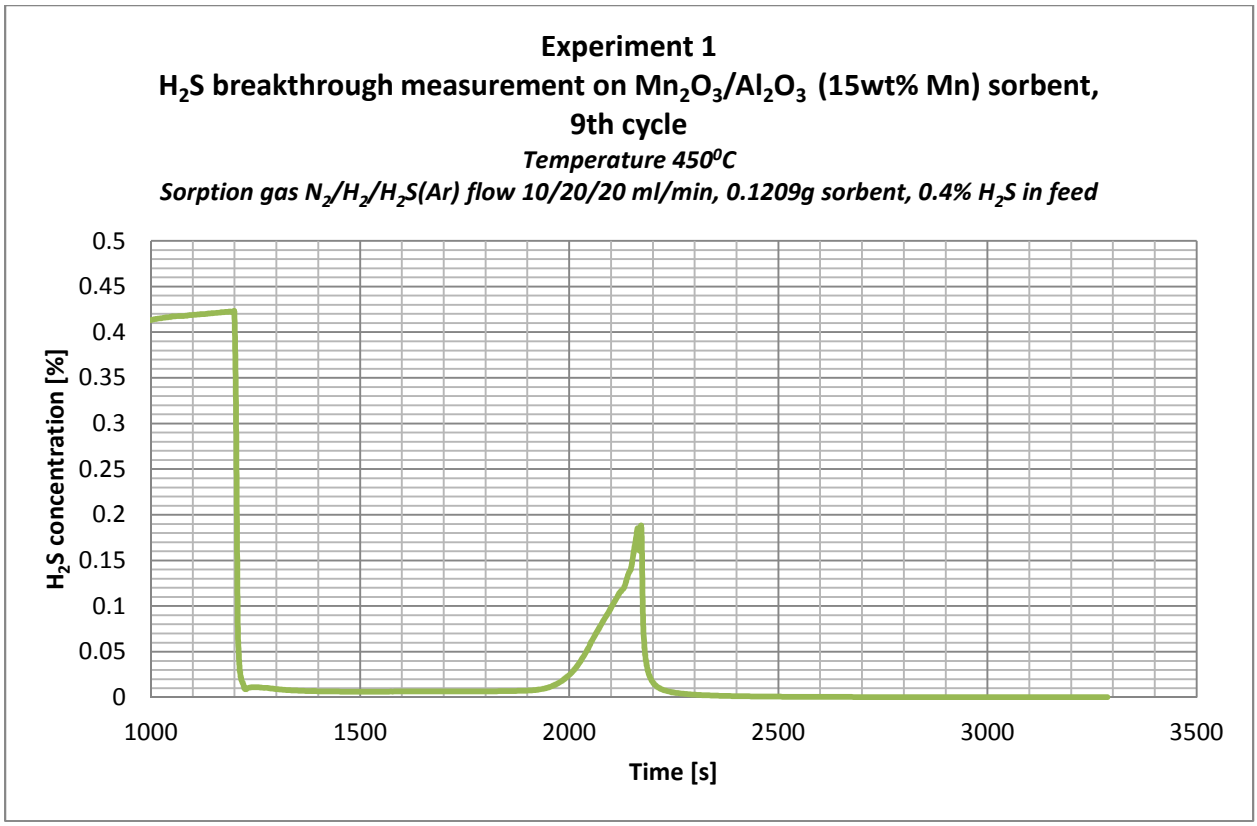
Experiment 1
H2S breakthrough measurement on Mn2O3/Al2O3 (15wt% Mn) sorbent, 9th cycle
Temperature 450⁰C
Sorption gas N2/H2/H2S(Ar) flow 10/20/20 ml/min, 0.1209g sorbent, 0.4% H2S in feed
H2S concentration [%]
0.5
0.45
0.4
0.35
0.3
0.25
0.2
0.15
0.1
0.05
0
1000
1500
2000
2500
3000
3500
Time [s]

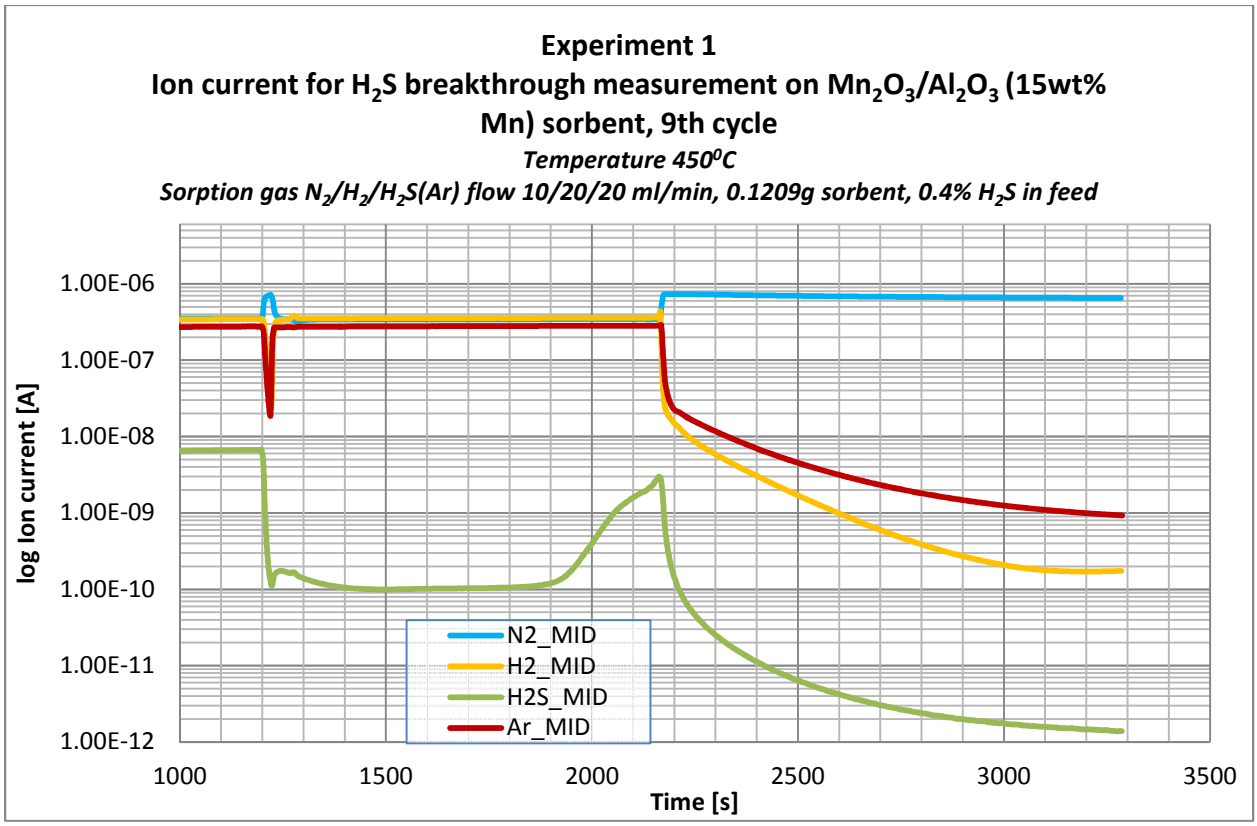
Experiment 1
Ion current for H2S breakthrough measurement on Mn2O3/Al2O3 (15wt% Mn) sorbent, 9th cycle
Temperature 450⁰C
Sorption gas N2/H2/H2S(Ar) flow 10/20/20 ml/min, 0.1209g sorbent, 0.4% H2S in feed
log Ion current [A]
1.00E-06
1.00E-07
1.00E-08
1.00E-09
1.00E-10
1.00E-11
1.00E-12
1000
1500
2000
2500
3000
3500
Time [s]
N2_MID
H2_MID
H2S_MID
Ar_MID

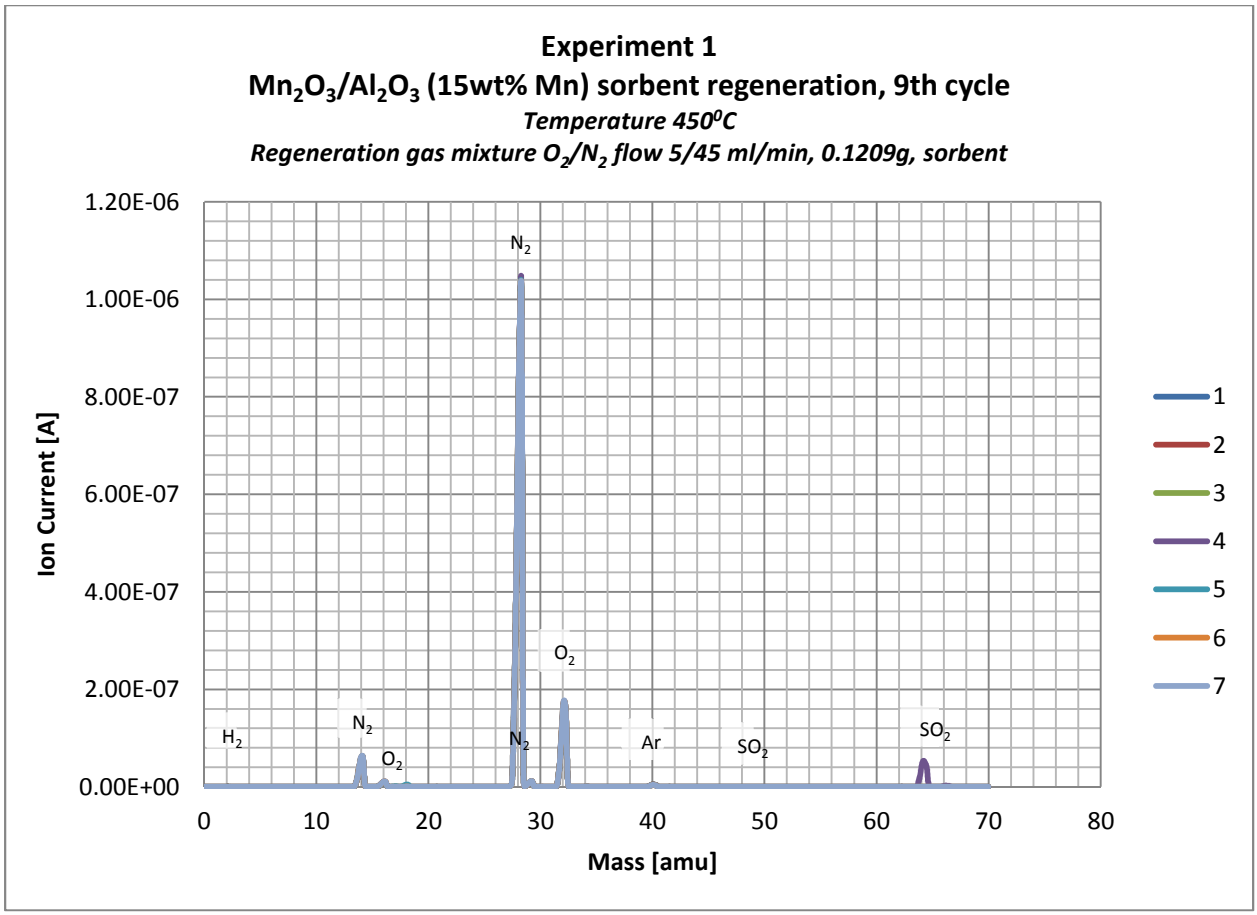
Experiment 1
Mn2O3/Al2O3 (15wt% Mn) sorbent regeneration, 9th cycle
Temperature 450⁰C
Regeneration gas mixture O2/N2 flow 5/45 ml/min, 0.1209g, sorbent
Ion Current [A]
1.20E-06
1.00E-06
8.00E-07
6.00E-07
4.00E-07
2.00E-07
0.00E+00
0
10
20
30
40
50
60
70
80
Mass [amu]
N2
O2
H2
N2
O2
N2
Ar
SO2
SO2
1
2
3
4
5
6
7

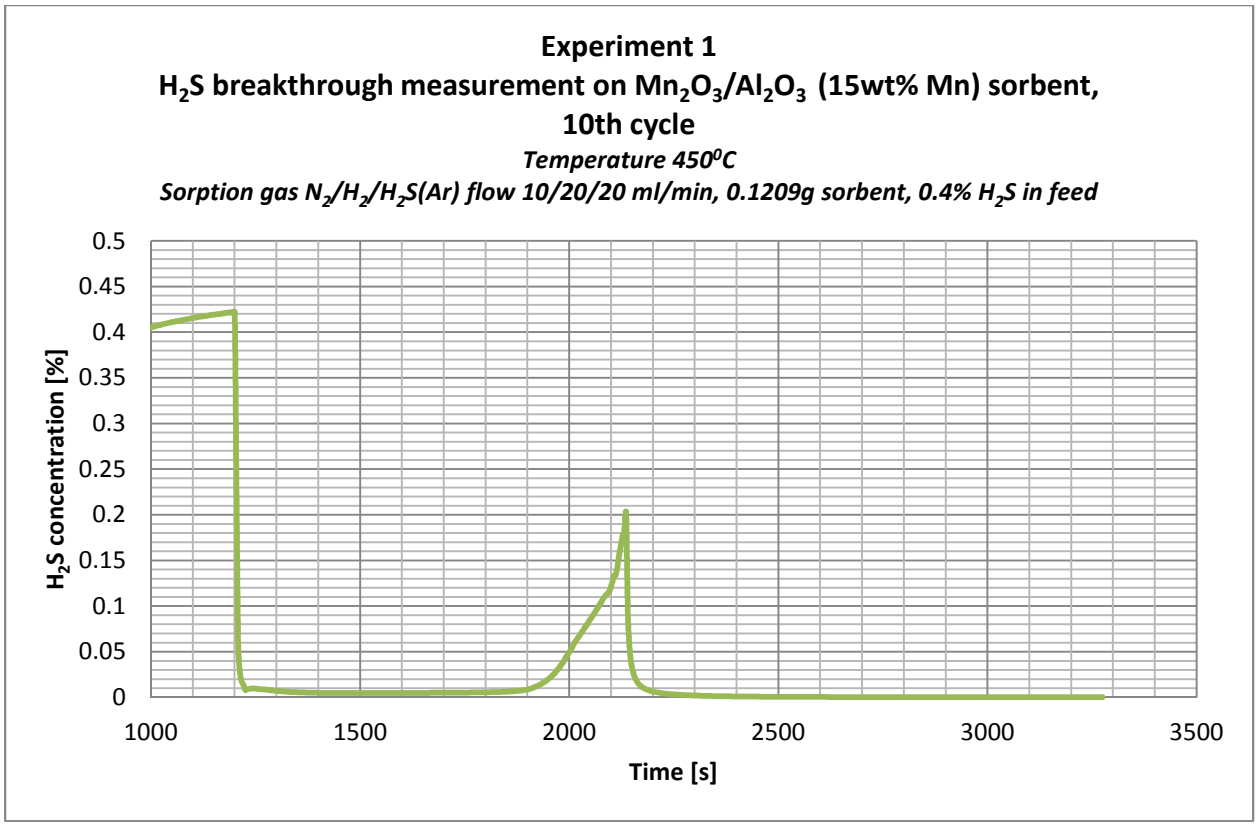
Experiment 1
H2S breakthrough measurement on Mn2O3/Al2O3 (15wt% Mn) sorbent, 10th cycle
Temperature 450⁰C
Sorption gas N2/H2/H2S(Ar) flow 10/20/20 ml/min, 0.1209g sorbent, 0.4% H2S in feed
H2S concentration [%]
0.5
0.45
0.4
0.35
0.3
0.25
0.2
0.15
0.1
0.05
0
1000
1500
2000
2500
3000
3500
Time [s]

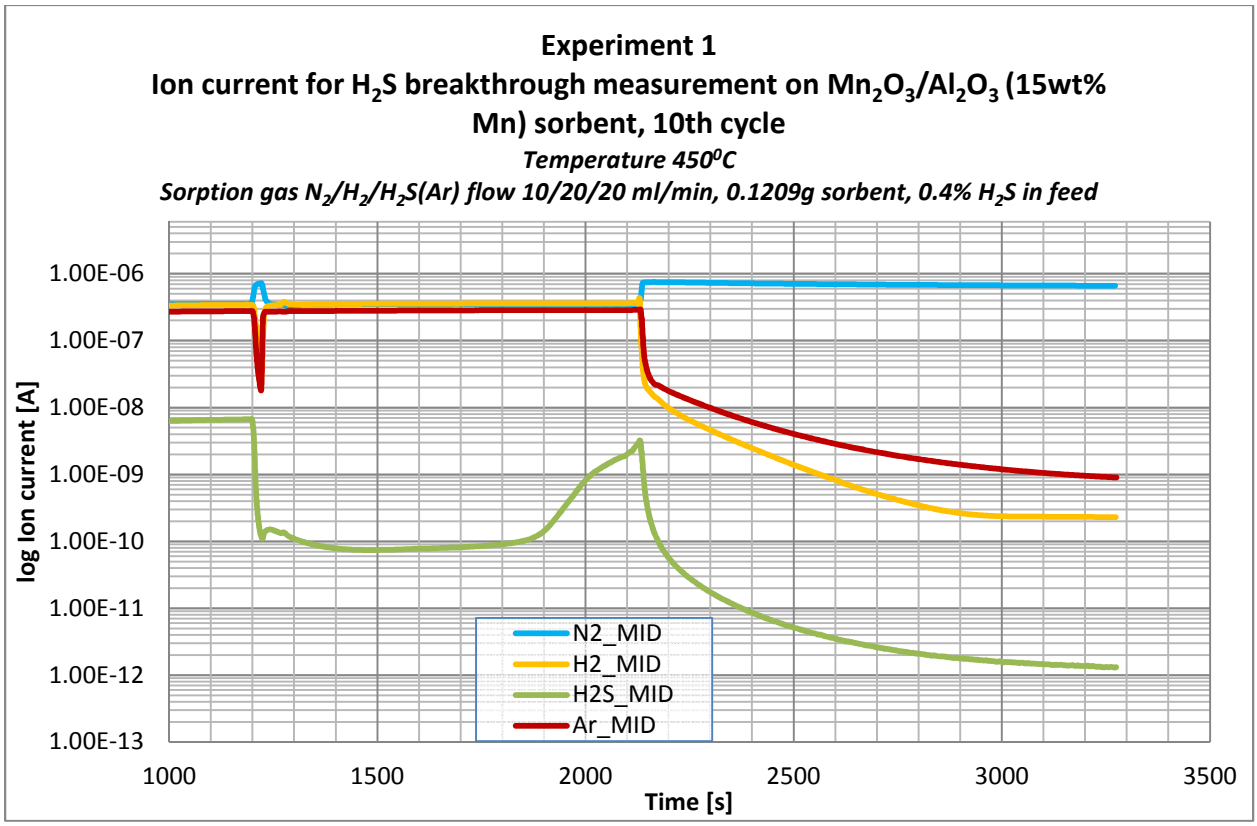
Experiment 1
Ion current for H2S breakthrough measurement on Mn2O3/Al2O3 (15wt% Mn) sorbent, 10th cycle
Temperature 450⁰C
Sorption gas N2/H2/H2S(Ar) flow 10/20/20 ml/min, 0.1209g sorbent, 0.4% H2S in feed
log Ion current [A]
1.00E-06
1.00E-07
1.00E-08
1.00E-09
1.00E-10
1.00E-11
1.00E-12
1.00E-13
1000
1500
2000
2500
3000
3500
Time [s]
N2_MID
H2_MID
H2S_MID
Ar_MID

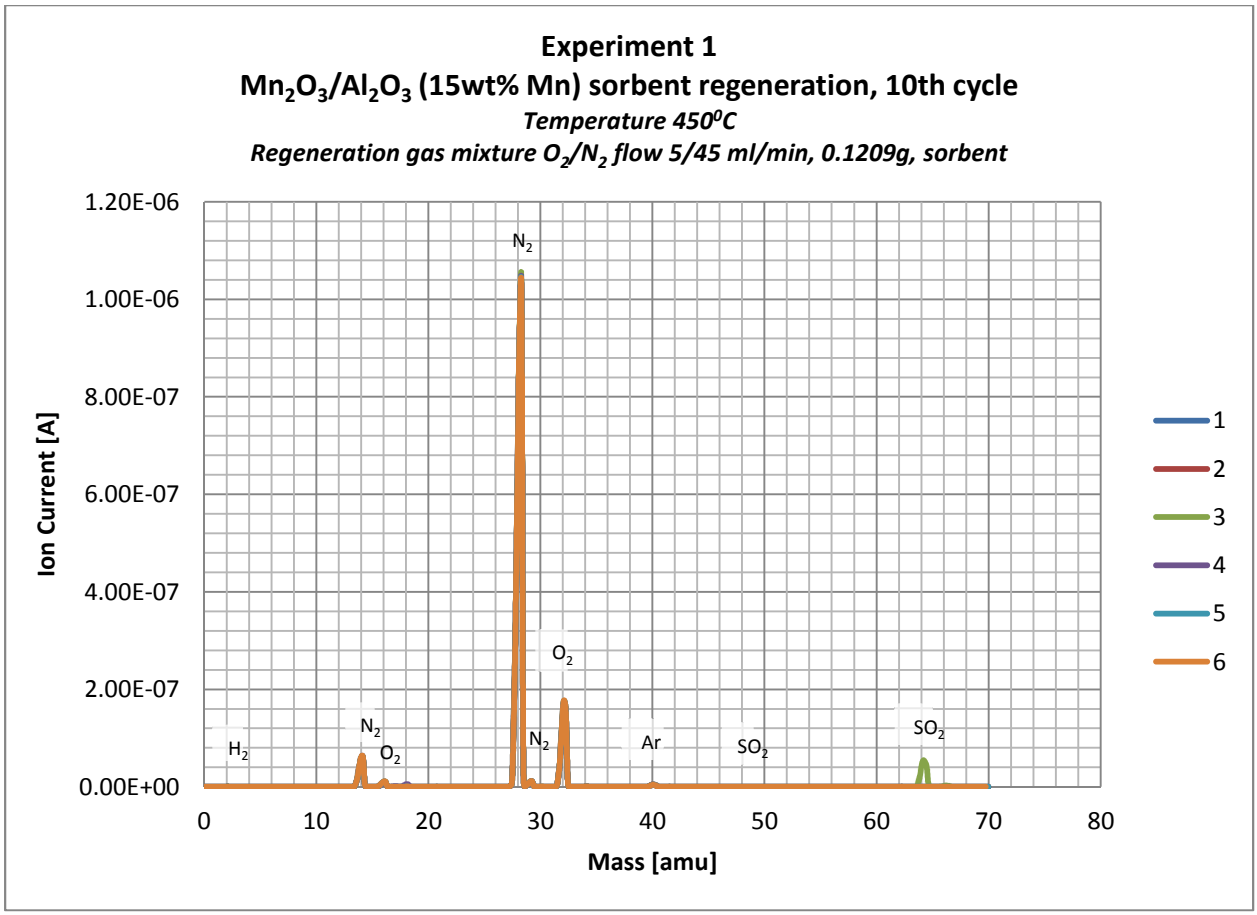
Experiment 1
Mn2O3/Al2O3 (15wt% Mn) sorbent regeneration, 10th cycle
Temperature 450⁰C
Regeneration gas mixture O2/N2 flow 5/45 ml/min, 0.1209g, sorbent
Ion Current [A]
1.20E-06
1.00E-06
8.00E-07
6.00E-07
4.00E-07
2.00E-07
0.00E+00
0
10
20
30
40
50
60
70
80
Mass [amu]
N2
O2
N2
H2
N2
O2
Ar
SO2
SO2
1
2
3
4
5
6

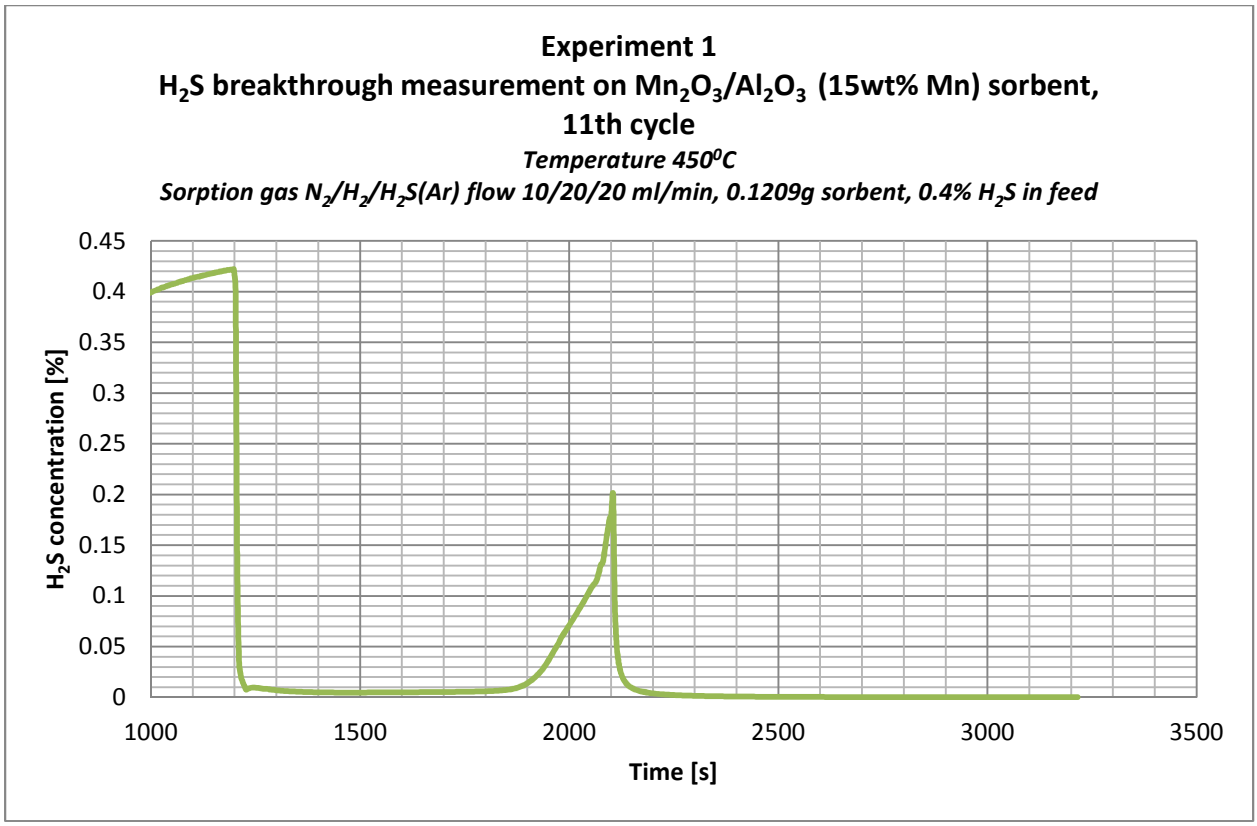
Experiment 1
H2S breakthrough measurement on Mn2O3/Al2O3 (15wt% Mn) sorbent, 11th cycle
Temperature 450⁰C
Sorption gas N2/H2/H2S(Ar) flow 10/20/20 ml/min, 0.1209g sorbent, 0.4% H2S in feed
H2S concentration [%]
0.45
0.4
0.35
0.3
0.25
0.2
0.15
0.1
0.05
0
1000
1500
2000
2500
3000
3500
Time [s]

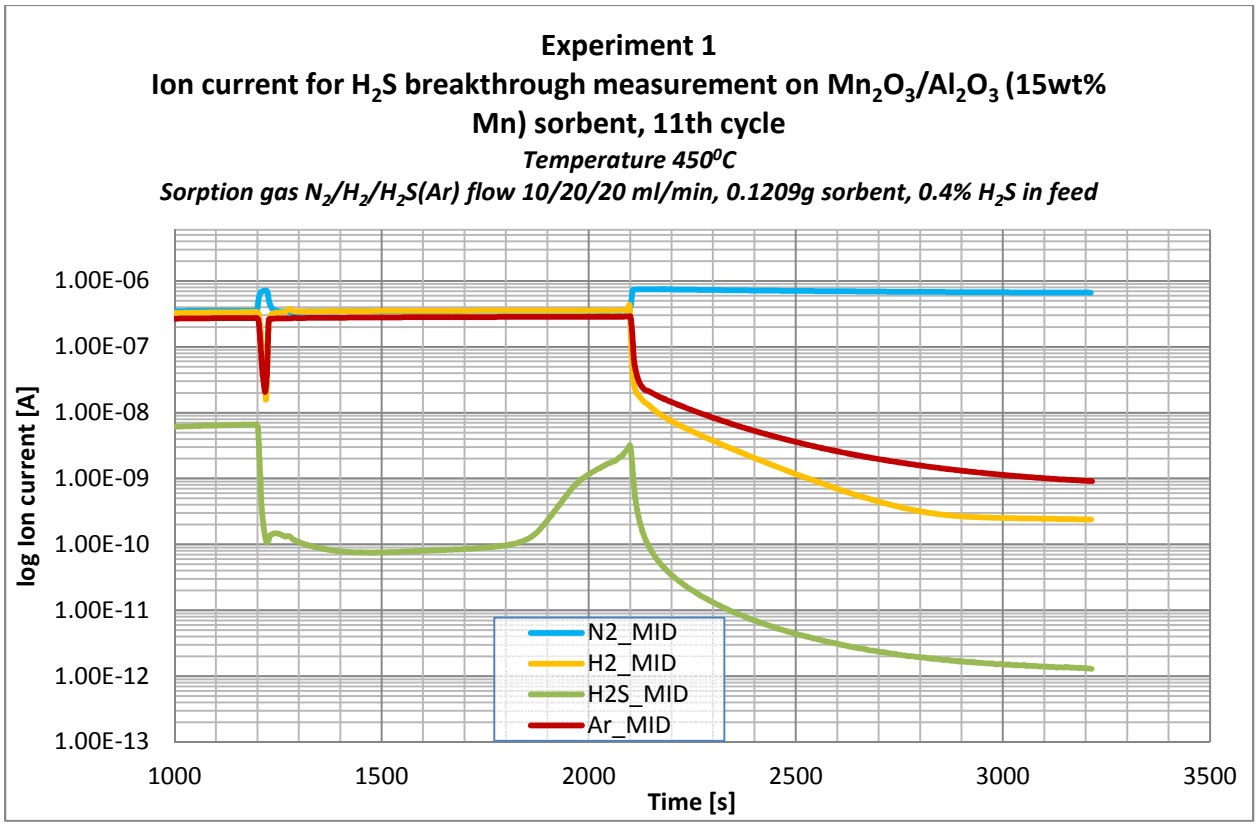
Experiment 1
Ion current for H2S breakthrough measurement on Mn2O3/Al2O3 (15wt% Mn) sorbent, 11th cycle
Temperature 450⁰C
Sorption gas N2/H2/H2S(Ar) flow 10/20/20 ml/min, 0.1209g sorbent, 0.4% H2S in feed
log Ion current [A]
1.00E-06
1.00E-07
1.00E-08
1.00E-09
1.00E-10
1.00E-11
1.00E-12
1.00E-13
1000
1500
2000
2500
3000
3500
Time [s]
N2_MID
H2_MID
H2S_MID
Ar_MID

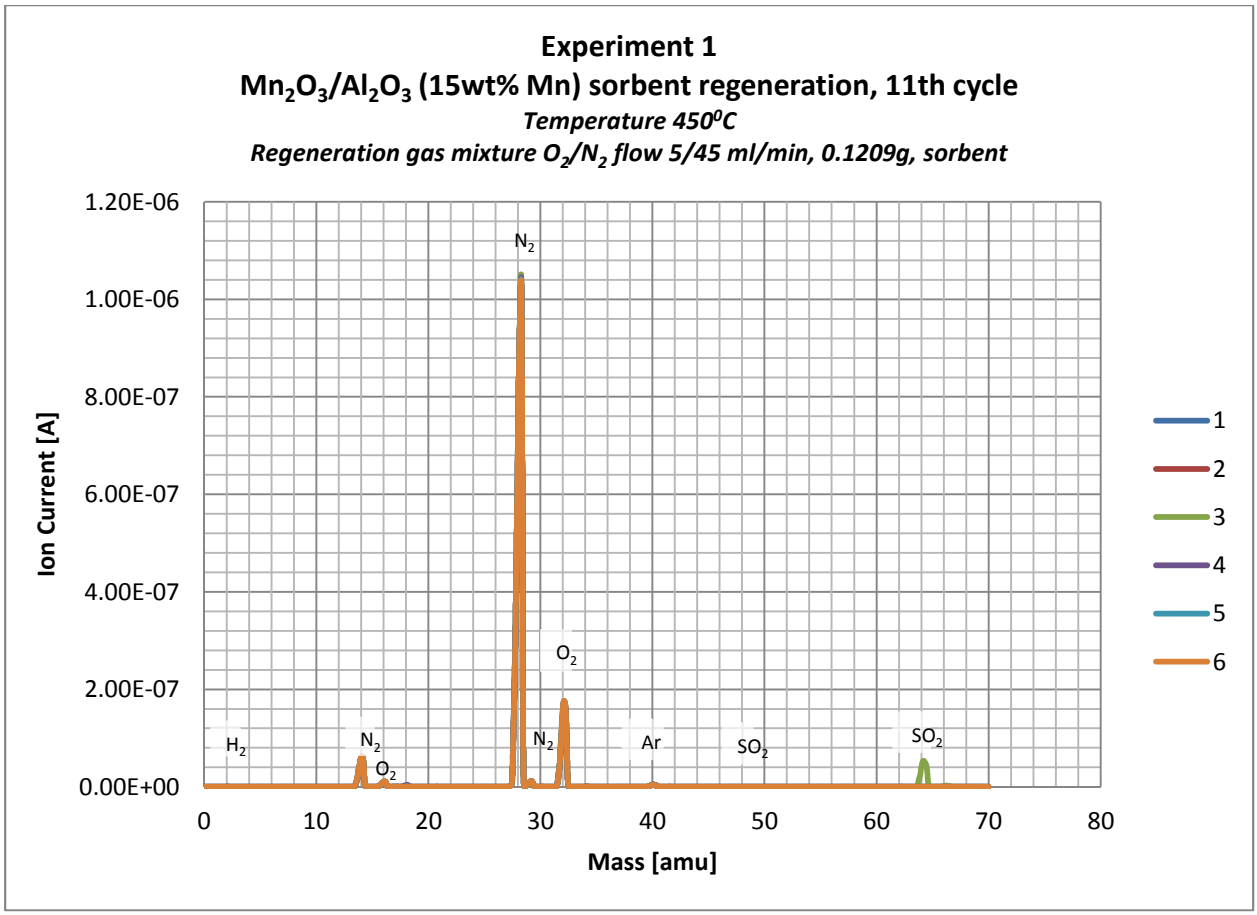
Experiment 1
Mn2O3/Al2O3 (15wt% Mn) sorbent regeneration, 11th cycle
Temperature 450⁰C
Regeneration gas mixture O2/N2 flow 5/45 ml/min, 0.1209g, sorbent
Ion Current [A]
1.20E-06
1.00E-06
8.00E-07
6.00E-07
4.00E-07
2.00E-07
0.00E+00
0
10
20
30
40
50
60
70
80
Mass [amu]
N2
O2
H2
N2
O2
N2
Ar
SO2
SO2
1
2
3
4
5
6

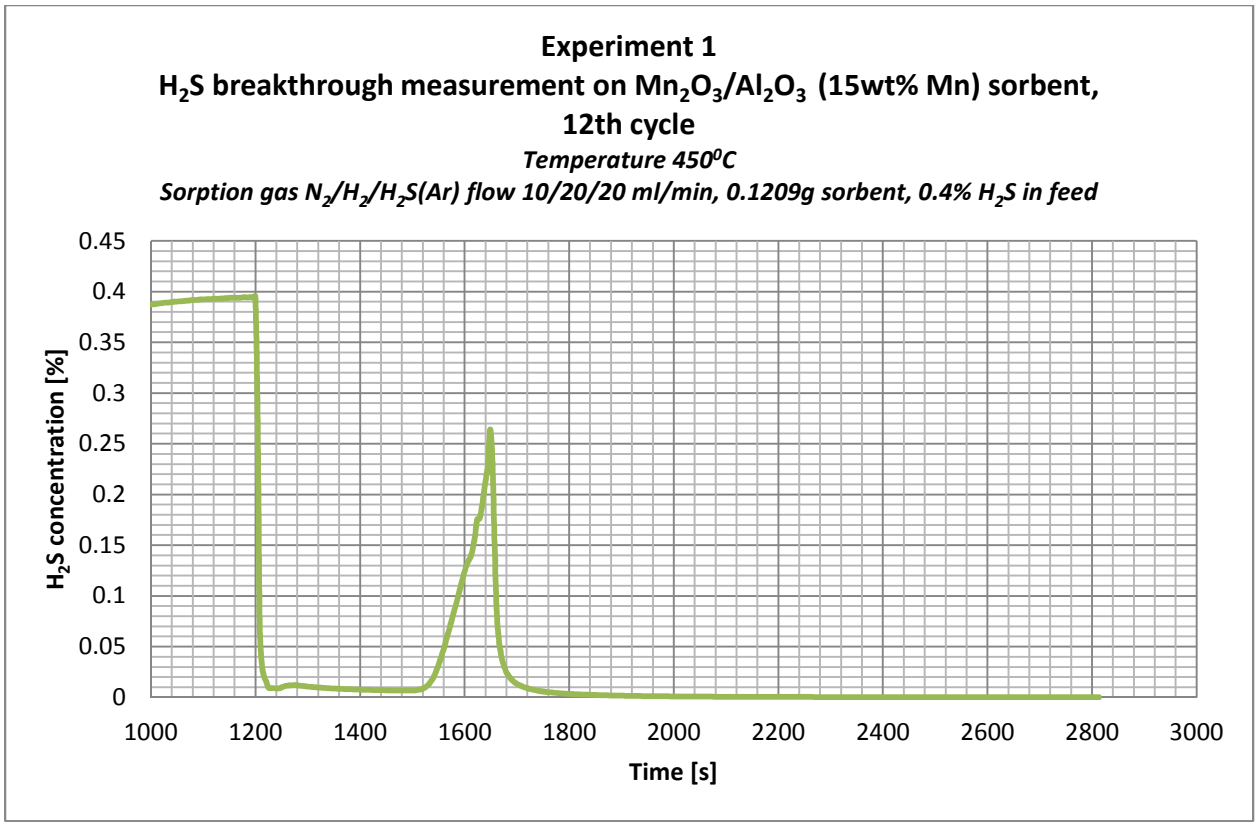
Experiment 1
H2S breakthrough measurement on Mn2O3/Al2O3 (15wt% Mn) sorbent, 12th cycle
Temperature 450⁰C
Sorption gas N2/H2/H2S(Ar) flow 10/20/20 ml/min, 0.1209g sorbent, 0.4% H2S in feed
H2S concentration [%]
0.45
0.4
0.35
0.3
0.25
0.2
0.15
0.1
0.05
0
1000
1200
1400
1600
1800
2000
2200
2400
2600
2800
3000
Time [s]

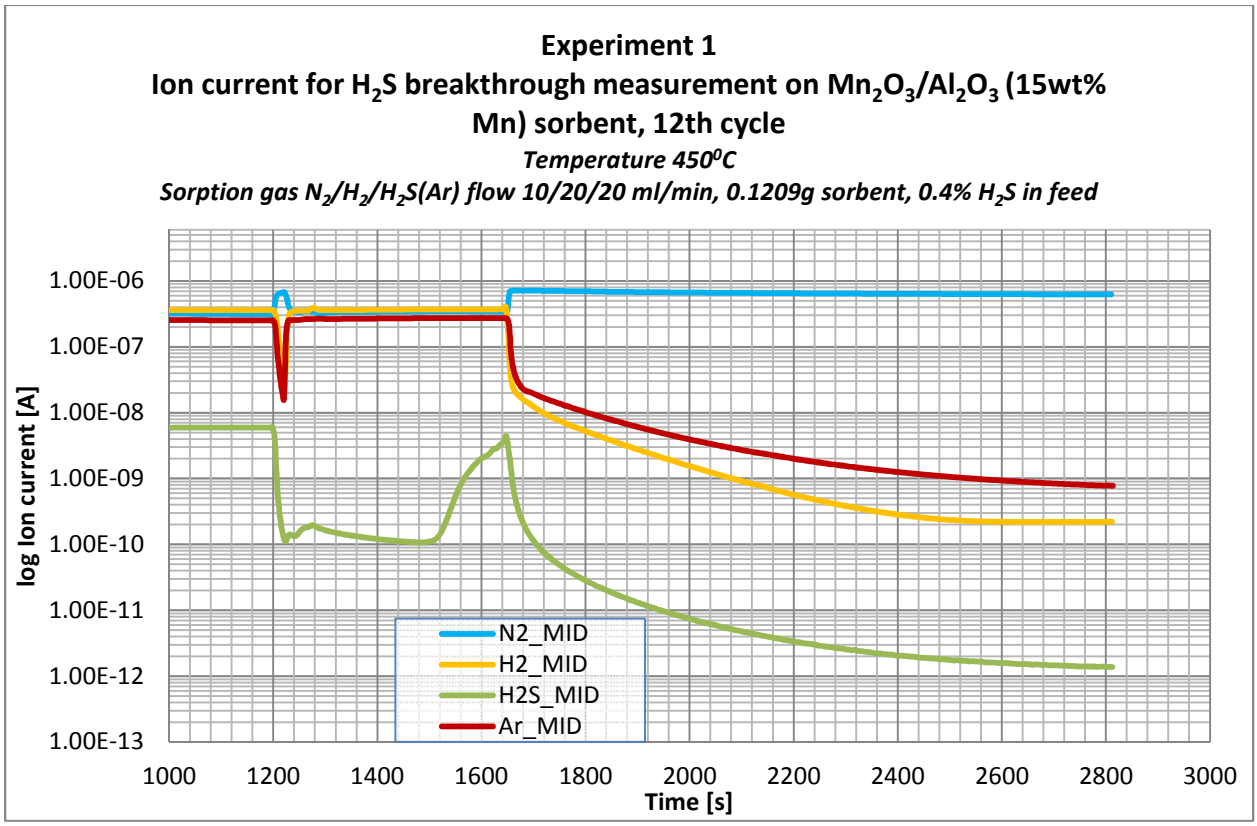
Experiment 1
Ion current for H2S breakthrough measurement on Mn2O3/Al2O3 (15wt% Mn) sorbent, 12th cycle
Temperature 450⁰C
Sorption gas N2/H2/H2S(Ar) flow 10/20/20 ml/min, 0.1209g sorbent, 0.4% H2S in feed
log Ion current [A]
1.00E-06
1.00E-07
1.00E-08
1.00E-09
1.00E-10
1.00E-11
1.00E-12
1.00E-13
1000
1200
1400
1600
1800
2000
2200
2400
2600
2800
3000
Time [s]
N2_MID
H2_MID
H2S_MID
Ar_MID

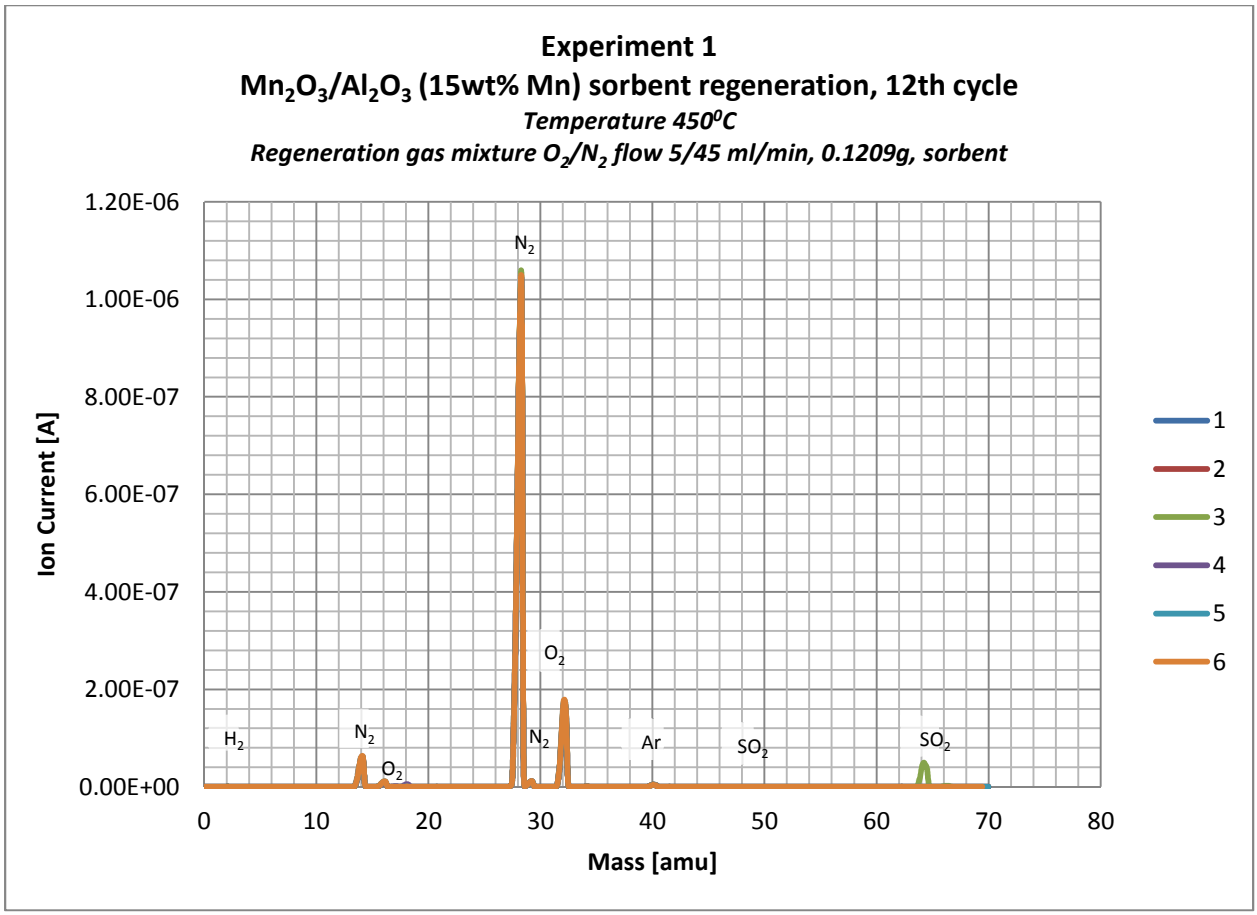
Experiment 1
Mn2O3/Al2O3 (15wt% Mn) sorbent regeneration, 12th cycle
Temperature 450⁰C
Regeneration gas mixture O2/N2 flow 5/45 ml/min, 0.1209g, sorbent
Ion Current [A]
1.20E-06
1.00E-06
8.00E-07
6.00E-07
4.00E-07
2.00E-07
0.00E+00
0
10
20
30
40
50
60
70
80
Mass [amu]
N2
O2
H2
N2
O2
N2
Ar
SO2
SO2
1
2
3
4
5
6

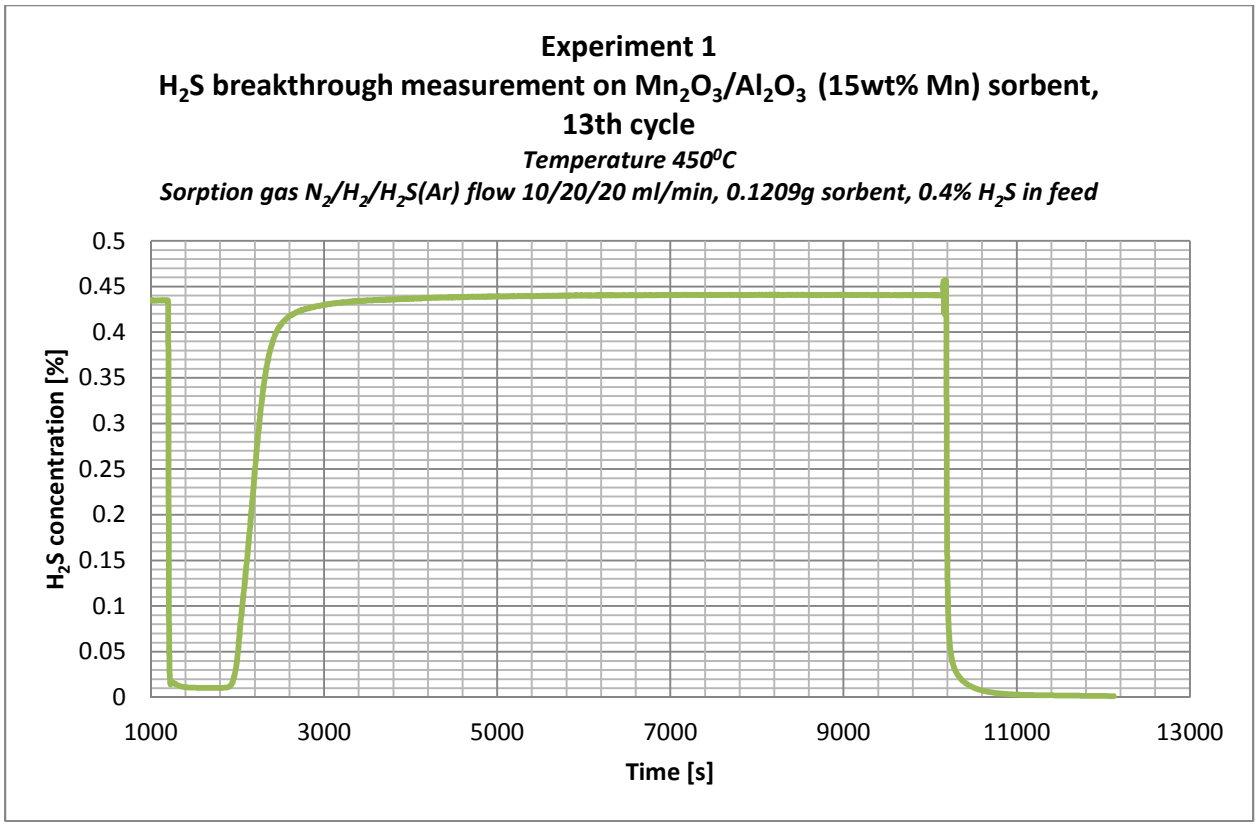
Experiment 1
H2S breakthrough measurement on Mn2O3/Al2O3 (15wt% Mn) sorbent, 13th cycle
Temperature 450⁰C
Sorption gas N2/H2/H2S(Ar) flow 10/20/20 ml/min, 0.1209g sorbent, 0.4% H2S in feed
H2S concentration [%]
0.5
0.45
0.4
0.35
0.3
0.25
0.2
0.15
0.1
0.05
0
1000
3000
5000
7000
9000
11000
13000
Time [s]

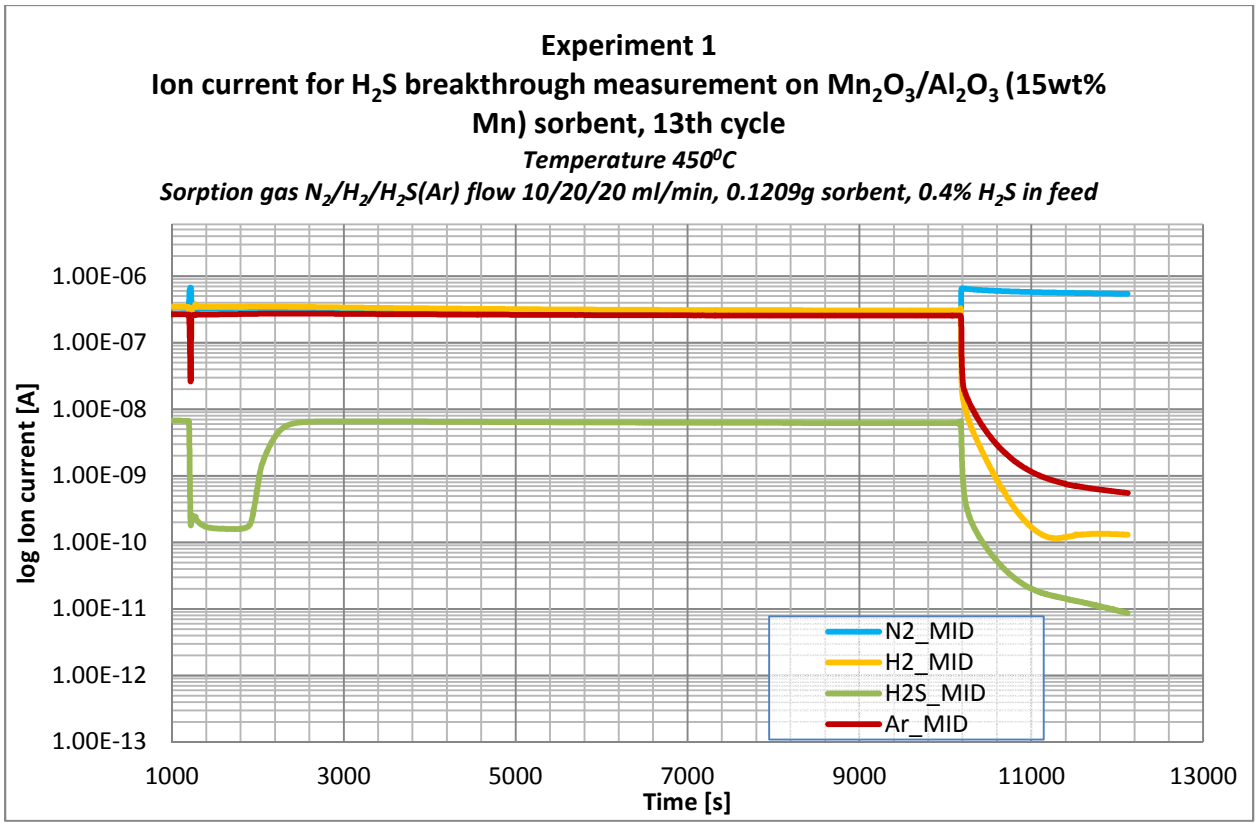
Experiment 1
Ion current for H2S breakthrough measurement on Mn2O3/Al2O3 (15wt% Mn) sorbent, 13th cycle
Temperature 450⁰C
Sorption gas N2/H2/H2S(Ar) flow 10/20/20 ml/min, 0.1209g sorbent, 0.4% H2S in feed
log Ion current [A]
1.00E-06
1.00E-07
1.00E-08
1.00E-09
1.00E-10
1.00E-11
1.00E-12
1.00E-13
1000
3000
5000
7000
9000
11000
13000
Time [s]
N2_MID
H2_MID
H2S_MID
Ar_MID

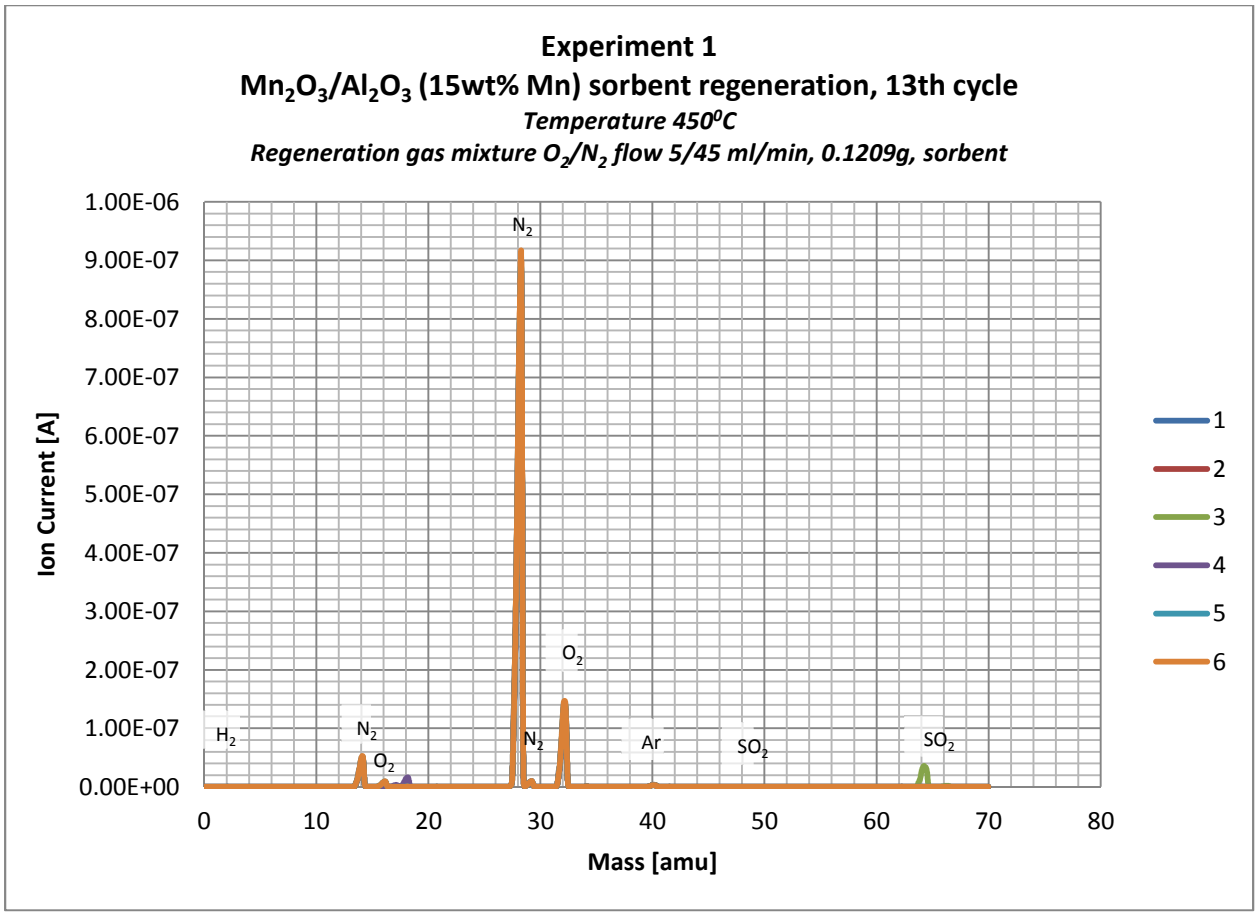
Experiment 1
Mn2O3/Al2O3 (15wt% Mn) sorbent regeneration, 13th cycle
Temperature 450⁰C
Regeneration gas mixture O2/N2 flow 5/45 ml/min, 0.1209g, sorbent
Ion Current [A]
1.00E-06
9.00E-07
8.00E-07
7.00E-07
6.00E-07
5.00E-07
4.00E-07
3.00E-07
2.00E-07
1.00E-07
0.00E+00
0
10
20
30
40
50
60
70
80
Mass [amu]
H2
N2
O2
N2
N2
O2
Ar
SO2
SO2
1
2
3
4
5
6

**Experiment 2**

**$H_2S$ breakthrough measurement on $Mn_2O_3/Al_2O_3$ (15wt% Mn) sorbent, 1st cycle**

***Temperature 450$^0$C***

***Sorption gas $N_2/H_2/H_2S$(Ar) flow 20/40/40 ml/min, 0.2417g sorbent, 0.4% $H_2S$ in feed***

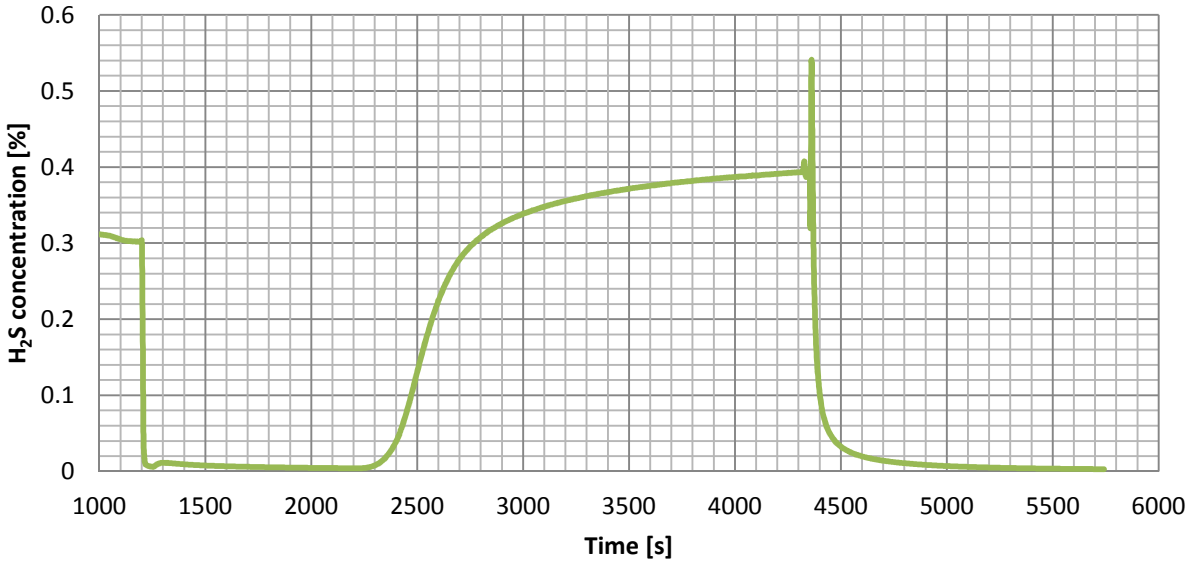


**Experiment 2**

**Ion current for $H_2S$ breakthrough measurement on $Mn_2O_3/Al_2O_3$ (15wt% Mn) sorbent, 1st cycle**

***Temperature 450$^0$C***

***Sorption gas $N_2/H_2/H_2S$(Ar) flow 20/40/40 ml/min, 0.2417g sorbent, 0.4% $H_2S$ in feed***

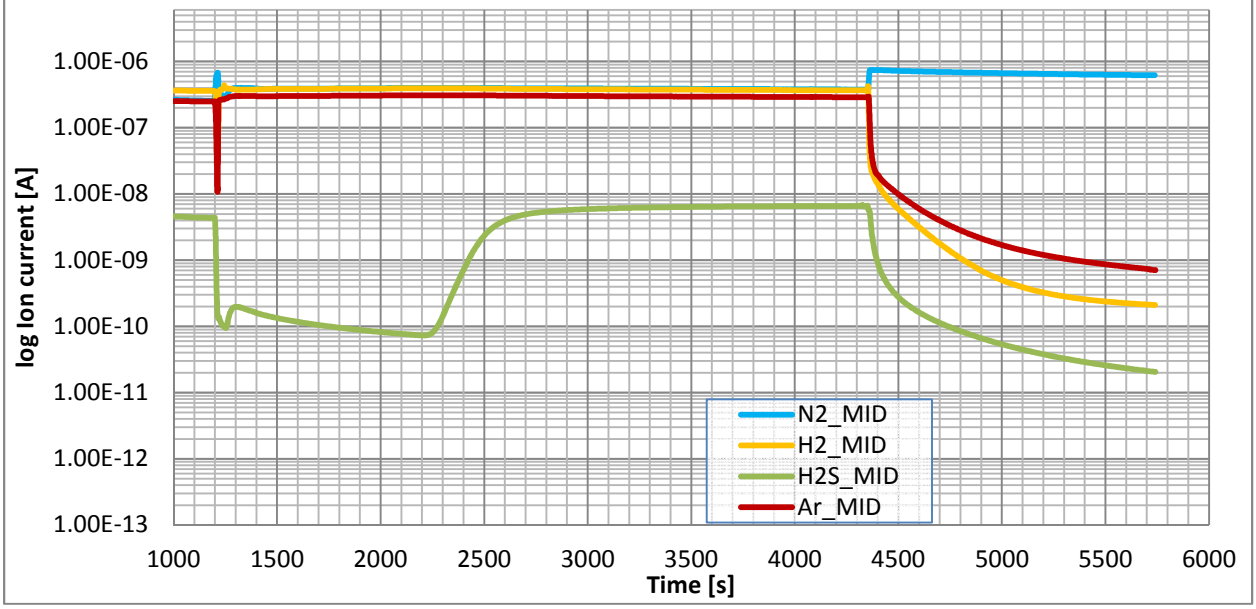

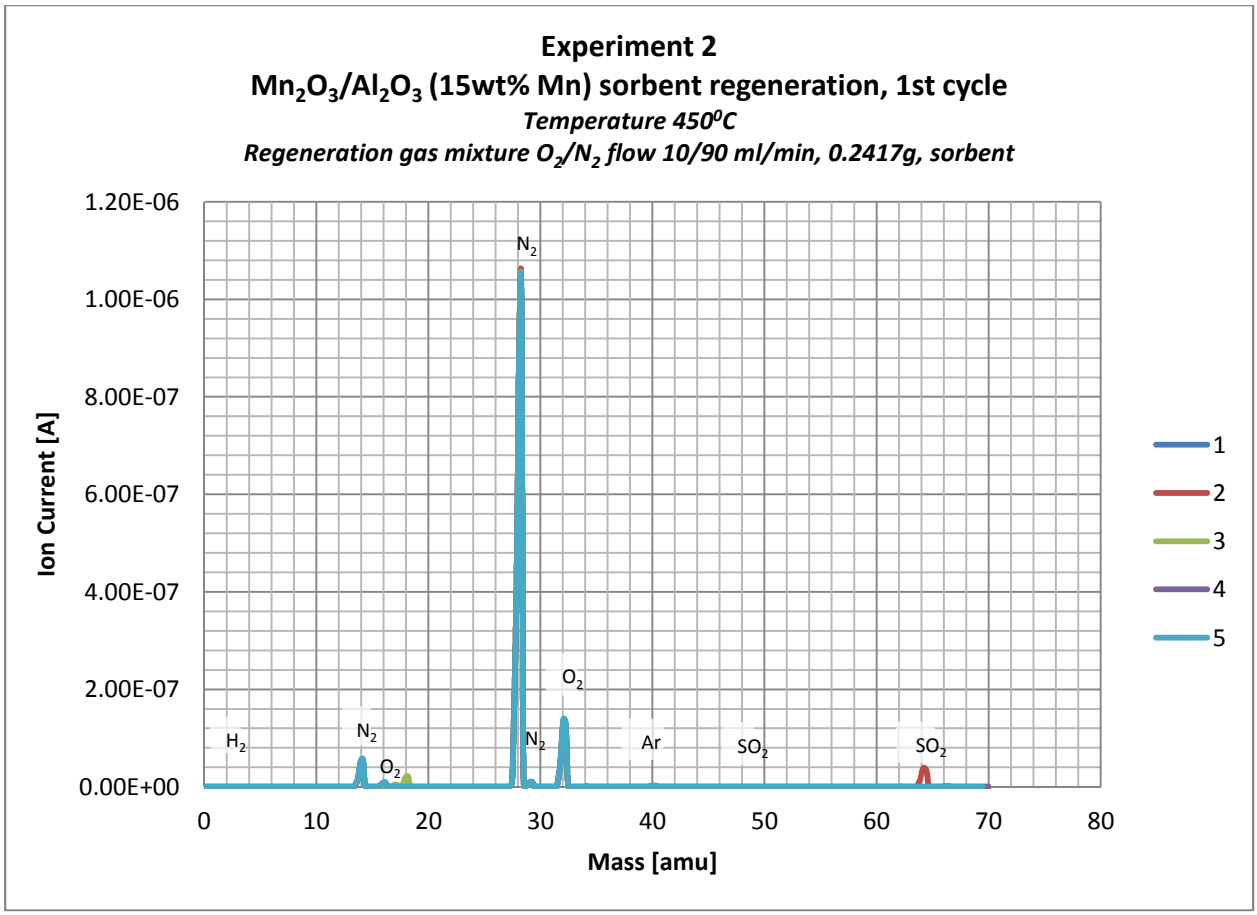
Experiment 2
Mn2O3/Al2O3 (15wt% Mn) sorbent regeneration, 1st cycle
Temperature 450⁰C
Regeneration gas mixture O2/N2 flow 10/90 ml/min, 0.2417g, sorbent
Ion Current [A]
1.20E-06
1.00E-06
8.00E-07
6.00E-07
4.00E-07
2.00E-07
0.00E+00
0
10
20
30
40
50
60
70
80
Mass [amu]
N2
O2
H2
N2
O2
N2
Ar
SO2
SO2
1
2
3
4
5

**Experiment 2**

**$H_2S$ breakthrough measurement on $Mn_2O_3/Al_2O_3$ (15wt% Mn) sorbent, 2nd cycle**

***Temperature 450$^0$C***

***Sorption gas $N_2/H_2/H_2S$(Ar) flow 20/40/40 ml/min, 0.2417g sorbent, 0.4% $H_2S$ in feed***

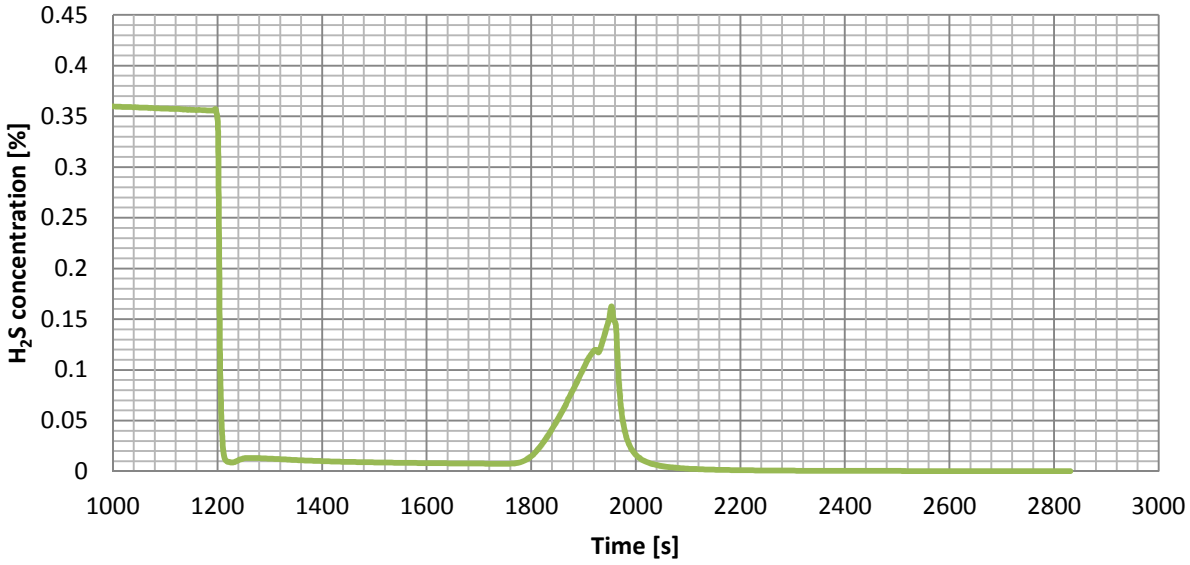


**Experiment 2**

**Ion current for $H_2S$ breakthrough measurement on $Mn_2O_3/Al_2O_3$ (15wt% Mn) sorbent, 2nd cycle**

***Temperature 450$^0$C***

***Sorption gas $N_2/H_2/H_2S$(Ar) flow 20/40/40 ml/min, 0.2417g sorbent, 0.4% $H_2S$ in feed***

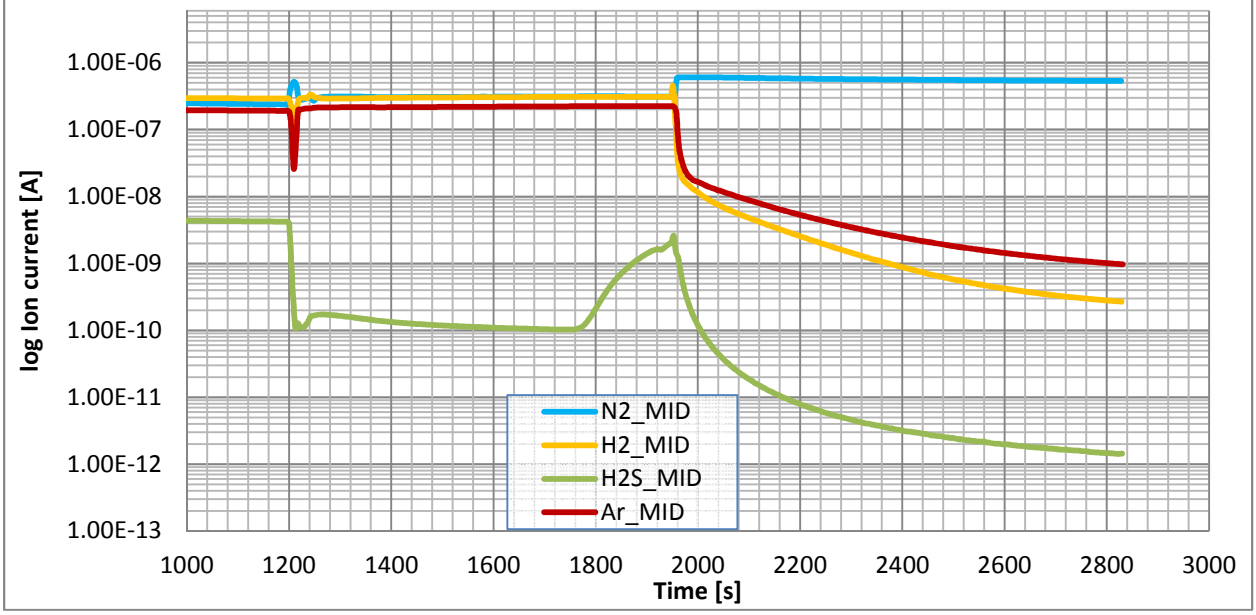

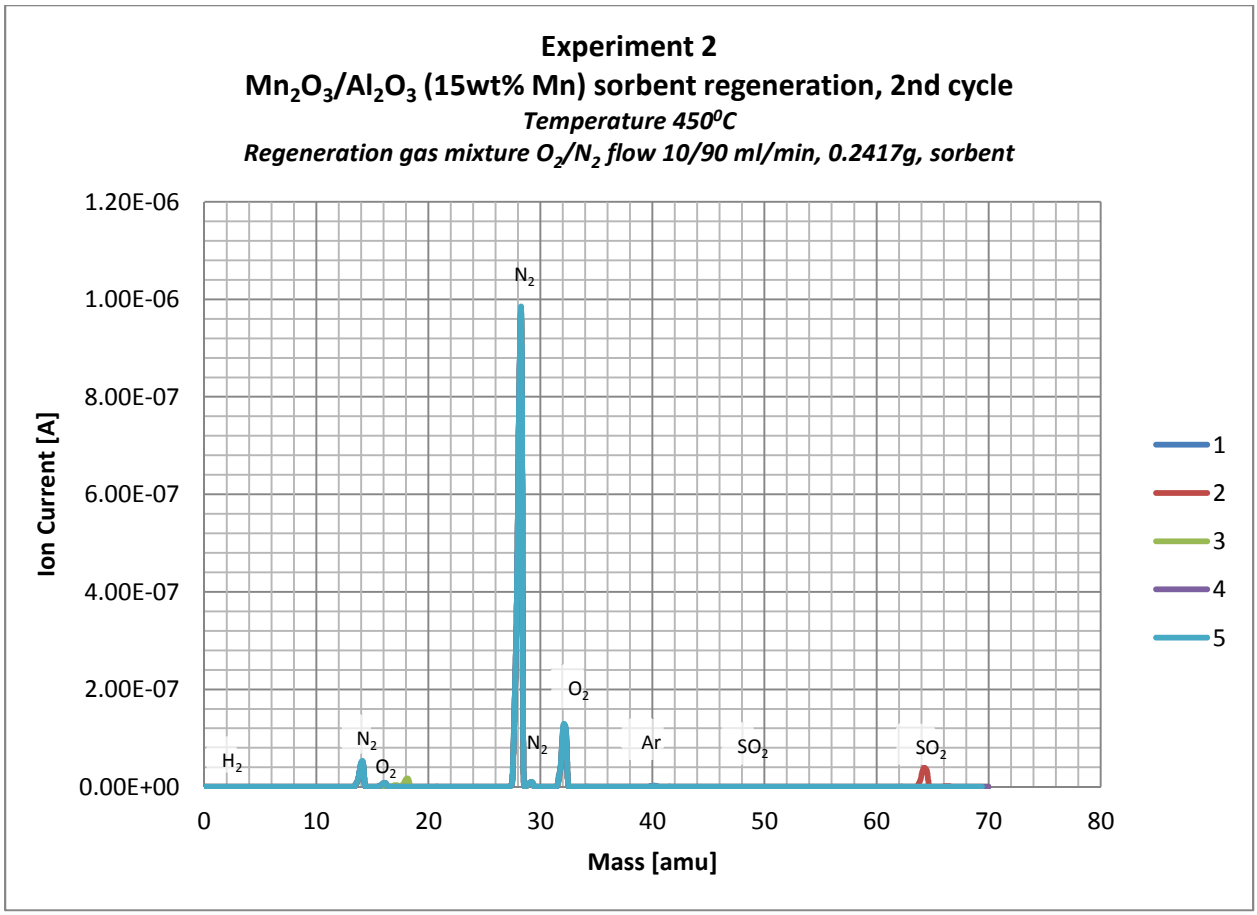
Experiment 2
Mn2O3/Al2O3 (15wt% Mn) sorbent regeneration, 2nd cycle
Temperature 450⁰C
Regeneration gas mixture O2/N2 flow 10/90 ml/min, 0.2417g, sorbent
Ion Current [A]
1.20E-06
1.00E-06
8.00E-07
6.00E-07
4.00E-07
2.00E-07
0.00E+00
0
10
20
30
40
50
60
70
80
Mass [amu]
N2
N2
O2
H2
N2
O2
Ar
SO2
SO2
1
2
3
4
5

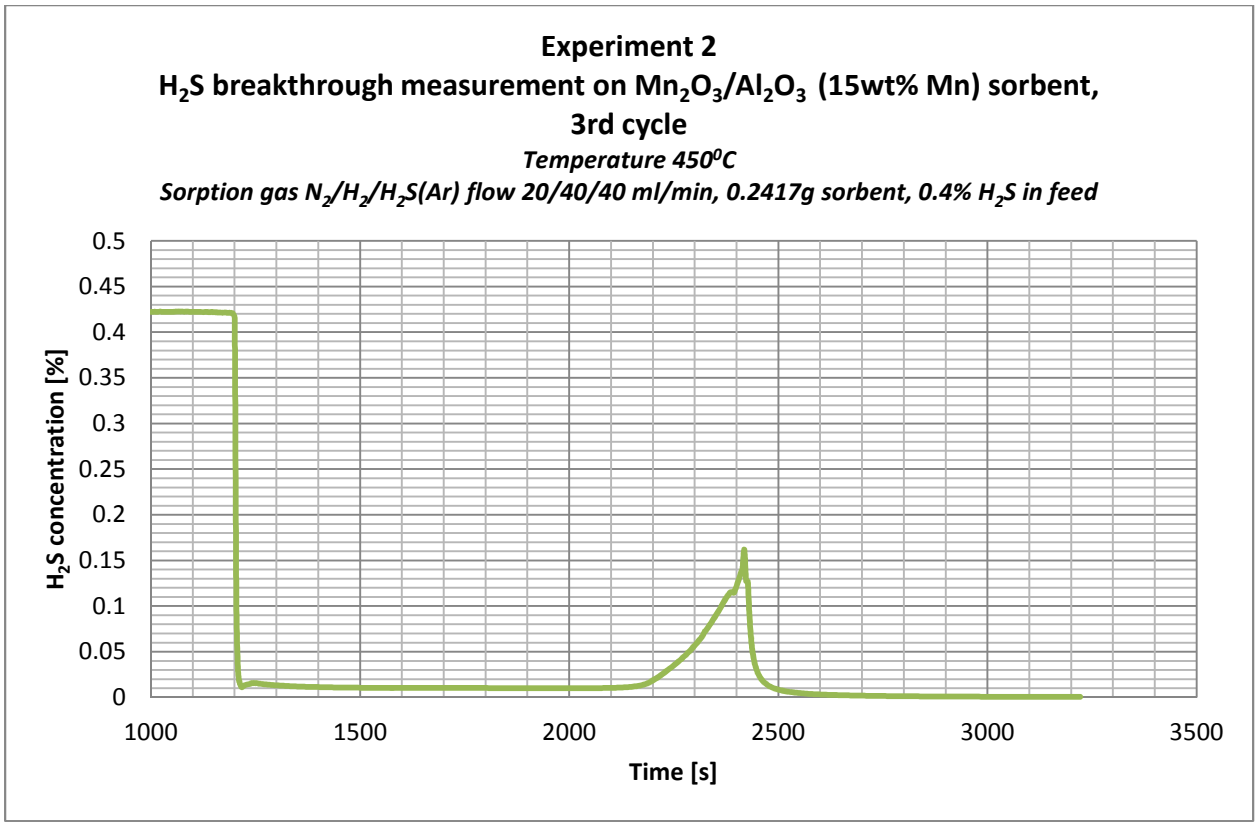
Experiment 2
H2S breakthrough measurement on Mn2O3/Al2O3 (15wt% Mn) sorbent, 3rd cycle
Temperature 450⁰C
Sorption gas N2/H2/H2S(Ar) flow 20/40/40 ml/min, 0.2417g sorbent, 0.4% H2S in feed
H2S concentration [%]
0.5
0.45
0.4
0.35
0.3
0.25
0.2
0.15
0.1
0.05
0
1000
1500
2000
2500
3000
3500
Time [s]

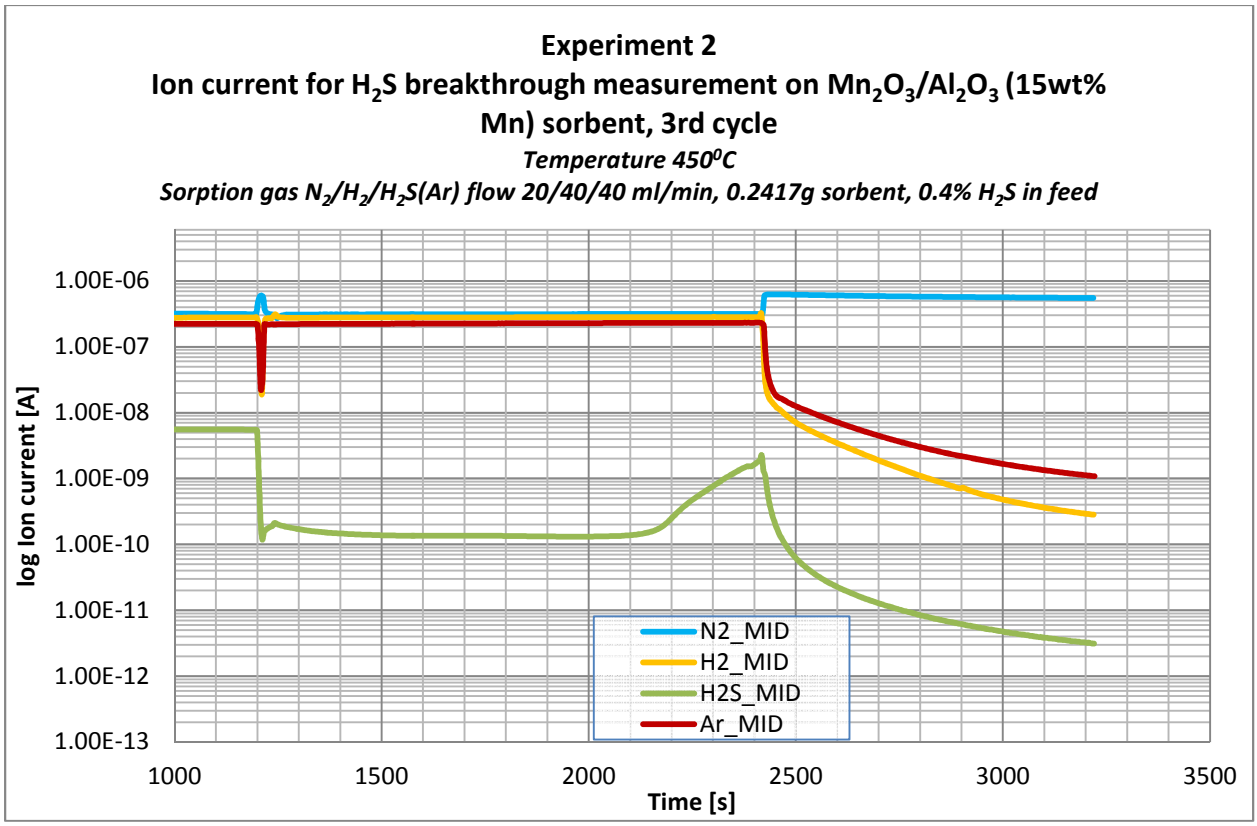
Experiment 2
Ion current for H2S breakthrough measurement on Mn2O3/Al2O3 (15wt% Mn) sorbent, 3rd cycle
Temperature 450⁰C
Sorption gas N2/H2/H2S(Ar) flow 20/40/40 ml/min, 0.2417g sorbent, 0.4% H2S in feed
log Ion current [A]
1.00E-06
1.00E-07
1.00E-08
1.00E-09
1.00E-10
1.00E-11
1.00E-12
1.00E-13
1000
1500
2000
2500
3000
3500
Time [s]
N2_MID
H2_MID
H2S_MID
Ar_MID

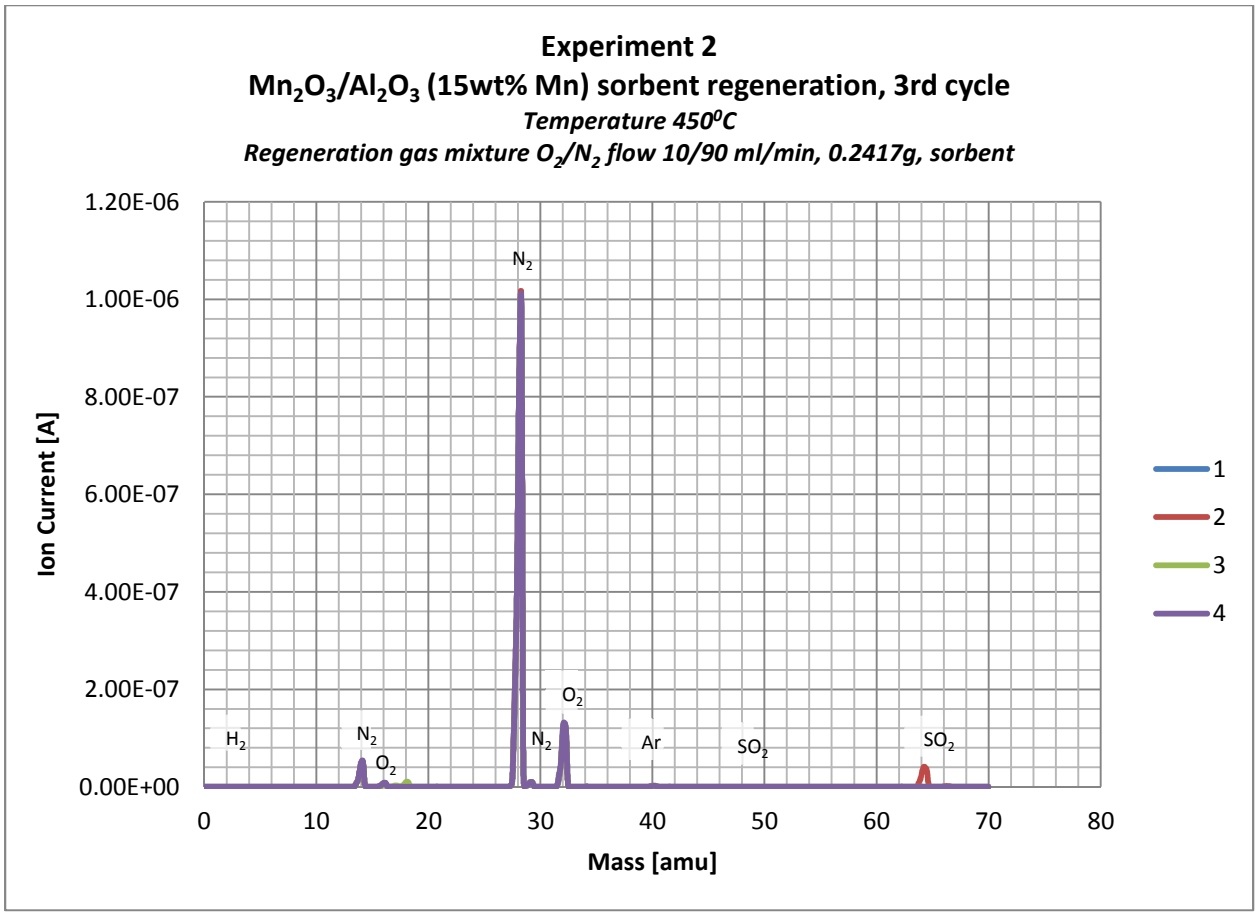
Experiment 2
Mn2O3/Al2O3 (15wt% Mn) sorbent regeneration, 3rd cycle
Temperature 450⁰C
Regeneration gas mixture O2/N2 flow 10/90 ml/min, 0.2417g, sorbent
Ion Current [A]
1.20E-06
1.00E-06
8.00E-07
6.00E-07
4.00E-07
2.00E-07
0.00E+00
0
10
20
30
40
50
60
70
80
Mass [amu]
H2
N2
O2
N2
N2
O2
Ar
SO2
SO2
1
2
3
4

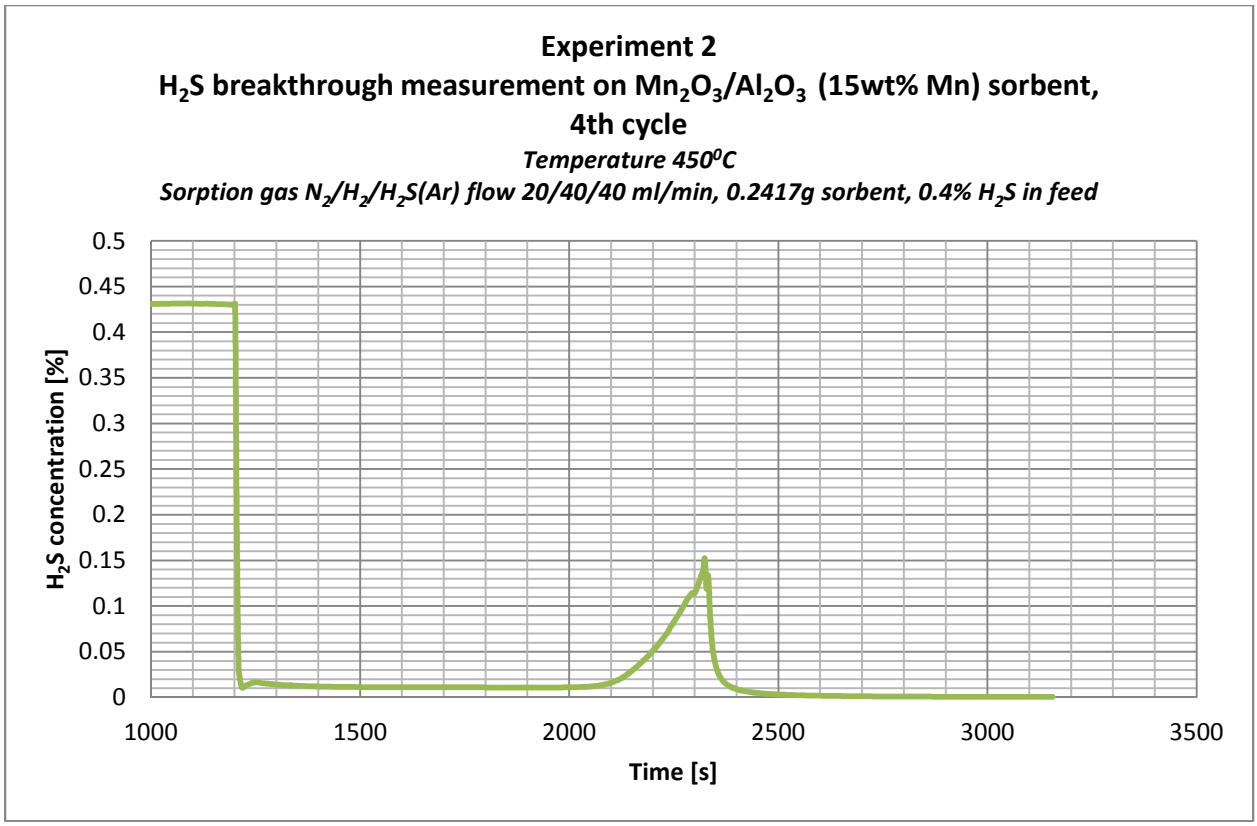
Experiment 2
H2S breakthrough measurement on Mn2O3/Al2O3 (15wt% Mn) sorbent, 4th cycle
Temperature 450⁰C
Sorption gas N2/H2/H2S(Ar) flow 20/40/40 ml/min, 0.2417g sorbent, 0.4% H2S in feed
H2S concentration [%]
0.5
0.45
0.4
0.35
0.3
0.25
0.2
0.15
0.1
0.05
0
1000
1500
2000
2500
3000
3500
Time [s]

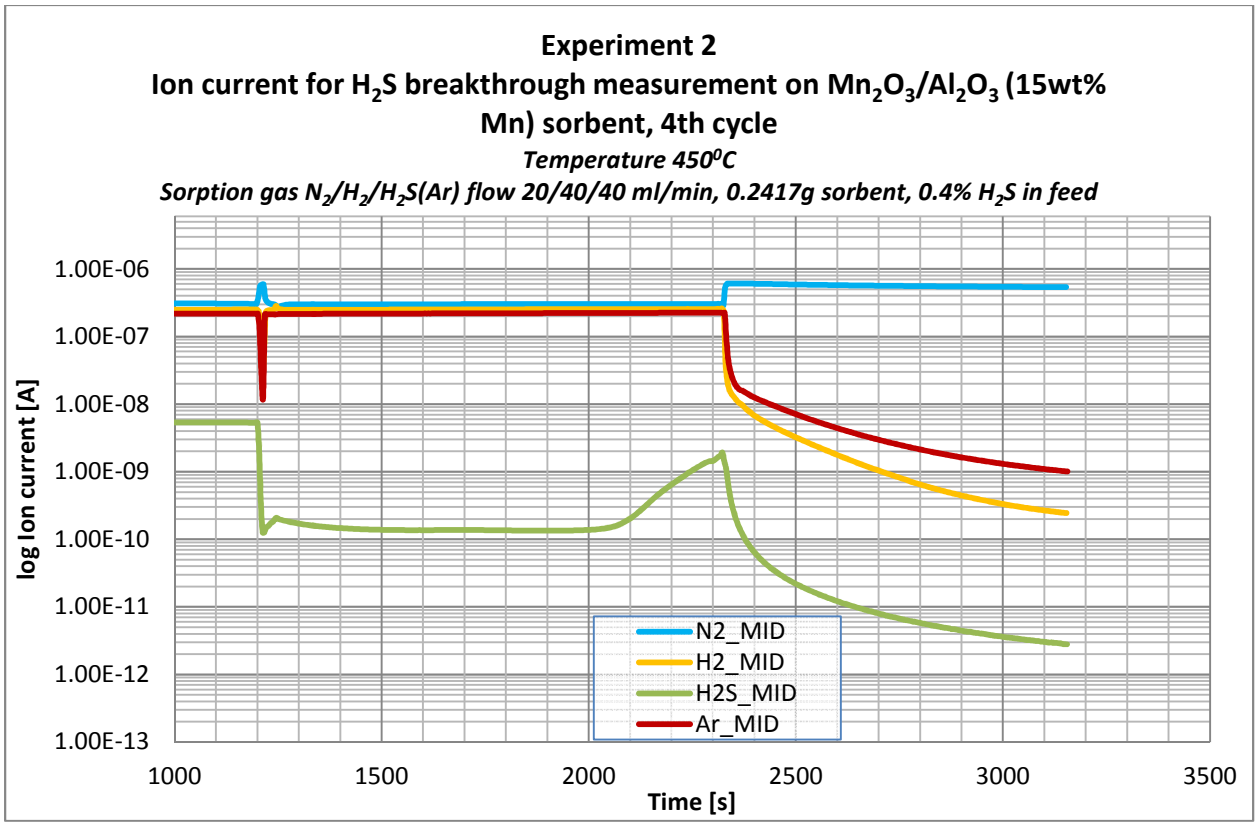
Experiment 2
Ion current for H2S breakthrough measurement on Mn2O3/Al2O3 (15wt% Mn) sorbent, 4th cycle
Temperature 450⁰C
Sorption gas N2/H2/H2S(Ar) flow 20/40/40 ml/min, 0.2417g sorbent, 0.4% H2S in feed
log Ion current [A]
1.00E-06
1.00E-07
1.00E-08
1.00E-09
1.00E-10
1.00E-11
1.00E-12
1.00E-13
1000
1500
2000
2500
3000
3500
Time [s]
N2_MID
H2_MID
H2S_MID
Ar_MID

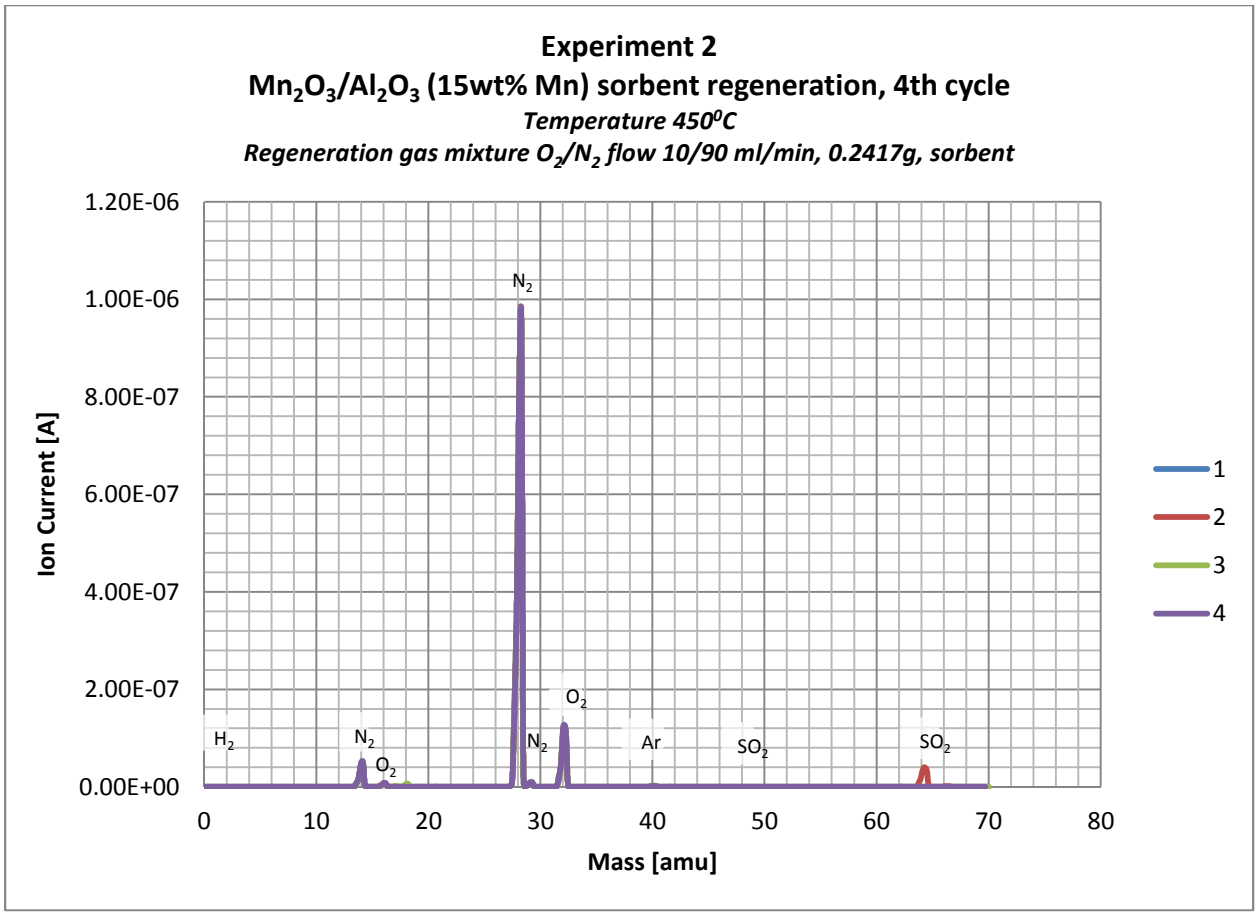
Experiment 2
Mn2O3/Al2O3 (15wt% Mn) sorbent regeneration, 4th cycle
Temperature 450⁰C
Regeneration gas mixture O2/N2 flow 10/90 ml/min, 0.2417g, sorbent
Ion Current [A]
1.20E-06
1.00E-06
8.00E-07
6.00E-07
4.00E-07
2.00E-07
0.00E+00
0
10
20
30
40
50
60
70
80
Mass [amu]
H2
N2
O2
N2
N2
O2
Ar
SO2
SO2
1
2
3
4

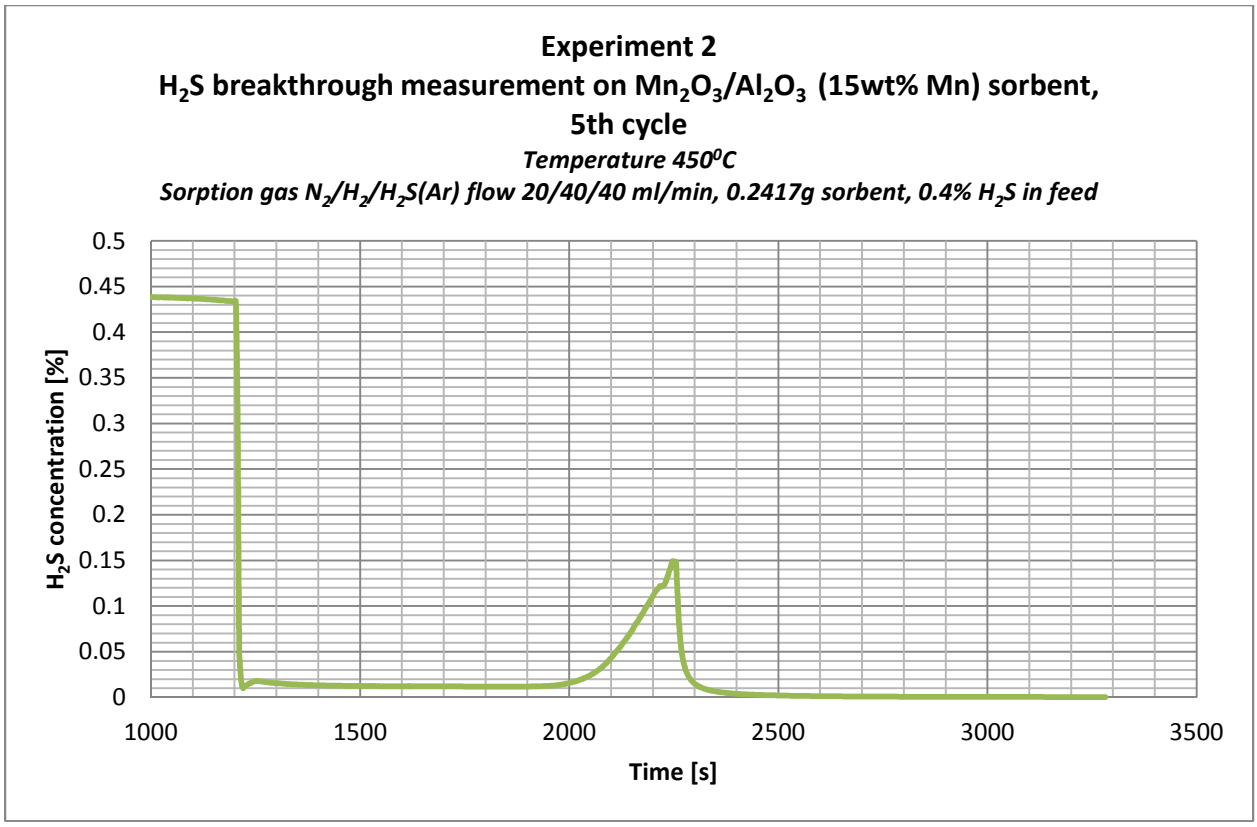
Experiment 2
H2S breakthrough measurement on Mn2O3/Al2O3 (15wt% Mn) sorbent, 5th cycle
Temperature 450⁰C
Sorption gas N2/H2/H2S(Ar) flow 20/40/40 ml/min, 0.2417g sorbent, 0.4% H2S in feed
H2S concentration [%]
0.5
0.45
0.4
0.35
0.3
0.25
0.2
0.15
0.1
0.05
0
1000
1500
2000
2500
3000
3500
Time [s]

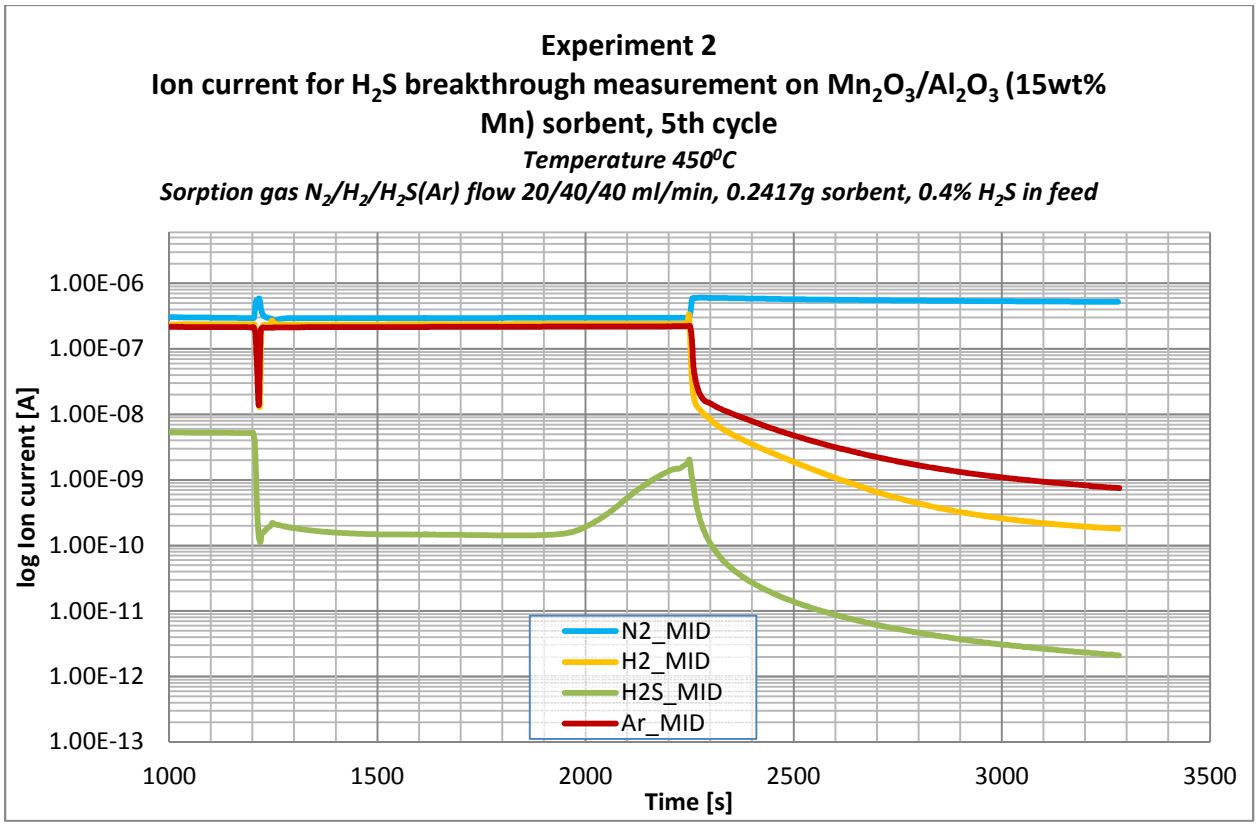
Experiment 2
Ion current for H2S breakthrough measurement on Mn2O3/Al2O3 (15wt% Mn) sorbent, 5th cycle
Temperature 450⁰C
Sorption gas N2/H2/H2S(Ar) flow 20/40/40 ml/min, 0.2417g sorbent, 0.4% H2S in feed
log Ion current [A]
1.00E-06
1.00E-07
1.00E-08
1.00E-09
1.00E-10
1.00E-11
1.00E-12
1.00E-13
1000
1500
2000
2500
3000
3500
Time [s]
N2_MID
H2_MID
H2S_MID
Ar_MID

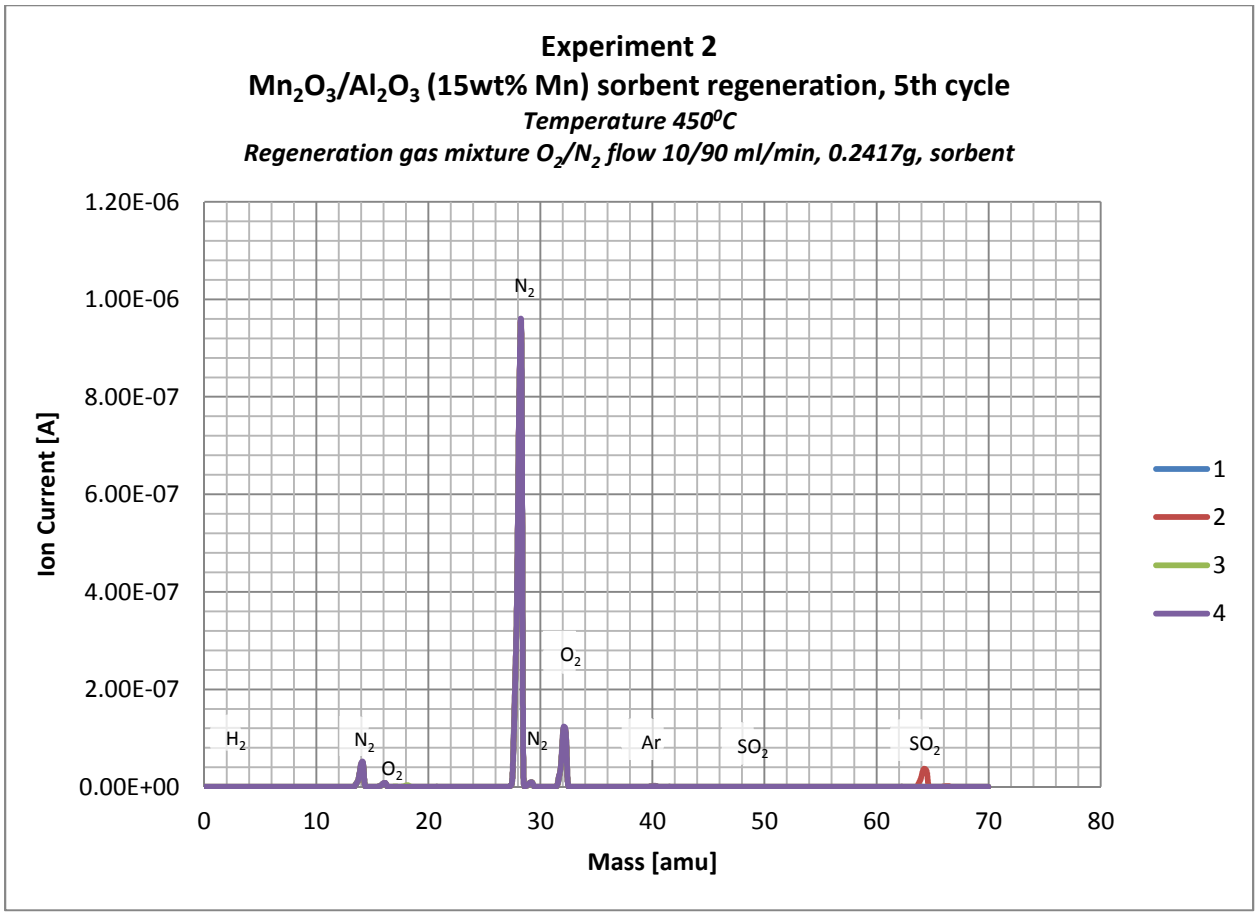
Experiment 2
Mn2O3/Al2O3 (15wt% Mn) sorbent regeneration, 5th cycle
Temperature 450⁰C
Regeneration gas mixture O2/N2 flow 10/90 ml/min, 0.2417g, sorbent
Ion Current [A]
1.20E-06
1.00E-06
8.00E-07
6.00E-07
4.00E-07
2.00E-07
0.00E+00
0
10
20
30
40
50
60
70
80
Mass [amu]
H2
N2
O2
N2
O2
N2
Ar
SO2
SO2
1
2
3
4

**Experiment 2**

**$H_2S$ breakthrough measurement on $Mn_2O_3/Al_2O_3$ (15wt% Mn) sorbent, 6th cycle**

***Temperature 450$^0$C***

***Sorption gas $N_2/H_2/H_2S$(Ar) flow 20/40/40 ml/min, 0.2417g sorbent, 0.4% $H_2S$ in feed***

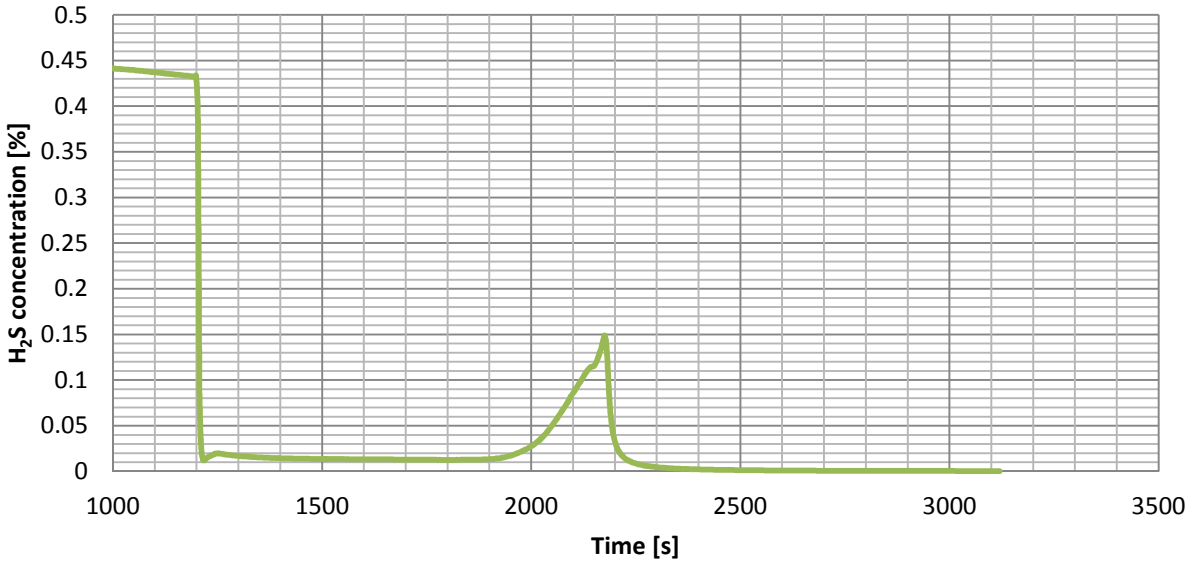


**Experiment 2**

**Ion current for $H_2S$ breakthrough measurement on $Mn_2O_3/Al_2O_3$ (15wt% Mn) sorbent, 6th cycle**

***Temperature 450$^0$C***

***Sorption gas $N_2/H_2/H_2S$(Ar) flow 20/40/40 ml/min, 0.2417g sorbent, 0.4% $H_2S$ in feed***

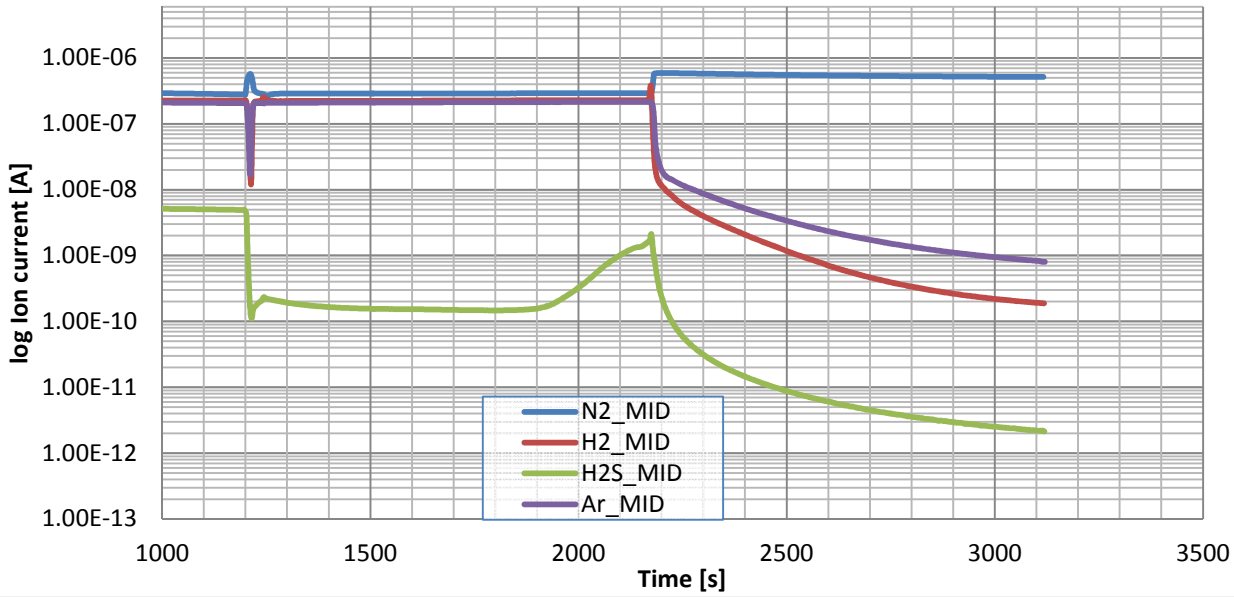

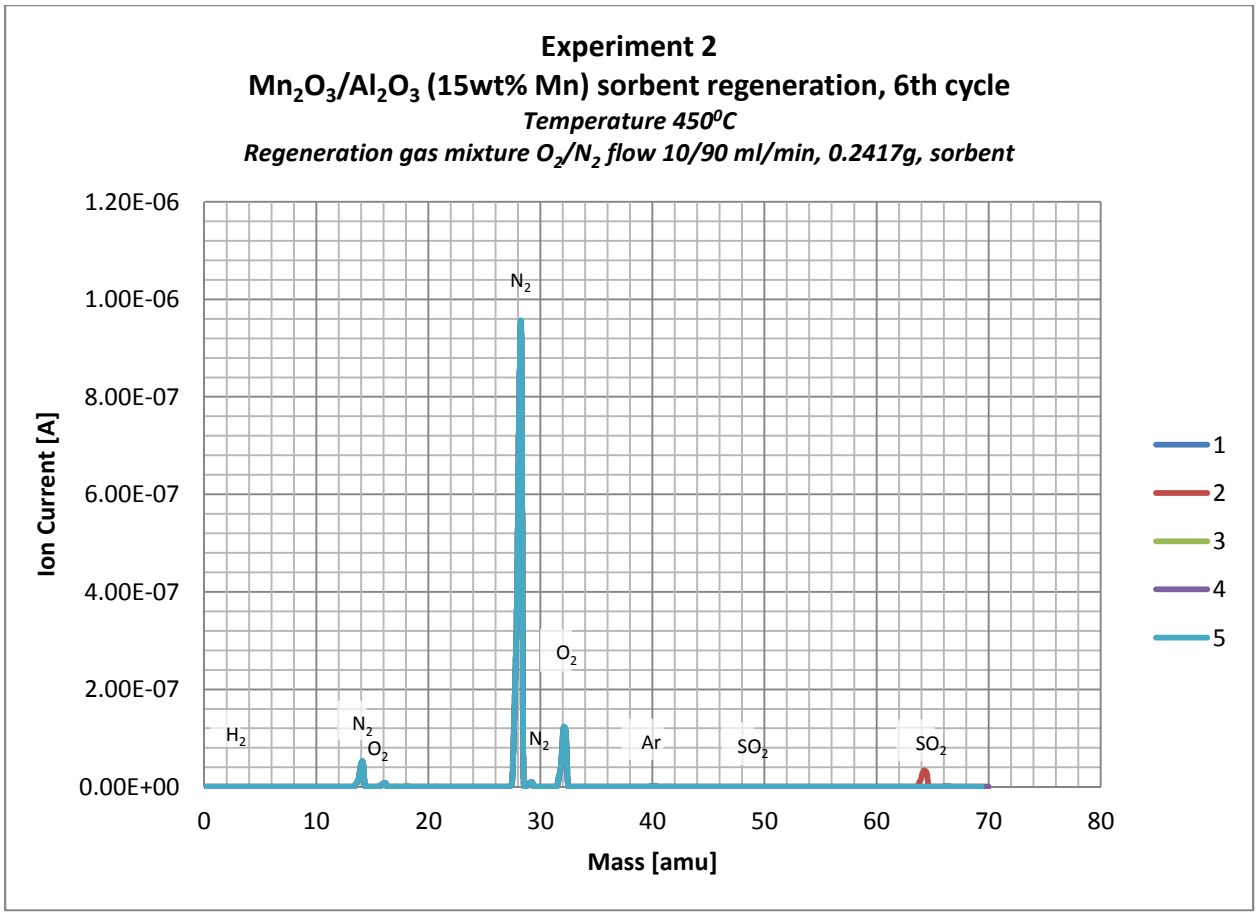
Experiment 2
Mn2O3/Al2O3 (15wt% Mn) sorbent regeneration, 6th cycle
Temperature 450⁰C
Regeneration gas mixture O2/N2 flow 10/90 ml/min, 0.2417g, sorbent
Ion Current [A]
1.20E-06
1.00E-06
8.00E-07
6.00E-07
4.00E-07
2.00E-07
0.00E+00
0
10
20
30
40
50
60
70
80
Mass [amu]
H2
N2
O2
N2
O2
N2
Ar
SO2
SO2
1
2
3
4
5

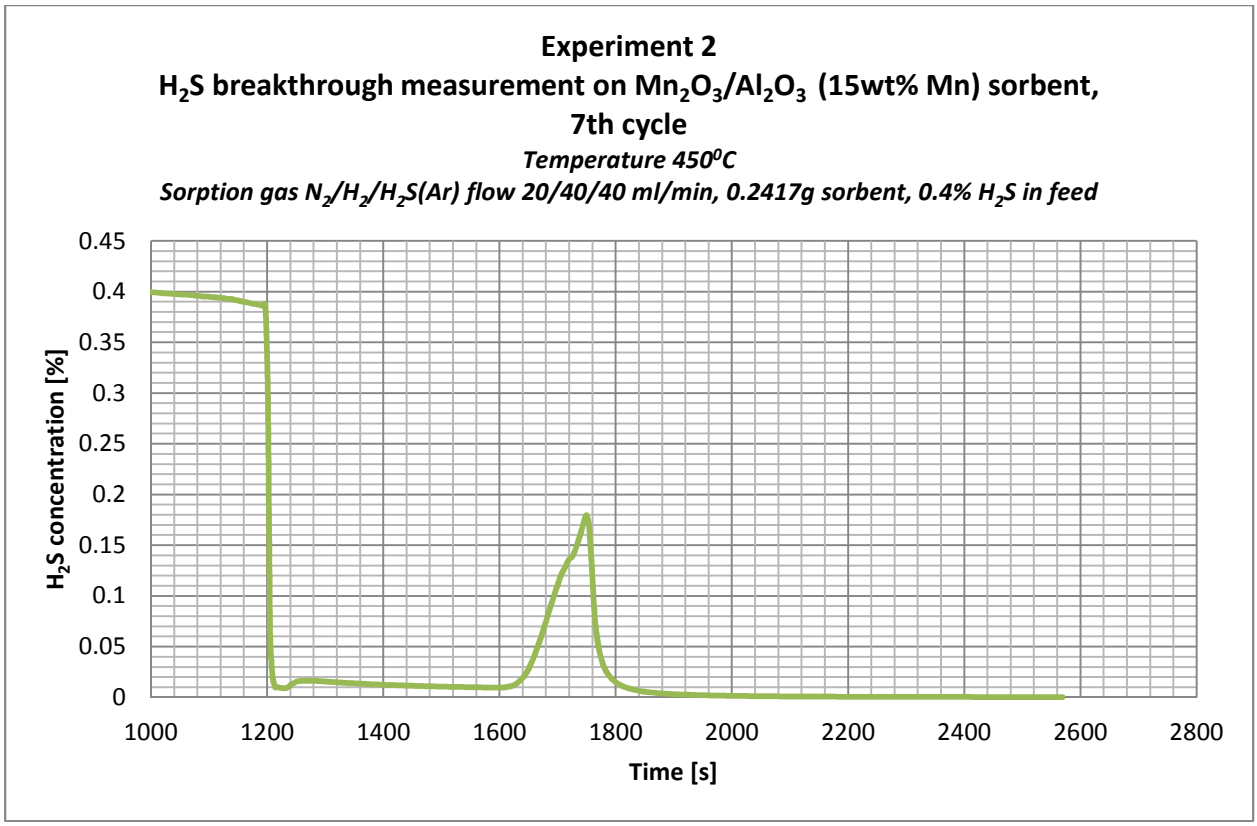
Experiment 2
H2S breakthrough measurement on Mn2O3/Al2O3 (15wt% Mn) sorbent, 7th cycle
Temperature 450⁰C
Sorption gas N2/H2/H2S(Ar) flow 20/40/40 ml/min, 0.2417g sorbent, 0.4% H2S in feed
H2S concentration [%]
0.45
0.4
0.35
0.3
0.25
0.2
0.15
0.1
0.05
0
1000
1200
1400
1600
1800
2000
2200
2400
2600
2800
Time [s]

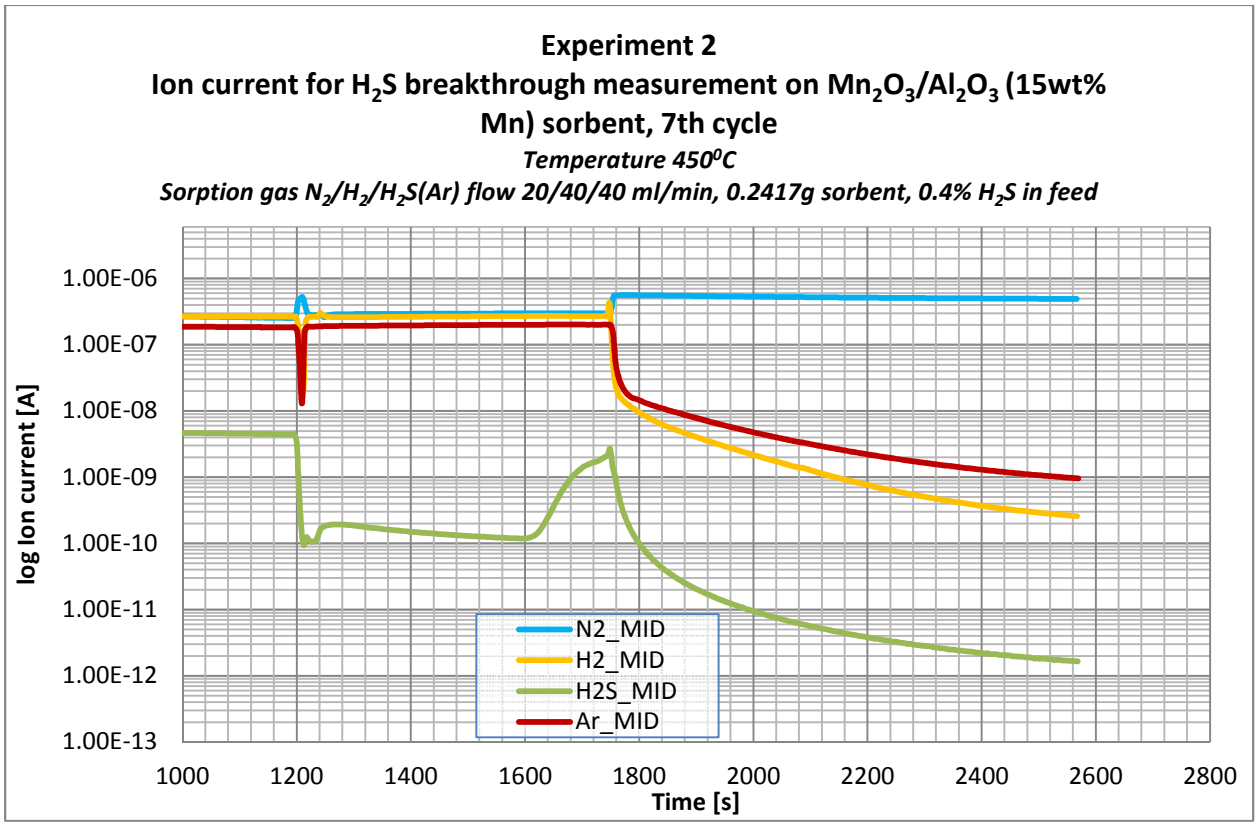
Experiment 2
Ion current for H2S breakthrough measurement on Mn2O3/Al2O3 (15wt% Mn) sorbent, 7th cycle
Temperature 450⁰C
Sorption gas N2/H2/H2S(Ar) flow 20/40/40 ml/min, 0.2417g sorbent, 0.4% H2S in feed
log Ion current [A]
1.00E-06
1.00E-07
1.00E-08
1.00E-09
1.00E-10
1.00E-11
1.00E-12
1.00E-13
N2_MID
H2_MID
H2S_MID
Ar_MID
1000
1200
1400
1600
1800
2000
2200
2400
2600
2800
Time [s]

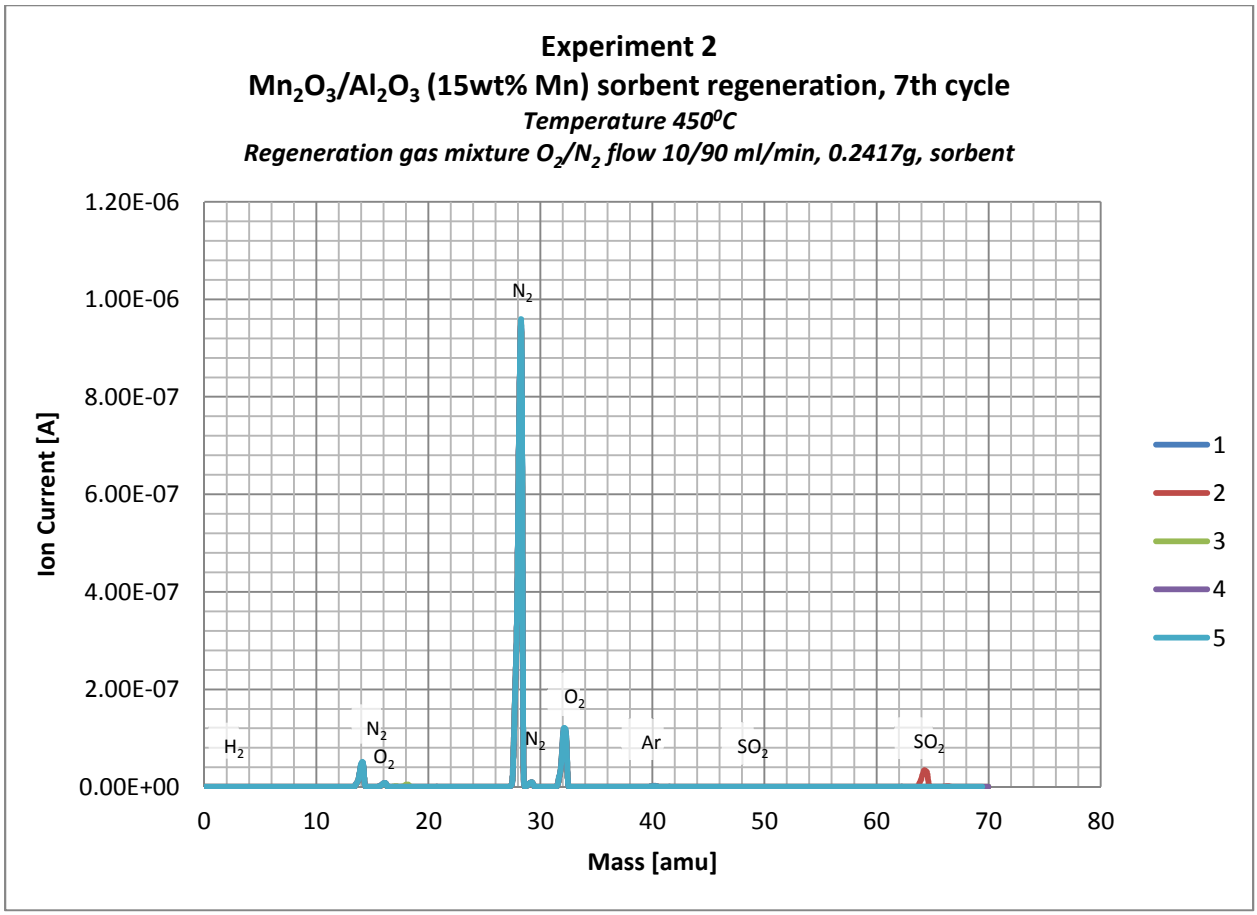
Experiment 2
Mn2O3/Al2O3 (15wt% Mn) sorbent regeneration, 7th cycle
Temperature 450⁰C
Regeneration gas mixture O2/N2 flow 10/90 ml/min, 0.2417g, sorbent
Ion Current [A]
1.20E-06
1.00E-06
8.00E-07
6.00E-07
4.00E-07
2.00E-07
0.00E+00
0
10
20
30
40
50
60
70
80
Mass [amu]
H2
N2
O2
N2
N2
O2
Ar
SO2
SO2
1
2
3
4
5

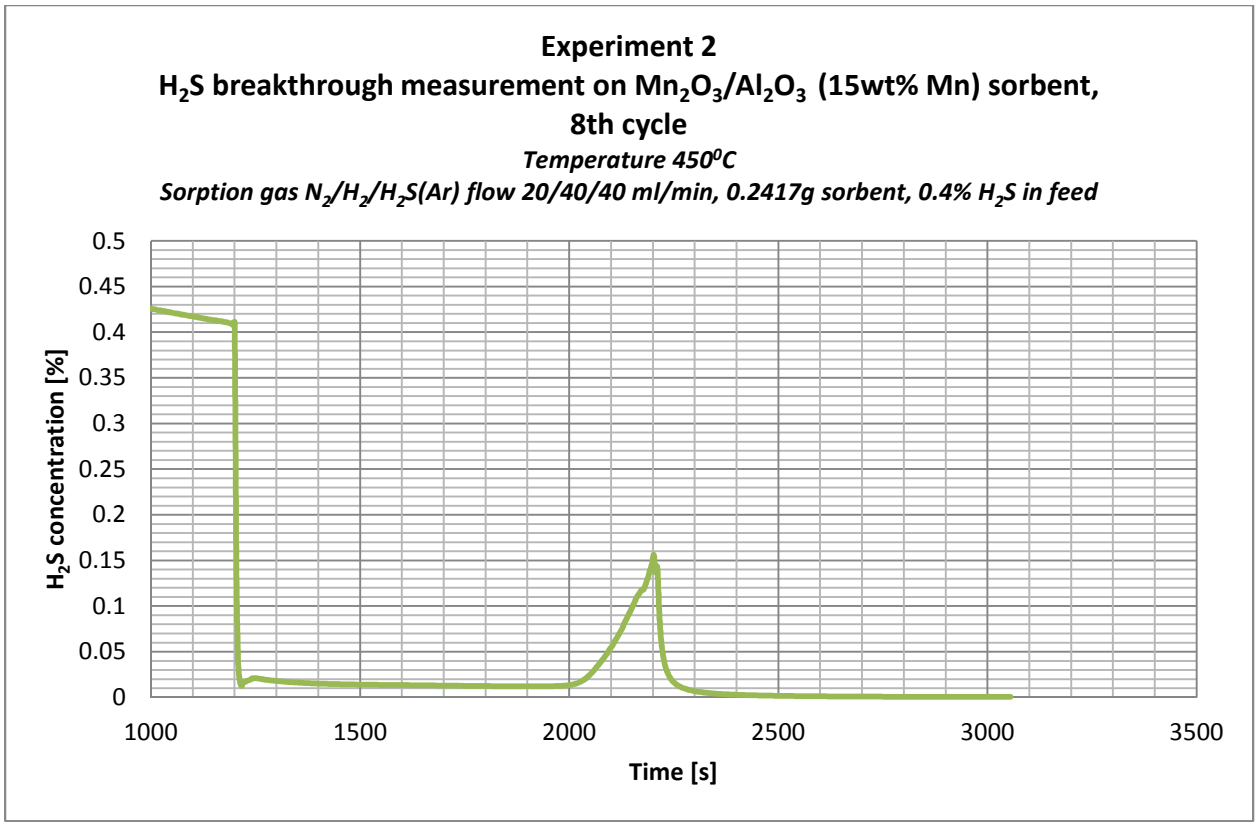
Experiment 2
H2S breakthrough measurement on Mn2O3/Al2O3 (15wt% Mn) sorbent, 8th cycle
Temperature 450⁰C
Sorption gas N2/H2/H2S(Ar) flow 20/40/40 ml/min, 0.2417g sorbent, 0.4% H2S in feed
H2S concentration [%]
0.5
0.45
0.4
0.35
0.3
0.25
0.2
0.15
0.1
0.05
0
1000
1500
2000
2500
3000
3500
Time [s]

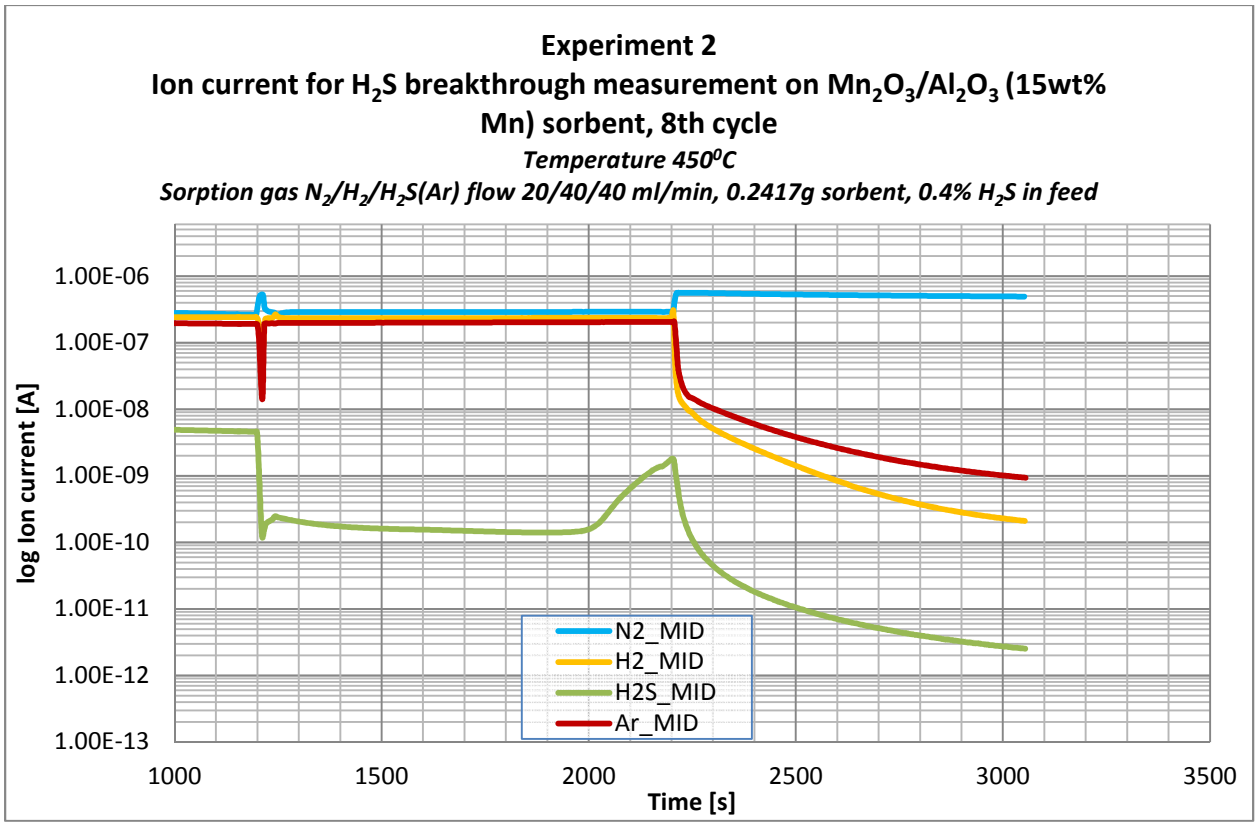
Experiment 2
Ion current for H2S breakthrough measurement on Mn2O3/Al2O3 (15wt% Mn) sorbent, 8th cycle
Temperature 450⁰C
Sorption gas N2/H2/H2S(Ar) flow 20/40/40 ml/min, 0.2417g sorbent, 0.4% H2S in feed
log Ion current [A]
1.00E-06
1.00E-07
1.00E-08
1.00E-09
1.00E-10
1.00E-11
1.00E-12
1.00E-13
1000
1500
2000
2500
3000
3500
Time [s]
N2_MID
H2_MID
H2S_MID
Ar_MID

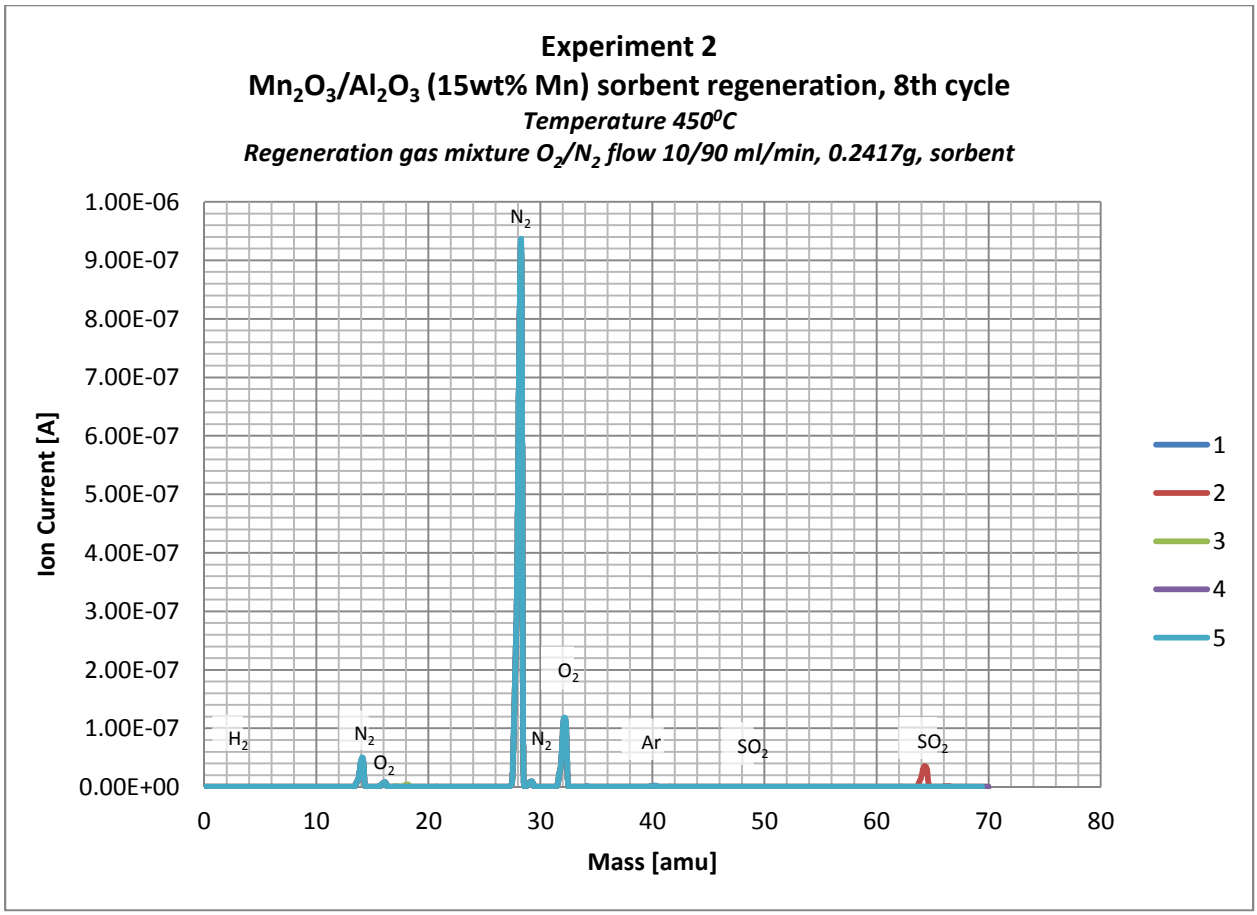
Experiment 2
Mn2O3/Al2O3 (15wt% Mn) sorbent regeneration, 8th cycle
Temperature 450⁰C
Regeneration gas mixture O2/N2 flow 10/90 ml/min, 0.2417g, sorbent
Ion Current [A]
1.00E-06
9.00E-07
8.00E-07
7.00E-07
6.00E-07
5.00E-07
4.00E-07
3.00E-07
2.00E-07
1.00E-07
0.00E+00
0
10
20
30
40
50
60
70
80
Mass [amu]
N2
O2
H2
N2
O2
N2
Ar
SO2
SO2
1
2
3
4
5

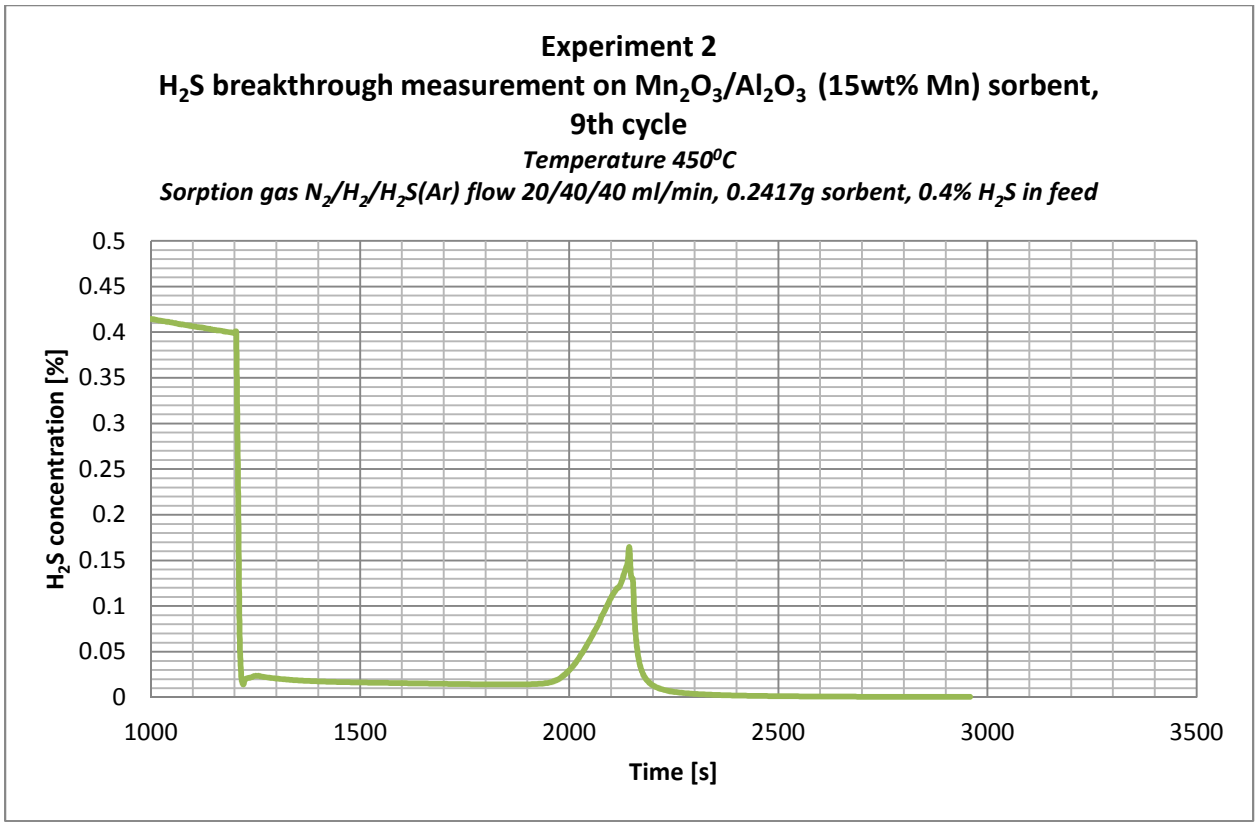
Experiment 2
H2S breakthrough measurement on Mn2O3/Al2O3 (15wt% Mn) sorbent, 9th cycle
Temperature 450⁰C
Sorption gas N2/H2/H2S(Ar) flow 20/40/40 ml/min, 0.2417g sorbent, 0.4% H2S in feed
H2S concentration [%]
0.5
0.45
0.4
0.35
0.3
0.25
0.2
0.15
0.1
0.05
0
1000
1500
2000
2500
3000
3500
Time [s]

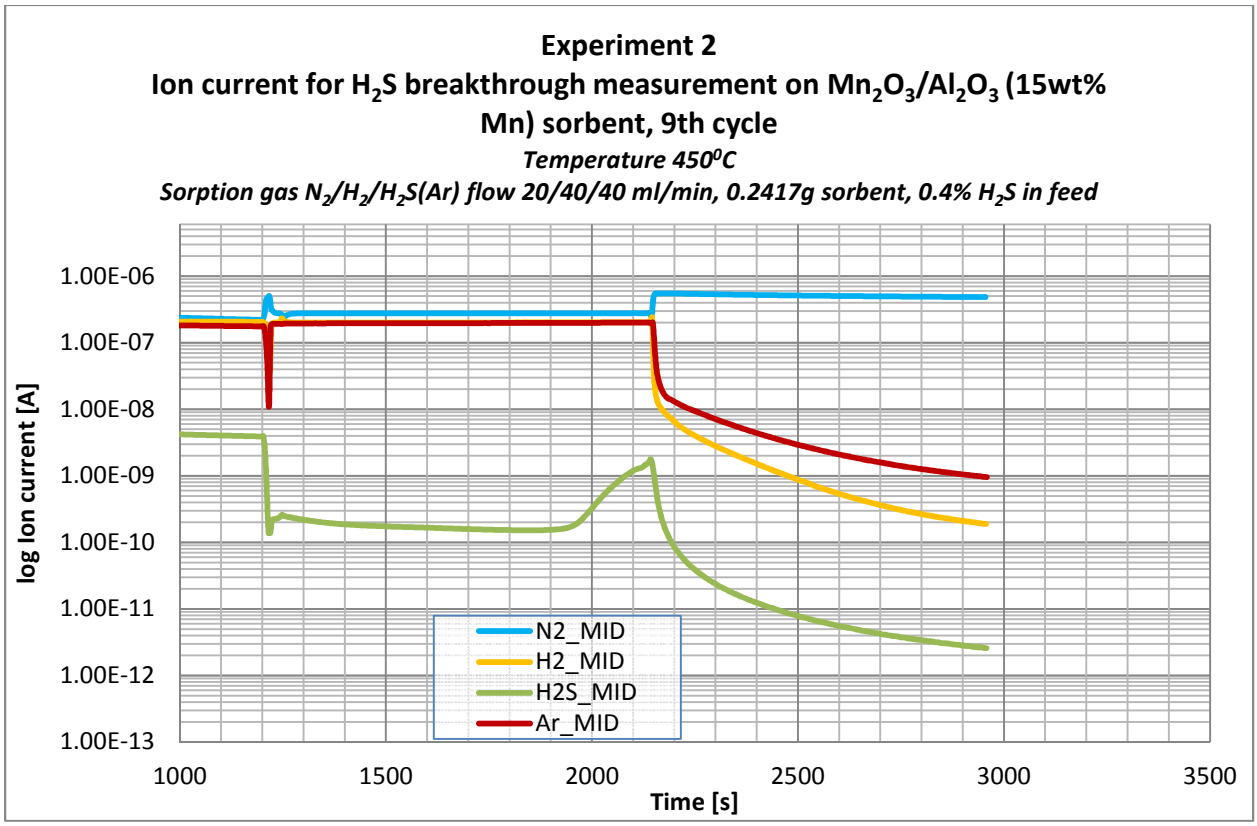
Experiment 2
Ion current for H2S breakthrough measurement on Mn2O3/Al2O3 (15wt% Mn) sorbent, 9th cycle
Temperature 450⁰C
Sorption gas N2/H2/H2S(Ar) flow 20/40/40 ml/min, 0.2417g sorbent, 0.4% H2S in feed
log Ion current [A]
1.00E-06
1.00E-07
1.00E-08
1.00E-09
1.00E-10
1.00E-11
1.00E-12
1.00E-13
1000
1500
2000
2500
3000
3500
Time [s]
N2_MID
H2_MID
H2S_MID
Ar_MID

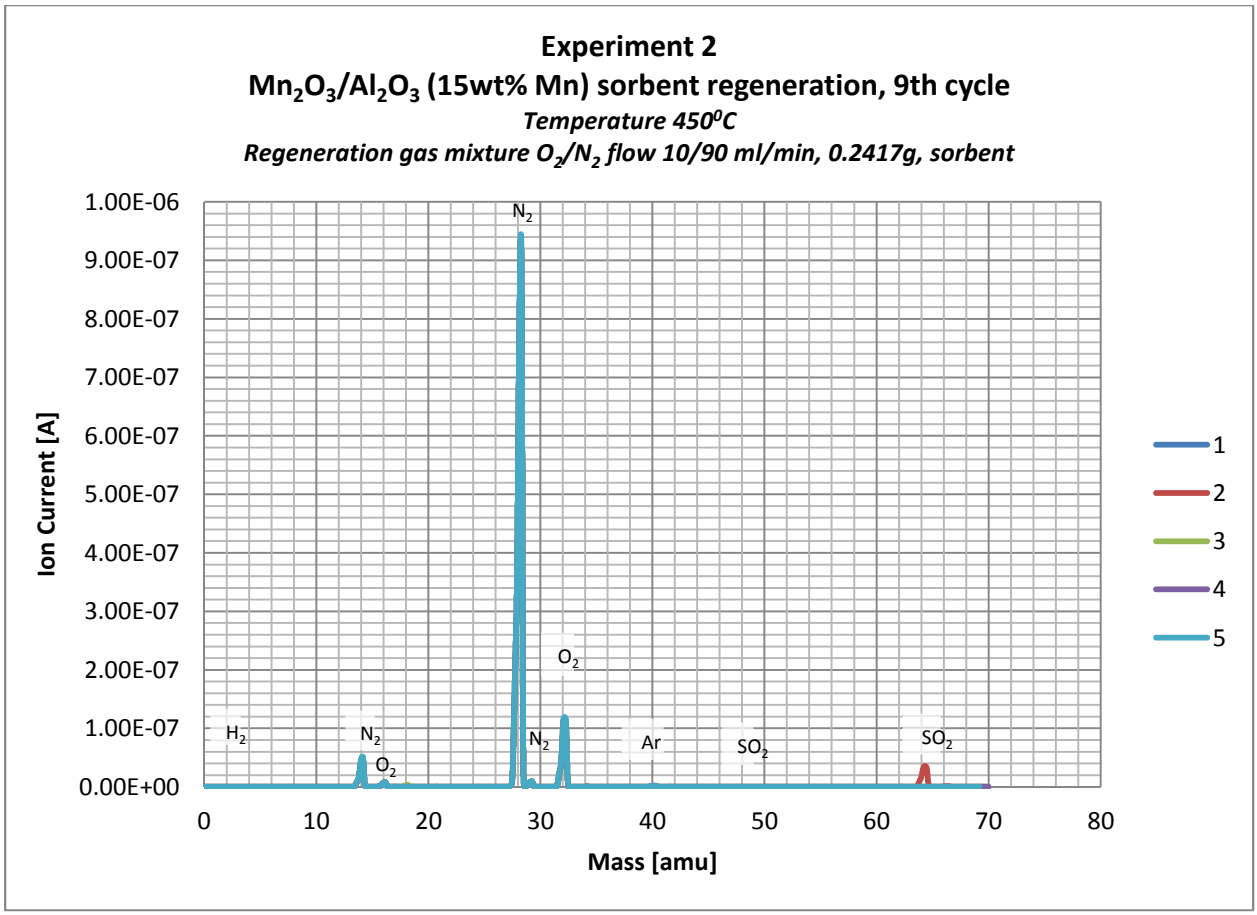
Experiment 2
Mn2O3/Al2O3 (15wt% Mn) sorbent regeneration, 9th cycle
Temperature 450⁰C
Regeneration gas mixture O2/N2 flow 10/90 ml/min, 0.2417g, sorbent
Ion Current [A]
1.00E-06
9.00E-07
8.00E-07
7.00E-07
6.00E-07
5.00E-07
4.00E-07
3.00E-07
2.00E-07
1.00E-07
0.00E+00
0
10
20
30
40
50
60
70
80
Mass [amu]
N2
O2
H2
N2
O2
N2
Ar
SO2
SO2
1
2
3
4
5

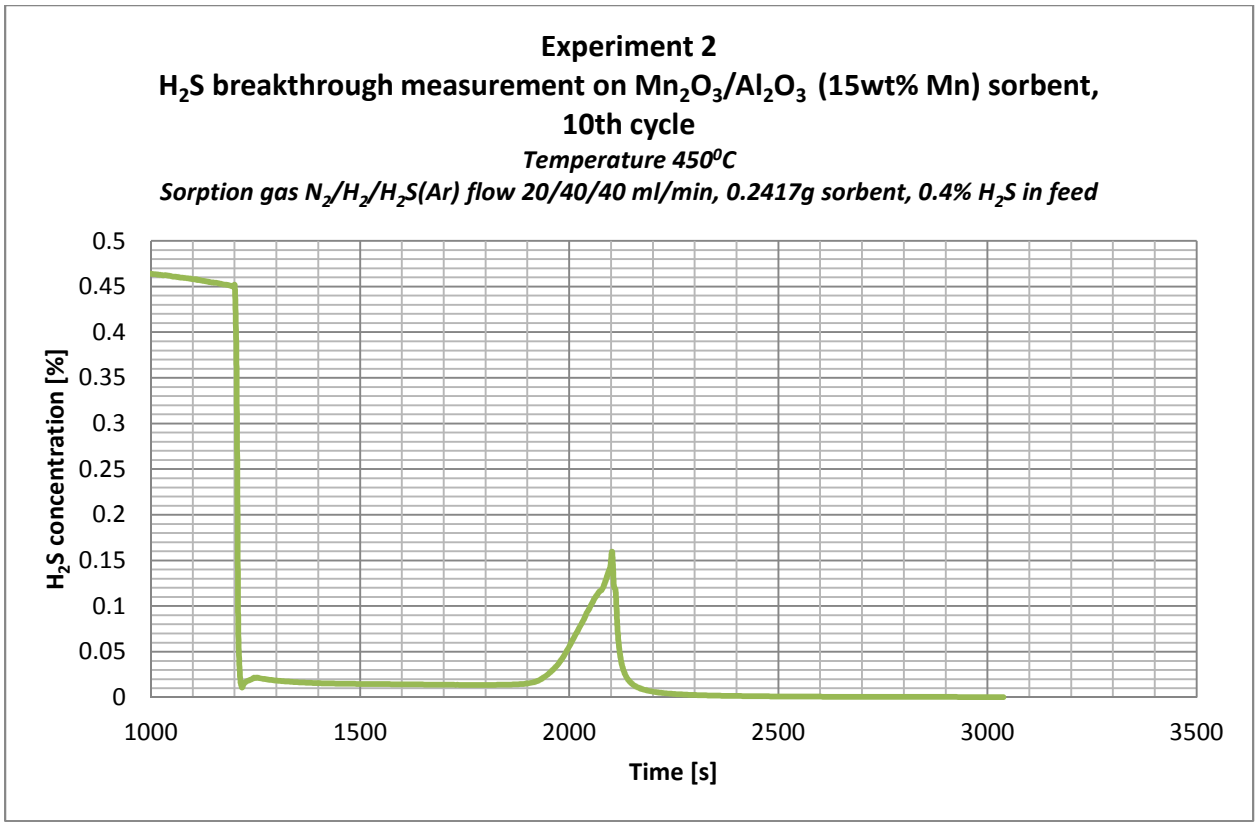
Experiment 2
H2S breakthrough measurement on Mn2O3/Al2O3 (15wt% Mn) sorbent, 10th cycle
Temperature 450⁰C
Sorption gas N2/H2/H2S(Ar) flow 20/40/40 ml/min, 0.2417g sorbent, 0.4% H2S in feed
H2S concentration [%]
0.5
0.45
0.4
0.35
0.3
0.25
0.2
0.15
0.1
0.05
0
1000
1500
2000
2500
3000
3500
Time [s]

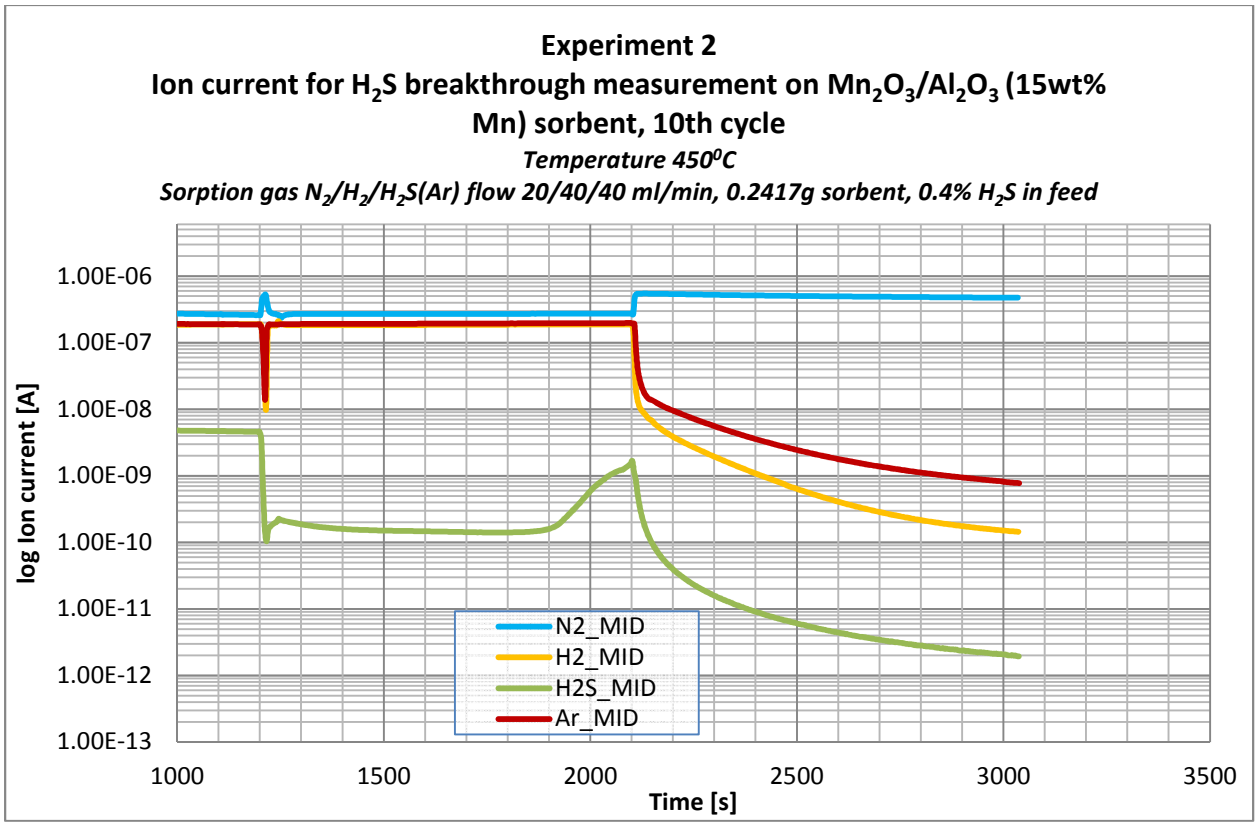
Experiment 2
Ion current for H2S breakthrough measurement on Mn2O3/Al2O3 (15wt% Mn) sorbent, 10th cycle
Temperature 450⁰C
Sorption gas N2/H2/H2S(Ar) flow 20/40/40 ml/min, 0.2417g sorbent, 0.4% H2S in feed
log Ion current [A]
1.00E-06
1.00E-07
1.00E-08
1.00E-09
1.00E-10
1.00E-11
1.00E-12
1.00E-13
1000
1500
2000
2500
3000
3500
Time [s]
N2_MID
H2_MID
H2S_MID
Ar_MID

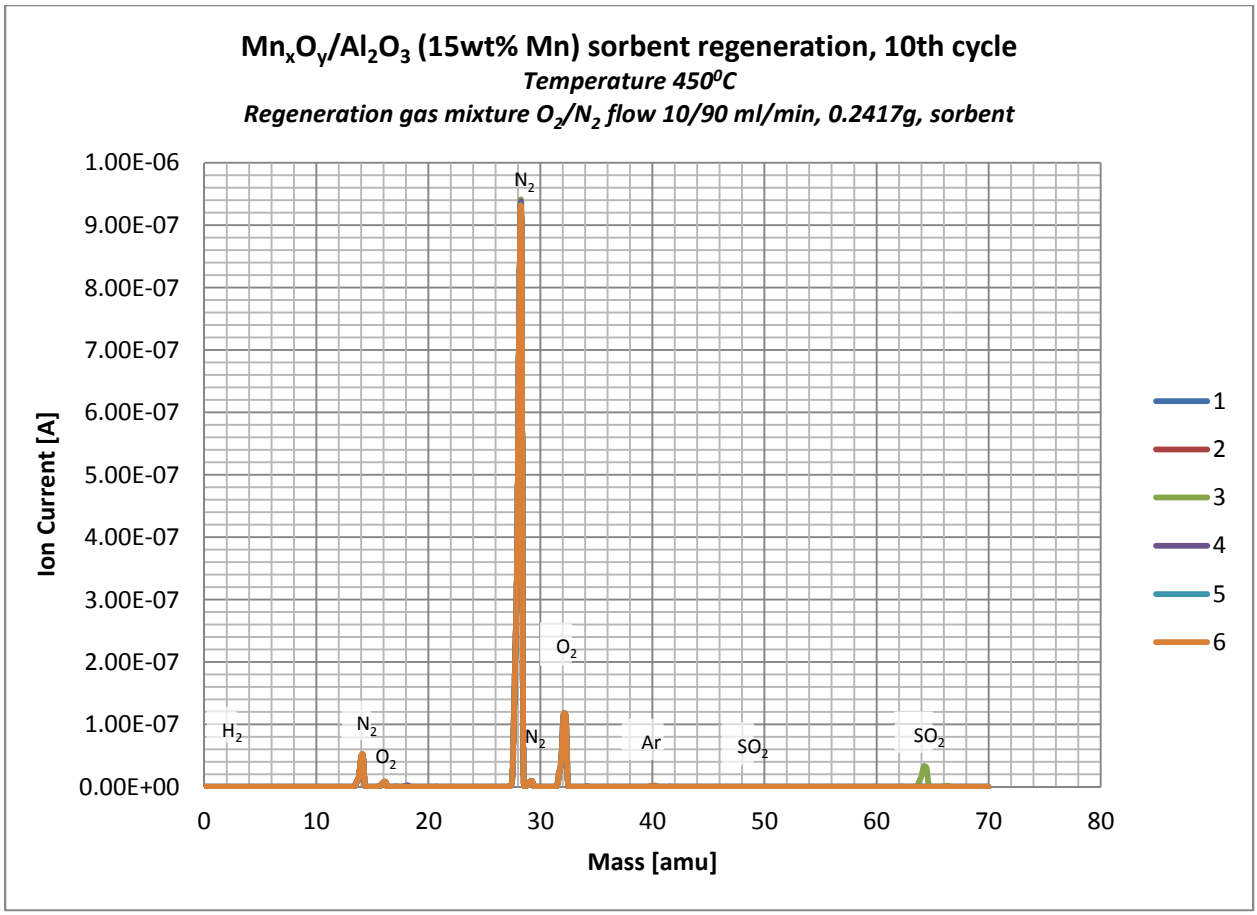
Mn$_x$O$_y$/Al$_2$O$_3$ (15wt% Mn) sorbent regeneration, 10th cycle
Temperature 450$^0$C
Regeneration gas mixture O$_2$/N$_2$ flow 10/90 ml/min, 0.2417g, sorbent
Ion Current [A]
1.00E-06
9.00E-07
8.00E-07
7.00E-07
6.00E-07
5.00E-07
4.00E-07
3.00E-07
2.00E-07
1.00E-07
0.00E+00
0
10
20
30
40
50
60
70
80
Mass [amu]
N$_2$
O$_2$
H$_2$
N$_2$
O$_2$
N$_2$
Ar
SO$_2$
SO$_2$
1
2
3
4
5
6

**Experiment 2**

**$H_2S$ breakthrough measurement on $Mn_2O_3/Al_2O_3$ (15wt% Mn) sorbent, 11th cycle**

***Temperature 450$^0$C***

***Sorption gas $N_2/H_2/H_2S$(Ar) flow 20/40/40 ml/min, 0.2417g sorbent, 0.4% $H_2S$ in feed***

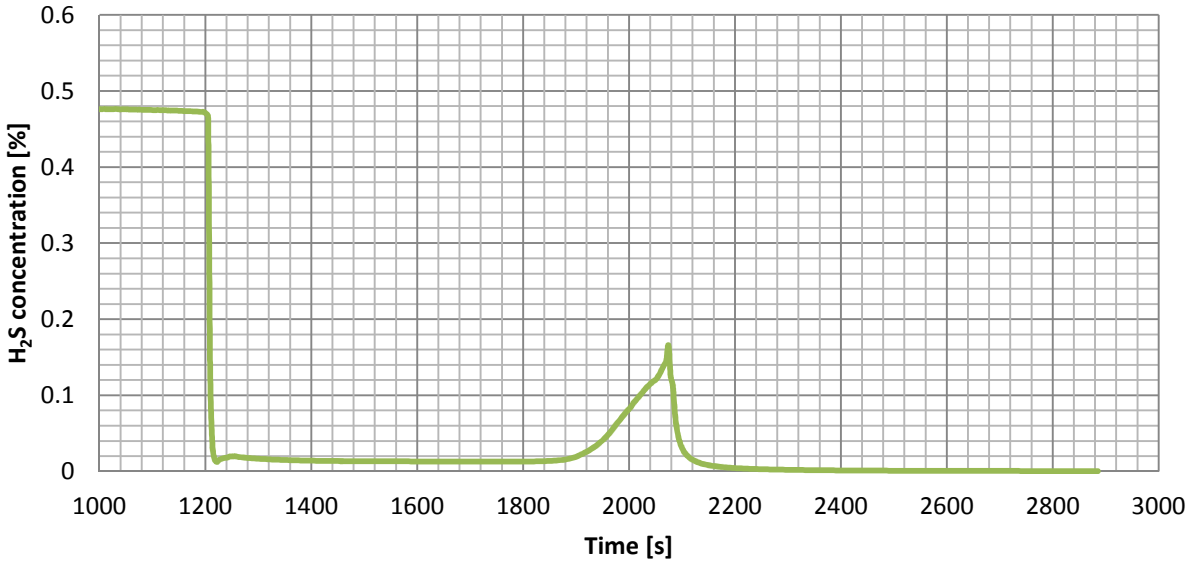


**Experiment 2**

**Ion current for $H_2S$ breakthrough measurement on $Mn_2O_3/Al_2O_3$ (15wt% Mn) sorbent, 11th cycle**

***Temperature 450$^0$C***

***Sorption gas $N_2/H_2/H_2S$(Ar) flow 20/40/40 ml/min, 0.2417g sorbent, 0.4% $H_2S$ in feed***

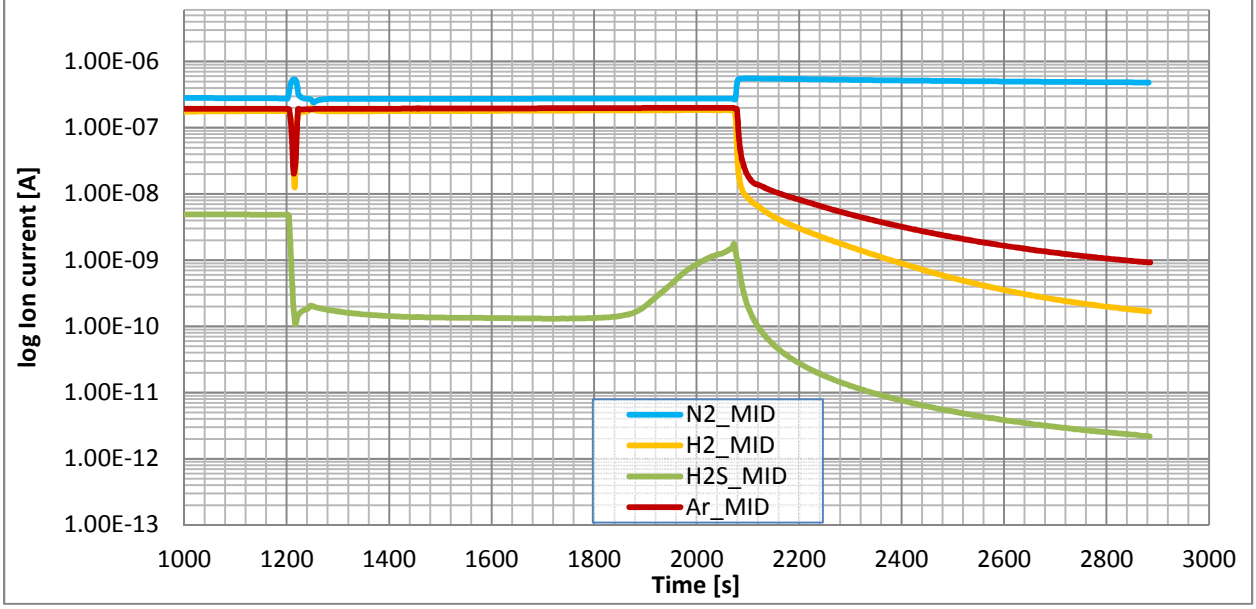

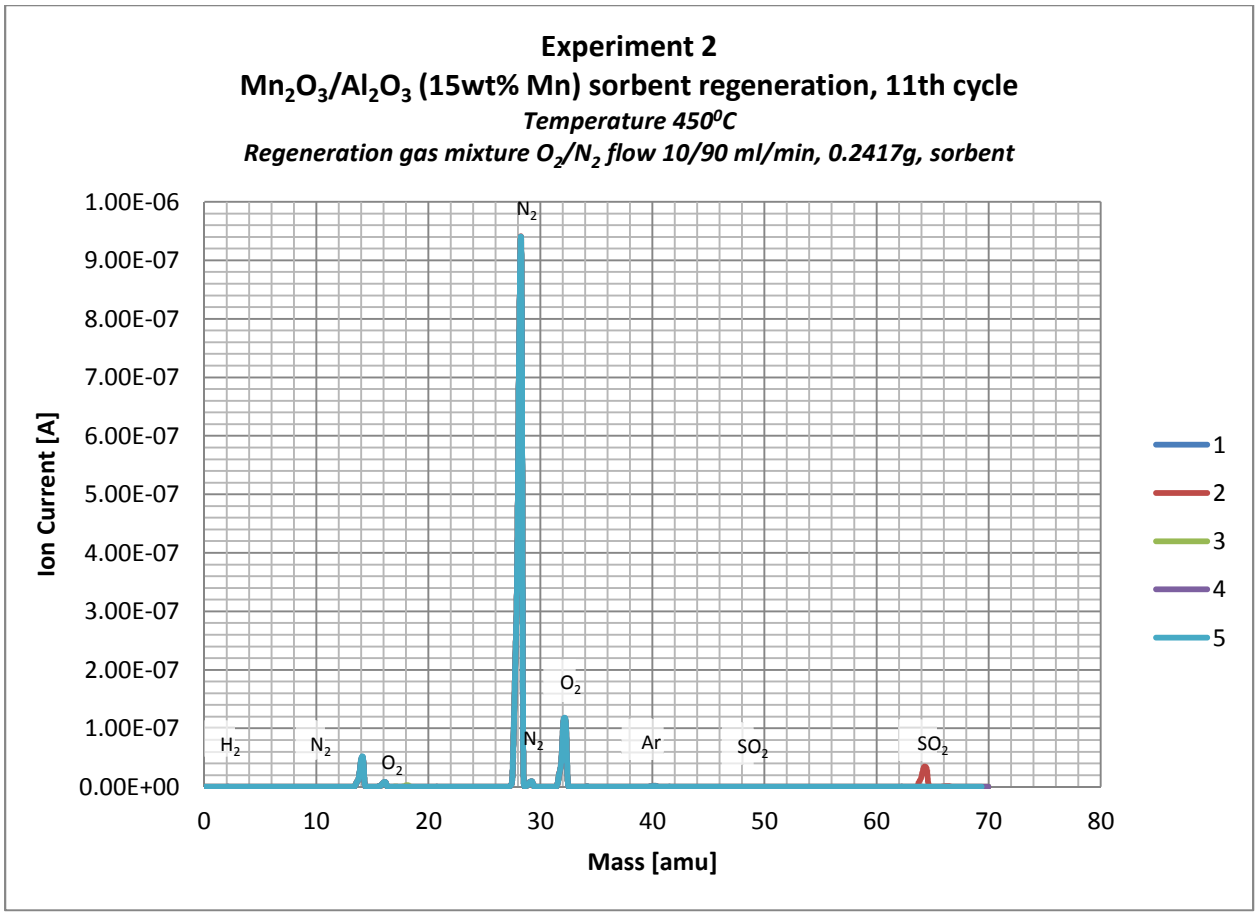
Experiment 2
Mn2O3/Al2O3 (15wt% Mn) sorbent regeneration, 11th cycle
Temperature 450⁰C
Regeneration gas mixture O2/N2 flow 10/90 ml/min, 0.2417g, sorbent
Ion Current [A]
1.00E-06
9.00E-07
8.00E-07
7.00E-07
6.00E-07
5.00E-07
4.00E-07
3.00E-07
2.00E-07
1.00E-07
0.00E+00
0
10
20
30
40
50
60
70
80
Mass [amu]
H2
N2
O2
N2
O2
N2
Ar
SO2
SO2
1
2
3
4
5

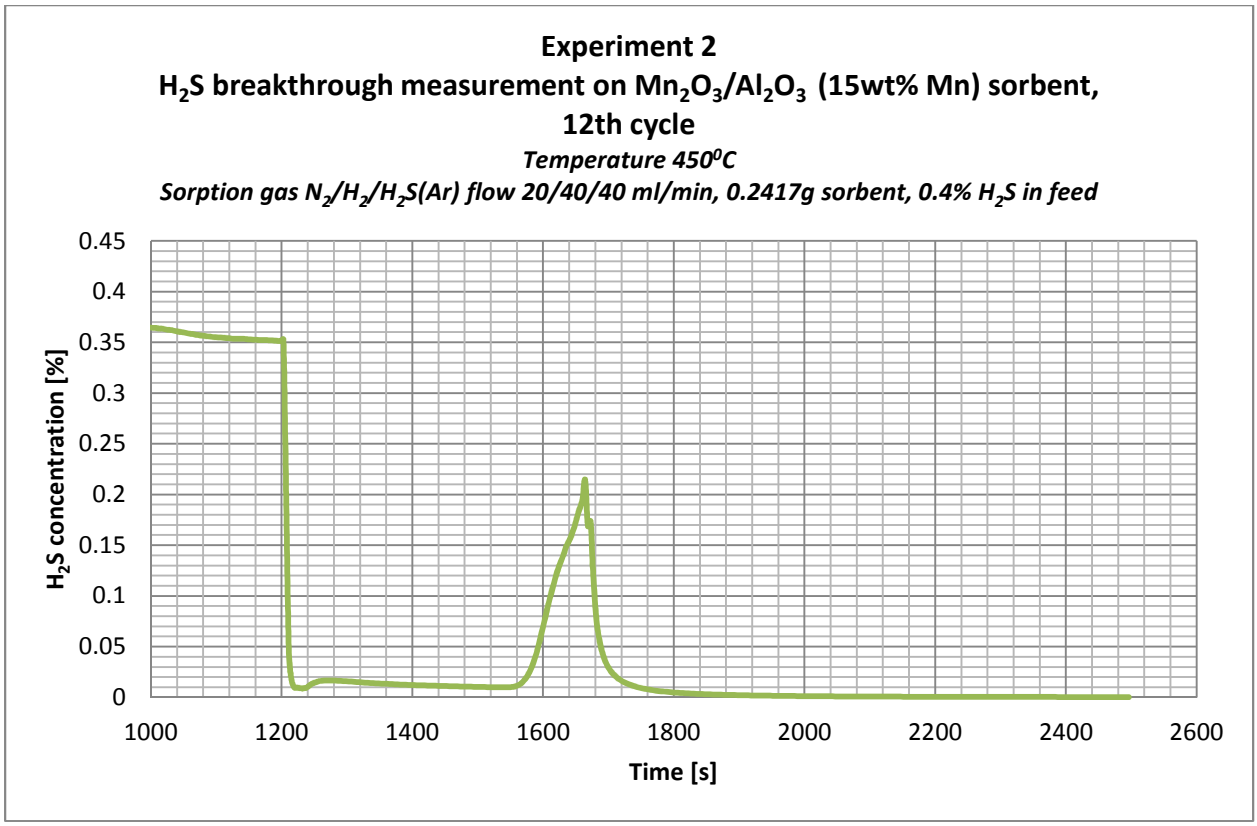
Experiment 2
H2S breakthrough measurement on Mn2O3/Al2O3 (15wt% Mn) sorbent, 12th cycle
Temperature 450⁰C
Sorption gas N2/H2/H2S(Ar) flow 20/40/40 ml/min, 0.2417g sorbent, 0.4% H2S in feed
H2S concentration [%]
0.45
0.4
0.35
0.3
0.25
0.2
0.15
0.1
0.05
0
1000
1200
1400
1600
1800
2000
2200
2400
2600
Time [s]

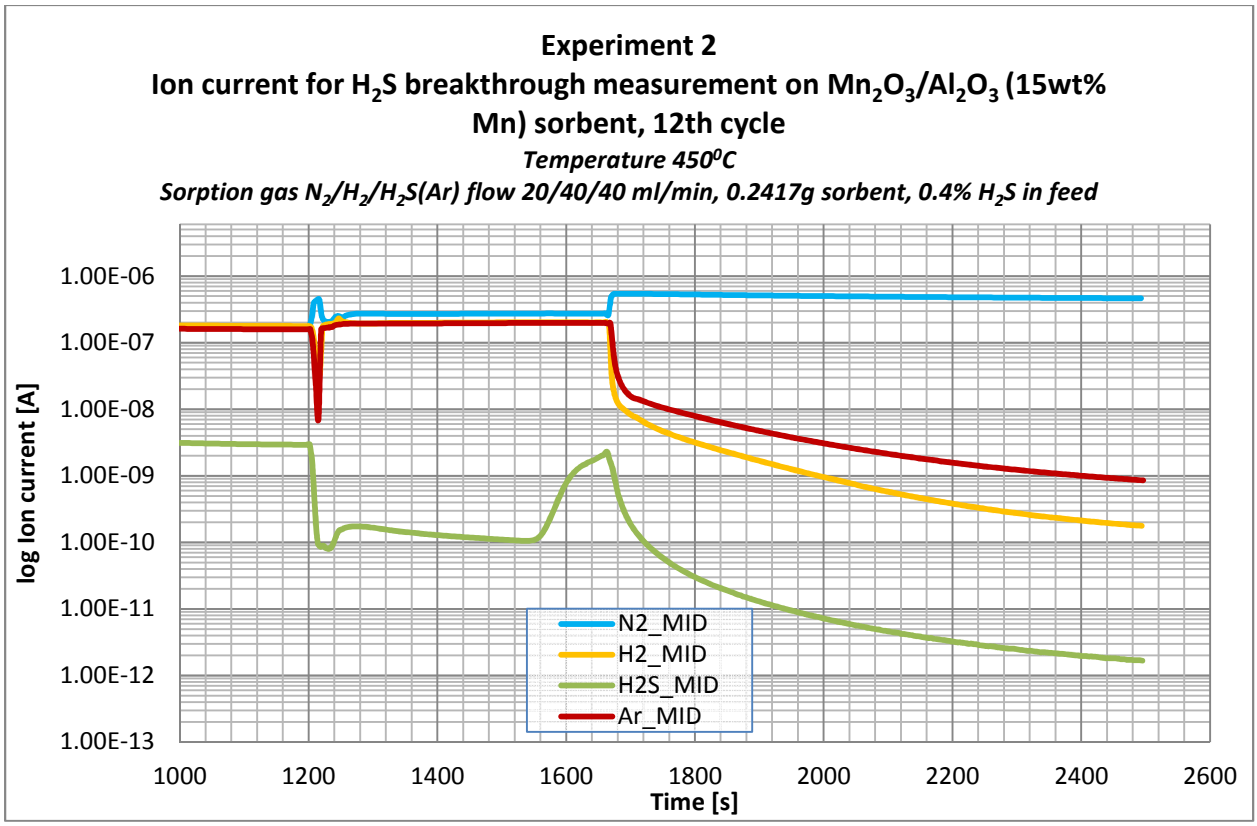
Experiment 2
Ion current for H2S breakthrough measurement on Mn2O3/Al2O3 (15wt% Mn) sorbent, 12th cycle
Temperature 450⁰C
Sorption gas N2/H2/H2S(Ar) flow 20/40/40 ml/min, 0.2417g sorbent, 0.4% H2S in feed
log Ion current [A]
1.00E-06
1.00E-07
1.00E-08
1.00E-09
1.00E-10
1.00E-11
1.00E-12
1.00E-13
1000
1200
1400
1600
1800
2000
2200
2400
2600
Time [s]
N2_MID
H2_MID
H2S_MID
Ar_MID

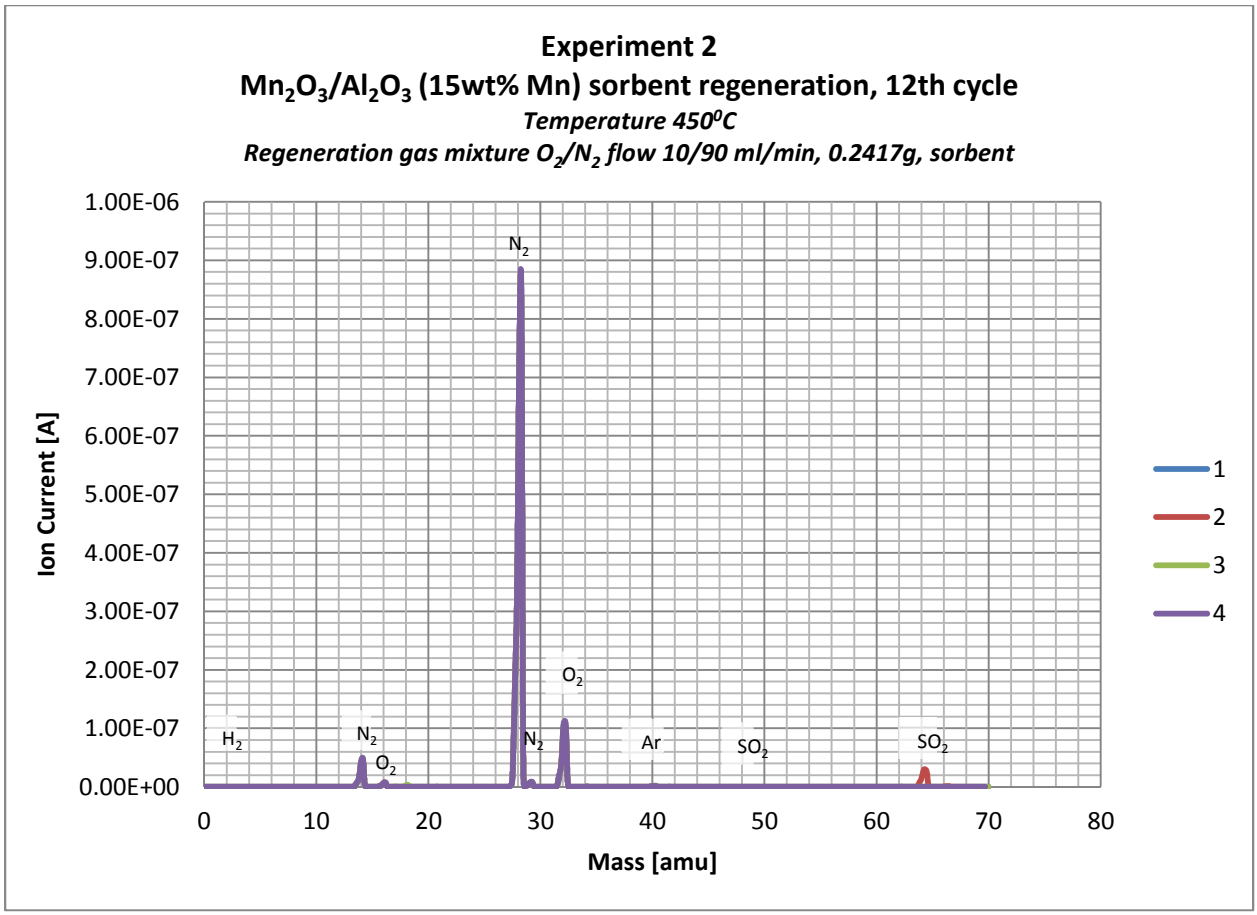
Experiment 2
Mn2O3/Al2O3 (15wt% Mn) sorbent regeneration, 12th cycle
Temperature 450⁰C
Regeneration gas mixture O2/N2 flow 10/90 ml/min, 0.2417g, sorbent
Ion Current [A]
1.00E-06
9.00E-07
8.00E-07
7.00E-07
6.00E-07
5.00E-07
4.00E-07
3.00E-07
2.00E-07
1.00E-07
0.00E+00
0
10
20
30
40
50
60
70
80
Mass [amu]
H2
N2
O2
N2
N2
O2
Ar
SO2
SO2
1
2
3
4

**Experiment 2**

**$H_2S$ breakthrough measurement on $Mn_2O_3/Al_2O_3$ (15wt% Mn) sorbent, 13th cycle**

***Temperature 450$^0$C***

***Sorption gas $N_2/H_2/H_2S$(Ar) flow 20/40/40 ml/min, 0.2417g sorbent, 0.4% $H_2S$ in feed***

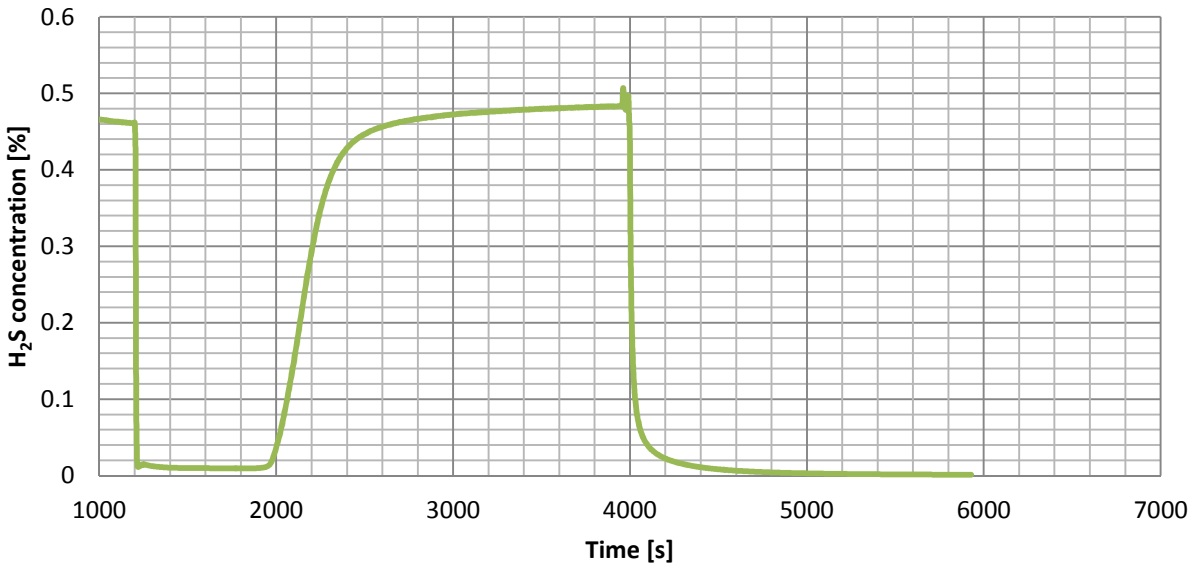


**Experiment 2**

**Ion current for $H_2S$ breakthrough measurement on $Mn_2O_3/Al_2O_3$ (15wt% Mn) sorbent, 13th cycle**

***Temperature 450$^0$C***

***Sorption gas $N_2/H_2/H_2S$(Ar) flow 20/40/40 ml/min, 0.2417g sorbent, 0.4% $H_2S$ in feed***

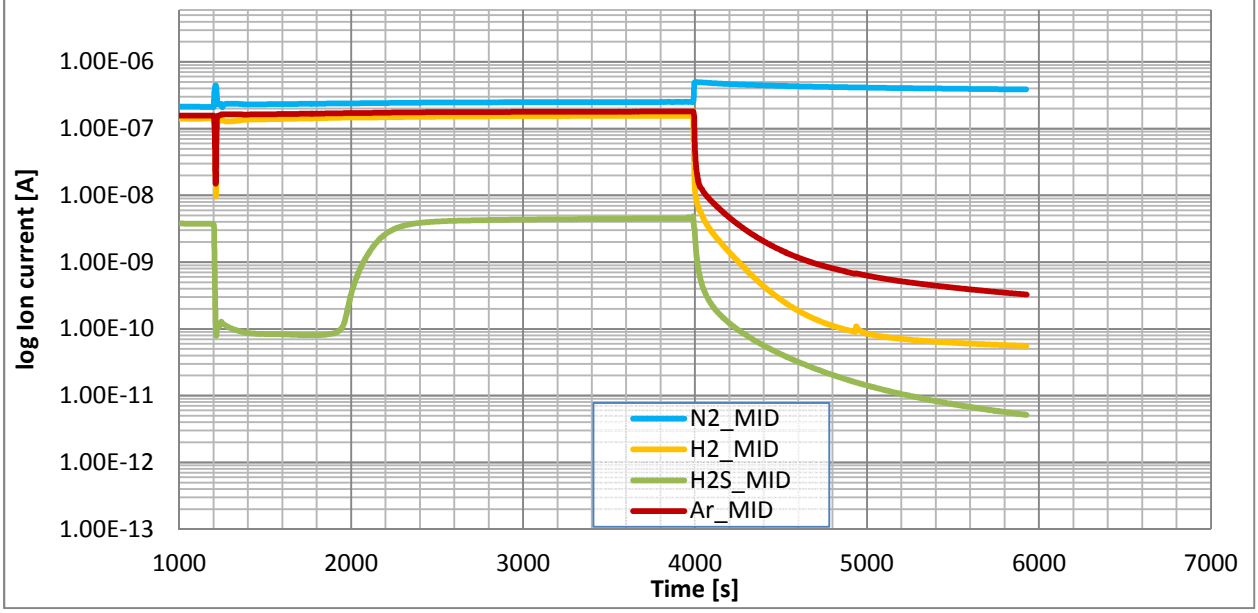

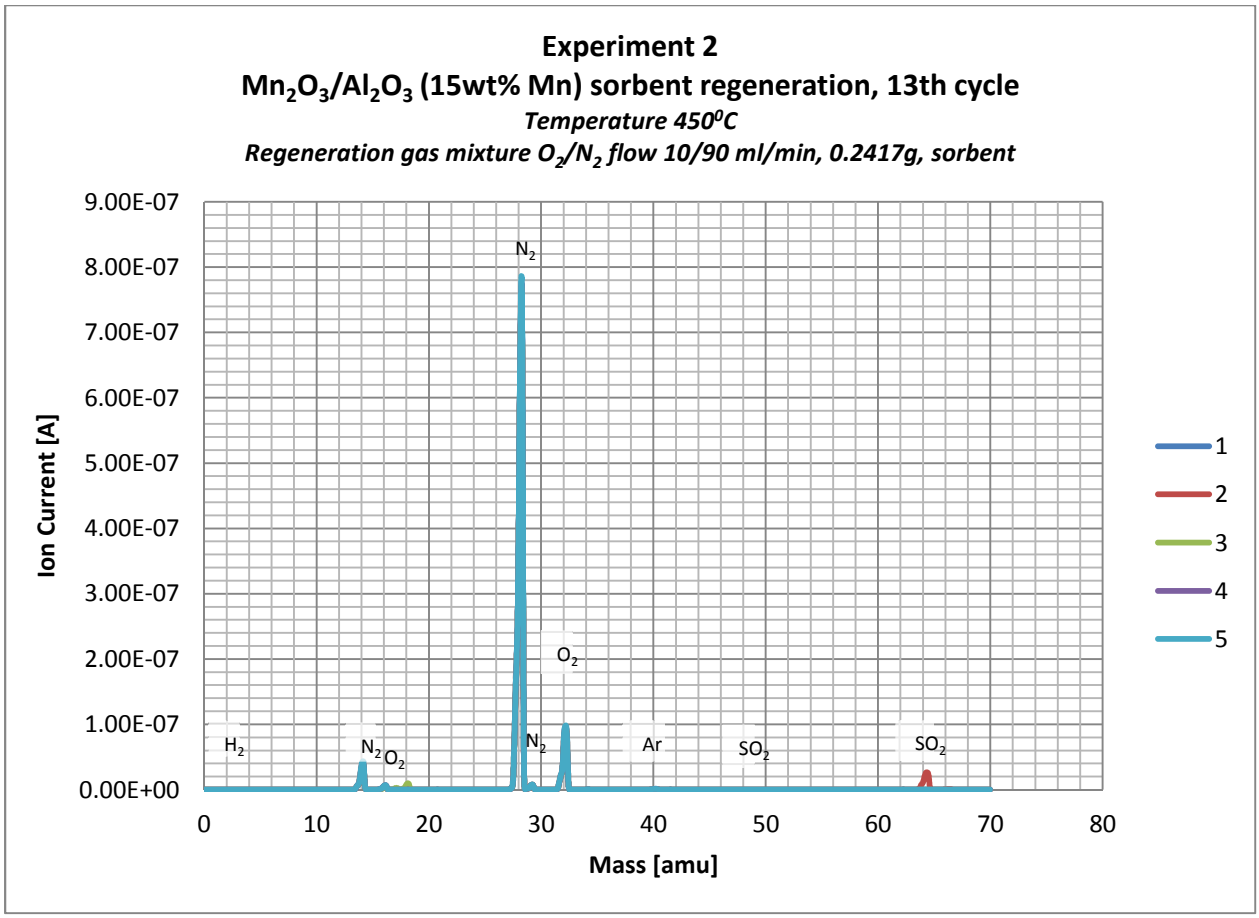
Experiment 2
Mn2O3/Al2O3 (15wt% Mn) sorbent regeneration, 13th cycle
Temperature 450⁰C
Regeneration gas mixture O2/N2 flow 10/90 ml/min, 0.2417g, sorbent
Ion Current [A]
9.00E-07
8.00E-07
7.00E-07
6.00E-07
5.00E-07
4.00E-07
3.00E-07
2.00E-07
1.00E-07
0.00E+00
0
10
20
30
40
50
60
70
80
Mass [amu]
N2
O2
H2
N2O2
N2
Ar
SO2
SO2
1
2
3
4
5

## *Appendix N Sorption cycle measurement results for $Mn_2O_3/Al_2O_3$ (30 wt.% Mn)*

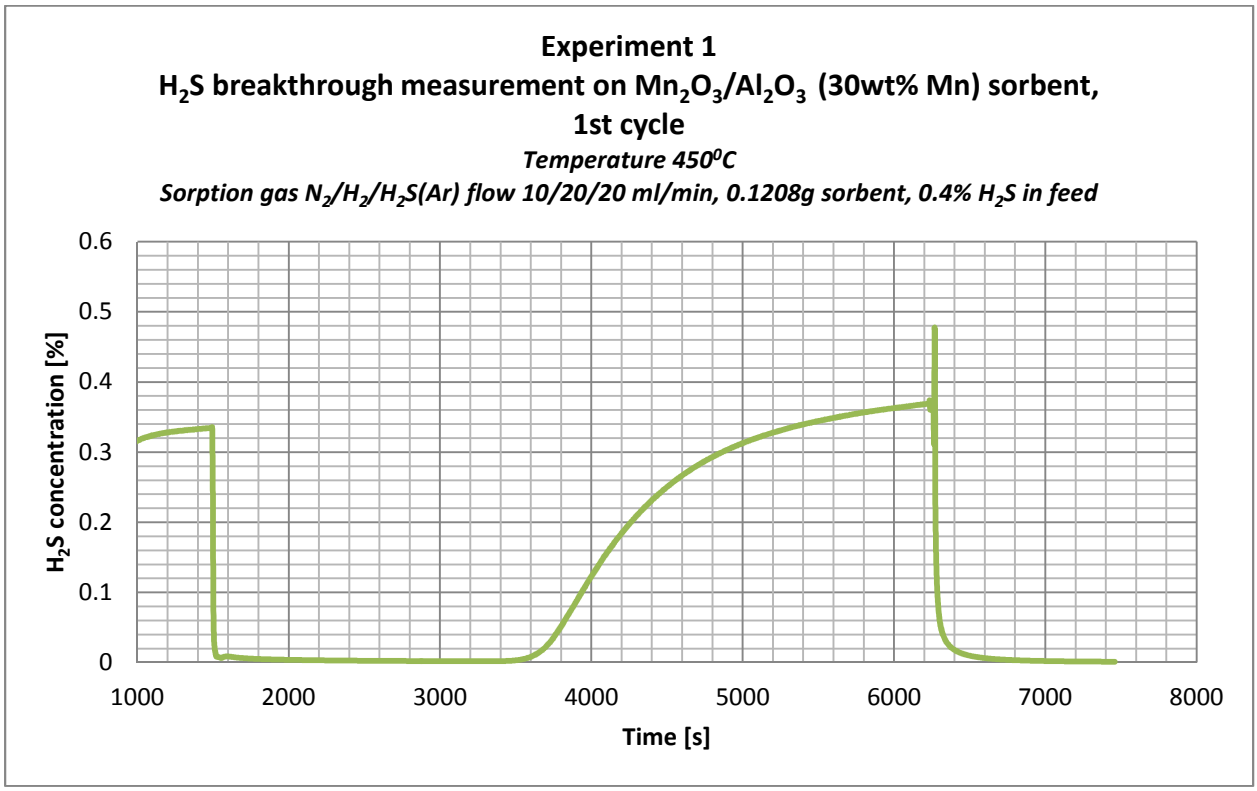


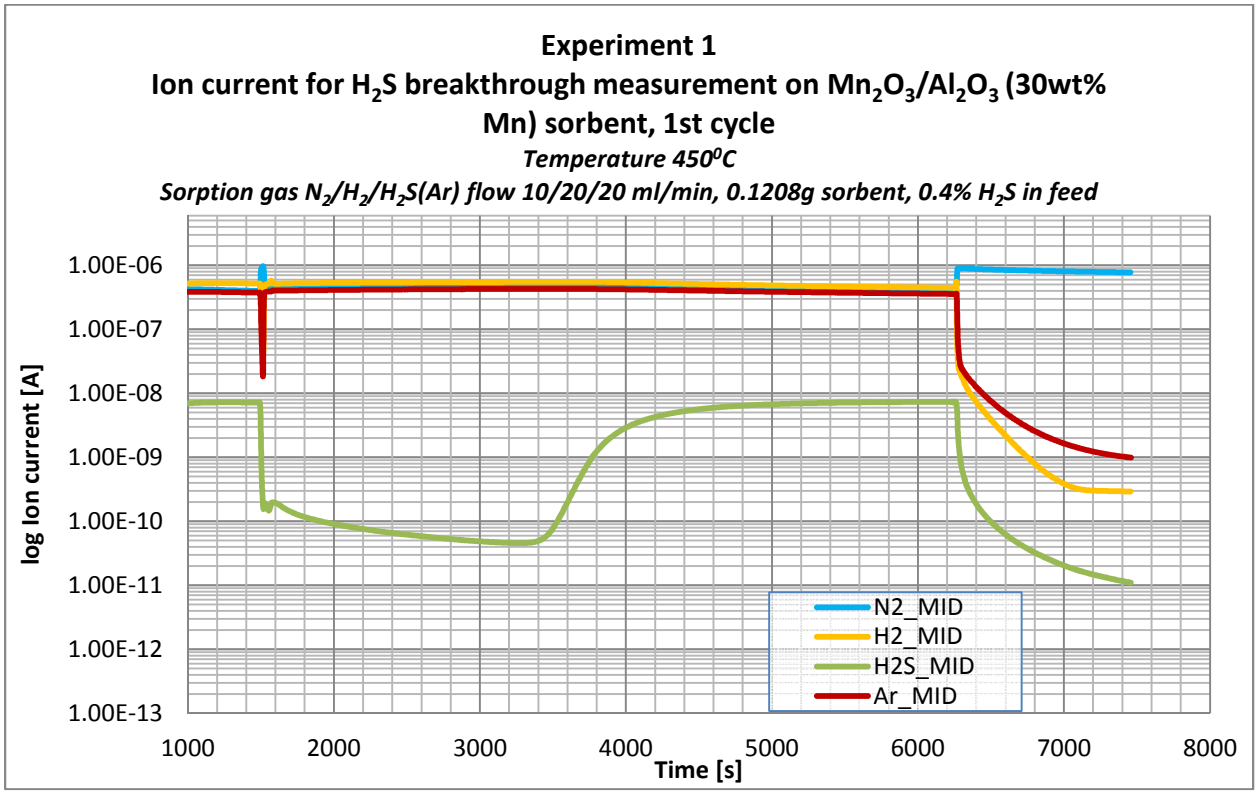

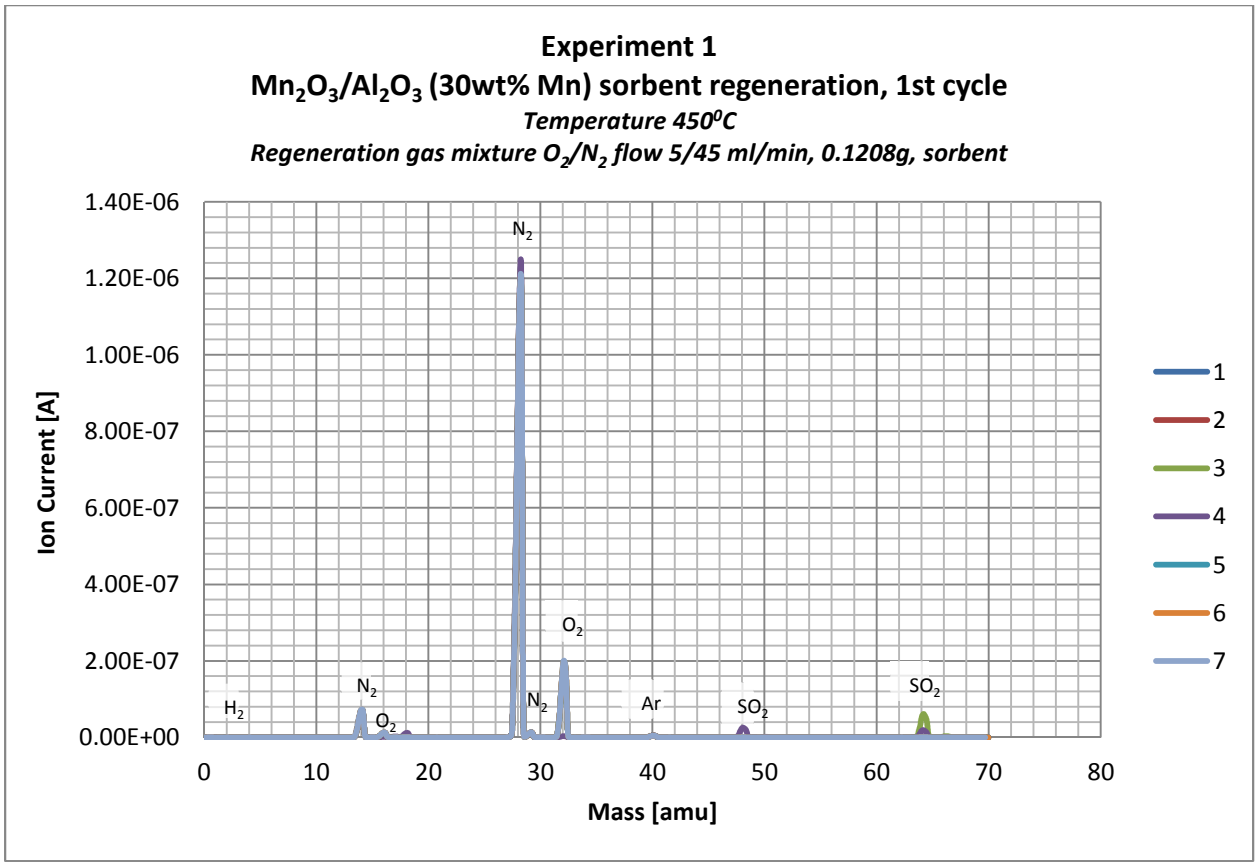
Experiment 1
Mn2O3/Al2O3 (30wt% Mn) sorbent regeneration, 1st cycle
Temperature 450⁰C
Regeneration gas mixture O2/N2 flow 5/45 ml/min, 0.1208g, sorbent
Ion Current [A]
1.40E-06
1.20E-06
1.00E-06
8.00E-07
6.00E-07
4.00E-07
2.00E-07
0.00E+00
0
10
20
30
40
50
60
70
80
Mass [amu]
N2
O2
H2
Ar
SO2
1
2
3
4
5
6
7

**Experiment 1**

**$H_2S$ breakthrough measurement on $Mn_2O_3/Al_2O_3$ (30wt% Mn) sorbent, 2nd cycle**

***Temperature 450$^0$C***

***Sorption gas $N_2/H_2/H_2S$(Ar) flow 10/20/20 ml/min, 0.1208g sorbent, 0.4% $H_2S$ in feed***

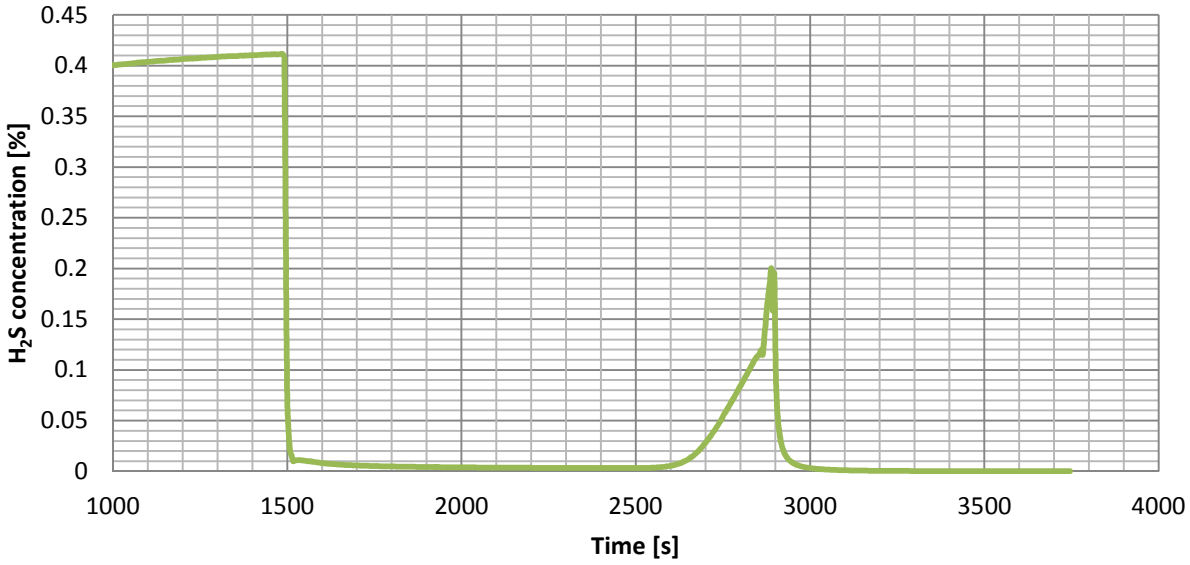


**Experiment 1**

**Ion current for $H_2S$ breakthrough measurement on $Mn_2O_3/Al_2O_3$ (30wt% Mn) sorbent, 2nd cycle**

***Temperature 450$^0$C***

***Sorption gas $N_2/H_2/H_2S$(Ar) flow 10/20/20 ml/min, 0.1208g sorbent, 0.4% $H_2S$ in feed***

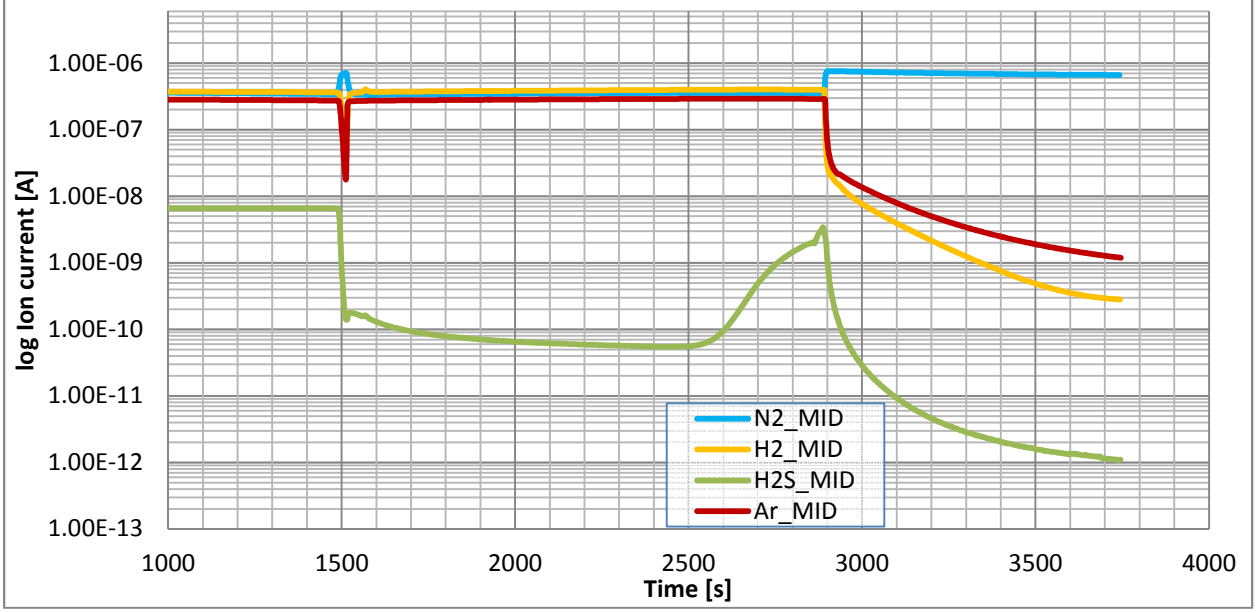

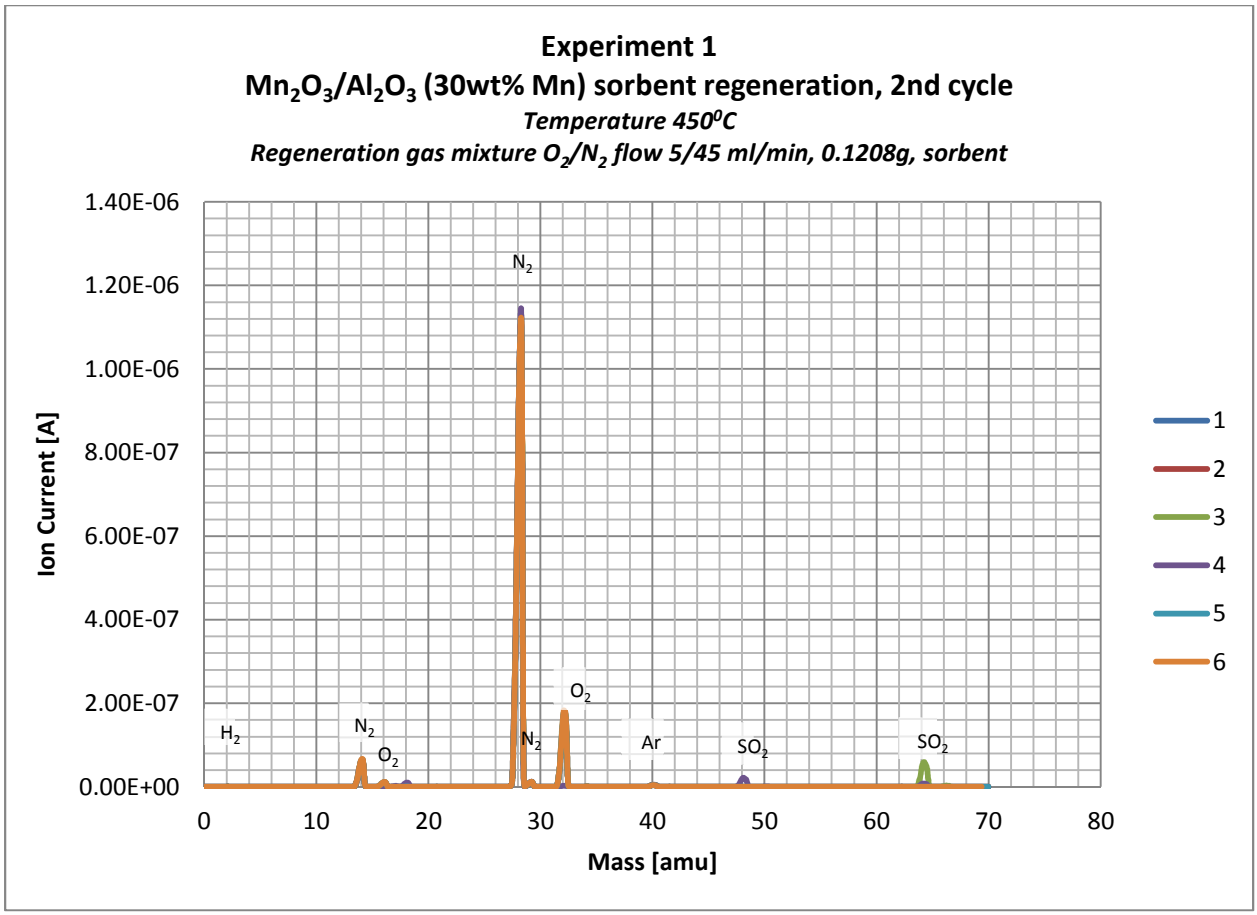
Experiment 1
Mn2O3/Al2O3 (30wt% Mn) sorbent regeneration, 2nd cycle
Temperature 450⁰C
Regeneration gas mixture O2/N2 flow 5/45 ml/min, 0.1208g, sorbent
Ion Current [A]
1.40E-06
1.20E-06
1.00E-06
8.00E-07
6.00E-07
4.00E-07
2.00E-07
0.00E+00
0
10
20
30
40
50
60
70
80
Mass [amu]
H2
N2
O2
N2
O2
N2
Ar
SO2
SO2
1
2
3
4
5
6

**Experiment 1**

**$H_2S$ breakthrough measurement on $Mn_2O_3/Al_2O_3$ (30wt% Mn) sorbent, 3rd cycle**

***Temperature 450$^0$C***

***Sorption gas $N_2/H_2/H_2S$(Ar) flow 10/20/20 ml/min, 0.1208g sorbent, 0.4% $H_2S$ in feed***

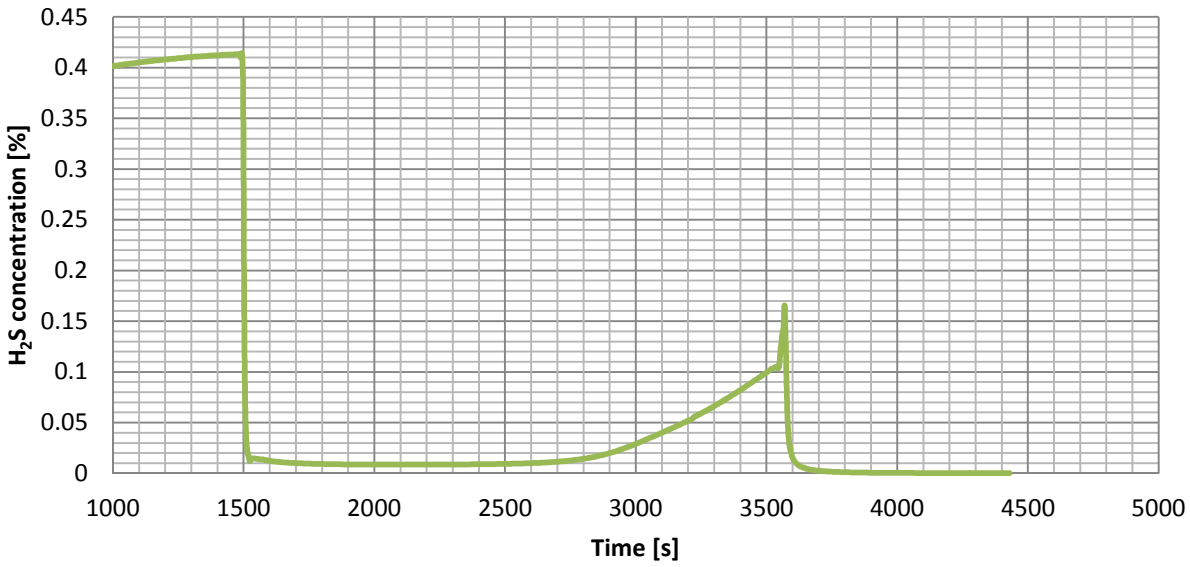


**Experiment 1**

**Ion current for $H_2S$ breakthrough measurement on $Mn_2O_3/Al_2O_3$ (30wt% Mn) sorbent, 3rd cycle**

***Temperature 450$^0$C***

***Sorption gas $N_2/H_2/H_2S$(Ar) flow 10/20/20 ml/min, 0.1208g sorbent, 0.4% $H_2S$ in feed***

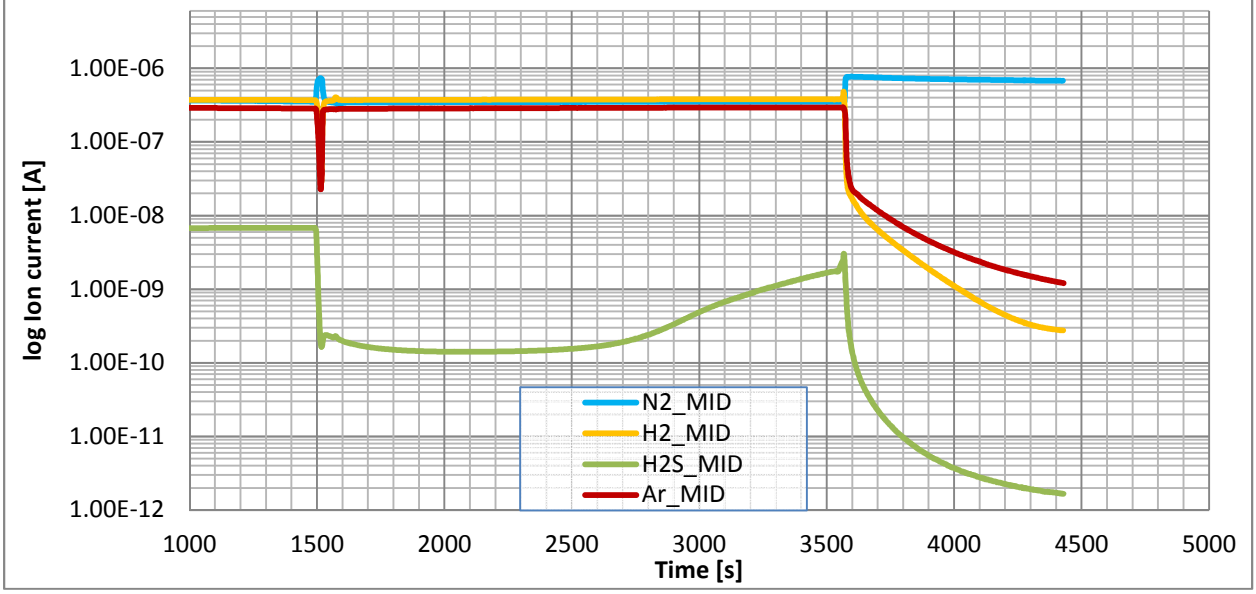

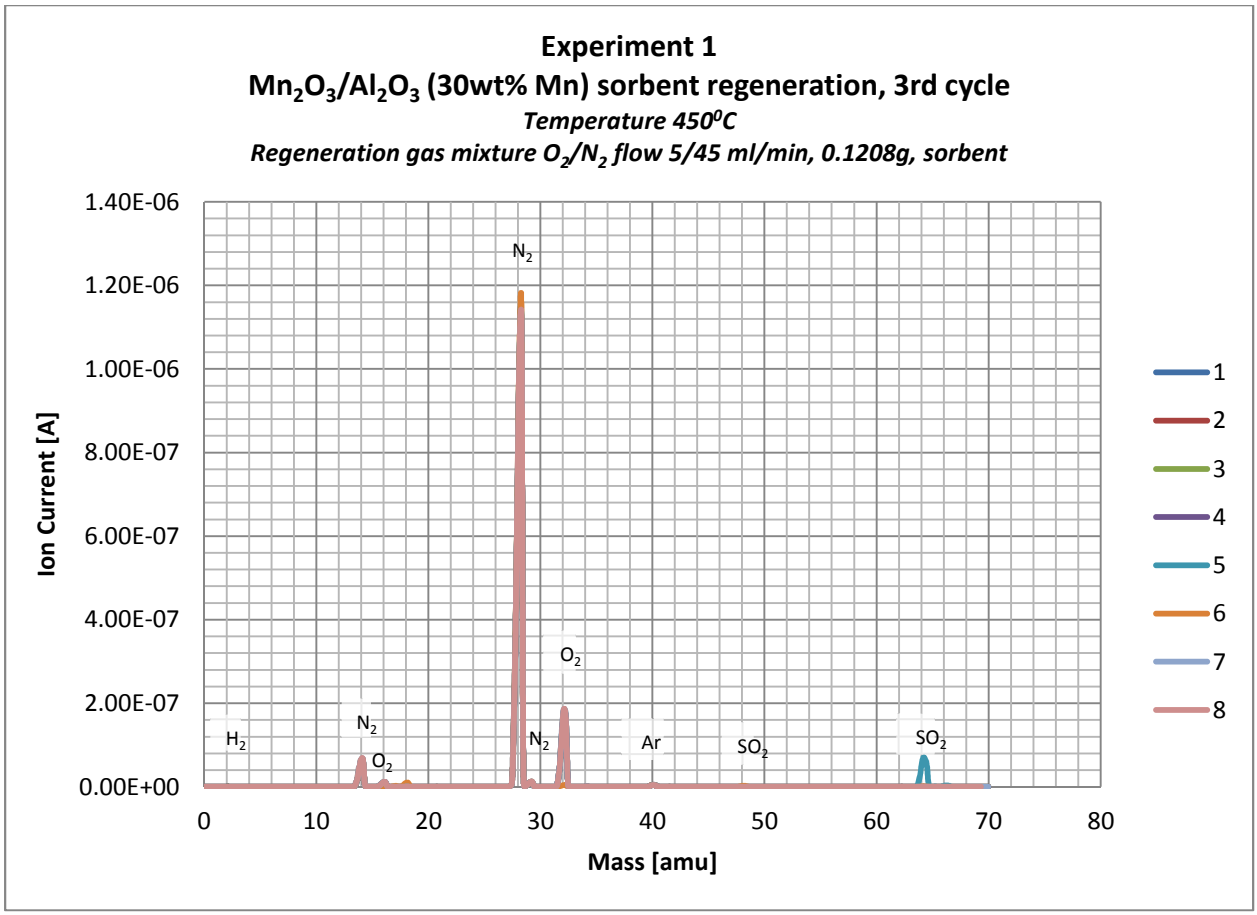
Experiment 1
Mn2O3/Al2O3 (30wt% Mn) sorbent regeneration, 3rd cycle
Temperature 450⁰C
Regeneration gas mixture O2/N2 flow 5/45 ml/min, 0.1208g, sorbent
Ion Current [A]
1.40E-06
1.20E-06
1.00E-06
8.00E-07
6.00E-07
4.00E-07
2.00E-07
0.00E+00
0
10
20
30
40
50
60
70
80
Mass [amu]
N2
O2
H2
N2
O2
N2
Ar
SO2
SO2
1
2
3
4
5
6
7
8

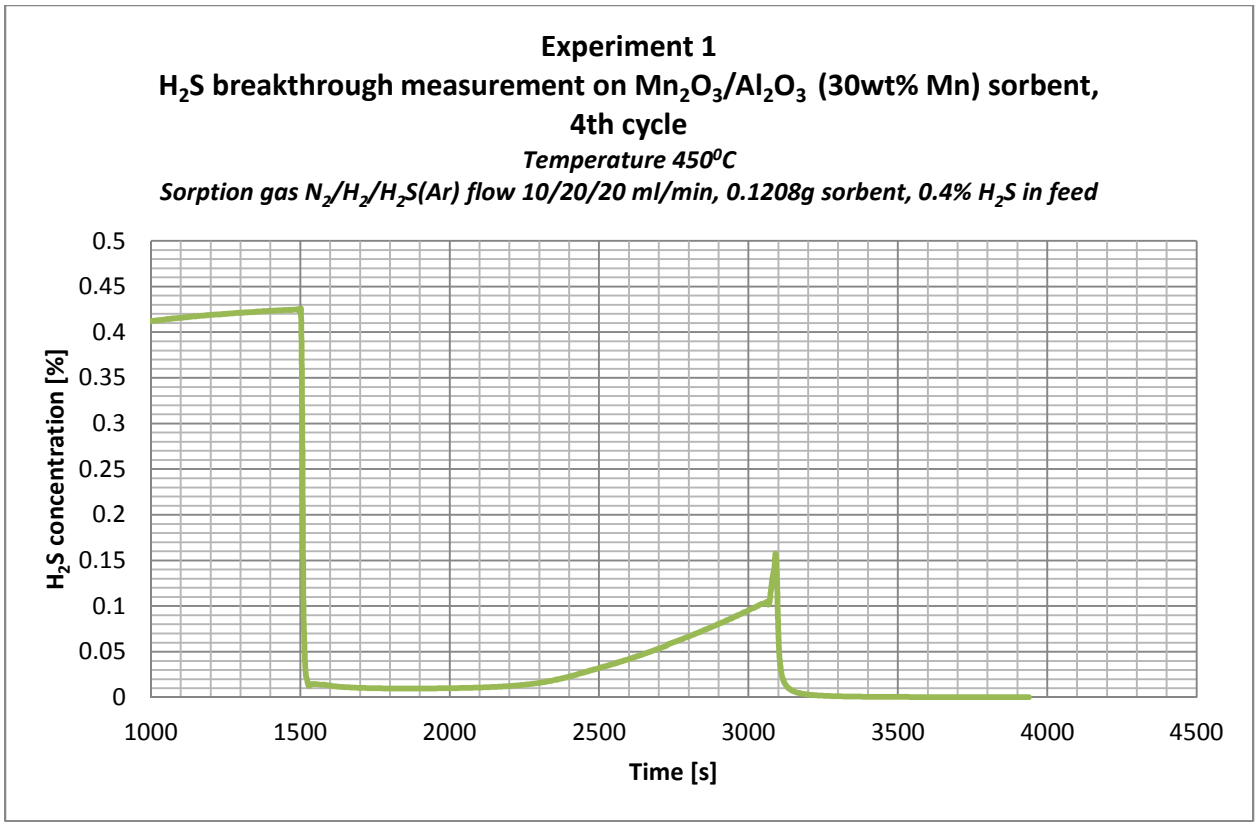
Experiment 1
H2S breakthrough measurement on Mn2O3/Al2O3 (30wt% Mn) sorbent, 4th cycle
Temperature 450⁰C
Sorption gas N2/H2/H2S(Ar) flow 10/20/20 ml/min, 0.1208g sorbent, 0.4% H2S in feed
H2S concentration [%]
0.5
0.45
0.4
0.35
0.3
0.25
0.2
0.15
0.1
0.05
0
1000
1500
2000
2500
3000
3500
4000
4500
Time [s]

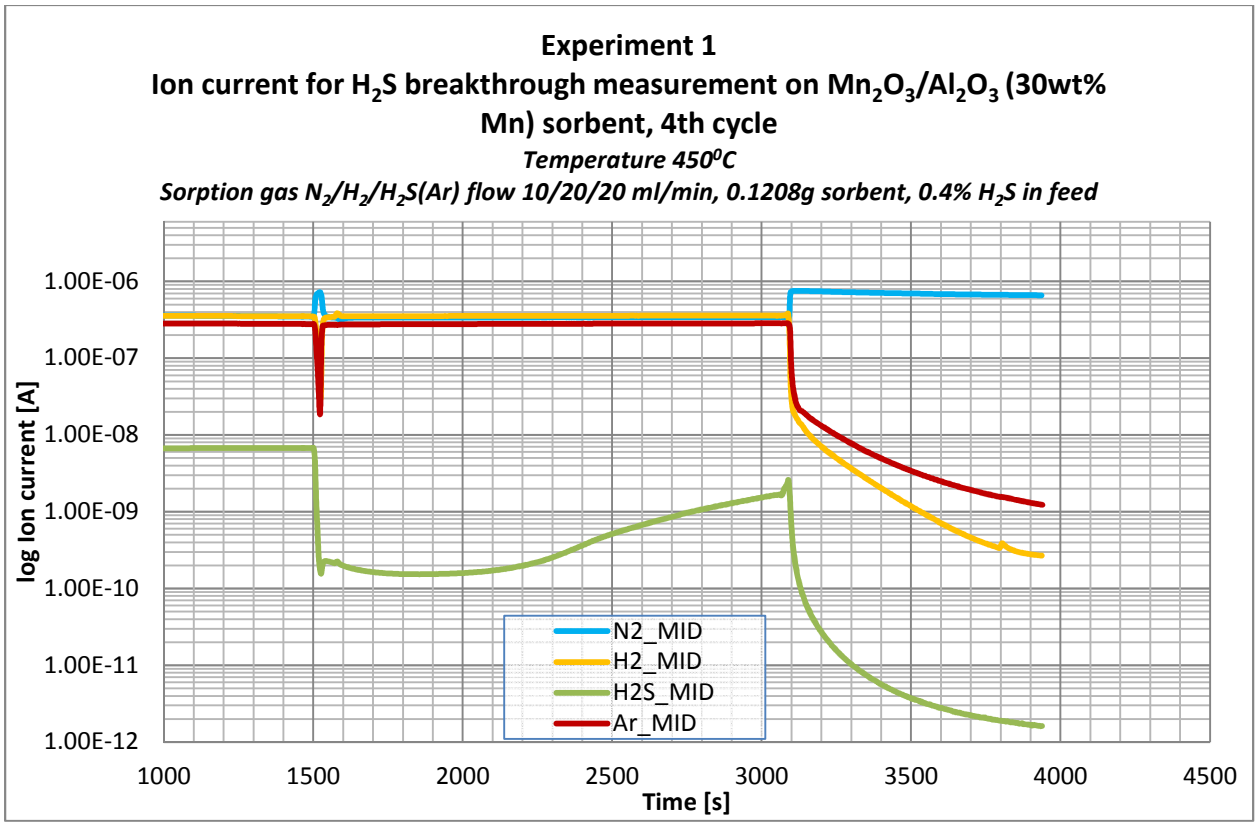
Experiment 1
Ion current for H2S breakthrough measurement on Mn2O3/Al2O3 (30wt% Mn) sorbent, 4th cycle
Temperature 450⁰C
Sorption gas N2/H2/H2S(Ar) flow 10/20/20 ml/min, 0.1208g sorbent, 0.4% H2S in feed
log Ion current [A]
1.00E-06
1.00E-07
1.00E-08
1.00E-09
1.00E-10
1.00E-11
1.00E-12
1000
1500
2000
2500
3000
3500
4000
4500
Time [s]
N2_MID
H2_MID
H2S_MID
Ar_MID

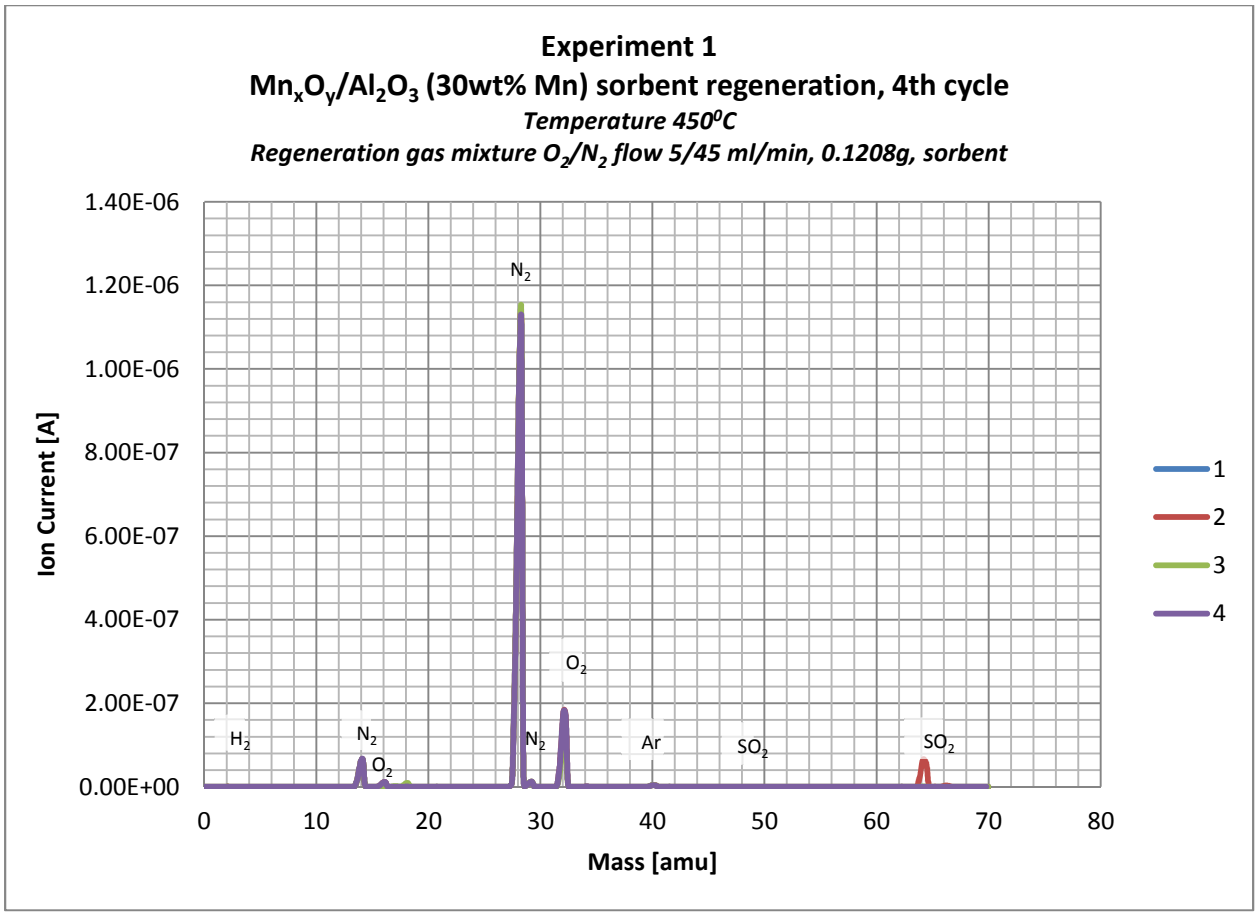
Experiment 1
Mn$_x$O$_y$/Al$_2$O$_3$ (30wt% Mn) sorbent regeneration, 4th cycle
Temperature 450$^0$C
Regeneration gas mixture O$_2$/N$_2$ flow 5/45 ml/min, 0.1208g, sorbent
Ion Current [A]
1.40E-06
1.20E-06
1.00E-06
8.00E-07
6.00E-07
4.00E-07
2.00E-07
0.00E+00
0
10
20
30
40
50
60
70
80
Mass [amu]
N2
O2
H2
N2
O2
N2
O2
Ar
SO2
SO2
1
2
3
4

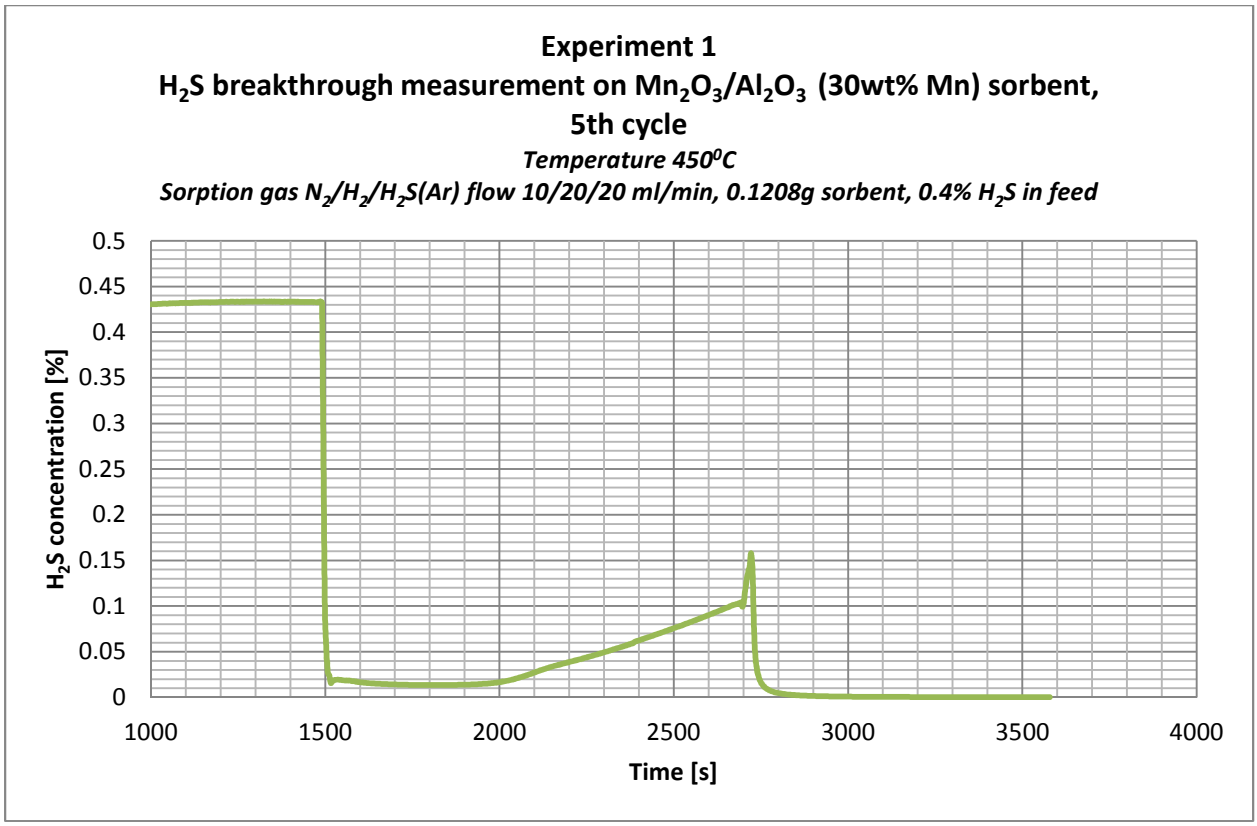
Experiment 1
H2S breakthrough measurement on Mn2O3/Al2O3 (30wt% Mn) sorbent, 5th cycle
Temperature 450⁰C
Sorption gas N2/H2/H2S(Ar) flow 10/20/20 ml/min, 0.1208g sorbent, 0.4% H2S in feed
H2S concentration [%]
0.5
0.45
0.4
0.35
0.3
0.25
0.2
0.15
0.1
0.05
0
1000
1500
2000
2500
3000
3500
4000
Time [s]

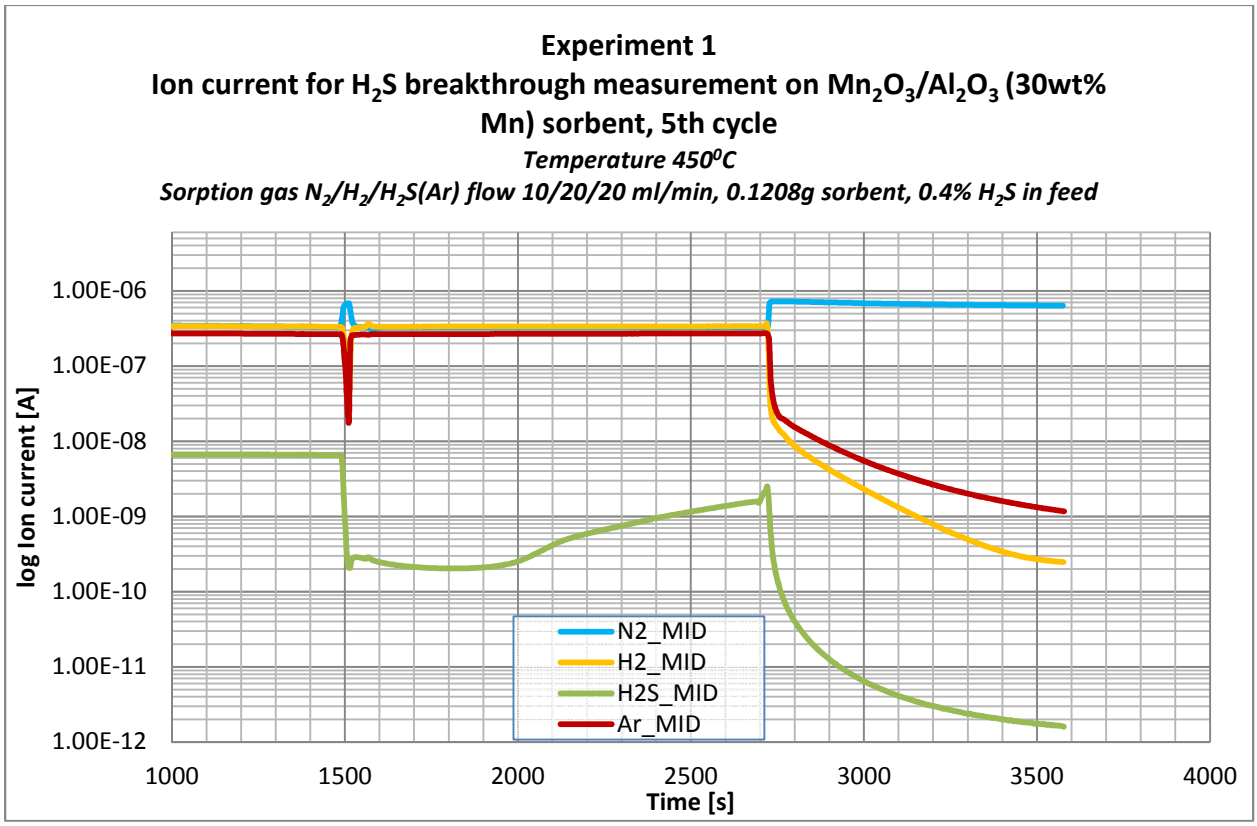
Experiment 1
Ion current for H2S breakthrough measurement on Mn2O3/Al2O3 (30wt% Mn) sorbent, 5th cycle
Temperature 450⁰C
Sorption gas N2/H2/H2S(Ar) flow 10/20/20 ml/min, 0.1208g sorbent, 0.4% H2S in feed
log Ion current [A]
1.00E-06
1.00E-07
1.00E-08
1.00E-09
1.00E-10
1.00E-11
1.00E-12
1000
1500
2000
2500
3000
3500
4000
Time [s]
N2_MID
H2_MID
H2S_MID
Ar_MID

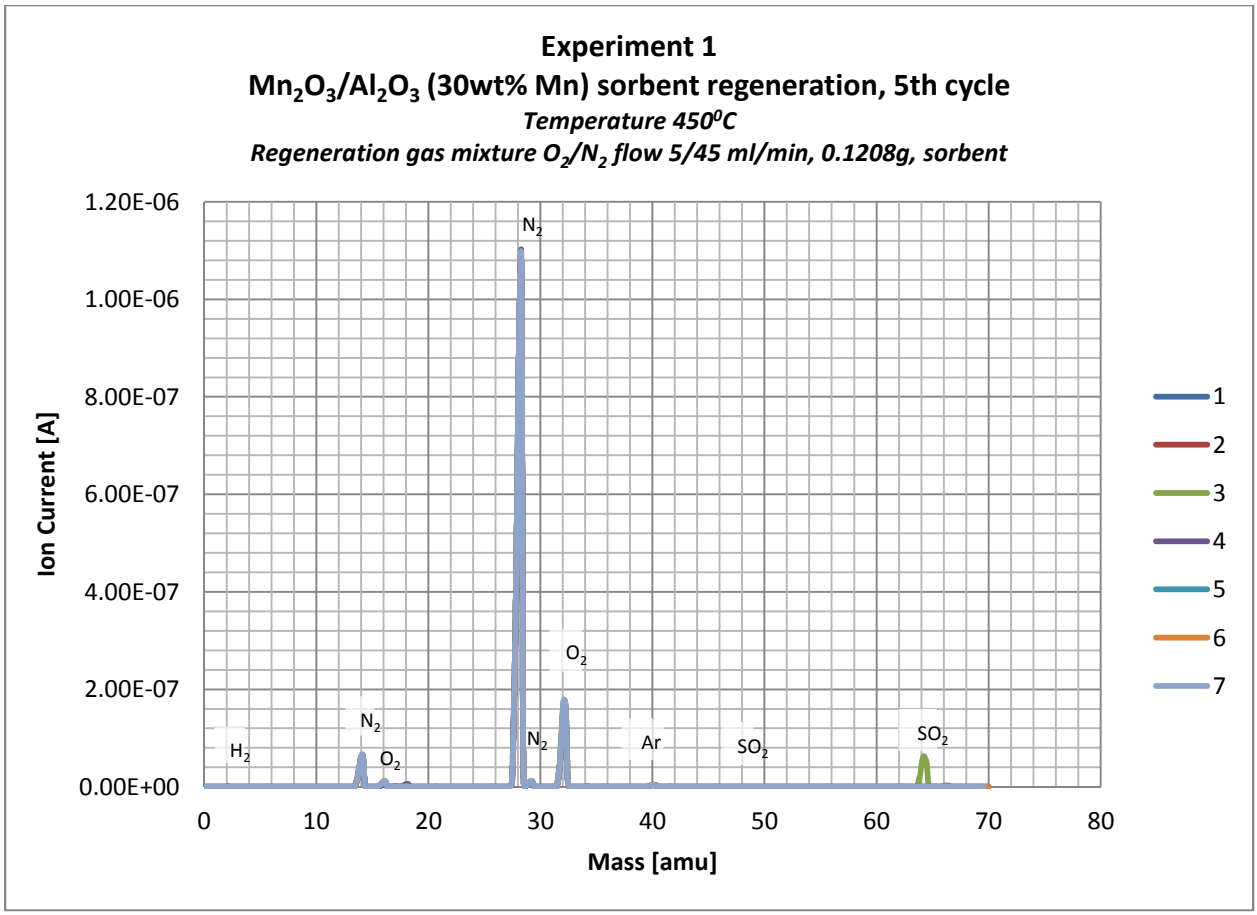
Experiment 1
Mn2O3/Al2O3 (30wt% Mn) sorbent regeneration, 5th cycle
Temperature 450⁰C
Regeneration gas mixture O2/N2 flow 5/45 ml/min, 0.1208g, sorbent
Ion Current [A]
1.20E-06
1.00E-06
8.00E-07
6.00E-07
4.00E-07
2.00E-07
0.00E+00
0
10
20
30
40
50
60
70
80
Mass [amu]
N2
O2
N2
H2
N2
O2
Ar
SO2
SO2
1
2
3
4
5
6
7

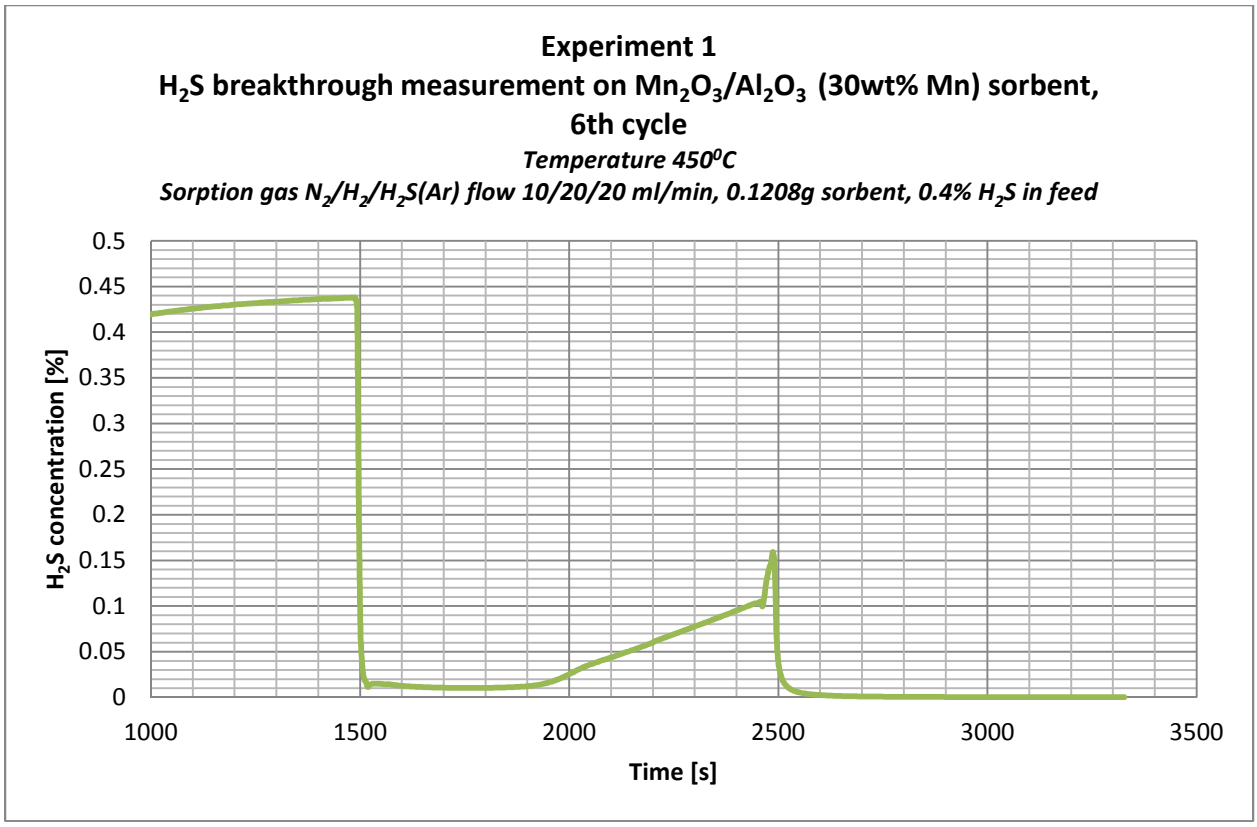
Experiment 1
H2S breakthrough measurement on Mn2O3/Al2O3 (30wt% Mn) sorbent, 6th cycle
Temperature 450⁰C
Sorption gas N2/H2/H2S(Ar) flow 10/20/20 ml/min, 0.1208g sorbent, 0.4% H2S in feed
H2S concentration [%]
0.5
0.45
0.4
0.35
0.3
0.25
0.2
0.15
0.1
0.05
0
1000
1500
2000
2500
3000
3500
Time [s]

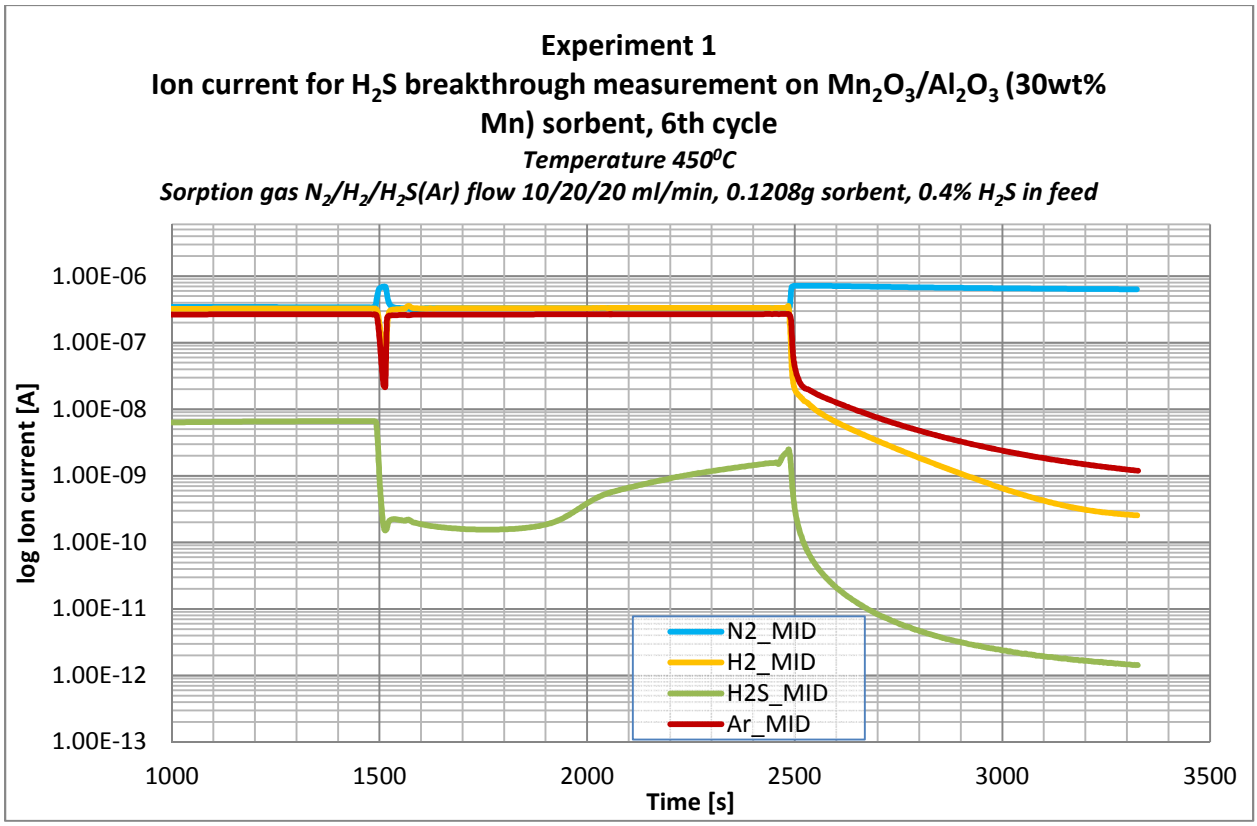
Experiment 1
Ion current for H2S breakthrough measurement on Mn2O3/Al2O3 (30wt% Mn) sorbent, 6th cycle
Temperature 450⁰C
Sorption gas N2/H2/H2S(Ar) flow 10/20/20 ml/min, 0.1208g sorbent, 0.4% H2S in feed
log Ion current [A]
1.00E-06
1.00E-07
1.00E-08
1.00E-09
1.00E-10
1.00E-11
1.00E-12
1.00E-13
1000
1500
2000
2500
3000
3500
Time [s]
N2_MID
H2_MID
H2S_MID
Ar_MID

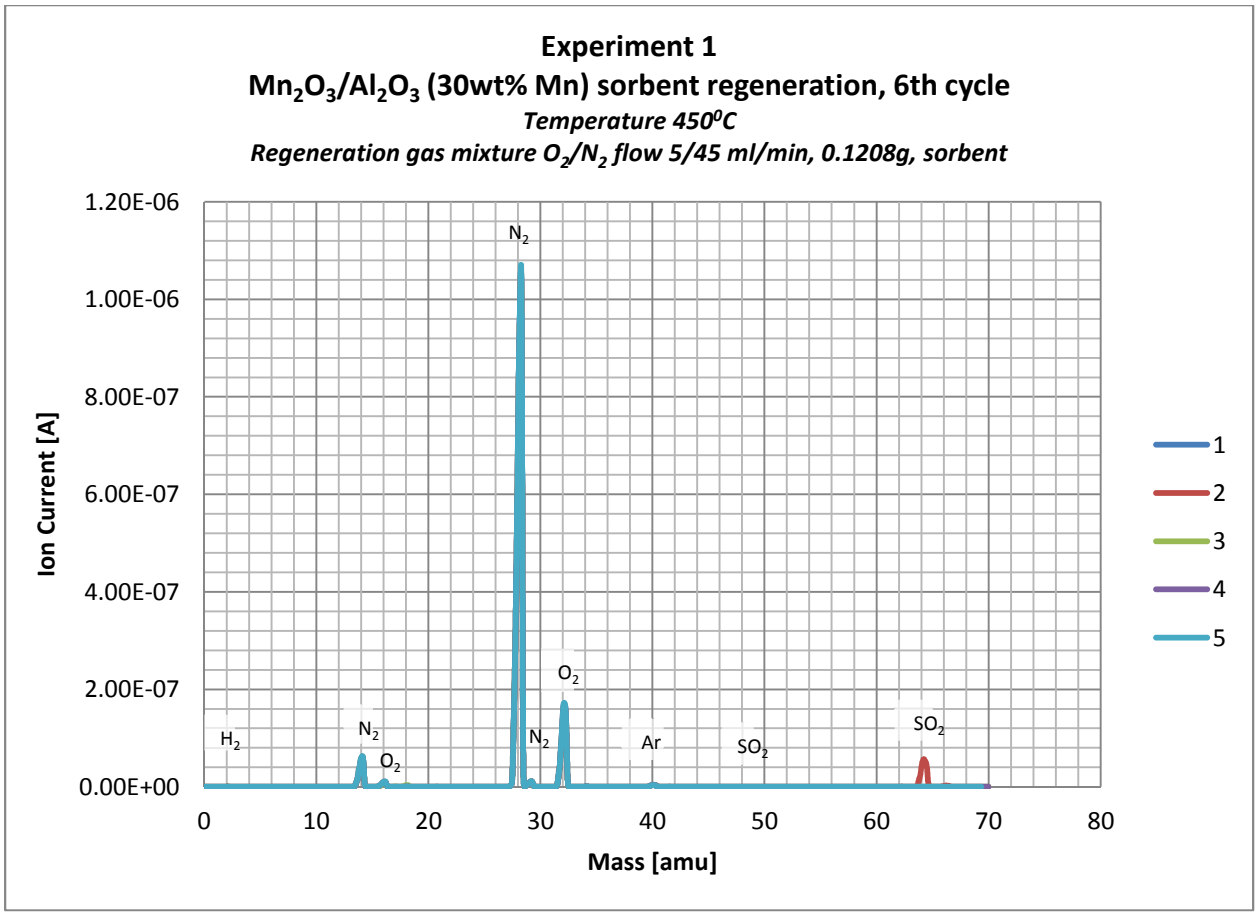
Experiment 1
Mn2O3/Al2O3 (30wt% Mn) sorbent regeneration, 6th cycle
Temperature 450⁰C
Regeneration gas mixture O2/N2 flow 5/45 ml/min, 0.1208g, sorbent
Ion Current [A]
1.20E-06
1.00E-06
8.00E-07
6.00E-07
4.00E-07
2.00E-07
0.00E+00
0
10
20
30
40
50
60
70
80
Mass [amu]
N2
O2
H2
N2
O2
N2
Ar
SO2
SO2
1
2
3
4
5

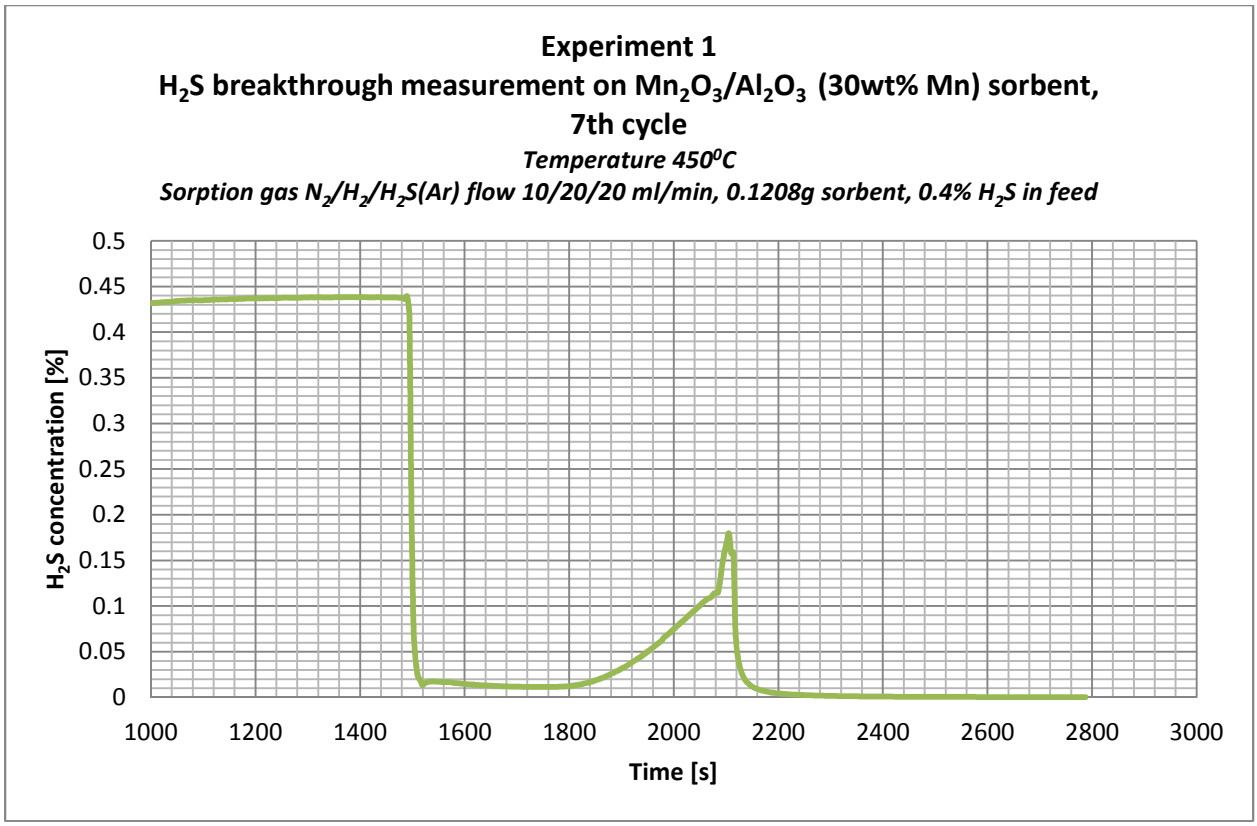
Experiment 1
H2S breakthrough measurement on Mn2O3/Al2O3 (30wt% Mn) sorbent, 7th cycle
Temperature 450⁰C
Sorption gas N2/H2/H2S(Ar) flow 10/20/20 ml/min, 0.1208g sorbent, 0.4% H2S in feed
H2S concentration [%]
0.5
0.45
0.4
0.35
0.3
0.25
0.2
0.15
0.1
0.05
0
1000
1200
1400
1600
1800
2000
2200
2400
2600
2800
3000
Time [s]

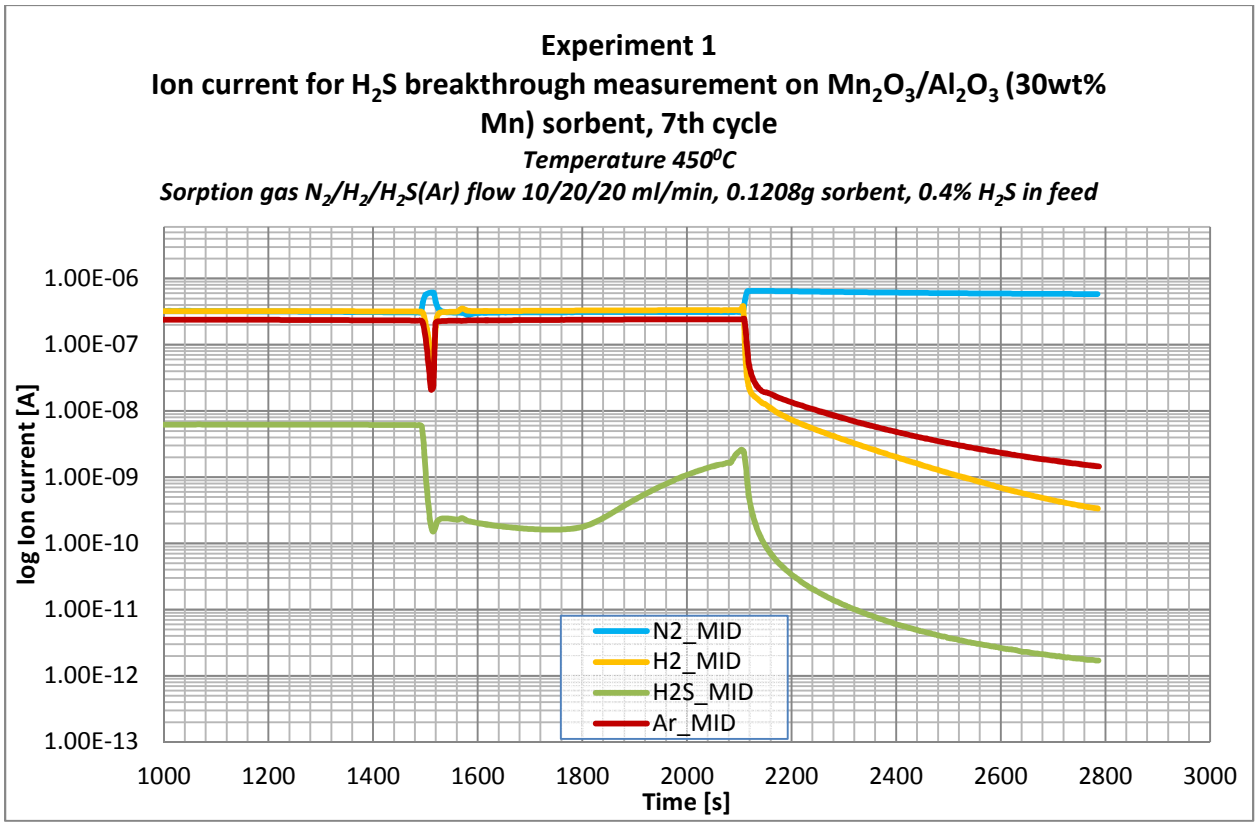
Experiment 1
Ion current for H2S breakthrough measurement on Mn2O3/Al2O3 (30wt% Mn) sorbent, 7th cycle
Temperature 450⁰C
Sorption gas N2/H2/H2S(Ar) flow 10/20/20 ml/min, 0.1208g sorbent, 0.4% H2S in feed
log Ion current [A]
1.00E-06
1.00E-07
1.00E-08
1.00E-09
1.00E-10
1.00E-11
1.00E-12
1.00E-13
1000
1200
1400
1600
1800
2000
2200
2400
2600
2800
3000
Time [s]
N2_MID
H2_MID
H2S_MID
Ar_MID

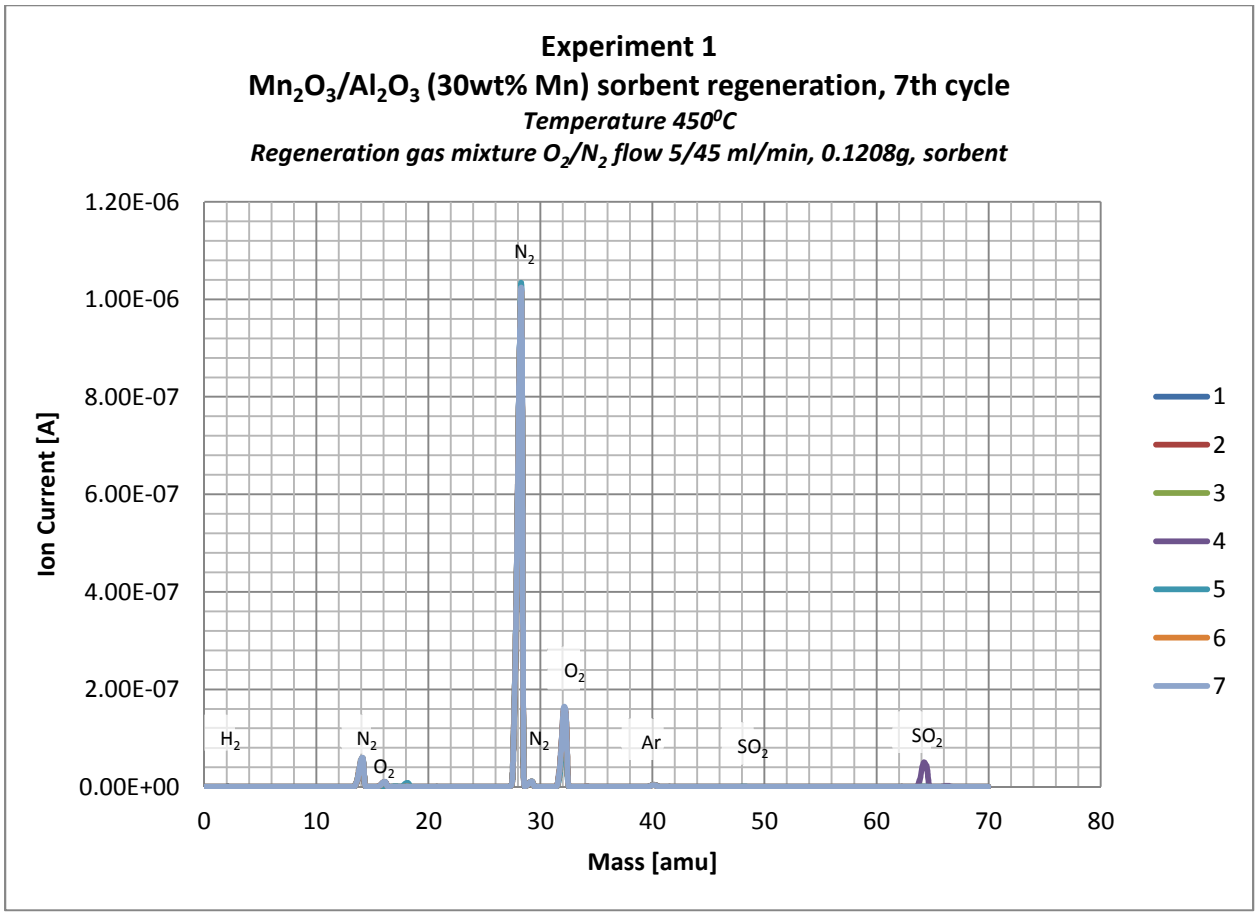
Experiment 1
Mn2O3/Al2O3 (30wt% Mn) sorbent regeneration, 7th cycle
Temperature 450⁰C
Regeneration gas mixture O2/N2 flow 5/45 ml/min, 0.1208g, sorbent
Ion Current [A]
1.20E-06
1.00E-06
8.00E-07
6.00E-07
4.00E-07
2.00E-07
0.00E+00
0
10
20
30
40
50
60
70
80
Mass [amu]
H2
N2
O2
N2
N2
O2
Ar
SO2
SO2
1
2
3
4
5
6
7

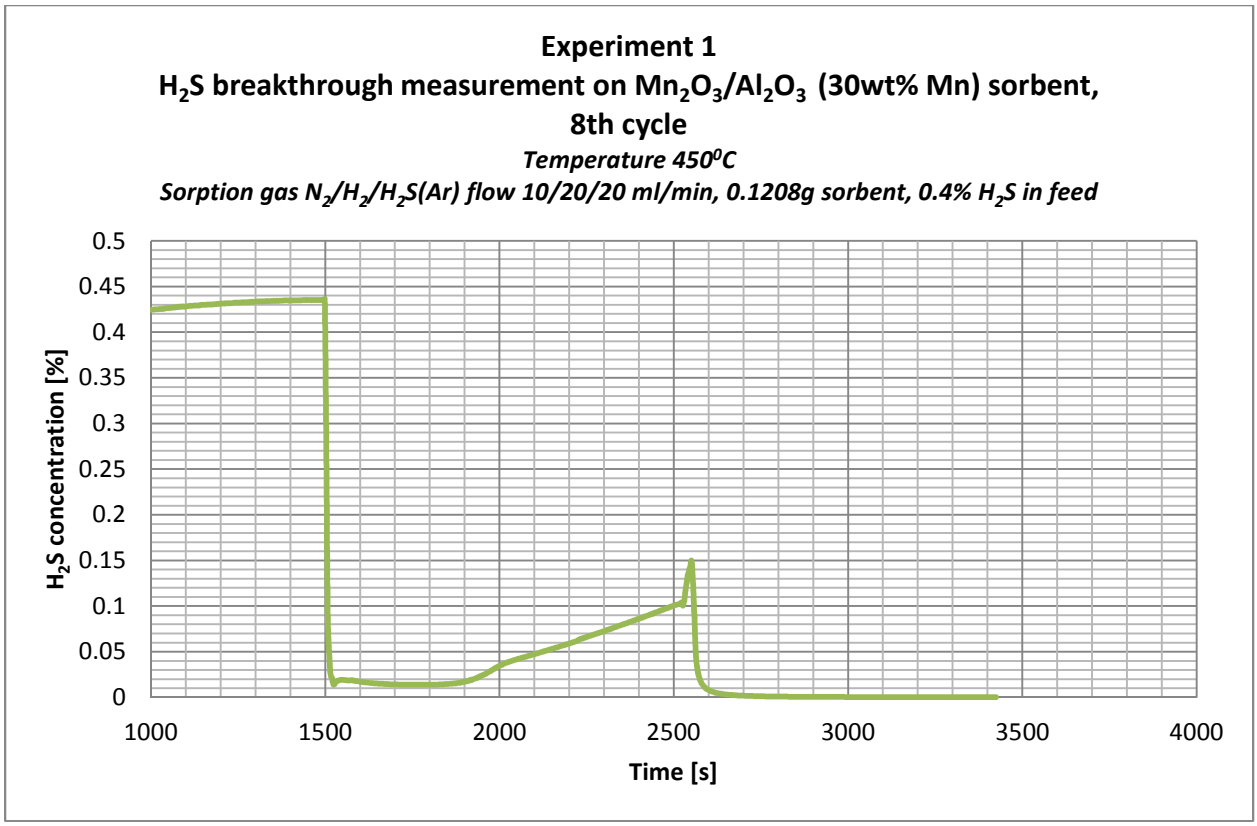
Experiment 1
H2S breakthrough measurement on Mn2O3/Al2O3 (30wt% Mn) sorbent, 8th cycle
Temperature 450⁰C
Sorption gas N2/H2/H2S(Ar) flow 10/20/20 ml/min, 0.1208g sorbent, 0.4% H2S in feed
H2S concentration [%]
0.5
0.45
0.4
0.35
0.3
0.25
0.2
0.15
0.1
0.05
0
1000
1500
2000
2500
3000
3500
4000
Time [s]

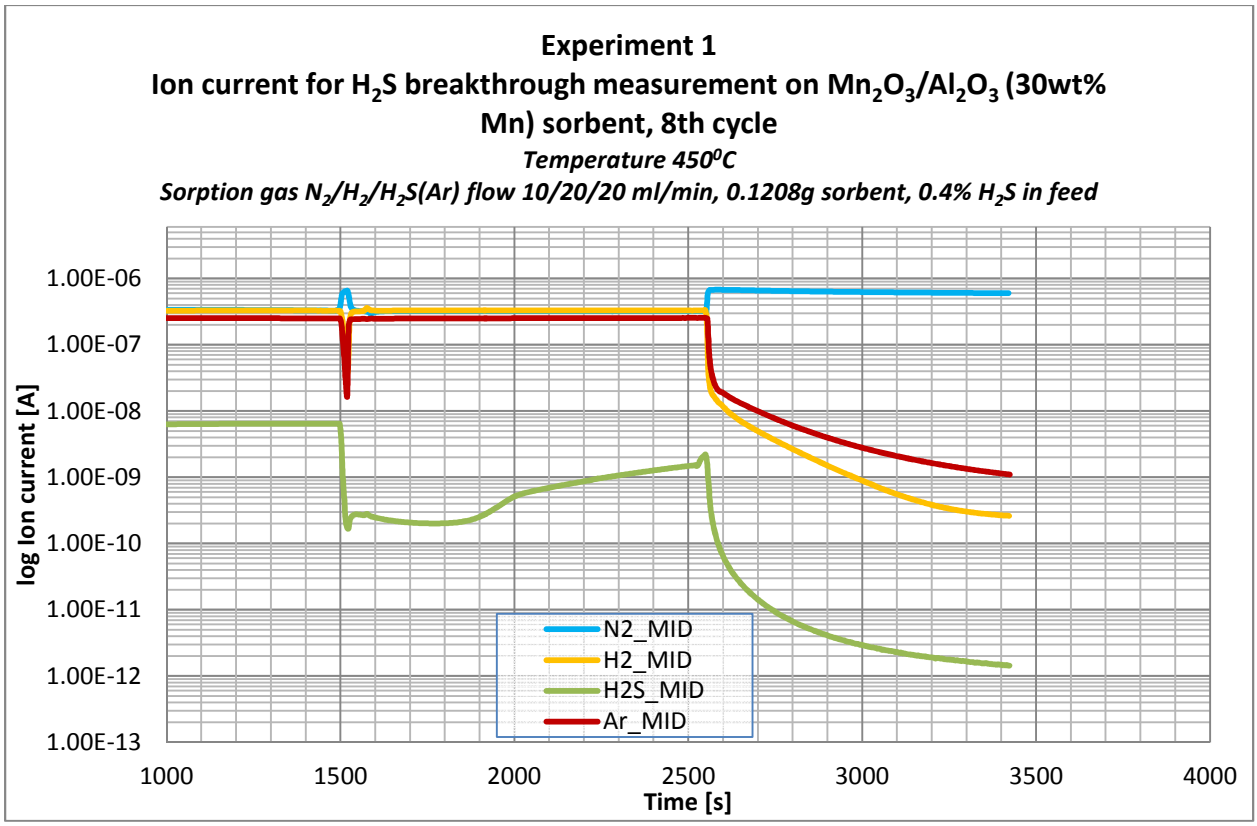
Experiment 1
Ion current for H2S breakthrough measurement on Mn2O3/Al2O3 (30wt% Mn) sorbent, 8th cycle
Temperature 450⁰C
Sorption gas N2/H2/H2S(Ar) flow 10/20/20 ml/min, 0.1208g sorbent, 0.4% H2S in feed
log Ion current [A]
1.00E-06
1.00E-07
1.00E-08
1.00E-09
1.00E-10
1.00E-11
1.00E-12
1.00E-13
1000
1500
2000
2500
3000
3500
4000
Time [s]
N2_MID
H2_MID
H2S_MID
Ar_MID

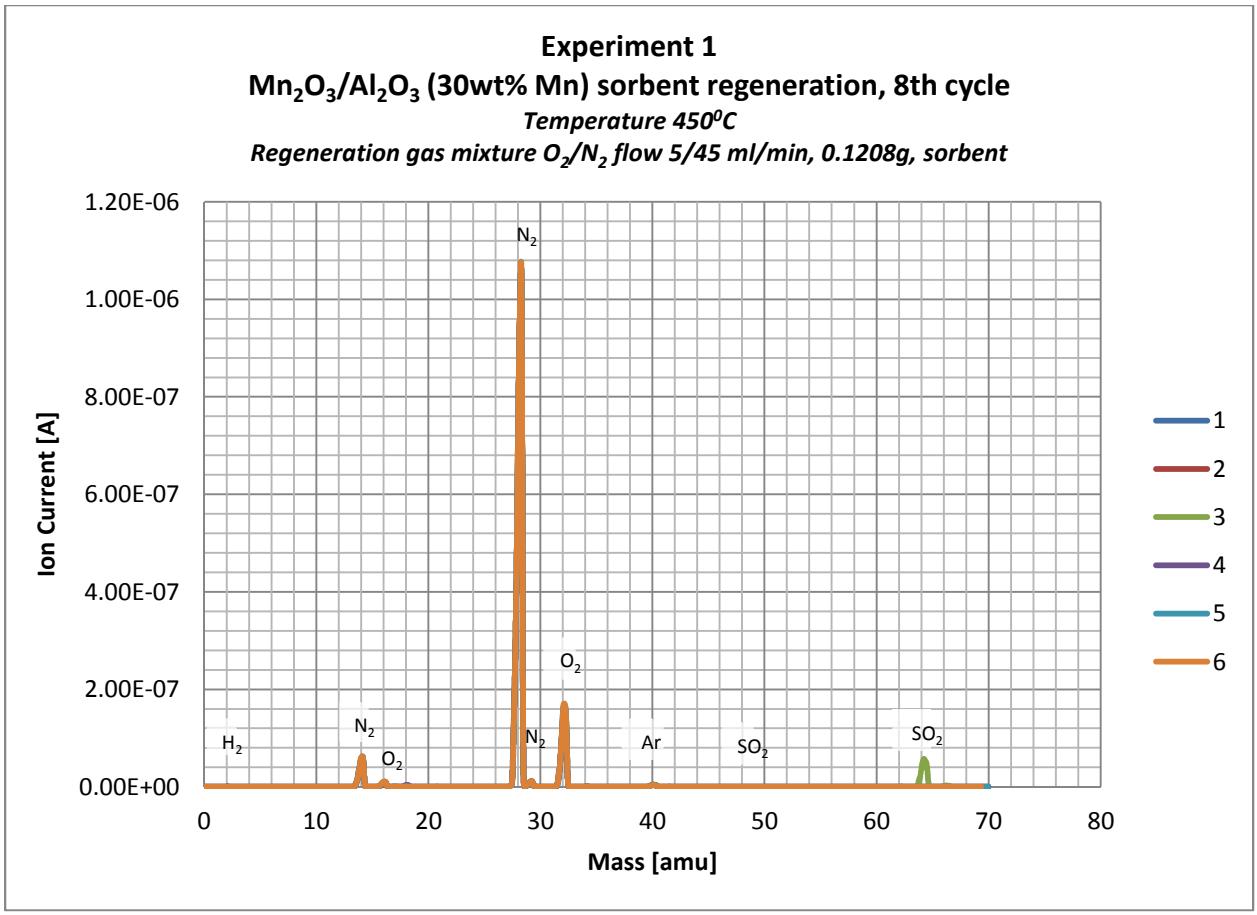
Experiment 1
Mn2O3/Al2O3 (30wt% Mn) sorbent regeneration, 8th cycle
Temperature 450⁰C
Regeneration gas mixture O2/N2 flow 5/45 ml/min, 0.1208g, sorbent
Ion Current [A]
1.20E-06
1.00E-06
8.00E-07
6.00E-07
4.00E-07
2.00E-07
0.00E+00
0
10
20
30
40
50
60
70
80
Mass [amu]
H2
N2
O2
N2
N2
O2
Ar
SO2
SO2
1
2
3
4
5
6

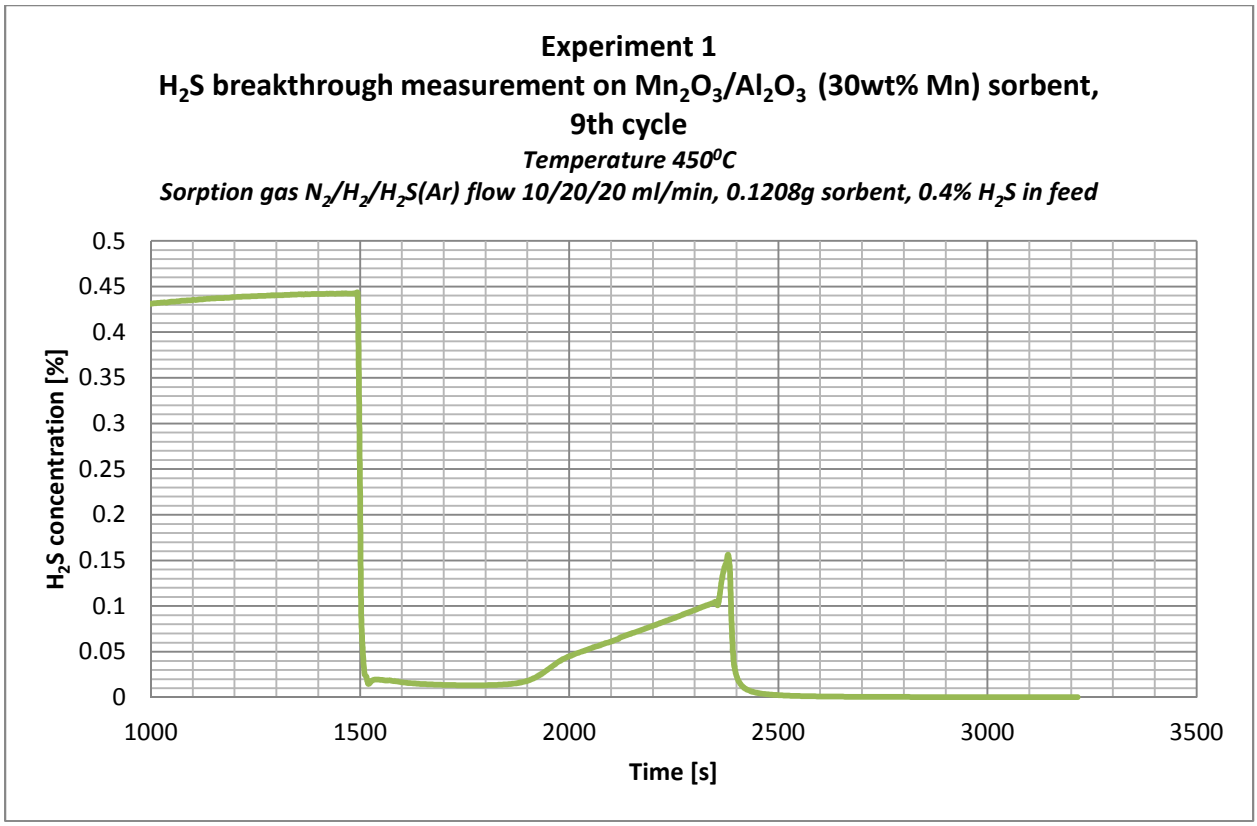
Experiment 1
H2S breakthrough measurement on Mn2O3/Al2O3 (30wt% Mn) sorbent, 9th cycle
Temperature 450⁰C
Sorption gas N2/H2/H2S(Ar) flow 10/20/20 ml/min, 0.1208g sorbent, 0.4% H2S in feed
H2S concentration [%]
0.5
0.45
0.4
0.35
0.3
0.25
0.2
0.15
0.1
0.05
0
1000
1500
2000
2500
3000
3500
Time [s]

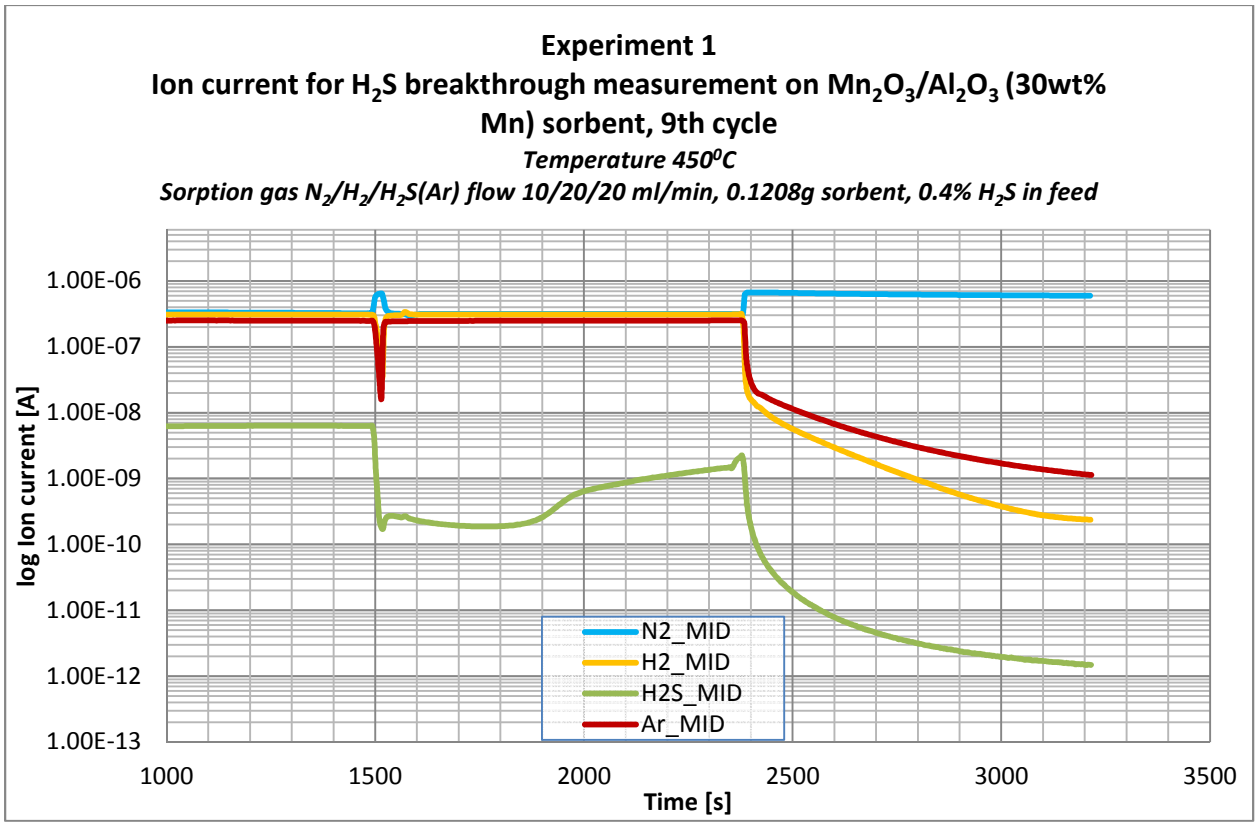
Experiment 1
Ion current for H2S breakthrough measurement on Mn2O3/Al2O3 (30wt% Mn) sorbent, 9th cycle
Temperature 450⁰C
Sorption gas N2/H2/H2S(Ar) flow 10/20/20 ml/min, 0.1208g sorbent, 0.4% H2S in feed
log Ion current [A]
1.00E-06
1.00E-07
1.00E-08
1.00E-09
1.00E-10
1.00E-11
1.00E-12
1.00E-13
1000
1500
2000
2500
3000
3500
Time [s]
N2_MID
H2_MID
H2S_MID
Ar_MID

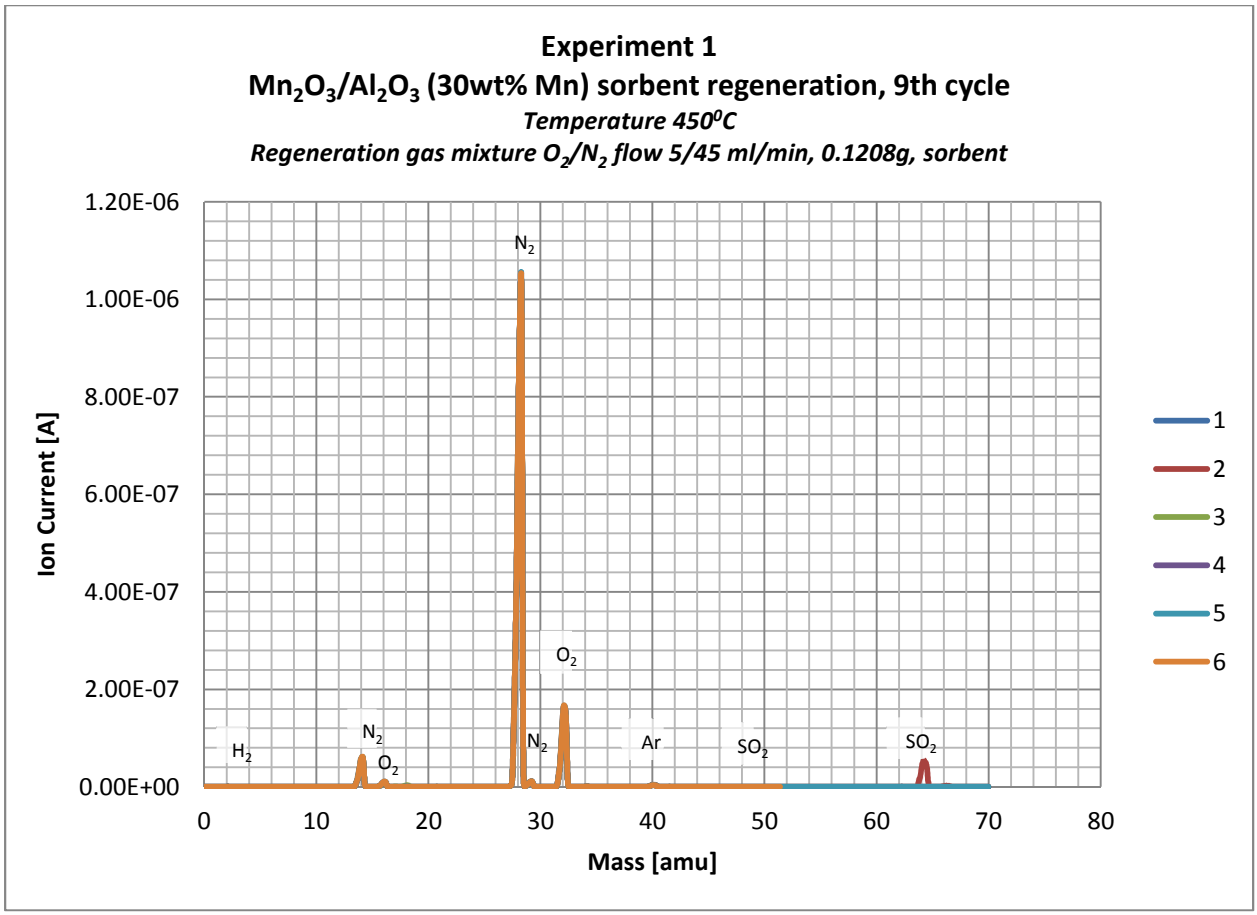
Experiment 1
Mn2O3/Al2O3 (30wt% Mn) sorbent regeneration, 9th cycle
Temperature 450⁰C
Regeneration gas mixture O2/N2 flow 5/45 ml/min, 0.1208g, sorbent
Ion Current [A]
1.20E-06
1.00E-06
8.00E-07
6.00E-07
4.00E-07
2.00E-07
0.00E+00
0
10
20
30
40
50
60
70
80
Mass [amu]
N2
O2
H2
N2
O2
N2
Ar
SO2
SO2
1
2
3
4
5
6

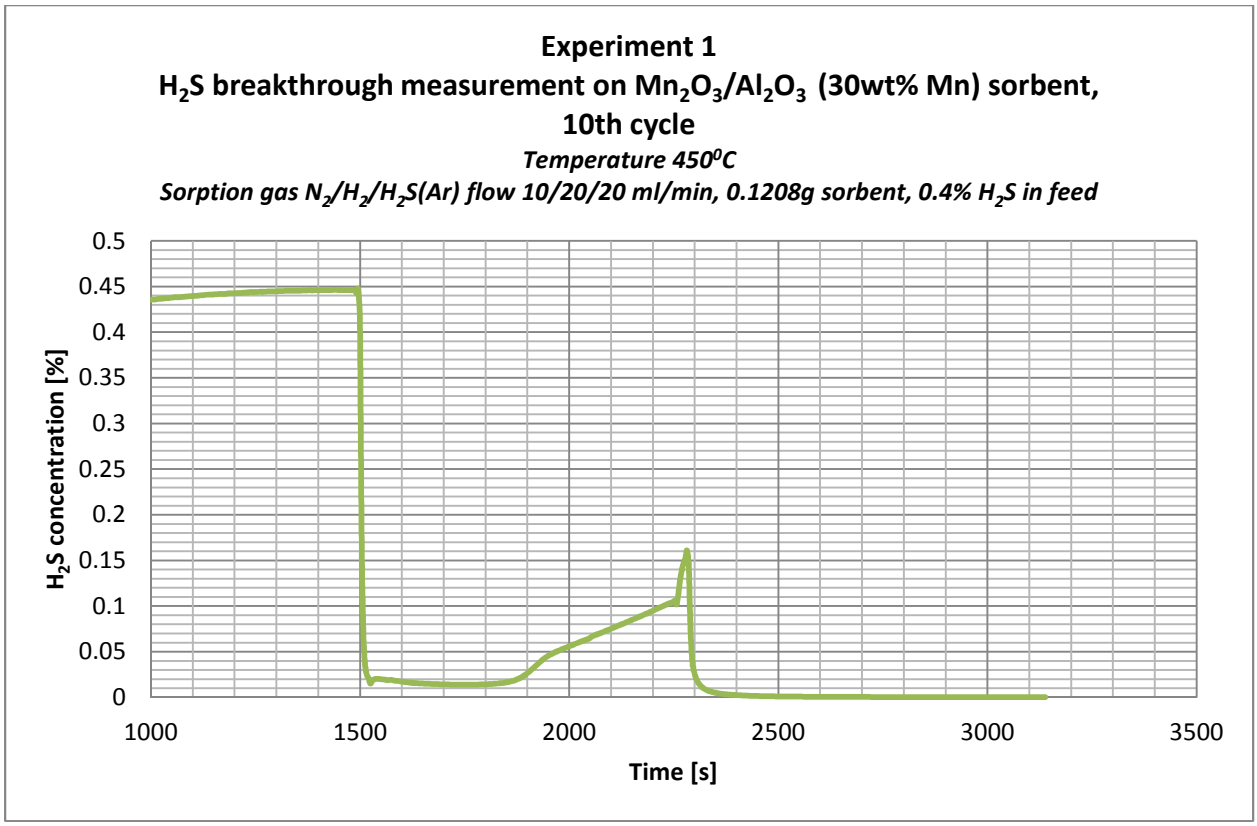
Experiment 1
H2S breakthrough measurement on Mn2O3/Al2O3 (30wt% Mn) sorbent, 10th cycle
Temperature 450⁰C
Sorption gas N2/H2/H2S(Ar) flow 10/20/20 ml/min, 0.1208g sorbent, 0.4% H2S in feed
H2S concentration [%]
0.5
0.45
0.4
0.35
0.3
0.25
0.2
0.15
0.1
0.05
0
1000
1500
2000
2500
3000
3500
Time [s]

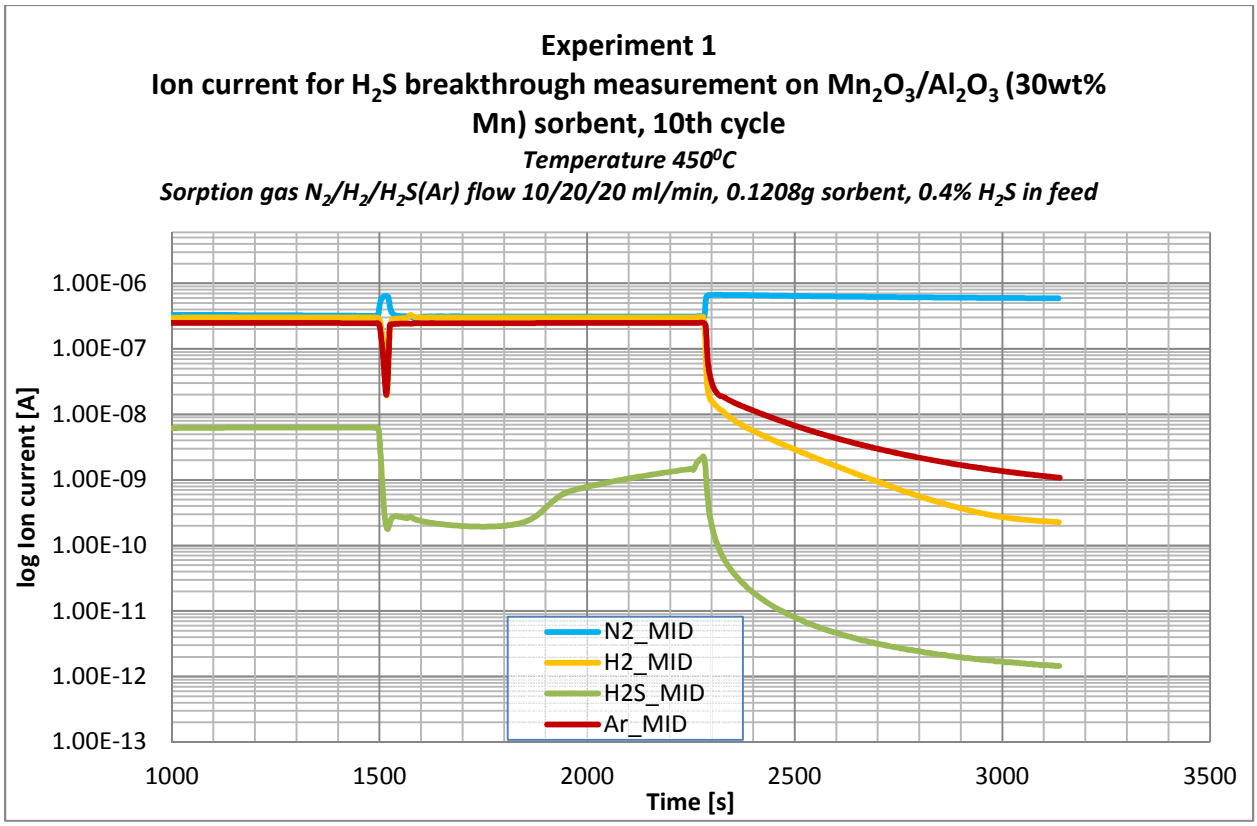
Experiment 1
Ion current for H2S breakthrough measurement on Mn2O3/Al2O3 (30wt% Mn) sorbent, 10th cycle
Temperature 450⁰C
Sorption gas N2/H2/H2S(Ar) flow 10/20/20 ml/min, 0.1208g sorbent, 0.4% H2S in feed
log Ion current [A]
1.00E-06
1.00E-07
1.00E-08
1.00E-09
1.00E-10
1.00E-11
1.00E-12
1.00E-13
1000
1500
2000
2500
3000
3500
Time [s]
N2_MID
H2_MID
H2S_MID
Ar_MID

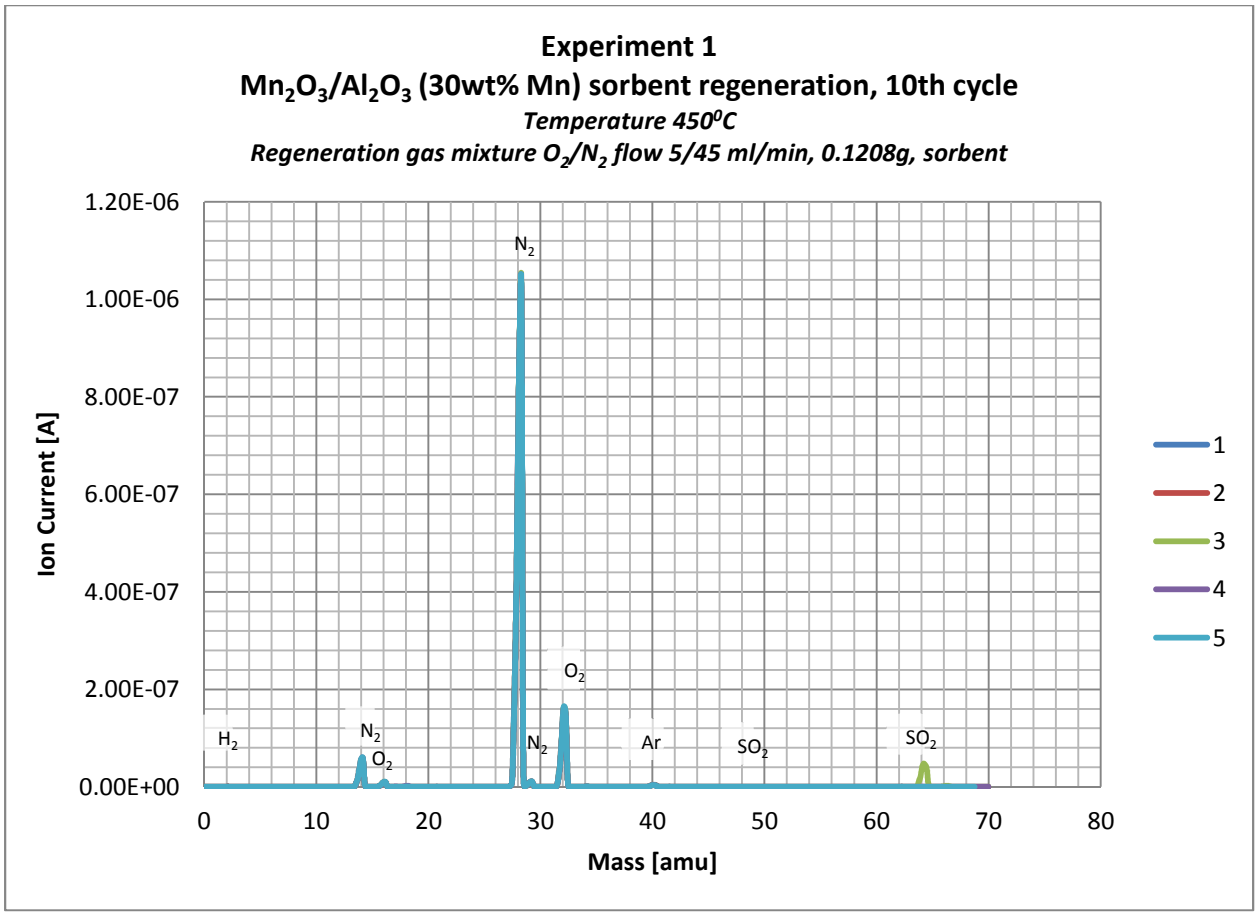
Experiment 1
Mn2O3/Al2O3 (30wt% Mn) sorbent regeneration, 10th cycle
Temperature 450⁰C
Regeneration gas mixture O2/N2 flow 5/45 ml/min, 0.1208g, sorbent
Ion Current [A]
1.20E-06
1.00E-06
8.00E-07
6.00E-07
4.00E-07
2.00E-07
0.00E+00
0
10
20
30
40
50
60
70
80
Mass [amu]
N2
O2
H2
N2
O2
N2
Ar
SO2
SO2
1
2
3
4
5

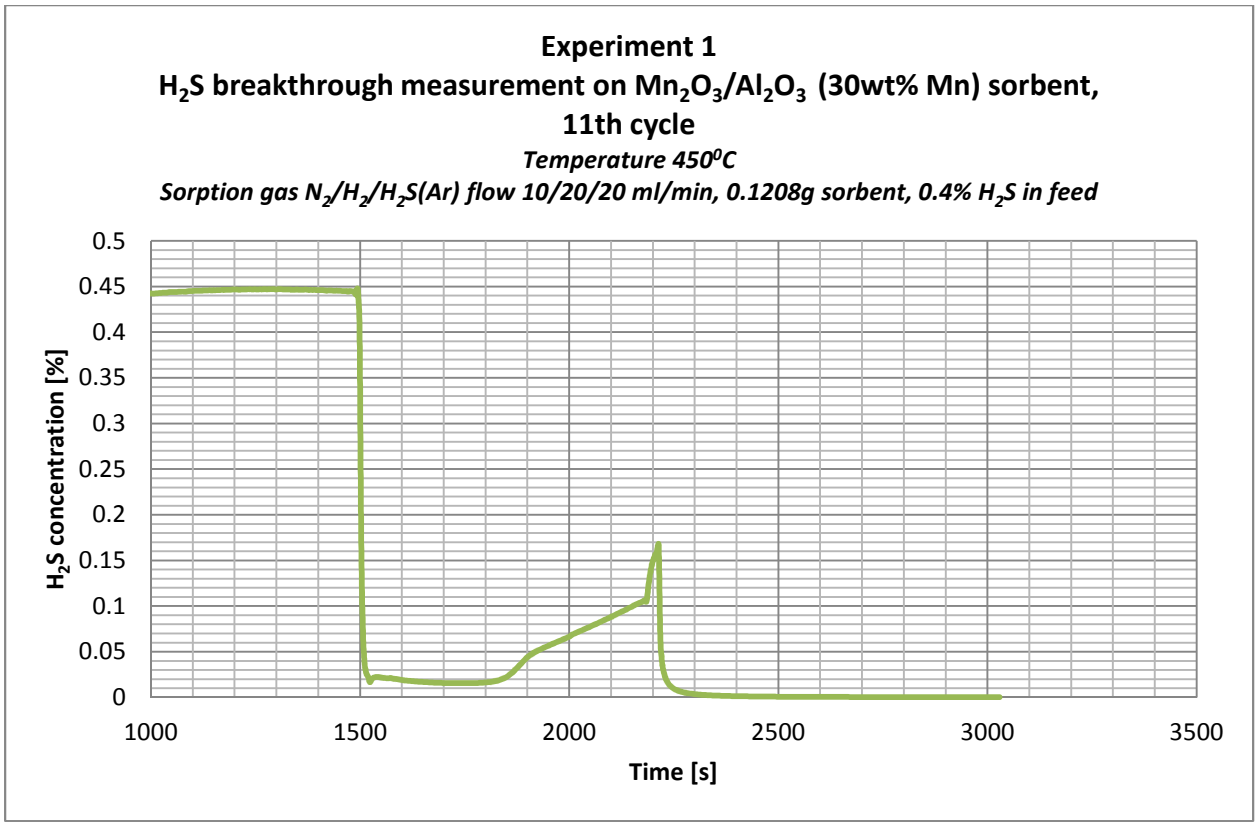
Experiment 1
H2S breakthrough measurement on Mn2O3/Al2O3 (30wt% Mn) sorbent, 11th cycle
Temperature 450⁰C
Sorption gas N2/H2/H2S(Ar) flow 10/20/20 ml/min, 0.1208g sorbent, 0.4% H2S in feed
H2S concentration [%]
0.5
0.45
0.4
0.35
0.3
0.25
0.2
0.15
0.1
0.05
0
1000
1500
2000
2500
3000
3500
Time [s]

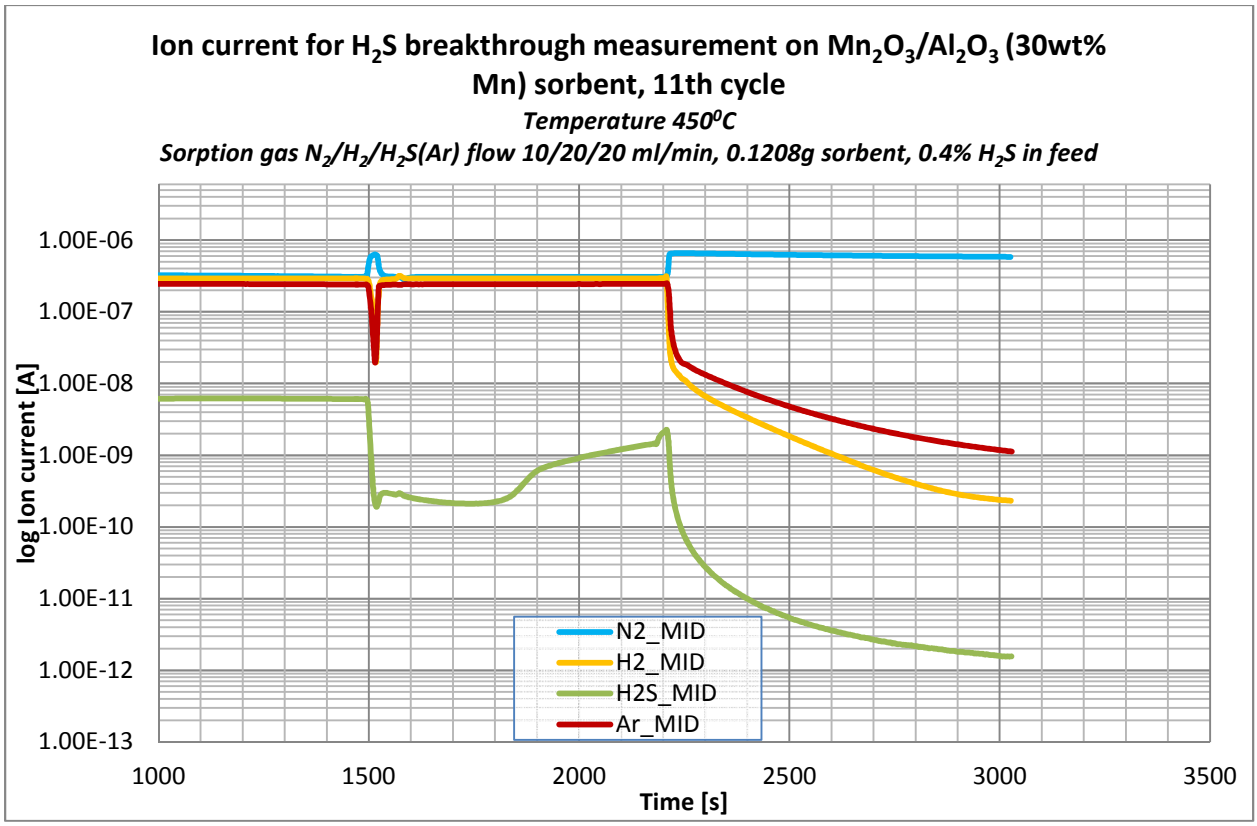
Ion current for H2S breakthrough measurement on Mn2O3/Al2O3 (30wt% Mn) sorbent, 11th cycle
Temperature 450⁰C
Sorption gas N2/H2/H2S(Ar) flow 10/20/20 ml/min, 0.1208g sorbent, 0.4% H2S in feed
log Ion current [A]
1.00E-06
1.00E-07
1.00E-08
1.00E-09
1.00E-10
1.00E-11
1.00E-12
1.00E-13
1000
1500
2000
2500
3000
3500
Time [s]
N2_MID
H2_MID
H2S_MID
Ar_MID

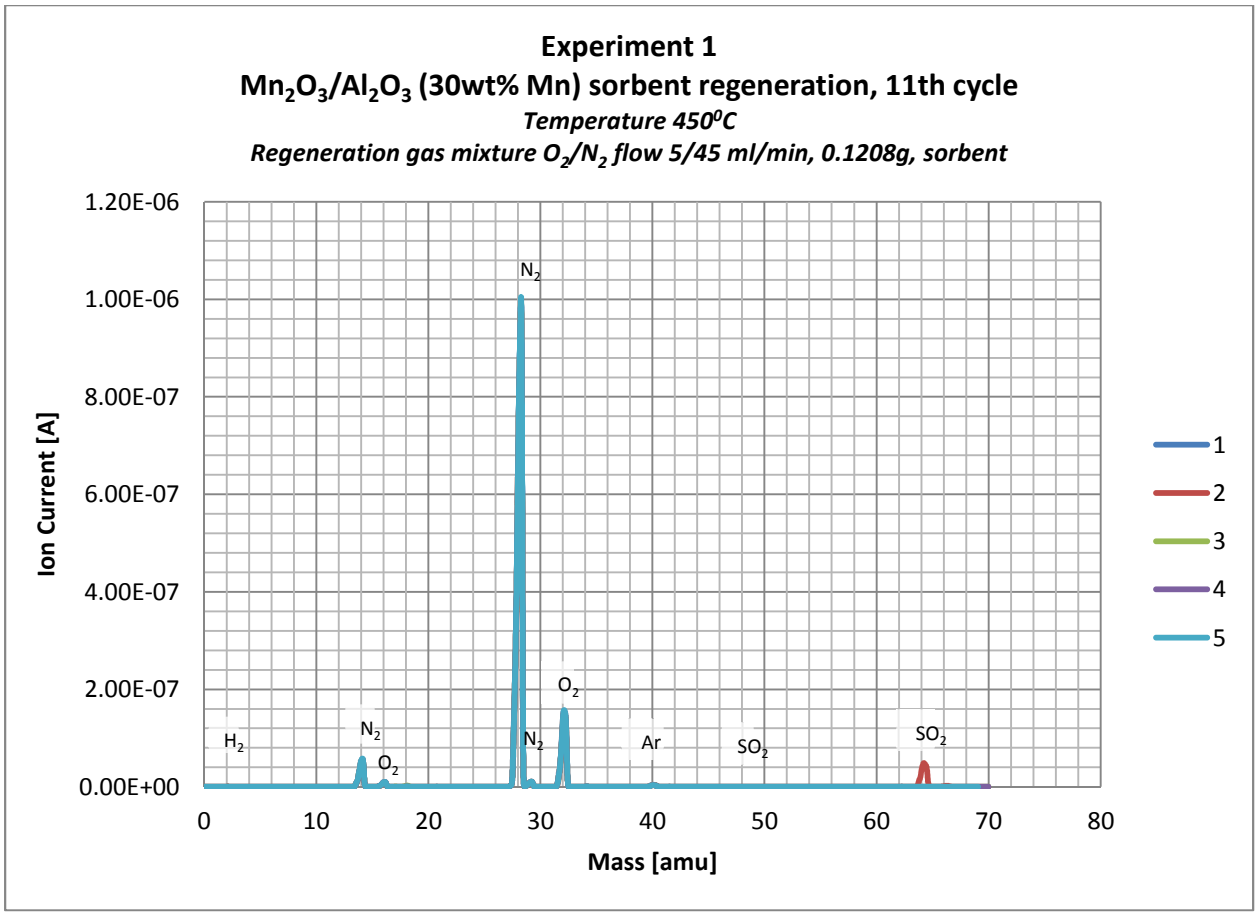
Experiment 1
Mn2O3/Al2O3 (30wt% Mn) sorbent regeneration, 11th cycle
Temperature 450⁰C
Regeneration gas mixture O2/N2 flow 5/45 ml/min, 0.1208g, sorbent
Ion Current [A]
1.20E-06
1.00E-06
8.00E-07
6.00E-07
4.00E-07
2.00E-07
0.00E+00
0
10
20
30
40
50
60
70
80
Mass [amu]
H2
N2
O2
N2
N2
O2
Ar
SO2
SO2
1
2
3
4
5

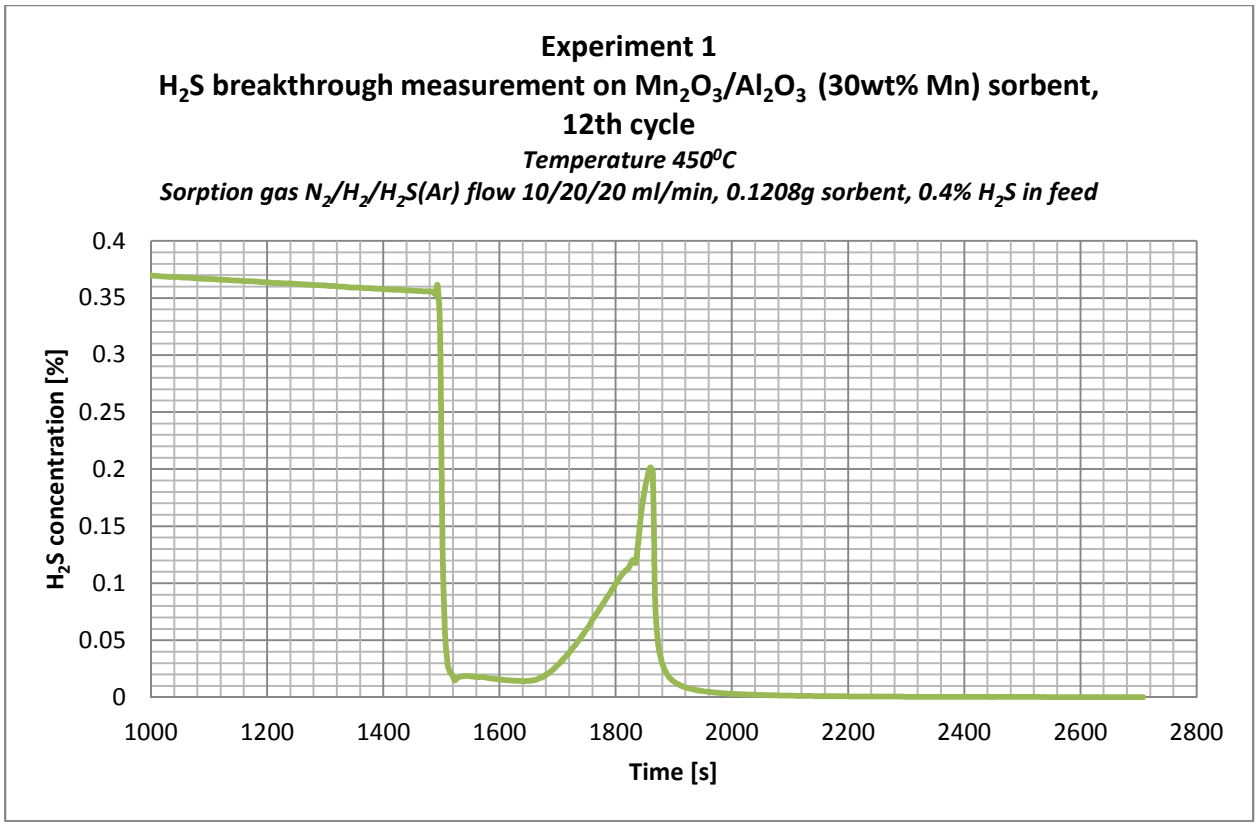
Experiment 1
H2S breakthrough measurement on Mn2O3/Al2O3 (30wt% Mn) sorbent, 12th cycle
Temperature 450⁰C
Sorption gas N2/H2/H2S(Ar) flow 10/20/20 ml/min, 0.1208g sorbent, 0.4% H2S in feed
H2S concentration [%]
0.4
0.35
0.3
0.25
0.2
0.15
0.1
0.05
0
1000
1200
1400
1600
1800
2000
2200
2400
2600
2800
Time [s]

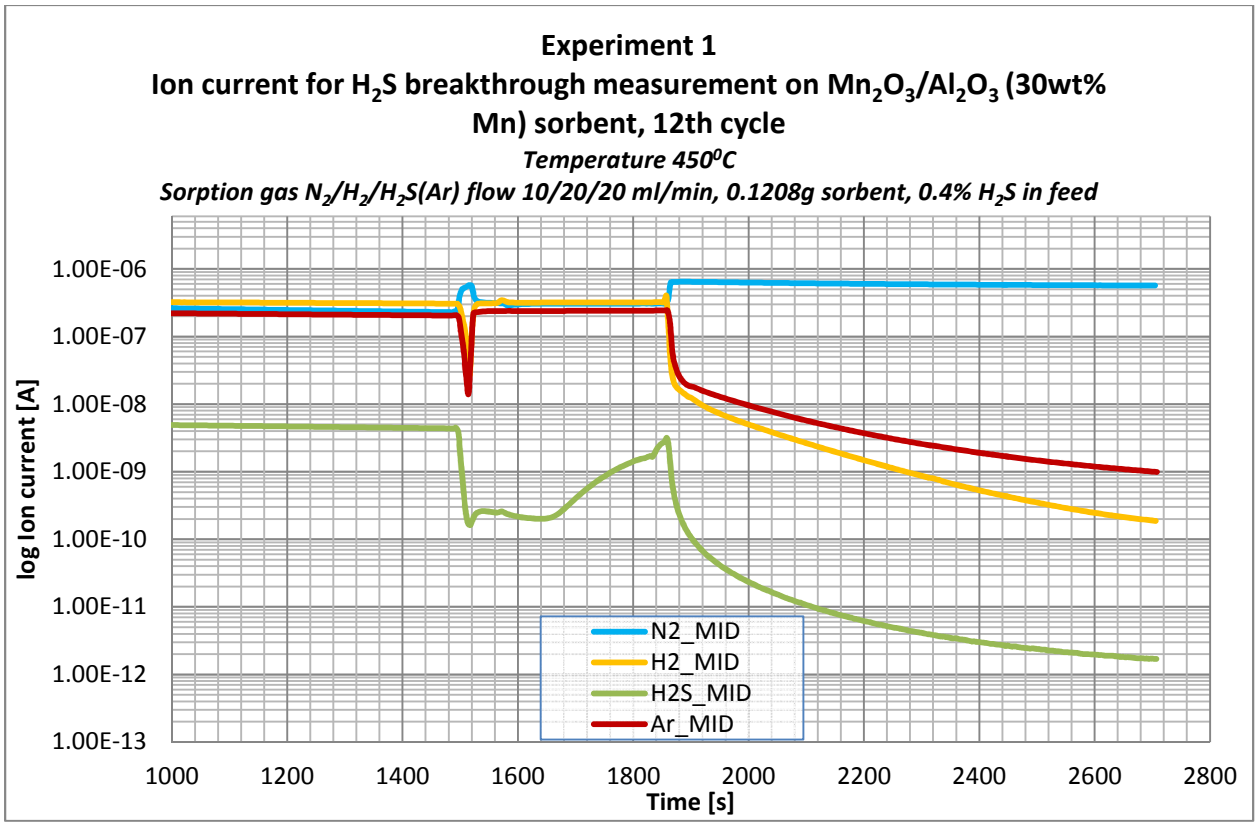
Experiment 1
Ion current for H2S breakthrough measurement on Mn2O3/Al2O3 (30wt% Mn) sorbent, 12th cycle
Temperature 450⁰C
Sorption gas N2/H2/H2S(Ar) flow 10/20/20 ml/min, 0.1208g sorbent, 0.4% H2S in feed
log Ion current [A]
1.00E-06
1.00E-07
1.00E-08
1.00E-09
1.00E-10
1.00E-11
1.00E-12
1.00E-13
1000
1200
1400
1600
1800
2000
2200
2400
2600
2800
Time [s]
N2_MID
H2_MID
H2S_MID
Ar_MID

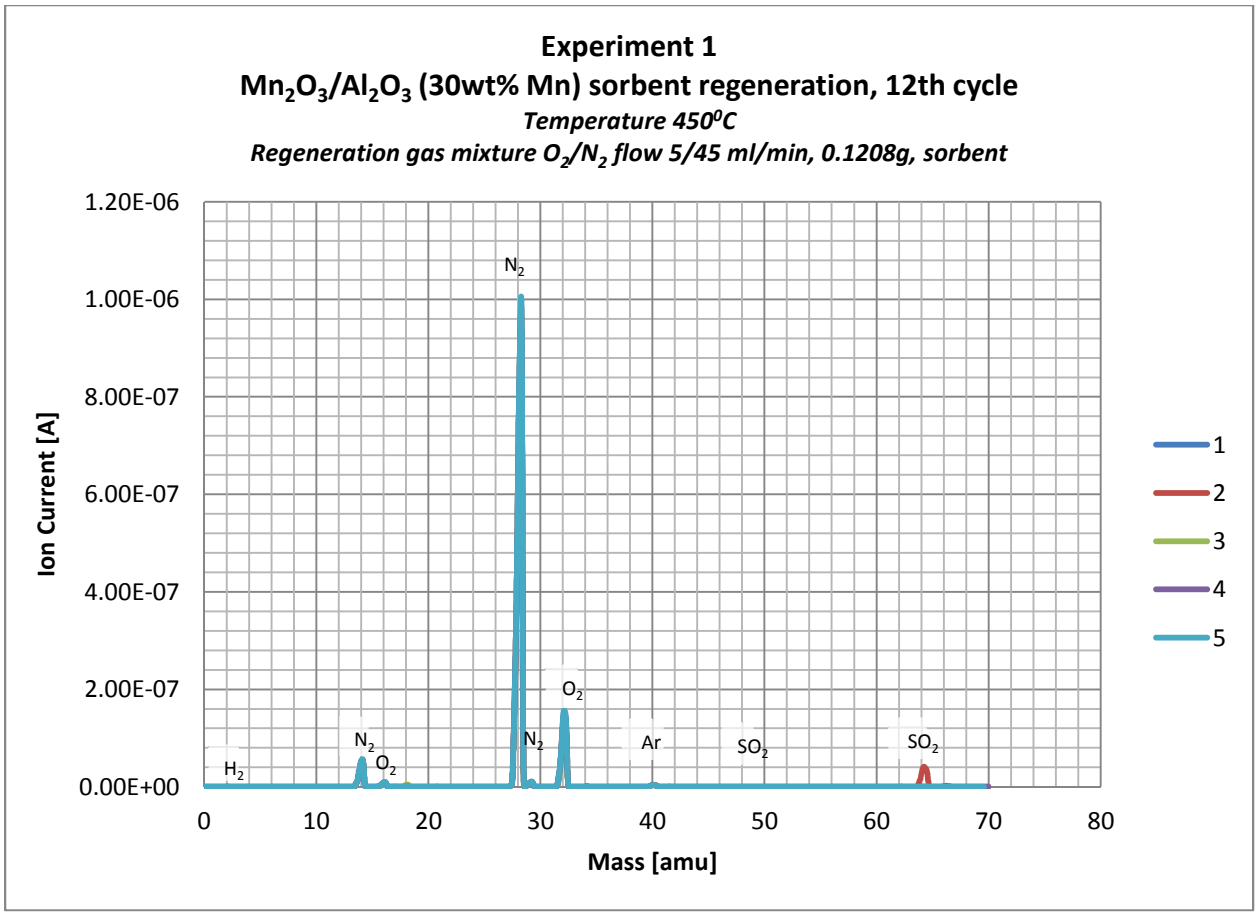
Experiment 1
Mn2O3/Al2O3 (30wt% Mn) sorbent regeneration, 12th cycle
Temperature 450⁰C
Regeneration gas mixture O2/N2 flow 5/45 ml/min, 0.1208g, sorbent
Ion Current [A]
1.20E-06
1.00E-06
8.00E-07
6.00E-07
4.00E-07
2.00E-07
0.00E+00
0
10
20
30
40
50
60
70
80
Mass [amu]
N2
O2
N2
H2
N2
O2
Ar
SO2
SO2
1
2
3
4
5

**Experiment 1**

**$H_2S$ breakthrough measurement on $Mn_2O_3/Al_2O_3$ (30wt% Mn) sorbent, 13th cycle**

***Temperature 450$^0$C***

***Sorption gas $N_2/H_2/H_2S$(Ar) flow 10/20/20 ml/min, 0.1208g sorbent, 0.4% $H_2S$ in feed***

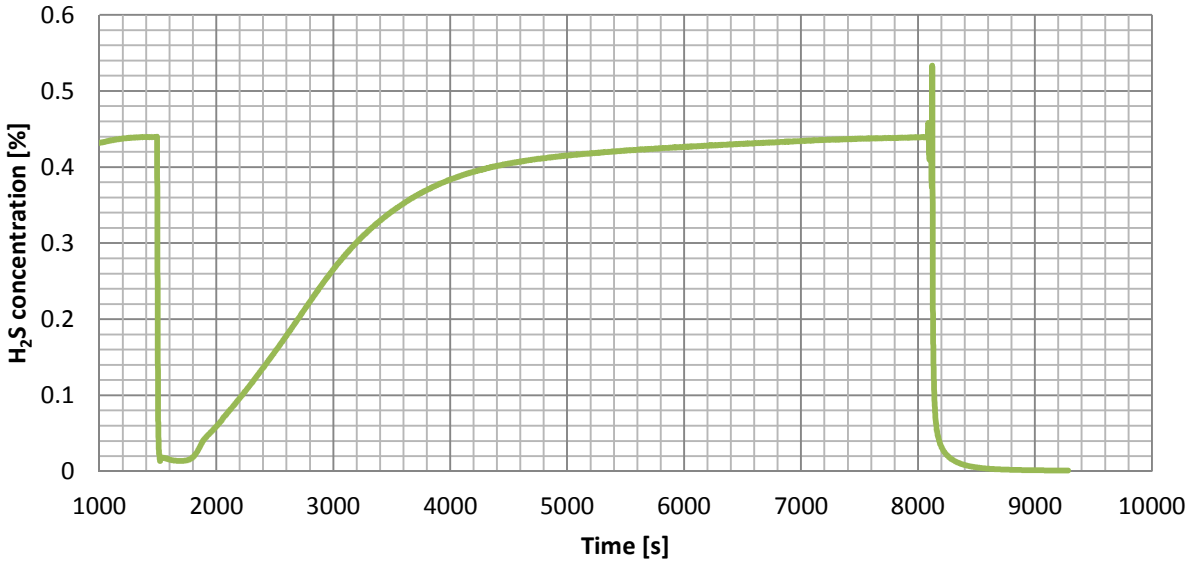


**Experiment 1**

**Ion current for $H_2S$ breakthrough measurement on $Mn_2O_3/Al_2O_3$ (30wt% Mn) sorbent, 13th cycle**

***Temperature 450$^0$C***

***Sorption gas $N_2/H_2/H_2S$(Ar) flow 10/20/20 ml/min, 0.1208g sorbent, 0.4% $H_2S$ in feed***

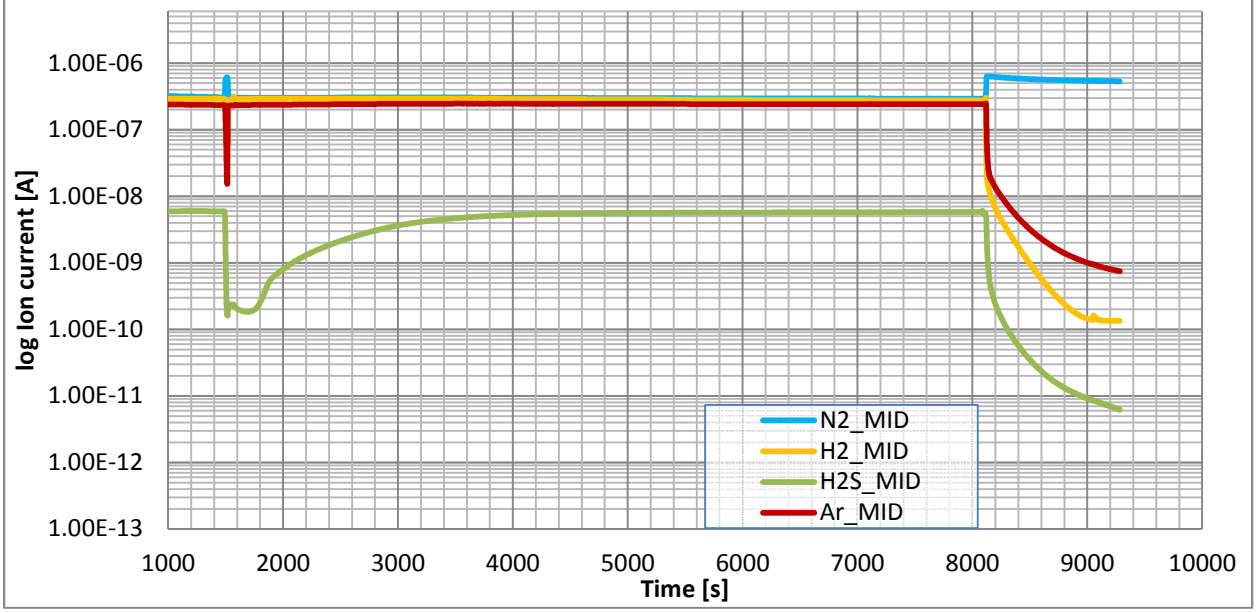

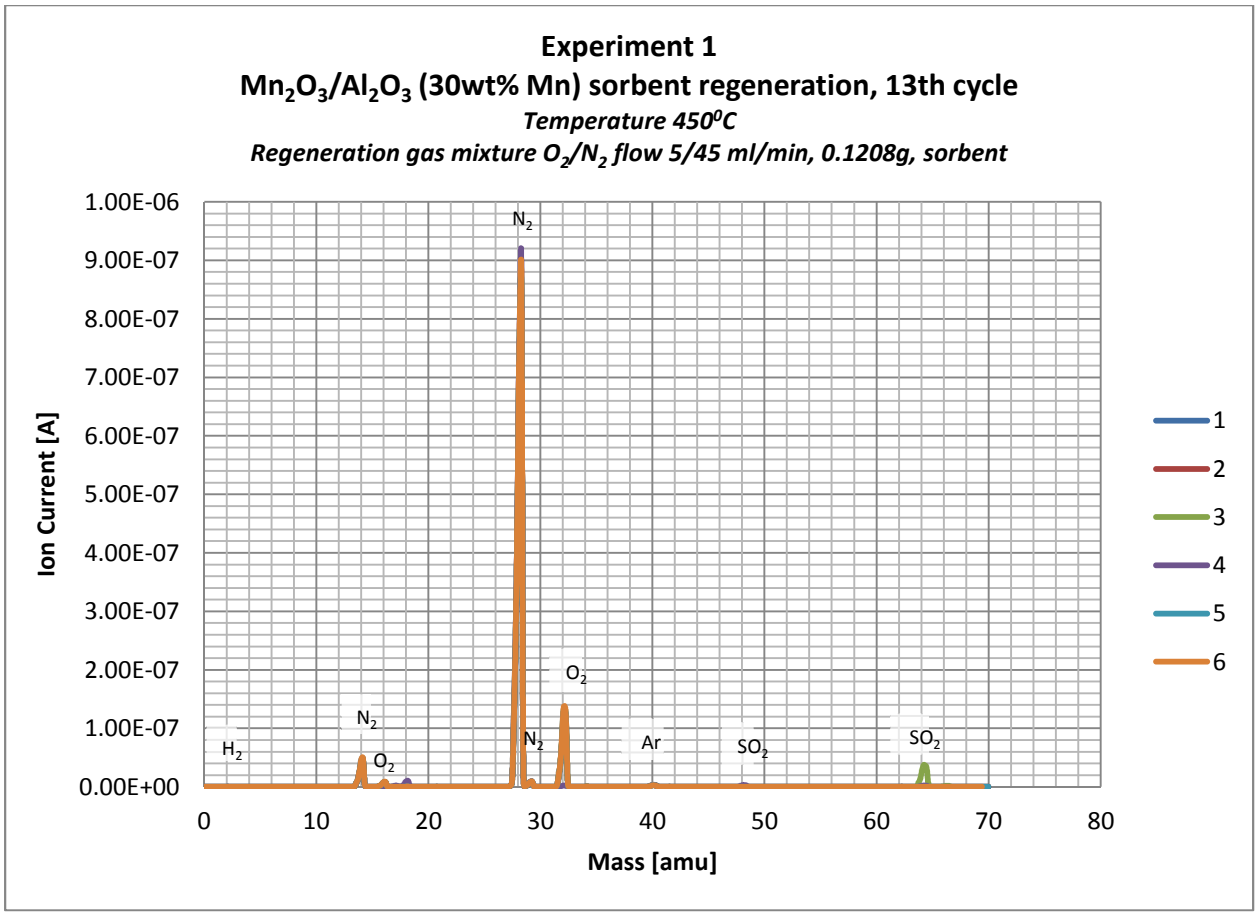
Experiment 1
Mn2O3/Al2O3 (30wt% Mn) sorbent regeneration, 13th cycle
Temperature 450⁰C
Regeneration gas mixture O2/N2 flow 5/45 ml/min, 0.1208g, sorbent
Ion Current [A]
1.00E-06
9.00E-07
8.00E-07
7.00E-07
6.00E-07
5.00E-07
4.00E-07
3.00E-07
2.00E-07
1.00E-07
0.00E+00
0
10
20
30
40
50
60
70
80
Mass [amu]
N2
O2
N2
H2
N2
O2
Ar
SO2
SO2
1
2
3
4
5
6

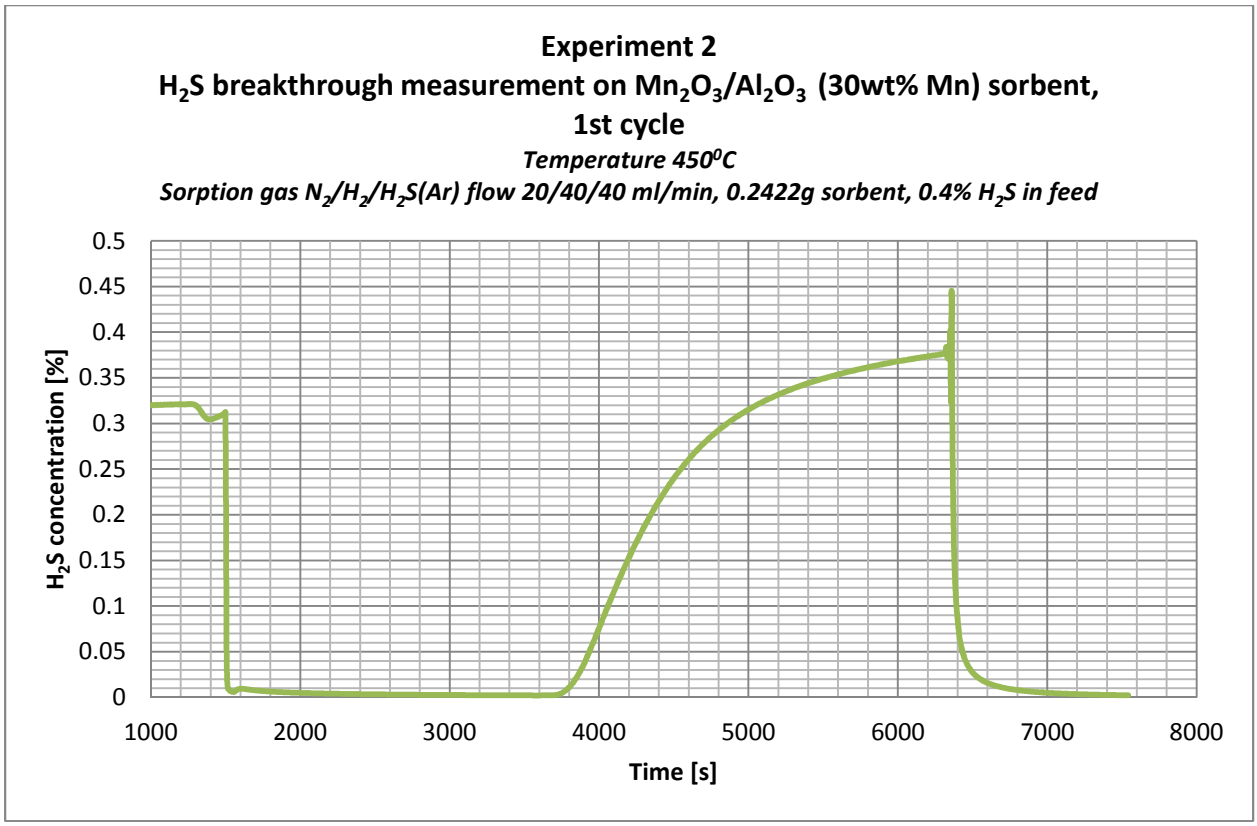
Experiment 2
H2S breakthrough measurement on Mn2O3/Al2O3 (30wt% Mn) sorbent, 1st cycle
Temperature 450⁰C
Sorption gas N2/H2/H2S(Ar) flow 20/40/40 ml/min, 0.2422g sorbent, 0.4% H2S in feed
H2S concentration [%]
0.5
0.45
0.4
0.35
0.3
0.25
0.2
0.15
0.1
0.05
0
1000
2000
3000
4000
5000
6000
7000
8000
Time [s]

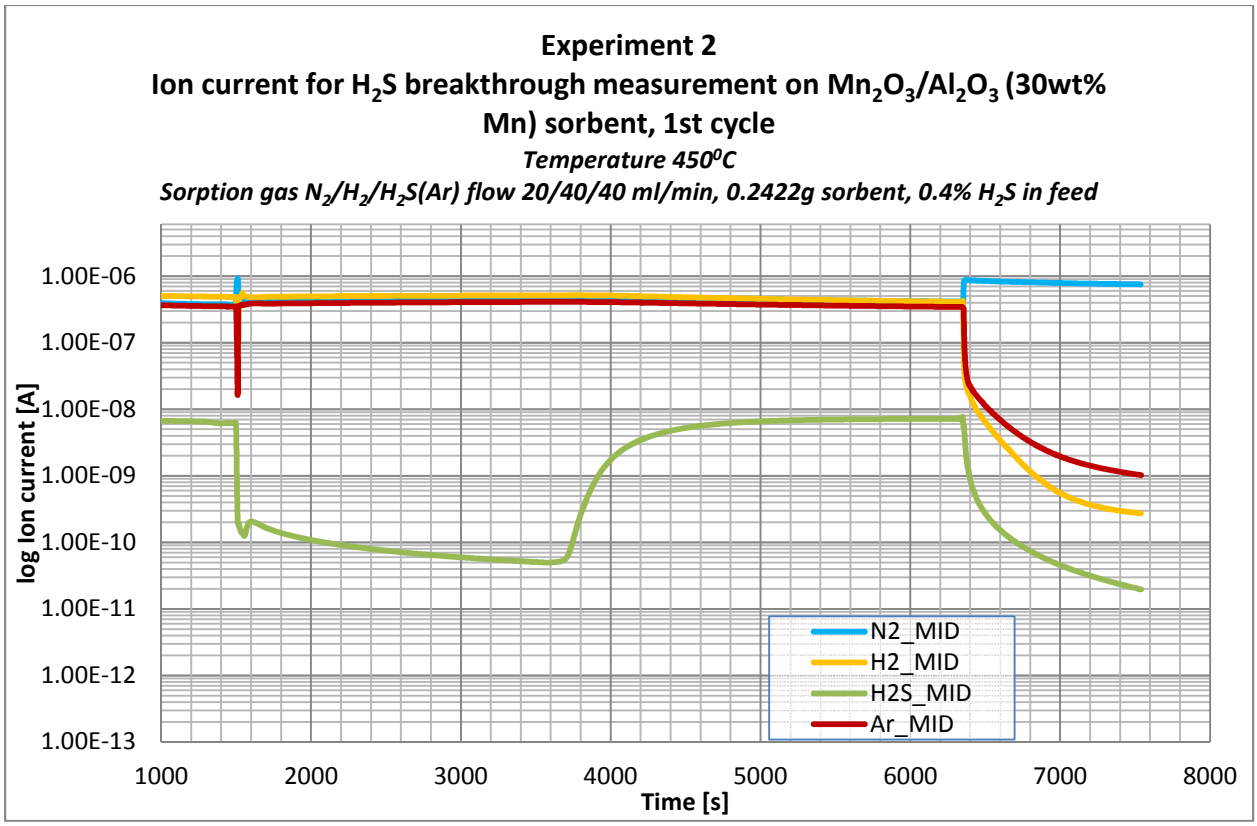
Experiment 2
Ion current for H2S breakthrough measurement on Mn2O3/Al2O3 (30wt% Mn) sorbent, 1st cycle
Temperature 450⁰C
Sorption gas N2/H2/H2S(Ar) flow 20/40/40 ml/min, 0.2422g sorbent, 0.4% H2S in feed
log Ion current [A]
1.00E-06
1.00E-07
1.00E-08
1.00E-09
1.00E-10
1.00E-11
1.00E-12
1.00E-13
1000
2000
3000
4000
5000
6000
7000
8000
Time [s]
N2_MID
H2_MID
H2S_MID
Ar_MID

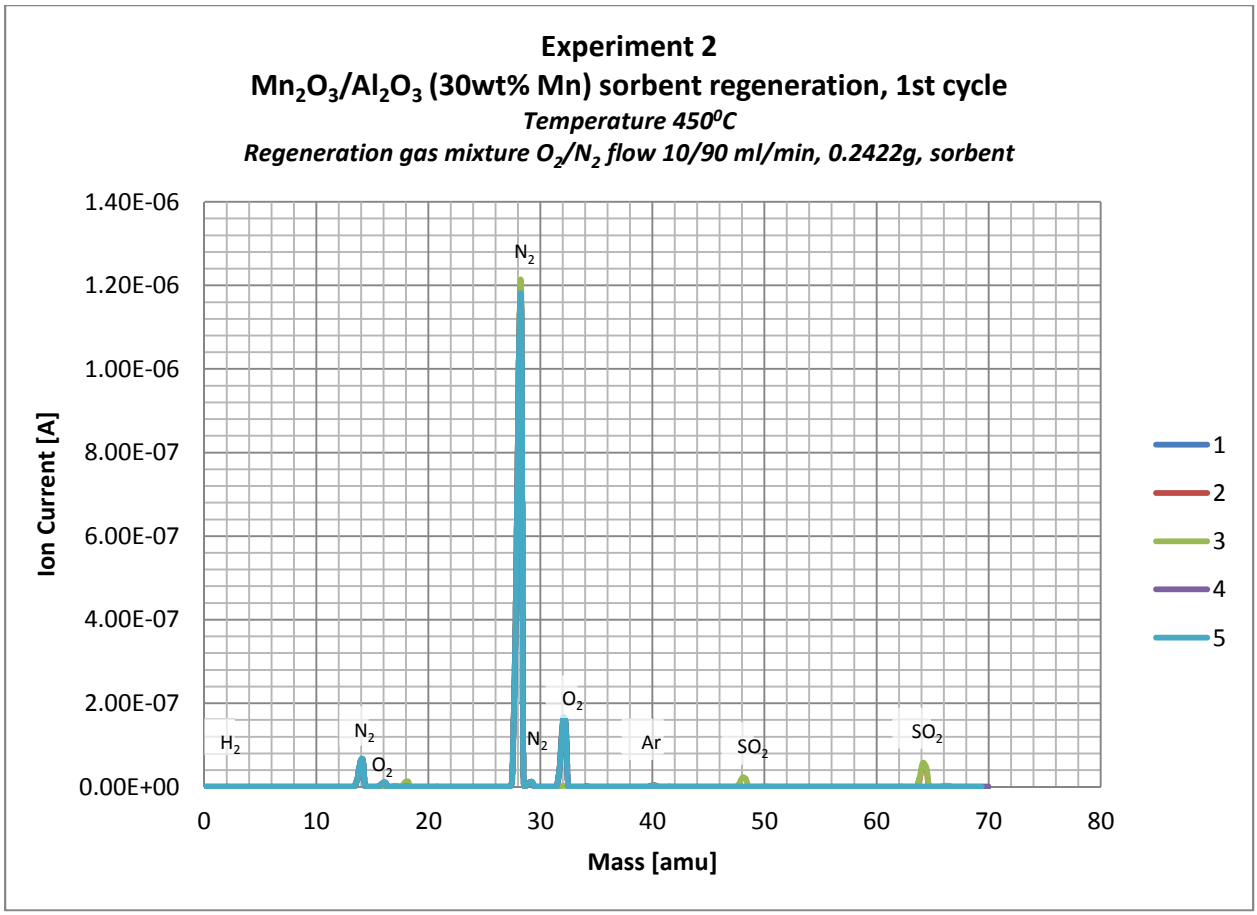
Experiment 2
Mn2O3/Al2O3 (30wt% Mn) sorbent regeneration, 1st cycle
Temperature 450⁰C
Regeneration gas mixture O2/N2 flow 10/90 ml/min, 0.2422g, sorbent
Ion Current [A]
1.40E-06
1.20E-06
1.00E-06
8.00E-07
6.00E-07
4.00E-07
2.00E-07
0.00E+00
0
10
20
30
40
50
60
70
80
Mass [amu]
H2
N2
O2
N2
N2
O2
Ar
SO2
SO2
1
2
3
4
5

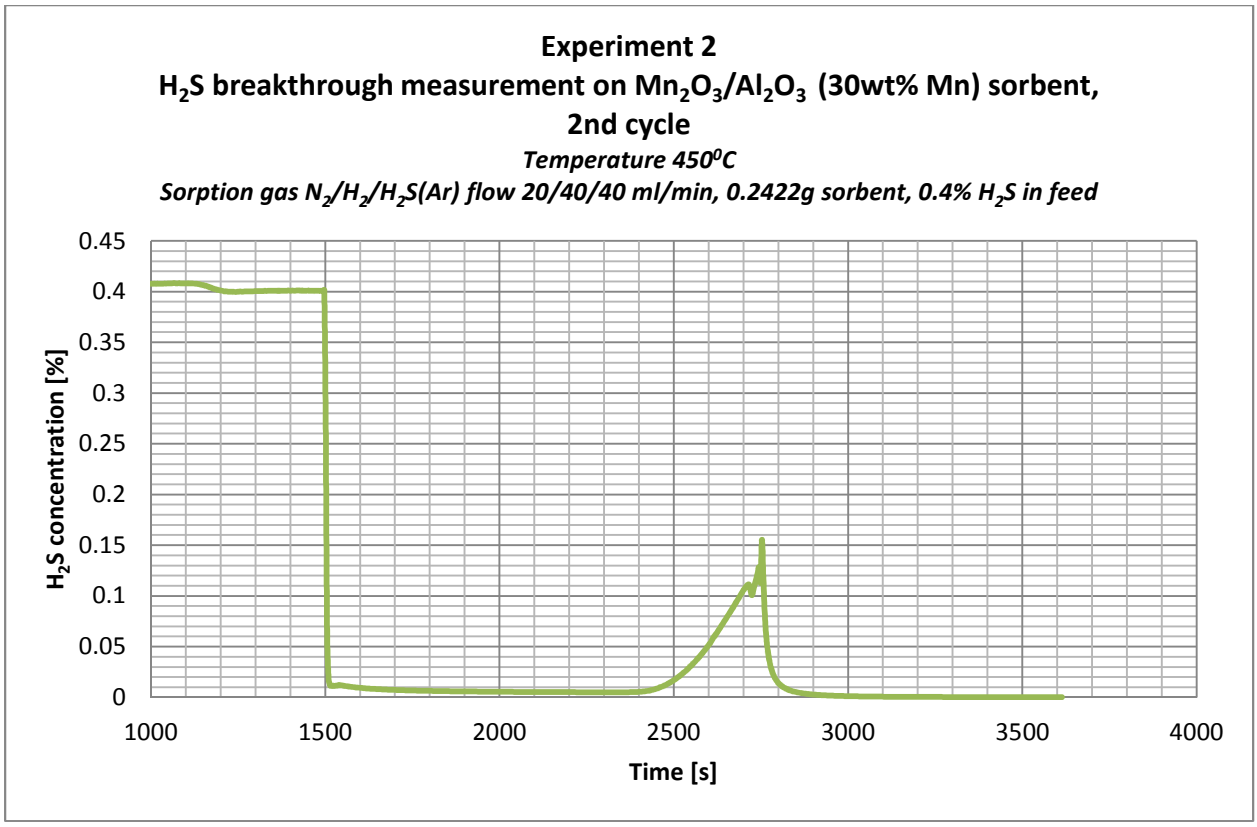
Experiment 2
H2S breakthrough measurement on Mn2O3/Al2O3 (30wt% Mn) sorbent, 2nd cycle
Temperature 450⁰C
Sorption gas N2/H2/H2S(Ar) flow 20/40/40 ml/min, 0.2422g sorbent, 0.4% H2S in feed
H2S concentration [%]
0.45
0.4
0.35
0.3
0.25
0.2
0.15
0.1
0.05
0
1000
1500
2000
2500
3000
3500
4000
Time [s]

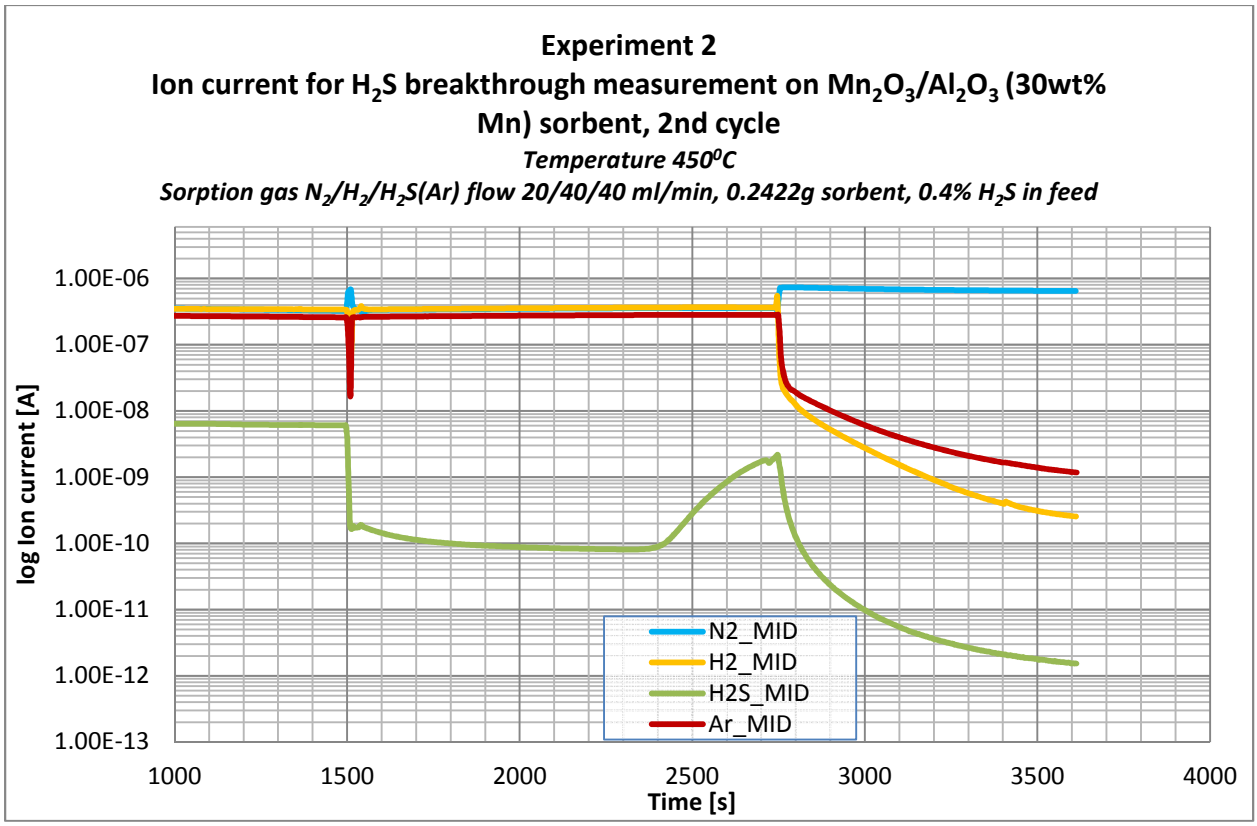
Experiment 2
Ion current for H2S breakthrough measurement on Mn2O3/Al2O3 (30wt% Mn) sorbent, 2nd cycle
Temperature 450⁰C
Sorption gas N2/H2/H2S(Ar) flow 20/40/40 ml/min, 0.2422g sorbent, 0.4% H2S in feed
log Ion current [A]
1.00E-06
1.00E-07
1.00E-08
1.00E-09
1.00E-10
1.00E-11
1.00E-12
1.00E-13
1000
1500
2000
2500
3000
3500
4000
Time [s]
N2_MID
H2_MID
H2S_MID
Ar_MID

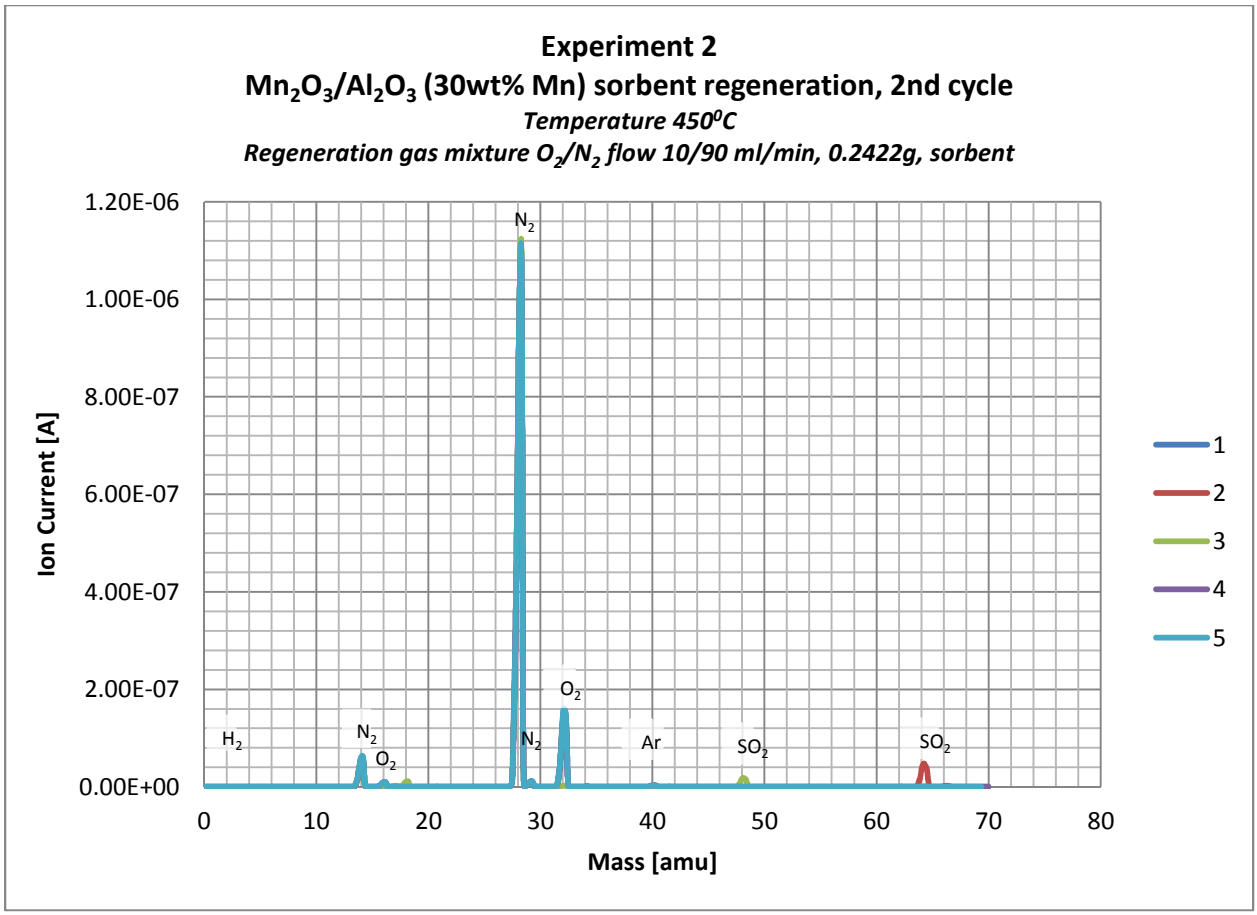
Experiment 2
Mn2O3/Al2O3 (30wt% Mn) sorbent regeneration, 2nd cycle
Temperature 450⁰C
Regeneration gas mixture O2/N2 flow 10/90 ml/min, 0.2422g, sorbent
Ion Current [A]
1.20E-06
1.00E-06
8.00E-07
6.00E-07
4.00E-07
2.00E-07
0.00E+00
0
10
20
30
40
50
60
70
80
Mass [amu]
N2
O2
H2
N2
O2
N2
Ar
SO2
SO2
1
2
3
4
5

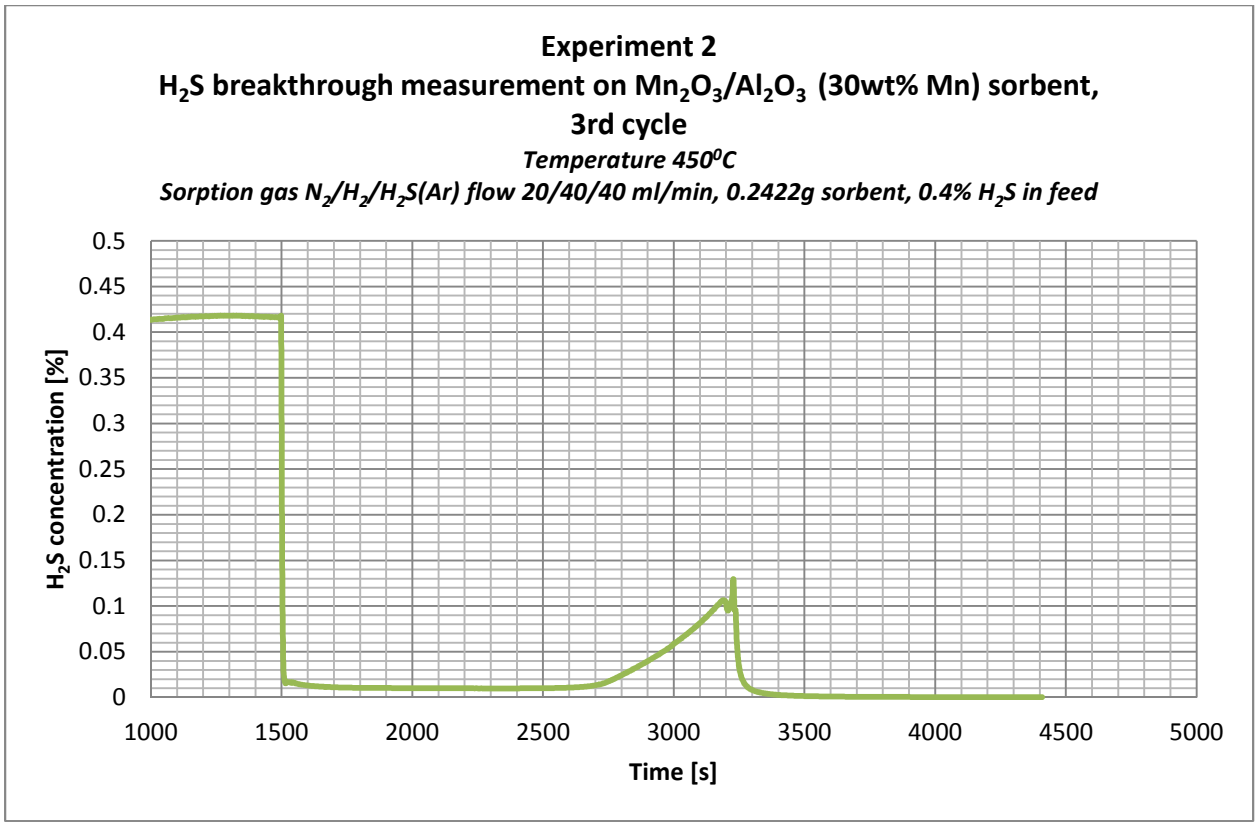
Experiment 2
H2S breakthrough measurement on Mn2O3/Al2O3 (30wt% Mn) sorbent, 3rd cycle
Temperature 450⁰C
Sorption gas N2/H2/H2S(Ar) flow 20/40/40 ml/min, 0.2422g sorbent, 0.4% H2S in feed
H2S concentration [%]
0.5
0.45
0.4
0.35
0.3
0.25
0.2
0.15
0.1
0.05
0
1000
1500
2000
2500
3000
3500
4000
4500
5000
Time [s]

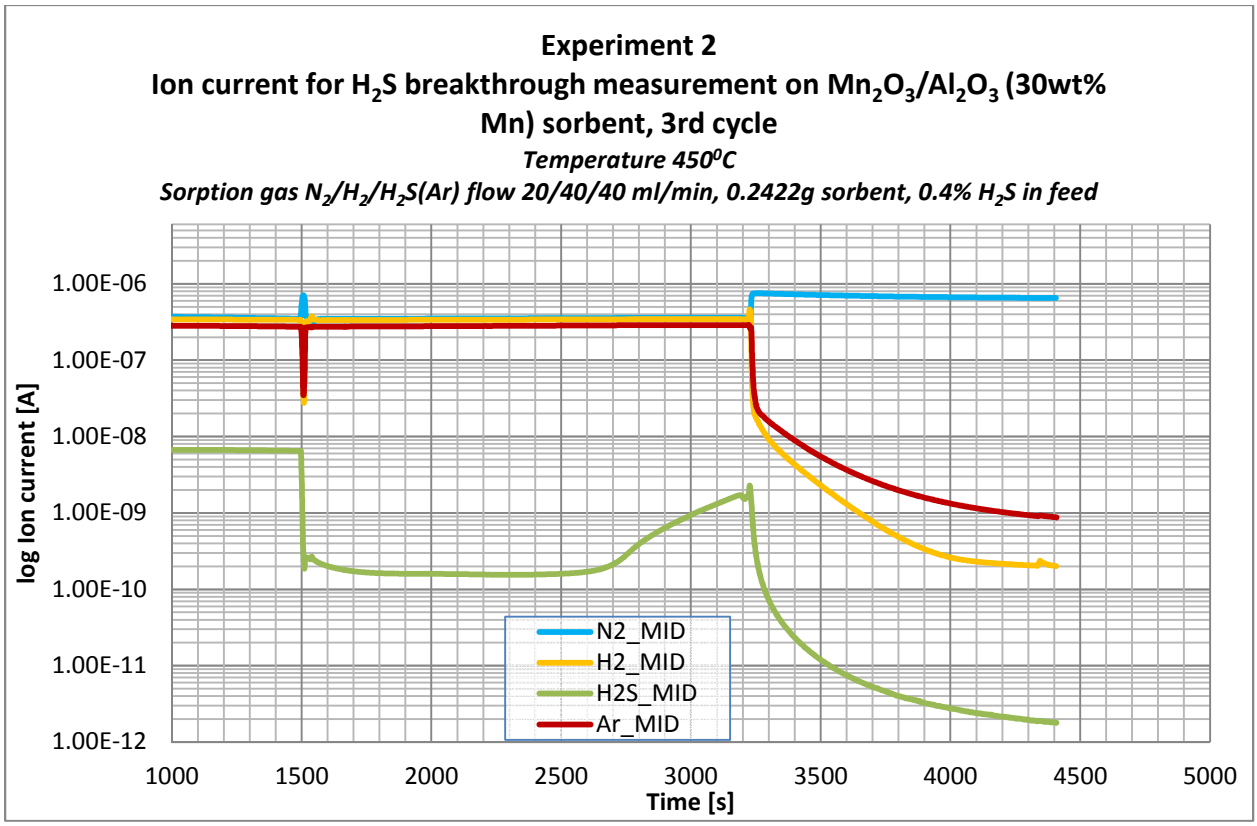
Experiment 2
Ion current for H2S breakthrough measurement on Mn2O3/Al2O3 (30wt% Mn) sorbent, 3rd cycle
Temperature 450⁰C
Sorption gas N2/H2/H2S(Ar) flow 20/40/40 ml/min, 0.2422g sorbent, 0.4% H2S in feed
log Ion current [A]
1.00E-06
1.00E-07
1.00E-08
1.00E-09
1.00E-10
1.00E-11
1.00E-12
1000
1500
2000
2500
3000
3500
4000
4500
5000
Time [s]
N2_MID
H2_MID
H2S_MID
Ar_MID

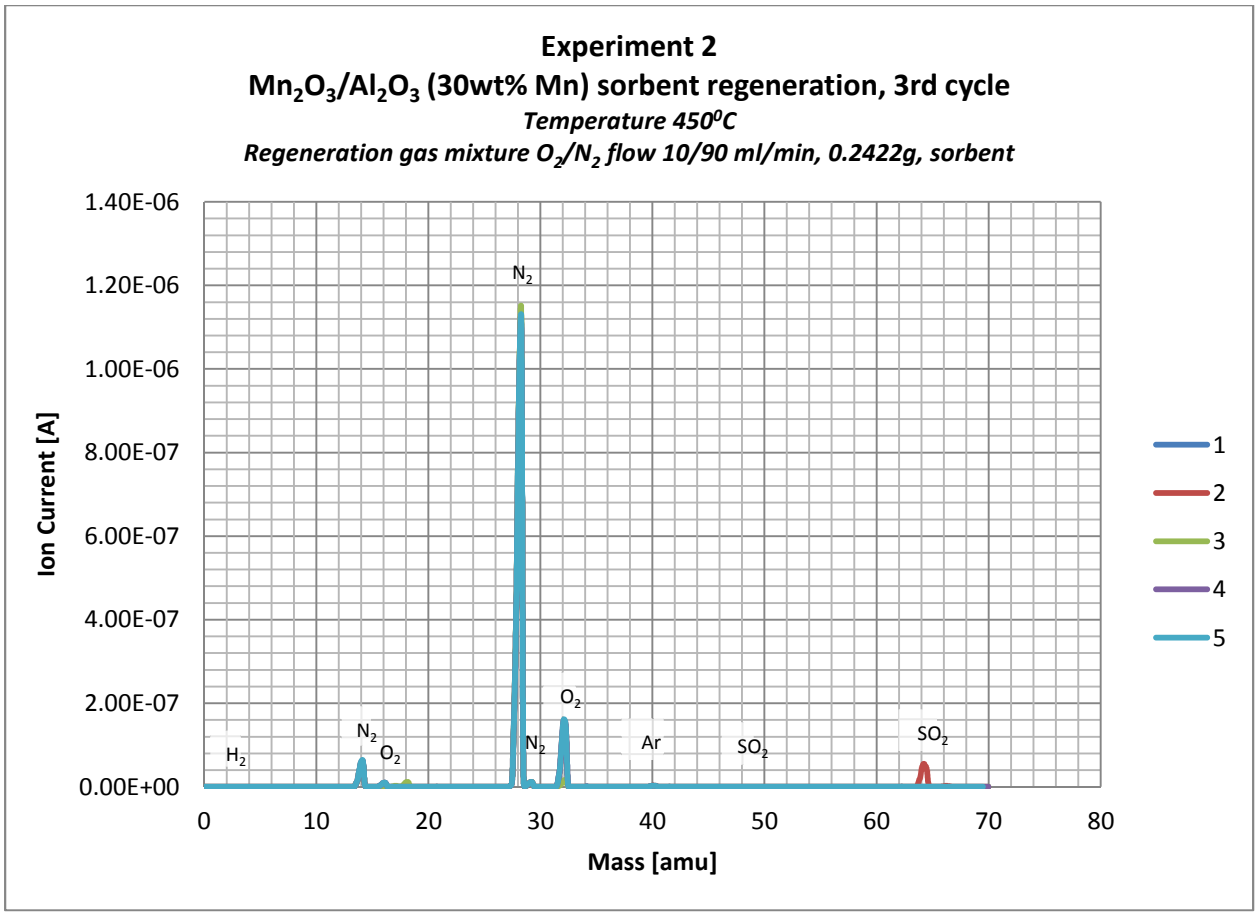
Experiment 2
Mn2O3/Al2O3 (30wt% Mn) sorbent regeneration, 3rd cycle
Temperature 450⁰C
Regeneration gas mixture O2/N2 flow 10/90 ml/min, 0.2422g, sorbent
Ion Current [A]
1.40E-06
1.20E-06
1.00E-06
8.00E-07
6.00E-07
4.00E-07
2.00E-07
0.00E+00
0
10
20
30
40
50
60
70
80
Mass [amu]
H2
N2
O2
N2
N2
O2
Ar
SO2
SO2
1
2
3
4
5

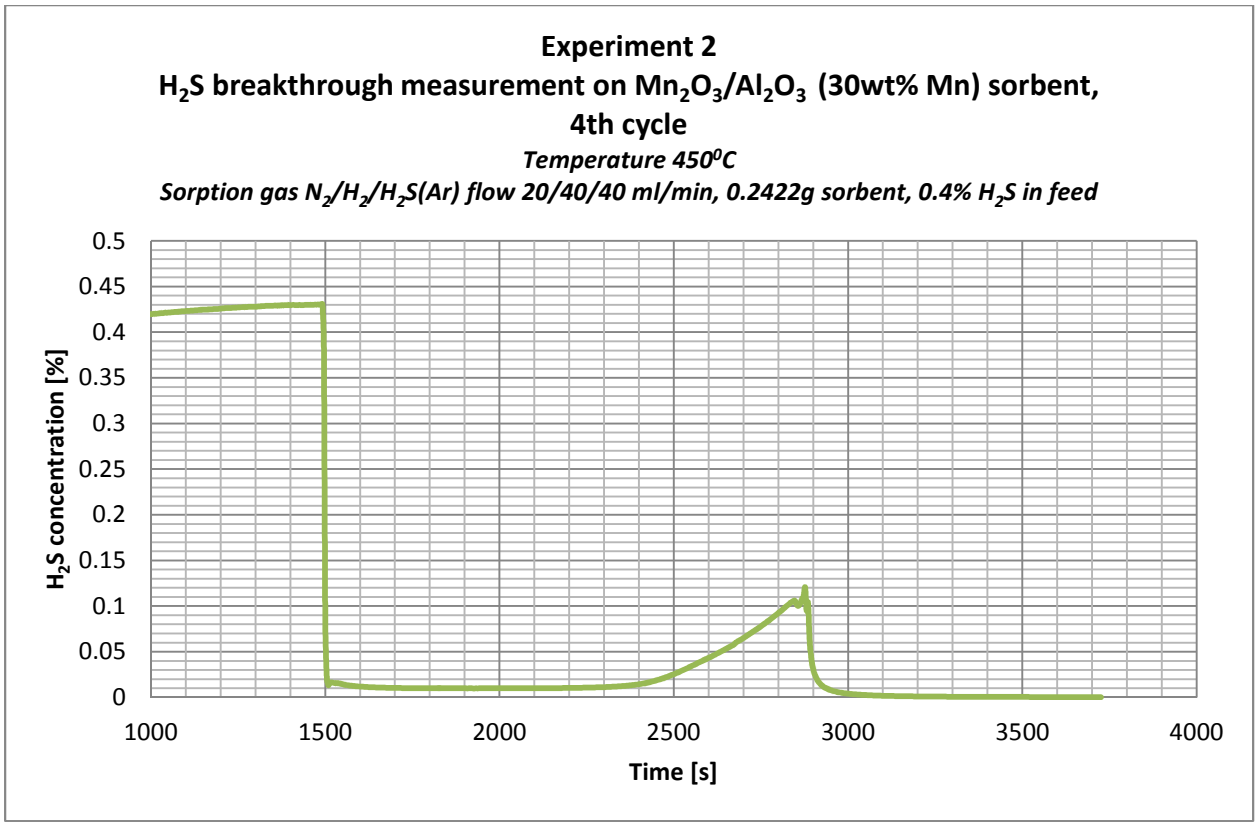
Experiment 2
H2S breakthrough measurement on Mn2O3/Al2O3 (30wt% Mn) sorbent, 4th cycle
Temperature 450⁰C
Sorption gas N2/H2/H2S(Ar) flow 20/40/40 ml/min, 0.2422g sorbent, 0.4% H2S in feed
H2S concentration [%]
0.5
0.45
0.4
0.35
0.3
0.25
0.2
0.15
0.1
0.05
0
1000
1500
2000
2500
3000
3500
4000
Time [s]

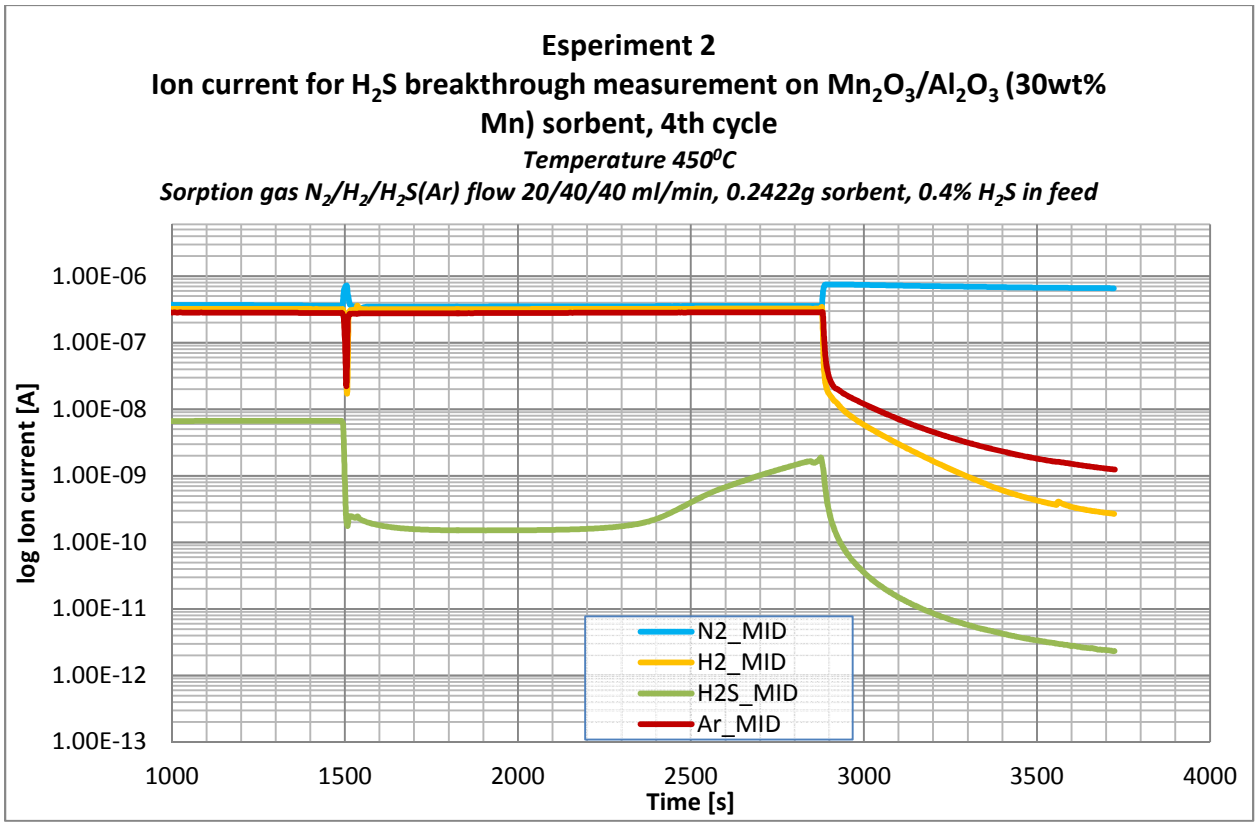
Esperiment 2
Ion current for H2S breakthrough measurement on Mn2O3/Al2O3 (30wt% Mn) sorbent, 4th cycle
Temperature 450⁰C
Sorption gas N2/H2/H2S(Ar) flow 20/40/40 ml/min, 0.2422g sorbent, 0.4% H2S in feed
log Ion current [A]
1.00E-06
1.00E-07
1.00E-08
1.00E-09
1.00E-10
1.00E-11
1.00E-12
1.00E-13
1000
1500
2000
2500
3000
3500
4000
Time [s]
N2_MID
H2_MID
H2S_MID
Ar_MID

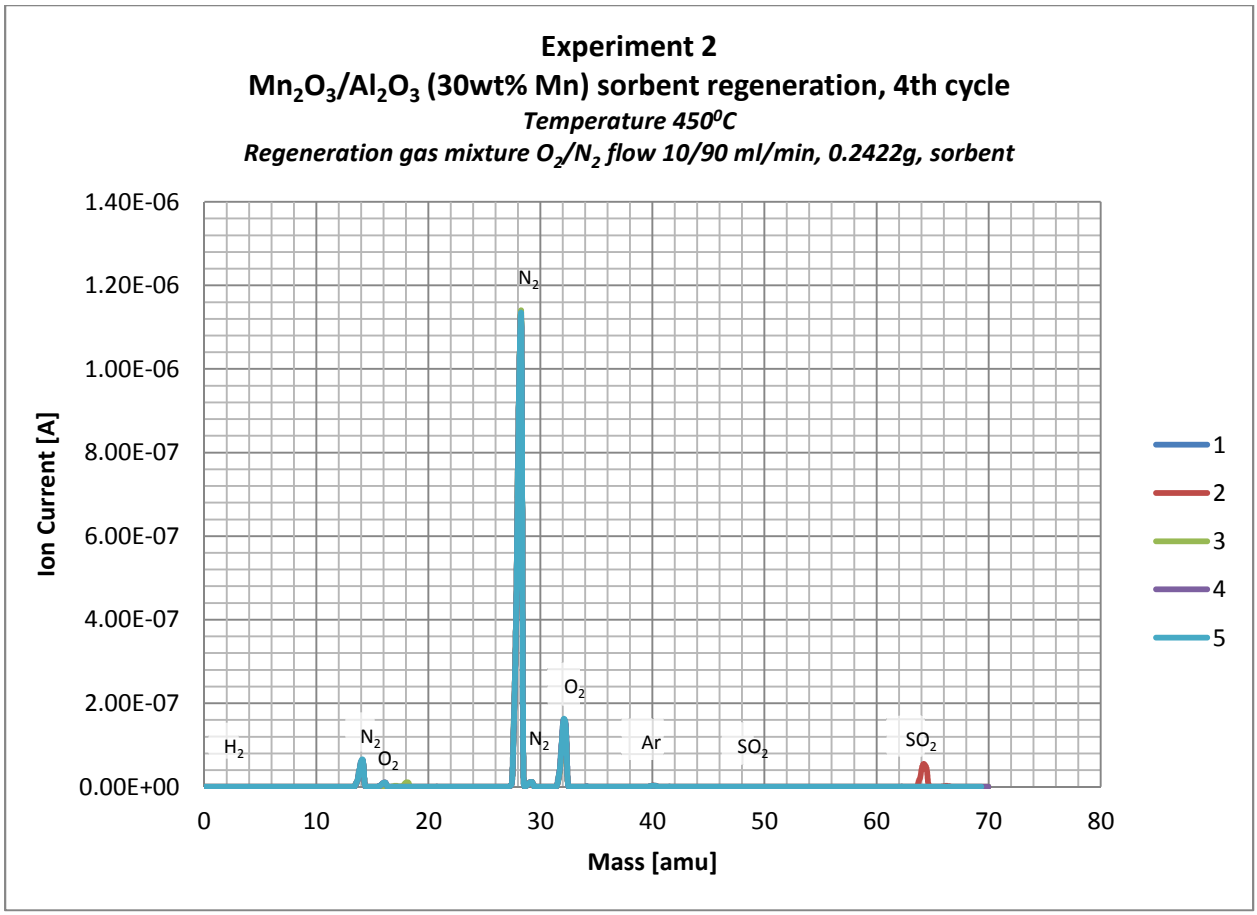
Experiment 2
Mn2O3/Al2O3 (30wt% Mn) sorbent regeneration, 4th cycle
Temperature 450⁰C
Regeneration gas mixture O2/N2 flow 10/90 ml/min, 0.2422g, sorbent
Ion Current [A]
1.40E-06
1.20E-06
1.00E-06
8.00E-07
6.00E-07
4.00E-07
2.00E-07
0.00E+00
0
10
20
30
40
50
60
70
80
Mass [amu]
N2
O2
H2
N2
O2
N2
Ar
SO2
SO2
1
2
3
4
5

**Experiment 2**

**$H_2S$ breakthrough measurement on $Mn_2O_3/Al_2O_3$ (30wt% Mn) sorbent, 5th cycle**

***Temperature 450$^0$C***

***Sorption gas $N_2/H_2/H_2S$(Ar) flow 20/40/40 ml/min, 0.2422g sorbent, 0.4% $H_2S$ in feed***

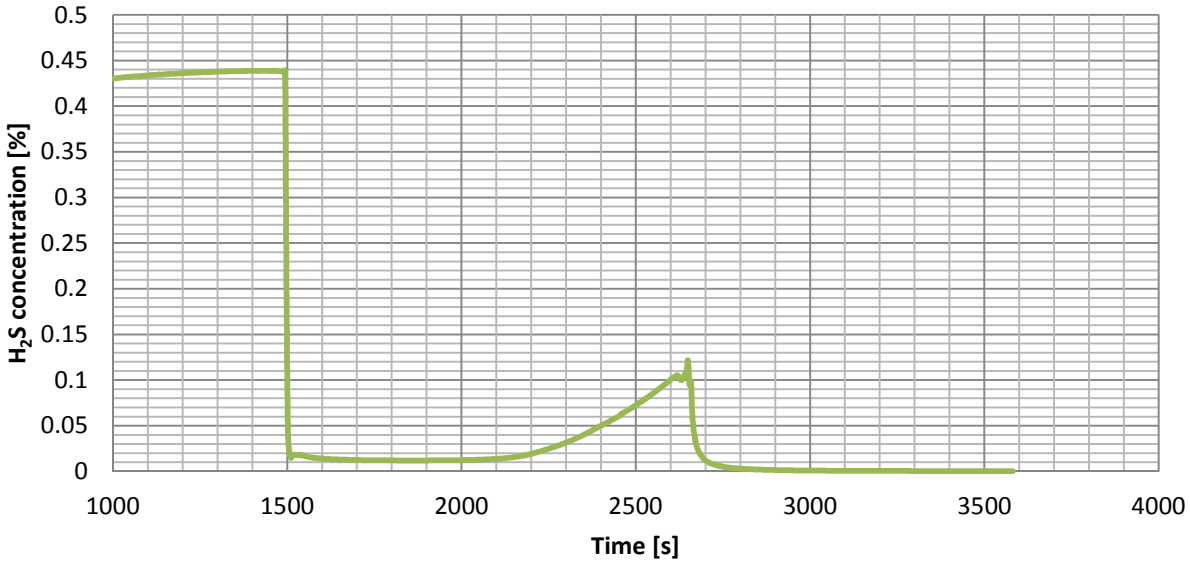


**Experiment 2**

**Ion current for $H_2S$ breakthrough measurement on $Mn_2O_3/Al_2O_3$ (30wt% Mn) sorbent, 5th cycle**

***Temperature 450$^0$C***

***Sorption gas $N_2/H_2/H_2S$(Ar) flow 20/40/40 ml/min, 0.2422g sorbent, 0.4% $H_2S$ in feed***

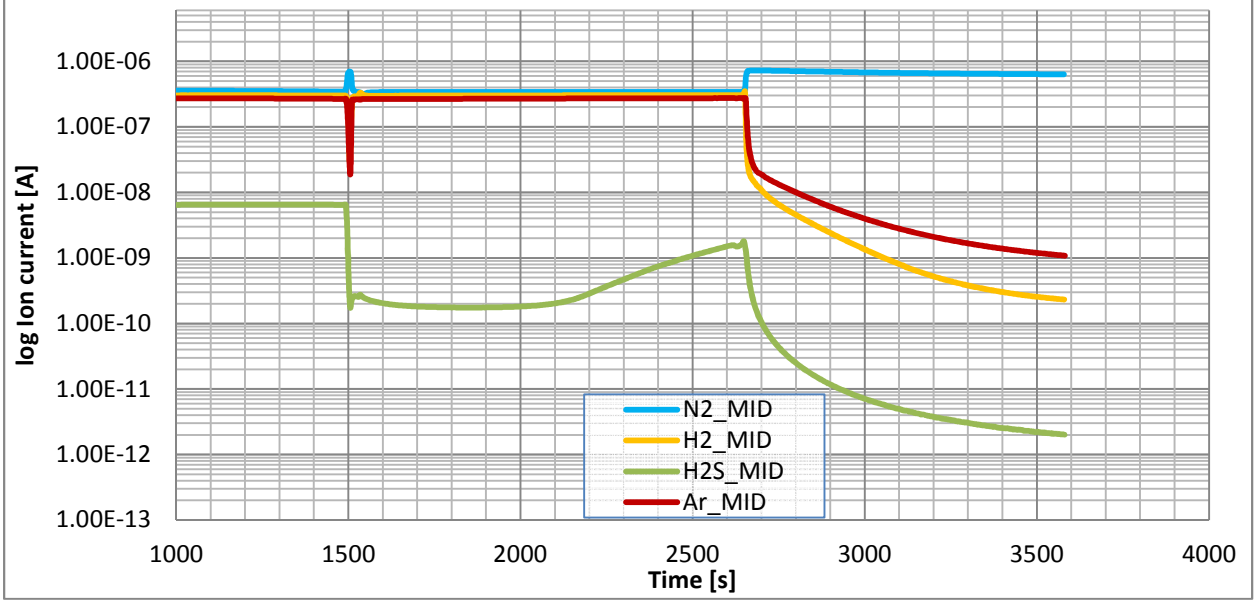

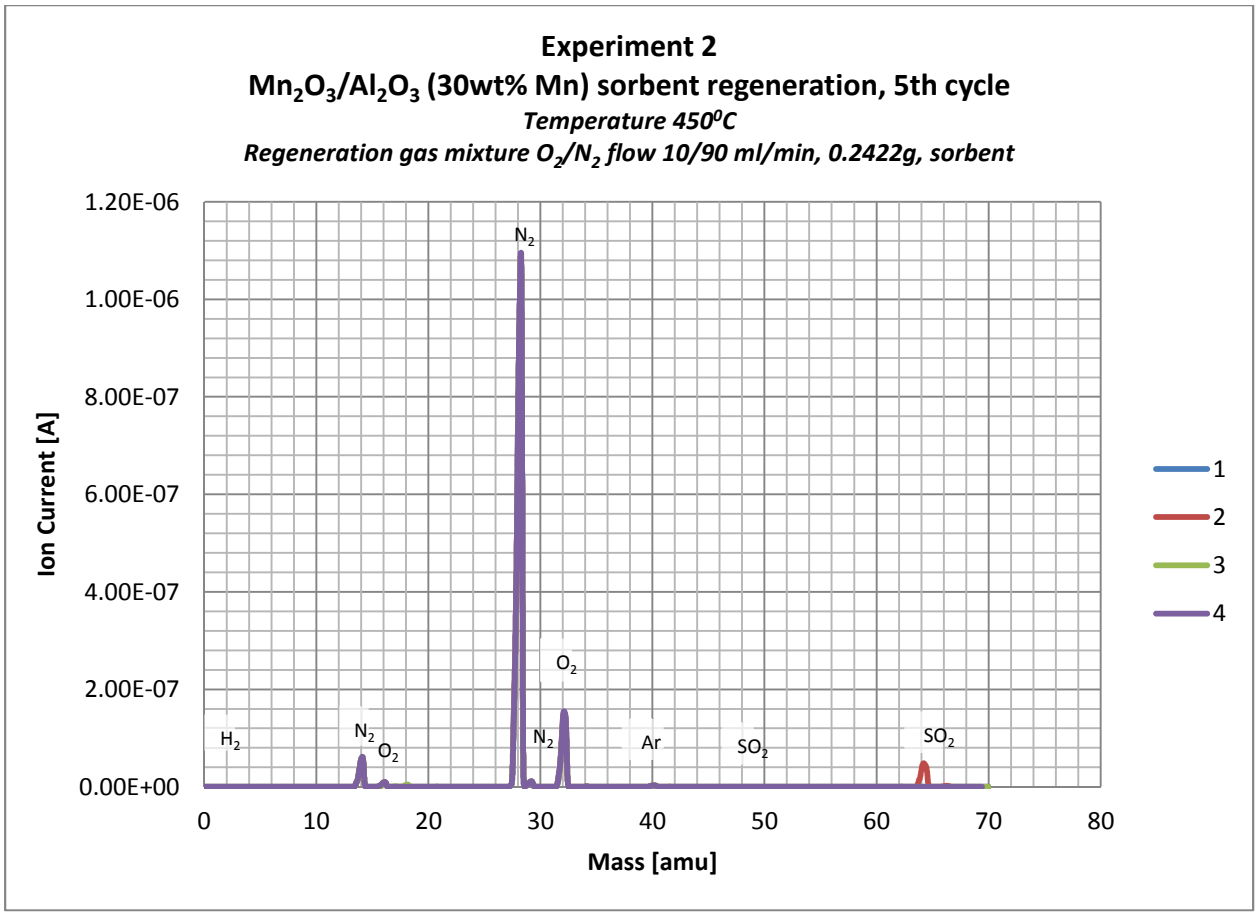
Experiment 2
Mn2O3/Al2O3 (30wt% Mn) sorbent regeneration, 5th cycle
Temperature 450⁰C
Regeneration gas mixture O2/N2 flow 10/90 ml/min, 0.2422g, sorbent
Ion Current [A]
1.20E-06
1.00E-06
8.00E-07
6.00E-07
4.00E-07
2.00E-07
0.00E+00
0
10
20
30
40
50
60
70
80
Mass [amu]
H2
N2
O2
N2
O2
N2
Ar
SO2
SO2
1
2
3
4

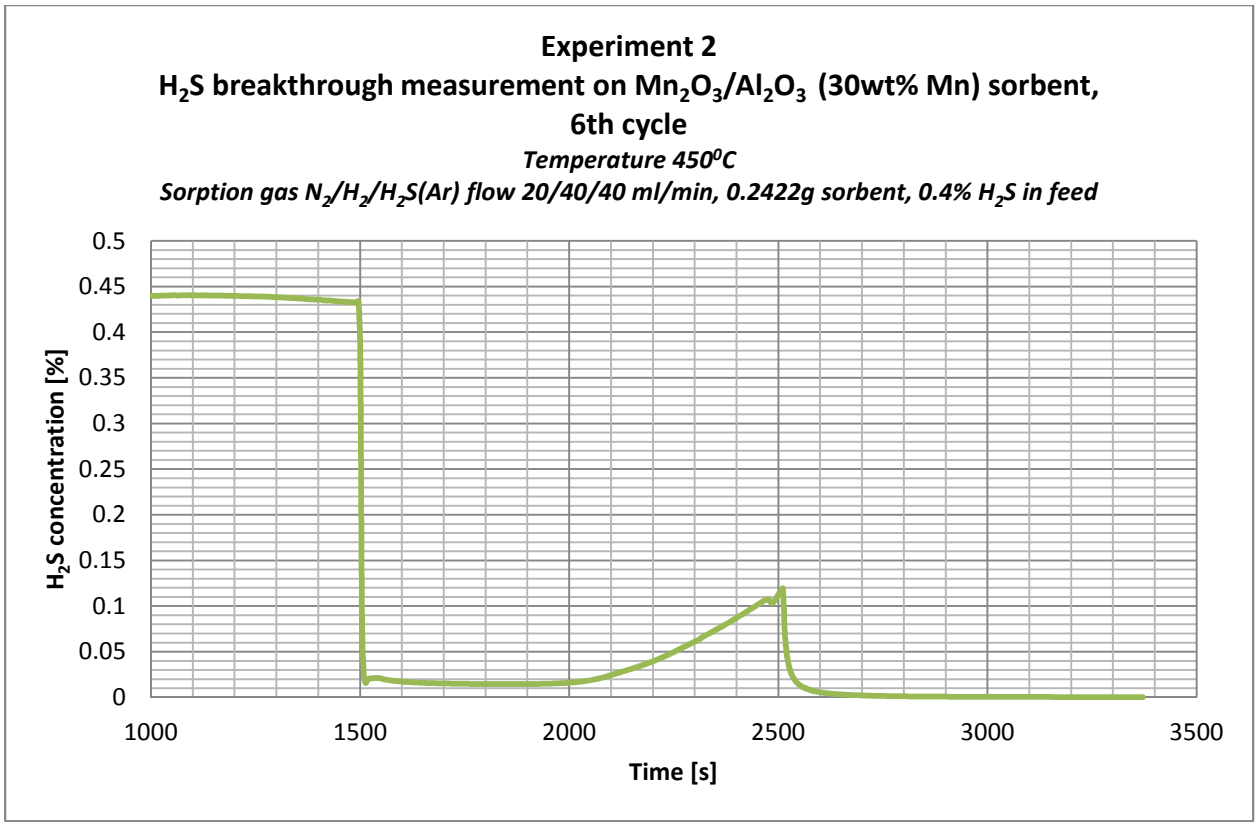
Experiment 2
H2S breakthrough measurement on Mn2O3/Al2O3 (30wt% Mn) sorbent, 6th cycle
Temperature 450⁰C
Sorption gas N2/H2/H2S(Ar) flow 20/40/40 ml/min, 0.2422g sorbent, 0.4% H2S in feed
H2S concentration [%]
0.5
0.45
0.4
0.35
0.3
0.25
0.2
0.15
0.1
0.05
0
1000
1500
2000
2500
3000
3500
Time [s]

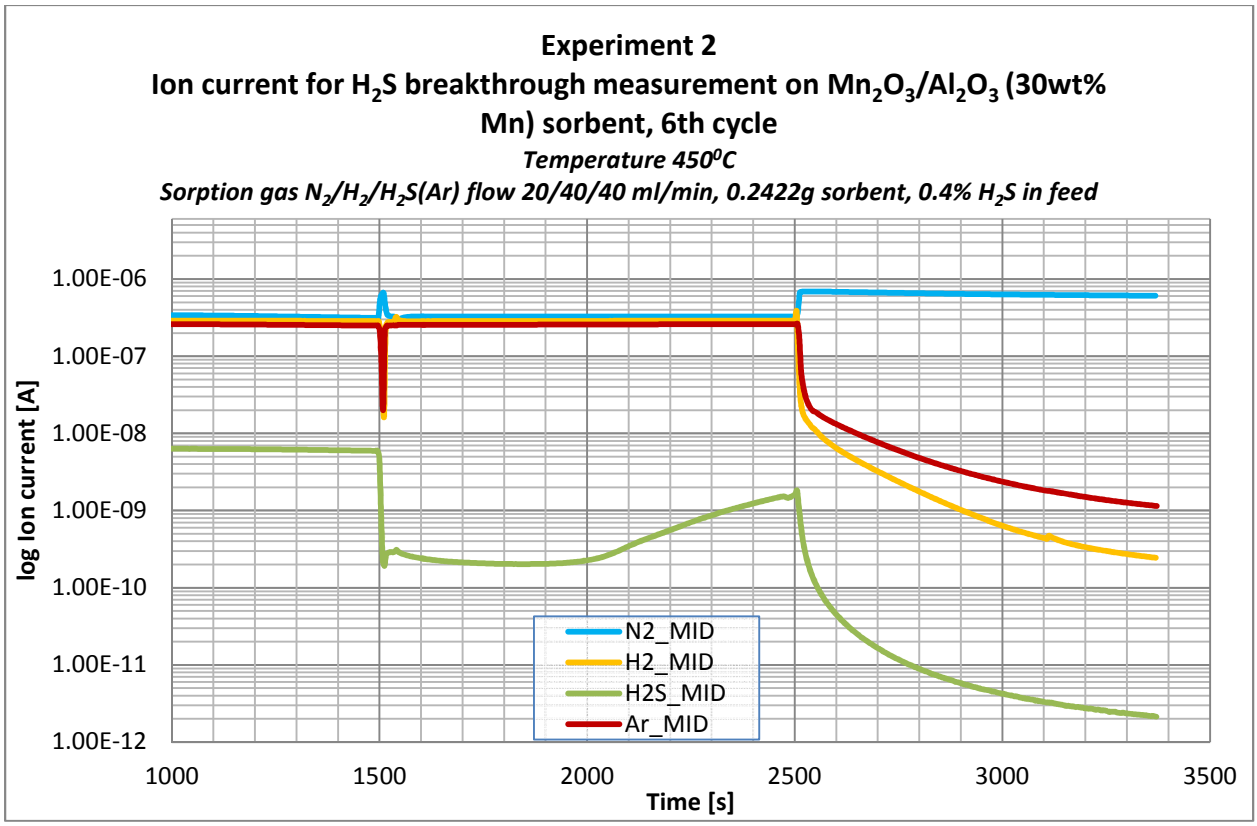
Experiment 2
Ion current for H2S breakthrough measurement on Mn2O3/Al2O3 (30wt% Mn) sorbent, 6th cycle
Temperature 450⁰C
Sorption gas N2/H2/H2S(Ar) flow 20/40/40 ml/min, 0.2422g sorbent, 0.4% H2S in feed
log Ion current [A]
1.00E-06
1.00E-07
1.00E-08
1.00E-09
1.00E-10
1.00E-11
1.00E-12
1000
1500
2000
2500
3000
3500
Time [s]
N2_MID
H2_MID
H2S_MID
Ar_MID

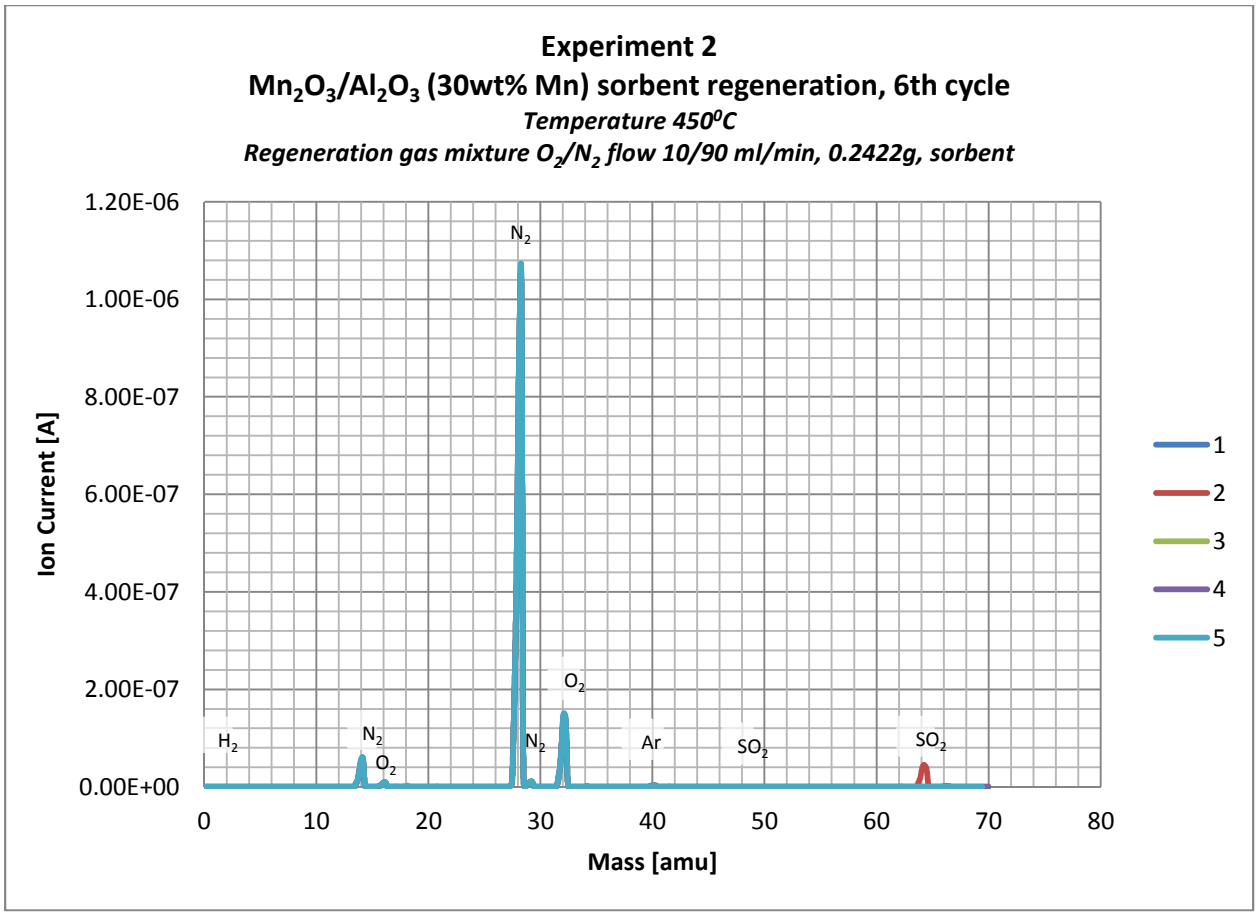
Experiment 2
Mn2O3/Al2O3 (30wt% Mn) sorbent regeneration, 6th cycle
Temperature 450⁰C
Regeneration gas mixture O2/N2 flow 10/90 ml/min, 0.2422g, sorbent
Ion Current [A]
1.20E-06
1.00E-06
8.00E-07
6.00E-07
4.00E-07
2.00E-07
0.00E+00
0
10
20
30
40
50
60
70
80
Mass [amu]
N2
O2
H2
N2
O2
N2
Ar
SO2
SO2
1
2
3
4
5

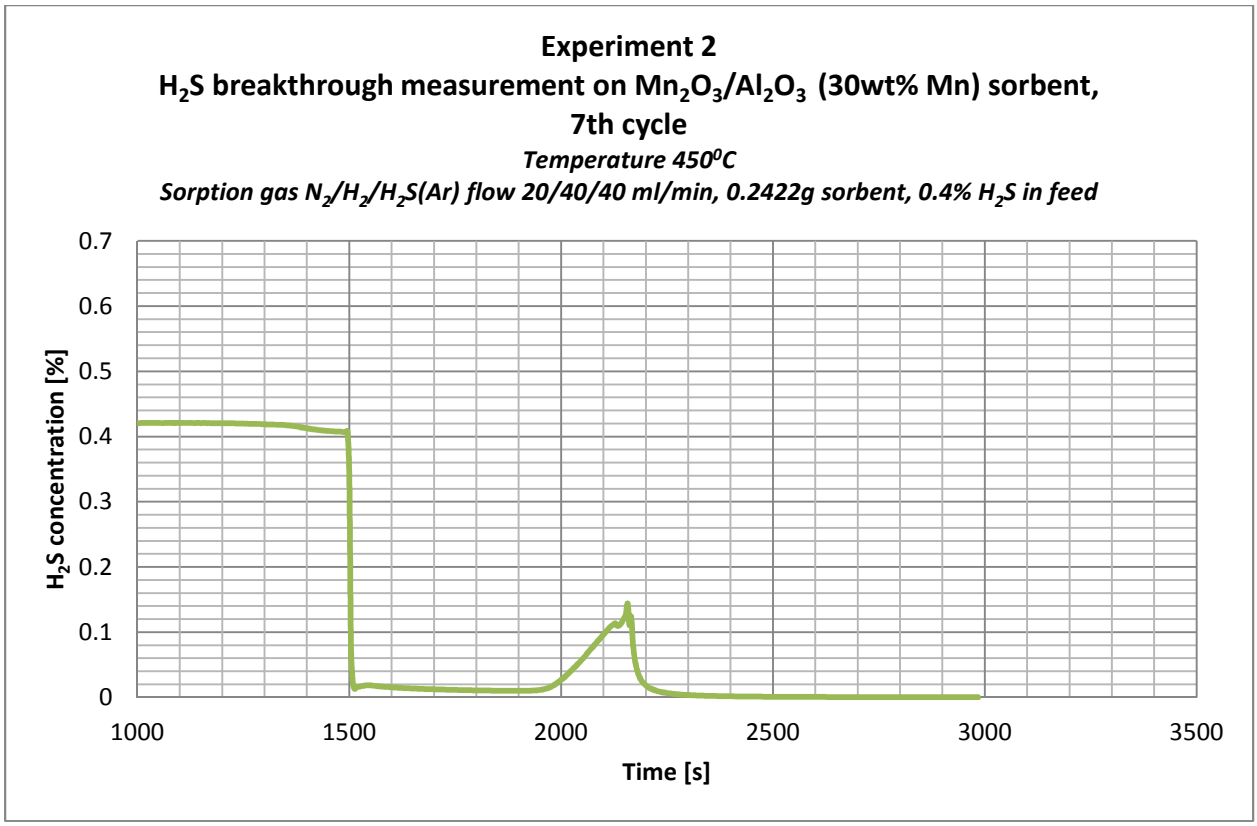
Experiment 2
H2S breakthrough measurement on Mn2O3/Al2O3 (30wt% Mn) sorbent, 7th cycle
Temperature 450⁰C
Sorption gas N2/H2/H2S(Ar) flow 20/40/40 ml/min, 0.2422g sorbent, 0.4% H2S in feed
H2S concentration [%]
0.7
0.6
0.5
0.4
0.3
0.2
0.1
0
1000
1500
2000
2500
3000
3500
Time [s]

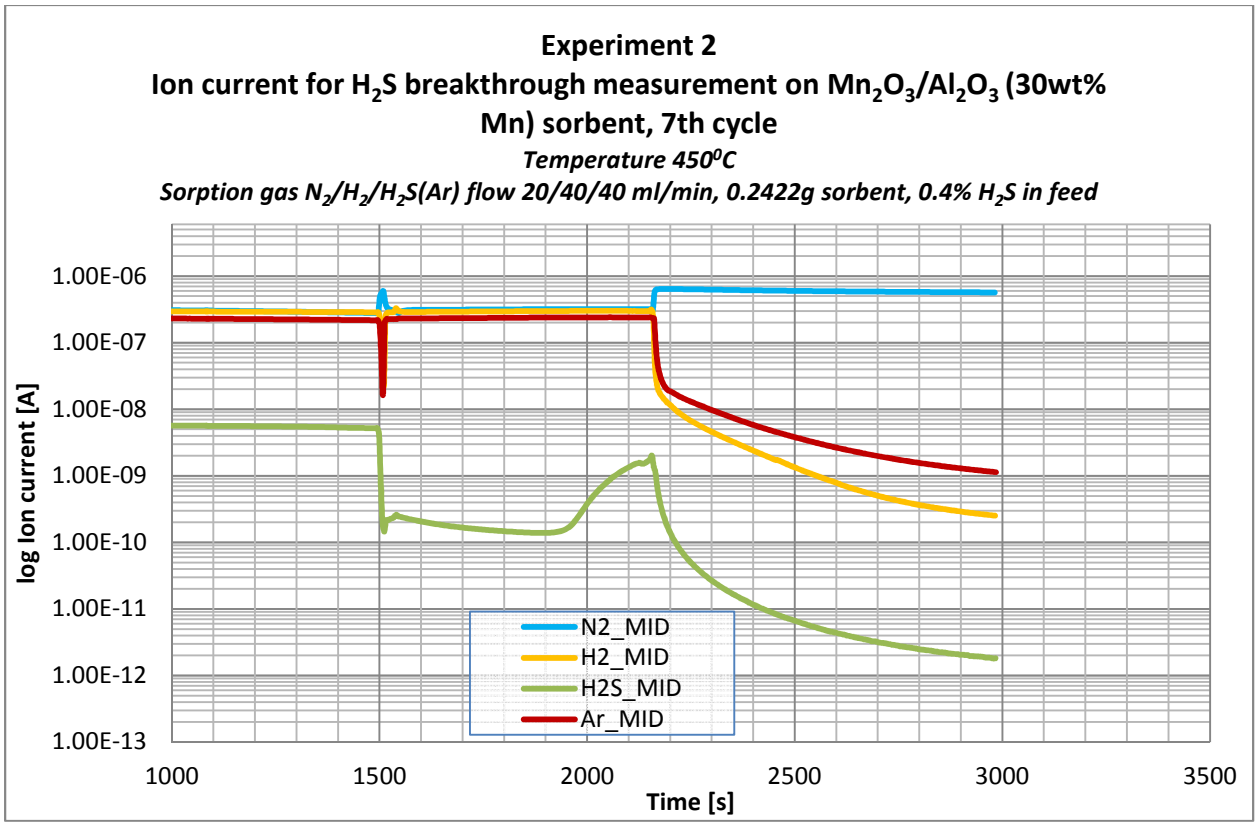
Experiment 2
Ion current for H2S breakthrough measurement on Mn2O3/Al2O3 (30wt% Mn) sorbent, 7th cycle
Temperature 450⁰C
Sorption gas N2/H2/H2S(Ar) flow 20/40/40 ml/min, 0.2422g sorbent, 0.4% H2S in feed
log Ion current [A]
1.00E-06
1.00E-07
1.00E-08
1.00E-09
1.00E-10
1.00E-11
1.00E-12
1.00E-13
1000
1500
2000
2500
3000
3500
Time [s]
N2_MID
H2_MID
H2S_MID
Ar_MID

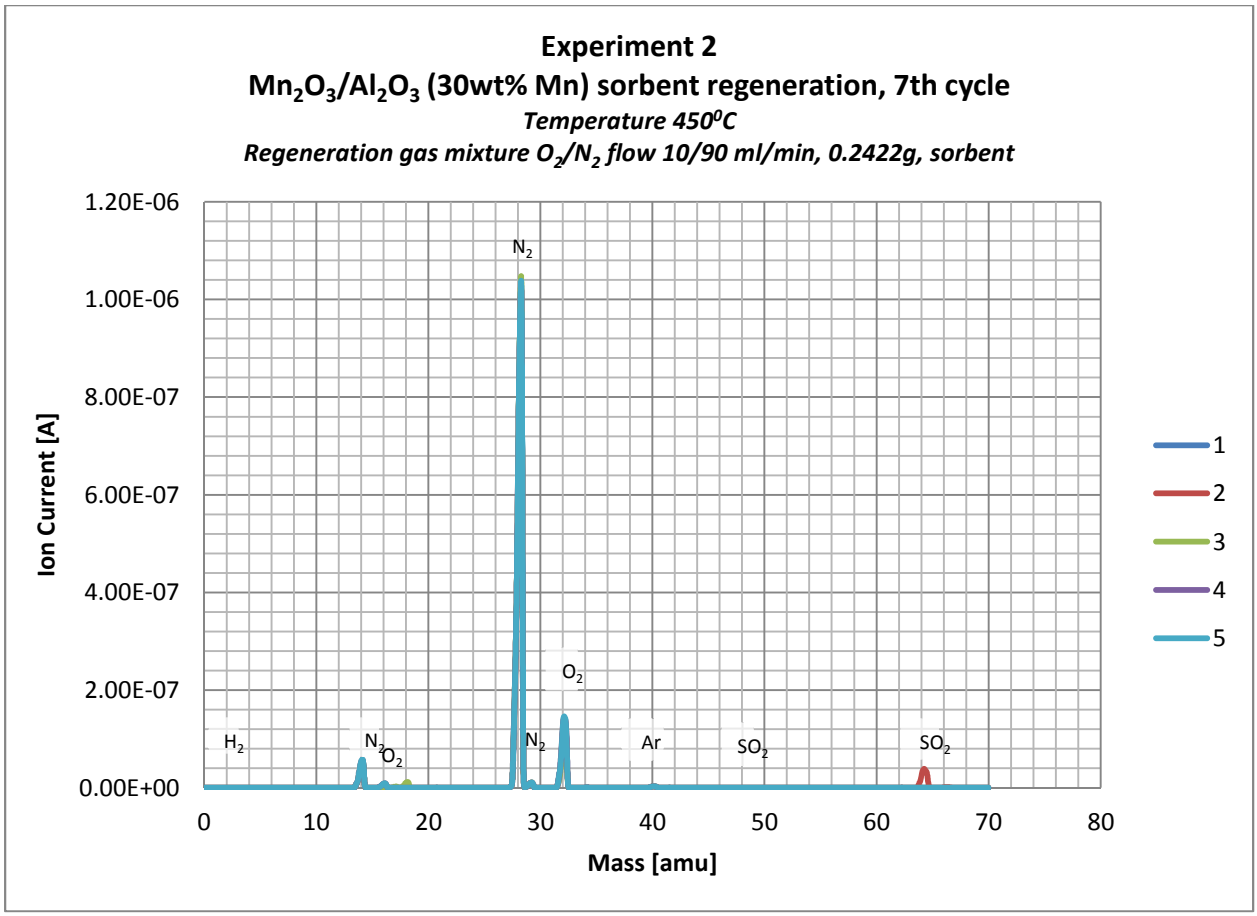
Experiment 2
Mn2O3/Al2O3 (30wt% Mn) sorbent regeneration, 7th cycle
Temperature 450⁰C
Regeneration gas mixture O2/N2 flow 10/90 ml/min, 0.2422g, sorbent
Ion Current [A]
1.20E-06
1.00E-06
8.00E-07
6.00E-07
4.00E-07
2.00E-07
0.00E+00
0
10
20
30
40
50
60
70
80
Mass [amu]
N2
O2
H2
N2
O2
N2
Ar
SO2
SO2
1
2
3
4
5

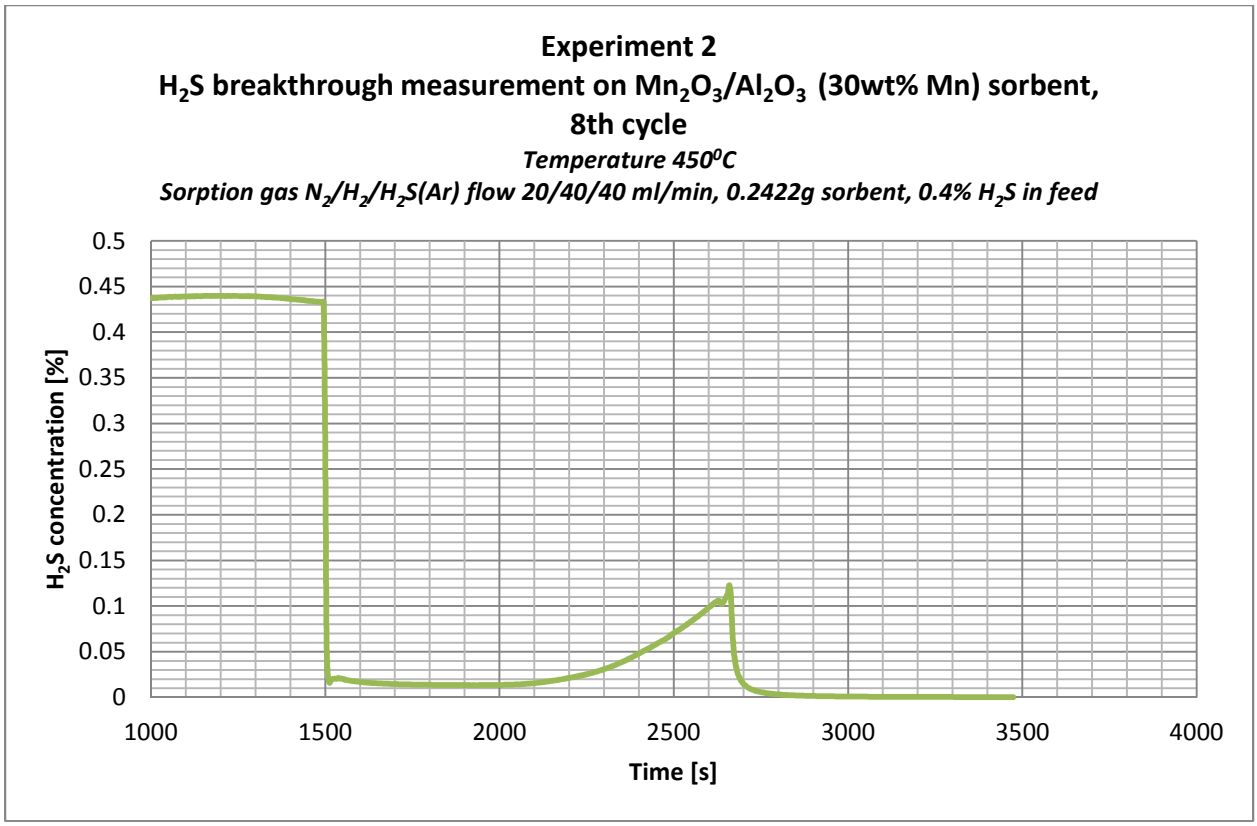
Experiment 2
H2S breakthrough measurement on Mn2O3/Al2O3 (30wt% Mn) sorbent, 8th cycle
Temperature 450⁰C
Sorption gas N2/H2/H2S(Ar) flow 20/40/40 ml/min, 0.2422g sorbent, 0.4% H2S in feed
H2S concentration [%]
0.5
0.45
0.4
0.35
0.3
0.25
0.2
0.15
0.1
0.05
0
1000
1500
2000
2500
3000
3500
4000
Time [s]

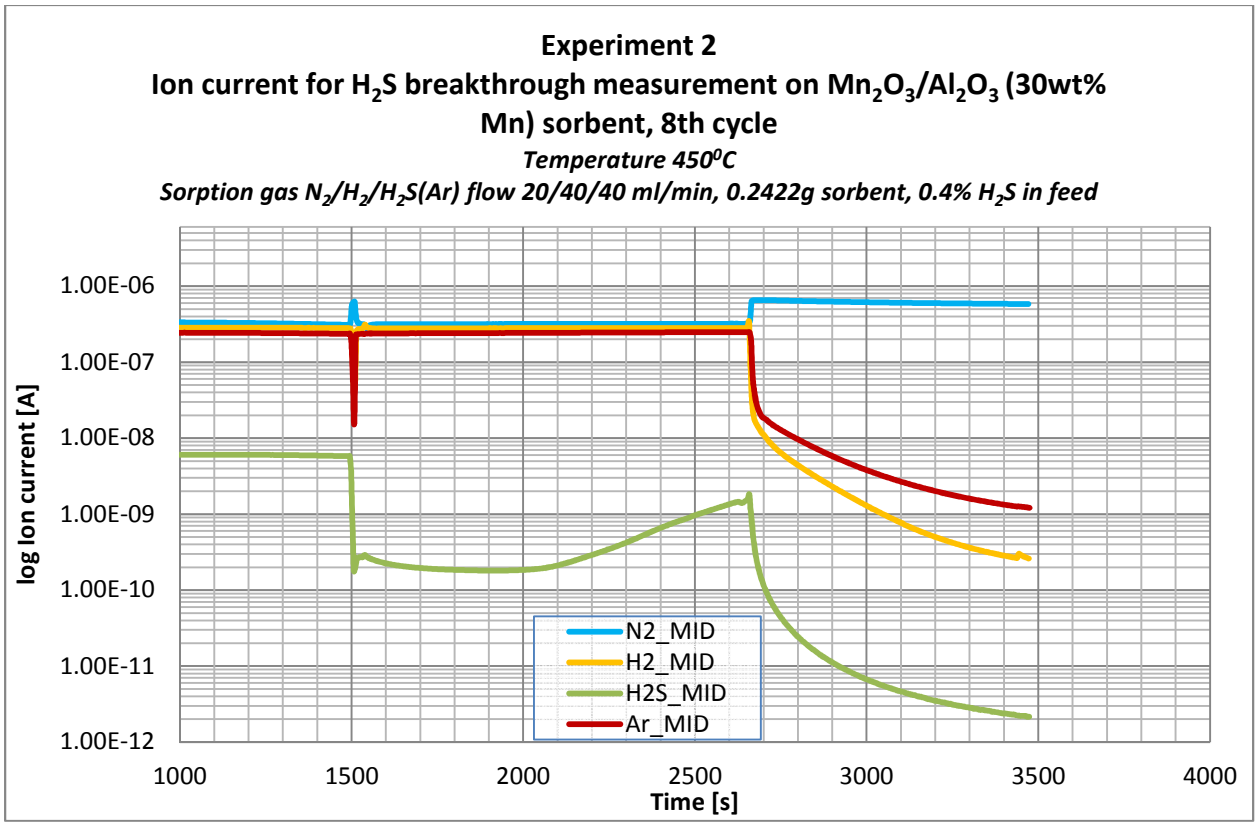
Experiment 2
Ion current for H2S breakthrough measurement on Mn2O3/Al2O3 (30wt% Mn) sorbent, 8th cycle
Temperature 450⁰C
Sorption gas N2/H2/H2S(Ar) flow 20/40/40 ml/min, 0.2422g sorbent, 0.4% H2S in feed
log Ion current [A]
1.00E-06
1.00E-07
1.00E-08
1.00E-09
1.00E-10
1.00E-11
1.00E-12
1000
1500
2000
2500
3000
3500
4000
Time [s]
N2_MID
H2_MID
H2S_MID
Ar_MID

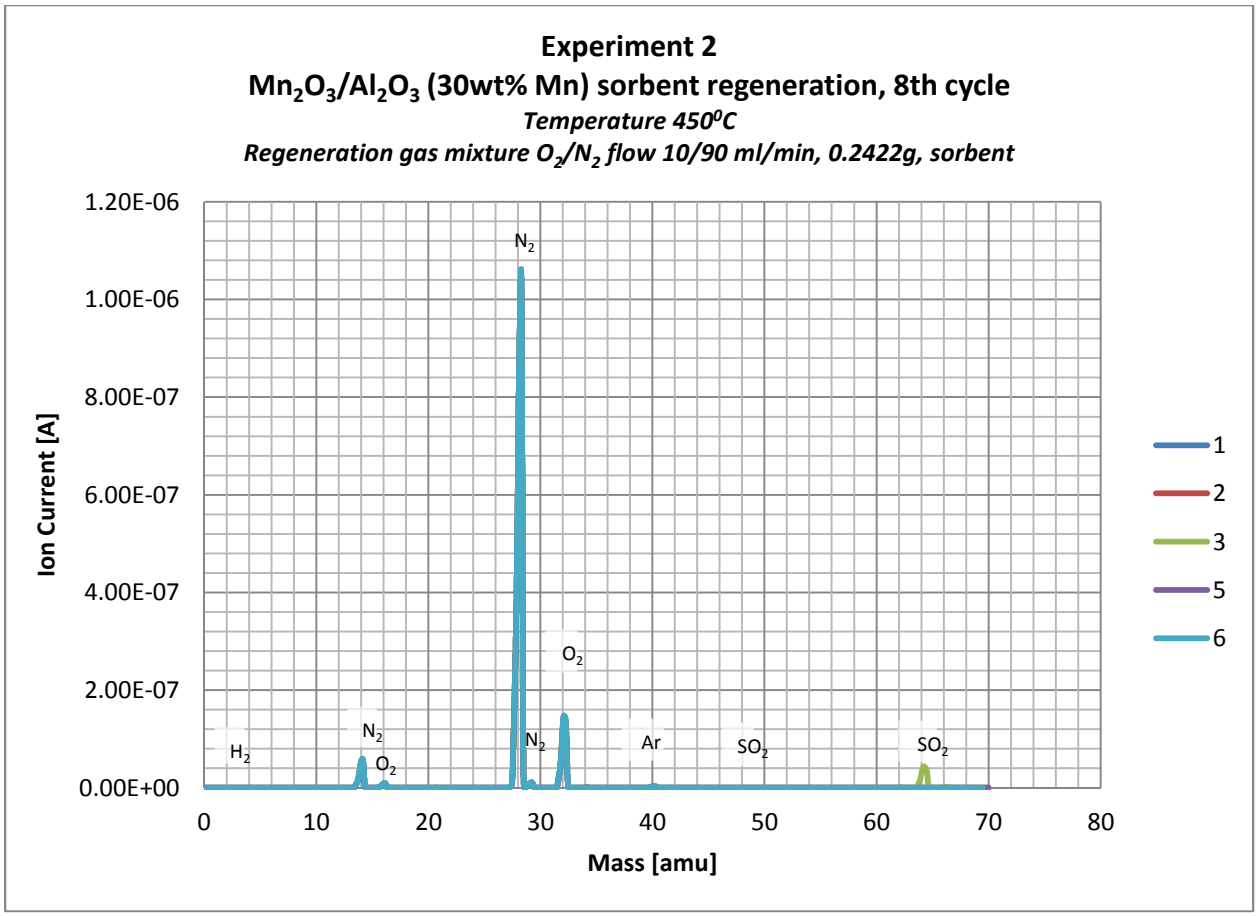
Experiment 2
Mn2O3/Al2O3 (30wt% Mn) sorbent regeneration, 8th cycle
Temperature 450⁰C
Regeneration gas mixture O2/N2 flow 10/90 ml/min, 0.2422g, sorbent
Ion Current [A]
1.20E-06
1.00E-06
8.00E-07
6.00E-07
4.00E-07
2.00E-07
0.00E+00
0
10
20
30
40
50
60
70
80
Mass [amu]
N2
O2
H2
N2
O2
N2
Ar
SO2
SO2
1
2
3
5
6

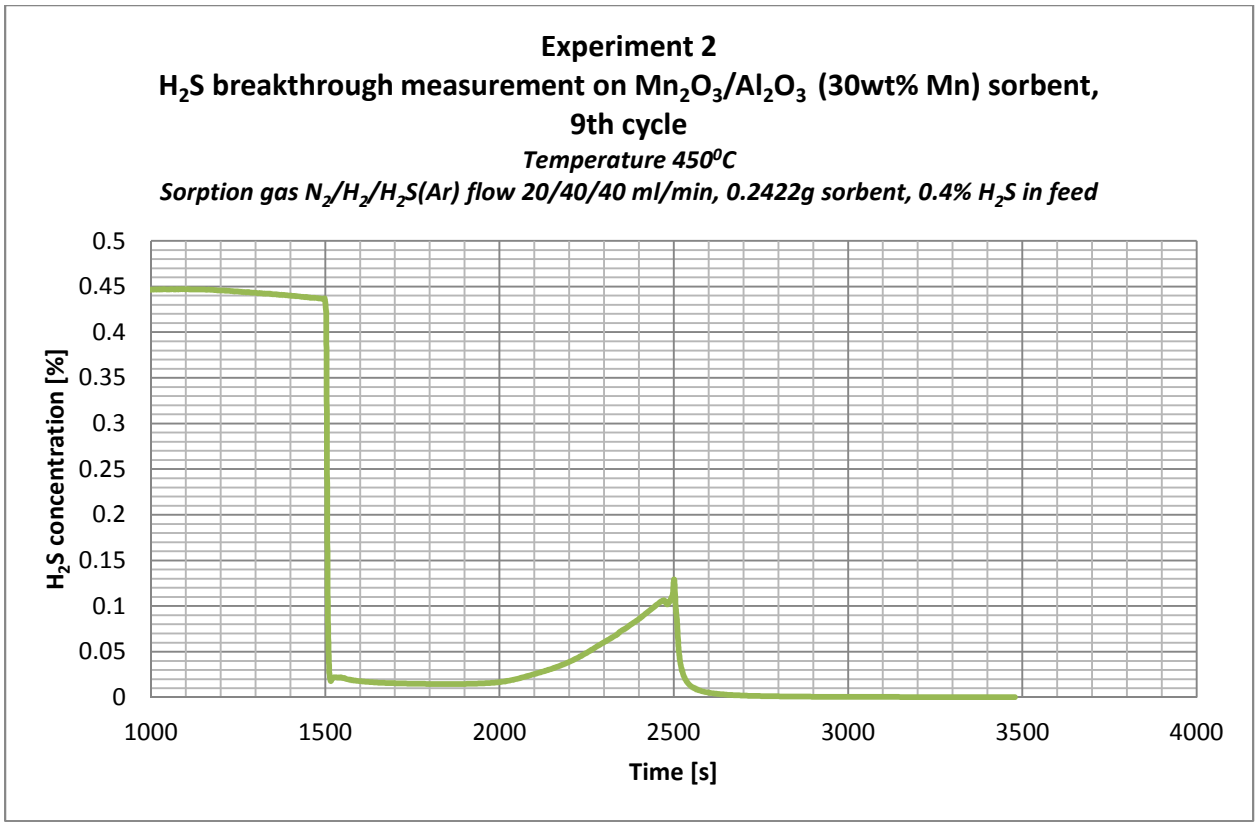
Experiment 2
H2S breakthrough measurement on Mn2O3/Al2O3 (30wt% Mn) sorbent, 9th cycle
Temperature 450⁰C
Sorption gas N2/H2/H2S(Ar) flow 20/40/40 ml/min, 0.2422g sorbent, 0.4% H2S in feed
H2S concentration [%]
0.5
0.45
0.4
0.35
0.3
0.25
0.2
0.15
0.1
0.05
0
1000
1500
2000
2500
3000
3500
4000
Time [s]

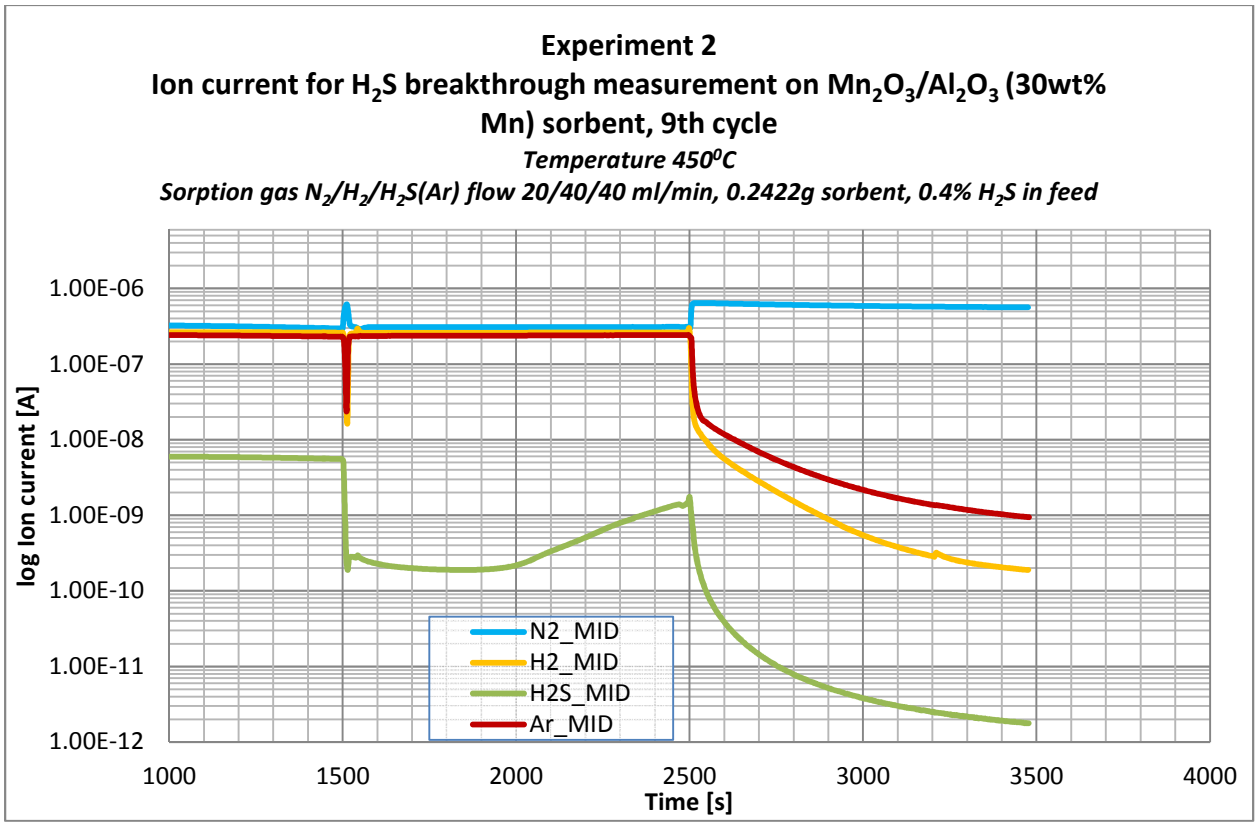
Experiment 2
Ion current for H2S breakthrough measurement on Mn2O3/Al2O3 (30wt% Mn) sorbent, 9th cycle
Temperature 450⁰C
Sorption gas N2/H2/H2S(Ar) flow 20/40/40 ml/min, 0.2422g sorbent, 0.4% H2S in feed
log Ion current [A]
1.00E-06
1.00E-07
1.00E-08
1.00E-09
1.00E-10
1.00E-11
1.00E-12
1000
1500
2000
2500
3000
3500
4000
Time [s]
N2_MID
H2_MID
H2S_MID
Ar_MID

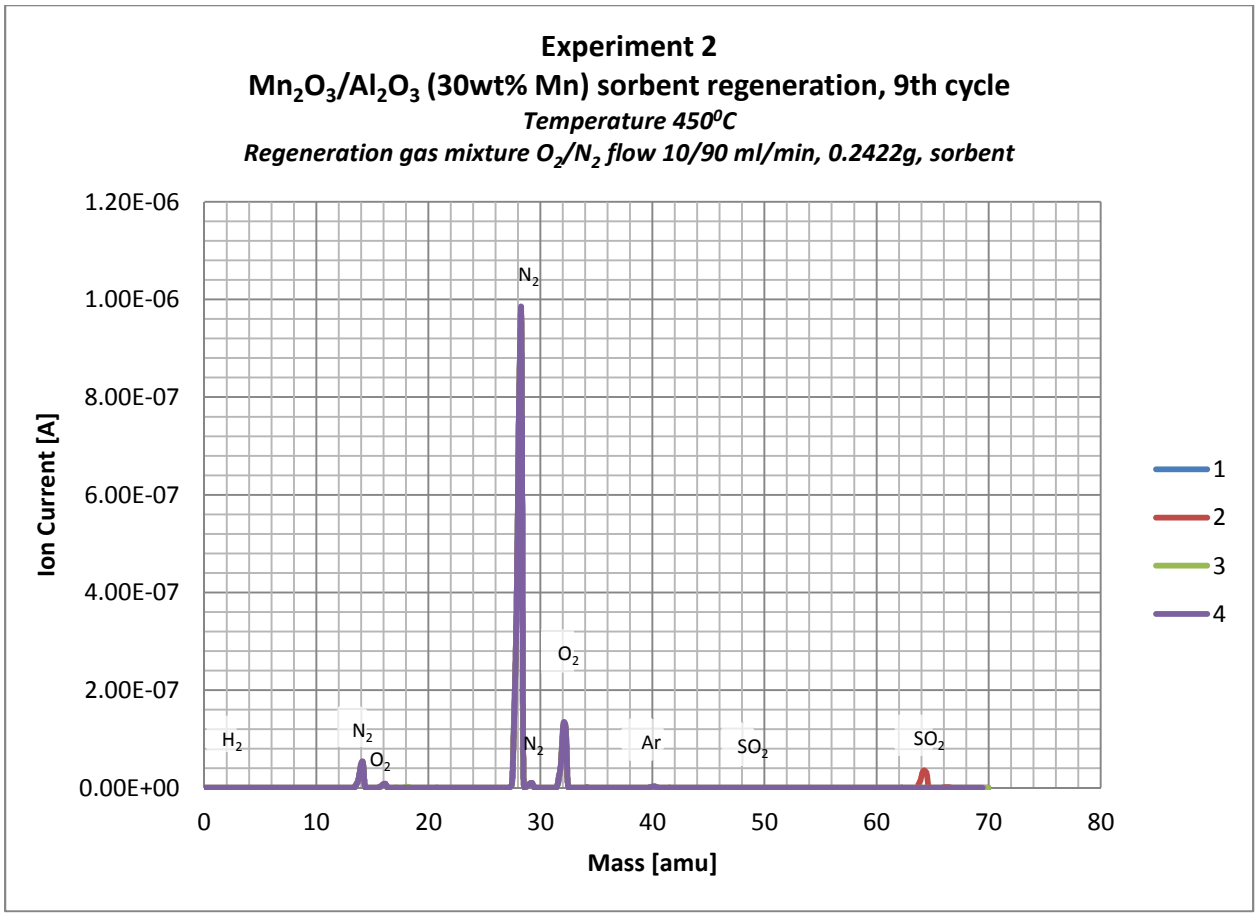
Experiment 2
Mn2O3/Al2O3 (30wt% Mn) sorbent regeneration, 9th cycle
Temperature 450⁰C
Regeneration gas mixture O2/N2 flow 10/90 ml/min, 0.2422g, sorbent
Ion Current [A]
1.20E-06
1.00E-06
8.00E-07
6.00E-07
4.00E-07
2.00E-07
0.00E+00
0
10
20
30
40
50
60
70
80
Mass [amu]
H2
N2
O2
N2
O2
Ar
SO2
SO2
1
2
3
4

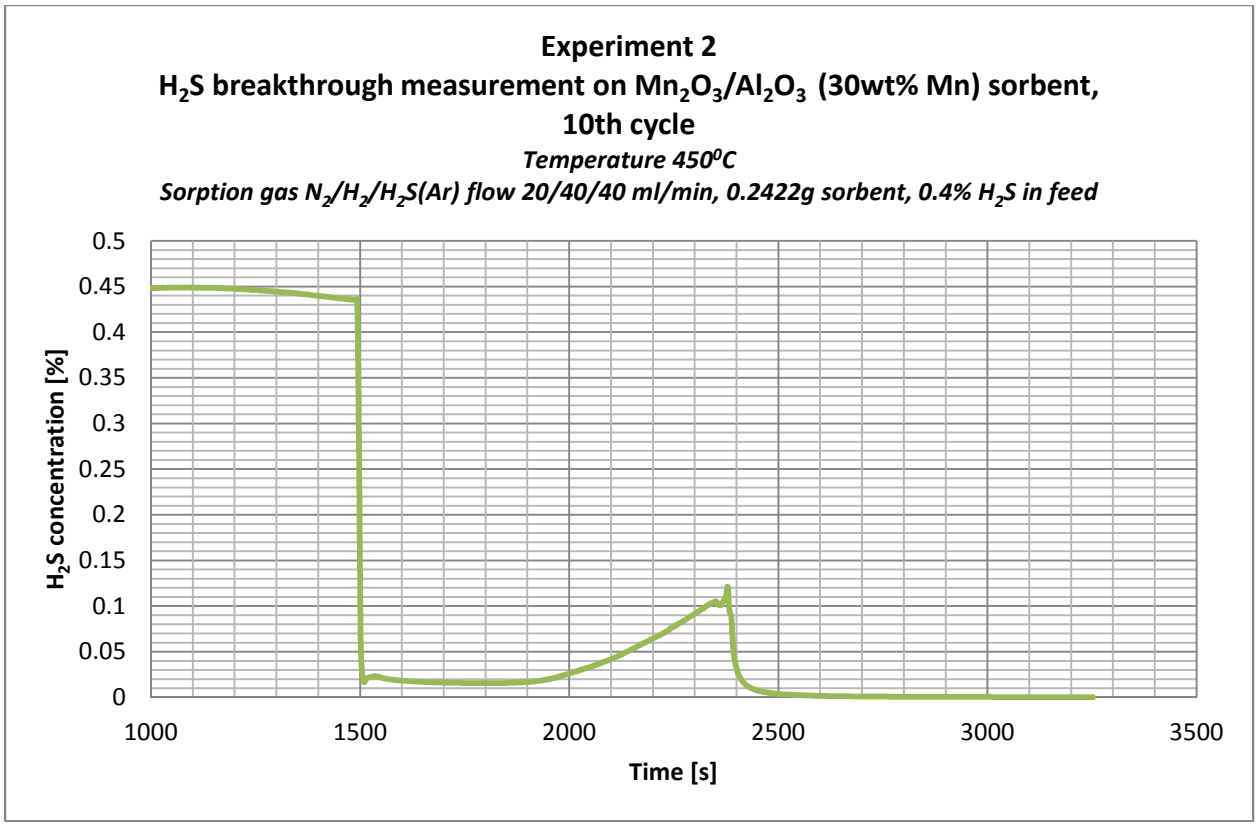
Experiment 2
H2S breakthrough measurement on Mn2O3/Al2O3 (30wt% Mn) sorbent, 10th cycle
Temperature 450⁰C
Sorption gas N2/H2/H2S(Ar) flow 20/40/40 ml/min, 0.2422g sorbent, 0.4% H2S in feed
H2S concentration [%]
0.5
0.45
0.4
0.35
0.3
0.25
0.2
0.15
0.1
0.05
0
1000
1500
2000
2500
3000
3500
Time [s]

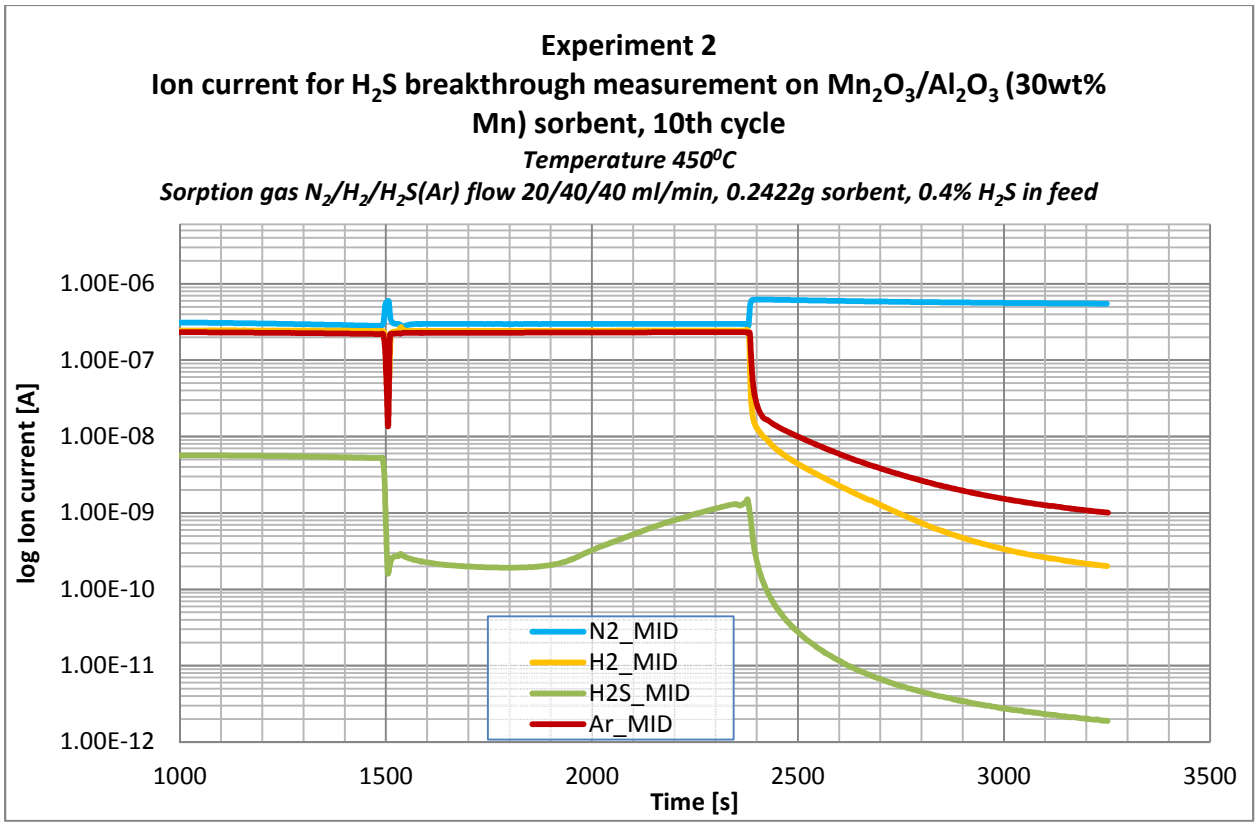
Experiment 2
Ion current for H2S breakthrough measurement on Mn2O3/Al2O3 (30wt% Mn) sorbent, 10th cycle
Temperature 450⁰C
Sorption gas N2/H2/H2S(Ar) flow 20/40/40 ml/min, 0.2422g sorbent, 0.4% H2S in feed
log Ion current [A]
1.00E-06
1.00E-07
1.00E-08
1.00E-09
1.00E-10
1.00E-11
1.00E-12
1000
1500
2000
2500
3000
3500
Time [s]
N2_MID
H2_MID
H2S_MID
Ar_MID

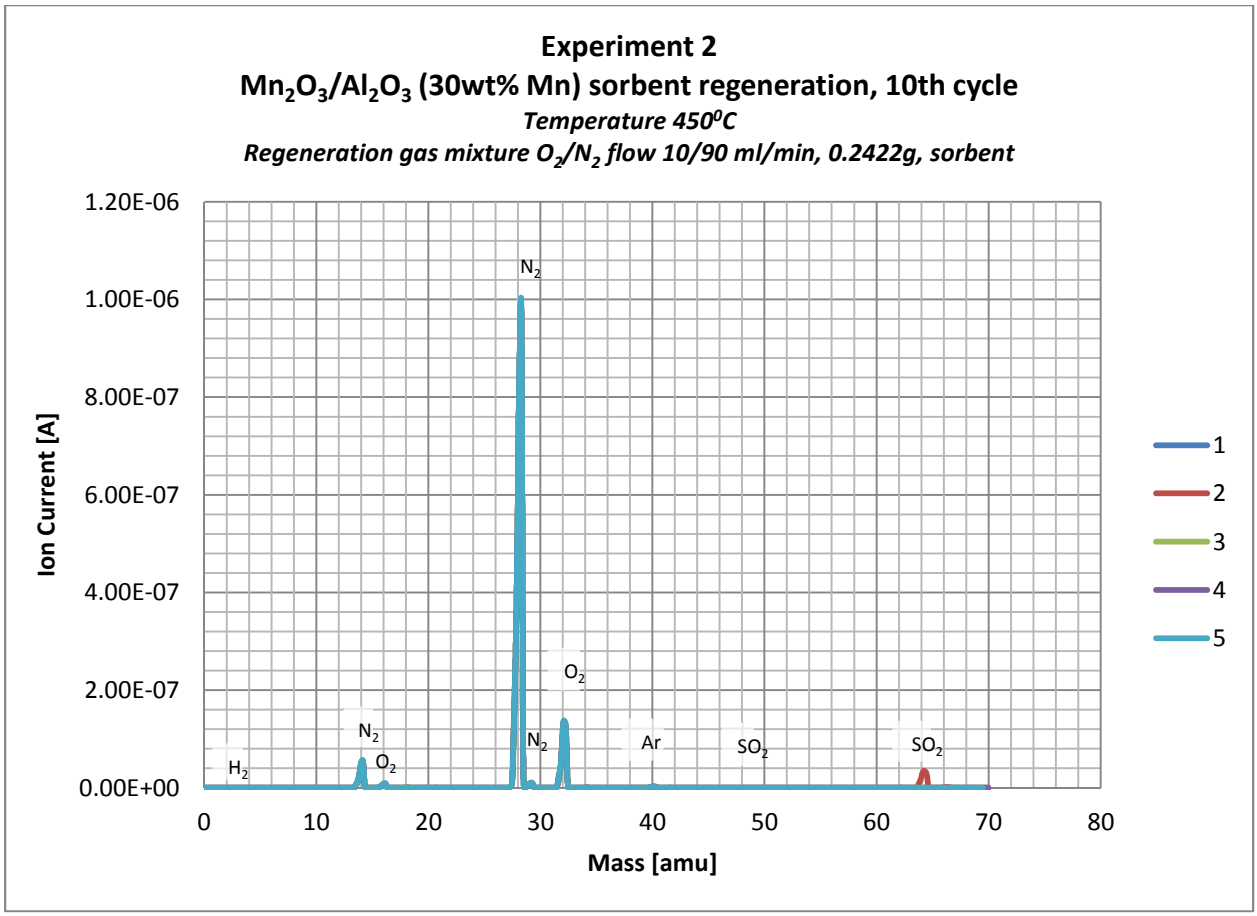
Experiment 2
Mn2O3/Al2O3 (30wt% Mn) sorbent regeneration, 10th cycle
Temperature 450⁰C
Regeneration gas mixture O2/N2 flow 10/90 ml/min, 0.2422g, sorbent
Ion Current [A]
1.20E-06
1.00E-06
8.00E-07
6.00E-07
4.00E-07
2.00E-07
0.00E+00
0
10
20
30
40
50
60
70
80
Mass [amu]
N2
O2
N2
N2
O2
H2
Ar
SO2
SO2
1
2
3
4
5

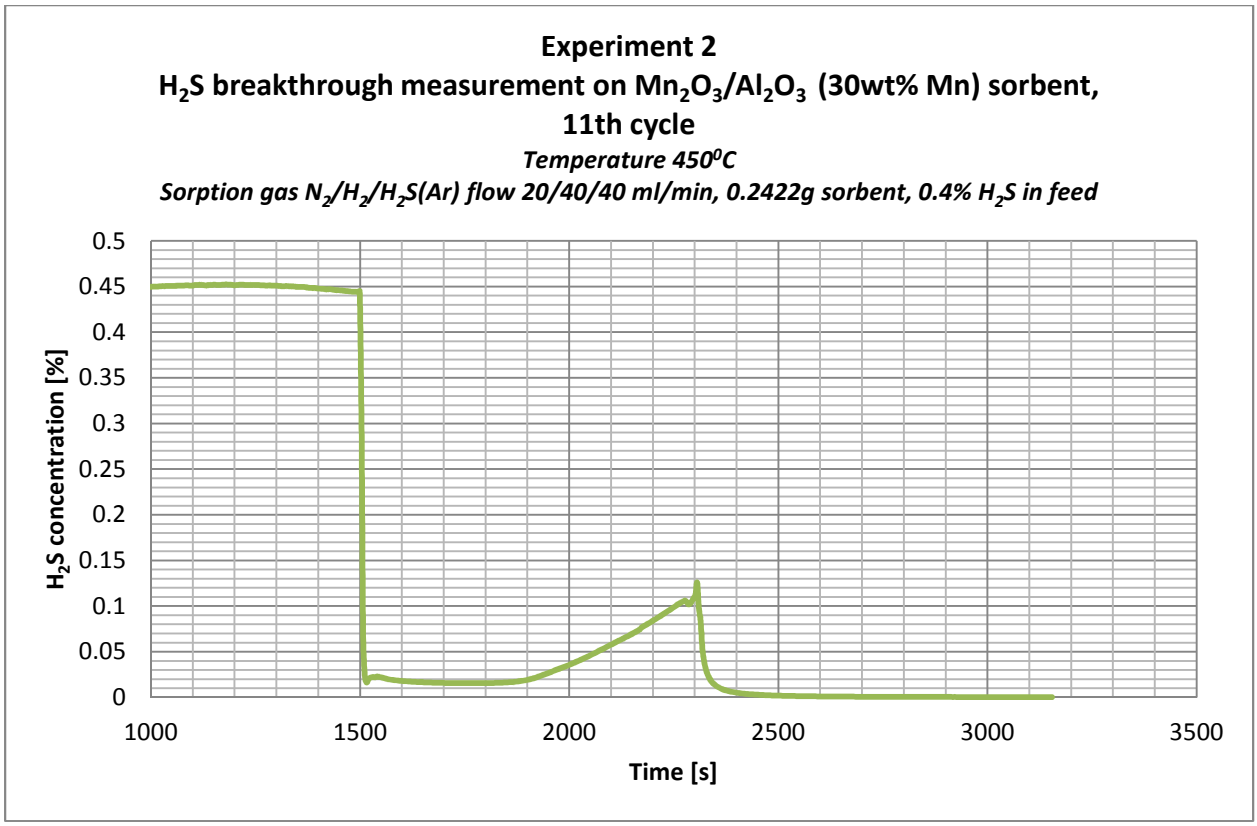
Experiment 2
H2S breakthrough measurement on Mn2O3/Al2O3 (30wt% Mn) sorbent, 11th cycle
Temperature 450⁰C
Sorption gas N2/H2/H2S(Ar) flow 20/40/40 ml/min, 0.2422g sorbent, 0.4% H2S in feed
H2S concentration [%]
0.5
0.45
0.4
0.35
0.3
0.25
0.2
0.15
0.1
0.05
0
1000
1500
2000
2500
3000
3500
Time [s]

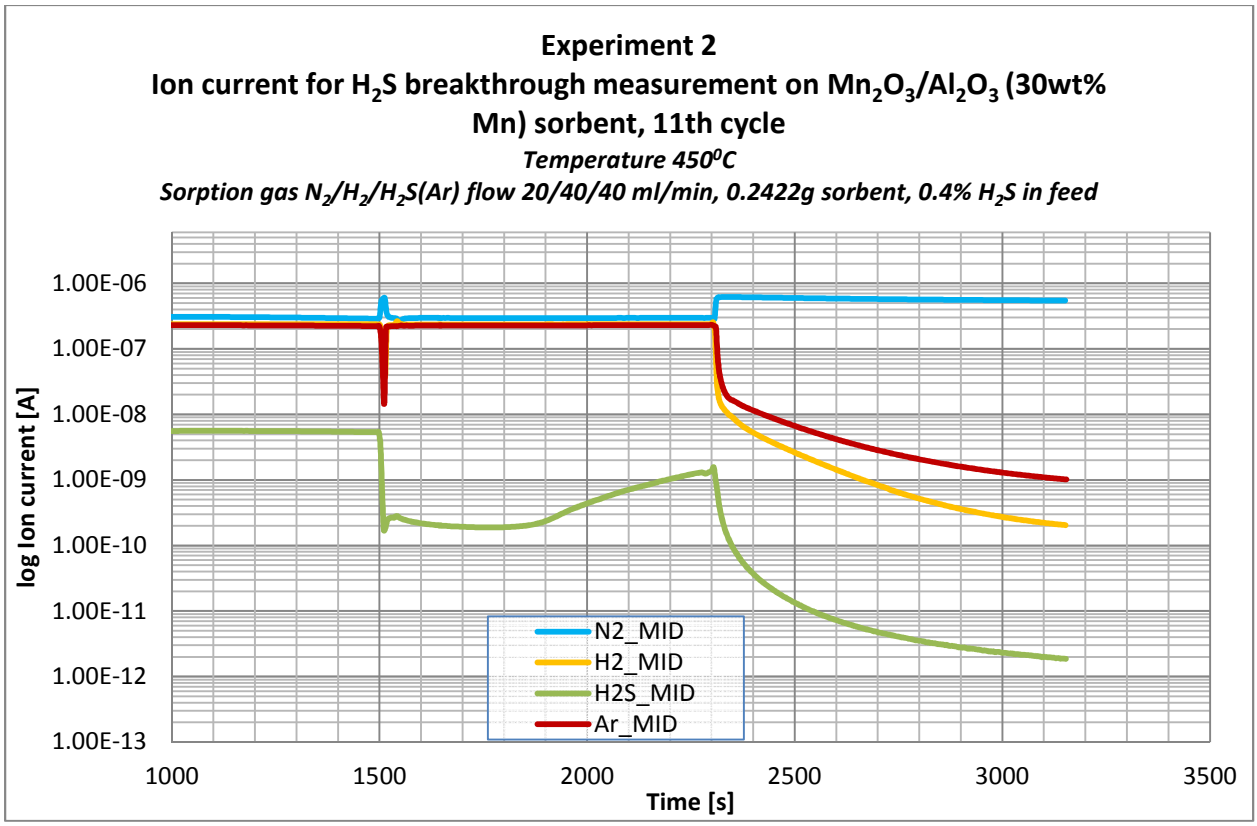
Experiment 2
Ion current for H2S breakthrough measurement on Mn2O3/Al2O3 (30wt% Mn) sorbent, 11th cycle
Temperature 450⁰C
Sorption gas N2/H2/H2S(Ar) flow 20/40/40 ml/min, 0.2422g sorbent, 0.4% H2S in feed
log Ion current [A]
1.00E-06
1.00E-07
1.00E-08
1.00E-09
1.00E-10
1.00E-11
1.00E-12
1.00E-13
1000
1500
2000
2500
3000
3500
Time [s]
N2_MID
H2_MID
H2S_MID
Ar_MID

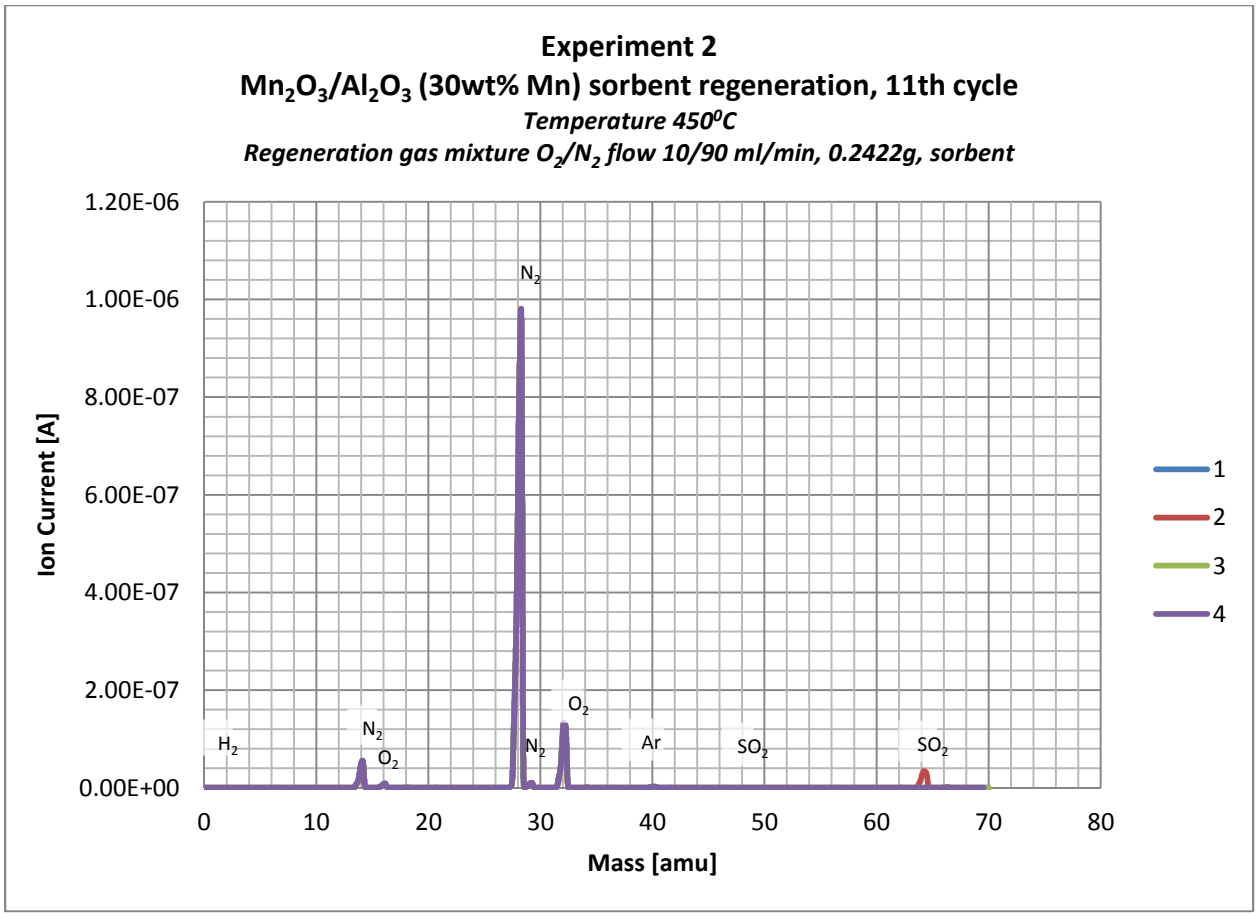
Experiment 2
Mn2O3/Al2O3 (30wt% Mn) sorbent regeneration, 11th cycle
Temperature 450⁰C
Regeneration gas mixture O2/N2 flow 10/90 ml/min, 0.2422g, sorbent
Ion Current [A]
1.20E-06
1.00E-06
8.00E-07
6.00E-07
4.00E-07
2.00E-07
0.00E+00
0
10
20
30
40
50
60
70
80
Mass [amu]
H2
N2
O2
N2
O2
N2
Ar
SO2
SO2
1
2
3
4

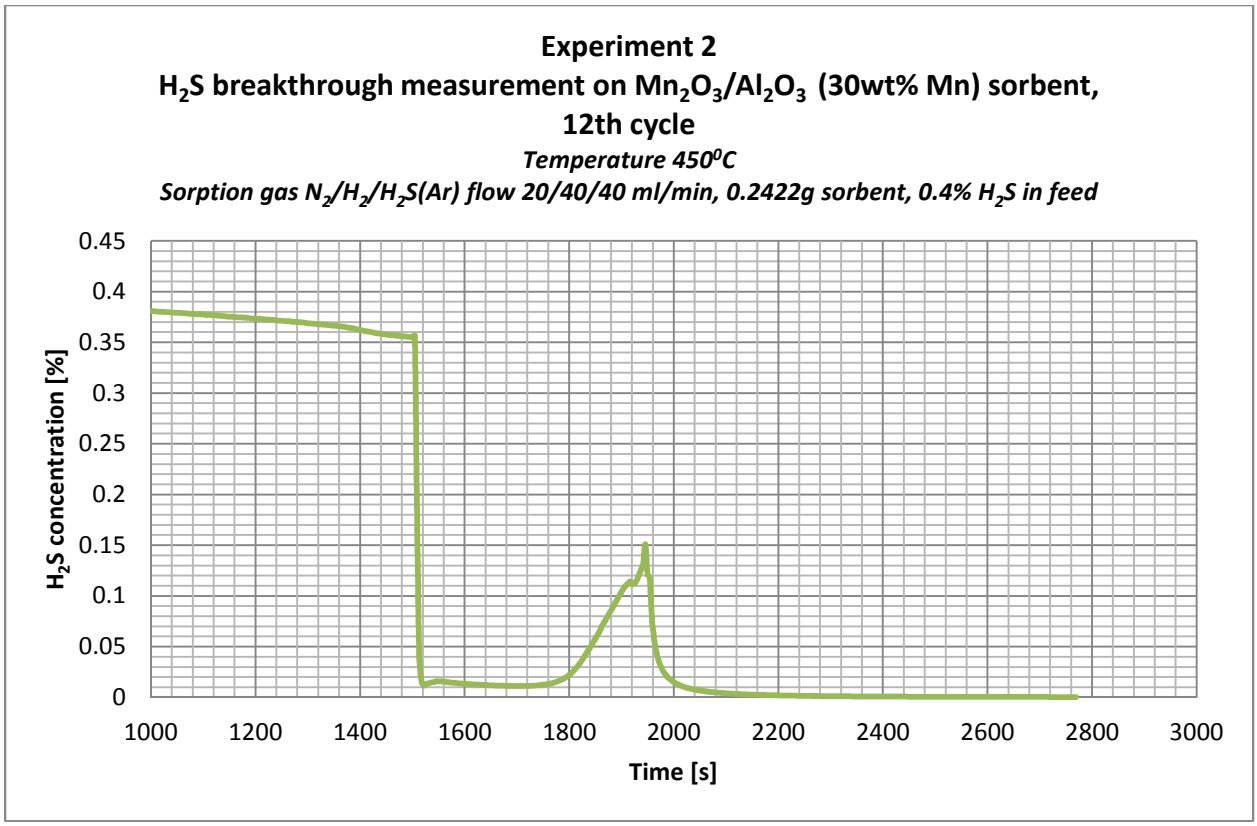
Experiment 2
H2S breakthrough measurement on Mn2O3/Al2O3 (30wt% Mn) sorbent, 12th cycle
Temperature 450⁰C
Sorption gas N2/H2/H2S(Ar) flow 20/40/40 ml/min, 0.2422g sorbent, 0.4% H2S in feed
H2S concentration [%]
0.45
0.4
0.35
0.3
0.25
0.2
0.15
0.1
0.05
0
1000
1200
1400
1600
1800
2000
2200
2400
2600
2800
3000
Time [s]

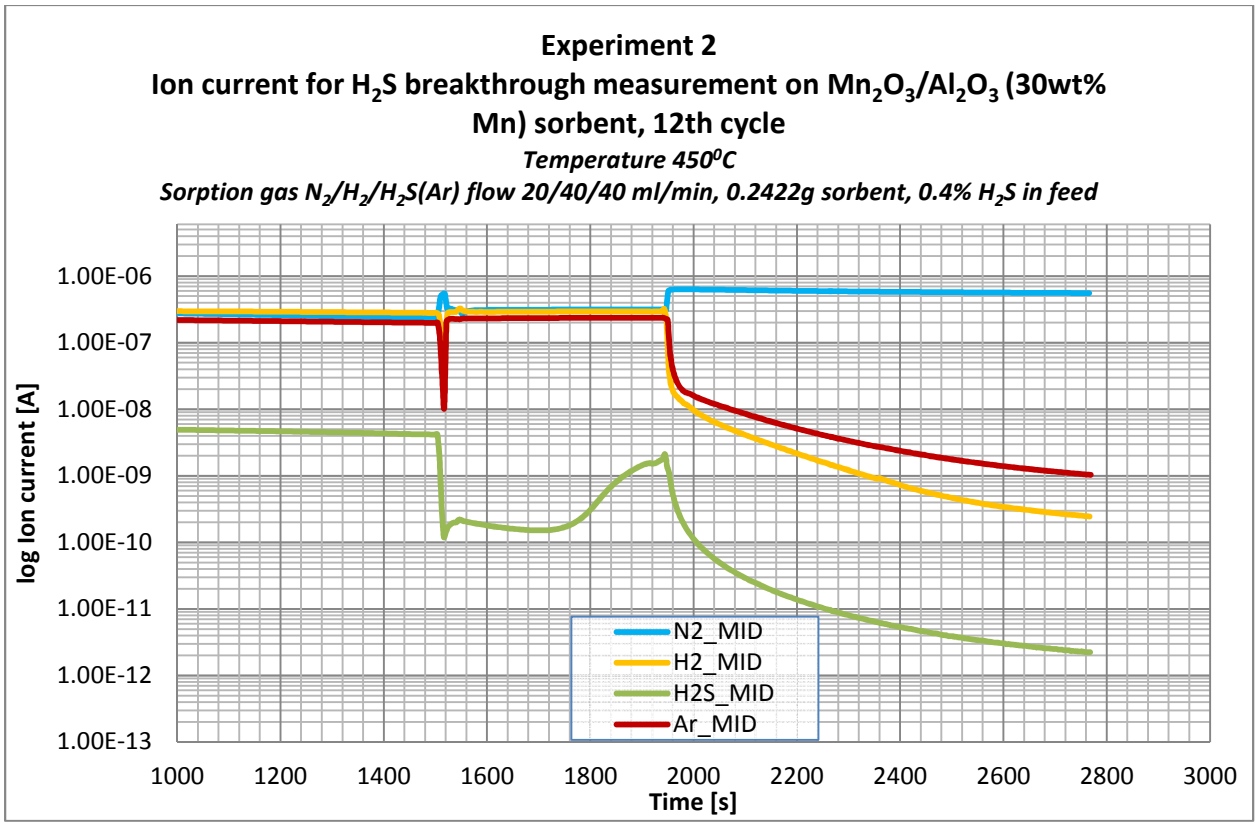
Experiment 2
Ion current for H2S breakthrough measurement on Mn2O3/Al2O3 (30wt% Mn) sorbent, 12th cycle
Temperature 450⁰C
Sorption gas N2/H2/H2S(Ar) flow 20/40/40 ml/min, 0.2422g sorbent, 0.4% H2S in feed
log Ion current [A]
1.00E-06
1.00E-07
1.00E-08
1.00E-09
1.00E-10
1.00E-11
1.00E-12
1.00E-13
1000
1200
1400
1600
1800
2000
2200
2400
2600
2800
3000
Time [s]
N2_MID
H2_MID
H2S_MID
Ar_MID

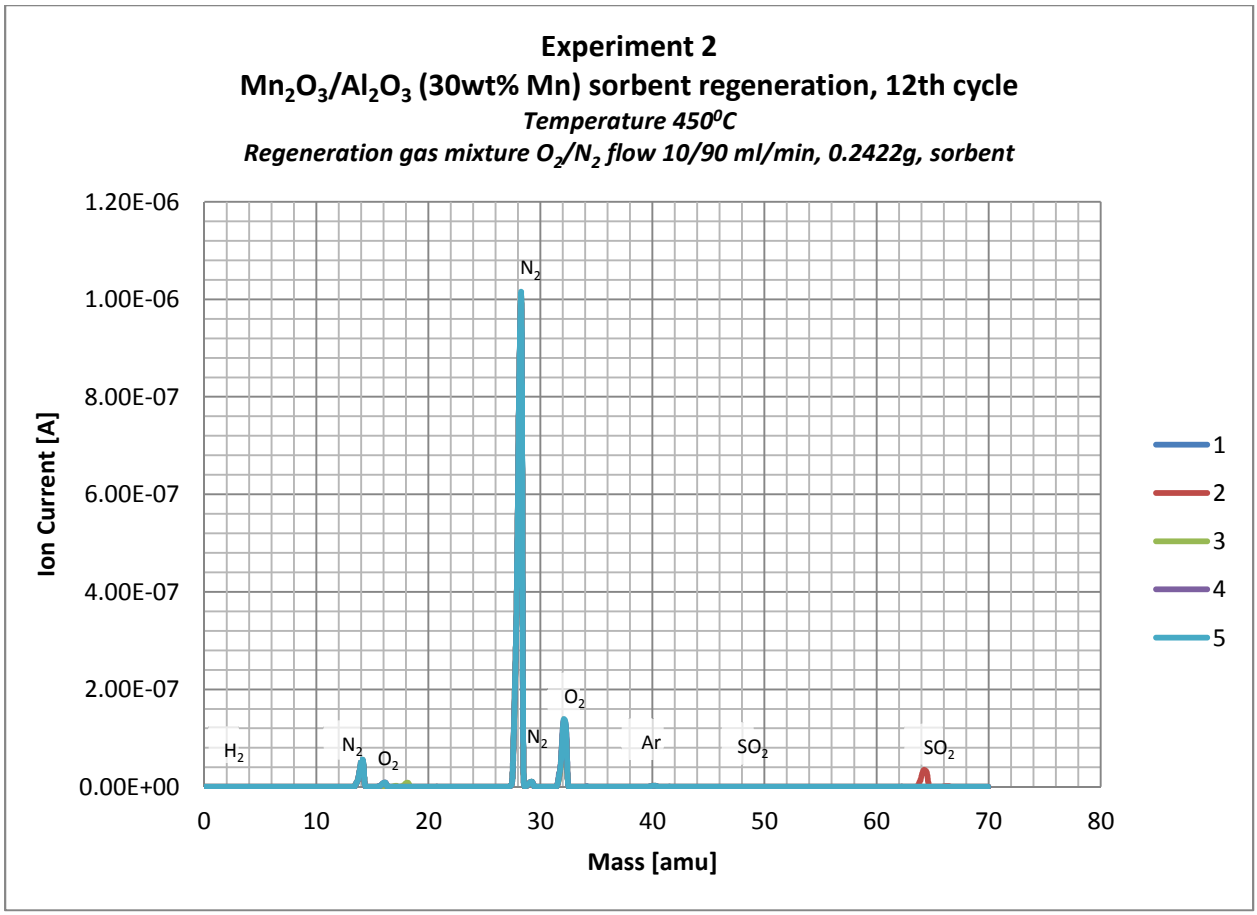
Experiment 2
Mn2O3/Al2O3 (30wt% Mn) sorbent regeneration, 12th cycle
Temperature 450⁰C
Regeneration gas mixture O2/N2 flow 10/90 ml/min, 0.2422g, sorbent
Ion Current [A]
1.20E-06
1.00E-06
8.00E-07
6.00E-07
4.00E-07
2.00E-07
0.00E+00
0
10
20
30
40
50
60
70
80
Mass [amu]
H2
N2
O2
N2
O2
N2
Ar
SO2
SO2
1
2
3
4
5

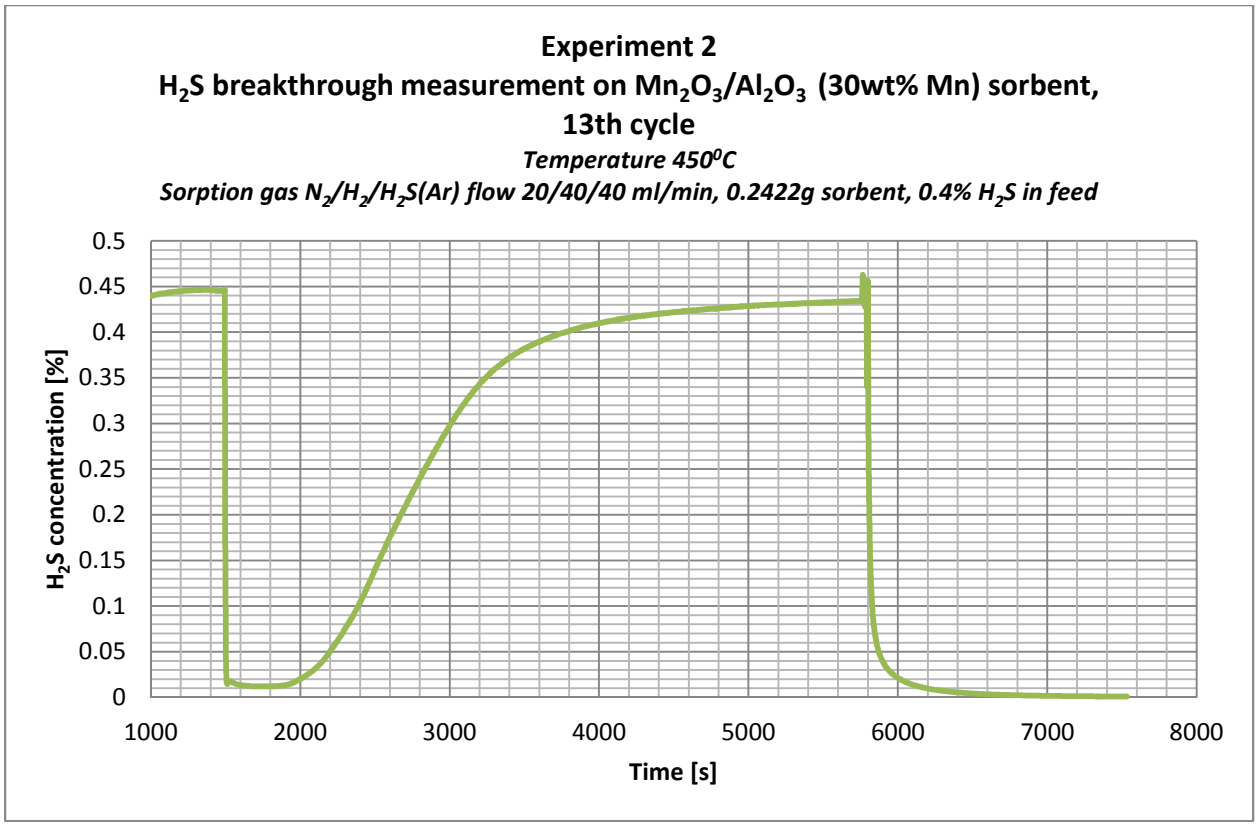
Experiment 2
H2S breakthrough measurement on Mn2O3/Al2O3 (30wt% Mn) sorbent, 13th cycle
Temperature 450⁰C
Sorption gas N2/H2/H2S(Ar) flow 20/40/40 ml/min, 0.2422g sorbent, 0.4% H2S in feed
H2S concentration [%]
0.5
0.45
0.4
0.35
0.3
0.25
0.2
0.15
0.1
0.05
0
1000
2000
3000
4000
5000
6000
7000
8000
Time [s]

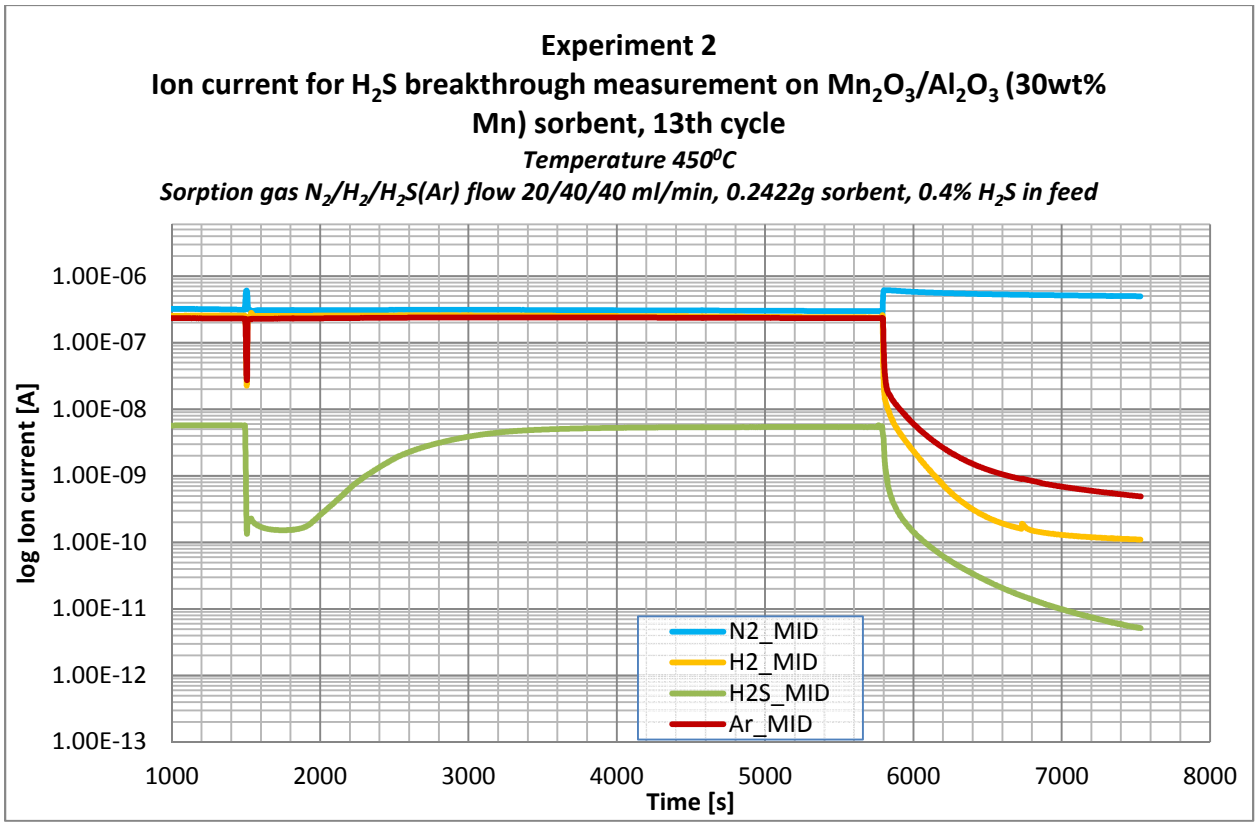
Experiment 2
Ion current for H2S breakthrough measurement on Mn2O3/Al2O3 (30wt% Mn) sorbent, 13th cycle
Temperature 450⁰C
Sorption gas N2/H2/H2S(Ar) flow 20/40/40 ml/min, 0.2422g sorbent, 0.4% H2S in feed
log Ion current [A]
1.00E-06
1.00E-07
1.00E-08
1.00E-09
1.00E-10
1.00E-11
1.00E-12
1.00E-13
1000
2000
3000
4000
5000
6000
7000
8000
Time [s]
N2_MID
H2_MID
H2S_MID
Ar_MID

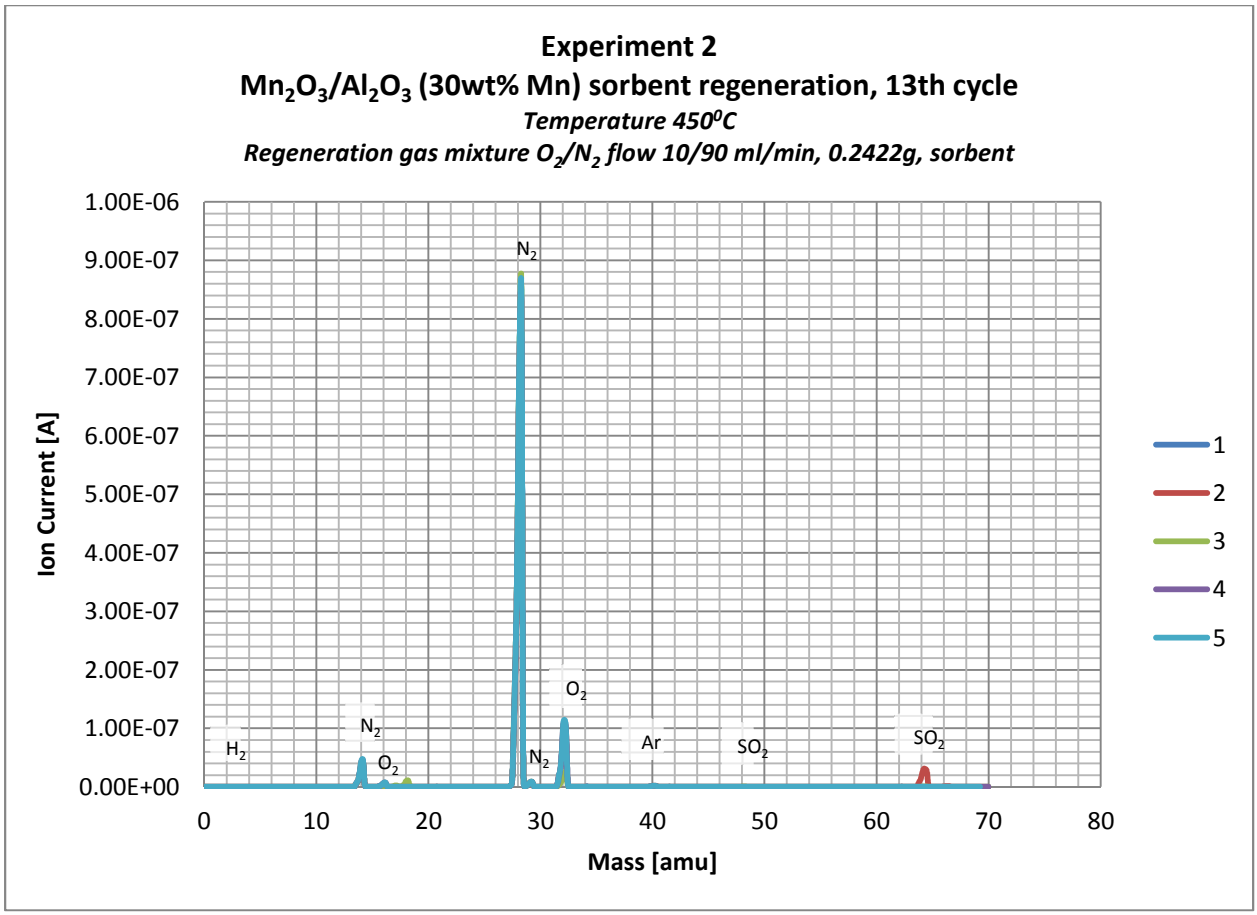
Experiment 2
Mn2O3/Al2O3 (30wt% Mn) sorbent regeneration, 13th cycle
Temperature 450⁰C
Regeneration gas mixture O2/N2 flow 10/90 ml/min, 0.2422g, sorbent
Ion Current [A]
1.00E-06
9.00E-07
8.00E-07
7.00E-07
6.00E-07
5.00E-07
4.00E-07
3.00E-07
2.00E-07
1.00E-07
0.00E+00
0
10
20
30
40
50
60
70
80
Mass [amu]
N2
O2
H2
Ar
SO2
1
2
3
4
5

# *Appendix O Sorbent sorption capacity calculations*

**Experiment 1**

**Calculating for $H_2S$ flow rate in $gH_2S/s$ sorption gas flow rate;**

The sorption gas flow is 10/20/20 ml/min for $N_2/H_2/H_2S$ (Ar)

Gas being used is approx. 1% $H_2S$ in Argon, therefore $H_2S$ flow rate is $\frac{1}{100}$ x 20 ml/min

= 0.2 ml/min

$= \frac{0.2\ x\ 10^{-3}}{60}$ l/min

$= 3.3\ x\ 10^{-6}$ l/s

Converting flow rate to mol/s (1 mol occupies 22.4 l) $= \frac{3.3\ x\ 10^{-6}}{22.4}$ mol$H_2S$/s

$= 1.5\ x\ 10^{-7}$ mol$H_2S$/s

Converting flowrate to g/s (1 mol of $H_2S$ has a molecular weight of 34g) $= 34\ x\ 1.5\ x\ 10^{-7}$g$H_2S$/s

$= \mathbf{5.0\ x\ 10^{-6}}$ **g$H_2S$/s**

**Experiment 2**

**Calculating for $H_2S$ flow rate in $gH_2S/s$ sorption gas flow rate;**

The sorption gas flow is 20/40/50 ml/min for $N_2/H_2/H_2S$ (Ar)

Gas being used is approx. 1% $H_2S$ in Argon, therefore $H_2S$ flow rate is $\frac{1}{100}$ x 40 ml/min

= 0.4 ml/min

$= \frac{0.4\ x\ 10^{-3}}{60}$ l/min

$= 6.6\ x\ 10^{-6}$ l/s

Converting flow rate to mol/s (1 mol occupies 22.4 l) $= \frac{6.6\ x\ 10^{-6}}{22.4}$ mol$H_2S$/s

$= 3.0\ x\ 10^{-7}$ mol$H_2S$/s

Converting flow rate to g/s (1 mol of $H_2S$ has a molecular weight of 34g) $= 34\ x\ 3.0\ x\ 10^{-7}$g$H_2S$/s

$= \mathbf{1.02\ x\ 10^{-5}}$ **g$H_2S$/s**

## $Mn_2O_3/Al_2O_3$ (15wt% Mn) sorbent

**Calculating for Maximum sorption capacity of sorbent used;**

Based on mass of sorbent used in Experiment 1 = 0.1209gSorbent

Mass of manganese in sorbent = $\frac{15}{100} x$ 0.1209 g

= 0.018g

Converting to mols of Mn (Molecular weight of Mn is 55g) = $\frac{0.018}{55}$ mols

= 0.00033 mol/0.1209gSorbent

According to sulfidation equation, molar ration of Mn to $H_2S$ is 1

Therefore, mols $H_2S$ required to fully saturate the prepared sorbent is 0.00033 mol/0.1209gSorbent

= 34 x 0.00033 g$H_2S$/0.1209 gSorbent

= 0.093 g$H_2S$/ gSorbent

***NB: The maximum sorption capacity is the same for Experiment 2 since both the flow rates and mass of sorbent are doubled***

## Experiment 1

**Mass weighed:** 0.1209g

Table A- 3 Sorption capacity for $Mn_2O_3/Al_2O_3$_15wt%, Experiment 1

| Cycle | *Time for sorption breakthrough curve to reach approx 0.02% | **Amount of $H_2S$ removed [$gH_2S$] | ***Sorption capacity [$gH_2S$/gSorbent] |
|---|---|---|---|
| 1 | 1024 | 5.18E-03 | 4.29E-02 |
| 2 | 632 | 3.20E-03 | 2.64E-02 |
| 3 | 1031 | 5.22E-03 | 4.31E-02 |
| 4 | 890 | 4.50E-03 | 3.72E-02 |
| 5 | 795 | 4.02E-03 | 3.33E-02 |
| 6 | 757 | 3.83E-03 | 3.17E-02 |
| 7 | 378 | 1.91E-03 | 1.58E-02 |
| 8 | 840 | 4.25E-03 | 3.52E-02 |
| 9 | 790 | 4.00E-03 | 3.31E-02 |
| 10 | 753 | 3.81E-03 | 3.15E-02 |
| 11 | 723 | 3.66E-03 | 3.03E-02 |
| 12 | 341 | 1.73E-03 | 1.43E-02 |
| 13 | 761 | 3.85E-03 | 3.18E-02 |

*Time is calculated as the difference between the time when the sorption gas is switched to the reactor and the time when the concentration increases to 0.02%

*Amount of $H_2S$ removed [$gH_2S$] = Time to reach approx. 0.02% [s] x $H_2S$ flowrate [$gH_2S$/s]

**Sorption capacity [$gH_2S$/gSorbent] = Amount of H2S removed [$gH_2S$] / Mass of sorbent used [gSorbent]

## Experiment 2

**Mass weighed:** 0.2417g

Table A- 4 Sorption capacity for $Mn_2O_3/Al_2O_3$_15wt%, Experiment 2

| Cycle | *Time for sorption breakthrough curve $H_2S$ concentration to reach approx 0.02% | **Amount of $H_2S$ removed [$gH_2S$] | ***Capacity [$gH_2S$/gSorbent] |
|---|---|---|---|
| 1 | 1160 | 1.17E-02 | 4.86E-02 |
| 2 | 616 | 6.23E-03 | 2.58E-02 |
| 3 | 1010 | 1.02E-02 | 4.23E-02 |
| 4 | 928 | 9.39E-03 | 3.89E-02 |
| 5 | 828 | 8.38E-03 | 3.47E-02 |
| 6 | 770 | 7.79E-03 | 3.22E-02 |
| 7 | 445 | 4.50E-03 | 1.86E-02 |
| 8 | 840 | 8.50E-03 | 3.52E-02 |
| 9 | 774 | 7.83E-03 | 3.24E-02 |
| 10 | 736 | 7.45E-03 | 3.08E-02 |
| 11 | 702 | 7.10E-03 | 2.94E-02 |
| 12 | 375 | 3.79E-03 | 1.57E-02 |
| 13 | 778 | 7.87E-03 | 3.26E-02 |

*Time is calculated as the difference between the time when the sorption gas is switched to the reactor and the time when the concentration increases to 0.02%

**Amount of $H_2S$ removed [$gH_2S$] = Time to reach approx. 0.02% [s] x $H_2S$ flowrate [$gH_2S$/s]

***Sorption capacity [$gH_2S$/gSorbent] = Amount of $H_2S$ removed [$gH_2S$] / Mass of sorbent used [gSorbent]

## $Mn_2O_3/Al_2O_3$ (30wt% Mn) sorbent

**Calculating for Maximum sorption capacity of sorbent used;**

Based on mass of sorbent used in Experiment 1 = 0.1208gSorbent

Mass of manganese in sorbent = $\frac{30}{100} x$ 0.1208 g

= 0.036g

Converting to mols of Mn (Molecular weight of Mn is 55g) = $\frac{0.036}{55}$ mols

= 0.00066 mol/0.1208gSorbent

According to sulfidation equation, molar ration of Mn to $H_2S$ is 1

Therefore, mols $H_2S$ required to fully saturate the prepared sorbent is 0.00066 mol/0.1208gSorbent

= 34 x 0.00066 g$H_2S$/0.1208 gSorbent

= 0.19 g$H_2S$/gSorbent

***NB: The maximum sorption capacity is the same for Experiment 2 since both the flow rates and mass of sorbent are doubled***

## Experiment 1

**Mass weighed:** 0.1208g

Table A- 5 Sorption capacity for $Mn_2O_3/Al_2O_3$_30wt%, Experiment 1

| Cycle | *Time for sorption breakthrough curve $H_2S$ concentration to reach approx 0.02% | **Amount of $H_2S$ removed [g$H_2S$] | ***Capacity [g$H_2S$/gSorbent] |
|---|---|---|---|
| 1 | 2196 | 1.11E-02 | 9.20E-02 |
| 2 | 1194 | 6.04E-03 | 5.00E-02 |
| 3 | 1410 | 7.13E-03 | 5.91E-02 |
| 4 | 765 | 3.87E-03 | 3.20E-02 |
| 5 | 554 | 2.80E-03 | 2.32E-02 |
| 6 | 487 | 2.46E-03 | 2.04E-02 |
| 7 | 370 | 1.87E-03 | 1.55E-02 |
| 8 | 429 | 2.17E-03 | 1.80E-02 |
| 9 | 420 | 2.12E-03 | 1.76E-02 |
| 10 | 383 | 1.94E-03 | 1.60E-02 |
| 11 | 349 | 1.77E-03 | 1.46E-02 |
| 12 | 192 | 9.71E-04 | 8.04E-03 |
| 13 | 316 | 1.60E-03 | 1.32E-02 |

*Time is calculated as the difference between the time when the sorption gas is switched to the reactor and the time when the concentration increases to 0.02%

**Amount of $H_2S$ removed [g$H_2S$] = Time to reach approx. 0.02% [s] x $H_2S$ flowrate [g$H_2S$/s]

***Sorption capacity [g$H_2S$/gSorbent] = Amount of $H_2S$ removed [g$H_2S$] / Mass of sorbent used [gSorbent]

## Experiment 2

**Mass weighed:** 0.2422g

Table A- 6 Sorption capacity for $Mn_2O_3/Al_2O_3$_30wt%, Experiment 2

| Cycle | *Time for sorption breakthrough curve $H_2S$ concentration to reach approx 0.02% | **Amount of $H_2S$ removed [$gH_2S$] | ***Capacity [$gH_2S$/gSorbent] |
|---|---|---|---|
| 1 | 2346 | 2.37E-02 | 9.80E-02 |
| 2 | 1019 | 1.03E-02 | 4.26E-02 |
| 3 | 1272 | 1.29E-02 | 5.31E-02 |
| 4 | 973 | 9.85E-03 | 4.07E-02 |
| 5 | 716 | 7.25E-03 | 2.99E-02 |
| 6 | 570 | 5.77E-03 | 2.38E-02 |
| 7 | 491 | 4.97E-03 | 2.05E-02 |
| 8 | 686 | 6.94E-03 | 2.87E-02 |
| 9 | 549 | 5.56E-03 | 2.29E-02 |
| 10 | 461 | 4.66E-03 | 1.93E-02 |
| 11 | 411 | 4.16E-03 | 1.72E-02 |
| 12 | 291 | 2.94E-03 | 1.22E-02 |
| 13 | 507 | 5.13E-03 | 2.12E-02 |

*Time is calculated as the difference between the time when the sorption gas is switched to the reactor and the time when the concentration increases to 0.02%

**Amount of $H_2S$ removed [$gH_2S$] = Time to reach approx. 0.02% [s] x $H_2S$ flowrate [$gH_2S$/s]

***Sorption capacity [$gH_2S$/gSorbent] = Amount of $H_2S$ removed [$gH_2S$] / Mass of sorbent used [gSorbent]

## *Appendix P Raman spectroscopy results*

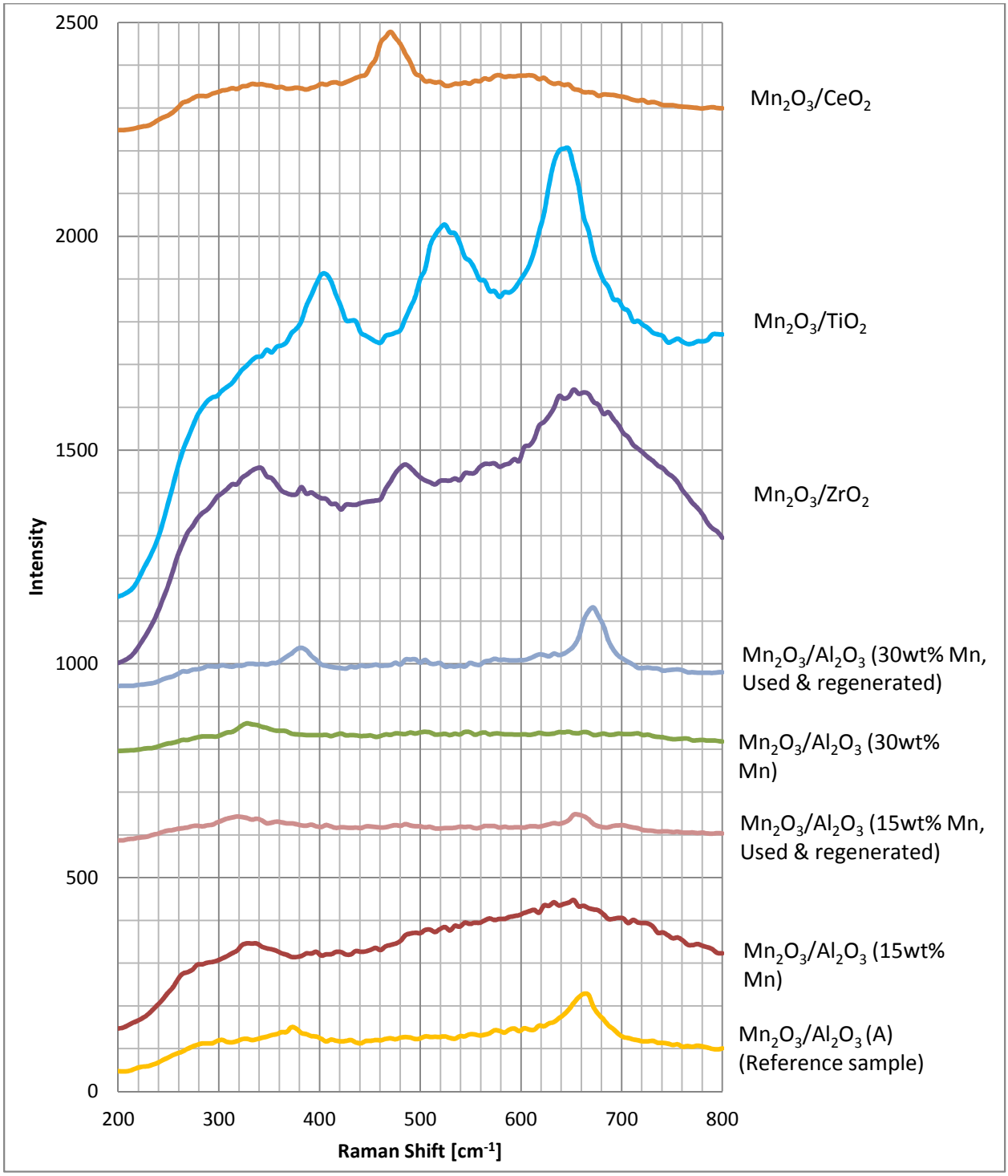


**Figure A 1 Raman spectra of the reference sample $Mn_xO_y$-$Al_2O_3$ (A) [49], the prepared sorbents; $Mn_2O_3/Al_2O_3$ (15wt% Mn), $Mn_2O_3/Al_2O_3$ (30wt% Mn), $Mn_2O_3/ZrO_2$, $Mn_2O_3/TiO_2$ and $Mn_2O_3/CeO_2$ sorbents, and the used and regenerated $Mn_2O_3/Al_2O_3$ (15wt%) and $Mn_2O_3/Al_2O_3$ (30wt%)**
**NB: Curves have been off-set along the y-axis for the sake of clarity and ease of comparison**